

https://dspace.org/

Atmospheric corrosion mapping of South Africa and the Greater Johannesburg Metropolitan Area (GJMA)

Janse Van Rensburg, Darelle Tania

2019

https://hdl.handle.net/10539/28770

Jane Van Rensburg, Darelle Tania (2019) Atmospheric corrosion mapping of South Africa and the Greater Johannesburg Metropolitan Area (GJMA), University of the Witwatersrand, Johannesburg, <http://hdl.handle.net/10539/28770>

Downloaded from a DSpace repository. https://dspace.org/

UNIVERSITY OF THE WITWATERSRAND, JOHANNESBURG

Atmospheric corrosion mapping of South Africa and the Greater Johannesburg Metropolitan Area (GJMA)

by

Darelle Tania Janse van Rensburg

A thesis submitted to the Faculty of Engineering and Built Environment, University of the Witwatersrand, in fulfilment of the requirements for the degree

Doctor of Philosophy (Materials and Metallurgy)

Supervisor: Prof. Lesley A. Cornish

Co-supervisor: Prof. Josias van der Merwe

Johannesburg, February 2019

© University of the Witwatersrand

Declaration

I declare that this thesis is my own work. It is being submitted for the Degree of Doctor of Philosophy at the University of the Witwatersrand, Johannesburg. It has not been submitted before for any degree or examination at any other University.



_____

Signature

14th day of February 2019 in Florida Hills.

Atmospheric corrosion mapping of South Africa and the Greater Johannesburg Metropolitan Area (GJMA)

ABSTRACT

The first corrosion map of South Africa (SA) was published in 1991. Since then only minor variations have been made to this map. However, due to the lack of differentiation of inland locations, overstatement of the corrosivity of environments, changes in international standards regarding the measurement of corrosive atmospheres, increased industrialisation of SA's large metropolitan areas, global climate change effects and improved mapping techniques, this chart has become outdated. The present study focused on the development of a new corrosion map for SA, with the emphasis placed on the provision of more detail concerning the atmospheric corrosivity of the Greater Johannesburg Metropolitan Area (GJMA) – SA's economic heartland.

In the study, historical published and unpublished corrosion data for South Africa were assimilated and analysed. The atmospheric corrosivity of the GJMA was also measured using ASTM G116 wire-on-bolt and ISO 9226:1992 open aluminium, zinc and copper wire helix devices, including ISO 9226:2012 flat mild steel and hot-dip galvanised steel coupons. Coated mild steel specimens were also exposed to determine the corrosive effects of the GJMA's atmosphere on organic materials. The morphologies and chemical compositions of the mild steel corrosion products, using SEM-EDS, FTIR and Raman spectroscopy, as well as pH and water-soluble salt measurement techniques were furthermore investigated, along with correlations between the measured corrosion data, and general meteorological and pollution parameters for the GJMA area.

The study showed that the corrosivity of SA's coastal environments decreases rapidly within the first 150 m from the ocean and that for most inland locations, very *low* (C1) to potentially *high* (C4) corrosive conditions may be expected, as per the ISO 9223 rating scheme. High correlations were also found between the first-year corrosion rates of mild steel, hot-dip galvanised steel, zinc, aluminium and copper. Moreover, it was confirmed that the corrosivity

of the GJMA is influenced by precipitation, humidity, PM_{10} and $PM_{2.5}$ particulate matter, as well as SO_2, NO_2, NO, CO and O_3 levels in the atmosphere, including wind direction and daily temperatures (maximum and minimum). Other factors found to affect the corrosivity of the GJMA's atmosphere are: elevations above sea and ground level; the presence of vegetation and large water bodies; topography; shielding and shading effects; the occurrence of an El Niño or La Nina event; and acid rain.

Moreover, it was established that the GJMA is most corrosive during spring and summer and that at least 90% of the area can be rated Upper-C2 (*low* to *medium*) corrosive. The results furthermore revealed high correlations between the ISO 9223 (1992 and 2012) corrosion monitoring devices and that wire-on-bolt (CLIMAT) units are better indicators of the impact of atmospheric pollutants on the 12- month corrosion rate of hot-dip galvanised steel than uncoated steel. A strong linear correlation was also found regarding the average corrosion rate of mild steel with every 20 mg/m^2 rise in the concentration of water-soluble salts in the corrosion product.

The East Rand of the GJMA rated most corrosive, with corrosion trouble spots identified at Aeroport, Bonaero Park, Brakpan, Chloorkop, Dalpark, Dunnottar, and Nigel. The Kagiso-Randfontein area was the only other area, outside the East Rand, that rated more corrosive. Extrapolations of the long-term corrosion rates of mild steel and hot-dip galvanised steel in the GJMA were additionally made based on logarithmic regressions of the 6-, 12-, 18- and 24-month corrosion data. Finally, geoprocessed (metal specific) corrosion maps were developed for the GJMA, subsequently incorporated into several corrosion maps for SA (also metal specific), to provide better clarity regarding SA's inland areas.

Keywords: Corrosion, atmosphere, South Africa, Greater Johannesburg, inland Metropolitan, wire-on-bolt, CLIMAT, ISO 9223, mapping, pollution, mild steel, hot-dip galvanised steel, aluminium, zinc, copper, coatings

Dedication / Nagedagtenis



In nagedagtenis van my Moeder - vir haar onvoorwaardelike liefde en wie my van jongs af aan ‘n akademiese kultuur blootgestel het.

(In memory of my Mother - for her unconditional love and whom has exposed me to an academical culture from an early age).

Susan Vermaakt

1939 to 2004

---o0o---

Acknowledgements

The author would like to express her sincerest gratitude to the following companies, institutions and persons in preparing this thesis.

Academic Advice

Professor Lesley A. Cornish

Professor Josias van der Merwe

Financial Support

Orytech (Pty) Ltd.

Department of Science and Technology

National Research Foundation

University of the Witwatersrand &

DST-NRF Centre of Excellence in Strong Materials

Hot Dip Galvanizers Association of Southern Africa

Facilities and Equipment

Orytech (Pty) Ltd.

University of the Witwatersrand

SGS - Johannesburg

City of Johannesburg – Environmental Department

All site owners

Materials

Orytech (Pty) Ltd.

Jotun SA

Powder-Lak (Pty) Ltd.

Optima Coatings

Permission to Publish

Eskom Holdings SOC Limited

South African Weather Services

City of Johannesburg

City of Ekurhuleni

General Advice and Editing

Sunette van Allemann, Verine Etsebeth, Markus Janse van Rensburg and Professor Lesley Cornish

Site- and Test-related Support

Onkgoptse Alfred Pheko

Tebogo Mokgomo

Dr. Rudolph Erasmus

General Support, Friendship and Love

My father, Les Vermaakt

My husband, Tinus

My children, Sunette, Markus, Riandé and Quinton,

and granddaughter, Leja

My assistant, Rulien Britz

My friend, Verine Etsebeth

and finally, but most importantly,

GOD THE ALMIGHTY

For having given me the ability, as well as mental and physical strength to complete this thesis… (*The heavens declare the glory of God; the skies proclaim the work of his hands: Psalm 19:1*)

Contents

Sec. no.	Description of Contents	Page no.
	Contents	viii
	List of figures	xiv
	List of tables	xxiv
	Nomenclature	xxvii
	List of abbreviations	xxix
	List of symbols	xxxiii
1	**CHAPTER 1 – INTRODUCTION – THE NEED FOR A NEW CORROSION MAP**	1
1.1	**Introduction**	1
1.2	**Shortfalls of the Callaghan map**	5
1.2.1	Lack of differentiation of inland areas	5
1.2.2	Overstatement of corrosion rates	6
1.2.3	Complicating the use of ISO 9223 to 9226, and ISO 12944 series of standards	7
1.2.4	Discouraging the use of more user- and environmentally-friendly coating systems	8
1.2.5	No reflection of increased industrialisation and global warming effects	9
1.3	**The need for detailed corrosion monitoring of the Greater Johannesburg Metropolitan Area (GJMA)**	10
1.4	**Primary research objectives and deliverables**	10
1.5	**Hypothesis**	11
1.6	**Research questions**	11
1.7	**Benefits and novelty of the research work**	13
1.8	**Research limitations**	14
1.9	**Structure of the thesis**	14
1.10	**Publications**	16
1.11	**Presentations**	16
2	**CHAPTER 2 – LITERATURE REVIEW**	17
2.1	**Atmospheric corrosion**	17
2.1.1	Corrosion	17
2.1.2	The atmosphere	17
2.1.3	The nature of atmospheric corrosion	19
2.1.3.1	*Atmospheric corrosion*	19
2.1.3.2	*The mechanism of atmospheric corrosion*	19
	Basic atmospheric corrosion	20
	Electrolyte formation	24
2.1.3.3	*Residence time of the thin film electrolyte/time of wetness (TOW)*	27
2.1.3.4	*Gas, aerosol and particle deposition*	29
2.1.3.5	*Salt production in marine environments*	30
2.1.3.6	*Dissolution of the metal and formation of the corrosion product*	31
2.1.4	Environmental and air quality parameters that influence atmospheric corrosion	31
2.1.4.1	*Precipitation, RH and acid rain*	32
2.1.4.2	*Temperature*	35
2.1.4.3	*Wind*	36
2.1.4.4	*Sunlight*	38

Sec. no.	Description of Contents	Page no.
2.1.4.5	*Topographical effects*	40
2.1.4.6	*Biomes and animal interaction*	42
2.1.4.7	*Oxygen*	43
2.1.4.8	*Chlorides*	43
2.1.4.9	*Sulphur-containing compounds*	44
2.1.4.10	*Nitrogen-containing compounds*	46
2.1.4.11	*Organic acids*	47
2.1.4.12	*Ozone, strong oxidants and hydrogen peroxide*	48
2.1.4.13	*Carbon dioxide (CO_2)*	49
2.1.4.14	*Time, initial period, and angle of exposure*	50
2.1.5	Atmospheric corrosion of carbon steel, hot-dip galvanised steel, aluminium, zinc and copper	51
2.1.5.1	*Carbon steel, irons (Fe), and alloy steels*	51
2.1.5.2	*Zinc (Zn) and hot-dip galvanising*	55
2.1.5.3	*Copper (Cu)*	58
2.1.5.4	*Aluminium (Al)*	60
2.1.6	Atmospheric corrosion classification	62
2.1.6.1	*BS EN 12500-2000 standard*	62
2.1.6.2	*CLIMAT (wire-on-bolt) classification*	62
2.1.6.3	*ISO classification*	65
2.1.7	Atmospheric corrosion monitoring	68
2.1.7.1	*Weight-loss/damage rate measurements*	69
2.1.7.2	*Weight-gain procedures*	71
2.1.7.3	*Online electrical resistance (ER) measurements*	72
2.1.7.4	*Linear polarisation resistance (LPR) and electrochemical impedance (EIS) techniques*	72
2.1.8	Modelling of atmospheric corrosion	72
2.1.9	Atmospheric corrosion maps	78
2.2	**The history of atmospheric corrosion monitoring in South Africa**	85
2.3	**Factors that may drive atmospheric corrosion in the GJMA**	94
2.3.1	Population and density	96
2.3.2	Development of the GJMA	97
2.3.3	Housing	98
2.3.4	Gold mine tailing dumps	99
2.3.5	The industrial heart	99
2.3.6	Airports	100
2.3.7	Transport	100
2.3.8	Railway	100
2.3.9	Gas, power and telecommunication infrastructure	100
2.3.10	Business and commercial infrastructure	101
2.3.11	Water	101
2.9.12	Dams, nature reserves, recreational parks and vegetation	101
2.9.13	Topography of the GJMA	102
2.2.14	General meteorology of the GJMA	102
2.2.15	General pollution of the GJMA	109
3	**CHAPTER 3 – METHODOLOGY**	113
3.1	**Atmospheric corrosion of South Africa – Data compilation**	113
3.2	**Corrosion monitoring of the GJMA – Experimental procedures**	114
3.2.1	Exposure sites	115

Sec. no.	Description of Contents	Page no.
3.2.2	Design and fabrication of test racks, and flat metal specimens	117
3.2.2.1	*Design, fabrication and installation of test racks*	117
3.2.2.2	*Preparation and chemical cleaning of flat, uncoated mild steel and hot-dip galvanised steel coupons*	120
3.2.3	Optical surface characterisation, morphology and chemical analysis of the mild steel corrosion products formed at the main and mini sites in the GJMA	122
3.2.4	ASTM G116-99 – Wire-on-bolt corrosion monitoring units	124
3.2.5	ISO 9226:1992 – Open wire helix (WH) units	125
3.2.6	Site inspections, and installations of test racks and other corrosion monitoring devices	127
3.2.7	Atmospheric corrosivity classification of the environments	127
3.3	**Preparation, exposure and evaluation/analysis of coated mild steel coupons**	128
3.3.1	Preparation of coated samples	128
3.3.2	Exposure of coated samples	129
3.3.3	Dry film thickness, chalking, degree of dirt retention, colour and gloss measurements of the coated samples	130
3.3.3.1	*Attenuated total reflectance – Fourier-transform infrared (ATR-FTIR) spectroscopy*	131
3.3.3.2	*Degree of chalking and dirt retention*	131
3.3.3.3	*Colour difference measurements*	131
3.3.3.4	*Gloss measurements*	132
3.3.3.5	*Attenuated total reflectance – Fourier-transform infrared (ATR-FTIR) spectroscopy*	133
3.4	**Meteorological and air quality data situation reports for the GJMA – used for interpretation of the corrosion results**	133
3.4.1	Meteorological data	134
3.4.1.1	*Temperature*	134
3.4.1.2	*Relative humidity, rainfall and acid rain*	136
3.4.1.3	*Wind speed and direction*	140
3.4.1.4	*Ultraviolet (UV) light radiation*	144
3.4.2	Air pollution effects	145
3.5	**Mapping procedures**	153
4	**CHAPTER 4 – RESULTS**	154
4.1	**Assimilations of existing published and unpublished atmospheric corrosion data for South Africa**	154
4.2	**Atmospheric corrosion of the GJMA**	154
4.2.1	Condition assessment of existing infrastructure at the 57 exposure sites	162
4.2.2	Corrosion indices (CLIMAT/wire-on-bolt units)	164
4.2.3	Aluminium, zinc, and copper wire helix (WH) corrosion rates	170
4.2.4	Flat metal panel corrosion rates	175
4.2.4.1	*Mild steel panels (MSPO) – Main sites*	175
4.2.4.2	*Hot-dip galvanised mild steel panels (GSP) – Main sites*	175
4.2.5	Mild steel panels (MSP) – Main and mini sites	176
4.2.6	Optical surface characterisation, morphology and chemical analysis of the mild steel corrosion products formed at the main and mini sites in the GJMA	183
4.2.6.1	*Optical surface characterisation of the corrosion product*	183
4.2.6.2	*Morphology of the mild steel corrosion product*	189
	Attenuated total reflectance (ATR) – Fourier transform infrared (FTIR) spectroscopy analysis	189
	Raman spectroscopy	189
4.2.6.3	*Chemical analysis of the mild steel corrosion products*	194

Sec. no.	Description of Contents	Page no.
	Scanning electron microscopy (SEM) and energy dispersive X-ray spectroscopy (EDS)	194
	Water-soluble salts and pH measurements	194
4.3	The effects of the GJMA atmosphere on organic coatings	199
4.3.1	Degree of corrosion of the coated panels	199
4.3.2	Changes in average coating thicknesses (DFTs)	199
4.3.3	Degree of chalking and dirt retention	204
4.3.4	Changes in 60° specular gloss levels	207
4.3.5	Changes in colour	209
4.3.6	Changes in the chemical structures of the coatings	209
5	**CHAPTER 5 - DISCUSSION**	212
5.1	**Atmospheric corrosivity of South Africa**	212
5.1.1	Mild (carbon) steel	212
5.1.2	Hot-dip galvanised mild steel	225
5.1.3	Pure zinc	228
5.1.4	Pure aluminium	232
5.1.5	Pure copper	236
5.1.6	Comparison of the different metal corrosion rates	237
5.1.7	Atmospheric (ACI), Industrial (ICI) and Marine (MCI) corrosion indices	239
5.1.8	Correlations of atmospheric corrosion data	242
5.1.9	Corrosivity rating of South Africa's macro atmosphere	244
5.2	**Atmospheric corrosivity of the GJMA**	244
5.2.1	Industrial, marine and atmospheric corrosion indices	244
5.2.1.1	*Industrial (ICI) corrosion indices*	244
5.2.1.2	*Marine corrosion indices (MCI)*	247
5.2.1.3	*Atmospheric corrosion indices (ACI)*	251
5.2.1.4	*Summary, correlations and preliminary mapping of the CLIMAT data*	255
5.2.2	Aluminium, zinc and copper wire helix (WH) corrosion rates	261
5.2.2.1	*Aluminium helices (Al-WH)*	261
5.2.2.2	*Zinc helices (Zn-WH)*	262
5.2.2.3	*Copper helices (Cu-WH)*	263
5.2.2.4	*Statistical analysis and preliminary mapping of the Al-WH, Zn-WH and Cu-WH data*	265
5.2.3	Mild steel (MSP) corrosion rates – Main sites	270
5.2.4	Hot-dip galvanised mild steel (GSP) corrosion rates – Main sites	281
5.2.5	Mild steel (MSP) corrosion rates - Main and mini sites	288
5.2.6	Visual condition assessments of existing infrastructure vs measured corrosion rates	295
5.2.7	Optical surface characterisation, morphology and chemical analysis of the mild steel corrosion products formed at the main and mini sites in the GJMA	296
5.2.7.1	*Optical surface characterisation of the mild steel corrosion product*	296
5.2.7.2	*Morphology of the mild steel corrosion product*	298
	Attenuated total reflectance (ATR) – Fourier transform infrared (FTIR) spectroscopy analysis	298
	Raman spectroscopy analysis	300
5.2.7.3	*Chemical analysis of the mild steel corrosion product*	302
	Scanning electron microscopy (SEM) and energy dispersive X-ray spectroscopy analysis (EDS)	302
	Water-soluble salts in the mild steel corrosion product	305
	pH measurements of the mild steel corrosion product	309
5.3	**Effects of the GJMA's atmosphere on organic coatings**	313
5.3.1	DFT film thickness (DFT) changes	314

Sec. no.	Description of Contents	Page no.
5.3.2	Degree of chalking and dirt retention	316
5.3.3	Changes in the 60° specular gloss levels	317
5.3.4	Changes in colour	319
5.3.5	Changes in chemical structure	320
5.4	**Physical, meteorological and pollution effects on the corrosivity of the GJMA**	324
5.4.1	Physical effects	324
5.4.1.1	*Topography and relief*	324
5.4.1.2	*Shading and vegetation*	326
5.4.1.3	*Waterbodies*	327
5.4.2	Meteorological effects	328
5.4.2.1	*Temperature*	328
5.4.2.2	*Humidity*	332
5.4.2.3	*Rainfall*	334
5.4.2.4	*Wind speed and direction*	336
5.4.2.5	*Overall impact of meteorological conditions*	338
5.4.2.6	*Ultraviolet (UV) light radiation*	339
5.4.3	Air pollution effects	340
5.4.3.1	*PM_{10} particulate matter*	343
5.4.3.2	*Sulphur dioxide (SO_2)*	345
5.4.3.3	*Nitrogen dioxide (NO_2)*	346
5.4.3.4	*Nitrogen oxide (NO)*	347
5.4.3.5	*$PM_{2.5}$ particular (dust) matter*	348
5.4.3.6	*Carbon dioxide (CO)*	348
5.4.3.7	*Ozone (O_3)*	348
5.4.3.8	*Visibility (haze) and El Niño event*	350
5.4.3.9	*Acid rain*	351
6	**CHAPTER 6 – ATMOSPHERIC CORROSION MAPS FOR SOUTH AFRICA AND THE GJMA**	352
6.1	**Introduction**	352
6.2	**Atmospheric corrosion maps for the Greater Johannesburg Metropolitan area (GJMA)**	353
6.2.1	GJMA – Industrial corrosion map	353
6.2.2	GJMA – 12-month mild steel corrosion map	355
6.2.3	GJMA – 12 month hot-dip galvanised mild steel corrosion map	357
6.2.4	GJMA – 12-month aluminium wire corrosion map	359
6.2.5	GJMA – 12-month zinc wire helix corrosion map	361
6.2.6	GJMA – 12-month copper wire helix corrosion map	363
6.3	**Atmospheric corrosion maps for South Africa**	366
6.3.1	South Africa – 12-month mild steel corrosion map	366
6.3.2	South Africa – 12-month hot-dip galvanised mild steel and pure zinc corrosion maps	369
6.3.3	South Africa – 12-month aluminium corrosion map	372
6.3.4	South Africa – 12-month copper corrosion map	374
6.3.5	South Africa – Corrosion map correlations	374
6.3.6	Comparison of GJMA and SA maps with those produced for other countries	376
7	**CHAPTER 7 – CONCLUSIONS**	377
7.1	**Atmospheric corrosivity of South Africa (SA)**	377

Sec. no.	Description of Contents	Page no.
7.2	**Atmospheric corrosivity of the Greater Johannesburg Metropolitan area (GJMA)**	379
7.2.1	Industrial, marine and atmospheric corrosion indices	379
7.2.2	Aluminium, zinc and copper wire helix (WH) corrosion rates	380
7.2.3	Mild steel corrosion rates – Main and mini sites	381
7.2.4	Hot-dip galvanised mild steel (GSP) corrosion rates – Main sites	384
7.2.5	Optical surface characterisation, morphology and chemical analysis of the mild steel corrosion products formed at the main and mini sites in the GJMA	385
7.2.6	Effects of the GJMA's atmosphere on organic coatings	387
7.2.7	Physical, meteorological and pollution effects on the corrosivity of the GJMA	388
7.3	**Atmospheric corrosion maps for South Africa and the GJMA**	391
7.3.1	Atmospheric corrosion maps for the GJMA	391
7.3.2	Atmospheric corrosion maps for South Africa	392
8	**CHAPTER 8 – RECOMMENDATIONS AND FUTURE PERSPECTIVE**	395
	REFERENCES	396
	APPENDICES	447
A	Population of the GJMA	448
B	GJMA site details	451
C	Metal specifications	454
D	Elcometer 135A & 135B Bresle patches – technical information sheet	459
E	Infrared control spectra of the different coatings.	460
F	Photographs of the GJMA exposure sites	464
G	CLIMAT results per season for the different main GJMA sites	483
H	ISO WH results per annum for the different main GJMA sites	484
I	Mild steel corrosion rates	485
J	Hot-dip galvanised corrosion rates	488
K	Pearson's product-moment correlation coefficients between the different corrosion monitoring results measured for the main GJMA sites	490
L	FTIR spectra of the mild steel corrosion products formed at selected sites in the GJMA	491
M	Raman spectral bands of the mild steel corrosion products formed at selected sites in the GJMA	494
N	SEM-EDS results of the mild steel corrosion products from the GJMA sites	495
O	DFT measurements of the coated samples before and after exposure at the main GJMA sites	497
P	Degree of chalking and dirt retention results	499
Q	Average 60° specular gloss levels of the coated samples before and after exposure at the different GJMA sites	500
R	Measured colour coordinates of coated samples before and after exposure	503
S	QCheck™ correlations (matches) of the coated samples before and after exposure	511
T	Papers and presentations	521

List of Figures

Figure no.	Description of Figure	Page no.
1.1	Callaghan's corrosion map of Southern Africa	2
1.2	Atmospheric corrosion map of Southern Africa – Leitch 1999	3
1.3	Atmospheric corrosion map of Southern Africa – Leitch 2006	4
2.1	Normal composition of the atmosphere	18
2.2	An adaptation of Roberge's schematic of the underlying mechanism of atmospheric corrosion of iron in a non-contaminated environment	20
2.3	Schematic diagram showing the effect of relative humidity on the corrosion rate of steel (in the absence of any pollutants)	26
2.4	Average rainfall map for South Africa	32
2.5	Average summer temperatures for South Africa	36
2.6	Prevailing summer and winter wind systems for South Africa	38
2.7	Average yearly solar irradiation levels for South Africa	40
2.8	A physical map of South Africa	41
2.9	The different terrestrial biomes of South Africa	42
2.10	The natural circulation of nitrogen	47
2.11	Changes in the atmospheric corrosion rate of carbon steel following different exposure periods at Elandsfontein	53
2.12	Changes in the atmospheric corrosion rate of hot-dip galvanised carbon steel after different exposure periods at Elandsfontein	58
2.13	An example of a CLIMAT unit, demonstrating the extent of corrosion of the different galvanic couples after 90 days of exposure in a highly aggressive marine site	63
2.14	Interrelationships between the ISO 9223-9226 procedures	66
2.15	Atmospheric corrosion map of Southern Africa – An adaptation of the Callaghan map	86
2.16	The HDGASA map – based primarily on Callaghan's data	89
2.17	Vosloo's, Pietersen's and Holtzhausen's pollution map of South Africa	90
2.18	Classification of airborne salinity by reference to continental and ocean conditions	92
2.19	Airborne salinity classification, including the wind conditions for the summer climatic situation	93
2.20	The Greater Johannesburg Metropolitan Area (GJMA)	95
2.21	Population densities in South Africa	97
2.22	Land-use categories (as percentages) of the total surface area of the CoJ	98
2.23	A 3D-view of the yellow gold mine tailing dumps along the gold-bearing reef of the GJMA	99
2.24	Relative humidity isograph for OR Tambo International Airport	103
2.25	Average monthly relative humidity for Johannesburg – as measured at OR Tambo International Airport	104
2.26	Annual rainfall distribution pattern for the CoJ	105
2.27	Climate graph for Johannesburg	107
2.28	Average monthly wind speed (in m/s) at OR Tambo International Airport	108
2.29	Average yearly wind speeds and directions at OR Tambo International Airport	108
2.30	Particulate matter with diameter 10 µm or less in µg/m^3 (2009 annual averages)	110
2.31	Particulate matter with diameter 2.5 µm or less in µg/m^3 (WHO May 2014 report)	110
2.32	Typical haze of pollution over the Greater Johannesburg area during wintertime	111

Figure no.	Description of Figure	Page no.
2.33	Average annual atmospheric pollution levels in Gauteng and its metropolitan areas	112
3.1	Positioning of the main and mini atmospheric corrosion monitoring sites in the GJMA	118
3.2	Typical set-up of a main corrosion monitoring site, comprising a 21-flat coated and uncoated mild steel coupon aluminium test rack, ASTM G116 wire-on-bolt and ISO 9226:1992 open wire helix corrosion monitoring units, attached to a steel structure at the Kagiso-Randfontein site	119
3.3	Typical set-up of a mini corrosion monitoring site, comprising a flat coupon test rack, with a holding capacity of two mild steel samples	120
3.4	Example of a CLIMAT corrosion monitoring unit	125
3.5	Example of an ISO open wire helix corrosion monitoring unit	126
3.6	Average monthly maximum temperatures for Johannesburg during the study period 2013 to 2015, as measured at OR Tambo International Airport	134
3.7	Average monthly minimum temperatures for Johannesburg during the study period 2013 to 2015, as measured at OR Tambo International Airport	134
3.8	Combined average monthly maximum and minimum temperatures for three weather stations in the GJMA for the study period 2013 to 2014	135
3.9	Average seasonal a) maximum and b) minimum temperatures for the GJMA during the study period, as measured at the Johannesburg Botanical Gardens and OR Tambo International Airport	135
3.10	Average monthly percentage relative humidity measurements recorded during the study period at the Johannesburg Botanical Gardens (Central GJMA) and OR Tambo International Airport (East Rand)	136
3.11	Average seasonal humidity levels for the GJMA during the study period, as measured at the Johannesburg Botanical Garden (Central GJMA) and OR Tambo International Airport (East Rand)	137
3.12	Average monthly percentage relative humidity levels for the GJMA – as measured at OR Tambo International Airport	137
3.13	Average monthly rainfall data for the GJMA area, as recorded at a) OR Tambo International Airport and b) the Johannesburg Botanical Gardens	138
3.14	Yearly rainfall data for the GJMA area, as recorded at OR Tambo International Airport and the Johannesburg Botanical Gardens	139
3.15	Average seasonal rainfall data measured for the central (Johannesburg Botanical Gardens) and eastern parts (OR Tambo International Airport) of the GJMA during Spring 2013 to Winter 2014	139
3.16	Total (dry plus wet) acid deposition rates for Gauteng and other parts of South Africa	140
3.17	Monthly wind roses for the period 2012 to 2014 – as measured at OR Tambo International Airport	141
3.18	Average seasonal wind speeds at the Johannesburg Botanical Gardens (Central GJMA) versus at the OR Tambo International Airport (East Rand)	143
3.19	Wind roses for the month of July, as recorded by SAWS (2014), from 2012 to 2014 for the Johannesburg Botanical Gardens	143
3.20	Wind roses for the month of July, as determined by SAWS (2014), from 2012 to 2014 for OR Tambo International Airport	144
3.21	Yearly and monthly sun hours and sunny days for the Johannesburg area	144
3.22	Yearly and monthly UV-index values for the Johannesburg area	145
3.23	Monthly average PM_{10} particulate concentrations for eight air quality/corrosion monitoring sites in the GJMA	146
3.24	Monthly average SO_2 concentrations for six air quality/corrosion monitoring sites	147

Figure no.	Description of Figure	Page no.
3.25	Monthly average NO_2 concentrations for some of the air quality/corrosion monitoring sites	147
3.26	Six-year mean (1996-2001) of global tropospheric NO_2 Vertical Column Density in 1015 molecules/m^2	148
3.27	Diurnal patterns in the average NO_2 concentrations for four of the GJMA air quality/corrosion monitoring sites	148
3.28	Monthly average NO concentrations for three of the eight air quality/corrosion monitoring sites	149
3.29	Monthly average $PM_{2.5}$ particulate concentrations for the Buccleuch air quality/corrosion monitoring site	150
3.30	$PM_{2.5}$ satellite measurements for Southern Africa	150
3.31	Monthly average CO concentrations for three of the air quality/corrosion monitoring GJMA sites	151
3.32	Monthly O_3 concentrations for some of the air quality/corrosion monitoring GJMA sites	151
3.33	Diurnal pattern of O_3 pollution in the GJMA	152
3.34	Yearly and monthly visibility data for the Johannesburg area	152
4.1	Historical atmospheric corrosion monitoring locations in South Africa – projected over an altitude map (in metres)	155
4.2	First-year (12-month) corrosion rates of mild (carbon) steel at various locations throughout South Africa (based on existing published and unpublished data)	156
4.3	First-year (12-month) corrosion rates of hot-dip galvanised steel at various locations throughout South Africa (based on existing published and unpublished data)	157
4.4	First-year (12-month) corrosion rates of pure zinc at various locations throughout South Africa (based on existing published and unpublished data)	158
4.5	First-year (12-month) corrosion rates of pure zinc at various locations throughout South Africa (based on existing published and unpublished data) – with the same key as Figure 3.8	159
4.6	First-year (12-month) corrosion rates of pure aluminium at various locations throughout South Africa (based on existing published and unpublished data)	160
4.7	First-year (12-month) corrosion rates of pure copper at various locations throughout South Africa (based on existing published and unpublished data)	161
4.8	Extent of metal loss and b) pitting of steel items at the Kagiso-Randfontein site	162
4.9	Atmospheric corrosion of hot-dip galvanised steel razor-wire at the Brakpan site	163
4.10	Atmospheric corrosion of hot-dip galvanised steel fencing and supports at the Doornkop exposure site	163
4.11	Measured Industrial Corrosion Indices (ICI values) for the 22 main sites in the GJMA during Spring 2013 and Summer 2013-2014	164
4.12	Measured Industrial Corrosion Indices (ICI values) for the main GJMA sites during Autumn 2014 and Winter 2014	164
4.13	Measured Marine Corrosion Indices (MCI values) for the main GJMA sites during Spring 2013 and Summer 2013-2014	165
4.14	Measured Marine Corrosion Indices (MCI values) for the main GJMA sites during Autumn 2014 and Winter 2014	165
4.15	Measured Atmospheric Corrosion Indices (ACI values) at the main GJMA sites during Spring 2013 and Summer 2013-2014	166
4.16	Measured Atmospheric Corrosion Indices (ACI values) at the main GJMA sites during Autumn 2014 and Winter 2014	166

Figure no.	Description of Figure	Page no.
4.17	Summations (∑) of the measured seasonal Industrial Corrosion Indices (ICI values) for the main GJMA sites (Spring 2013 to Winter 2014)	167
4.18	Summations (∑) of the measured seasonal Marine Corrosion Indices (MCI values) for the main GJMA sites (Spring 2013 to Winter 2014)	168
4.19	Summations (∑) of the measured Atmospheric Corrosion Indices (ACI values) for the main GJMA sites - during Spring 2013 to Winter 2014	168
4.20	Summations of the seasonal fluctuations of the average ICI values for the major regions of the GJMA (Spring 2013 to Winter 2014)	169
4.21	Summations of the measured average seasonal MCI values for the different major regions of the GJMA (Spring 2013 to Winter 2014)	169
4.22	Sum totals and seasonal fluctuations of the measured average ACI values for the different major regions of the GJMA - during Spring 2013 to Winter 2014	170
4.23	Measured 12-month aluminium wire helix corrosion rates for the 22 main sites in the GJMA	171
4.24	Measured 12-month zinc wire helix corrosion rates for the 22 main sites in the GJMA	171
4.25	Measured 12-month copper wire helix corrosion rates for the 22 main sites in the GJMA	172
4.26	Average 12-month aluminium wire helix corrosion rates for the different regions of the GJMA	172
4.27	Average 12-month zinc wire helix corrosion rates for the different regions of the GJMA	173
4.28	Measured 12-month copper wire helix corrosion rates for the different regions of the GJMA	173
4.29	Average 12-month copper wire helix corrosion rates for the northern suburbs of the GJMA	174
4.30	Summations (∑) of the 12-month corrosion rates of aluminium, zinc and copper for the 22 main GJMA exposure sites	174
4.31	Changes in the 6-, 12-, 18- and 24-month corrosion rates of duplicate sets of mild steel panels (MSP) for 21 of the main exposure sites	175
4.32	Changes in the 12-, 18- and 24-month corrosion rates of duplicate sets of hot-dip galvanised steel panels (GSP) at 21 of the main exposure sites	176
4.33	12-month average corrosion rates of galvanised steel, aluminium, zinc and copper, as measured for the different parts of the GJMA	176
4.34	Average 12-month corrosion rates of mild steel, as measured at the main and mini sites in the GJMA	179
4.35	Average 12-month corrosion rates of mild steel, as measured at the main and mini sites in the different regions of the GJMA	180
4.36	12-month corrosion rates of mild steel at the main and mini sites located in the Eastern region of the GJMA	181
4.37	12-month corrosion rates of mild steel at the main and mini sites located in the Southern region of the GJMA	181
4.38	12-month corrosion rates of mild steel at the main and mini sites located in the Central part of the GJMA	182
4.39	12-month corrosion rates of mild steel at the main and mini sites located in the Northern region of the GJMA	182
4.40	12-month corrosion rates of mild steel at the main and mini sites located in the Western part of the GJMA	183
4.41	Micrographs (x20 magnification) of the morphologies of the corrosion products formed on the 12-month flat mild steel specimens at the GJMA exposure sites	184

Figure no.	Description of Figure	Page no.
4.42	Micrograph (x20 magnification) of the corrosion product of a mild steel specimen exposed at the Princess site – Note the yellowish-white spots	188
4.43	Micrographs (x20 magnification) of the corrosion products of the mild steel specimens following (a) 6 months and (b) 12 months of exposure at the Kagiso-Randfontein site	188
4.44	Micrographs (x20 magnification) of the corrosion products of the mild steel specimens following (a) 6 months and (b) 12 months of exposure at the Florida Hills site	189
4.45	Typical FTIR spectrum of the 12-month corrosion product formed on the mild steel specimens at exposed in the GJMA. The above spectrum was taken for the mild steel samples exposed at Ruimsig	190
4.46	Raman spectrum of a combination of γ-FeOOH and α-FeOOH found in the corrosion product of the Alexandra site	191
4.47	Raman spectrum of a combination of γ-FeOOH, α-FeOOH and Fe_3O_4 found in the corrosion product of the Chloorkop site	191
4.48	Raman spectrum of amorphous carbon found in the corrosion product of the Kagiso-Randfontein site	192
4.49	Raman spectrum of a combination of α-Fe_2O_3 and β-FeOOH found in the corrosion product of the Chloorkop site	192
4.50	Raman spectrum of a combination of γ-FeOOH and $Fe(OH_3)$ found in the corrosion product of the Chloorkop site	193
4.51	Raman spectrum of a combination of γ-FeOOH and Fe_3O_4 found in the corrosion product of the Nasrec site	193
4.52	Typical scanning electron micrograph (in BSE mode) of the scraped corrosion products of the mild steel panels	194
4.53	EDS spectrum indicating the elementals of the corrosion product from the mild steel panels exposed at the Chloorkop site	195
4.54	Oxide compositions of the corrosion products of the mild steel specimens exposed at the different GJMA sites, versus their respective 12-month corrosion rates	196
4.55	Water-soluble salt levels of the corrosion products versus the 12-month corrosion rates of the mild steel at the different GJMA sites	197
4.56	pH measurements of the mild steel corrosion products originating from the different GJMA sites	198
4.57	Conditions of the coated mild steel samples (Systems A to D) after 24 months of exposure at the Kagiso-Randfontein site	200
4.58	Sum ($\sum$) differences between the average thicknesses of the various coatings before and after 24 months of exposure at the main GJMA sites	202
4.59	Average percentage changes in the mean thicknesses of the different coatings at the main GJMA sites – after 24 months of outdoor weathering	202
4.60	Average percentage changes in the DFTs of the various coating systems exposed at the main GJMA exposure sites over a period of 24 months	203
4.61	Sum ($\sum$) percentage changes in the average DFTs of Systems D to G after 24 months of outdoor weathering at the main GJMA sites	203
4.62	Percentage changes in the average DFTs of System E after 24 months of exposure at the main GJMA sites	204
4.63	Extent of chalking and dirt retention by tape pull-off testing of the different coated surfaces exposed at a) Braamfontein, b) Chloorkop, c) Kagiso-Randfontein and d) Chamdor	205
4.64	Degree of chalking and dirt retention of the mild steel specimens coated with an alkyd coating system (System G) after 24 months of exposure at a) Aeroport, b) Braamfontein and c) Chloorkop	206

Figure no.	Description of Figure	Page no.
4.65	Sum (∑) ratings of the degree of chalking and dirt retention of the different coatings after 24 months of exposure at the main sites in the GJMA	206
4.66	Sum (∑) ratings of the degree of chalking and dirt retention of the different coating systems	207
4.67	Percentage change in the average gloss levels of the different coating systems after 24 months of exposure at the main sites in the GJMA	208
4.68	Sum (∑) changes in the average gloss levels (GU) of Coating Systems A, B, C, F and G, after 24 months of exposure at the main sites in the GJMA	208
4.69	Summations (∑) of the slight colour differences (ΔE) of Systems A to G, after 24 months of exposure at the main sites in the GJMA	209
4.70	Average QCheck™ correlations of the FTIR spectra of the coated surfaces before and after cleaning with their control references – following 24 months of exposure at the main GJMA sites	210
4.71	QCheck^{TM} correlations between the ATR-FTIR spectra (chemical 'fingerprints') of the different coatings following 24 months of exposure at the main sites and their control spectra	211
5.1	Salt deposits versus distance from the ocean	215
5.2	Climatic regions of South Africa	218
5.3	The Great Escarpment and the Central Plateau	220
5.4	A flyer by Greenpeace showing a worldwide concern regarding the increased pollution of the Secunda and Emalahleni (Witbank) areas	222
5.5	First-year (12-month) corrosion rates of mild steel, measured at numerous sites in South Africa, versus their approximate distances from the ocean	223
5.6	First-year (12-month) corrosion rates of mild steel, measured at numerous sites in South Africa, versus their relative altitudes (elevations above sea level)	224
5.7	First-year (12-month) corrosion rates of mild steel, measured at numerous sites in South Africa, versus their relative altitudes (elevations above sea level)	224
5.8	First-year (12-month) corrosion rate of hot-dip galvanised mild steel at various sites in South Africa, versus their distances from the ocean	228
5.9	First-year (12-month) corrosion rate of zinc at exposure sites in South Africa versus their distances from the ocean	232
5.10	First-year (12-month) corrosion rates of aluminium, measured at numerous sites in South Africa, versus their relative altitudes (elevations above sea level)	234
5.11	First-year (12-month) corrosion rates of copper, measured at numerous sites in South Africa, versus their relative altitudes (elevations above sea level)	237
5.12	Countrywide average 12-month corrosion rates of mild steel, hot-dip galvanised mild steel, pure zinc, aluminium and copper	238
5.13	Average first-year (12-month) corrosion rates of mild steel, hot-dip galvanised steel, aluminium, zinc, and copper at varying distance spans from the ocean	238
5.14	Average Atmospheric (ACI), Industrial (ICI) and Marine (MCI) corrosion indices with different distance spans from the ocean	242
5.15	Corrosivity rating of South Africa's macro atmosphere, based on the ISO 9223:2012 rating scheme, from inland to coastal environments	244
5.16	A superimposed wind rose for OR Tambo International Airport indicating the strength and predominant direction of the wind during May 2012 to 2014	249

Figure no.	Description of Figure	Page no.
5.17	A superimposed wind rose for OR Tambo International Airport indicating the strength and predominant direction of the wind during the month of July 2012 to 2014	250
5.18	Differences in the average seasonal daily maximum temperatures during 2012 to 2014	252
5.19	Differences in the average rainfall figures for Spring, Summer, Autumn and Winter 2012 to 2014	253
5.20	Measured PM_{10} levels for the main air quality monitoring sites of the City of Johannesburg Metropolitan Municipality – during July 2004 to September 2015	254
5.21	Average seasonal variations in the ICI, MCI and ACI values for the GJMA atmosphere, over the period September 2013 (spring) to September 2014 (winter)	255
5.22	A map representation of the yearly average ICI values of the GJMA	257
5.23	A map representation of the yearly average MCI values of the GJMA	258
5.24	A map representation of the yearly average ACI values of the GJMA	259
5.25	Close-up views of the aluminium vs copper (a), aluminium vs mild steel (b), and aluminium vs nylon (c) surfaces of the wire-on-bolt units exposed at the Brakpan site during Spring 2013	260
5.26	A map representation of the 12-month corrosion rates of aluminium helices in the GJMA	267
5.27	A map representation of the 12-month corrosion rates of zinc helices in the GJMA	268
5.28	A map representation of the 12-month corrosion rates of copper helices in the GJMA	269
5.29	The Eastrand Mall site located next to OR Tambo International Airport. Note the presence of the low-flying aircraft and the oil-like stains on the mild steel panel surface	271
5.30	Linear regression of (a) 6-versus 12-month corrosion rates of mild steel, and 12-month corrosion rates of mild steel versus the 12-month corrosion rates of (b) aluminium, (c) zinc and (d) copper, as measured at the main sites in the GJMA	273
5.31	Measured linear relationship between the 6- and 18-month corrosion rates of mild steel at the main sites in the GJMA	277
5.32	Measured linear relationship between the 12- and 18-month corrosion rates of mild steel at the main locations in the GJMA	277
5.33	Linear regression of the measured 12- and 24-month corrosion rates of mild steel at the main sites in the GJMA	278
5.34	Linear regression of the measured 18- and 24-month corrosion rates at the main sites in the GJMA	279
5.35	Regression analysis of the average measured 6-, 12-, 18- and 24-month corrosion rates of mild steel at the main sites in the GJMA	280
5.36	Linear regressions of the 12-month corrosion rates of hot-dip galvanised steel versus the 12-month corrosion rates of (a) aluminium, (b) zinc and (c) copper, as well as (d) uncoated mild steel, as measured at the main sites in the GJMA	283
5.37	Linear regression of the 18-month versus 12-month corrosion rates of hot-dip galvanised steel, as measured at the main sites in the GJMA	285
5.38	Regression analysis of the average 12-, 18- and 24-month corrosion rates of galvanised steel, as measured at the main sites in the GJMA	287
5.39	Map representation of the 12-month corrosion rates of mild steel at the main and mini sites in the GJMA - revealing two outlier locales	290

Figure no.	Description of Figure	Page no.
5.40	The gold mine tailings dump located next to the Kagiso-Randfontein site	298
5.41	Linear regression analysis of the average 12-month corrosion rate of mild steel at the various GJMA sites, versus 20 mg/m^2 rises in the concentration of water-soluble salts in the corrosion products	307
5.42	Measured 6- and 12-month water-soluble salt concentrations of the corroded mild steel specimens versus the 12-month corrosion rate of pure zinc at the East Rand sites	308
5.43	Measured 6- and 12-month water-soluble salt concentrations of the corroded mild steel specimens versus the 12-month corrosion rate of pure zinc at the West Rand sites	308
5.44	Linear regression analysis of the pH values of the corrosion products versus the 12-month corrosion rates of mild steel, as recorded at the different GJMA main and mini sites	310
5.45	Pourbaix diagrams for a) iron, b) copper, c) zinc and d) aluminium at 25°C	312
5.46	Average PPMC coefficients between the FTIR spectra of the different coatings after exposure in the GJMA environment and their respective control spectra, as well as opposed to the changes in the corrosivity of the local environments	323
5.47	Illustration showing that the concentrations of air fumes decrease with an increase in altitude and distance from the sources of pollution	325
5.48	Shielding and shading effects at Delta Park	326
5.49	Blaauwpan Lake located next to the Bonaero Park corrosion monitoring locale, causing a spike in backdrop humidity levels	327
5.50	Average seasonal corrosion indices (as percentage weight loss) for the GJMA measured during the period August/September 2013 to August/September 2014: a) ICI, b) MCI and c) ACI	330
5.51	The effect of air temperature on the atmospheric corrosion rate of carbon steel: a) during rain and b) at drying out of a film of moisture during a constant RH of 75%	332
5.52	PPMC coefficients between the average seasonal changes in %RH versus variations of the CLIMAT corrosion indices	334
5.53	PPMC coefficients for the mean seasonal rainfall values versus the CLIMAT indices for the central and eastern parts of the GJMA	335
5.54	PPMC coefficients between the average seasonal wind speeds and the cyclic CLIMAT corrosion indices for the central and eastern regions of the GJMA	337
5.55	Average PPMC coefficients and standard deviations for the meteorological parameters and the atmospheric corrosivity measurements of the GJMA – excluding any pollution effects	338
5.56	Measured 12-month corrosion rates of mild steel at the different air quality/corrosion monitoring sites of the GJMA	341
5.57	Measured average ICI, MCI and ACI values for the various air quality/corrosion monitoring sites of the GJMA	342
5.58	Measured 12-month corrosion rates of aluminium, zinc and copper at the different air quality/corrosion monitoring sites of the GJMA	343
5.59	Overall corrosivity rating of the various air quality/corrosion monitoring sites – based on the rankings of their 12-month corrosion rates of mild steel, aluminium, zinc and copper	343
5.60	Ranking order of the different air quality/corrosion monitoring sites based on their average PM_{10} particulate matter concentrations	344

Figure no.	Description of Figure	Page no.
5.61	PPMC coefficients between the rankings for PM_{10} particulate matter concentration and the different corrosion monitoring results at the various sites	344
5.62	Ranking order of the different air quality/corrosion monitoring sites (excluding the Delta Park and Newtown locales) based on their average SO_2 concentrations	345
5.63	Sum changes in the *ΔL**- value (which represents lightness or fading) regarding the CIE *L*a*b* – colour space coordinates	450
6.1	IDW interpolated atmospheric corrosion map of the Greater Johannesburg Metropolitan Area – based on yearly average Industrial Corrosion Indices (ICI), as measured during August 2013 to September 2014	354
6.2	IDW interpolated atmospheric corrosion map of the Greater Johannesburg Metropolitan Area – based on the 12-month corrosion rate of mild steel, as measured during August 2013 to September 2014	356
6.3	IDW interpolated atmospheric corrosion map of the Greater Johannesburg Metropolitan Area – based on the 12-month corrosion rate of hot-dip galvanised mild steel, as measured during August 2013 to September 2014	358
6.4	IDW interpolated atmospheric corrosion map of the Greater Johannesburg Metropolitan Area – based on the 12-month corrosion rate of aluminium, as measured during August 2013 to September 2014	360
6.5	IDW interpolated atmospheric corrosion map of the Greater Johannesburg Metropolitan Area – based on the 12-month corrosion rate of zinc, as measured during August 2013 to September 2014	362
6.6	IDW interpolated atmospheric corrosion map of the Greater Johannesburg Metropolitan Area – based on the 12-month corrosion rate of copper, as measured during August 2013 to September 2014	364
6.7	Atmospheric corrosion map of South Africa – based on the 12-month corrosion rate of mild steel	367
6.8	Atmospheric corrosion map of South Africa – based on ISO 9223:2012 corrosivity rating scheme	368
6.9	Atmospheric corrosion map of South Africa – based on the 12-month corrosion rate of hot-dip galvanised mild steel	370
6.10	Atmospheric corrosion profiling of South Africa – based on the 12-month corrosion rate of pure zinc	371
6.11	Atmospheric corrosion map of South Africa – based on the 12-month corrosion rate of pure aluminium	373
6.12	Atmospheric corrosion profiling of South Africa – based on the 12-month corrosion rate of pure copper	375
A.1	Population densities of the different towns and suburbs of the GJMA study area	450
E.1 – E.7	Infrared control spectra of the different coatings	460
F.1-F228	Exposure photographs – The GJMA Exposure Sites	464
I.1	Measured 6-month corrosion rates of duplicate sets of mild steel panels (MSP) at 21 of the main exposure sites	486
I.2	Measured corrosion rates of mild steel after 18 months of exposure at the main sites in the GJMA	486
I.3	Measured 24-month corrosion rates of mild steel at the main GJMA sites	487
J.1	Average 12-month corrosion rates of duplicate sets of hot-dip galvanised steel panels (GSP) at 21 of the main exposure sites	489
L.1	Typical FTIR spectra of the rust layers of the mild steel samples exposed at different sites – Note the similarity of the spectra	491

Figure no.	Description of Figure	Page no.
L.2	Outlier spectra regarding the typical FTIR spectrum of the corrosion product of mild steel in the GJMA area	492
L.3	FTIR spectrum of the corrosion product of mild steel exposed at the Lenasia site for 12 months	493
S.1	Changes in the amplitudes/intensities of the peaks of the functional groups of System D, i.e. the water-based acrylic coating, at Aeroport (dark blue), Jabavu (Soweto) (purple), Kagiso-Randfontein (green) and Newtown (red), after 24 months of exposure at the main sites in the GJMA	513
S.2	Changes in the amplitudes/intensities of the peaks of the functional groups of System E (water-based acrylic coating) at Aeroport (dark blue), Jabavu (Soweto) (purple), Kagiso-Randfontein (green) and Newtown (red), after 24 months of exposure at the main sites in the GJMA	514
S.3	Changes in the amplitudes/intensities of the peaks of the functional groups of System G (alkyd high gloss enamel coating) at Aeroport (dark blue), Jabavu (Soweto) (purple), Kagiso-Randfontein (green) and Newtown (red), after 24 months of exposure at the main sites in the GJMA	515
S.4	Reduced intensities of the FTIR peaks of System D (water-based acrylic coating) at Aeroport (dark blue), Jabavu (Soweto) (purple), Kagiso-Randfontein (green) and Newtown (red), after 24 months of exposure at the main sites in the GJMA	516
S.5	Reduced intensities of the FTIR peaks of System E (water-based acrylic coating) at Aeroport (dark blue), Jabavu (Soweto) (purple), Kagiso-Randfontein (green) and Newtown (red), after 24 months of exposure at the main sites in the GJMA	517
S.6	Reduced changes of the FTIR peaks of System C (aliphatic acrylic polyurethane coating) at Aeroport (dark blue), Jabavu (Soweto) (purple), Kagiso-Randfontein (green) and Newtown (red), after 24 months of exposure at the main sites in the GJMA	518
S.7	Reduced changes in the intensities of the FTIR peaks of System B (polysiloxane coating) at Aeroport (dark blue), Jabavu (Soweto) (purple), Kagiso-Randfontein (green) and Newtown (red), after 24 months of exposure at the main sites in the GJMA	519
S.9	Reduced changes in the intensities of the FTIR peaks of System F (polyester powder coating) at Aeroport (dark blue), Jabavu (Soweto) (purple), Kagiso-Randfontein (green) and Newtown (red), after 24 months of exposure at the main sites in the GJMA	520

List of Tables

Table no.	Description of Table	Page no.
1.1	General structure of the thesis	15
2.1	CLIMAT test - five levels of corrosivity	63
2.2	Categories of corrosivity of atmospheres based on the 12-month corrosion rates of mild (carbon) steel, zinc, copper and aluminium	67
2.3	Approximate levels of uncertainty for the measurement of the corrosivity of atmospheres based on actual corrosion rates and estimated rates obtained via the dose-response models	75
2.4	Approaches followed for atmospheric corrosion mapping, including their strengths and weaknesses	82
2.5	Annual climate variables for Johannesburg	107
2.6	Air quality data for Gauteng/Greater Johannesburg and its surrounding areas	112
4.1	Average 12-month corrosion rates of duplicate sets of mild steel specimens exposed at 22 main and 35 mini sites in the GJMA, with margin of uncertainty of about ± 5%.	177
5.1	Average first-year (12-month) corrosion rate of aluminium within varying distance spans from the ocean	233
5.2	Average first-year corrosion rate of copper within varying distance spans from the ocean	236
5.3	Average ACI, ICI and MCI data for South Africa, within varying distance spans from the ocean	240
5.4	Significant (95%) rank correlations between the atmospheric corrosion data of South Africa	242
5.5	Aluminium corrosion rate from ISO 9223 (International Organization for Standardization 2012) and Doyle and Wright (1982)	243
5.6	Sensitivities of iron, aluminium, zinc and copper to corrosive atmospheric species	265
5.7	Revised corrosivity categories of the atmosphere - adapted from International Organization for Standardization	294
5.8	Comparisons between the measured 12-month corrosion rates of mild steel, with a margin of error of about 5%, versus the visual condition assessments of select sites in GJMA	296
5.9	Significant PPMC coefficients between the water-soluble salt levels of the corroded mild steel surfaces and the average 12-month corrosion rates of the different metals, as well as the CLIMAT indices, derived from the different corrosion monitoring procedures	307
5.10	PPMC coefficients between the pH values of the corrosion products of the mild steel specimens versus the 12-month corrosion rates of mild steel, hot-dip galvanised steel, aluminium, zinc and copper, as well as opposed to the ICI, MCI and ACI values	311
5.11	PPMC coefficients between the changes in the average DFTs of the various coating systems after 24 months of outdoor weathering at the main GJMA sites	316
5.12	PPMC coefficients between the changes in the average gloss levels of the coating systems after 24 months of exposure, and the 12-month corrosion rates of mild steel, galvanised steel, aluminium, zinc and copper at the different sites	318
5.13	PPMC coefficients between the total colour differences (ΔE) of the coating systems after 24 months, and the 12-month corrosion rates of mild steel, galvanised steel, aluminium, zinc and copper at the various locales	320

Table no.	Description of Table	Page no.
5.14	PPMC coefficients for the FTIR (chemical 'fingerprint') matches of the control versus the after-exposure spectra, with the DFT, gloss, chalking and colour (ΔE) differences of the coating systems after 24 months of exposure, as well as in comparison with the 12-month corrosion rates of mild steel, galvanised steel, aluminium, zinc and copper at the different locales	321
6.1	Significant (95%) rank correlations between the different corrosion maps for South Africa	374
A.1	The different zones and populations of the CoJ Metropolitan Municipality's section of the GJMA	448
A.2	Sections of the Ekurhuleni Metropolitan Municipality forming part of the GJMA	449
A.3	Sections of the Mogale Local Municipality included in the GJMA study	449
A.4	Sections of the Randfontein Local Municipality included in the GJMA study	449
B.1	Geographical information and general descriptions of the main atmospheric corrosion monitoring locations in the GJMA	451
B.2	Geographical information and general descriptions of the mini atmospheric corrosion monitoring locations in the GJMA	452
C.1	Typical physical and chemical properties of the low-carbon (mild) steel flat metal panels used for corrosion monitoring, and preparation of the hot-dip galvanised and coated mild steel specimens	454
C.2	Typical physical and chemical properties of the hot-dip galvanised coating	455
C.3	Typical physical and chemical properties of the aluminium wire used for manufacturing of the ISO WH-Al units	456
C.4	Typical physical and chemical properties of the zinc wire used for manufacturing of the ISO WH-Zn units	457
C.5	Typical physical and chemical properties of the copper wire used for manufacturing of the ISO WH-Cu units	458
G.1	ICI, MCI and ACI (CLIMAT) results (as percentage weight loss) for the periods Spring 2013 to Winter 2014 for the different main GJMA sites, with an uncertainty of measurement of about 5%	483
H.1	12-month helix wire corrosion rates (in µm/a) for the GJMA, measured during August-September 2013 to August-September 2014, with an uncertainty of measurement of about 5%.	484
I.1	Measured 6-, 12-, 18- and 24-month corrosion rates of mild steel at 21 of the main GJMA sites, during August 2013 to September 2015 (with an uncertainty of measurement of about 5%).	485
J.1	12-, 18- and 24-month corrosion rates of hot-dip galvanised steel specimens exposed at 21 of the main GJMA sites, with an uncertainty of measurement of about 5%	488
K.1	Pearson's product-moment correlation coefficients between the different corrosion monitoring results measured for the main GJMA sites	490
M.1	Raman spectral bands of the mild steel corrosion products formed at selected sites in the GJMA	494
N.1	SEM-EDS results of the mild steel corrosion products from the GJMA sites	495
O.1	Dry film thicknesses (DFTs) of the coated samples before (BE) and after (AE) exposure at the main GJMA sites, with an uncertainty of measurement of about 2.5 µm	497
O.2	Percentage change in the average dry film thicknesses (DFTs) of the different coated samples after 24 months of exposure at the main GJMA sites, with an accuracy of measurement of about 2.5 µm, with an uncertainty of measurement of about 1%.	498

Table no.	Description of Table	Page no.
P.1	Degree of chalking and dirt retention results, with a level of uncertainty of about 20%.	499
Q.1	Average 60° specular gloss levels (in GU) of the coated samples before exposure at the different GJMA sites, with an uncertainty of measurement of about 2.5%.	500
Q.2	Average 60° specular gloss levels of the coated samples after 24 months of exposure at the different GJMA sites, with an uncertainty of measurement of about 2.5%.	501
Q.3	Changes in the average 60° specular gloss levels (in GU) of the different coated samples after 24 months of exposure at the GJMA sites, with an uncertainty of measurement of about 2.5%.	502
R.1	Measured colour coordinates of Coating System A before exposure	503
R.2	Measured colour coordinates of Coating System B before exposure	504
R.3	Measured colour coordinates of Coating System C before exposure	505
R.4	Measured colour coordinates of Coating System D before exposure	506
R.5	Measured colour coordinates of Coating System E before exposure	507
R.6	Measured colour coordinates of Coating System F before exposure	508
R.7	Measured colour coordinates of Coating System G before exposure	509
R.8	Colour changes (ΔE) per sample after exposure at the GJMA	510
S.1	QCheck^{TM} correlations (matches) (before cleaning) between the FTIR 'fingerprints' of the different coated specimens after exposure at the main GJMA sites and their respective control spectra	511
S.2	QCheck^{TM} correlations (matches) (after cleaning) between the FTIR 'fingerprints' of the different coated specimens after exposure at the main GJMA sites and their respective control spectra	512
T.1	List of papers prepared for publishing	521
T.2	List of presentations given at conferences and seminars	521

Nomenclature

Term	Description of Term
Acrylic	Typically, a coating made-up of pigments and fillers that are suspended in an acrylic resin emulsion
Aliphatic	Organic substances in which the carbon and hydrogen atoms are joined as open chains
Alkyd	Typically, an oil-based, single-component convertible (chemically curing), air drying coating, that is formed via the reaction of glycerol and a dicarboxylic acid or its anhydride
Amphoteric	A metal oxide or hydroxide which can react with an acid or base
Chalking	The formation of a powdery product (loose pigments) on the surface of a coating due to breakdown of the binder when exposed to long-term ultraviolet light radiation
Coat	Single layer of paint
Coating system	Term used that encompasses the surface preparation and different paint layers of a specific surface protection procedure
Dirt retention	Tendency of a coating to retain dust and other surface contaminants that are unlikely to be removed by rain or mere washing of the surfaces
East Rand	The eastern part of the Witwatersrand
Epoxy	Two-component convertible (chemically-curing) polymer coating containing epoxide groups
Eskom	Eskom Holdings SOC Ltd.
Film	Homogenous layer of paint
Fynbos	Hard-leaved, evergreen (sclerophyllous) shrubs
Gloss level	Sheen or reflective level
Highveld	South Africa’s inland plateau
Irradiation	Process through which an object or surface is exposed to radiation
ISOCORRAG	An international testing programme concerning the corrosion monitoring of numerous countries throughout the world that resulted in the development and publishing of ISO 9223-9226 standards
MICAT	The International Ibero-American Programme involving the atmospheric corrosion monitoring of 14 countries
RAL	A colour matching system developed by the German RAL gGmbH
Outlier	A result differing significantly from all the other results
Photochemical	Chemical effects due to light
Photolysis	The breakdown of molecules by light
Polyester	A synthetic resin coating in which the polymer units are combined via ester groups

Polysiloxane	A highly durable polymer top coating with a silicon-oxygen backbone
Polyurethane	An organic coating of which the polymers are linked using urethane groups
Post-curing	Additional curing of a polymeric material when exposed to heat or radiation
Regression	Measuring of the mean value of one variable versus that of another
Roodekransrif	A rocky ridge in the Ruimsig (Roodepoort) area
Single-component	Paint comprising only one liquid part
Solstice	When the sun reaches its highest northerly and southerly positions above the Earth
Surface tolerant	Coating tolerant to marginally prepared surfaces
Time of wetness	Time during which relative humidity is higher than 80% and temperature more than 0°C
Two-component	Paint comprising two liquid or powder parts
Under-film creep	Also known as undercutting corrosion that develops underneath the coating at a scribe, edge, or mechanically damaged area
Vaal Triangle	A triangular section of land formed by the towns of Vereeniging, Vanderbijlpark and Sasolburg
West Rand	The western part of the Witwatersrand
Wind rose	Graphic representation of the wind speed and wind direction for a specific area

List of Abbreviations

Abbreviation	Description
ACI	Atmospheric corrosion index
AE	After exposure
AFSA	Aluminium Federation of South Africa
AISI	American Iron and Steel Institute
Al-WH	Aluminium wire helix
ASM	American Society for Metals
ASTM	ASTM International
ATR	Attenuated total reflectance
BE	Before exposure
CBD	Central business district
CDD	Chloride-deposition density
CI	Confidence interval of the calculated mean
CIE	Commission Internationale de l'Eclairage
CL	Confidence level
CLIMAT	CLassify Industrial and Marine ATmospheres)
CoJ	City of Johannesburg
CRH	Critical relative humidity
ISOCORRAG	ISO corrosion programme
CSIR	Council for Scientific Industrial Research
Cu-WH	Copper wire helix
CV	Coefficient of variation
DEA	Department of Environmental Affairs
DFT	Dry film thickness (in micrometres/microns)
DRH	Deliquesce relative humidity
DIY	Do it yourself

Abbreviation	Description
EDS	Energy dispersive X-ray spectroscopy
EPA	Environmental Protection Agency
ERH	Efflorescence relative humidity
Eq.	Equation
FTIR	Fourier transform infrared
Galv	Galvanising
GDP	Gross Domestic Product
GIS	Geographic information system
GJMA	Greater Johannesburg Metropolitan Area
GPS	Global positioning satellite
GSP	Galvanised steel panel
HDGASA	Hot Dip Galvanizers Association of Southern Africa
ICI	Industrial corrosion index
IDW	Inverse distance weighted
Inc.	Incorporated
ISO	International Organization for Standardization
ISO-WH	ISO 9223:1992 open wire helix corrosion monitoring unit
JHB	Johannesburg
KZN	KwaZulu-Natal
MCI	Marine corrosion index
MDRH	Mutual deliquescence relative humid
MDS	Dimethyl sulphide
MICAT	MICAT cooperative programme
MS	Mild steel
MSP	Mild steel panel
n.d.	No date

Abbreviation	Description
N1	National route in South Africa that runs from Beite Bridge to Cape Town
NACE	National Association of Corrosion Engineers
NRF	National Research Foundation
OR Tambo	Oliver Reginald Tambo International Airport
PM_{10}	Particulate matter with diameter 10 µm or less
$PM_{2.5}$	Particulate matter with diameter 2.5 µm or less
PPMC	Pearson product-moment correlation
QD	Quick-dry
R	Rand
RH	Relative humidity
SA	South Africa
SAAQIS	South African Air Quality Information System
SABS	South African Bureau of Standards
SANS	South African National Standards
SAWS	South African Weather Service
SEM	Scanning electron microscopy
TCI	Total corrosion index
TM	Trade mark
TOW	Time of wetness
UHI	Urban heat island
US	United States
US$	US dollars
USA	United States of America
UV	Ultraviolet
VOC	Volatile organic compound
vs	Versus

Abbreviation	Description
WH	Wire helix
WHO	World Health Organisation
Zn-WH	Zinc wire helix

List of Symbols

SYMBOL	DESCRIPTION
~	Approximate
λ	Lamda – Greek symbol for wavelength
∑	Sum
µm/a	Micrometres per annum
µm/y	Micrometres per year
3D	Three dimensional
a*	Red/green (chroma)
b*	Yellow/blue (hue)
BSk	Cold semi-arid climate
C1	Very low corrosive
C2	Low corrosive
C3	Moderate corrosive
C4	High corrosive
C5	Very high corrosive
CO	Carbon dioxide
CX	Extreme corrosive
g/(m^2·a)	Gram per square metre annum
GU	Gloss unit
ha	Hectares
HO_2	Hydroperoxyl
Hours/a	hours per annum
kV	Kilovolt
L*	Lightness
mg/(m^2·d)	Milligrams per square metre day
mm/kV	Millimetre per kilovolt (insulator creepage voltage)

SYMBOL	DESCRIPTION
MW	Megawatt
nm	Nanometre
NO	Nitrogen oxide
NO_2	Nitrogen dioxide
NO_x	Nitrogen oxides
O_3	Ozone
OH^-	Hydroxide
PM_{10}	Particulate matter with diameter 10 µm or less
$PM_{2.5}$	Particulate matter with diameter 2.5 µm or less
ppb	Parts per billion
ppm	Parts per million
r	Pearson product-moment coefficient
R^2	R-squared of the correlation
r_{av}	10-year average corrosion rate
R_{corr}	12-month / first-year corrosion rate
r_{corr}	12-month / first-year corrosion rate
Ri	Degree of rusting as per the ISO 4629-3 pictorial standard
r_{lin}	Steady-state corrosion rate
SO_2	Sulphur dioxide
SO_x	Sulphur oxides
ΔE	Colour difference

CHAPTER 1

INTRODUCTION – THE NEED FOR A NEW CORROSION MAP

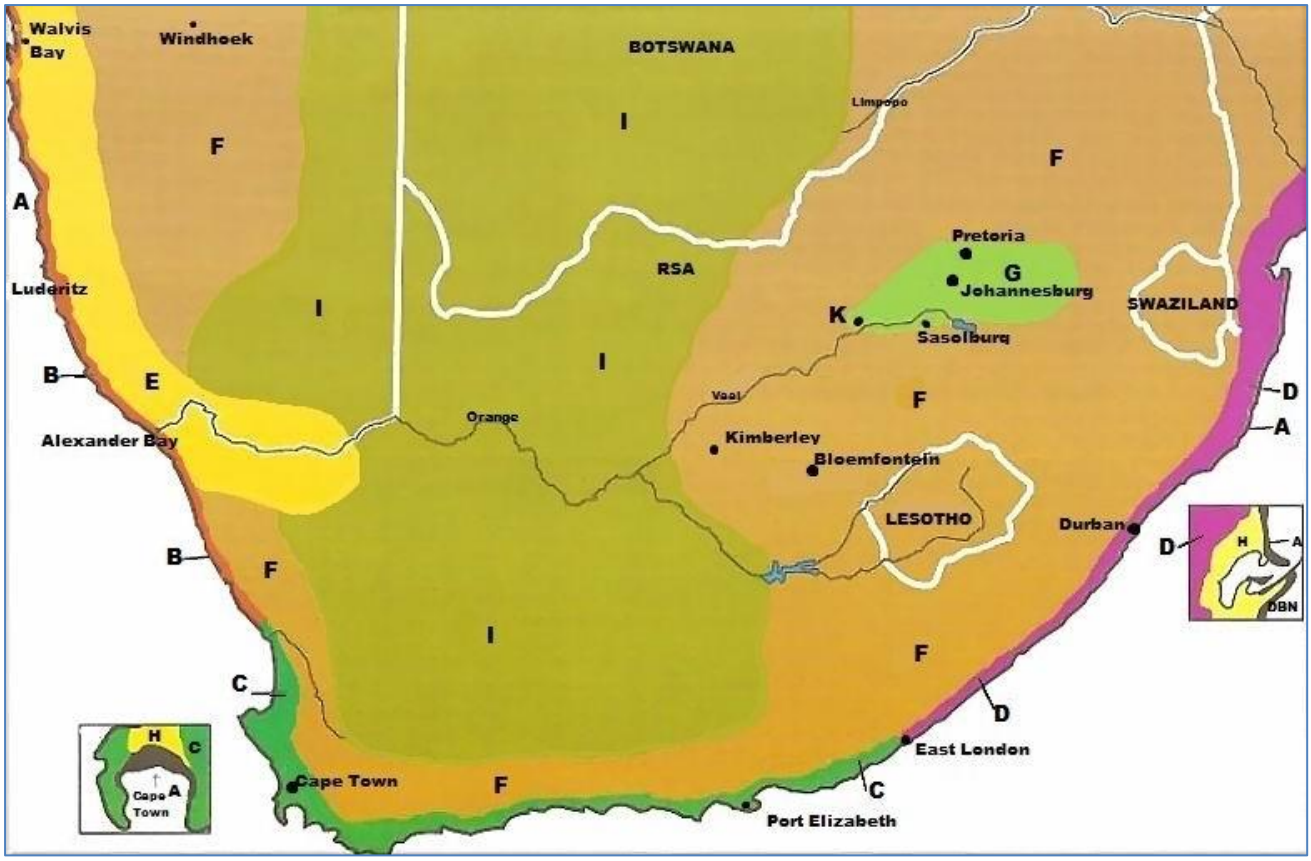
1.1 INTRODUCTION

More than twenty years ago, Brian Callaghan, of the Council for Scientific Industrial Research (CSIR), developed the first corrosion map of Southern Africa (henceforth referred to as the Callaghan map). This map, **Figure 1.1**, was produced from atmospheric corrosion monitoring work carried out between 1970 and 1990 (Callaghan 1991). Since its publication, the corrosion engineering and protective coatings industries in South Africa have used this map extensively to:

- predict the service life of metals when exposed to different corrosive atmospheres;
- forecast the corrosivity of environments during plant design and construction, and
- facilitate the specification and selection of suitable organic and inorganic protective systems for various corrosive conditions.

Callaghan's map has undergone only minor adaptations since 1991 (AECI Paints n.d.; HDGASA 2005; Leitch 2006; Janse van Rensburg 2010). This was contrary to the fact that his atmospheric corrosion monitoring studies were carried out at only eleven sites, namely, five primary and six subsidiary locations (Callaghan 1991), of which sixty per cent were situated along the South African and Namibian coastlines.

Moreover, the map is mostly extrapolated. Leitch highlighted this shortcoming in 2006, consequently conducting several atmospheric corrosion studies to provide greater detail to the Callaghan map (**Figures 1.2 & 1.3**).



Code	Description	Map Colour	Type of corrosion	Mild steel corrosion rate(µm/a)	Galvanised steel sheet life in years
A	Intertidal to 5 km inland		Severe marine	100 – 300	Up to 3
B	Desert marine (Mists)		Severe marine	80 – 100	0.5 – 2
C	Temperate marine		Marine	30 – 50	3 – 7
D	Sub-tropical marine		Medium to severe marine	50 – 80	3 – 5
E	Desert inland dry		Desert	< 5	> 30
F	Inland		Rural	10 – 20	> 20
G	Inland urban		Inland industrial	15 – 40	5 – 15
H	Urban coastal		Marine industrial	50 – 150	1 – 3
I	Inland arid		Semi desert	5 - 10	> 30

Figure 1.1 Callaghan's corrosion map of Southern Africa (Callaghan 1991).

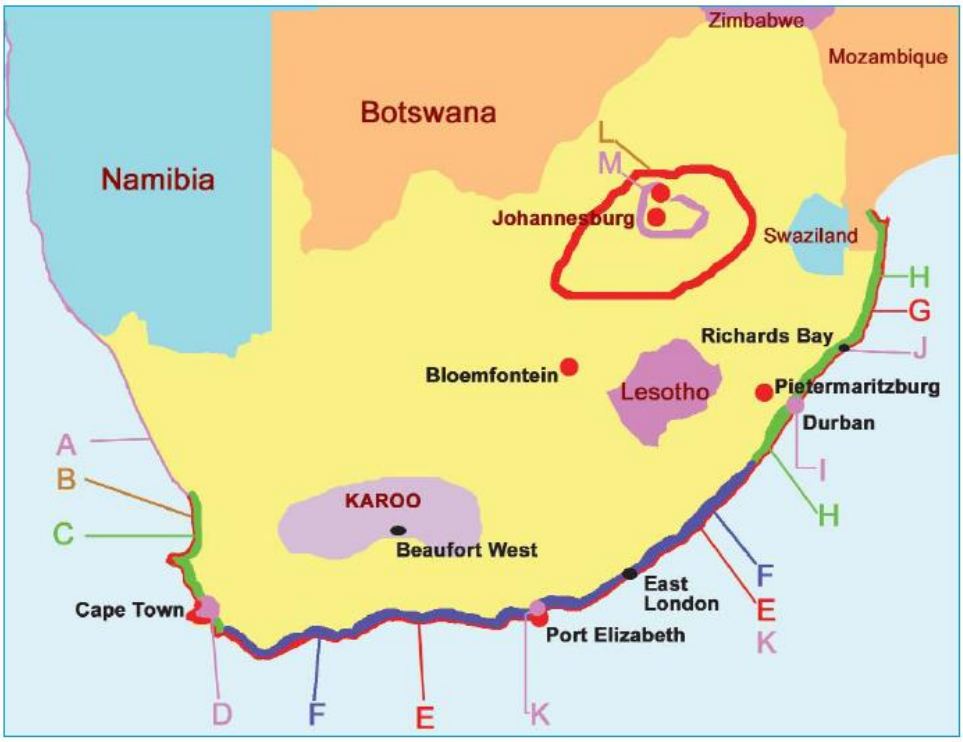
https://researchspace.csir.co.za/dspace/bitstream/handle/10204/10510/Callaghan%201991.pdf?sequence=1&isAllowed=y

While Callaghan attempted to include some inland sites in his original corrosion monitoring studies, none were in the present-day Greater Johannesburg Metropolitan Area (henceforth referred to as GJMA and previously known as the Witwatersrand). Comprehensive corrosivity profiling of South Africa's major metropolitan areas, especially inland, had also not been carried out.

MAP NOT PUBLICLY AVAILABLE

Figure 1.2 Atmospheric corrosion map of Southern Africa (Leitch 1999).

http://www.corrosioninstitute.org.za/#



Code	Geographic area	Distance from ocean	Description	ISO Category	Comments
A	Namibia and NW Cape shoreline	To 5 km	Desert shoreline and coastal fog zone	Above C5	N. of Olifants River
B	W. Cape-Atlantic shoreline	To 3 km	Arid shoreline with fog and strong winds	Above C5	False Bay to Olifants River
C	W. Cape coastal	To 5-15km	Coastal area	C4	To a range of fallout of salt aerosols
D	W. Cape urban	To 25 km	Coastal urban/industrial	C5	Cape Town and surrounds
E	S. and E. Cape shoreline	To 1 km	Temperate shoreline	C5	Distance from ocean varies with terrain
F	S. and E. Cape and Natal South coast	To 5 to 10 km	Temperate coastal	C4	Distance from ocean varies with terrain
G	KZN shoreline	To 4 km	Subtropical shoreline	Above C5	KZN to Maputo
H	KZN coastal	To 15 to 25 km	Subtropical coastal	C4	
I	Durban urban	To 10 km	Urban and industrial, inland and shoreline	Upper C5	Amanzimtoti to Durban North
J	Durban urban	To 15 km	Urban and industrial, inland of shoreline	Lower C5	
K	Coastal cities	To 10 to 15 km	Industrial and heavy traffic areas	Lower C5	Areas of Port Elizabeth, East London, Pinetown
L	Highveld general area	-	Rural and suburban areas	C3	
M	Highveld urban and industrial	-	High-traffic urban, or close to heavy industry	C4	East Rand, areas of Pretoria, Witbank

Figure 1.3 Atmospheric corrosion map of Southern Africa (Leitch 2006).

http://www.corrosioninstitute.org.za/#

1.2. SHORTFALLS OF THE CALLAGHAN MAP

1.2.1 Lack of Differentiation of Inland Areas

Based on the Callaghan map (**Figure 1.1**) (Callaghan 1991), the corrosivity of the GJMA is grouped with Pretoria, Vereeniging, Vanderbijlpark, Sasolburg, Emalahleni (formerly known as Witbank) and Middleburg – in other words, the area highlighted in lime green or indicated by 'G'. Moreover, as shown in the legend of this map, this region is given an expected corrosion rate for carbon (mild) steel of 15 μm/a to 40 μm/a (micrometres per annum) (Callaghan 1991).

Notwithstanding, studies by Callaghan (1991), Nixon (1993), Gnoinski & Ramothlola (1994) and Leitch (2006), showed that the Eastern Highveld region (the section of South Africa's inland plateau, spanning from Ekurhuleni to Emalahleni) tends to be more polluted and potentially more corrosive than many of the urban and rural areas in and around Johannesburg and Pretoria. This is because of the continuous burning of coal at Sasol Secunda (South Africa's largest synthetic fuel producer), and at several closed-circuit and dry-cooling coal-fired power stations located in this region, combined with the environmental pollution from open-cast coal mines and other large industrial plants (Callaghan 1991; Gnoinski & Ramothlola 1994; Van Tienhoven 1999). Currently, Kusile, a large new dry-cooling coal-fired power station is also being constructed in this region.

Sasolburg, Vereeniging and Vanderbijlpark, together known as the Vaal Triangle, are also recognised as highly polluted towns (Van Tienhoven 1999), primarily because of the production of petrochemical products from natural gas at Sasol Sasolburg, the burning of coal at a 3708 MW (megawatt) coal-fired power generating plant (Eskom 1988), and milling of steel at ArcelorMittal in Vanderbijlpark (South African Iron and Steel Institute 2012). However, the differentiation mentioned above in the corrosivity of the atmosphere is not evident in the Callaghan map.

1.2.2 Overstatement of Corrosion Rates

It may be debated that the predicted corrosion rate of mild steel for the Highveld region, 15-40 μm/a (**Figure 1.1**) is still relevant today, although this would only be valid providing the map was based on the first- and second-year corrosion results of mild steel. In 1999, Leitch suggested that it was based on the CSIR's average ten-year corrosion exposure results, subsequently acknowledged by Callaghan in 2012. This implied that the corrosion rates given in the Callaghan map were potentially significantly over-stated, particularly when compared to the guiding values specified in ISO 9224 (International Organization for Standardization 2012b) for the average corrosion rates of mild steel during the first ten years of exposure. Leicth also advanced this argument in 1999.

Assuming this to be true and that the map is based on the CSIR's average ten-year exposure results, then the projected first-year corrosion rate of mild steel in the Highveld region would be in the order of 39-88 μm/a, placing this area in the *moderate* (C3) to *very high* (C5) atmospheric corrosivity categories (International Organization for Standardization 2012a).

Noteworthy is that the ISO 9223 (2012) classification system is currently used worldwide for the rating of the corrosivity of environments. It comprises six levels of corrosivity, namely C1 (*very low*), C2 (*low*), C3 (*moderate*), C4 (*high*), C5 (*very high*) and CX (*extreme)* (International Organization for Standardization 2012a) (Refer to **Table 2.2**). While the C3 to C5 classifications may apply to some of the 'hotspots' in the Highveld area, in particular, because of specific sources of pollution, it is doubtful whether this classification is relevant to the whole region. By accepting this designation, it would mean that the corrosivity of the Highveld area is like many coastal atmospheres, which is logically not the case.

Also of note is that while ISO 9223:2012 is used extensively to classify the corrosivity of atmospheres, based on environmental data and/or actual corrosion rate measurements of metal specimens (International Organization for Standardization 2012a), it refers to ISO 9224 for the long-term service life predictions of standard materials of construction (International Organization for Standardization 2012b). (Refer also to Section 2.1.6.2).

These guiding values were derived from the average and steady-state corrosion rates of the different metals and alloys during the first ten years of service and reportedly, based on many exposure programmes and actual service performances of materials (Knotkova 2005; International Organization for Standardization 2012a). While the ten-year results, tabled in the CSIR's report (Callaghan 1991) seem to correlate better with the ten-year guideline values given in ISO 9224 (International Organization for Standardization 2012b), some values still do not match the corrosivity ranges provided in this standard.

1.2.3 Complicating the Use of ISO 9223 to 9226, and ISO 19244 Series of Standards

The grouping of several major towns and cities under the same corrosivity range in the Callaghan map complicates the use of standards such as ISO 9223 and ISO 9224, as well as the application and interpretation of other related International Standards, namely ISO 12944 (Parts 5 and 6) (International Organisation for Standardisation 2018a, 2018b).

Important to keep in mind is that it is not the author's intention to discredit the Callaghan corrosion map, but to highlight the need for greater detailed mapping of South Africa, mainly since international standards are currently used in combination with many plant-related corrosion protection specifications.

Several of the ISO Standards, relating to corrosion monitoring and coating laboratory testing procedures, have also been adopted by the Standards Division of the South African Bureau of Standards (SABS), henceforth referred to as SANS (South African National Standards). For example, SANS ISO 12944:1998 (Parts 1 to 8) series of standards (South African Bureau of Standards 1998a) have been wholly adopted from the original ISO 12944:1998 (Parts 1 to 8) series of standards. These first-issue standards cover the directions to follow regarding the general corrosion protection of steel structures by protective systems. Part 5:1998, for example, titled "*Paints and varnishes – Corrosion protection of steel structures by protective systems, Part 5: Protective paint systems*", can be used to select coating systems for different corrosive atmospheres (regarding C1 to C5 categories as per the ISO 9223:1992 standard). Nevertheless, it also refers to ISO 12944-Part 2 (International Organization for Standardization 1998a), which in turn references ISO 9223 and ISO 9226 (International

Organization for Standardization 1992a, 1992b), as the methodologies to use for classification of the environment into the different corrosivity categories. ISO 9226:1992 in turn, refers to ISO 9224 (International Organization for Standardization 1992b). Strong interrelationships between these standards exist, which are currently widely used for the design and corrosion protection of plants and equipment throughout South Africa. Noteworthy is that due to the recent 2017 and 2018 updates of the ISO 12944 series of standards, the SANS ISO 12944:1998 series of standards have become outdated and will likely be revised/withdrawn.

1.2.4 Discouraging the Use of More User- and Environmentally-friendly Coating Systems

ISO 12944:1998 (Part 6), also adopted and published as SANS 12944-6:1998 (South African Bureau of Standards 1998b), specifies the laboratory procedures to be used for the testing of organic and inorganic coatings for the different corrosive atmospheres. Regarding this standard, different water condensation and neutral salt spray testing periods, ranging from 48 hours to 1440 hours, are specified for coatings to be used in *low* (C2) to *very high* (C5) corrosive atmospheres. Therefore, in applying the Callaghan map to predict the corrosivity of the Highveld area, the user of the SANS equivalent or ISO 12944-6 standard would be uncertain as to which testing procedures to follow for this region, which may ultimately result in the incorrect specification of corrosion protection systems.

Based on the testing requirements of SANS or ISO 12944-6, for example, a water-based acrylic coating may hypothetically qualify as a highly durable paint system for a *low* (C2) corrosive environment, in which case it would have a predicted durability of more than 15 years (International Organisation for Standardisation 1998c; South African Bureau of Standards 1998c). On the other hand, the same coating is likely wholly inadequate for a *moderate* (C3) atmosphere in the same region, in which case its expected durability is only 2 to 5 years. Purely from a life-cycle costing point of view, significant calculation errors can be made by using generalised rating systems for large geographical areas, rather than more detailed results.

It may be contended that ‘over-specification’ is at least better than ‘under-specification’ and that from a life-cycle costing point of view, lower long-term maintenance costs may

be expected in using more durable systems. Still, over-specification often results in the preclusion of more user- and environmentally friendlier corrosion protection systems, which may be suitable for a less corrosive environment. Having a more detailed corrosion profile of the atmosphere in the Highveld region may encourage the potential use of water-based and low VOC (volatile organic compound) corrosion protection systems.

According to the London Metal Exchange (2012), which is the "*international standard for metal commodity pricing*" (About.com - Part of the New York Times Company 2012), between 2006 and 2007, there was a dramatic increase in the price of zinc worldwide. This increase in the cost of zinc has had a significant impact on South Africa's corrosion protection industry from a pricing point of view, particularly combined with the closure of Exxaro's Zincor company in 2011, which was South Africa's only zinc refinery (Moolman 2012). Noteworthy is that zinc is not only used in coatings to enhance their corrosion resistance properties (e.g. as zinc chromate, zinc phosphate, and zinc dust) but also as a corrosion protection system on its own in the hot-dip galvanised, electroplated and metal-sprayed forms. For corrosion protection suppliers, the vending of zinc-rich materials has, therefore, become a problem (Dulux Protective Coatings 2012).

Moreover, because of the increase in the zinc price, local end-users have been more willing to use organic coatings for the long-term corrosion protection of mild steel. This is an alternative to hot-dip galvanising - known to provide long-term corrosion protection of steel surfaces. It is therefore understood that the use of environmentally acceptable coatings under these conditions would be of further benefit.

1.2.5 No Reflection of Increased Industrialisation and Global Warming Effects

During the last three decades, the Highveld and Vaal Triangle regions have seen dramatic changes from an industrialisation point of view. This reality combined with the problem of global warming, resulting from increasing environmental pollution (Biodiversity and Conservation Biology Department 2012), have likely altered earlier meteorological patterns and data used for the extrapolation of the Callaghan map. Since 1991, significant advances have also been made in the meteorological and pollution

monitoring of environments. The Callaghan map does not reflect any of these technological advances and global changes.

1.3 THE NEED FOR DETAILED CORROSION MONITORING OF THE GREATER JOHANNESBURG METROPOLITAN AREA (GJMA)

Given the above-highlighted issues, the need for a more detailed corrosion map of South Africa has been identified. This process, however, is a long-term endeavour, likely to be carried out in different phases and over many years. During 2007 to 2012, Eskom Holdings SOC Ltd (the leading electricity producer of South Africa and henceforth referred to as Eskom) contracted the author (on behalf of Orytech Pty. Ltd.) to carry out atmospheric corrosion monitoring at 77 of its power generating, transmission and distribution sites - positioned throughout South Africa (Janse van Rensburg 2010). Based on the results of this work, it became apparent that greater focus needed to be placed on the Highveld and Vaal Triangle areas, of which the 'Greater Johannesburg Metropolitan Area' or GJMA forms a significant part.

This area covers the City of Johannesburg Metropolitan Municipality, the East Rand, and West Rand, and extends from east to west about 100 km and from south to north, 60 km. It includes Soweto, Roodepoort, Sandton, Randburg, Alexandra, Germiston, Randfontein, Nigel, Midrand, Orange Farm, Vosloorus, Kempton Park, Boksburg, Benoni, Alberton and Springs (Wikipedia.com 2017a; Google Inc. 2017a).

1.4 PRIMARY RESEARCH OBJECTIVES AND DELIVERABLES

It is important to stress that the primary aim of this thesis is not to provide a complete review and study of all the mechanisms of atmospheric corrosion (from macro to electrochemical levels), or of the interconnected equations by which the processes occur. The primary research objectives are:

i) To provide sufficient insight into the different factors and mechanisms that influence atmospheric corrosion, with greater emphasis placed on those factors

that have a significant impact on the atmospheric corrosion of South Africa and the GJMA.

ii) To compile new geoprocessed (metal specific) corrosion maps for South Africa, based on assimilations of historical published and unpublished, as well latest corrosion monitoring data for the GJMA, that can be used for cost-effective corrosion protection solutions.

1.5 HYPOTHESIS

Atmospheric corrosivity of South Africa's inland areas, mainly the GJMA, is not homogenous, as shown in Callaghan's map, but heterogeneous, due to seasonal, geographical, climatological and pollution variations. Detailed corrosion mapping of this area is, therefore, necessary to provide greater clarity regarding atmospheric corrosion in South Africa.

1.6 RESEARCH QUESTIONS

The primary research questions are:

- What is the nature of atmospheric corrosion?
- What are the general factors that influence atmospheric corrosion?
- Which methods are most practical and cost-effective for the atmospheric corrosivity monitoring of significant inland (metropolitan) environments in South Africa?
- What modelling techniques are used for atmospheric corrosion mapping?
- What are the general atmospheric corrosion mechanisms and corrosion products of carbon steel, hot-dip galvanised steel, aluminium, copper and zinc?
- What are the benefits of atmospheric corrosion maps?
- What are the strengths and weaknesses of the existing corrosivity maps?
- What is the history of atmospheric corrosion monitoring in South Africa?
- What are the key factors that drive atmospheric corrosion in the GJMA?

- Based on existing (published and unpublished data), how does atmospheric corrosion of mild steel, hot-dip galvanised steel, aluminium, zinc and copper change throughout South Africa?
- What are the potential errors and uncertainties about the existing (published and unpublished) atmospheric corrosion data of South Africa?
- What are the seasonal variables regarding atmospheric corrosion at selected sites in the GJMA, based on their Atmospheric (ACI), Industrial (ICI) and Marine (MCI) Corrosivity Indices?
- What are the 12-month atmospheric corrosion rates of mild steel, hot-dip galvanised mild steel, aluminium, zinc and copper at 57 sites in the GJMA?
- How does atmospheric corrosion vary between distinct regions in the GJMA?
- How do the periods of exposure impact on the atmospheric corrosion rates of mild steel and hot-dip galvanised steel?
- What are the potential errors and uncertainties about the latest atmospheric corrosion data of the GJMA?
- What are the key factors of atmospheric corrosion in the GJMA, based on conductivity and pH measurements, as well as elemental composition analysis of the corrosion products?
- What is the typical morphology of the corrosion product formed on mild steel in the GJMA?
- To what extent do the latest atmospheric corrosion trends relate to existing meteorological and pollution data for the GJMA?
- How do the most recent atmospheric data correlate with previous atmospheric corrosion studies of this region?
- Where are the atmospheric corrosion ‘hotspots’ in the GJMA?
- How does the atmospheric corrosivity of the GJMA influence the photochemical breakdown of organic materials?
- What is the variability of the ISO 9223:2012 corrosivity rating in South Africa and the GJMA?
- How do the corrosion rates of mild steel, hot-dip galvanised mild steel, aluminium, copper and zinc vary throughout South Africa and the GJMA?

1.7 BENEFITS AND NOVELTY OF THE RESEARCH WORK

This thesis considers the corrosion profiling of the atmosphere at 57 sites in and around the GJMA, adding to the current South African knowledge base and facilitating revisions of the South African corrosion map. The novelty of this work lies in the substantial number of sites involved in the study – making it one of the largest of its kind in South Africa. Corrosion profiling of a large metropolitan area was also carried out for the first time in South Africa.

Other academic contributions include:

- the unique study area that was chosen;
- the new geographic information system (GIS) presentation format of published and unpublished research data;
- identification of the primary corrosion factors involved at the selected GJMA sites; and
- the seasonal and annual corrosion profiling of potential 'hotspots' in and around Johannesburg.

Moreover, ISO 9223:1992 (International Organization for Standardization 1992a) copper wire corrosion data are presented in a public format for the first time in South Africa. The results have also been used to predict the residual life of selected bronze statues in South Africa, of which the data are published separately from this thesis.

The unique application of the Bresle water-soluble salt contamination test (International Organization for Standardization 2006), with associated pH measurements of the corrosion products, are furthermore advanced.

Apart from the measurement of atmospheric corrosivity at 57 inland locations, organic coated steel specimens were also exposed as potential indicators of the ultraviolet (UV) light radiation and pollution levels at the different locales. Additionally, the photochemical breakdown effects of these water-based, and low and high volatile organic compound (VOC) coatings were explored. This information enables the specification of more environmentally-friendly materials for the GJMA.

An additional benefit of this study involves the Consumer Protection Act No. 68 of 2008. Since its enactment in 2008, material and coating manufacturers, and suppliers have

been forced to carry out more rigorous testing of their products, which is to ensure that the South African consumer is well informed and protected from poorly performing goods and exaggerated claims (Janse van Rensburg 2011). However, this may only materialise by knowing how various materials perform under different environmental conditions.

1.8 RESEARCH LIMITATIONS

Investigation of the seasonal variables of the atmospheric corrosivity of only 22 out of the 57 sites in the GJMA was carried out - this was due to time and cost constraints. Furthermore, although the measured and estimated corrosion data were based on the exposure of many units at various sites, it only covered one exposure period per location, namely from August 2013 to September 2015. Therefore, long-term climatic and pollution changes that may affect the corrosion rates of metals are not included in the results. Also, due to cost constraints, meteorological and air quality data of only eight of the 57 sites were available for comparison with the corrosion data.

1.9 STRUCTURE OF THE THESIS

Table 1.1 presents the general layout of the thesis.

Table 1.1 General structure of the thesis.

Chapter No.		Description
Chapter 1		**Introduction – The need for a new corrosion map** (Background to the study)
Chapter 2		**Literature review**
	2.1	Atmospheric corrosion
	2.2	The history of atmospheric corrosion in South Africa
	2.3	Factors that may drive atmospheric corrosion in the GJMA
Chapter 3		**Methodology**
	3.1	Atmospheric corrosion of South Africa – Data compilation
	3.2	Corrosion monitoring of the GJMA – Experimental procedures
	3.3	Meteorological and air quality data situation reports for the GJMA
	3.4	Mapping procedures
Chapter 4		**Results**
	4.1	Assimilations of existing published and unpublished atmospheric corrosion data for South Africa
	4.2	Atmospheric corrosion of the GJMA
	4.3	The effects of the GJMA atmosphere on organic coatings
Chapter 5		**Discussion**
	5.1	Statistical analyses and interpretation of existing atmospheric corrosion data for South Africa
	5.2	Atmospheric corrosion of the GJMA
	5.3	Effects of the GJMA atmosphere on organic coatings
	5.4	Effects of physical, meteorological and pollution parameters on the corrosivity of the GJMA
Chapter 6		**Atmospheric corrosion maps for South Africa and the GJMA**
Chapter 7		**Conclusions and key/novel findings**
Chapter 8		**Recommendations and future perspective**

1.8 PUBLICATIONS

Based on the work presented in this thesis, four papers were prepared, namely:

- Corrosion mapping of South Africa' s macro atmosphere;
- Atmospheric corrosion profiling of the Greater Johannesburg Metropolitan Area (GJMA);
- Atmospheric corrosion and residual life expectancy estimates of bronze statues in South Africa; and
- Photochemical degradation of organic materials in the Greater Johannesburg Metropolitan Area (GJMA).

1.9 PRESENTATIONS

The author also gave presentations of this work at selected South African conferences and seminars, namely:

- AfriCORR – 2014 Conference in Pretoria (28 to 30 July 2014) - Atmospheric corrosion profiling of the Greater Johannesburg Metropolitan Area – The start of a new corrosion map;
- AfriCORR – 2016 Conference in Midrand (25 to 29 July 2016) - A preliminary updated atmospheric corrosivity map of South Africa - based on historical published and unpublished data;
- Corrosion Institute of Southern Africa – Gauteng branch – Atmospheric corrosion of zinc and hot-dip galvanising in South Africa (8 June 2017);
- Corrosion Institute of Southern Africa - Western Cape branch – Atmospheric corrosion of zinc and hot-dip galvanising in South Africa (22 June 2017); and
- AfriCORR – 2018 Conference in Johannesburg (July 2018) - Atmospheric corrosion maps of South Africa and the Greater Johannesburg Metropolitan Area (GJMA).

CHAPTER 2

LITERATURE REVIEW

2.1 ATMOSPHERIC CORROSION

2.1.1 Corrosion

'Corrosion' is defined as the breakdown of materials due to environmental effects (Uhlig 1963; Fontana 1987; Roberge 2012), and principally applies to metals. However, since materials, e.g. plastics, rubbers, paints and ceramics similarly degrade because of environmental exposure, some scholars maintain that it is also applicable to non-metallic materials (Fontana 1987; Leygraf et al. 2016). For this thesis, the term 'corrosion' correspondingly relates to the breakdown of metallic and non-metallic materials, since the photochemical degradation effects of coatings in the GJMA are also investigated.

2.1.2 The Atmosphere

In corrosion studies, the term 'atmosphere' applies to indoor and outdoor open ambient air conditions. From an outdoor perspective, Earth's atmosphere encompasses six layers (Cottis et al. 2010; Botkin & Keller 2010) of which the bottom layer that extends from the ground up to 10-20 km (Botkin & Keller 2010) is called the troposphere, where the air is at its densest and in which weather occurs (Kerrod 1983; Botkin & Keller 2010). This study deals with the corrosion of materials in the lower tropospheric layer only.

Cottis et al. (2010) and Botkin & Keller (2010) state that the atmosphere is not a static system, but changes continuously, due to the exchange of gases via plants, the sea, biological organisms, volcanic eruptions, weathering processes, as well as human interaction. The composition of the uncontaminated atmosphere surrounding Earth includes nitrogen (~78%), oxygen (~21%), argon (~0.9%), carbon dioxide (~0.03-0.04%) and water vapour (Botkin & Keller 2010; Encyclopaedia Britannica 2018a). The remaining constituents comprise trace gases, such as neon, helium, krypton, and xenon (Encyclopaedia Britannica 2018a). Accordingly, Seinfeld & Pandis (1997) indicate that

the general composition of the atmosphere includes several additional gases (**Figure 2.1**).

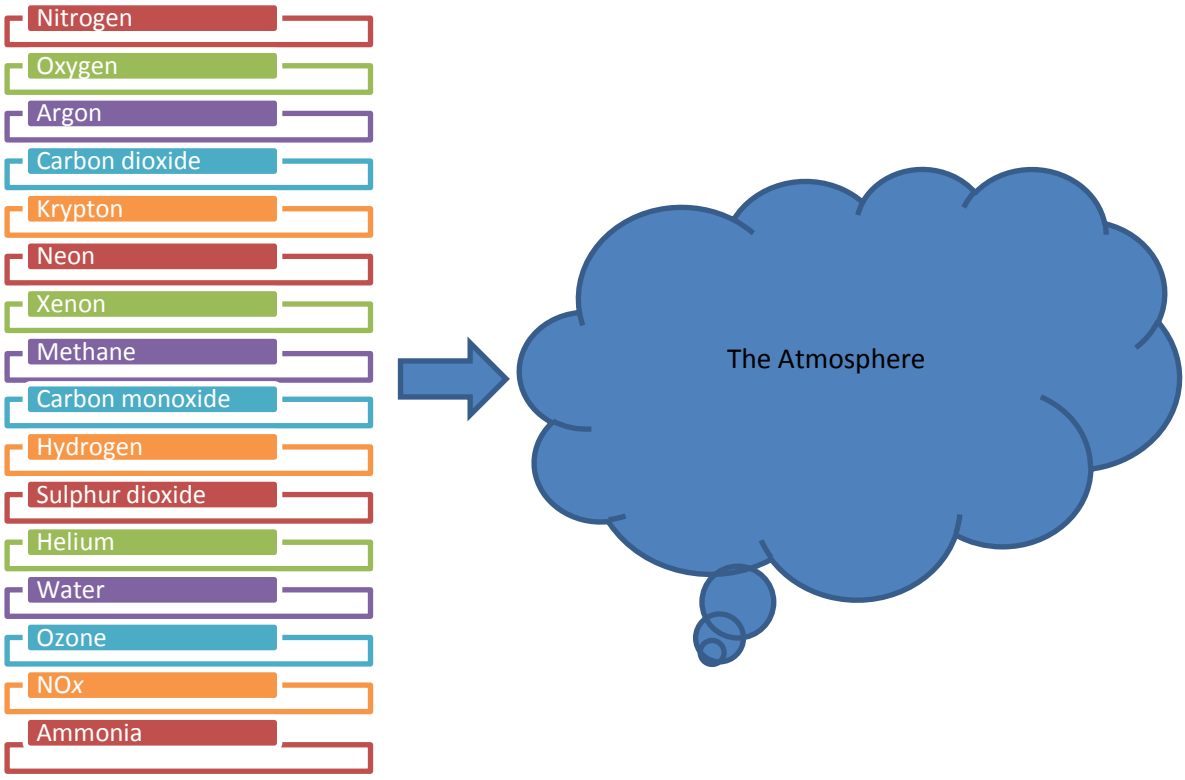


Figure 2.1 Normal composition of the atmosphere - Adapted from Seinfeld and Pandis (1997).

Apart from oxygen and carbon dioxide, the permanent gases are primarily inert, implying that they do not readily react with other elements to form new chemical substances. In contrast, oxygen plays a crucial role in many atmospheric corrosion oxidising processes, while carbon dioxide, which is a significant trace gas (~three volumes in 10 000) (Encyclopaedia Britannica 20018b) affects Earth's weather (The Gale Encyclopedia of Science 2008) and can also influence the passivation of materials, e.g. hot-dip galvanising (McEwan 2004).

From an atmospheric corrosion perspective, the focus is placed on those gases that:

i. promote/control the wetting of material surfaces via the formation of hygroscopic salts;
ii. encourage the change of the pH of the electrolyte, and

iii. promote/control the solubility of the corrosion product (Cottis et al. 2010).

2.1.3 The Nature of Atmospheric Corrosion

2.1.3.1 Atmospheric corrosion

In terms of metals, 'atmospheric corrosion' is an electrochemical process (Uhlig 1963; Kerrod 1983; Fontana 1987; Leygraf et al. 2016) and defined as the degradation of materials (Fontana 1987; Leygraf et al. 2016) when exposed to the gases, aerosols, and particles (International Organization for Standardisation 1998c) in the atmosphere. However, non-metallic materials may also degrade due to exposure to the environment (Leygraf et al. 2016).

Since atmospheric corrosion of metals is electrochemical, the process entails the flow of an electric current, i.e. the movement of electrons between two materials - one a solid substrate and the other a liquid, or melt (an electrolyte) (Encyclopaedia Britannica 2008a, 2018c). NACE International (2002) defines an "*electrolyte as a chemical substance containing ions that migrate in an electric field*".

2.1.3.2 The mechanism of atmospheric corrosion

Initially, scholars have understood that atmospheric corrosion involves merely a metal in contact with water and oxygen (Payne 1961; Fontana 1987, Rincon et al. 2000). However, later studies have shown that the process is enormously complex, due to many variables involved, and triggered only by a thin film of moisture on the metal surface (Payne 1961; Uhlig 1963; Fontana 1987; Tullmin & Roberge 2000; Cole 2017; Roberge 2012; Leygraf et al. 2016). Since an electrolyte is a fundamental requirement for electrochemical corrosion, the conditions under which it develops, its constituency and residence time on the steel surface are essential aspects that required further investigation. Therefore, during the past three decades or so, significant strides have been made regarding the chemical, electrochemical and physical processes involved in atmospheric corrosion (Leygraf et al. 2016).

Basic atmospheric corrosion principals

The electrolyte acts as a medium for the flow of oxidised metal ions from the anode to the cathode, as well as delivering the reduction species to the cathode. However, it also acts as a solvent for the dissolution of atmospheric constituents, e.g. gases or particulates (Leygraf et al. 2016; Encyclopaedia Britannica 2008a). For corrosion to take place, both the cathodic and anodic sites of the base metal must be immersed/covered in the same electrolyte (McEwan 2004).

The anode is the position/site at which electrons are released via a process of oxidation of the metal, and the cathode, the site where the electrons are consumed via a reduction reaction (Uhlig 1963; Fontana 1987; McEwan 2004; Tullmin & Roberge 2000; Roberge 2012; Leygraf et al. 2016). **Figure 2.2** presents an adaptation of Roberge's (2012) schematic of the underlying mechanism of atmospheric corrosion of iron in a non-contaminated environment.

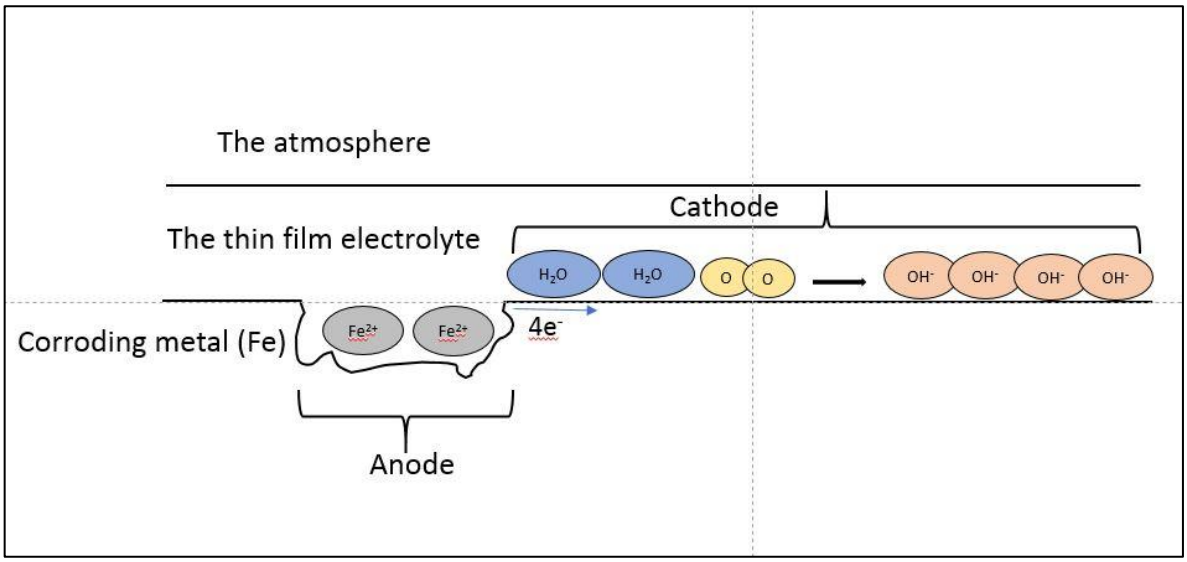


Figure 2.2 An adaptation of Roberge's (2012) schematic of the underlying mechanism of atmospheric corrosion of iron in a non-contaminated environment.

In the presence of a neutral or slightly acidic electrolyte (in other words an uncontaminated atmosphere), the typical balancing reactions that develop at the anodic and cathodic sites on an iron surface are given by Uhlig (1963), Fontana (1987), Callaghan (1991), Tullmin & Roberge (2000), and Roberge (2012) as:

Anodic reaction (oxidation reaction): $2Fe \longrightarrow 2Fe^{2+} + 4e^-$ **Eq. 2.1**

Cathodic reaction (oxygen reduction): $O_2 + 2H_2O + 4e^- \longrightarrow 4OH^-$ **Eq. 2.2**

The corrosion product is formed when the hydroxides migrate to the anodic zone, forming hydrated Fe_2O_3 (Uhlig 1963; Fontana 1987; Tullmin & Roberge 2000), of which the complete balanced reaction is:

$4Fe + 3O_2 + 2H_2O \longrightarrow 2Fe_2O_3.H_2O$ **Eq. 2.3**

The corrosion reaction is influenced in various ways. The cathodic (reduction) reaction (**Equation 2.2**) may be influenced by a low concentration or diffusion rate of oxygen, and the anodic (oxidation) reaction (**Equation 2.1**), can be reduced by the limited supply of moisture and corrosive-stimulating chemical species (Stratmann et al. 1987; Schweitzer 1999). The anodic and cathodic sites are also often separated from each other (Leygraf et al. 2016). This occurrence was first demonstrated by Evans in 1926 via drop experiments, which provided significant insight regarding the nature of the atmospheric corrosion process (Morton 2013). Using ferroxyl indicator (affected by the pH of the solution) in his pitting corrosion experiments, Evans applied small droplets of an aqueous sodium chloride solution on mild steel whereafter the formation of the cathodic and anodic sites was investigated. The results showed that even though oxygen is initially evenly dissolved throughout the salty droplets, leading to the even formation of anodic and cathodic sites through the drops, with time, the oxygen in the droplet becomes depleted via reduction. Consequently, the anodic and cathodic sites separate, causing oxygen reduction to occur along the perimeters of the drops, owing to easier access.

Leygraf et al. (2016) reported that because of the free availability of oxygen to the thin liquid layer on the surface, the anodic rather than the cathodic reaction tends to drive the corrosion rate. However, protective coatings, surface deposits, oils and crevices, in the presence of water, which may cause more localised forms of corrosion attack, can significantly reduce oxygen's availability to the cathode (Tullmin & Roberge 2000). Dissimilar metals in contact with each other may also markedly increase the severity of atmospheric corrosion (Fontana 1987; Callaghan 1991). Under these conditions, the rate of corrosion process is instead controlled by the cathodic reaction, whereas the

dissolution of the metal depends on the formation of a corrosion product, its solubility in the electrolyte and the development of passive oxide films (Fontana 1987; Tullmin & Roberge 2000). Kelly and co-workers also showed with their computational model that the cathodic reaction can have a limiting effect on the localised corrosion of wetted Type 316 stainless steel (Cui et al. 2005).

Misawa et al. (1974), as condensed by Morcillo et al. (2012), postulated the following mechanism (**Equations 2.4 & 2.5**) for the atmospheric corrosion of irons. Firstly, atmospheric oxidised ferrous ions are said to dissolve into a neutral or slightly acidic thin moisture layer on the steel surface, resulting in the precipitation of lepidocrocite (γ- FeOOH) (**Equation 2.4**). The precipitation and crystallisation of γ-FeOOH are then advanced by wet-dry cyclic conditions.

$$Fe \xrightarrow{\text{dissolution}} Fe^{2+} \xrightarrow{\text{hydrolysis}} FeOH^{+} \xrightarrow{\text{oxidation and precipitation}} \gamma\text{-FeOOH}. \qquad \textbf{Eq. 2.4}$$

Secondly, SO_2 in the atmosphere is known to lower the pH of rainwater. Consequently, a low pH moisture film on a superficially rusted steel surface will tend to dissolve the γ- FeOOH, resulting in the precipitation of amorphous ferric oxyhydroxide upon drying. The latter is then converted to goethite (α-FeOOH), using OH^- (hydroxyl ions) supplied by the rain (**Equation 2.5**).

$$\gamma\text{-FeOOH} \xrightarrow{\text{dissolution \& precipitation}} FeO_xOH_{3-2x} \xrightarrow{\text{solid state transformation}} \alpha\text{-FeOOH}. \qquad \textbf{Eq. 2.5}$$

However, in 1987, Stratmann et al. proposed the division of the corrosion process of iron into three stages, namely:

i. *Wetting of the dry surface* – During the initial wetting stage of the metal surface, the dissolution of Fe at the anode is in equilibrium by the reduction of Fe(III) at the cathode in the rust layer. Also, the O_2 reduction reaction at the cathode is slow, and the corrosion process is mainly driven by the dissolution of the metal, which is limited to the amount of reducible FeOOH in the rust layer (Stratmann et al. 1987; Morcillo et al. 2012);
ii. *Wet surface* – After the reducible FeOOH has been consumed, the O_2 reduction reaction becomes the cathodic reaction as in **Equation 2.2**. It is said that the dissolution rate of the iron is controlled by the diffusion-limited current density

(DLCD) of the O_2 reduction reaction on the surfaces of the pores. Since the corrosion product pores are filled with electrolyte, the corrosion rate is slowed down during this stage, as the diffusion rate of O_2 is lower in the liquid than in gas phase (Stratmann et al. 1987; Morcillo et al. 2012);

iii. *Drying-out of the surface* – During the final stage, as the surface begins to dry, resulting in thinning of the electrolyte film on the inner rust layer surface, a rapid increase in the reduction reaction takes place due to the increased diffusion of O_2. Consequently, the rate of corrosion is high, with the O_2 reduction once more becoming the cathodic reaction. Additionally, the reduced Fe(II) formed during Stage 1, can be re-oxidised by O_2. Consequently, because of the increased corrosion rate, the drying-out stage of the whole wet-dry cycle tends to dominate the extent of the metal loss. During the final stage, due to the re-oxidisation of γ- FeOOH and other ferrous oxides, goethite forms, as well as γ-FeOOH is regenerated (Stratmann et al. 1987; Morcillo et al. 2012).

Since Evans' initial work, electrolyte drop experiments have proven valuable pertaining to the study of the atmospheric corrosion of different materials from a laboratory perspective, especially about the development of localised corrosion effects. According to Frankel (1998), and Frankel & Sridharb (2008), localised corrosion can be divided into the following steps:

i) the breakdown of the passive oxide film - initiated above a critical potential;
ii) the formation of small pits, of which many become stable during this stage and cease to develop any further;
iii) the steady growth of the corrosion sites – some of which can grow large; and
iv) providing the correct conditions prevail, re-passivation or termination of the corrosion attack – below a lower potential.

Pitting corrosion studies involving materials that form passive oxide layers e.g. aluminium, its alloys, and stainless steels have also been conducted by Tsutsumi et al. (2007), Frankel & Sridharb (2008), Li et al. (2011), Maier & Frankel (2011), Morton & Frankel (2013), Davenport et al. (2014) & Cook et al. (2017). In this regard, Tsutsumi et al. (2007) showed that the initiation of corrosion pits in Type 304 stainless steel may occur under "*sufficient low humidity conditions*", while Davenport et al. (2014) reported

that changes in the relative humidity (RH) might cause partial or complete re-passivation of pits, occasionally forming new pits. Conversely, Cook et al.'s (2017) study revealed that nitrate tends to inhibit pitting corrosion of Types 304L and 316L stainless steels under magnesium salt droplets when the deposition density ratio of nitrate and chloride ions is above a critical value.

Electrolyte formation

Relative humidity (RH) is the critical player in the rate of atmospheric corrosion (Mansfield 1979; Roberge 2012) and a function of temperature that describes the amount of moisture that exists in a gaseous mixture of air and water vapour (Castillo 2011). Concerning atmospheric corrosion, the thin electrolyte layer, mostly water (Kerrod 1983; Efunda 2016), forms in different ways, i.e. either directly via rain, dew, fog, spray, snow or vapour condensation (Cottis et al. 2010; Leygraf et al. 2016) due to high %RH in the atmosphere, or indirectly by the deliquescence of salts (deposited via impacting or diffusion to the surface), e.g. chloride-bearing salts (Cottis et al. 2010; Leygraf et al. 2016).

Leygraf et al. (2016) state that the initial stages of atmospheric corrosion involve the instantaneous reaction of water vapour with the metal surface, via the bonding of the oxygen atom to the metal or another positively charged surface contaminant. The main driving force for the dissociation of water is the formation of metal-oxygen and metal-hydroxyl bonds, which function as sites for additional water adsorption, with added exposure to the atmosphere. Consequently, more and more monolayers of moisture are formed, with the ultimate number of films being dependant on the RH, the time of exposure and the substrate properties (Cottis et al. 2010; Leygraf et al. 2016).

Cottis et al. 2010 and Leygraf et al. (2016) further report that the amount of moisture layer build-up depends on the hydrophobic or hydrophilic nature of the surface, the density of surface defects and RH. It is also said that the number of monolayers of moisture increases with a rise in RH and that it is generally recognised that below 60% RH, the electrolyte film is too thin to sustain the electrochemical corrosion process (Cottis et al. 2010). Moreover, adsorbed hygroscopic aerosols may further attract moisture, causing an additional rise in the number of water molecules at a specific RH

than predicted (Leygraf et al. 2016). The porosity and roughness of the surface also influence the extent of water adsorption (Leygraf et al. 2016).

The dissolved ions in the electrolyte, responsible for the transfer of the charge present in the corrosion cell, are provided by pollutants and natural salts present in the atmosphere (Cottis 2010; Roberge 2012), while the concentration of the electrolyte, is determined by the relative humidity (Mi 2013). The critical RH at which significant corrosion of metal occurs is termed the Critical Relative Humidity (CRH) (Brown and Masters 1982; Callaghan 1991; Tullmin & Roberge 2000) (**Figure 2.3**) (McEwan (2004, 30). This concept was introduced by Vernon in 1931, whose studies revealed an increase in the corrosion rate of steel at an approximate RH of 60%, and an even higher increase at 80% in the presence of 0.01% sulphur dioxide (SO_2). Lobnig et al. (1996a) described CRH as "*an effective RH at which a surge in moisture pickup of a compound occurs*". However, nowadays it is considered that CRH is instead governed by the vapour pressure of hydrated salts, e.g. chlorides and sulphates present in the corrosion product or on the base metal (Lloyd n.d.; Brown & Masters 1982).

CRH is not constant for all metals (Brown and Masters 1982), surface contaminants or environments, but varies depending on the type of the material, affinity of the corrosion product and other surface deposits to absorb moisture, as well as the presence and concentration of atmospheric pollutants (Brown and Masters 1982; Tullmin & Roberge 2000; Li et al. 2013). Although, as cited by Li et al. (2013), in an unpolluted atmosphere, the "*primary critical relative humidity*" for clean metal surfaces appears to be reasonably similar, namely 66%, but changes when the surfaces are covered with corrosion product or salt deposits.

The method by which salts or other chemical substances absorb moisture from the atmosphere to form an electrolyte is termed 'deliquescence' (Schinderholtz & Kelly 2012). Providing the air is sufficiently humid, all soluble salts deliquesce (Encyclopaedia Britannica 2018d). However, substances that absorb moisture or wet, without dissolving into the electrolyte, it said to exhibit a hygroscopic nature, e.g. dust (McEwan 2004).

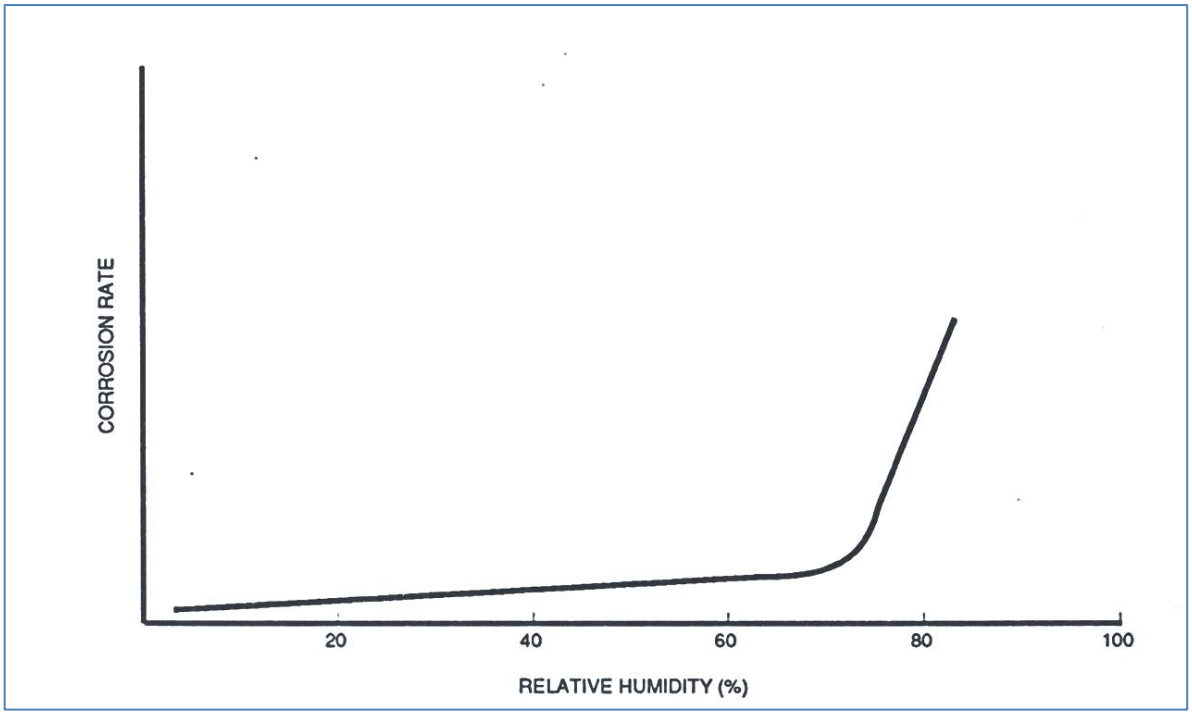


Figure 2.3 Schematic diagram showing the effect of %RH on the corrosion rate of steel (in the absence of any pollutants) – McEwan (2004). http://www.corrosioninstitute.org.za/#

The point at which salts or crystalline materials start to absorb large quantities of moisture is termed the Deliquescence Relative Humidity (DRH) (Schinderholtz & Kelly 2012). Each salt has a unique DRH (Wexler et al. 2011; Schinderholtz & Kelly 2012), for example, for magnesium chloride it is 32-34% (Montgomery et al. 2011; Roberge 2012; Schinderholtz & Kelly 2012; Cook et al. 2017), ammonium chloride 80% (Schinderholtz & Kelly 2012) and for sodium chloride, 75-77% (Montgomery et al. 2011; Roberge 2012; Schinderholtz & Kelly 2012). However, the deliquescence point of a salt mixture, which is typically more encountered in atmospheric corrosion and lower than its pure salt components, is referred to as the Mutual Deliquescence RH (MDRH) (Schinderholtz & Kelly 2012).

Deliquescence of deposited salts (solid to liquid) (Schindelholz et al. 2014) is a function of temperature, particle shape and size (Schinderholtz & Kelly 2012) and depends on whether the salt's DRH is lower or higher than atmospheric RH. If, RH > DRH, moisture is taken up by the salts. Conversely, when RH < DRH, moisture is driven out (Cottis et al. 2010). The latter process is referred to as efflorescence (Schindelholz et al. 2014), and the stage controlled by the ERH (efflorescence relative humidity).

Recent droplet studies have also shown that regarding chloride salt deposition, if the mass per unit area (also known as chloride-deposition density (CDD)) of the salt is greater, a larger volume of electrolyte forms (at constant RH), leading to an increased corrosion rate (Davenport et. al. 2014; Street et al. 2015). Moreover, the thickness of the electrolyte layer also plays an important role, e.g. in the case of zinc surfaces (Roberge 2012).

2.1.3.3 Residence time of the thin film electrolyte/time of wetness (TOW)

The residence time of the thin film electrolyte on the metal surface is called the time of wetness (TOW) and is frequently used in corrosion prognostics and environmental corrosivity classification (Schinderholtz & Kelly 2012). TOW is also commonly defined as the time that surfaces remain wet for significant corrosion to occur. It is symbolised as τ, and described in the renowned ISO 9223-9226:2012 model for corrosive atmospheres (International Organization for Standardization 2012a-d) as the time the RH in the air is more than 80%, while the temperature is above 0°C.

Consistent with Cole et al. (1999), Ahmad (2006) and the International Organization for Standardization (2012a), the time that surfaces remain wet, either because of rain, condensation, or other wetting processes, is a significant determinant of the rate of atmospheric corrosion. Accordingly, the ISO-TOW concept carries a much higher weighting than air-borne sulphur dioxide (P) and salinity (S) in the ISO 9223-9226:2012 model. Based on the ISO model, when RH exceeds 80% for more than 5500 hours/a (hours/annum), the environment is classified as *moderately* (C3) to *highly* (C4) corrosive – that is regarding the corrosion of unalloyed carbon steel (International Organization for Standardization 2012a). This is in the absence of any significant depositions of sulphur dioxide ($P_d \leq 10$ mg/(m^2·d) and salinity ($S_d \leq 1500$ mg/(m^2·d). In contrast, however, when the deposition rates of sulphur dioxide and salinity are at their highest levels, that is when $P_d \leq 200$ mg/(m^2·d) and $S_d \leq 1500$ mg/(m^2·d), but time of wetness is at its lowest ($\tau \leq 10$), the environment may be classified as only *low* (C2) corrosive.

Criticism of the ISO-TOW concept is that although it is considered useful in atmospheric corrosion studies, it is not founded on basic principles (Cole et al. 1999). As a result, other models have been developed to predict the formation and evaporation of a

moisture film on surfaces, e.g. TCD (time of condensation) (Cole et al. 1999), which is defined as:

TCD = time when TCON > 0 **Eq. 2.6**

TCON, the tendency to condensation, is given as the difference between the vapour concentration of the air (A_{vc}) and the saturation vapour concentration of the surface (S_{svc}) required for condensation (Cole et al.1999). Even though the TCD model was found to be more accurate and fundamentally based regarding the prediction of the formation of the electrolyte layer than ISO-TOW, the latter concept is still seen and used as an acceptable procedure (Cole et al. 1999).

Schinderholtz & Kelly (2012) reported that the notion of what is meant by 'wet' has also been contentious. Consequently, these researchers have provided a comprehensive review of the current state of the concept of TOW, its determination, issues and limitations, as well as improvement avenues in the field. Based on their paper, the main parameters that influence TOW are:

- the wettability of the surface, which is controlled by:
    - the surface roughness, defects and cleanliness;
    - the liquid drop size, its geometry and gravity;
    - the capillary action via surface pores; and
    - precursor films and secondary spreading.
- the modes of wetting:
    - dry deposition (via the combined influences of gravitational sedimentation, impaction, and diffusion);
    - cloud and fog droplet deposition on surfaces via settling and impaction, known as occult deposition; and
    - precipitation - rain, snow, sleet and hail.
- sorption:
    - sorption of moisture occurs via adsorption, dew condensation, capillary condensation, and deliquescence modes, which are governed by temperature, water activity, surface geometry and composition.

- the methods of drying:
    - evaporation – which is controlled by the difference in the water vapour pressure of the electrolyte and the ambient air;
    - dewetting – which is the natural withdrawal of a liquid film from a non-wetting surface; and
    - runoff - where a water film or drop leaves a tilted surface altogether due to the force of gravity, e.g. hot-dip galvanised roofs. In this regard, the runoff tends to wash off surface contaminants and corrosion product that has accumulated on a surface by dry deposition (Schinderholtz & Kelly 2012).

2.1.3.4 Gas, aerosol and particle deposition

Apart from being a prerequisite for electrochemical reactions, the electrolyte also acts as a solvent for atmospheric gases, aerosols and particulates that may deposit on the surfaces, which are given by Leygraf et al. (2016):

- in the gaseous form: as sulphur dioxide (SO_2); nitrogen dioxide (NO_2); hydrogen chloride (HCl); carbon dioxide (CO_2); ammonia (NH_3); hydrogen sulphide (H_2S); oxygen (O_2); nitric acid (HNO_3); hydrogen peroxide (H_2O_2); formaldehyde (HCHO); and
- in the particulate form: as sodium chloride (NaCl); sodium sulphate (Na_2SO_4); ammonium sulphates ($(NH_4)_2SO_4 \cdot NH_4HSO_4$); and ammonium chloride (NH_4Cl).

(Selected airborne pollutants that influence atmospheric corrosion are discussed in further detail in Sections 2.1.4.7 to 2.1.4.13).

Following the deposition of the air pollutants on the surface or in the thin electrolyte layer, several chemical and electrochemical reactions may occur, e.g. SO_2 may be transformed into sulphuric acid (H_2SO_4) and NO_2 into nitric acid (HNO_3) (McEwan 2004; Leygraf et al. 2016). Due to the daily drying and wetting of these surfaces, the concentration and pH of the electrolyte layer also fluctuates (Leygraf et al. 2016).

The deposition rates of the gases, aerosols, and particulate matter on surfaces furthermore influence atmospheric corrosion processes. In this regard, the primary

mechanisms for outdoor aerosols and particle deposition are given by Cottis et al. (2010) as:

i. gravitational settling;
ii. turbulence diffusion; and
iii. momentum-dominated impact.

Cottis et al. (2010) state the efficiency of deposition largely depends on the size of the aerosol or particle. For example, for particles with a diameter of ~1 µm, the primary deposition mechanism is turbulent diffusion, while for larger particles with a diameter of ~5 µm, the momentum-dominated impact method prevails. In the case of ~20 µm diameter particles, the primary mode of deposition is gravitational settling.

Different approaches (Haynie 1988; Spence et al. 1992; Klassen & Roberge 2000; Cole et al. 2007) have been followed to predict the deposition rate of gases, aerosols and particles in the atmosphere, particularly in coastal regions. Cole & Paterson (2004b) reported that the deposition efficiency of aerosols increases significantly for aerosol greater than 20 µm, while the object shape is also of importance. For example, on an exposed plate placed at approximately 45°, more salts are deposited than on a salt candle. The deposition also varies across the surfaces of a structure and tends to be higher along the edges due to higher turbulence in these areas. Moreover, the roughness of the surface may increase the deposition of aerosols by about 25% (e.g. in forest areas).

The aerosol residence is controlled by convection, gravity and aerosol scavenging by cloud drops, raindrops and physical objects, such as trees and buildings (Cole et al. 2003a). Cole et al. (2003a) further report that in dry environments, exhibiting reduced rainfall and low ground coverage, marine aerosol transport is likely to be favoured than in more humid and higher rainfall climates, with forest cover.

2.1.3.5 Salt production in marine environments

The production of airborne salts along coastlines is mainly influenced by surf action and white-caps in the ocean (Cole et al. 2003a). Cole et al. (2003a) further state that white-caps of ocean waves vary with latitude, seasons, tides, ocean currents, etc. and that

tropical seas produce fewer marine aerosols, with lower marine corrosion near equatorial regions.

2.1.3.6 Dissolution of the metal and formation of the corrosion product

Leygraf et al. (2016) reported that the dissolution of the metal is initially encouraged by the dissolved ions in the electrolyte, by a proton-and-ligand-induced process, which also weakens the bonds between the metal atoms and their neighbours. However, the dissolution process may similarly be stimulated by ultraviolet (UV) light exposure, e.g. copper in H_2S polluted environments. It is further said that following pairing of the metal ions with preferred counterions in the electrolyte, e.g. silver (Ag^{+}) with sulphur (S^{2-}) rather than with sulphate (SO_4^{2-}), to a level of supersaturation, the ion pairs precipitate via a complicated nucleation process into the solid state (Leygraf et al. 2016).

Moreover, with more extended exposure, the number and size of the precipitated nuclei increases, until the complete metal surface is covered. Further growth depends on the thickness and protective qualities of the corrosion product layer, as well as its hindering of the movement of the corrosive ions to the metal substrate (Leygraf et al. 2016).

2.1.4 Environmental and Air quality Parameters that Influence Atmospheric Corrosion

A range of factors affects the initial and subsequent rates of atmospheric corrosion of metals and their alloys (Montgomery et al. 2011). These causes can be divided into several categories, namely weathering, pollution, biological, mechanical, incompatibility and usage effects (Brown & Masters 1982), including the angle of metal exposure (Dean et al. 2005; Vera & Ossandon 2014), elevations above sea and ground level, as well as shielding effects (Janse van Rensburg 2010; Cole et al. 2003c, 2013).

It is important to acknowledge that these factors do not always have a negative impact on atmospheric corrosion. Some, for example, rain, may not only result in wetting of the surfaces or the solubilising of corrosion products but may also wash away pollutants that can otherwise accelerate the corrosion process (McEwan 2004; Vera & Ossandon 2014).

2.1.4.1 Precipitation, RH and acid rain

Precipitation may occur in the form of rain, hail, condensation, fog, frost, sleet and snow, as well due to high RH (McEwan 2004; Botkin & Keller 2010; Cottis et al. 2011; Roberge 2012; Leygraf et al. 2016). Consequently, metals exposed in environments exhibiting heavy and continuous rainfall, mist, and high RH - indicating prolonged TOW, tend to show higher atmospheric corrosion rates (Morcillo et al. 2015), compared to exposure to drier conditions. In this context, the higher rainfall areas in South Africa (**Figure 2.4**) (My Cyberwall 2017) are expected to exhibit increased corrosivity compared to the drier regions.

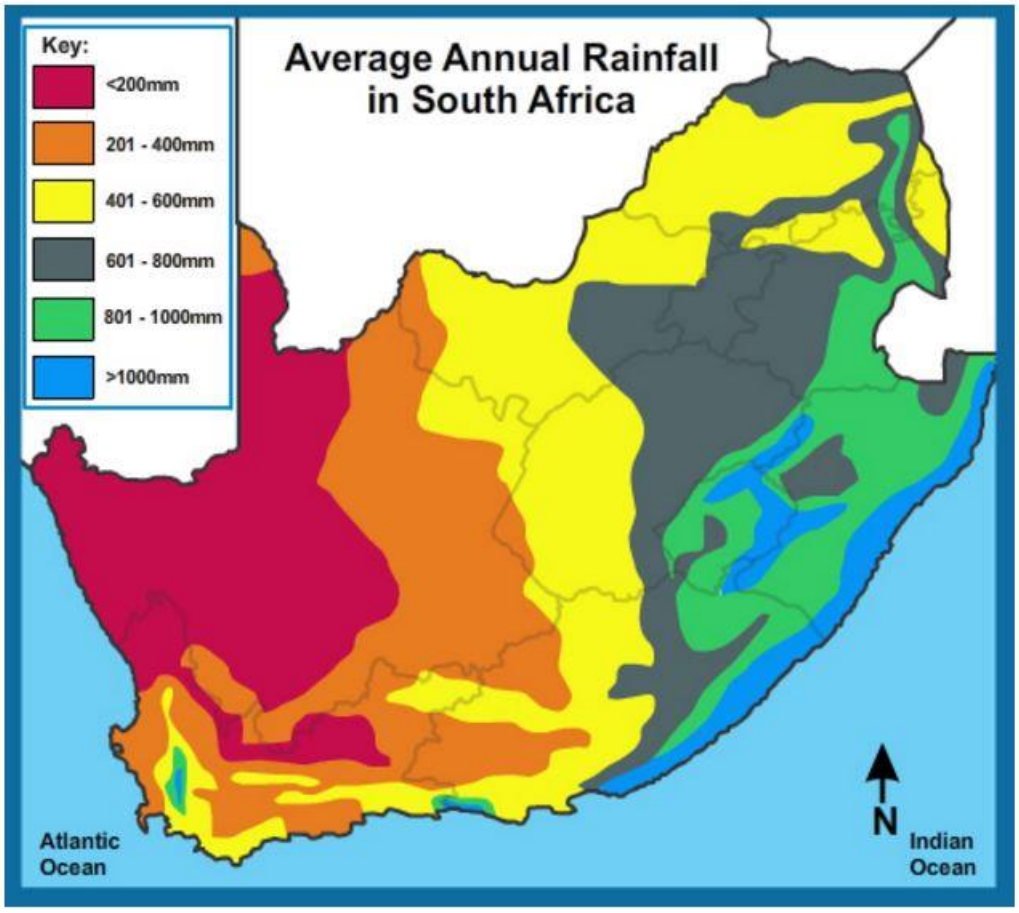


Figure 2.4 Average rainfall map for South Africa (My Cyberwall 2017), showing that the higher rainfall areas are mostly located in the eastern parts of the country, where potentially higher corrosion rates may be expected.

https://www.mycyberwall.co.za/get-smart/geography/grade-5/rainfall

According to Vargel (2004), at ambient temperatures, air is considered:

- dry, when RH < 30%;
- normal, when 50% < RH < 60%;
- humid, when RH > 80%; and
- saturated, when RH – 100%.

Consequently, in desert and semi-desert areas, RH rarely exceeds 10-20%, while it ranges between 40% and 60% in temperate climates and may reach 90-95% in tropical zones. TOW not only varies from one locality to another, but also by month and year. The type, size and orientation of the metal surface exposed to a corrosive atmosphere also determine TOW (Dean et al. 2005).

As aforementioned, the pH of the thin film electrolyte is influenced by atmospheric pollutants that are taken up by the moisture in the air, via the metal surface, or participate in the corrosion process. Botkin & Keller (2010) affirm that the pH of pure rainfall is typically 5.6 and that of uncontaminated distilled water, 7. The slight acidity of normal rainwater may be attributed to the build-up of naturally occurring sulphur oxides (SO_x), nitrogen oxides (NO_x) and because carbon dioxide (CO_2) dissolves into it, forming a weak carbonic acid (Encyclopedia.Com 2008; US Environmental Protection Agency 2016).

Due to pollution, e.g. caused by the burning of fossil fuel (coal, natural gas and gasoline) and wood, elevated levels of SO_x and NO_x are emitted into the atmosphere. The US Environmental Protection Agency (2016) states that two-thirds of SO_x and one-fourth of NO_x in the atmosphere come from electric power generators. Further air pollution sources include vehicles, manufacturing, oil refineries and other industries. The emissions from these sources are converted by reactions with oxygen and water vapour to sulphuric and nitric acids in the atmosphere, which can be blown by the wind for long distances - in many directions from where the first emissions took place. This causes acid rain, which is the "*precipitation in which the pH is below 5.6*" (Botkin & Keller 2010). McEwan (2004) states that the acidity of rainwater can increase to a pH of 3, which is ten times more acidic than a pH of 4 (Botkin & Keller 2010) and 160 times more acidic than a pH of 5.6.

The deposition of acid rain often occurs close to and downwind of fossil fuel power plants, as well as near other areas where fossil fuel burning takes place, resulting in the emission of SO_x and NO_x. However, HCl emissions from coal-fired power stations also participate in the formation of acid rain (Botkin & Keller 2010).

Other pollutants that contribute to the acidity of rain are volatile organic compounds (VOC), which are carbon-hydrogen (C-H) containing compounds (Botkin & Keller 2010) that readily become vapours or gases (Encyclopedia.Com 2008). Sources of VOC include thinners, solvents and degreasing agents (Encyclopedia.Com 2008; Botkin & Keller 2010).

The primary variables affecting acid rain on an area include general air movement, climate, topography, geology and air transport systems around the Earth. Pollutants are converted into H_2SO_4 and HNO_3 by mixing with clouds of water vapour. Conversely, wind-blown alkaline (e.g. sodium-, potassium- and calcium-based) dust passing more freely through the air, may neutralise atmospheric acidity. This phenomenon is often seen in drier climates (Encyclopedia.Com 2008).

Acid rain is a significant cause of the corrosion of building materials, galvanised steel, paint, plastic, cement, masonry, marble and metal statues or other fabricated items (Botkin & Keller 2010), as well as of motor vehicles in industrial areas. Metals most affected by acid rain include bronze, copper, nickel, zinc, and certain types of steel. Consistent with Botkin and Keller (2010), classical buildings in Athens (Greece), are severely affected by acid rain, which has accelerated in the twentieth century due to air pollution.

The fact that regular rain does not necessarily have an adverse impact on the corrosion of metal surfaces is of note. Although rainfall may facilitate the corrosion process because of surface wetting, it also reduces the levels of contaminants on the metal surface due to its rinsing/washing effect (McEwan 2004). Montgomery et al. (2011) state that rain rinses away pollutants, while mist deposits more pollutants, and dew reactivates surface contaminants.

2.1.4.2 Temperature

Temperature is indeed a major influencing player when it comes to the varying meteorological conditions of regions (**Figure 2.5**) (South African Tours and Travel.com 2016). This is particularly true regarding the %RH in the atmosphere, dew point, the solubility of pollutants in wet films on metal surfaces, the drying time of surfaces, acceleration of electrochemical corrosion rates, and the formation effect of wind, etc.. Consequently, the north-western region of South Africa is typically classified as a desert to semi-desert environment, where low atmospheric corrosion rates may be anticipated.

Temperature can also directly or indirectly increase the pollution levels of the atmosphere, e.g. during winter when higher levels of SO_x, NO_x and CO_2 gases are forced into the air because of the burning of coal and other forms of fossil fuel for heating purposes (DEA 2017a).

Temperature primarily affects atmospheric corrosion processes in two ways (Dean & Reiser 2002; Roberge 2012). First, as a rule of thumb, the temperature can increase the corrosion rate of a metal surface two-fold, with every 10°C rise in temperature. Secondly, due to the temperature lag of materials, compared to ambient air (during night times, in particular), it may encourage condensation of moisture on metal surfaces (Dean & Reiser 2002; Roberge 2012). This occurs at the dewpoint, which is the temperature at which condensation and evaporation from a surface are in equilibrium (Roberge 2012).

One of the significant deficiencies of the ISO 9223 corrosivity of atmospheres classification model is that temperature is not included as a variable (International Organization for Standardization 2012a). It is only mentioned that the model applies to conditions where the ambient temperature of the environment is more than 0°C since, at temperatures below the freezing point of water, corrosion of iron, aluminium, copper and zinc is considered negligible (Uhlig 1963). Since corrosion is a chemical process, Dean and Reiser (2002) affirm that there must be a temperature effect. However, a problem regarding measuring ambient temperature is that the metal surfaces are often dry when the measurements are taken. Ideally, therefore, they recommend that dew point temperature should be measured.

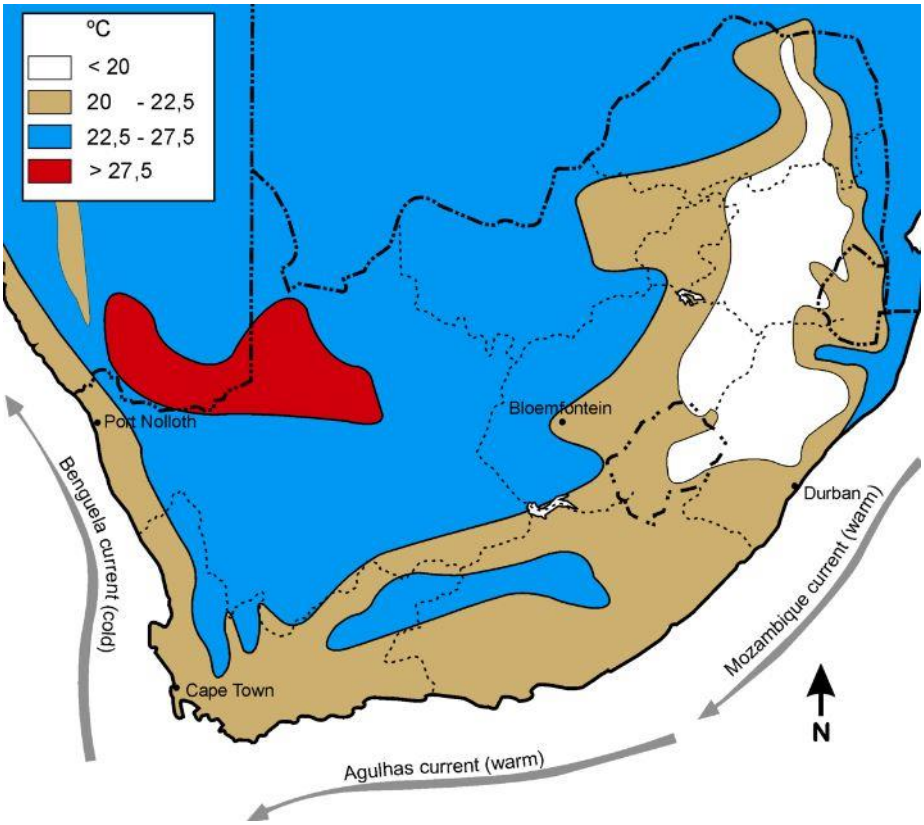


Figure 2.5 Average summer temperatures for South Africa (South African Tours and Travel.com 2016). http://www.south-africa-tours-and-travel.com/south-africa-climate.html

The temperature may also decrease the oxygen concentration on the metal surface and in turn, reduce the corrosion process (McEwan 2004; Vera & Ossandon 2014). Seasonality effects during summer and winter periods are likewise encountered.

Due to the increasing global threat of 'Climate Change', researchers such as Cole & Paterson (2006) and Li et al. (2013) believe that the increase in the mean annual temperature of the Earth, over periods of time (Botkin & Keller 2010), will ultimately impact on the atmospheric corrosion rates of materials.

2.1.4.3 Wind

Purnell's Dictionary of Science (Kerrod 1983) defines wind as "*air in motion*" and the result of pressure and temperature differences in the atmosphere (Brunt 1952). Wind is highly variable in duration, place, and intensity, for example, wind can increase in speed over hilltops or may be channelled through a mountain pass (Botkin & Keller 2010).

Considering atmospheric corrosion, wind direction and velocity (speed) play prominent roles (ASM International 2006). In the southern hemisphere, between the 30 to 60th parallels, the wind blows primarily from the north-west, which is called the prevailing westerlies (Kerrod 1983). Corrosive aerosols and particulates that are ejected into the atmosphere, e.g. sea spray and windblown dust are not only carried by the wind for long distances from their source, but the aerosols may also be directed towards specific areas or industrial installations.

Figure 2.6 (Maskew Miller Longman (Pty) Ltd 2013) shows the directions of the prevailing winds during summer and winter for South Africa. Evidently, during summertime, the South East Trade Wind may be a significant driving force of atmospheric corrosion along the South African coastline.

Roberge (2012) contends that high correlations exist between wind speed and the deposition and capture of aerosols. Consequently, since aerosol particles have a finite mass and are subject to gravity, studies relating to the inland migration of sea salts have shown that the large particles (> 10 µm diameter) are often deposited by the wind in the region of 400-600 m from the shoreline (Roberge 2012).

Cottis et al. (2010) suggest that the wind plays a significant role in the cleaning of surfaces, particularly in dry environments. This is because the wind may carry abrasive particles, either to or from surfaces. It can also drastically reduce the temperature rise of surfaces. Furthermore, wind can result in the loss of adhesion of corrosion products, exposing fresh metal to further corrosion (Vera & Ossandon 2014). High wind speeds may erode surfaces (Del Angel et al. 2015) and can encourage atmospheric corrosion at marine sites when industrial air pollutants are channelled towards an area (ASM International 2006).

Like rain, the wind may also be beneficial from an atmospheric corrosion reduction point of view, in the sense that surfaces that are exposed to wind dry out faster (Del Angel et al. 2015). Conversely, the evaporation of water, because of wind, increases the concentration of any salts that may be present on the surface.

MAP NOT PUBLICLY AVAILABLE

Figure 2.6 Prevailing summer and winter wind systems for South Africa (Maskew Miller Longman (Pty) Ltd 2013). https://za.pearson.com/

2.1.4.4 Sunlight

Like temperature, the impact of sunlight on atmospheric corrosion processes may be viewed as having a three-way effect. Firstly, solar heating may increase surface temperature and thus increase evaporation rates or reduced TOW. This interaction between sunlight radiation, increased surface temperature and reduced evaporation rates is depicted in **Figure 2.7** (Evwind 2017), which shows that typically, the high sunlight irradiation levels in the north-western parts of South Africa result in dry, elevated temperature desert-like environments.

However, sunlight also affects the performance of organic materials and can lead to the embrittlement and cracking of polymeric products (ASM International 2006). Cole & Paterson (2006) mention that on a bright day, with a wind speed of 5 m/s and air moisture level of 75% RH, a 200 µm film of moisture evaporates within an hour after sunrise. Conversely, on a cloudy, windless day, the same layer of moisture does not disappear after 4 hours of daytime. Due to the rise in surface temperature, sunlight may theoretically also increase the corrosion rate.

Sunlight may also promote photochemical changes of naturally occurring atmospheric compounds or pollutants, or of the material surfaces themselves. For example, ozone (O_3) may be produced by the photolysis of NO_2 and SO_2 by the photolysis of carbonyl sulphide (OCS) (Cottis et al. 2010), while sunlight may degrade organic coated surfaces to such an extent that corrosion processes of the steel substrate may be initiated. In this regard, paint exposure studies, conducted over many years along the South African coastline (Janse van Rensburg 2000), have shown that concerning specific types of epoxy coatings, 5-30% of the film thickness may be lost per annum when exposed to sunlight. This is because of varying photo-oxidative, photolytic, and thermo-oxidative changes, resulting in the breakage of the polymer chains - producing free radicals, reducing the molecular weight, as well as causing degradation of the mechanical properties (Yousif & Haddad 2013).

Factors that affect the impact of solar radiation and heating of material surfaces include cloud formation, overhangs of natural landscapes, human-made constructions, trees (Botkin & Keller 2010) and air pollution. For example, smog, which is a noncombustible by-product of fossil fuel, can be photolysed by sunlight to form O_3 (Druzik 1985).

Concerning the degradation of organic materials, Hare (1992) states that the impact of UV light radiation increases directly with a rise in the intensity of radiation. The latter depends on factors such as distance from the equator, orientation in a northerly or southerly direction (depending on the relevant hemisphere), the hours of sunlight exposure, shielding effects by nearby infrastructure, vegetation and even landscapes, as well as the generic type and formulation of the coating.

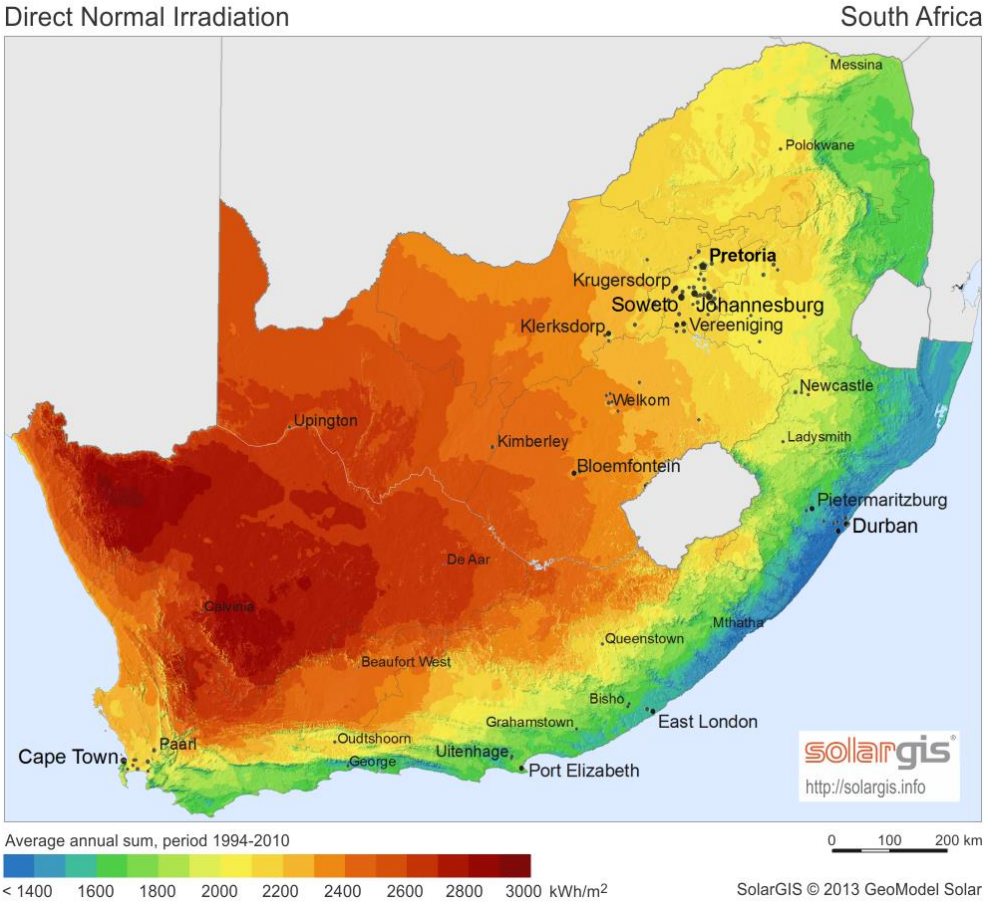


Figure 2.7 Average yearly solar irradiation levels for South Africa (Evwind 2017). https://www.evwind.es/2017/02/06/enel-brings-two-new-south-african-pv-plants/58722

Photochemical breakdown of materials occurs in open atmospheres, with or without the presence of any pollutants, and is mainly due to exposure to sunlight and other controlling factors such as air, temperature, and water (Janse van Rensburg & Calitz 2004; Mark 2007; Stoye & Freitag 2008). Stoye & Freitag (2008) observed that the ageing or weathering of coatings is the sum of all irreversible chemical and physical processes. Solar radiation also results in the heating of surfaces, which is influenced by the colour of the item (Stoye & Freitag 2008).

2.1.4.5 Topographical effects

Land contours, e.g. mountains and valleys have a significant impact on the transport and deposition rates of airborne salts and other pollutants. They may also influence wind speed and wind direction, as well as result in the shielding of areas of interest, consequently reducing atmospheric corrosion (Roberge 2011). From a South Africa

context, **Figure 2.8** (Maskew Miller Longman (Pty) Ltd 2013) indicates a reduced relief all along the shoreline, which allows salts to be carried further inland than in more mountainous terrains.

Likewise, the height of exposed metal surfaces above ground and sea levels may have an impact on atmospheric corrosion rates. Hernandez et al. (2011) and Janse van Rensburg (2010) found that altitude and height above ground and sea level play essential roles in the atmospheric corrosion levels of marine environments. Consequently, an area that is located on a cliff or top of a tower or steel structure may show reduced corrosivity when compared to a zone situated at the same distance from the ocean, but at a lower altitude. Del Angel et al. (2015) also investigated this occurrence in Chile and Mexico. However, the higher positioning of a structure above ground level may also expose it to a more open atmosphere, thus potentially increasing the corrosion rate. Moreover, the exposure of metal surfaces above or near natural water bodies encourages atmospheric corrosion. This is primarily due to an increase in RH of the surrounding environment.

MAP NOT PUBLICLY AVAILABLE

Figure 2.8 A physical map of South Africa (Maskew Miller Longman (Pty) Ltd 2013) https://za.pearson.com/

2.1.4.6 Biomes and animal interaction

The availability of water determines the size of plants existing in a region (Botkin & Keller 2010). In tropical areas, tall leafy trees may act as windshields or pollution accumulators (Nowak 2002) and limit the dispersion of ground-level airborne pollutants. Trees may also result in the prolonged drying out of surfaces (increased TOW in other words).

As rainfall lessens, the size of the plants decreases to small trees, then to scrubs and grasses, and then to scattered plants (Botkin & Keller 2010). This change is depicted in **Figure 2.9** (OpenStax CNX 2017), which shows the most recent classification of the biomes in South Africa. As plant growth decreases towards the western parts of South Africa, the extent of shielding offered by the plants also lessens. Consequently, the atmospheric corrosion of metal surfaces located along arid coastlines may sometimes be more pronounced than those positioned along tropical or Mediterranean seashores. This appears to be particularly true in the South African and Namibian context (Barnett 2006). Refer also to Section 5.1.

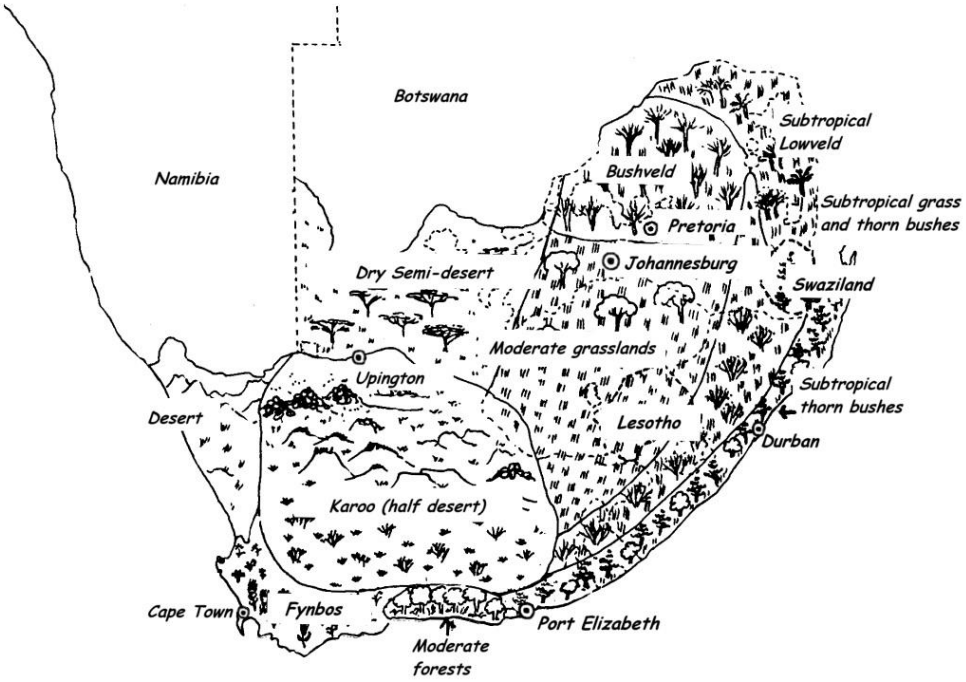


Figure 2.9 The different terrestrial biomes of South Africa (OpenStax CNX 2017).
http://archive.cnx.org/contents/669116d7-d148-4af9-905d-4dcdf17cde56@1#graphics1.png

Bird droppings, specifically in excessive amounts, may additionally affect general atmospheric corrosion processes. Huang & Lavenburg (2011) claim that bird droppings from pigeons in urban areas have been found to contain silicon (Si), carbon (C), nitrogen (N), calcium (Ca), potassium (K), oxygen (O), phosphorous (P), chlorine (Cl), sulphur (S) and even fluorine (F). Of these elements, N, P, Cl, S, and F readily participate in atmospheric corrosion processes, particularly the halides, which are considered aggressive corrosive species (Hernandez et al. 2011).

Animal and human waste, such as horse and cattle manure, contains NH_3, which increases the atmospheric corrosivity of nearby environments (Roberge 2012). The atmosphere near sewage farms will therefore often be more corrosive than in areas located further away from the plants. King et al. (1982) also identified this phenomenon in Melbourne (Australia), where an increase in atmospheric corrosion was found near sewage farms.

2.1.4.7 Oxygen

Oxygen is a primary driver of the atmospheric corrosion process (McEwan 2004; Leygraf et al. 2016). It is readily taken up by moisture on metal surfaces, therefore stimulating any oxidation reaction (Syed 2006; Leygraf et al. 2016). In the absence of oxygen, corrosion processes are reduced. However, this is not particularly relevant in the case of open atmospheres, where oxygen makes up one-fifth of the air (Kerrod 1983) and is thus freely available to participate in atmospheric corrosion processes.

In the upper atmosphere (stratosphere), an allotrope of oxygen occurs, namely, O_3 (Kerrod 1983), which may influence corrosion processes even further (see Section 2.1.4.11 in this regard).

2.1.4.8 Chlorides

Chloride deposition on metal surfaces is known as a critical factor of many atmospheric corrosion processes. This applies in particular to metal components located close to the sea. Alcántara et al. (2015) found a clear correlation in wave height, marine wind (direction and speed), and the deposition of chloride (Cl^-) in marine atmospheres. In these environments, pitting corrosion of zinc, aluminium and stainless steels are of notable importance (McEwan 2004). This is because the marine salts dissolve in the

thin electrolyte film, raising its conductivity and destroying passive films (Alcántara et al. 2015).

Studies (Allam et al. 1991; Montgomery et al. 2011; Morcillo et al. 2011) have indicated that although chlorides are incorporated into the first corrosion products, they are not necessarily retained in the long-term. The reason for this is that the concentration of ferrous and ferric chloride in the corrosion product decreases, unless a new supply of chlorides to the anodic areas is sustained (Montgomery et al. 2011; Morcillo et al. 2011). The thick layer of the corrosion product that forms also reduces the exposure of the substrate to chlorides over time (Allam, Arlow & Saricimen 1991; Montgomery et al. 2011). Consequently, the corrosion rate of metals is often reduced with an increase in exposure time.

Moreover, the type of chloride affects the corrosion rate of metals. Montgomery et al. (2011), Roberge (2012) and Leygraf et al. (2016) mention that due to the hygroscopic nature of $MgCl_2$ in sea salt or mist, atmospheric corrosion is enabled to take place at a lower RH (at 33-34% RH) than in the solitary presence of NaCl (at 75-77% RH). It is further stated that the original corrosion products formed between the metal substrate and the environment affect the long-term corrosion of the metal.

2.1.4.9 Sulphur-containing compounds

The primary sulphur-containing compounds in the atmosphere are SO_2, H_2S, dimethyl sulphide (DMS or CH_3SCH_3), carbon disulphide (CS_2) and OCS (Cottis et al. 2010). SO_2, a precursor to acid rain (Botkin & Keller 2010; Roberge 2012), is moderately soluble in water (Leygraf et al. 2016). It is also a gas made by the burning of sulphur-containing sources or fossil fuels (Botkin & Keller 2010; Roberge 2012; Leygraf et al. 2016) that plays a significant role in atmospheric corrosion in urban and industrial atmospheres (McEwan 2004; Syed 2006; Roberge 2012; Leygraf et al. 2016).

SO_2 is also adsorbed on metal surfaces, exhibits high solubility in water, about 2 600 times more than oxygen (Li et al. 2013) and tends to form H_2SO_4 in the presence of surface moisture films (Kerrod 1983; McEwan 2004; Botkin & Keller 2010; Leygraf et al. 2016). Moreover, it exhibits high bleaching and sterilising effects (Kerrod 1983). In urban

atmospheres, SO_2 concentrations are said to vary significantly and can exceed the levels of any other atmospheric gas, except CO_2 (Leygraf et al. 2016).

Natural sources of SO_2 include ocean spray, volcanic emissions, sub-terrains (Kerrod 1983) and H_2S, which is emitted from the decay of organic matter (Encyclopedia.Com 2008; US Environmental Protection Agency 2016). The formation of H_2SO_4 in the atmosphere, which lowers the pH of rain and aerosols (Leygraf et al. 2016), takes place using the following chemical reactions (Virtual Chembook 2003):

$SO_2 + H_2O \longrightarrow H_2SO_3$ (sulphur dioxide and water forming sulphurous acid) **Eq. 2.7**

and

$SO_3 + H_2O \longrightarrow H_2SO_4$ (sulphur trioxide and water forming sulphuric acid) **Eq. 2.8**

H_2SO_4 acid is highly corrosive and gives rise to a series of salts, known as sulphates (Kerrod 1983). Other sulphur-containing compounds participating in atmospheric corrosion processes include various sulphates (SO_4^{2-}), sulphides (S^-) and sulphonic acids (which are strong organic acids of general formula RSO_2OH, e.g. benzene sulphonic acid, oxides) (Kerrod 1983).

The principal sources of H_2S are wetlands, plants, soils, volcanos, and sewage farms, whereas DMS is produced in waste and sea waters by microorganisms (Jeon et al. 2009; Cottis et al. 2010). When oxidised, it is a source of methane sulphonic acid and SO_2. The former chemical compound is also a primary source of "*sulphate cloud condensation nuclei (CCN)*", and consequently, a direct contributor to acid rain (Cottis et al. 2010).

Vargel (2004) gives the SO_2 concentrations of typical atmospheres as:

- rural: 0-0.1 mg/m^3;
- urban: 0.1-0.3 mg/m^3; and
- industrial: > 0.3 mg/m^3.

2.1.4.10 Nitrogen-containing compounds

Nitrogen (N_2) makes up 78% by volume of air and can form several oxides (NO_x), e.g. nitric oxide (NO), NO_2, dinitrogen tetroxide (N_2O_4) and nitrous oxide (N_2O) (Kerrod 1983; Botkin & Keller 2010; Cottis et al. 2010). Nitrogen oxides ($NO + NO_2$) (Cottis et al. 2010) are the primary cause of smog in urban areas (Roberge 2012), of which the reddish colour may be attributed to NO_2 (Kerrod 1983). Moreover, it is a significant precursor of HNO_3 (Arroyave et al. 2002; Botkin & Keller 2010), which is extremely soluble in water (Leygraf et al. 2016).

Syed (2006), Botkin & Keller (2010) and Leygraf et al. (2016) state that most of the nitrogen oxides are produced as NO during combustion processes, which is oxidised to NO_2 using the following reaction:

$$2NO + O_2 \longrightarrow 2NO_2 \qquad \textbf{Eq. 2.9}$$

When moving further from the source, it is additionally oxidised by O_3, as indicated by **Equation 2.10**:

$$NO + O_3 \longrightarrow NO_2 + O_2 \qquad \textbf{Eq. 2.10}$$

The main industrial sources of NO_x include electric power generators, vehicles, manufacturing plants, oil refineries, and other industries (US Environmental Protection Agency 2016). As in the case of SO_2, NO_x is also a product of fuel combustion (Cottis et al. 2010), particularly in and around urban areas, where it is an exhaust fume from vehicles (Arroyave et al. 2002; Roberge 2012).

Roberge (2012) mentions that 50% of the haze or smog in modern cities may be ascribed to a combination of sulphuric and nitric acids. Nitric acid (HNO_3) is a potent oxidising agent and the "*parent*" of nitrates (Kerrod 1983), which are the salts and esters of nitric acid (Encyclopaedia Brittanica 2018d). Cottis et al. (2010) indicate that NO_x decreases significantly with increasing distance from urban sources.

NO_x also occurs naturally in the atmosphere, although, the primary sources are micro-organisms in soils and electric discharge (lightning) storms. Reportedly, 33% of the sulphur and nitrogen discharges in the United States comes from these environmental

sources (Encyclopedia.Com 2008). **Figure 2.9** presents Kerrod's (1983) illustration of the natural processes by which nitrogen from the air is 'fixed' or removed from the atmosphere, and ultimately returned there.

NH_3 is also a primary gas in the atmosphere and originates naturally from the ocean (Leygraf et al. 2016), animal waste and soil emissions (Cottis et al. 2010). Other sources of NH_3 include fertilisers, cropland emissions, chemical processing plants and sewage farms (Cottis et al. 2010; Leygraf et al. 2016), with the single most significant source being high animal population (Leygraf et al. 2016). Since NH_3 exhibits high solubility (Leygraf et al. 2016) and is quickly absorbed by surfaces, including by water droplets, its residence time is short (Cottis et al. 2010). NH_3 may react with HCl and HNO_3 directly to form ammonia salts, and is also a major aerosol component (Cottis et al. 2010). In SO_2-polluted environments, it can also react with oxidised SO_2 to form $(NH_4)_2SO_4$ (Leygraf et al. 2016). Since NH_3 is a base, it is furthermore seen as a counterbalance for several gases that are acidic (Leygraf et al. 2016).

DIAGRAM NOT PUBLICLY AVAILABLE

Figure 2.10 The natural circulation of nitrogen – adapted from Kerrod (1983).

https://www.amazon.co.uk/Purnells-Concise-Dictionary-Science-Kerrod/dp/0361053460

2.1.4.11 Organic acids

Even in small concentrations, organic acids in the atmosphere, such as formic acid (HCOOH) and acetic acid (CH_3COOH) influence the atmospheric corrosion levels (Syed 2006) of several metals (Leygraf et al. 2016). These pollutants originate from industrial, biogenic, and volcanic processes, although the most common source is due

to the incomplete combustion of wood and other vegetation (Cottis et al. 2010; Leygraf et al. 2016), as well as the reactions of photochemical smog (Leygraf et al. 2016). Organic acid concentrations in urban areas are typically in the 1-10 ppbv (parts per billion based on volume) range, which in the presence of moisture, may result in metal corrosion (Leygraf et al. 2016).

Tétreault et al. (2013) found that organic acid vapours, e.g. HCOOH may influence the corrosion of copper. Reportedly, levels of HCOOH more than 0.4 ppmv (parts per million based on volume) affect the appearance of copper at 75% RH, and at levels higher than 4 ppmv, the weight of copper increases at both 54% and 75% RH, due to oxidation. Acetic acid vapours found in industrial atmospheres may also originate from food processing plants or paper industries, from the decomposition of raw materials (Syed 2006).

2.1.4.12 Ozone, strong oxidants, and hydrogen peroxide

Even though the stratosphere holds most of the Earth's ozone, it can be carried into the troposphere by so-called "*tropopause folding events*" (Cottis et al. 2010). O_3 is a gaseous chemically-reactive air pollutant (Whitmore et al. 1987), as well as a powerful oxidant that may also be produced by complex reactions between pollutants emitted by consumer products, vehicles, factories, evaporation of paints and industrial plants (California Environmental Protection Agency 2015). This can also result from the burning of fuels, in particular via NO_x emissions. It is a significant component of smog, and its action may be comparable to bleach (California Environmental Protection Agency 2015).

During daytime, NO_2 may be photolysed by sunlight to form NO and atomic oxygen O, followed by the rapid reaction of atomic oxygen with molecular oxygen to form O_3 (Druzik 1985). The reactions are as follows (Cottis et al. 2010; Leygraf et al. 2016):

$$NO_2 \xrightarrow{\text{Visible and ultraviolet light}} NO + O \qquad \textbf{Eq. 2.11}$$

and

$$O + O_2 \longrightarrow O_3 \qquad \textbf{Eq. 2.12}$$

O_3 may also react with NO at night. Consequently, strong daily fluctuations in the levels of O_3 in the atmosphere exist. Base levels of O_3 are given as approximately 20-25 ppb, which may rise to 200-400 ppb near NO_x emitting sources (Cottis et al. 2010).

Druzik (1985) mentions that O_3 has been found to fade dyes (in paper and textiles) and colour pigments in paints, as well as reduce the service life of natural rubber. It is furthermore reported to be involved in corrosion processes (Leygraf et al. 2016) and in polymers, O_3 may result in the breaking of chains and cross-links (Druzik 1985). In metals, though, Graedel et al. (1984) have found that the corrosive attack of H_2S can be significantly increased by solar radiation and atmospheric O_3. This indicates that in urban areas, the increased levels of corrosion are due to a "*complex sequence of multicomponent photochemical processes*" (Druzik 1985).

O_3 also enhances oxidation of silver and iron, whereas damp or wet aluminium reacts with O_3 - causing corrosion (Druzik 1985). Moreover, the production of H_2O_2 is closely linked to photochemical activity and forms from radical-radical reactions, as indicated by **Equation 2.13** (Cottis et al. 2010).

$$HO_2 + HO_2 \longrightarrow H_2O_2 + O_2 \qquad \textbf{Eq. 2.13}$$

These radicals usually form because of the oxidation of hydrocarbons. However, in high NO_x polluted environments, the radicals may react with NO, resulting in a decrease of the H_2O_2 levels. H_2O_2 is the main oxidant found in clouds, fog, and rain. Other oxidants include OH^- and HO_2 (Cottis et al. 2010).

2.1.4.13 Carbon dioxide (CO_2)

CO_2 is a primary constituent of the atmosphere (Botkin & Keller 2010) and emitted because of natural cycles in vegetation and the ocean (Leygraf et al. 2016). However, it is also released into the air by anthropogenic activities, via the combustion of fossil fuels (Botkin & Keller 2010; Leygraf et al. 2016).

The formation of carbonic acids that may lead to the accelerated corrosion of metal surfaces, due to CO_2 pollution in urban environments, has been established (Guttman 1982). Regarding zinc metal surfaces, though, the formation of zinc carbonates is necessary to ensure the long-term protection of the surfaces. McEwan (2004) states

that in the absence of CO_2 under humid conditions, the corrosion of zinc coatings may be rapidly increased. This is due to the formation of zinc oxides and hydroxides - also commonly referred to as 'white rust'. Consequently, the zinc carbonate layers must be maintained.

Guttman (1982) suggests that CO_2 may decrease the effect of SO_2 pollution on metal surfaces, e.g. on steel and copper, which is probably due to the nature of the corrosion products that are formed. Conversely, high CO_2 levels may cause carbonisation of concrete, resulting in a decrease in its alkalinity and therefore, a potential increase in the corrosion of any reinforcement steel that may be embedded in the concrete (McEwan 2004). This problem is especially noticeable in the buildings of the University of Johannesburg, where the relevant authorities have been battling with reinforcement corrosion for many years.

2.1.4.14 Time, initial period, and angle of exposure

It is known that for most materials, atmospheric corrosion rates decrease with an increase in time, which is associated with the formation of protective corrosion product layers (Callaghan 1991; ASM International 2006; Janse van Rensburg 2010; Leygraf et al. 2016). However, where the corrosion rate is sufficiently high, thus preventing the formation of a proper protective layer(s) (ASM International 2006), high corrosion rates may be maintained, resulting in extremely high levels of metal loss, e.g. carbon steel in CX corrosive environments (Janse van Rensburg 2010; International Organization for Standardization 2012a).

However, the initial corrosion rates and period of exposure may have a significant impact on the variation of corrosion rates (ASM International 2006; Li et al. 2013). Montgomery et al. (2011) report that studies have shown that several site-specific factors often influence the initial and later atmospheric corrosion of metals, e.g. time of the year of first exposure, massive storms, and exposure to increased pollution levels.

The angle and direction of exposure are also of importance (Vera et al. 2003). Horizontal surfaces are more affected by corrosion than vertical surfaces. This is due to increased TOW of flat or small-angled surfaces, following periods of water precipitation. The direction of the exposure may furthermore determine whether the metal will be more

affected by salts or pollutants in the atmosphere. For example, seaward-facing surfaces are commonly more affected by corrosion than those facing in the opposite direction (Callaghan 1991; McEwan 2004).

2.1.5 Atmospheric Corrosion of Carbon Steel, Hot-Dip Galvanised Steel, Aluminium, Zinc and Copper

2.1.5.1 Carbon steels, irons (Fe) and alloy steels

Carbon steel (hot or cold rolled) and irons (Fe), e.g. cast and ingot, are used extensively in the construction and manufacturing industries. Accordingly, the mechanisms associated with the atmospheric corrosion of these materials have been widely studied. Carbon steels are known for their typical reddish-brown corrosion product, known as 'rust' when oxidised in moist environments (Fontana 1987). Rust comprises a variety of oxides, hydrated oxides, oxyhydroxides and different crystalline and amorphous substances of iron (Morcillo et al. 2011; Leygraf et al. 2016).

Freudenberger et al. (2009), Alcántara et al. (2015) and Leygraf et al. (2016) state that lepidocrocite (γ-FeOOH) is the first crystalline product that forms, which is transformed into various other iron minerals, e.g. goethite (α-FeOOH), of which the volume may be six to eight times greater than the actual metal loss (Freudenberger et al. 2009). A comprehensive study has also been made by Stratmann (1990) about the effect of cyclic (dry-wet-dry) exposure conditions on the formation of the rust layer, which tended to favour the creation of the less soluble compounds (Leygraf et al. 2016).

In SO_2 polluted environments, iron sulphate ($FeSO_4$) is known to form at the metal surface. However, it is hydrolysed to FeOOH, with SO_4^{2-} being liberated by the reaction (Barton 1976; Fyfe 1994; Graedel 1996; Syed 2006). This leads to a reduction in the pH of the electrolyte, which may increase the corrosion rate. However, it is likely that this effect is of less importance due to the protecting qualities of the hydroxide and oxide corrosion products that form (Syed 2006). In H_2S-rich environments, while FeS may form initially, it is also unstable and readily removed from the steel surface in a low pH environment, forming again H_2S, which enhances the corrosion process further (Salas et al. 2012). Conversely, in a wet CO_2-rich environment, iron carbonate scale may develop, which can be protective or non-protective (Corrosion Source 2018). The

corrosion rate of the steel is initially high due to exposure to the carbonic acid but then decreases with the formation of the iron carbonate scale layers. In high CO polluted environments, carbonyl may slowly form, but also tends to be unstable in low pH conditions (Heusler & Cartledge 1961).

Conversely, in marine atmospheres, high proportions of β-FeOOH (akageneite) are found in the corrosion products of steel (Kamimura et al. 2002; De la Fuente et al. 2011; Morcillo et al. 2011), which notably accelerate corrosion processes (Morcillo et al. 2015). Apart from akageneite, Alcántara et al. (2015) also reported high magnetite (Fe_3O_4) contents in the corrosion product of mild steel exposed to a marine atmosphere.

According to the ISOCORRAG Programme (Knotkova et al. 2010), for which the main aim was to provide actual corrosion data based on the ISO 9223 to ISO 9226 procedures, the first-year corrosion rates of unalloyed flat carbon steel coupons (Cu 0.03-0.10%, P < 0.07%) worldwide, at 54 sites and in 14 countries, ranged from 0.8 μm/a to 373.0 μm/a (micrometres/annum). During this study, the lowest value was recorded at Oymyakon, which is a rural area (a selo) in the Sakha Republic of Russia (Rohli 2017) and interestingly, outside of Antarctica, one of the coldest settled locales of the world (Encyclopaedia Britannica 2008b). On the contrary, the highest corrosion rate of carbon steel was measured at Fort Sherman, a coastal site, which is located at Toro Point in Panama (Leonard 2015), near the Pacifica entrance to the Panama Canal (Encyclopaedia Britannica 2008c). This site is classified as a tropical marine environment (Knotkova et al. 2010).

At most of the sites, the corrosion rate of carbon steel decreased due to the protective nature of the corrosion products formed on the metal surfaces (Knotkova et al. 2010). This trend was also affirmed during studies conducted by Janse van Rensburg (2010) at more than 50 sites in South Africa, over a period of three years. See also **Figure 2.11** (Mokgatlhe & Janse van Rensburg 2012).

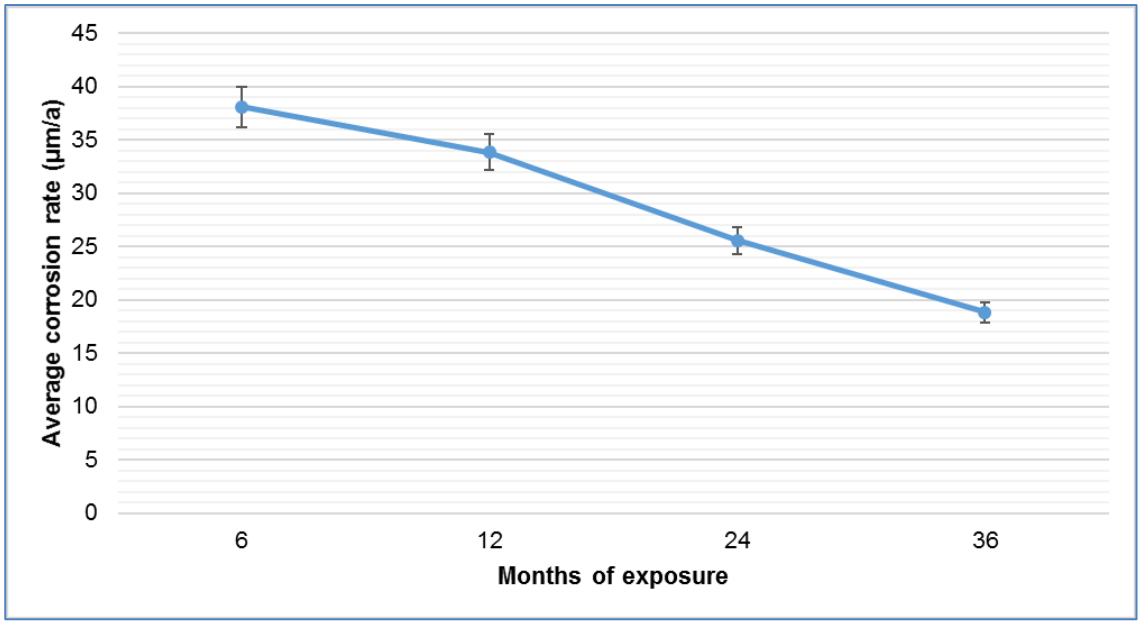


Figure 2.11 Changes in the atmospheric corrosion rate of carbon steel following different exposure periods at Elandsfontein (a rural environment in Mpumalanga, South Africa) – Adapted from Mokgatlhe & Janse van Rensburg (2012).

Li et al. (2013) reported that the corrosion rates of mild steel in different atmospheric environments could generally be summarised as follows:

- Rural: 4-65 µm/a;
- Urban: 23-71 µm/a;
- Industrial: 26-175 µm/a; and
- Marine: 26-104 µm/a.

In many cases, the carbon contents of steel, cast irons and "*commercially pure*" irons, such as ingot iron and Armco iron, have a negligible effect on the general corrosion resistance of these steels (Fontana 1987). In the case of low-alloy steels, however, the carbon is alloyed with chromium, nickel, copper, molybdenum, phosphorous, and vanadium, which add to the corrosion resistance of these materials. Lloyd (n.d.) reports that weathering or slow-rusting steels, containing 0.2-0.3% copper and slight additions of other elements, corrode at roughly one third to one quarter the rate of plain steels.

Since 1920, stainless steels have been developed for their resistance to corrosion (Leygraf et al. 2016). Chromium is the primary alloying element, of which the steel must contain at least 11 wt% (Fontana 1987), which provides a stable abundantly-rich

chromium passive layer of only a few nanolayers that tends to improve with time (Leygraf et al. 2016). However, when atmospheric corrosion occurs, it is inclined to be localised in pits, which at first form next to inhomogeneities like crevices and inclusions/flaws in the passive layer (McEwan 2004; Leygraf et al. 2016; Mohammed-Ali 2016). However, if not re-passivated, these pits propagate further (Leygraf et al. 2016).

Due to the long-term corrosion resistance properties of stainless steels, their corrosion rates, pitting depths, pit propagation, microstructure, composition, nobility, differences in grain size, and corrosion product staining or coverage, have been studied extensively (Wallinder et al. 2003; Leygraf et al. 2016), as well as in many different environments. For example, Davenport et al. (2014) reported that the morphology of the corrosion pits of stainless steel is affected by the presence of residual ferrite, and that dense covers may affect pit stability. Similarly, Mohammed-Ali (2016) from Davenport's group identified critical factors of the pitting corrosion of Types 304L and 316L stainless steels in $MgCl_2$ droplets as being the influence of residual ferrite on pit morphology, the critical chloride density below which pits do not propagate, and the CRH above which pits cannot form. Street et al. (2015), on the other hand, showed that the pitting corrosion was strongly RH dependant and that at high CDD, satellite pits formed around the perimeter of broad, shallow dish regions.

Leygraf et al. (2016) reported atmospheric mass losses for Type 304 stainless steel of 0.2-0.5 $mg.m^{-2}.a^{-1}$ and for Type 316, 0.1 $mg.m^{-2}.a^{-1}$, which are significantly lower than in the case of carbon and weathering steels. However, their main corrosive environments are stated as areas high in SO_2, chlorides and particulates, low to moderate rainfall zones, areas with moderate to high RH, high-temperature sites with high RH, as well as locations with elevated temperatures but low RH (Leygraf et al. 2016).

In South Africa, Callaghan (1991) reported corrosion rates for Types 430, 304 and 316 stainless steels of less than 0.0025 µm/a in a rural (low-pollution) environment after 20 years of exposure. Conversely, 0.24 µm/a, 0.04 µm/a and 0.03 µm/a, were recorded for the same stainless steel types, correspondingly, in a severe marine environment, also after 20 years of exposure. Moreover, it was found that the trend in the corrosion rates amongst the stainless steels followed the alloying content of the steel.

Consequently, the 316 alloy (18Cr/10Ni/3Mo) exhibited better corrosion resistance than the 304 alloy (18Cr/10Ni), which in turn performed better than the 430 alloy (17% Cr).

The most common types of stainless steels used in the construction industry are the 304, 304L, 316 and 347 austenitic grades (containing chromium and nickel) (Roberge 2012), which are favoured for their high corrosion resistance in atmospheric environments. Conversely, the molybdenum-bearing steels, e.g. 316, are more resistant to pitting and H_2SO_4 conditions (Fontana 1987; Llewellyn & Hudd 1998).

The ferritic stainless steels, e.g. Type 430, containing only chromium, have been developed to resist stress corrosion cracking. Although more corrosion resistant than the martensitic grades, e.g. Type 410, they are typically inferior to the austenitic grades (Fontana 1987).

2.1.5.2 Zinc (Zn) and hot-dip galvanising

Zinc (Zn) is used extensively in the corrosion protection industry as a barrier and cathodic or sacrificial protective system. Since Zn is anodic to steel and for that matter, exhibits a negative potential to most other metals, it tends to sacrifice itself during corrosion processes. The corrosion resistance of Zn coatings stems from the formation of top layers, e.g. Zn carbonate, which is mainly insoluble in water (Schultz & Thiele 2012).

Corrosion of Zn under normal conditions is an oxidation reaction, comprising two equal half-reactions (**Equations 2.15-2.18**) that can be presented by the following responses (Schultz & Thiele 2012):

At the anode:

$$Zn \longrightarrow Zn^{2+} + 2e^- \qquad \textbf{Eq. 2.15}$$

At the cathode:

$$2H^+ + 2e^- \longrightarrow H_2 \qquad \textbf{Eq. 2.16}$$

$$O_2 + 2H_2O + 4e^- \longrightarrow 4OH^- \qquad \textbf{Eq. 2.17}$$

$$2H_2O + 2e^- \longrightarrow H_2 + 2OH^- \qquad \textbf{Eq. 2.18}$$

According to Schultz & Thiele (2012), **Equation. 2.16** at the cathode prevails in an acidic environment. In neutral waters, though, **Equation 2.17** is dominant and responsible for the cathodic partial reaction of corrosion. In oxygen-deficient waters, **Equation 2.18** prevails.

Zinc hydroxide [$Zn(OH)_2$] forms as a voluminous solid white corrosion product (McEwan 2004), which upon drying, forms zinc oxide (ZnO) (zincite). Schultz & Thiele (2012) report that $Zn(OH)_2$ and ZnO have both amphoteric natures, which implies that they are soluble at low and high pH values. Furthermore, in water under normal pH and atmosphere, $Zn(OH)_2$ and ZnO reacts with CO_2 (when present), forming stable (insoluble) zinc carbonate ($Zn_5(OH)_6(CO_3)_2$), using the following reaction:

$$5Zn(OH)_2 + 2CO_2 \longrightarrow Zn_5(OH)_6(CO_3)_2 + 2H_2O \qquad \textbf{Eq. 2.19}$$

Providing this protective layer is maintained, Zn exhibits low corrosion rates. However, in the absence of O_2 and CO_2, or when exposed to low and high pH or other aggressive environments, corrosion of Zn rapidly takes place. Studies of the oxide layers of Zn by Cui et al. (2017) showed that in tropical marine-industrial environments in China, the depth and width of pitting corrosion of the Zn surfaces increased with time, while the corrosion is progressively transformed into a uniform pattern. The main crystalline components of the corrosion product were found to be simonkolleite ($Zn_5\,Cl_2[OH]_8{\cdot}H_2O$), sodium zinc chlorohydroxy-sulphate ($NaZn4Cl[OH]_6SO_4{\cdot}6H_2O$) and zinc hydroxyl carbonates ($Zn_5[CO_3]_2[OH]_6$) and ZnO. A decrease in the corrosion rate of the Zn was also observed and attributed to the protective qualities of the ($Zn_5\,Cl_2[OH]_8{\cdot}H_2O$). Cole (2017) provided a comprehensive review of the latest research about the atmospheric corrosion of galvanised steel and Zn and reported that the ZnO in the corrosion product might likely drive the oxygen reduction process.

During the ISOCORRAG Programme, the first-year corrosion rate of Zn flat metal coupons (98.5% pure Zn) worldwide was found to range between 0.2 μm/a and 17.5 μm/a, averaging at about 2 μm/a (Knotkova et al. 2010). This is about 20 times slower than the average corrosion rate measurement of carbon steel. The lowest value was recorded at San Juan in Argentina, which is a rural (subtropical) area (American Society for Testing and Materials 2000). Conversely, the highest corrosion rate of Zn

flat panel coupons was measured at the Panama Fort Sherman coastal site (Knotkova et al. 2010).

Contrary to the carbon steel, the corrosion rate of the pure Zn coupons remained reasonably constant over an eight-year exposure period (Knotkova et al. 2010). This phenomenon was also identified by Callaghan (1991), during his twenty-year corrosion monitoring programme of South Africa's macro atmosphere. Consequently, the service life of hot-dip galvanising coating is often quoted as being proportional to its thickness, providing the layer is sound and continuous (Galvanizers Association of Australia 2011).

The notion that the service life of the hot-dip galvanised coating is directly related to its thickness is not entirely accurate, however, since it is essential to keep in mind that hot-dip galvanising involves the application of a Zn melt to carbon steel surfaces. During the galvanising process, metallurgical bonds form between the molten Zn and steel substrate (McEwan 2004), resulting in the formation of hard iron-zinc gamma, delta, and zeta layers, as well as an eta (pure zinc) outer layer. McEwan (2004) states that in most environments, the Fe-Zn layers exhibit approximately 30% better resistance to corrosion than the pure Zn layer. Consequently, a slight decrease in the corrosion rate of hot-dip galvanising with time is theoretically more probable. This hypothesis was supported by corrosion monitoring work conducted by Janse van Rensburg (1994, 2010) at numerous locations throughout South Africa during which it was shown that for most sites, a small decrease in the corrosion rate of hot-dip galvanising might be anticipated with an increase in time. Refer also to **Figure 2.12** (Mokgatlhe & Janse van Rensburg 2012) in this regard.

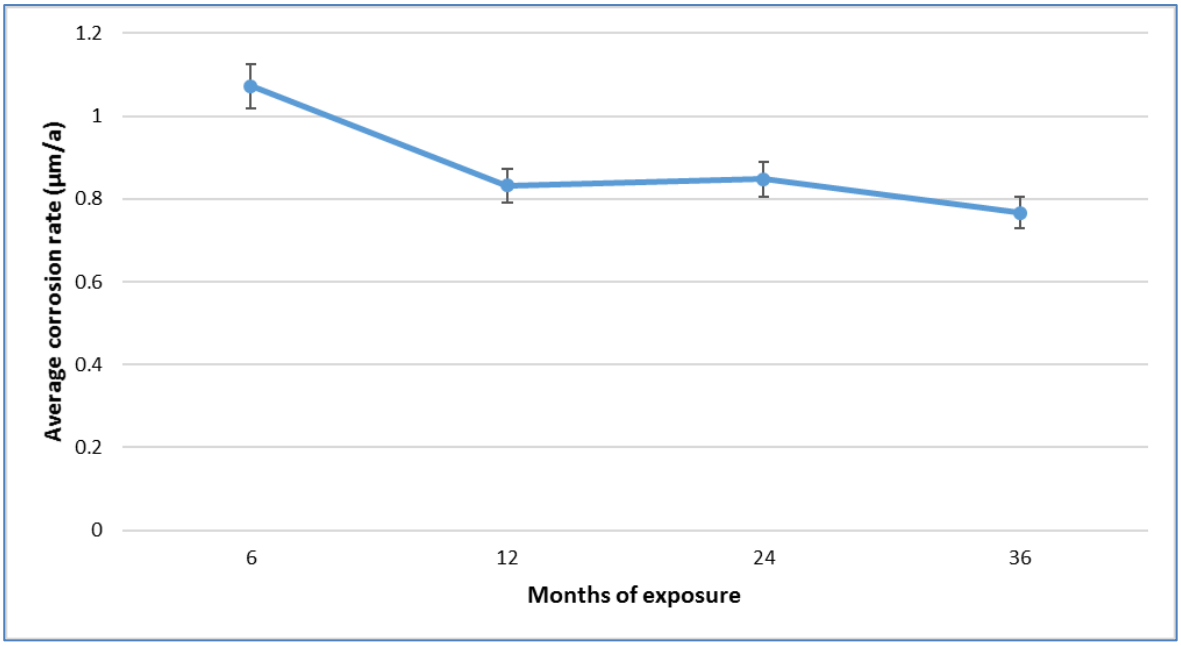


Figure 2.12 Changes in the atmospheric corrosion rate of hot-dip galvanised carbon steel after different exposure periods at Elandsfontein (a rural environment in Mpumalanga, South Africa) – Adapted from Mokgatlhe & Janse van Rensburg (2012).

2.1.5.3 Copper (Cu)

Copper (Cu) is produced mainly for electro-technical and architectural industries. It is furthermore used to form alloys, such as brasses (Cu-Zn), bronzes (Cu-Sn), and nickel silvers (Knotkova & Kreislova 2007; Leygraf et al. 2016). Fontana (1987) states that Cu exhibits good corrosion resistance properties and does not readily corrode in acidic environments, except when O_2 and oxidising agents are present. However, Rice et al. (1981) found during their laboratory studies that the corrosion rate of copper is sensitive to RH, SO_2, H_2S, O_3, HCl, and chlorine (Cl_2) concentrations.

Roberge (2012) reports that Cu and its alloys exhibit excellent corrosion resistance in rural, industrial, and marine environments, However, in NH_3 polluted atmospheres, it may be prone to stress corrosion cracking, particularly in Cu-Zn alloys containing more than 20% zinc. Long-term atmospheric exposure of Cu also changes its mechanical properties (i.e. strength and ductility) as corrosion extends over the entire surface exposed to the corrosive environment (Knotkova & Kreislova 2007).

When Cu is exposed to a moist environment, it develops a dark brownish protective oxide layer. This layer thickens with time (months to years), due to reaction with air

pollutants, e.g. SO_2 and chloride, providing a green patina, which is often considered aesthetically pleasing (Knotkova & Kreislova 2007; Kreislova 2015). However, in some cases, the patina remains black/dark brown despite being of significant age (FitzGerald et al. 2006). In their examination studies of patina samples from Brisbane, Denmark, Sweden, France, USA and Austria, FitzGerald et al. (2006) attributed this phenomenon to the [Fe]/[Cu] ratio. Accordingly, they reported that providing the patina is suitably thick, and the [Fe]/[Cu] ratio is reduced, then the patina is green, whereas if the [Fe]/[Cu] ratio is ~10 at.%, then the patina is rust brown.

As in the case of other metals, the corrosion resistance of Cu is associated with the formation of its protective patinas (Kreislova 2015). In urban areas, the main patina that is formed is cuprite (Cu_2O), which reacts with SO_2 from the atmosphere, forming posnjakite ($Cu_4SO_4(OH)_6.xH_2O$) and brochantite ($Cu_4SO_4(OH)_6$, which are green patinas. Antlerite and malachite may also be found in urban areas as patinas. In marine environments, however, the Cu_2O layer is covered by a voluminous green-blueish copper chloride patina, called atacamite ($Cu_2Cl(OH)_3$) (Wallinder et al. 2002; Syed 2006; Leygraf et al. 2016).

According to the Cu exposure results of the comprehensive ISOCORRAG Programme, the first-year corrosion rate of Cu flat metal coupons (99.5% pure), worldwide, measured from 0.1-5.5 μm/a, averaging at about 1.6 μm/a (Knotkova et al. 2010). This is nearly 28 times slower than the corrosion rate of carbon steel and approximately 1.3 times less than the corrosion rate of pure Zn. Like the carbon steel exposure panels, the lowest value was recorded at Oymyakon and the highest at the Panama Fort Sherman coastal site.

Callaghan (1991) found that the corrosion rate of new Cu in low corrosive environments in South Africa initially started off at a higher rate, but then tapered off, with an increase in time. However, in more aggressive settings, e.g. marine, the corrosion rate remained constant or higher than usual. Regarding the corrosion rates of Cu-Zn alloys, Leygraf et al. (2016) reported that these are typically lower than in pure Cu in low chloride polluted environments. However, in chloride-rich marine environments, the difference is less distinct. Conversely, the corrosion rate of Cu-Zn is said to be significantly lower than Cu in low chloride-containing urban and rural environments, whereas the opposite is correct

pertaining to severe marine environments. Though, the difference tends to decrease with an increase in distance from the ocean.

During the UN ECE International Co-operative Programme on Effects on Materials including Historic and Cultural Monuments (Knotkova & Kreislova 2007), as well as the ISOCORRAG programme (Kreislova 2015), the 12-month (r_{corr}) and 10-year (r_{av}) average corrosion rates of Cu-Sn alloy were found to be approximately two-thirds and one-third, respectively, of pure Cu.

2.1.5.4 Aluminium (Al)

Aluminium (Al) is the most frequently used non-ferrous metal globally and together with its various alloys, often used in aircraft construction, building materials, electrical conductors, chemical and food-processing equipment, etc. (Encyclopaedia Britannica 2008d). Vargel (2004) reports that following 1950, the use of aluminium has significantly increased in the building sector for the manufacturing of cladding, curtain walls, roofing sheet, metallic fittings, street signs, etc..

Granting that aluminium is less noble than steel and chemically active, it tends to corrode slowly under atmospheric conditions due to the presence of a robust amorphous oxide (γ-Al_2O_3) layer (Graedel 1989; Lobnig et al. 1996b; Leygraf et al. 2016), exhibiting low solubility over the pH range of 4 to 8.6 (Lobnig et al. 1996b). In uncontaminated atmospheres, $Al(OH)_3$ or $Al_2O_3 \cdot 3H_2O$ (bayerite) and other hydrated oxides and hydroxides may also form (Leygraf et al. 2016b). In SO_2 polluted environments, however, primary aluminium sulphates and amorphous aluminium sulphate hydrate mainly tend to develop (Lobnig et al. 1996b), while in chloride-rich (marine) environments, the chloride may destroy the passive oxide film, resulting in the formation of primarily $Al(OH)_3$, together with amorphous $Al_2(SO_4)_3 \cdot nH_2O$ (n = 4, 5) and less soluble aluminium hydroxysulphates ($Al_4SO_4(OH)_{10}$) (Leygraf et al. 2016).

Aluminium tends to corrode by pitting rather than by uniform corrosion (McEwan 2004; Melchers 2015). Consequently, several studies have been conducted to investigate the pitting corrosion of aluminium. For example, Hernandez et al. (2011) have carried out atmospheric corrosion studies of aluminium in archipelagic subtropical environments. According to their research, the pit densities on aluminium were significantly affected

by the concentration of pollutants and the wetness of the atmospheres. Also, a direct linear correlation between the pitting parameters and the chloride level in the atmosphere was found. However, the effect of SO_2 was established to be less significant, although laboratory tests showed that the addition of sulphate ions to chloride-containing solutions encouraged the growth of broader pits. Melchers (2015) also investigated the time-dependent development of aluminium pitting corrosion and showed that the collection of corrosion products over the pit mouths likely produces localised anoxic conditions within pits. This leads to autocatalytic conditions, which is consistent with observations of hydrogen evolution from pits.

Apart from pitting, other corrosion problems of aluminium and its alloys include exfoliation, filiform (filament-like form or corrosion) (Hernandez et al. 2011), crevice, intergranular and stress corrosion cracking, which occurs when the protective oxide layer dissolves or suffers damage, depending on the environmental conditions involved (AFSA 2011). In general, aluminium exhibits excellent corrosion resistance in rural, industrial and marine atmospheres (Callaghan 1991; Janse van Rensburg 2010; Knotkova et al. 2010; AFSA 2011).

Leygraf et al. (2016) summarised the atmospheric corrosion processes of aluminium as follows:

i. The interaction between H_2O and the initial aluminium surface oxide film leading to the formation of a porous AlOOH layer, with the added growth of other aluminium oxides/hydroxides;
ii. Adsorption of sulphate or chloride ions on the oxidised surface, resulting in the thinning of the oxide layer or the formation of local pits, and the simultaneous dissolution of aluminium ions;
iii. The growth of less soluble amorphous aluminium sulphate hydrate in the presence of sulphate ions and its potential conversion into aluminium hydroxysulphate; and
iv. Local growth of soluble aluminium chloride or hydroxychlorides and the possible alteration back to aluminium hydroxide.

During the ISOCORRAG Programme, the first-year corrosion rate of aluminium flat panel coupons (99.5% pure) worldwide was found to range between 0.03 μm/a and

1.70 μm/a, averaging at about 0.4 μm/a (Knotkova et al. 2010). This is approximately 100 times slower than the corrosion rate of steel, five times slower than zinc and roughly four times slower than copper. The lowest value was again recorded at San Juan in Argentina, whereas the highest value was measured at Auby in France, which is classified as a heavy industrial site. Like various other metals, even though the corrosion rate of aluminium is slow, it tends to taper off with time (Callaghan 1991).

2.1.6 Atmospheric Corrosion Classification

2.1.6.1 BS EN 12500-2000 standard

Traditionally, as per British Standard BS EN 12500-2000 (British Standards Institution 2000a), five types of primary atmospheres have been recognised regarding atmospheric corrosion, namely rural, urban, industrial, marine and marine industrial. This method for the classification of the environment has been widely used due to its simplicity (Callaghan 1991; Nixon & Janse van Rensburg 1992; McEwan 2004; Adikari et al. 2014). From a critique point of view, however, Mikhailov et al. (2004) described the old system as only qualitative in nature, while Hernandez et al. (2011) contended that this primary classification of corrosive atmospheres was limited, since the wind may produce marine or polluted environments at locations much further away from the coastline or actual sources of pollution. Independently, though, the standard was withdrawn in February 2012 (British Standards Institution 2018) and replaced with the ISO Classification system discussed in Section 2.1.6.3.

2.1.6.2 CLIMAT (Wire-on-bolt) Classification

Galvanic couple corrosion studies by way of the threaded bolt and wire test were first carried out by Compton & Mendizza (1955a; 1955b). However, based on further work done by Doyle & Goddard (1966), the CLIMAT (ATCORR) (CLassify Industrial and Marine ATmospheres) classification technique evolved into a rapid method for the corrosivity measurement of atmospheres. Consistent with this CLIMAT procedure, now standardised as ASTM G116 (ASTM International 2004), the average percent weight loss of aluminium wire, wrapped around approximate 100 mm long threaded nylon, copper and carbon steel bolts, are used to classify the corrosivity of atmospheres into five, non-linear levels (Carter 1982; Li et al. 2013) (**Table 2.1**) (See also **Figure 2.13**.)

Table 2.1 CLIMAT test - five levels of corrosivity (Carter 1982).

Rating	ICI (aluminium wire-on-copper bolt)	MCI (aluminium wire-on-mild steel bolt)	ACI (aluminium wire-on-nylon bolt)
Negligible	<1	<2	<0.4
Moderate	1.1 to 2	2 to 5	0.5 to 1
Moderately severe	2.1 to 4	5.1 to 10	1.1 to 1.5
Severe	4.1 to 7	10.1 to 20	1.6 to 3.0
Very severe	>7.1	>20	>3.1

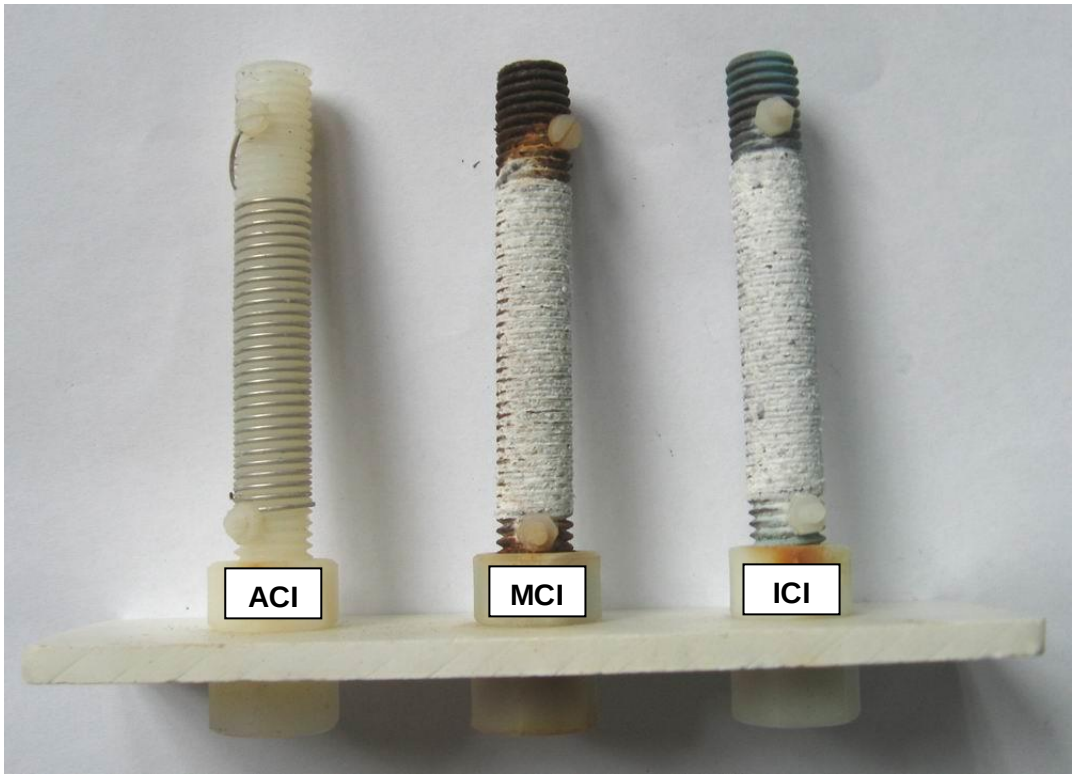


Figure 2.13 An example of a CLIMAT unit, demonstrating the extent of corrosion of the different galvanic couples after 90 days of exposure in a highly aggressive marine site.

The *aluminium-nylon* couple is used as a reference specimen (Carter 1982; ASTM International 2004) to separate general and crevice corrosion from galvanic effects. In this regard, Carter (1982) states that usually, ACI couples will seldom provide values greater than 3.0. Therefore, when higher ACIs are measured in combinations with "*normal*" MCIs, some atypical source of corrosivity may be expected. Moreover, the *aluminium-nylon* couple is used to measure the Atmospheric Corrosion Index (ACI), i.e. the general level of corrosivity of the atmosphere to aluminium (Carter 1982). While this

couple emphasises the influence of moisture on the corrosivity of the environment, it may also be affected by Cl^-, SO_2, smoke and dust particles that are present in the atmosphere (Leitch 1994).

The *aluminium-steel* couple is used to determine the Marine Corrosion Index (MCI) (Carter 1982) and tends to emphasise the effects of moisture and Cl^-, and to a lesser extent, SO_2 present in the atmosphere. Conversely, the *aluminium-copper* galvanic couple is affected by humidity, SO_4^{2-} and Cl^- found in the environment, and thus gives the Industrial Corrosion Index (ICI) (Carter 1982; Leitch 1994). Correlations of these quantitative indices for numerous sites have been established, particularly regarding aluminium. However, other galvanic-couples have also been used (Carter 1982).

Due to the small surface area of the anode material (wire) in comparison with the large cathode (threaded bolt), galvanic corrosion is accelerated. The corrosion process is increased even further due to the tight crevice that exists between the wire and the bolt (ASTM International 2004).

Since its inception, this procedure has been widely used by industrial and academic researchers in South Africa, as well as in other parts of the world to monitor and classify the corrosivity of environments (Callaghan 1991; Nixon 1991, 1993; Nixon & Janse van Rensburg 1992; Nixon 1993; Janse van Rensburg 1994; Leitch 2003; Janse van Rensburg 2010; Delgado & Vera 2013).

While the procedure has proven useful for the monitoring of the seasonal fluctuations of corrosive atmospheres, it has been found to be too sensitive in severe marine environments, often producing invalid results (Janse van Rensburg 2010). Li et al. (2013) similarly derived this conclusion and gave other limitations of the wire-on-bolt procedure as:

i) the lack of indicating the relative atmospheric corrosivity of an environment;

ii) the fact that the Industrial, Marine and Atmospheric Corrosion Indices (ICI, MCI and ACI) do not reflect the actual corrosion rates of aluminium; and

iii) the data do not provide accurate information regarding the deterioration behaviour of metallic components.

Moreover, the morphology of the base metal corrosion attack or its impact on the mechanical properties of this metal cannot be evaluated by this procedure (ASTM International 2004).

Nonetheless, in 2013, Delgado & Vera reported that the CLIMAT procedure was still an adequate method for the classification of atmospheres. This was since during their study of the corrosivities of various sites in Chile; it was found that the CLIMAT results were in line with the classifications obtained by other methodologies, e.g. ISO 9223, which required a higher number of measurements. Consequently, they concluded that the use of this procedure implied lower costs in the implementation of samples and less time spent on analysis. Morcillo et al. (2010) concurred that the CLIMAT test is easy and economical to use.

2.1.6.3 ISO Classification

Presently, the ISO 9223 scheme is mostly used to classify the corrosivity of indoor and outdoor environments, from *very low* (C1) to the *extreme* (CX) (International Organization for Standardization 2012a). This quantitative rating system (Mikhailov et al. 2004) was developed by a Working Group (TC156/WG4) of the International Standard Organization (ISO) during the ISOCORRAG Program of 1986 to 1998, and involved the exposure of mild (carbon) steel, copper, zinc and aluminium coupons at 51 sites in 14 countries over the world (Dean & Reiser 2002; Knotkova et al. 2010; Roberge 2012). Based on the research done, two classification procedures were developed (**Figure 2.14**) (International Organization for Standardization 2012a):

i. Determination of the corrosivity of atmospheric environments based on the 12- month corrosion losses of carbon steel, aluminium, zinc and copper; and
ii. Estimation of the corrosivity of atmospheres based on dose-response functions for TOW, SO_2 and Cl^-.

Consistent with the ISO 9223 (2012) corrosivity classification scheme, six corrosivity categories were established, as shown in **Table 2.2**.

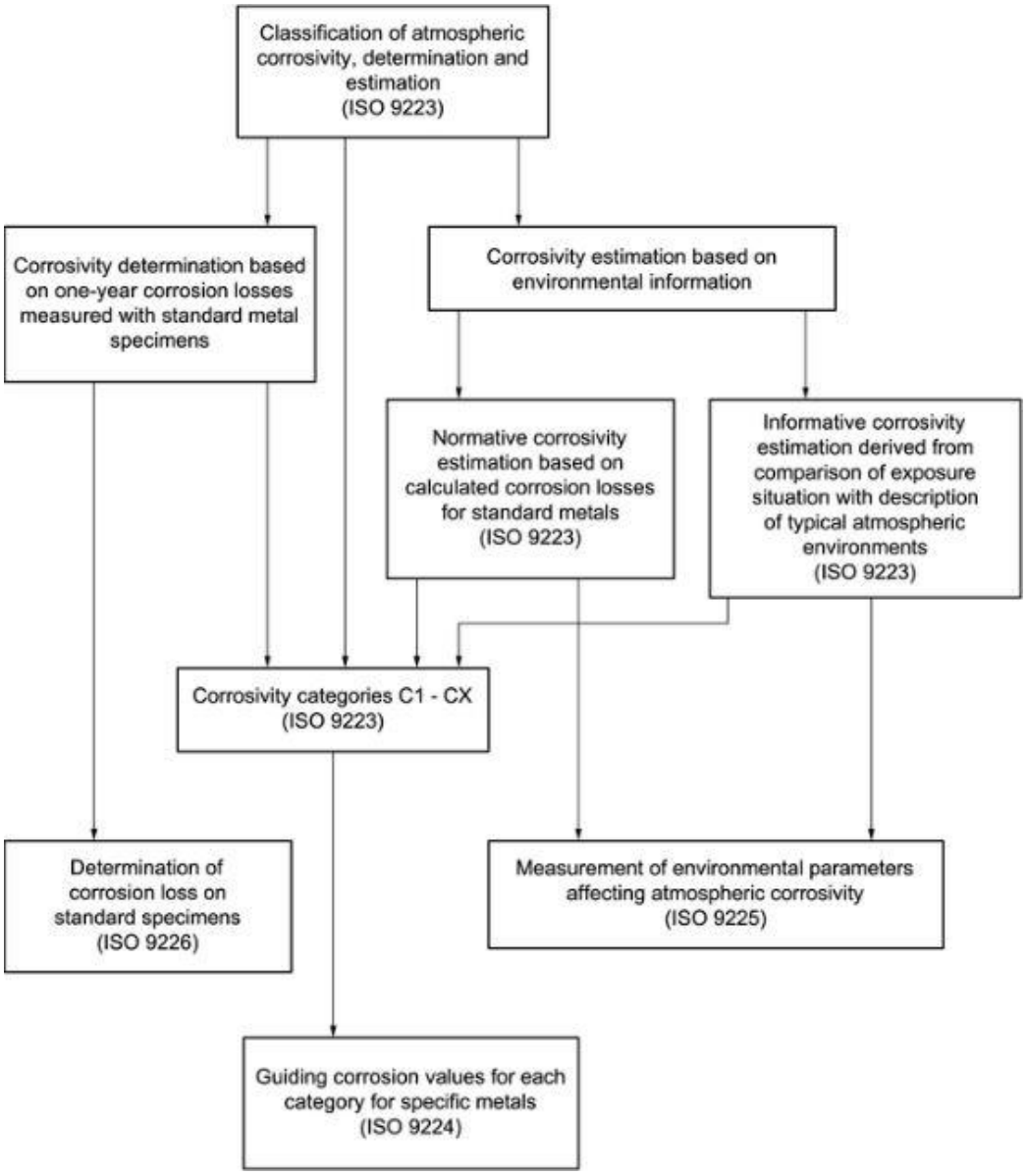


Figure 2.14 Interrelationships between the ISO 9223-9226 procedures (International Organization for Standardization 2012a).

https://www.iso.org/obp/ui/#iso:std:iso:9223:ed-2:v1:en

Table 2.2 Categories of corrosivity of atmospheres based on the 12-month corrosion rates of mild (carbon) steel, zinc, copper and aluminium – Adapted from International Organization for Standardization (2012a, 4).

Corrosivity category	General description	Corrosivity	Corrosion rate of mild steel	Corrosion rate of aluminium)	Corrosion rate of zinc	Corrosion rate of copper
C1	Indoors, and desert to rural	Very low	As per ISO 9223 (2012) https://www.iso.org/obp/ui/#iso:std:iso:9223:ed-2:v1:en NOT PUBLICLY AVAILABLE			
C2	Rural to light industrial	Low				
C3	Moderate industrial or marine	Medium				
C4	High industrial or marine	High				
C5	Severe / heavy industrial or marine	Very high				
CX	Extreme marine	Extreme				

Note: The corrosion rate of aluminium is given in g/(m^2·a) due to its localised nature, mainly pitting.

While the ISO system was well received and has been extensively used for the corrosivity classification of environments, using both procedures (Mikhailov et al. 2004), the estimation method, whereby TOW and the deposition rates of SO_2 and Cl^- are used to predict the corrosion rates of carbon steel, zinc, copper and aluminium, has been questioned. This is since the procedure only considers three atmospheric corrosion parameters, ignoring important variables such as NO_x, H_2S, CO_2, temperature, rainfall, wind speed, etc. (Adikari et al. 2014). As aforementioned, Cole et al. (1999) also questioned the ISO-TOW definition.

Mikhailov et al. (2004) similarly contended that the first method (mass loss procedure) was more reliable, therefore it was included in the normative part of the standard, whereas the second method (assessing the corrosivity categories via TOW and the deposition rates of SO_2 and Cl^-) was included in the informative part of the standard. This thesis is dedicated to the first, mass loss procedure of assessing the corrosivity of South Africa's and the GJMA's macro atmospheres, using the ISO 9223 and ISO 9226 procedures (International Organization for Standardization 2012a, 2012d).

In the first issues of these standards in 1992, an open wire (aluminium, zinc or copper) helix procedure was introduced for the measurement of the corrosivity of the environment, as an alternative to the use of flat metal specimens. Although this procedure has subsequently been withdrawn (International Organization for Standardization 2012d), it has been used extensively for the corrosivity classification of numerous sites throughout South Africa (Leitch 1999; Leitch 2006; Janse van Rensburg 2010; Janse van Rensburg 2015), as well as during the ISOCORRAG study (Knotkova et al. 2010). However, Carter (1982) considered the CLIMAT unit more robust than the ISO wire helix device.

2.1.7 Atmospheric Corrosion Monitoring

Atmospheric corrosion monitoring via passive mass loss procedures, visual inspection or real-time, and in-line data acquisition methods is performed under industrial, practical operating or laboratory simulation conditions (Roberge 2012). As mentioned by Roberge (2012), corrosion monitoring is often difficult since:

- different forms of corrosion are often present;
- corrosion may generally be spread over the test surface or more localised in nature, e.g. at pits, crevices, edges and around fasteners;
- corrosion rates may vary considerably, even over short distances; and
- no single corrosion monitoring technique can measure or detect these variable conditions.

2.1.7.1 Weight-loss/damage rate measurements

Weight-loss/damage rate measurements of standard metal specimens (flat plate and coil units/coupons) are universal methods used to characterise the corrosivity of atmospheres. Consequently, several standard methodologies exist, e.g.:

- ASTM G1 (ASTM International 2003a) - Standard practice for preparing, cleaning, and evaluating corrosion test specimens;
- ASTM G92 (ASTM International 1986) - Standard practice for characterisation of atmospheric test sites;
- ASTM G116 (ASTM International 2004) - Standard practice for conducting wire-on-bolt test for atmospheric galvanic corrosion; and
- ISO 9226 (International Organization for Standardization 2012d) – Corrosion of metals and alloys - Corrosivity of atmospheres - Determination of corrosion rate of standard specimens for the evaluation of corrosivity.

These standards have been developed to determine the actual corrosion rates of metals and their alloys under different environmental conditions. Following measurement, the weight-loss results may then be used to classify the corrosivity of environments, e.g. as per the CLIMAT or ISO 9223 corrosivity rating schemes (**Tables 2.1 & 2.2**) (Carter 1982; International Organization for Standardization 2012a). These 'weight-loss' corrosion monitoring techniques are considered easy and cost-effective to use (Roberge 2012; Delgado & Vera 2013), especially with regards to large-scale or country-wide corrosion studies (Janse van Rensburg 2010; Knotkova et al. 2010; Delgado & Vera 2013). Moreover, real-world weight-loss methods have several advantages over laboratory testing techniques, namely:

- they provide the most direct measure of the corrosion effect (Leygraf et al. 2016);
- they are often much closer to end-user applications (Roberge 2012);
- they can be carried out over periods of a few months to many years (Callaghan 1991; Janse van Rensburg 2010; Roberge 2012);
- various materials can be tested simultaneously (Callaghan 1991; Janse van Rensburg 2010; Knotkova et al. 2010);
- flat coupons or bimetallic couplings may reveal directional information concerning corrosive agents (Roberge 2012);

- the coupons can be exposed to environmental conditions that may not be accurately simulated in the laboratory (Roberge 2012); and
- the coupons can be tested in duplicate or triplicate (measuring scatter), as well as fabricated to simulate such conditions as welding, residual stresses or crevices (Roberge 2012).

An additional benefit is that following exposure, the corroded coupons may be used to measure pit density or depth measurements, as well for studying the morphologies and chemical compositions of the corrosion products. Many pitfalls exist, however, which can be avoided or limited by following the guidance of standards such as ASTM G4-1 (2014) (Roberge 2012), entitled, "*Standard guide for conducting corrosion tests in field applications*".

The principal technique involves the exposure of small flat plate or wire specimens, with known weights to environments for specific periods. Following exposure, the devices are removed, chemically cleaned, often with an aqueous acidic solution to remove the corrosion products that have formed on the metal surfaces, whereafter the samples are reweighed and the corrosion rates/indices determined.

ASTM G15 (ASTM International 1990) and ISO 9226 (International Organization for Standardization 2012d) defines the term 'corrosion rate' (r_{corr}) as the amount of corrosion occurring in unit time, e.g. mass change per unit area per unit time or penetration per unit time, and is calculated by means of **Equation 2.20**:

$$Corrosion\ rate\ of\ metal = \frac{\Delta m}{At} \qquad \textbf{Eq. 2.20}$$

where:

the corrosion rate (r_{corr}) is in g/m^2.annum (g/m^2. a)
Δm is the mass loss (g);
A is the surface area (m^2); and
t is the exposure time in years.

Alternatively, the corrosion rate may be calculated in micrometres per annum (µm/a) (**Equation 2.21**).

$$Corrosion\ rate\ of\ metal = \frac{\Delta m}{At\rho} \qquad \textbf{Eq. 2.21}$$

where:

the corrosion rate (r_{corr}) is in μm/a;

Δm is the mass loss (g);

A is the exposed surface area (m^2);

t is the exposure time in years; and

ρ is the density of the metal (g/cm^3) (International Organization for Standardization 2012d).

Long-term measuring of different meteorological and pollution factors such as TOW, SO_2, Cl^-, etc., often accompany the exposure of metallic coupons to the environment. Consequently, these atmospheric corrosion studies tend to be longstanding, e.g. one to five, ten, fifteen or even twenty years in duration (Callaghan 1991; Janse van Rensburg 1994, 2010; Knotkova et al. 2010). While relatively inexpensive, weight-loss programmes can become costly when linked to simultaneous monitoring of weather and pollution parameters. An added disadvantage is the chemical stripping treatment that may remove some of the non-corroded base metal. According to Leygraf et al. (2016), presently a mass loss detection limit of about 10 mg/m^2 is possible, which in the case of some of the more corrosion resistant metals, e.g. copper, can correspond to a few months of outdoor exposure in mildly corrosive environments. However, this disadvantage of the weight-loss procedure is less significant when materials are exposed to highly corrosive conditions.

2.1.7.2 Weight-gain procedures

Atmospheric corrosion measurements can also be done via weight-gain procedures. Leygraf et al. (2016) report that the weight-gain analysis of metallic coupons, rather than the weight-loss method, require no removal of the corrosion product. Consequently, much smaller mass gains can be measured in comparison with the weight-loss process. However, a significant drawback is that the mass increase of a metal coupon may not necessarily imply corrosion, but can also be due to humidity sorption and dust deposition. Also, some of the corrosion product may be lost due to exfoliation of the steel surfaces (Janse van Rensburg 2015). Consequently, lower corrosion rates may be measured than are valid.

2.1.7.3 Online electrical resistance (ER) measurements

Online ER measurements, based on increases in the ohmic resistances of thin metal films due to atmospheric corrosion, have the advantage that atmospheric corrosion measurements can be made *in situ* (Leygraf et al. 2016). They are also useful for measuring short-term corrosion events (ASTM International 2003b). While the detection limit is only a few milligrams per square metre, i.e. when the resistance of the corrosion product is high, and the corrosion is uniform, resistance sensor measurements tend to overstate the corrosivity of environments (Leygraf et al. 2016). A further disadvantage is that these systems often involve the use of rather expensive corrosion-sensors/probes, data loggers, computer hardware, and software, etc. (Colloby 1995). Therefore, they become too costly to use in the case of large-scale, country-wide corrosion monitoring programmes. The possibility of theft and power supply interruptions are also significant deterrents.

2.1.7.4 Linear polarisation resistance (LPR) and electrochemical impedance (EIS) techniques

Atmospheric corrosion monitoring may also be carried out by different linear polarisation resistance (LPR) and electrochemical impedance (EIS) procedures. These methods involve the application of small "*artificial electronic perturbations in the form of a direct- or alternating-current signal to particular sensor elements and measuring the resulting electrochemical signal response*" (Tullmin & Roberge 2000). The use of such techniques for large-scale country-wide corrosion monitoring programmes is, however, impractical and would be extremely costly.

2.1.8 Modelling of Atmospheric Corrosion

Simultaneous measurements of environmental parameters and corrosion were done for the first time in the 1990s. Subsequently, tremendous effort has been made about the linkage of atmospheric corrosion of materials with the environmental parameters that influence it (Graedel & Leygraf 2001). Additionally, due to the significant improvements in portable computing and communication technologies (Roberge 2012), the modelling of atmospheric corrosion has become extremely popular, since models:

- contribute to knowledge and understanding;

- help in the interpretation of experimental data;
- assist in the testing of theories, and
- allow projections to be made about the vulnerability of a given system to corrosion (Leygraf 2016).

Modelling of atmospheric corrosion commonly involves the correlation of pollution, RH, temperature, TOW, rainfall, wind direction, etc., with the corrosivity rates of metals and alloys to predict the probable corrosivity of an atmosphere. These models are based on the knowledge that the corrosion of metals under atmospheric conditions depends on the TOW, adsorption of water on the metal face, temperature, the type and concentration of chemical pollutants in the air, time of exposure of the metals, as well as by other influencing factors (Mikhailovsky 1982). However, due to the instability of atmospheric processes, the accuracy of mathematical atmospheric corrosion models is often questioned (Mikhailovsky 1982; Hernandez et al. 2011). Limits of parametric models that link climate and pollutant variables with the mass loss of metal specimens, as determined by field exposures include:

i) the models from different countries are often unlike;
ii) the models cannot be applied accurately in areas significantly different from the regions in which they were derived (Cole et al. 2011); and
iii) weak to moderate correlation coefficients frequently exist (Kelly et al. 2007).

One of the most common methods used to describe atmospheric corrosion damage as a function of time is via the linear bilogarithmic law (**Equation 2.22**) (Pourbaix 1982; Feliu et al. 1993; Adikari et al. 2014), since the atmospheric corrosion is typically not linear, but tends to reduce with time due to the build-up of corrosion products (Adikari et al. 2014).

$$C = kt^n \qquad \textbf{Eq. 2.22}$$

or

$$Log_{10}C = log_{10}k + nlog_{10}t \qquad \textbf{Eq. 2.23}$$

where:

C is the corrosion loss; and
t is the exposure time.

The atmospheric behaviour of a specific metal at a location is defined by k and n, with k representing the initial corrosion during the first year of exposure and n, a measure of the long-term reduction in the corrosion rate of materials, which is directly related to the metal type, the atmospheric and exposure conditions. By defining k and n, as functions of atmospheric variables (**Equations 2.24-25**), this power law equation can be generalised to any location (Adikari et al. 2014).

$$k = f(\mathrm{TOW}, \mathrm{Cl^-}, \mathrm{SO_2}, \mathrm{T}, \text{etc..}) \qquad \textbf{Eq. 2.24}$$

$$n = F(\mathrm{TOW}, \mathrm{Cl^-}, \mathrm{SO_2}, \mathrm{T}, \text{etc..}) \qquad \textbf{Eq. 2.25}$$

Subsequently, the relationship between these variables is determined using field exposure programmes and statistical analysis. However, in some cases, the rate of corrosion is given as a direct function of atmospheric variables, with the relationships between the corrosion and environmental parameters also being determined via field exposure programmes (Adikari et al. 2014).

$$C = f(\mathrm{TOW}, \mathrm{Cl^-}, \mathrm{SO_2}, \mathrm{T}, \text{etc..}) \qquad \textbf{Eq. 2.26}$$

The ISOCORRAG Collaborative Exposure Programme involved the exposure of flat metal coupons, i.e. mild steel, aluminium, zinc and copper at 51 sites throughout the world. Simultaneously, RH, temperature (T), salt deposition (measured by salt candles) and SO_2 deposition were determined at each site. Successively, the statistical correlations between the corrosion rates and environmental parameters were established as dose/response functions, which were incorporated into ISO 9223 for predictive purposes.

An example of the dose-response function for calculation of the first-year corrosion loss of mild steel is given as **Equation 2.27** (International Organization for Standardization 2012a).

$$r_{\mathrm{corr}} = 1.77 \cdot P_{\mathrm{d}}^{0.52} \cdot \exp(0.020 \cdot \mathrm{RH} + f_{\mathrm{St}}) + 0.102 \cdot S_{\mathrm{d}}^{0.62} \cdot \exp(0.033 \cdot \mathrm{RH} + 0.040 \cdot T) \qquad \textbf{Eq. 2.27}$$

$f_{\mathrm{St}} = 0.0150 \cdot (T - 10)$ when $T \leq 10$ °C; otherwise $-0{,}054 \cdot (T - 10)$

$N = 128$, $R^2 = 0.85$

where:

r_{corr} is first-year corrosion rate of metal, expressed in micrometres per annum (µm/a);

T is the annual average temperature, expressed in degrees Celsius (°C);

RH is the annual average relative humidity, expressed as a percentage (%);

Pd is the annual average SO_2 deposition, expressed in milligrams per square metre per day [mg/(m^2·d)]; and

Sd is the annual average Cl^- deposition, expressed in milligrams per square metre per day [mg/(m^2·d)].

Based on the atmospheric corrosion results of the ISOCORRAG Programme (Knotkova et al. 2010; International Organization for Standardization 2012a), however, it was found that the levels of uncertainty of the measured corrosion rates of exposed metal specimens versus their estimated corrosion rates based on the ISO 9223 dose/response functions were high (**Table 2.3**).

Table 2.3 Approximate levels of uncertainty for the measurement of the corrosivity of atmospheres based on actual corrosion rates and estimated rates obtained via the dose-response models - after Knotkova (2005).

Metal Type	Determination	Estimation
Carbon steel	± 2%	-33% to 50%
Zinc	± 5%	-33% to 50%
Copper	± 2%	-33% to 50%
Aluminium	± 5%	-50% to 100%

Starting in September 1987, a model was also developed by the International Cooperative Programme on Effects on Material (ICP Materials), involving 39 exposure sites in 14 countries. Several meteorological and pollution parameters, i.e. time, temperature, rainfall and RH, and SO_2, O_3 and acid concentrations were measured (Tidblad et al. 1999). Based on the different models derived, the corrosion of a metal was expressed in mass loss (ML) as a function of the aforementioned climatic and pollution variables, given for zinc (**Equation 2.28**) (Adikari et al. 2014) as:

$$\mathrm{ML} = 1.4(\mathrm{SO_2})^{0.22}\exp[0.018\mathrm{RH}+f(T)]t^{0.85} + 0.029\mathrm{Rain}[\mathrm{H^+}]t \qquad \textbf{Eq. 2.28}$$

where:

- ML is mass loss (g/m^2);
- t is exposure time;
- RH is relative humidity (%);
- T is average annual temperature (°C);
- $f(T)$ is $a(T\text{-}10)$, when T<10°C, otherwise $b(T\text{-}10)$, with a and b being constant values depending on the specific metal;
- $\mathrm{SO_2}$ is sulphur dioxide concentration in µg/m^3;
- Rain is the average annual rainfall (in mm); and
- $\mathrm{H^+}$ is the hydrogen ion concentration in the precipitation (in mg/L).

In 2017, based on the integration of the ISOCORRAG, ICP/UNECE and MICAT (MICAT cooperative programme: "*Ibero-American Atmospheric Corrosivity Map*") atmospheric corrosion databases, Chico et al. (2017) established global damage functions (DF) between the first year corrosion rate of carbon steel in different atmospheres, and available environmental and pollution variables.

Regarding non-marine atmospheres, the climatological and pollution parameters mutual to all three databases and included in the analysis were temperature, RH and $\mathrm{SO_2}$ pollution. Since all three parameters were found to be statistically significant, the resulting regression equation (**Equation 2. 29**) explained 72.5% of the dependent variables.

$$C = -26.32 + 0.43\ T + 0.45\ \mathrm{RH} + 0.82\ \mathrm{SO_2};\ (\mathrm{R^2} = 0.725)\ (N = 333) \qquad \textbf{Eq. 2.29}$$

where:

- C is the annual corrosion of carbon steel, in µm;
- T is annual average temperature, in °C;
- RH is the annual average relative humidity, in %; and
- $\mathrm{SO_2}$ is the $\mathrm{SO_2}$ pollution, in mg/m^2.day.

However, in marine atmospheres, the statistically significant variables used for the analysis were $\mathrm{Cl^-}$, $\mathrm{SO_2}$ and TOW, with the resulting regression equation (**Equation 2.30**) explaining only 47.4% of the dependant variables

$$C = -24.50 + 0.75\ \mathrm{Cl^-} + 0.67\ \mathrm{SO_2} + 77.32\ \mathrm{TOW}\ (\mathrm{R^2} = 0.474)\ (N = 206) \qquad \textbf{Eq. 2. 30}$$

where:

C is the annual corrosion of carbon steel, in µm;

Cl^- is chloride pollution, in mg/m^2.day;

TOW is time of wetness, annual fraction of number of hours/year in which RH is greater than 80% and $T > 0$°C; and

SO_2 is the SO_2 pollution, in mg/m^2.day.

Due to the limitations of parametric models (Cole et al. 2003a), a holistic model approach for atmospheric corrosion was developed by I.S Cole and associates, dealing with the multifaceted environments that occur in atmospheric corrosion from macro through to meso to local, micro, surface response to micron and lastly electrochemical scales (Cole et al. 2011). According to Cole et al. (2011), 'macro' refers to major meteorological environments, 'meso' denotes areas with sizes up to 100 km^2, 'local' is the immediate surrounding area of a building, whereas 'micro' refers to the absolute proximity of a material surface, 'surface response' implies mainly the physical responses of a surface, e.g. deposition and retention of pollutants, or condensation and evaporation. Lastly, 'micron' refers to interactions within the metal/oxide/electrolyte interfaces. Being fundamentally based, these models can be applied outside the data sets from which they originate (Cole et al. 2003a).

The holistic model approach, primarily designed for Australian (marine) atmospheric conditions, has been published as several papers, namely:

- Part 1 – Theoretical framework for production, transportation and deposition of marine salts (Cole et al. 2003a);
- Part 2 – Experimental measurement of deposition of marine salts in a number of long range studies (Cole et al. 2003b);
- Part 3 – Effect of natural and man made landforms on deposition of marine salts in Australia and south-east Asia (Cole et al. 2003c);
- Part 4 – Geographic information system for predicting airborne salinity (Cole et al. 2004a)
- Part 5 – Factors controlling deposition of salt aerosol on candles, plates and buildings (Cole & Paterson 2004b);
- Part 6 – From wet aerosol to salt deposit (Cole et al. 2004c); and
- Part 7 - Cleaning of salt from metal surfaces (Cole & Paterson 2013).

In 2011, Cole and partners applied their multi-scale model of atmospheric corrosion to the corrosion of steel, zinc, and aluminium in the Infrastructure and Aerospace industries. The outcome of this sequence of modules was the capability to forecast the "*state*" of a surface (every three hours) on various infrastructure types for localities throughout Australia. It is said that the term "*state*" could be that the surface has dried, wet from rain or moist from the wetting of hygroscopic salts (Cole et al. 2011).

Since empirical and statistical models give little information about the underlying physicochemical phenomena that determine the corrosion processes, other mechanistic models of atmospheric corrosion have also been developed (Simillion et al. 2014). These are, for example, microscopic models of isolated corrosion phenomena, namely crevice corrosion (Evitts 1997; Raunio 2015), corrosion under porous layers, pitting corrosion (Tsutsumi et al. 2007; Davenport et al. 2014; Krouse et al. 2014), as well as the modelling of local electrochemical methods (Simillion et al. 2014).

According to Adikari et al. (2014), models are only beneficial if they can be validated and provide sensible results so that predictions can be tested, which depend on the relevance and accuracy of the data collected, the level of understanding of the primary parameters, and the observations. Once corroborated, they can be utilised to approximate the required intervals between maintenance and remedial actions, evaluating the effectiveness of different corrosion mitigation approaches, assisting in the choice of suitable materials and coatings, as well as performing sensitivity analysis regarding underlying assumptions.

2.1.9 Atmospheric Corrosion Maps

Infrastructure relating to housing, business, public service, telecommunications, transport, power generation, electricity supply, radio/television broadcasting, aviation, mining and manufacturing are mostly exposed to open atmospheres and therefore, are susceptible to corrosion. According to NACE (EPA News 2014), the most recent corrosion cost study, sponsored by the United States of America (USA) Federal Highway Administration, was carried out in 2002. The results of this survey showed that in 2002, more than US$276-billion per year was spent in the USA to address corrosion

problems and implement preventative procedures. This number equates to approximately 3% of the USA's Gross Domestic Product (GDP).

Similar studies have also been conducted in other countries (Tullmin & Roberge 2000; EPA News 2014), including in South Africa in 1986 (Slabbert 1986). During the South African study, which covered the mining, power generation, shipping and transportation sectors, corrosion protection preventative measures, metal losses and replacement costs were estimated at R1 250-million/annum or US$625-million/annum. This number was based on an exchange rate of approximately US$1: R2 (BusinessTech 2016a) in those days, which amounted to roughly 5% of South Africa's GDP.

In line with The World Bank's (2017) numbers, South Africa's GDP in 2015 was US$314.6- billion (approximately R4 403-billion). By applying the 2002 USA figure of 3% of the national GDP as the cost of corrosion per annum, this means that at least R132-billion is spent annually in South Africa in trying to combat or prevent corrosion problems. Of this amount, atmospheric corrosion is viewed as a significant contributor, namely more than 50% or R66-billion (Li et al. 2013; Natesan et al. 2015). However, Badea et al. (2011) put this figure closer to 80%.

Atmospheric corrosion mapping is considered essential to the specification and selection of materials (Li et al. 2013), including in the management of infrastructure and mitigation of corrosion problems. Consequently, atmospheric corrosion maps have been developed for continents (Tullmin & Roberge 2000), islands (Rincon et al. 2000; Santana et al. 2001; Roberge 2012), countries (Callaghan 1991; Roberge 2012; Li et al. 2013; Natesan et al. 2015), large metropolitan areas (King et al. 1982; Tullmin & Roberge 2000), towns, industrial/operational plants, and even aircraft and aerospace operational centres (Kennedy Space Centre) (Tullmin & Roberge 2000).

The primary purpose is typically to provide a diagram that presents the regional corrosion behaviour (Adikari et al. 2014) of different metals and alloys, exposed to varying corrosive atmospheres. Corrosion maps are also considered extremely useful in most engineering fields, e.g. research, design, construction, maintenance, and operations, as well as from a public perspective. Roberge (2012) notes that corrosion maps are "*powerful tools for communicating information related to geographical landscapes*", which may also provide the following potential benefits:

- assisting with cost-effective corrosion protection solutions (Callaghan 1991) by aiding with the selection of suitable materials and protective coatings (Santana et al. 2001; International Organization for Standardization 2012a; South African Bureau of Standards 2013; Natesan et al. 2015);
- helping with risk-based planning, and the design of industrial and private works (Rincon et al. 2000; Janse van Rensburg 2010);
- forecasting of corrosion problems (Janse van Rensburg & Calitz 2004; Janse van Rensburg 2010);
- aiding in critical asset management (Janse van Rensburg 2010);
- assisting with the service-life predictions of materials (Janse van Rensburg 2010; International Organization for Standardization 2012a);
- enabling the development of best operating procedures (Janse van Rensburg 2010);
- assisting with comparisons between different corrosion protection systems (Janse van Rensburg 2010);
- improving plant sustainability (Janse van Rensburg 2010);
- improving life-cycle costing of new and maintenance materials (Janse van Rensburg 2010);
- assisting with the forecast of maintenance and inspections (Santana et al. 2001; Janse van Rensburg 2010);
- avoiding the use of more expensive corrosion resistant alloys by allowing the timeous maintenance of less corrosion-resistant materials; and
- assisting with the tailoring of site-specific corrosion protection specifications (Janse van Rensburg & Calitz 2004; Janse van Rensburg 2010).

Atmospheric corrosion maps are also advantageous in the sense that they provide potential means to assess the effects of pollution (King et al. 1982) and climate change (Cole & Paterson 2010; Li et al. 2013) on materials and the environment.

The principal methodologies followed in the corrosion mapping of large areas (Li et al. 2013) include:

A. Direct measurements of the corrosion rates of metals in regions of interest;
B. Classification using climatological results and the deposition rates of atmospheric pollutants; and
C. Classification using corrosion rate measurements, together with climatological variables and deposition rates of atmospheric contaminants.

Table 2.4 provides a summary of some of the approaches followed for the development of atmospheric corrosivity maps. As per the summarised data, it is apparent that concerning the accuracy and best understanding of the regional behaviour of atmospheric corrosion, the more sites, materials and corrosion mechanisms, as well as meteorological and pollutions variables that can be measured, over extended periods to determine long-term trends, the better. Also, about indoor and micro atmospheres, the use of generalised corrosivity data on a macroscopic scale is of little or no value (Tullmin & Roberge 2000).

From a South African perspective, country-wide measurement of the significant climatological and pollution parameters that affect atmospheric corrosion, combined with the direct analysis of atmospheric corrosion is considered unlikely at present. This conclusion has also been drawn by Prof. R. Sanderbergh (2016) of the University of Pretoria during his preliminary investigation concerning the potential modelling of the corrosivity of South Africa's macro atmosphere. This is since most air quality monitoring stations in South Africa presently do not measure atmospheric Cl^- concentrations, and those that do monitor SO_2 levels are not always reliable.

Consequently, with regards to the current corrosivity mapping of South Africa's and the GJMA's atmospheres, the approach is more like those used by King et al. (1982), Li et al. (2011) and Natesan et al. (2015), i.e. site-specific and contour-based, with the difference that mapping is also done using geoprocessing software. According to Tullmin & Roberge (2000), a grid pattern of sites can provide detailed corrosion mapping of regions, which can be valuable for planning, plant design and maintenance of infrastructure points of view.

Table 2.4 Approaches followed for atmospheric corrosion mapping, including their strengths and weaknesses.

Country	Methodology uses	Study period	Metal(s) used	Assumptions	Benefits	Limitations	References
South Africa	*Methodology A* Direct measurements of atmospheric corrosion at selected sites, representing principal corrosive atmospheres, i.e. rural, industrial, marine, marine-industrial sites.	20 years.	Mild steel, COR-TEN, zinc, copper, aluminium (3S, M57S, 5OS, B51S, D65S) stainless steel (430, 304, 316 3CR12).	Atmospheric corrosion occurs uniformly.	Provide the user with a basic understanding of the corrosion of mild steel and zinc, mainly along the coastal areas of South Africa. Corrosion products could be examined. Varied materials over many years evaluated.	Based on only eleven sites. Limited inland cities included. Overrating of the atmospheric corrosion of marine and inland environments. Exposure of metal specimens at a few isolated sites - providing insufficient information to the rate of corrosion of a country. Significant extrapolations.	Callaghan (1991)
India	*Methodology C* Direct measurements of atmospheric corrosion at 40 sites, with climatic and pollution parameter measurements at some of the locations.	One-year studies over a period of 11 years.	Mild steel, hot-dip galvanised steel, zinc and aluminium.	Atmospheric corrosion occurs uniformly. Some climatic and pollution parameters are viewed as more critical than others.	The corrosion behaviour of different metals studied.	The maps are area and not region specific.	Natesan et al. (2015)
Canary Isles	*Methodology C* Quantifying the corrosion experienced by metal specimens at 39 sites across three islands as per ISO 9223, including correlations with environmental parameters such as TOW, Cl^- and SO_2, and the influence of atmospheric salinity and its dependence on distance from the ocean.	Three years.	Mild steel.	Atmospheric corrosion occurs uniformly. Some climatic and pollution parameters viewed as more critical than others.	Includes direct measurement and dose/response estimation of the corrosion of mild steel, exhibiting high correlations. More detailed approach.	The width of the coastal outline exaggerated to correspond to a coastal strip of 500 m from the shoreline.	Santana et al. (2001)

Table 2.4 *Continued.*

Country	Methodology uses	Study period	Metal(s) used	Assumptions	Benefits	Limitation	References
Melbourne (Australia)	*Methodology A* Grid pattern (2 km apart) direct measurement of atmospheric corrosion at 300 sites, followed by contoured mapping by plotting procedure.	One to two years.	Special copper-bearing alloy steel that corrodes uniformly.	Atmospheric corrosion occurs uniformly.	Reveals corrosion trouble spots. Less expensive than the continuous monitoring of corrosive pollutants, e.g. Cl^- and SO_2.	The method requires many sites. Results may change from one year to the next.	King et al. (1982)
Sydney, Perth, Brisbane, Canberra, Adelaide, Melbourne, and Hobart (Australia)	*Methodology A* Direct measurements of atmospheric corrosion at selected sites. Not more than four sites per city.	Unknown.	Unknown.	Atmospheric corrosion occurs uniformly.	Less costly. Corrosion products could be examined.	Exposing metal specimens at a few isolated sites does not provide enough information to the rate of corrosion of a large city.	Martin & King (1981)
Catalonia (Spain)	*Methodology C* Direct measurements of atmospheric corrosion at 42 sites, including correlations with some climatic variables and SO_2.	Three years.	Carbon steel, aluminium, zinc, copper, brass and stainless steel.	Atmospheric corrosion occurs uniformly. Some climatic and pollution parameters viewed as more critical than others.	Corrosion products could be examined.	May change with time.	Costa (1987)
New Zealand	*Methodology C* Direct measurements of atmospheric corrosion at 39 sites, including correlations with 30-year trends of climatic parameters.	One year.	Mild steel and hot-dip galvanised steel	Atmospheric corrosion occurs uniformly. Some climatic and pollution parameters viewed as more critical than others.	Corrosion products could be examined.	Impossible to derive a clear relationship between variations in New Zealand's climate over the thirty-year period and atmospheric behaviour. The maps have limitations in their zone boundaries for some regions. Change in the corrosion rate with time. Different starting times of testing.	Li et al. (2013)

Table 2.4 *Continued.*

Country	Methodology uses	Study period	Metal(s) used	Assumptions	Benefits	Limitation	References
Sao Luis City (Brazil)	*Methodology C* Monitoring of the atmospheric deposition rates of Cl^-, SO_2 and dust at 15 sites, and correlations with meteorological data, as well as direct measurements of the atmospheric corrosion rates of metals. Mapping was done using geoprocessing software – ArcView 9.0 GIS (Geographic Information System) developed by ESRI.	Monthly over a period of < 1 year.	Mild steel, hot-dip galvanised steel, aluminium and copper.	Atmospheric corrosion occurs uniformly. Some climatic and pollution parameters are viewed as more critical than others.	Materials used in the electricity distribution and transmission lines were studied. Various climatological and pollution parameters were measured. Corrosion products could be examined. Better visualisation of the local corrosivity could be defined, according to the shading chloride concentration gradient shown on the map. More detailed approach.	The map considers atmospheric corrosion behaviour only in the critical period (dry season).	Sica et al. (2007)

2.2 THE HISTORY OF ATMOSPHERIC CORROSION MONITORING IN SOUTH AFRICA

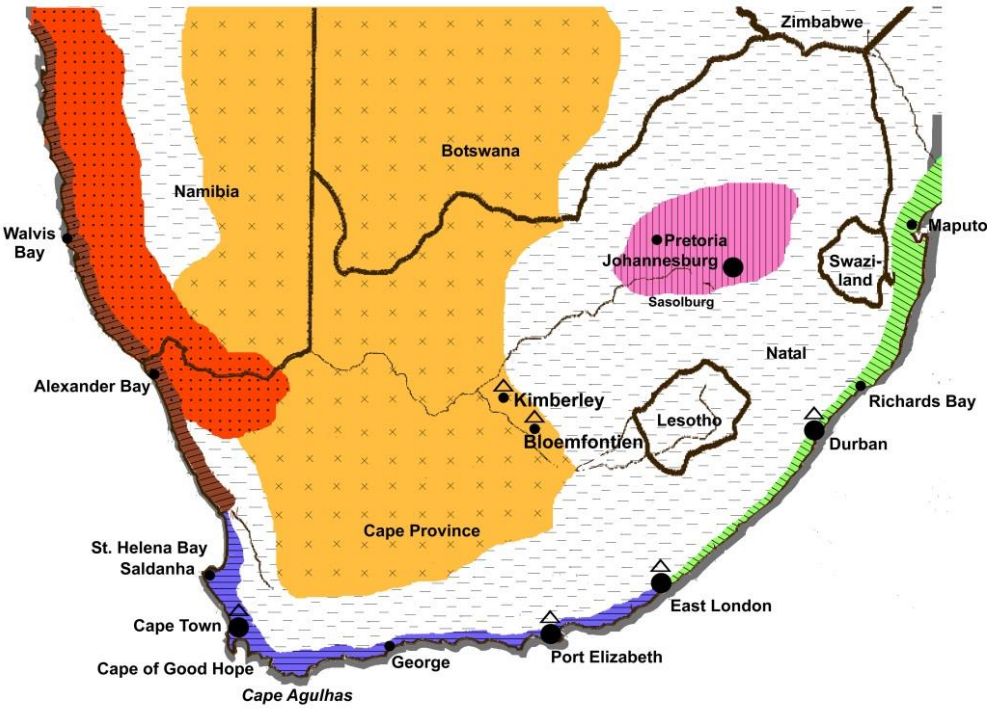
Pre-1970, several small atmospheric corrosion monitoring studies were conducted in South Africa. The CSIR (1975) and Callaghan (1991) provided comprehensive overviews of these very early exposure programmes. Of importance is that most of the initial studies primarily focused on the corrosion of aluminium in coastal atmospheres, located for instance in Durban, East London, and Port Elizabeth. However, the atmospheric corrosion of ingot iron, zinc, copper, sheet alloys (AISI Type 302), stainless steel, mild steel, lead and Monel was also investigated (Callaghan 1991).

Post-1970 to the early 1990s, the first national exposure programme was conducted by Brian G. Callaghan on behalf of the CSIR, over a period of 20 years (Callaghan 1991). His initial work involved two four-year exposure programmes, one of which included the exposure of a range of metals and alloys, while the other entailed metallic coatings on steel substrates at several sites throughout South Africa (CSIR 1975).

Due to shortcomings identified regarding the long-term trends of these early exposure studies, a twenty-year exposure programme was initiated. Callaghan's work, conducted at sites located in Cape Town, Port Elizabeth, Gobabeb, Standfontein, Walvis Bay, Pretoria, Sasolburg, False Bay, Durban, Simonstown and East London, culminated in the publication of the Callaghan map in 1991 (**Figures 1.1 & 2.15**).

During Callaghan's studies, quantitative 1-, 2-, 5-, 10- and 20-year corrosion rates were provided for mild steel, COR-TEN A, zinc, copper, aluminium (2S, 3S, M57S, 5OS, B51S and D65S), stainless steel (430, 304 and 316) and 3CR12 (pickled) (Callaghan 1991) .

From 1990 to 1993, Eskom also conducted atmospheric corrosion studies along the Eastern, Southern and Western Cape coastlines (Gross & Nixon 1993). This study mainly involved the exposure of wire-on-bolt (CLIMAT/ATCORR) units; manufactured corresponding to ASTM G116:1999 (ASTM International 2004) procedures, to the corrosive marine atmospheres.



Key:	Description	Type of corrosion	Mild steel corrosion rate µm/year	Galvanised steel sheet life in years
	Inland arid	Semi desert	5 – 10	> 30
	Inland	Rural	10 – 20	> 20
	Inland dry	Desert	< 5	> 30
	Inland urban	Inland industrial	15 – 40	5 – 15
	Inland	Industrial	10 – 30	5 – 15
	Sub-tropical marine	Medium to severe marine	50 – 80	3 – 5
	Desert marine (mists)	Severe marine corrosion	80 – 100	0.5 – 2
	Temperate Marine	Marine	30 – 50	3 – 7
	Intertidal to 5 km inland	Severe marine corrosion	100 – 300	Up to 3

Figure 2.15 Atmospheric corrosion map of Southern Africa - An adaptation of the Callaghan (1991) map by Janse van Rensburg (2005).

A five-year corrosion study was simultaneously launched relating to the atmospheric corrosivity of sites in other areas along the South African coastline, as well as in the Southern and Eastern Highveld regions. This work was carried out by Nixon (1993), Janse van Rensburg (1994), Colloby (1995) and Northcott (1999). It involved the exposure of mild steel, copper, aluminium, zinc, galvanised mild steel, stainless steel and 3CR12 panels to different corrosive atmospheres. Changes in the electrical resistance of iron, zinc, copper, and aluminium were also investigated (Colloby 1995). These studies were mainly conducted at locations near Melkbosstrand, Klienzee, Richards Bay, Kriel, Sasolburg, Elandsfontein, Bethal (Palmer), Volksrust and Vanderbijlpark.

During 1991 to 1994, a three-year project was also launched by the CSIR in the Eastern parts of the Gauteng Highveld region. This project was in conjunction with Eskom, namely at Pretoria, Grootpan (close to Ogies), Elandsfontein, and Verkykkop (in Volksrust) (Nixon & Janse van Rensburg 1992; Nixon 1993; Gnoinski & Ramothlola 1994; Janse van Rensburg 1994). The purpose of the CSIR research work carried out by Gnoinski, Ramothlola, and Tullmin (1994), was mainly to determine the effectiveness of a rapid method for the assessment of atmospheric corrosion.

Numerous atmospheric corrosion tests were also carried out by John E. Leitch, over a period of more than 20 years (Leitch 2003). This work was done mainly on behalf of Hulett Aluminium (Pty) Ltd., the CSIR, Eskom, and other interested parties. During earlier years, Leitch's work primarily involved the exposure of wire-on-bolt units to different corrosive atmospheres - to classify the atmospheres of sites using the CLIMAT method (Doyle & Goddard 1966). However, with the inception of the ISO corrosivity classification procedures in 1992, described in detail in ISO 9226:1992 (International Organization for Standardization 1992b), most of Leitch's studies in his later years were conducted in accordance with the open wire helix (zinc and aluminium) method (Leitch 1999; Leitch 2006).

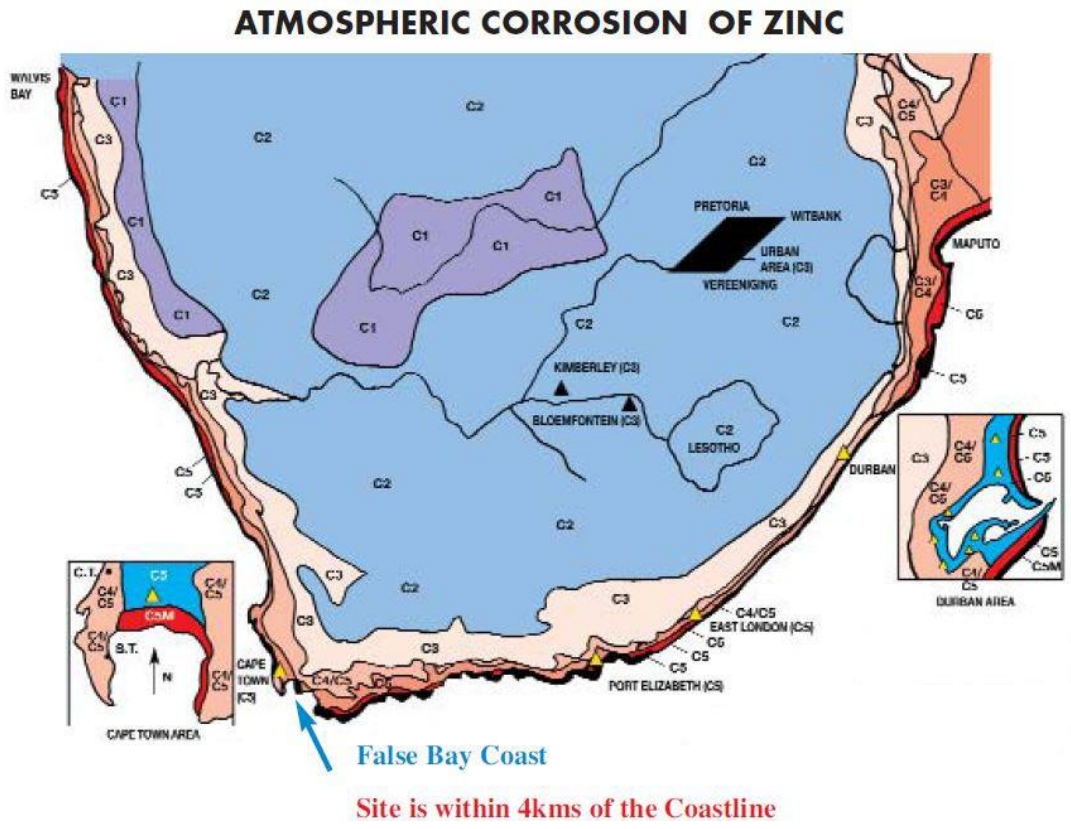
Leitch's work culminated in the publication of an updated corrosion map of South Africa in 1999 (Leitch 1999) (**Figure 1.2**), and again in 2003 (Leitch 2003) (**Figure 1.3**), with the latter chart having been subsequently incorporated into SANS 1796:2013 (South African Bureau of Standards 2013).

Leitch's maps were hailed in the sense that they represented the first attempts by a South African researcher to classify the corrosivity of atmospheric environments based on the ISO 9223 and ISO 9226 procedures (International Organization for Standardization 1992a, 1992b). Leitch employed the ISO 9226:1992 open wire helix technique at Cape Town, Mossel Bay, Port Elizabeth, Durban, Umhlanga and Richards Bay (Leitch 2003).

The Hot Dip Galvanizers Association of Southern Africa (HDGASA) also published an updated atmospheric corrosion map of zinc (after the Callaghan map) based on the ISO 9223:1992 classification system (HDGASA 2005). This map is presented in **Figure 2.16**.

Additional work worth mentioning is that of Vosloo of Eskom, in partnership with Pietersen and Holtzhausen of the University of Stellenbosch (Pietersen et al. 2004). Their studies mainly involved the development of an insulator pollution severity application map for South Africa (**Figure 2.17**), which significantly added to the knowledge base about atmospheric pollution in South Africa. Calitz & Potgieter (2005) also conducted atmospheric corrosion studies of overhead power transmission conductors at a marine site near Koeberg Nuclear Power Station, situated along the Western Cape coastline.

During 2001 to 2004, the CSIR provided limited atmospheric corrosion data for one site in Johannesburg in a collaborative study with eleven other countries in Asia and Africa, as part of the Swedish International Development Agency (SIDA) funded Programme on Regional Air Pollution in Developing Countries (RAPIDC) (Tidblad et al. 2007). This study entailed actual corrosion measurements of carbon steel, zinc, and copper, over 1-, 2- and 4-year periods, as well as estimations of the corrosion rates of these metals, based on the ISO 9223:1992 dose-response model (Foax et al. 2009). Of note is that the estimations for the corrosion rates of zinc and copper in Johannesburg were significantly higher than the actual measured values. This was based on the ISO 9223 dose-response functions for SO_2 (International Organization for Standardization 1992a).



Corrosion category	Description of environment	Corrosion rate (average loss of steel in µm/a)	Corrosion rate (average loss of zinc in µm/a)
C1	Interior: dry	≤ 1.3	≤ 0.1
C2	Interior: occasional condensation Exterior: exposed rural inland	> 1.3 to 25	0.1 to 0.7
C3	Interior: high humidity, some air pollution Exterior: urban inland or mild coastal	> 25 to 50	0.7 to 2.1
C4	Interior: e.g. swimming pools and chemical plants Exterior: industrial inland or urban coastal	> 50 to 80	2.1 to 4.2
C5-I or C5-M	Exterior: industrial with high humidity or high salinity coastal	> 80 to 200	4.2 to 8.4

Figure 2.16 The HDGASA map – based primarily on Callaghan's data (HDGASA 2005).

https://www.scribd.com/document/272793619/Corrosion-Resistance-for-Steel

NOT PUBLICLY AVAILABLE

Key

Pollution Classification	mm/kV	
Light	16	
Medium	21	
Heavy	25	
Very Heavy	≥ 31	

Figure 2.17 Vosloo's, Pietersen's and Holtzhausen's pollution map of South Africa – taken from Janse van Rensburg (2005).

The AEI (Agricultural Engineering Institute) also launched an eleven-year atmospheric exposure programme on five diverse types of agricultural wire at seven sites in South Africa. Findings of this work, which dates to December 1990, are currently still used to provide recommendations regarding suitable fencing materials in different corrosive environments (O'Donnell et al. n.d.). Materials tested included light galvanised, heavy

galvanised, aluminium coated, Galfan, and 3CR12 wire, which was exposed at Bathurst and Riviersonderend. Work in this field was also conducted by R.J Bronkhorst and K.L Rodseth (O'Donnell et al., n.d.).

Janse van Rensburg (2005) initiated one of the most significant atmospheric corrosion programmes in South Africa. This study, on behalf of Eskom, was carried out between 2005 and 2010, involving atmospheric corrosion monitoring of 50 sites throughout South Africa - covering inland and coastal regions. Janse van Rensburg also conducted smaller studies at other locations. Selections and statistical analysis of this work are made public for the first time in the results and discussion chapters of the thesis, as well as in the form of new corrosion maps for South Africa (based on different metal types).

In June 2012, Slamova et al. (2012) carried out a potential mapping of atmospheric corrosion of the world's coastal environments. In order to enable the approximation of the distribution of sea salt levels in the coastal areas of the world, two approaches were followed, namely:

a) a "*geo-statistical analysis method… for interpolating chloride deposition data*" and;

b) "*modelling of the environmental conditions… affecting source and distribution of airborne salinity*".

According to Slamova et al. (2012), the evaluation of atmospheric corrosion of the coastal regions was based on the ISO 9223 methodology (International Organization for Standardization 2012a). The result was the mapping of atmospheric corrosion in coastal areas on a worldwide basis, including South Africa (as indicated in **Figures 2.18 & 2.19**). However, examining Slamova et al.'s (2012) maps, it is evident that the corrosivity of South Africa's coastline has been dramatically overstated, particularly moving inland. According to the Callaghan (1991) map, as well as subsequent work done by Leitch (1999, 2003, 2006) and Janse van Rensburg (1994, 2010), it has been found that the corrosivity of South Africa's coastline decreases rapidly within the first 5 km from the sea, due to the settling of salts, changing topographical, shielding and environmental conditions. These changes, however, are not reflected in the Slamova et al. (2012) maps.

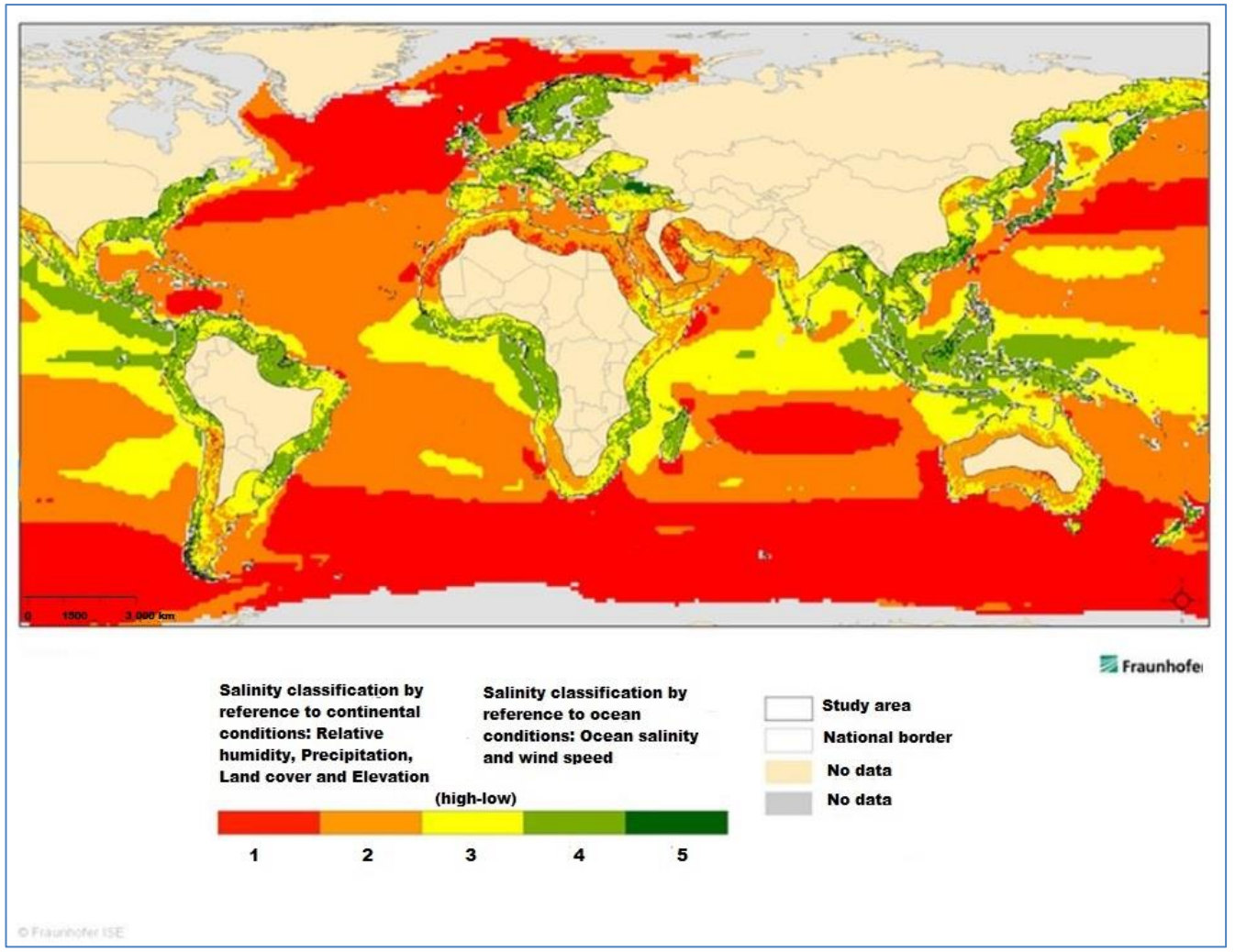


Figure 2.18 Classification of airborne salinity by reference to continental and ocean conditions (Slamova et al. 2012).
https://www.researchgate.net/publication/233841501_Mapping_atmospheric_corrosion_in_coastal_regions_methods_and_results

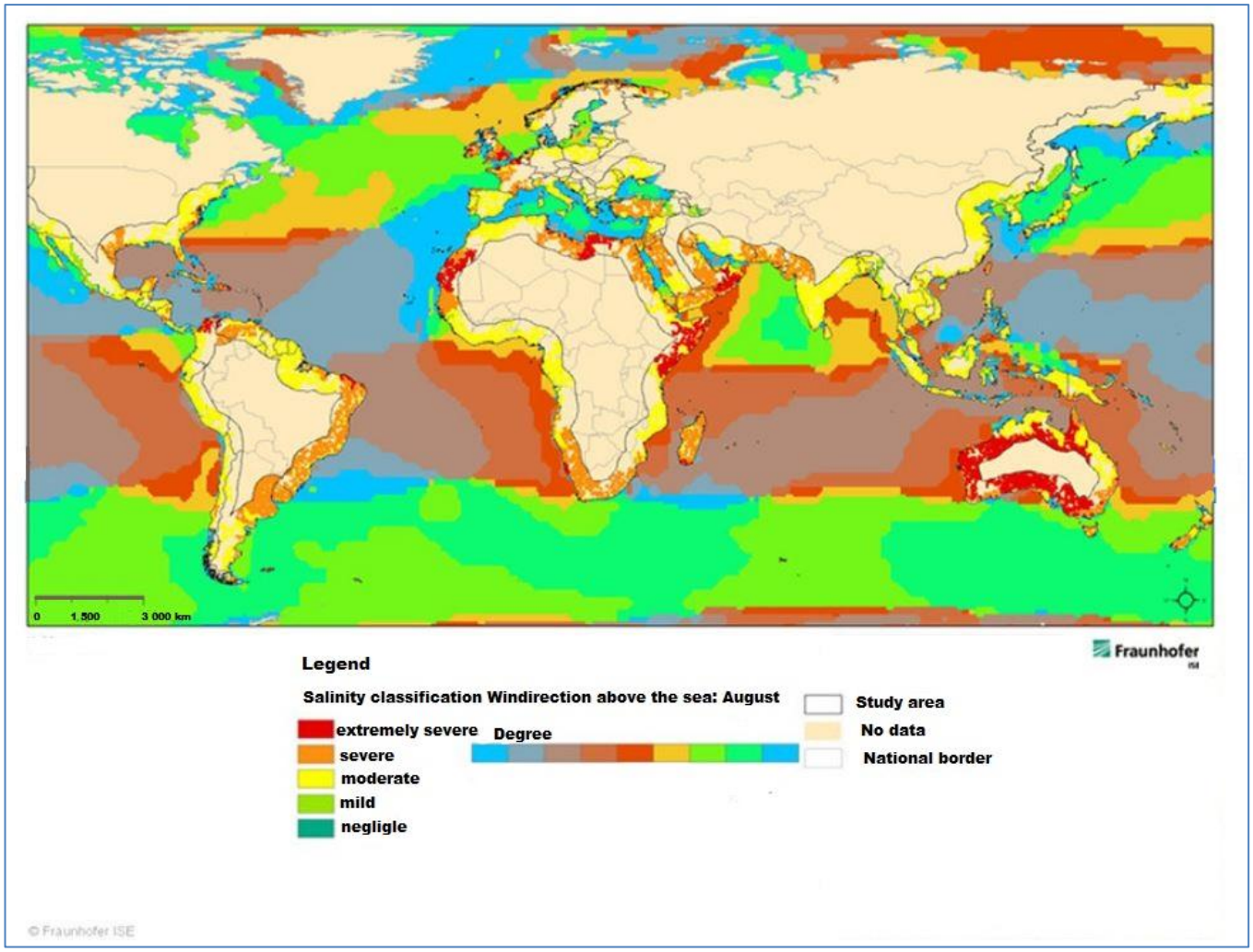


Figure 2.19 Airborne salinity classification, including the wind condition for the summer climatic situation (Slamova et al. 2012).

https://www.researchgate.net/publication/233841501_Mapping_atmospheric_corrosion_in_coastal_regions_methods_and_results

Based on a critical review of the different studies mentioned above, shortcomings relating to the atmospheric corrosion data of South Africa's inland and metropolitan areas were identified. This necessitated further investigation. Consequently, the latest study was launched in 2013, involving the atmospheric corrosion monitoring of 57 sites in and around the GJMA. This work was funded by Orytech (Pty) Ltd, the University of the Witwatersrand (Wits), the DST-NRF Centre of Excellence in Strong Materials and the HDGASA, of which the methodology, results, and conclusions are discussed in Chapters 3 to 7 of the thesis.

During the same period, the University of Pretoria conducted their preliminary work concerning the modelling of the corrosive conditions of South Africa's atmosphere (Sandenberg 2016). Unfortunately, the work was halted due to a lack of available countrywide air quality data.

2.3 FACTORS THAT MAY DRIVE ATMOSPHERIC CORROSION IN THE GJMA

The Greater Johannesburg Metropolitan Area (GJMA), also known as the Witwatersrand or Rand, located in the province of Gauteng/"Place of Gold", is considered the heartland of the South African economy (Jonathan Ball Publishers 2014; South Africa.info 2015). It is also one of the fastest growing metropolitan areas in Africa (Mathee & von Schirnding 2003).

It is a big mining, industrial, business, residential and even rural expanse that extends from east to west (Nigel to Randfontein) for about 80 km and from north to south (Diepsloot to Orange Farm), 63 km (**Figure 2.20**) (Google Inc. 2016a). It covers the City of Johannesburg (CoJ) Metropolitan Municipality, the East Rand and West Rand, which includes several important centres. The region is located roughly at a latitude of 25° 55′ to 26° 56′ South, and a longitude of 27°.41′ to 28° 52′ East, with a total estimated surface area of 3 389 km² (about 20% of Gauteng Province's surface area) (Google Inc. 2016a).

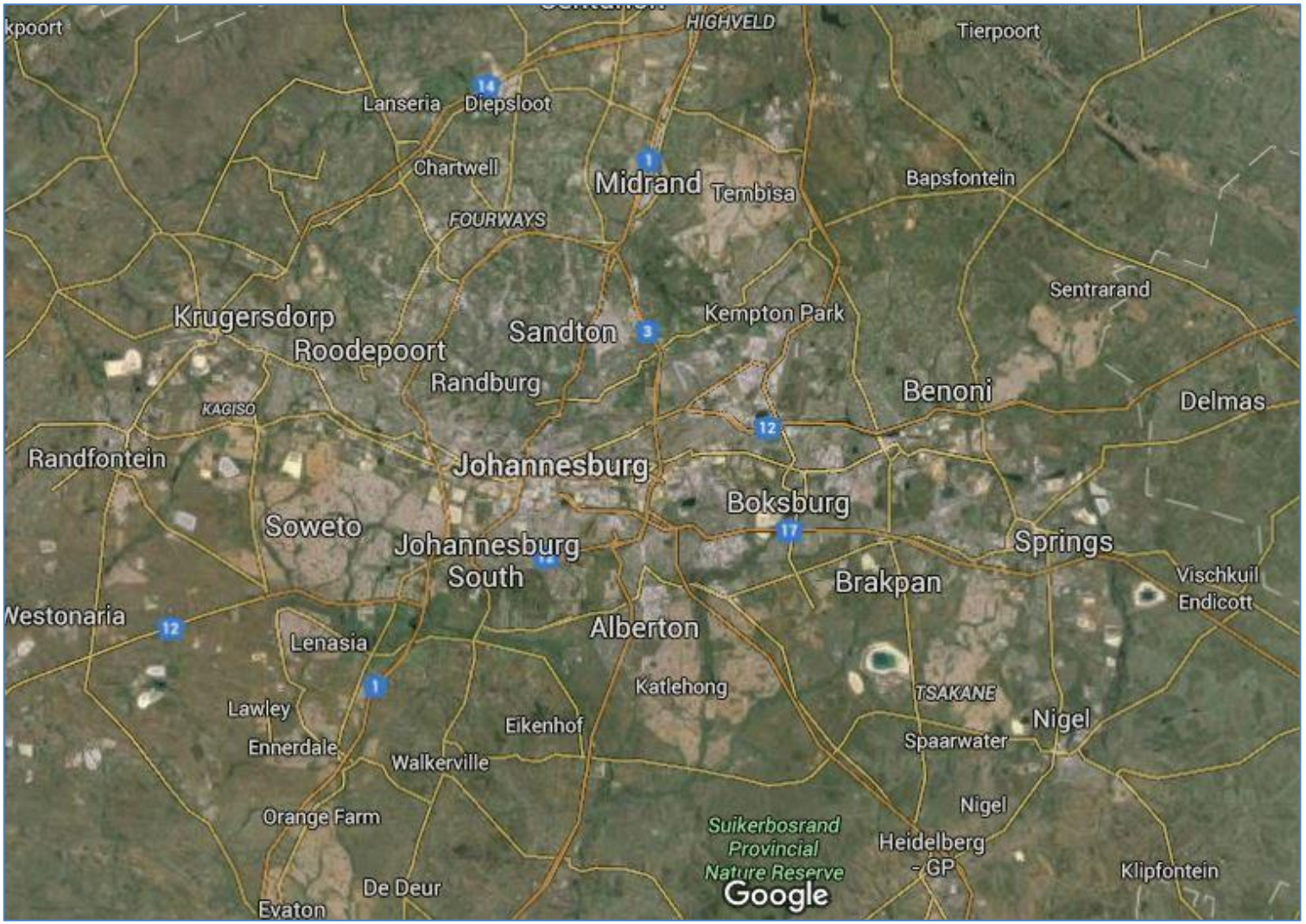


Figure 2.20 The Greater Johannesburg Metropolitan Area (GJMA) – Source: Google Inc. (2016a).

Given that a primary objective of this study was to provide a corrosion profile map of the GJMA, this section of the thesis aims to deliver a comprehensive sketch of the study area, by outlining various socio-economical, meteorological, topographical, biome and environmental parameters that may influence atmospheric corrosion processes in the region. Some of the data presented in this chapter have been sourced from newspapers and websites, as well as from local and governmental reports, making it difficult to evaluate the quality thereof. However, these data were only consulted where other suitable literature (e.g. peer-reviewed articles and books) were unavailable.

2.3.1 Population and Density

Based on the 2017 mid-year population estimates by Statistics South Africa (Statistics South Africa 2017b), it was projected that Gauteng is home to more than 14 million people, which encompasses approximately 25% of South Africa's total population of 56.5 million inhabitants. See also **Figure 2.21** (Brand South Africa 2017). This places the GJMA area in the upper 15 largest urbanised areas in the world (De Wet et al. 2008).

The region also has the highest population density in South Africa (Du Toit 2001), at 863 people/km^2 (based on Statistics South Africa's 2016 projected figure). The total surface area of Gauteng is 16 548 km^2 (Oxford University Press Southern Africa (Pty) Ltd 2006).

In accordance with Statistics South Africa's data, as adapted by Adrian Frith (2016), the respective populations of the different zones of the CoJ Metropolitan Municipality alone were indicated in 2011 as approximately 4.4 million people. Additionally, populated sections of the Ekurhuleni Metropolitan Municipality, Mogale Local Municipality and Randfontein Local Municipality were included in the GJMA study (**Appendix A – Tables A.1 – A.4**).

Consequently, the total estimated population of the GJMA study area is just below seven million people (as calculated from the Census 2011 data). Noteworthy is that the Johannesburg's CBD, as well as the Apartheid-era institutionalised 'township' areas, exhibit the highest population densities, e.g. Alexandra, Ivory Park, Mayibuye and Tembisa (**Appendix A - Figure A.1**).

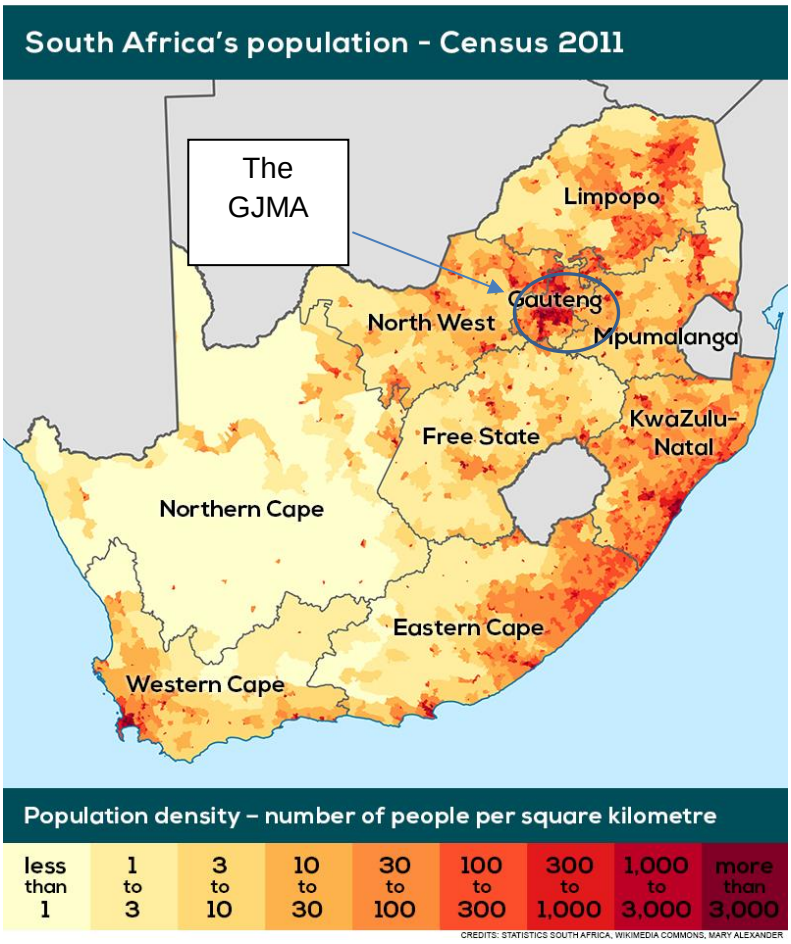


Figure 2.21 Population densities in South Africa – Source: Brand South Africa (2017).

https://www.brandsouthafrica.com/people-culture/people/south-africas-population

2.3.2 Development of the GJMA

The development of Johannesburg and its surrounding areas was initially founded on gold mining (South African History Online 2011). However, since the initial discovery of gold, numerous supporting businesses and industries have sprouted along the 'gold-bearing reef' of the Witwatersrand Basin (City of Johannesburg 2008), resulting in the growth of a large multi-nodal metropolitan region (City of Johannesburg 2007a). At present, the GJMA's leading economic sectors include finance, business, community, and social services, as well as manufacturing and trade (Why Joburg.com 2016; Local Government 2016). Johannesburg today is the headquarters to various multinational corporations and the transportation hub of Southern Africa (Junior Worldmark Encyclopedia of World Cities 2016). According to Statistics South Africa (2017a), Johannesburg is also the single largest metropolitan contributor to the economy in

South Africa, adding approximately 16% (R117 billion) to the national reserves (City of Johannesburg 2003).

The land-use as indicated by the City of Johannesburg Metropolitan Municipality in 2009, is presented in **Figure 2.22** (based on the City of Johannesburg's (2009)) data.

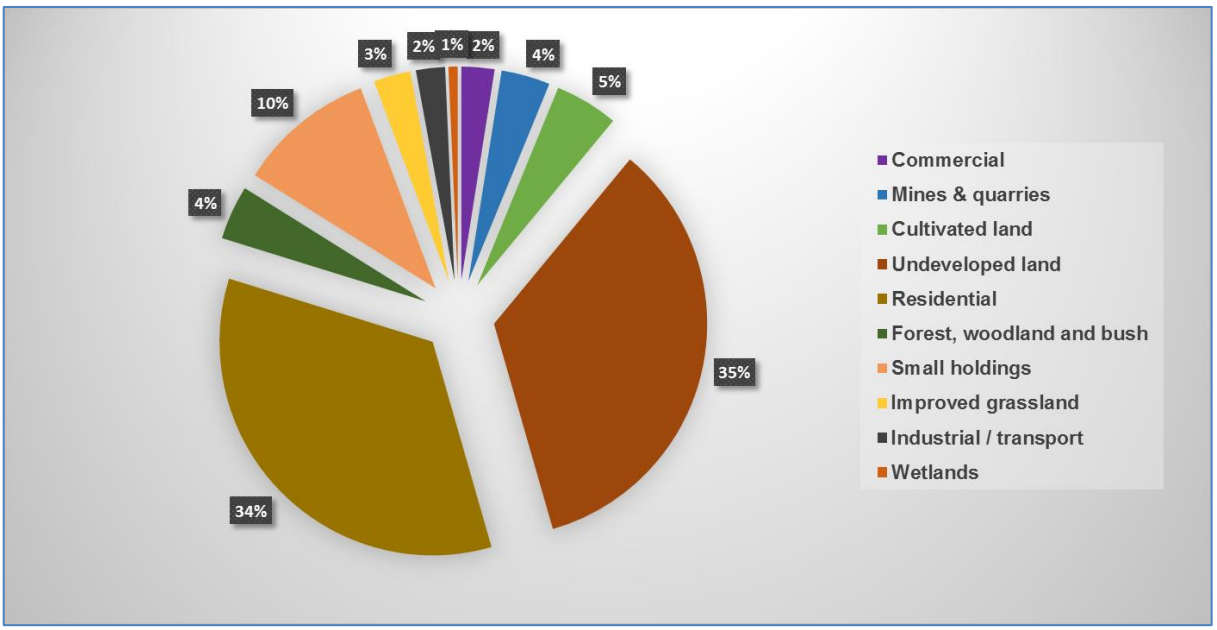


Figure 2.22 Land-use categories (as percentages) of the total surface area of the CoJ – Based on the City of Johannesburg's (2009) data.

2.3.3 Housing

Housing ranges from open-spaced, well-developed residential regions and estates, to highly dense townhouse complexes and apartment blocks, as well as large sprawling informal settlements (Mathee & von Schirnding 2003), and shantytowns, spread mainly on the outskirts of the cities, towns and suburbs. Apart from vast residential areas, the region also enfolds large recreational parks (e.g. Kliprivierberg Nature Reserve, Melville and Northcliff Koppies, Delta Park, Emmerentia Dam and Florida Lake) set aside for nature conservation and community recreation. Regarding the CoJ alone, about 88% of housing is classified as formal residential and near 8% as informal settlements (Cooper 2016). Nuttall and Mbembe (2007) correctly describe Johannesburg and its surrounding areas, as a "*complex mélange of city and township*".

2.3.4 Gold Mine Tailing Dumps

The GJMA is known for its massive yellow-white gold mine tailing dumps, spread primarily to the east and west of the CoJ, reaching as far as Randfontein to the west and Nigel to the east (Stassen 2015) (**Figure 2.23**) (Google Inc. 2017a).



Figure 2.23 A 3D-view of the yellow gold mine tailing dumps along the gold-bearing reef of the GJMA – Source: Google Inc. (2017a).

It is estimated that the gold mines in this region cover approximately 400 km^2 (Vidal 2011; Stassen 2015), roughly 8% of the total surface of the GJMA. However, as the "*waste gold-bearing ore*" dumps are presently being reprocessed (Why Joburg.com 2016), particularly those located to the south (Mathee & von Schirnding 2003), these may disappear from Johannesburg's landscape in the foreseeable future. Nonetheless, mining currently continues in the West Rand (Mathee & von Schirnding 2003). It is important to note that according to the well-known environmental activist, Mariette Lieferink, the dumps are considered a primary source of local water and atmospheric pollution (Vidal 2011).

2.3.5 The Industrial Heart

The industrial heartland of the GJMA is located mainly towards the west, south-east, east and to the north-eastern parts of the region, in and around Germiston, Edenvale, Isando and Modderfontein. The latter suburb is the home of four large explosive factories, three acid plants (for sulphuric and nitric acids production) and two acid regeneration facilities (Jonathan Ball Publishers 2014).

Germiston is said to exhibit the highest density of factories in South Africa, involving mainly the manufacturing of engineering components, building materials, chemicals, explosives, ammunition, tools, glass, furniture and textiles (Jonathan Ball Publishers 2014). To the north-east of the CoJ, at Chloorkop, chlorine, caustic soda and chloralkali derivative plants are produced (NCP Chlorchem 2011-2017).

2.3.6 Airports

The GJMA is home to at least four airports, namely OR Tambo, Lanseria, Rand and Grand Central, although smaller airfields also exist. OR Tambo, which is located to the east in Kempton Park, and Lanseria (positioned to the west) are both international airports. The former is Africa's most significant and busiest airport with an air traffic movement of 212 580 flights per annum or approximately 582 flights per day (Airports Company South Africa 2016).

2.3.7 Transport

The Johannesburg Metropole is engulfed by a network of highways and standard roads, which according to a 2011 South African Tom Tom survey, carry more than 3.8 million drivers on Johannesburg's roads every day (Jonckie 2011). It is claimed that the Ben Schoeman Highway is the busiest road in South Africa (Manana 2011), with at least 180 000 vehicles using this section of the N1 highway between Johannesburg and Pretoria during rush-hour per day (Engineering News 2008).

2.3.8 Railway

Rail infrastructure also exists, primarily commuting people in and out of the Johannesburg CBD, the East Rand, Soweto and Roodepoort. A rapid electrically driven rail network (approximately 80 km in length) runs between Pretoria and the Johannesburg CBD, as well as between Sandton and OR Tambo International Airport (Bohlweki Environmental (Pty) Ltd 2002; Gautrain 2016).

2.3.9 Gas, Power and Telecommunications Infrastructure

The GJMA has a well-developed power network, which includes two operational coal-fired power stations (Kelvin A and Kelvin B), located in the eastern parts of the region, with a combined power generating capacity of 600 MW (Kelvin Power 2016).

According to Census 2011 statistics, about 91% of the city's households have electricity (Cooper 2016). The Johannesburg Metropolitan area is also serviced by a natural gas reticulation network, namely Egoli Gas. The gas is supplied by Sasol and stored at a facility in Langlaagte. The gas network extends to Midrand in the north, Bruma in the east, Orange Farm in the south and Roodepoort in the west (Egoli Gas 2016).

2.3.10 Business and Commercial Infrastructure

The corporate heart is located more in the centre and northern parts of the region. During the past 15 to 20 years or so, the leading business centre of the GJMA has shifted towards Sandton, which is located to the north of the CoJ. This area is at present seen as the new financial centre of South Africa (Gauteng Conference Centre 2016).

2.3.11 Water

It is often maintained that Johannesburg is the only significant Metropole not located close to a significant natural water source, e.g. river, lake or the sea (City of Johannesburg 2003; City Lodge Blog 2012). However, the area has at least twelve smaller river systems, meandering through its suburbs (City of Johannesburg 2013; Gauteng Conference Centre 2016).

2.3.12 Dams, Nature Reserves, Recreational Parks and Vegetation

As per the different departments of the City of Johannesburg, the city has 18 500 ha of developed and undeveloped open space or green areas. This includes 4 443 ha of open veld, in excess of 2 000 parks (Mayuchi 2008), a zoo (55 ha) (Johannesburg City Parks and Zoo 2016), 35 cemeteries, 17 nature reserves, rivers and hiking trails (87 ha), pavements, botanical gardens (80 ha), 106 dams and numerous bird sanctuaries (63 ha) (City of Johannesburg 2007b).

Noteworthy is the fact that many trees are found in the region. There are over ten million trees (Hardy & Nel 2015), of which 1.6 million are street trees (Mayuchi 2008). It is claimed that the planting of trees in urban areas may change local climatic conditions and cause an urban heat island (UHI) effect, referring to urban areas where the surface temperature is higher than the surrounding areas (Hardy & Nel 2015). Trees may increase or reduce local temperatures, remove air pollutants (particulate matter, O_3,

SO_2, NO_2, and CO), reduce the emissions of VOCs, as well as decrease building energy usage (e.g. using shading and blocking of winds (Nowak 2002). Consistent with Hardy & Nel (2015), those areas with the highest vegetation in the GJMA, tend to exhibit lower ambient temperatures than less vegetated areas, whereas densely populated regions tend to be warmer than sparsely populated places. The UHI effect is the highest in the Northern Suburbs in the evenings, as well as in areas where building density is high. Conversely, it is the lowest in locations near dams and streams, as well as in highly dense vegetated areas.

From an untransformed perspective, the biome of the region may be classified as temperate grasslands (Oxford University Press Southern Africa (Pty) Ltd 2006).

2.3.13 Topography of the GJMA

The GJMA is located at an elevation ranging from 5700-5930 feet (1740-1810 meters) (Junior Worldmark Encyclopedia of World Cities 2016) in the eastern plateau of South Africa (Oxford University Press 2004), known as the Highveld or “Rand” (Junior Worldmark Encyclopedia of World Cities 2016). The CoJ stretches across the Witwatersrand, a protruding rocky ridge in the region, which falls to the north and south. The ridge runs mainly through the City in an east-west direction. Towards the north and west, the GJMA has rolling hills, whereas the eastern parts consist of rolling plains (Gauteng Conference Centre 2016).

2.3.14 General Meteorology of the GJMA

The general climate of the Greater Johannesburg may be classified as temperate (not too warm or too cold), with typical warm, wet summers and cloudless, cold, dry winters (Oxford University Press Southern Africa (Pty) Ltd 2006; Jonathan Ball Publishers 2014). The temperature of the region is significantly influenced by its higher altitude (City of Johannesburg 2003). Consequently, temperatures tend to be lower than in other areas at similar elevations.

Rainfall, which occurs mostly in the afternoons as brief electrical storms (Gauteng Department of Agriculture and Rural Development 2011; Jonathan Ball Publishers 2014), happens during summer from November to March. The yearly average is between 600 mm and 800 mm (Oxford University Press 2004), which is approximately

17% below the world average. However, the average annual figures vary significantly, making drought a 20% to 25% probability (Oxford University Press Southern Africa (Pty) Ltd 2006), for example during 2015, when Johannesburg and the rest of South Africa, experienced one of the worst droughts on record due to an El Niño event. This was caused by the natural warming of the surfaces water of the Pacific Ocean – transpiring every two to seven years (News24 2015). Also, hail frequently occurs during summer (Gauteng Department of Agriculture and Rural Development 2011).

Figure 2.24 (Callaghan 1991; McEwan 2004) presents a dated (before 1984) relative humidity isograph for OR Tambo International Airport. As shown, the percentage moisture in the atmosphere of the GJMA region tends to be higher from mid-spring to mid-autumn, as well as during night-time, from approximately 8:00 p.m. to 8:00 a.m. The average annual relative humidity is given as approximately 60%, ranging from about 47% in August to near 71% in February (ClimaTemps.com 2017a). See also **Figure 2.25**, which has been derived from ClimaTemps.com's (2017a) data.

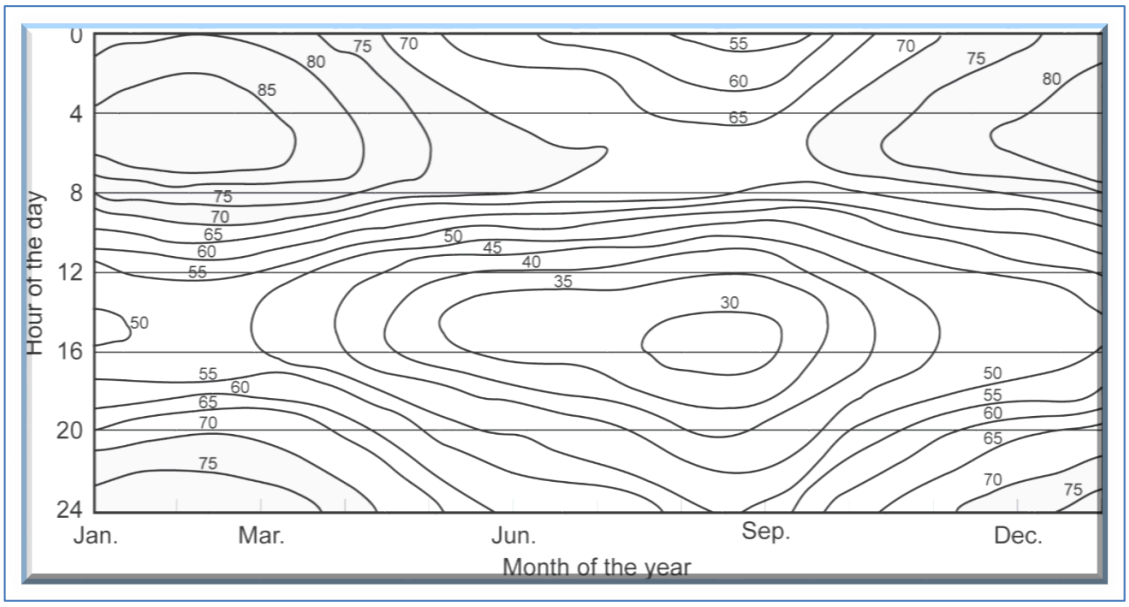


Figure 2.24 Relative humidity isograph (before 1984) for OR Tambo International Airport - Sources: Callaghan (1991) and McEwan (2004).

http://www.corrosioninstitute.org.za/#

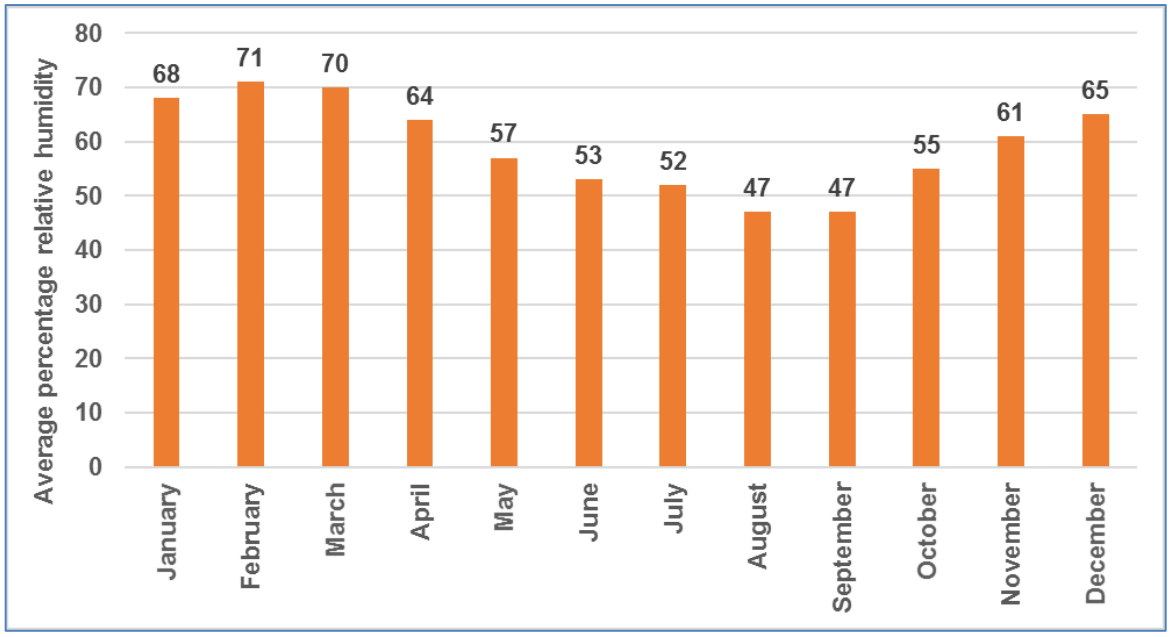


Figure 2.25 Average monthly relative humidity for Johannesburg – as measured at OR Tambo International Airport – Derived from ClimaTemps.com's (2017a) data.

As stated by ClimaTemps.com (2017b), Johannesburg may be classified as having a "*mid-latitude steppe/semi-arid cold climate (Köppen-Geiger classification: BSk*)" and is located near the warm temperate dry forest biome (as per the Holdridge life zones system of bioclimatic classification). The average temperature per annum is given as approximately 16°C and the mean monthly temperature change equal to 10°C, indicating that the "*continentality type is hyperoceanic, subtype barely hyperoceanic*" (ClimaTemps.com 2017b).

The Highveld area is also known for significant diurnal temperature fluctuations, especially during the winter months, making dew and frost common (McEwan 2004; Gauteng Department of Agriculture and Rural Development 2011). The latter is a frequent occurrence during the winter months in the southern areas of the GJMA, due to the dry, cold and windless conditions (Gauteng Department of Agriculture and Rural Development 2011). The average daily maximum temperature during June (winter) is approximately 18°C and during January (summer), 26°C (South African Weather Services 2014), as measured at the OR Tambo International Airport weather station.

According to Statistics South Africa (2004), the highest rainfall recorded in the Johannesburg area was in 1917, 1903 mm, and the lowest in 1992, 509 mm. (Statistics

South Africa 2004). The highest rainfall often corresponds with the rocky ridge that runs east-west across the GJMA, with typically Northcliff, Melville Koppies, Houghton, etc. (**Figure 4.26**) experiencing elevated levels (City of Johannesburg 2003). The lack of moisture in the Johannesburg atmosphere during the chilly winter months is also illustrated in **Figures 2.24 & 2.25** (Callaghan 1991; McEwan 2004; ClimaTemps.com 2017a).

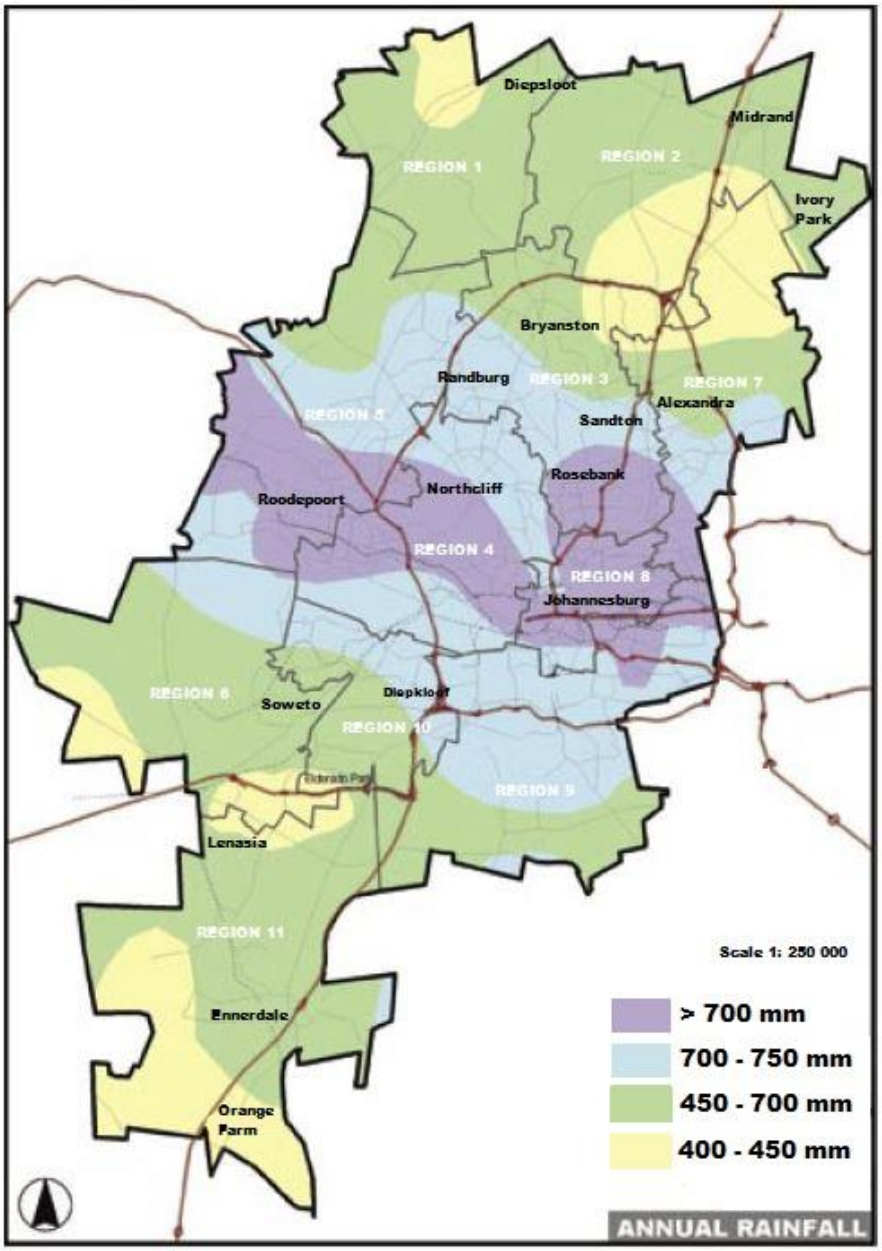


Figure 2.26 Annual rainfall distribution pattern for the CoJ – Adapted from City of Johannesburg (2003).

During winter, the area is known for general mild sunny days and sometimes bitter cold nights, especially in the South (Jonathan Ball Publishers 2014), decreasing to an average minimum temperature of roughly 5ºC in June, as measured at OR Tambo International Airport (South African Weather Services 2014). Regular cold fronts with cold southerly winds can result in nightly temperatures decreasing to below 0°C (South African Weather Services 2014; South Africa.info 2015).

Snow may also occur, although rarely. The daily average temperature of the GJMA increases slightly (by about 1°C) from south to north (moving towards Pretoria), and from west to east (moving towards Emalahleni). This may be attributed to changing altitudes and movement towards the equator (Gauteng Conference Centre 2016).

Due to the global climate change, Barney Kgope, the Director of Air Quality and Climate of the Department of Environmental Management indicated that based on climate models, Johannesburg is likely to become not only warmer (by about 2.3ºC) by 2056-2065, but also increasingly humid (City of Johannesburg 2012).

Using ClimaTemps.com's (2017b) (**Figure 2.27**) weather data for Johannesburg, the annual climatic averages are given as indicated in **Table 2.5**.

The windiest time of the year (as measured at the OR Tambo International Airport Weather Station), is from August to March, when the average wind speed varies from 4-5 m/s (**Figure 2.28** – derived from South African Weather Services (SAWS) 2014 results). A wind rose for Johannesburg, based on 2007 to 2016 data, is presented in **Figure 2.29** (SAWS 2017). The graph illustrates that the most frequent wind direction during the year at OR Tambo International Airport is in a south-easterly to a southerly direction, with average wind speeds reaching up to 8-11 m/s.

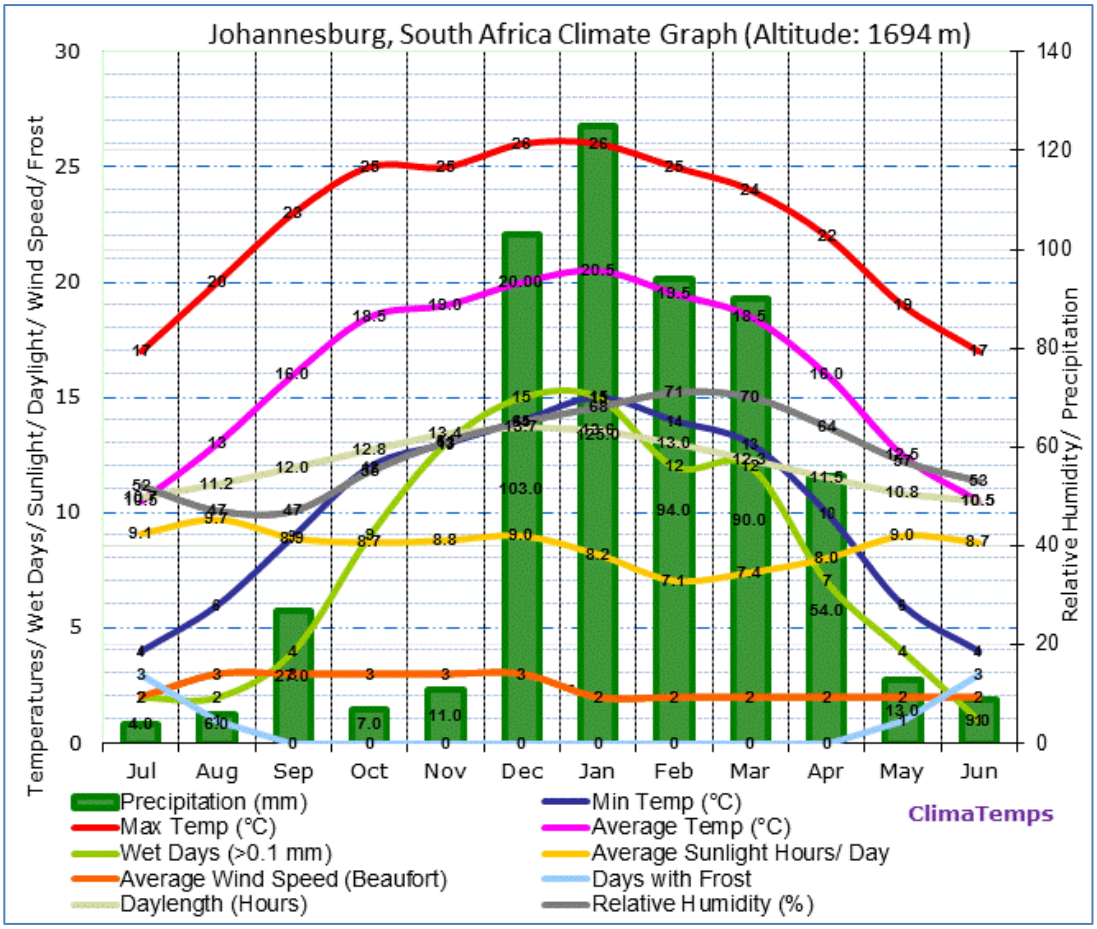


Figure 2.27 Climate graph for Johannesburg – Source: ClimaTemps.com (2017b).

http://www.johannesburg.climatemps.com/

Table 2.5 Annual climate variables for Johannesburg – Adapted from ClimaTemps.com (2017b).

Climate variable	Annual mean	Annual monthly minimum	Annual monthly maximum
Mean max temperature (°C)	22	17 (June and July)	26 (December and January)
Average temperature (°C)	16	11 (June and July)	21 (January)
Average minimum temperature (°C)	10	4 (June and July)	15 (January)
Average precipitation (mm)	543	4 (July)	125 (January)
Number of wet days (*Percentage probability of rain on a day*)	96 (*26%*)	1 (*3%*) (June)	15 (*48%*) (December and January)
Average sunlight hours per day	8 h 42′	7 h 25′ (March)	9 h 42′ (August)
Average daylight hours per day	12 h 00′	11 h 13′ (August)	13 h 44′ (December)
Percentage of sunny (*cloudy*) daylight hours	72 (*27*)	60 (*40*) (February)	87 (*13*) (August and June)
Sun altitude at noon on the 21st day (°)	63.3	40.4 (June)	87.2 (December)

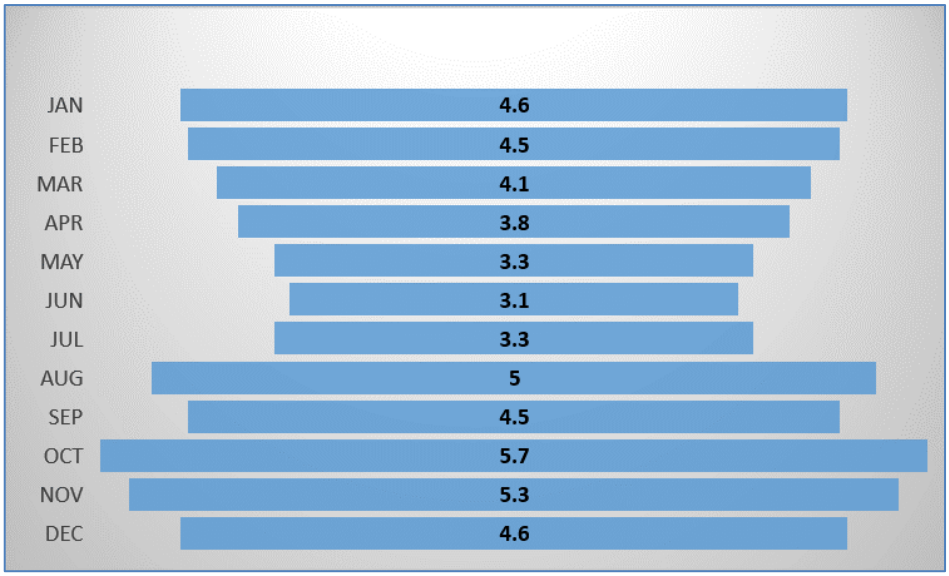


Figure 2.28 Average monthly wind speed (in m/s) at OR Tambo International Airport - Based on SAWS (2014) data.

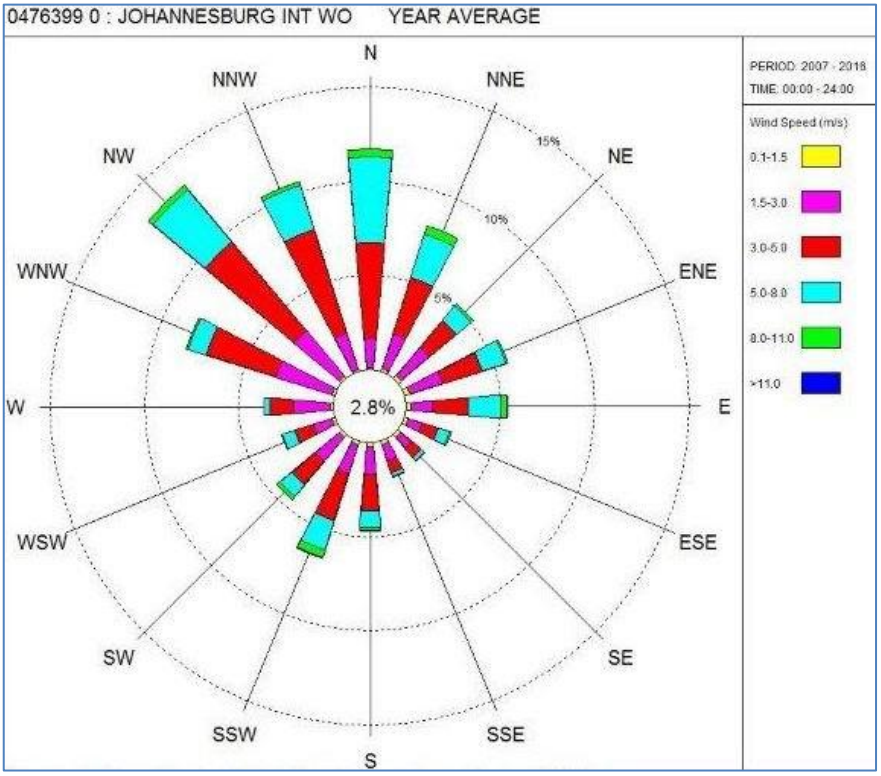


Figure 2.29 Average yearly wind speeds and directions at OR Tambo International Airport - Source: SAWS (2017).

2.3.15 General Pollution of the GJMA

In 2013, Johannesburg was said to be the seventh most polluted city in the world's biggest economies (2OceansVibe News 2013). This claim was based on measured PM_{10} (particles of 10 microns or less) levels taken by the World Health Organisation (WHO) during 2009, of 1600 cities (located in 91 countries). However, it needs to be mentioned that at the time of the survey, only a few cities were monitored (News24 2014). Since then, however, the WHO's database has grown extensively with over 3000 cities being monitored, which subsequently resulted in Hartebeespoort (located to the west of Johannesburg) being rated in 2016 as the 162nd most air polluted area in the world (BusinessTech 2016b). Johannesburg is reportedly more polluted than Paris and Montreal – See **Figure 2.30** by The Economist (2013) and **Figure 2.31** by Clean Planet Solutions (2015).

Johannesburg's CBD and some of its suburban areas display several environmental problems. These are mainly water pollution (from industrial effluents and sewage), air pollution from industry and vehicle emissions, dust from the gold mine tailing dumps, as well as litter and excess refuse caused by overcrowding (Junior Worldmark Encyclopedia of World Cities 2016).

The highest levels of air pollution are commonly measured during the winter periods (**Figure 2.32**), due to the burning of coal and fossil fuels, e.g. SO_2, particulate matter, fine mode aerosols, etc. (Piketh et al. 2007). This is because of the dry, cold, windless conditions (**Figure 2.28**) (SAWS 2014) and temperature inversion effects (Mathee & von Schirnding 2003; Bennett 2017), which causes atmospheric pollutants to become trapped close to the ground, resulting in the formation of a "*haze of pollution*" and acid rain (United Nations Human Settlements Programme (UN-Habitat) 2014).

According to Mathee & von Schirnding (2003), atmospheric pollution in the Greater Johannesburg are mainly attributable to:

i) the rapid sprawling and crowding of townships and informal settlement areas;

ii) the emissions of pollutants from various industrial plants/sites – due to inadequate control and lack of enforcement of existing legislation; and

iii) the emissions from motor vehicles.

The levels of air pollutants, e.g. NO_2 and particulate matter tend to increase in the mornings and early night-time, due to an increase in coal burning and heating activities (Annegarn 2007; Piketh et al. 2007). The highest levels of ground-level O_3 are measured during spring and summer (Piketh et al. 2007) since it is a secondary pollutant that is formed by interaction with sunlight.

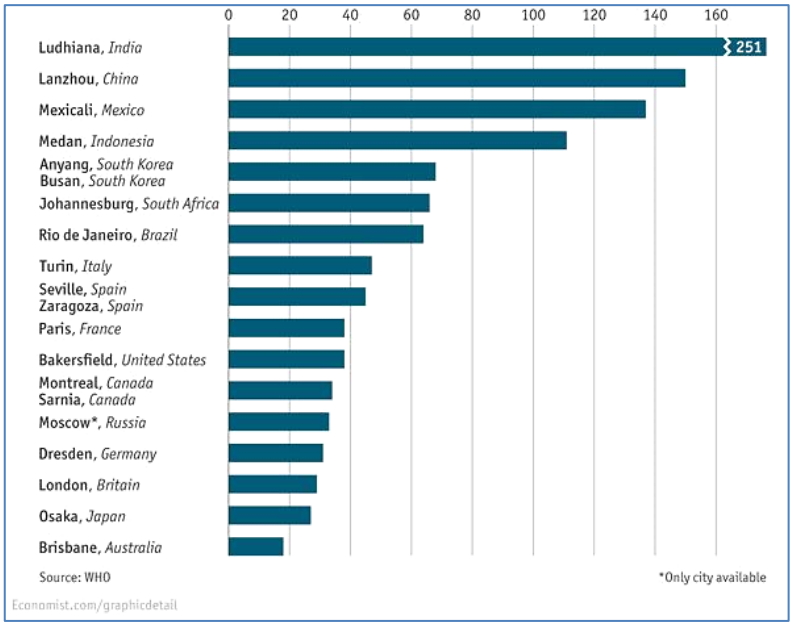


Figure 2.30 Particulate matter with diameter 10 µm or less in µg/m^3 (2009 annual averages) – Source: The Economist (2013). http://www.economist.com/blogs/graphicdetail/2013/01/daily-chart-11?fsrc=rss

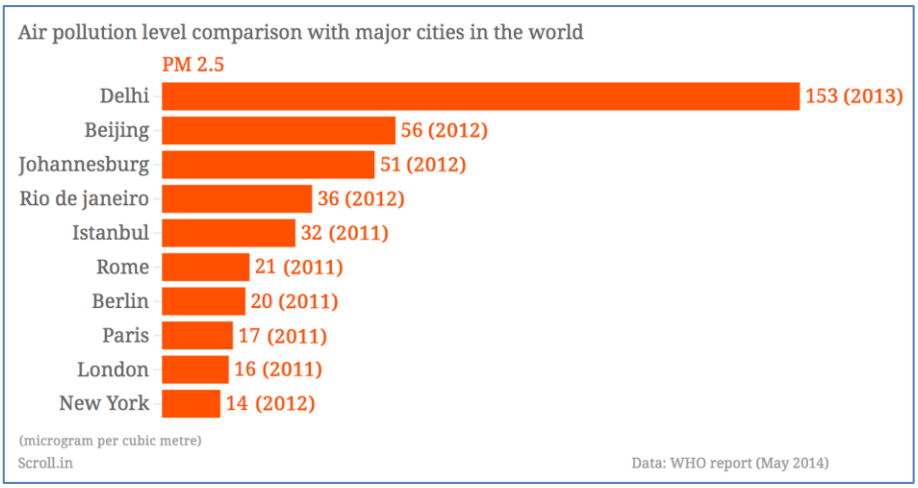


Figure 2.31 Particulate matter with diameter 2.5 µm or less in µg/m^3 (WHO May 2014 report) – Source: Clean Planet Solutions (2015).

www.who.int/phe/health_topics/.../WHO_AAP_database_May2016_v3web.xlsx



Figure 2.32 Typical haze of pollution over the Greater Johannesburg area during wintertime.

Consistent with air quality data (**Table 2.6**) (City of Johannesburg 2003; Zunckel et al. 2005; Tidblad et al. 2007; Lourens 2012), the most significant contributors to air pollution in the region are due to fossil fuel burning, i.e. coal, oil, natural gas, diesel and petrol, to produce electricity and power vehicles. See also **Figure 2.33**. The primary sources are CO_2, SO_2, O_3, particulate matter (PM_{10} and $PM_{2.5}$) and NO_x. CoJ's air quality data indicate that the PM_{10} levels tend to be at their highest in the 'township' areas, e.g. Soweto, Daveyton, Katlehong, Vosloorus, Orange Farm, Alexandra, etc. (City of Johannesburg 2007c), due to the burning of wood, coal and paraffin.

These sources encourage the formation of an urban island heat effect, as well as acid deposition in the area. Moreover, greenhouse gases, causing ozone depletion, also promote global warming. These are all factors that may influence atmospheric corrosion or 'breakdown' of metallic and non-metallic materials in the GJMA.

Table 2.6 Air quality data for Gauteng/Greater Johannesburg and its surrounding areas.

Air quality variable	Average annual concentration	Reference
Carbon dioxide	1.52-12.60 ppm (average ~3.3 ppm)	(Zunckel et al. 2005)
Sulphur dioxide	5.50-15.50 ppb (average ~10.0 ppb)	(Zunckel et al. 2005; Tidblad et al. 2007; Lourens 2012)
Nitrogen dioxide	17.13-48.00 ppb (average ~27.7 ppb)	(Zunckel et al. 2005; Tidblad et al. 2007)
Nitrogen oxide	3.1-150.0 ppb (average ~48 ppb)	(Zunckel et al. 2005)
Oxides of nitrogen	9.9-182.9 ppb (average ~76 ppb)	(Zunckel et al. 2005)
Particulate matter (PM_{10} & $PM_{2.5}$)	21-132 µg/m^3 (average ~68 µg/m^3)	(Zunckel et al. 2005; Tidblad et al. 2007)
Chloride	~0.1 µg cm^{-2} $month^{-1}$	(Tidblad et al. 2007)
Ozone	35-70 ppb (average ~74 ppb)	(City of Johannesburg 2003; Tidblad et al. 2007; Lourens 2012)
Benzene	1.06-2.23 ppb (average ~1.8 ppb)	Zunckel et al. 2005; Lourens 2012)
Toluene	2.56-5.66 ppb (average ~3.7 ppb)	(Zunckel et al. 2005; Lourens 2012)
Ethylbenzene	~0.45 ppb	(Lourens 2012)
Xylene	0.23-7.35 ppb (average ~2.6 ppb)	(Zunckel et al. 2005; Lourens 2012)

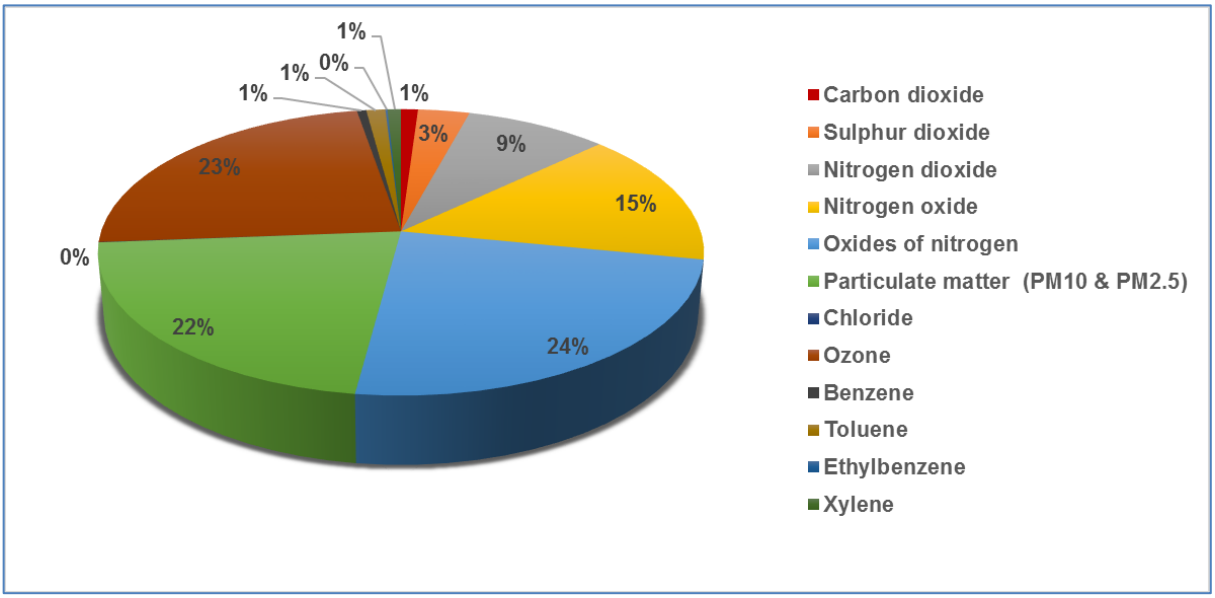


Figure 2.33 Average annual atmospheric pollution levels in Gauteng and its metropolitan areas – derived from the data in **Table 2.6** (City of Johannesburg 2003; Zunckel et al. 2005; Tidblad et al. 2007; Lourens 2012).

CHAPTER 3

METHODOLOGY

3.1 ATMOSPHERIC CORROSION OF SOUTH AFRICA - DATA COMPILATION

The first year or 12-month atmospheric corrosion rates of mild steel, aluminium, zinc and copper from all available South African published and unpublished datasets, spanning more than three decades (as outlined in Section 2.2), were collected. Due to the lack of enough detail, some of the results were excluded. In totality, data were compiled for close to 100 locations. Due to the sensitive and proprietary nature of some of the data sets, the full disclosure of the list of sites has been omitted from this thesis. Also, in a few cases, particularly concerning the old CSIR (1975) and Callaghan (1991) results, the Global Positioning Satellite (GPS) coordinates of the test sites were guesstimated based on verbal descriptions of the locations of the sites. In these cases, the exact positions of the locales may be inaccurate by one square kilometre. However, the sites in question were mainly positioned inland where the impact of this discrepancy on the overall findings of the current study would have been reduced. Also, based on the objectives of the historical studies, the assumption was made that the test racks were placed in locations to measure 'macro' rather than 'micro' atmospheres.

As for the GPS coordinates of the other locales, these were either recorded during the initial set-ups of the sites, with a Garmin GPS receiver, with an accuracy of < 15 m, or determined via Google Maps, which is not exact. However, as stated by a representative of Google (Tengs 2016), the imagery may vary from less than a meter resolution in main cities to 15 m resolution for most of the earth's surface, with a global base resolution of one kilometre. Since their database is continuously updated, Google Maps do not give a specific resolution for any geographic region. However, as per independent research findings, the coordinates of the Google Map model may be erroneous by several metres.

The corrosion data were subsequently compiled in a Microsoft Excel spreadsheet, together with the determined or estimated GPS coordinates and projected distances from the nearest coast and altitudes, based on Google Maps measurements, for the

different sites. Subsequently, the results were statistically analysed in totality, as well as in sub-sets to calculate the averages and standard deviations for different spans (< 150 m, < 1 km, 1-3 km, 3-10 km, 10-30 km and > 30 km) from the ocean, in addition to regional perspectives.

Since the 12-month corrosion results for the historical sites were derived over a period of more than 30 years, the estimated level of uncertainty of the data, particularly predating 2005, was high, likely 30% or more, because of the following potential variables:

- different descaling treatment processes;
- different starting times;
- different climatic and pollution conditions;
- alternate exposure angles;
- different low-carbon steel, hot-dip galvanised steel, aluminium, zinc and copper materials;
- alternative chemical cleaning procedures; and
- different measurement accuracies.

For example, studies done by Janse van Rensburg (2015) have shown that the variability of the 12-month corrosion rate of mild steel can be as high as about 33% due to a mere change in the initial surface cleaning process, e.g. abrasive blast-cleaning vs mill finishing. The former procedure was particularly popular during Eskom's earlier studies.

Also, concerning the CSIR (1975) results, exposure of the metal specimens was done at an inclination of 30° from the horizontal, facing North, whereas all the Eskom and Janse van Rensburg samples were exposed at an angle of 45° to the horizontal. This would have impacted significantly on the outcome of the results.

3.2 CORROSION MONITORING OF THE GJMA - EXPERIMENTAL PROCEDURES

Concerning the corrosion mapping of the GJMA, wire-on-bolt, open wire helix and plate metal specimens, as well as coated mild (carbon) steel coupons were utilised for the

atmospheric corrosion monitoring of 57 sites over periods of 6, 12, 18 and 24 months of exposure. The metal types and corrosion monitoring devises used during the historical South African corrosion studies governed the choice of the materials for the current GJMA study - enabling comparison and final merger of the results. While long-term corrosion monitoring studies are preferred to establish yearly trends, the present study period was limited to 24 months, due to time and financial restrictions. Also, in terms of ISO 9223, a monitoring period of 12 months is sufficient for the corrosivity rating of environments (International Organization for Standardization 2012a).

3.2.1 Exposure Sites

One of the current study's primary objectives was to provide an atmospheric corrosion map for the GJMA, which could be incorporated into the new charts for South Africa. Therefore, the chosen corrosion monitoring sites of the GJMA needed to be representative of the geographical zones in which they were located, and, as far as possible, evenly distributed throughout the study area.

Broadly, the corrosion monitoring sites were selected based on the locations of significant suburbs, towns, cities, industrial plants and other important areas associated with the GJMA. The sites were also chosen to coincide with existing air quality monitoring locales managed by the Environmental Department of the City of Johannesburg, namely Soweto, Orange Farm, Alexandra, Ivory Park, Delta Park, Diepsloot, Newtown and Buccleuch. Since the safety of a site was of the utmost importance, some of the potential locales were slightly re-positioned to comply with this criterion.

Nixon & Janse van Rensburg (1992) and Janse van Rensburg (1994, 2010, 2015) also identified several additional factors that needed to be taken into consideration during the selection of suitable atmospheric corrosion monitoring sites in South Africa. These are:

- the ease with which access could be obtained to the site on a regular basis;
- the ease with which site staff would assist during the inspection of the corrosion samples (where applicable) – for example, due to safety concerns, many sites could only be visited, while being escorted by suitably qualified site personnel.

The willingness or reluctance of these individuals to assist with inspections could, therefore, have influenced the success of the exposure programme;

- the known corrosive conditions of a site – the more corrosion data available for a location, the more pertinent data could be obtained;
- the availability of open space at a site to allow for the proper positioning of the test racks, without significant interference from nearby buildings, fences or vegetation;
- the general safety of the location – some areas are more prone to hijackings, vandalism and theft. Within the South African context, this reality impacted significantly on the potential use of specific locations;
- the perceived importance of a place or site – the results from individual sites could potentially be of higher value due to their proximity to large industrial areas, townships, etc.; and
- the site also needed to be representative of an environment to be examined, for example residential, business, industrial, mining and recreational.

Also, consideration was given to the requirements of international standards relating to the real-world exposure testing of materials, e.g. ISO 2810, (International Organization for Standardization 2004b) and ASTM D1014 (ASTM International 2009).

Following proper selection of suitable locations, a total of 57 sites were established during late August to middle September 2013. Of these locales, 22 sites (henceforth referred to as the 'main/primary' sites) were earmarked for more detailed corrosion monitoring of the environment, of which eight locations coincided with current and historical air quality monitoring sites of the Environmental Department of the City of Johannesburg. The remaining 35 locales (henceforth referred to as the 'mini' sites) were used to cover the gaps regarding the overall corrosivity of the Greater Johannesburg's atmosphere.

The positioning of the sites is given in **Figure 3.1**, whereas relevant geographical information relating to the different locales, such as site names, general descriptions, altitudes (elevations above sea level) and GPS coordinates, are presented in **Appendix B - Tables B.1 & B.2**. The most northerly, easterly, southerly and westerly sites in the study area were Diepsloot, Nigel, Orange Farm and Randfontein, respectively.

Tables B.1 & B.2 (Appendix B) show that the sites represented a broad range of general environmental zones, namely farming, business, industrial, mining, recreational, residential, agricultural (field), township and traffic.

3.2.2 Design and Fabrication of Test Racks, and Flat Metal Specimens

3.2.2.1 Design, fabrication and installation of test racks

The test rack frames were fabricated from anodised aluminium to ensure that they remained unaffected by corrosion for the duration of the study. The lightweight properties of aluminium also facilitated ease of transportation and installation of the racks.

Existing, low-cost designs by Orytech (Janse van Rensburg 2015) were used in the manufacturing of the frames, which were riveted together with aluminium fasteners. The samples were insulated from each other using high-density polyethylene (HDPE) insulation bobbins to prevent galvanic corrosion. The size of the rack depended on the number of samples to be exposed and the duration of the corrosion monitoring period.

Concerning the 22 primary corrosion monitoring sites, the rack size measured 500 x 700 mm, with a design sample holding capacity of 21 (76 x 152 x 0.8 mm) flat steel (coated and blank) coupons (**Figure 3.2**). This type of frame enabled the exposure of eight mild steel panels (referred to as MSP), six hot-dip galvanised steel (referred to as GSP) and seven painted mild steel specimens to an environment for 24 months. The design removal intervals of the test coupons were as follows:

i) two mild steel specimens every 6, 12, 18 and 24 months of exposure;

ii) two hot-dip galvanised panels every 12, 18 and 24 months of exposure; and

iii) seven coated steel panels, which remained on the test racks for the full 24-month period, before removal.

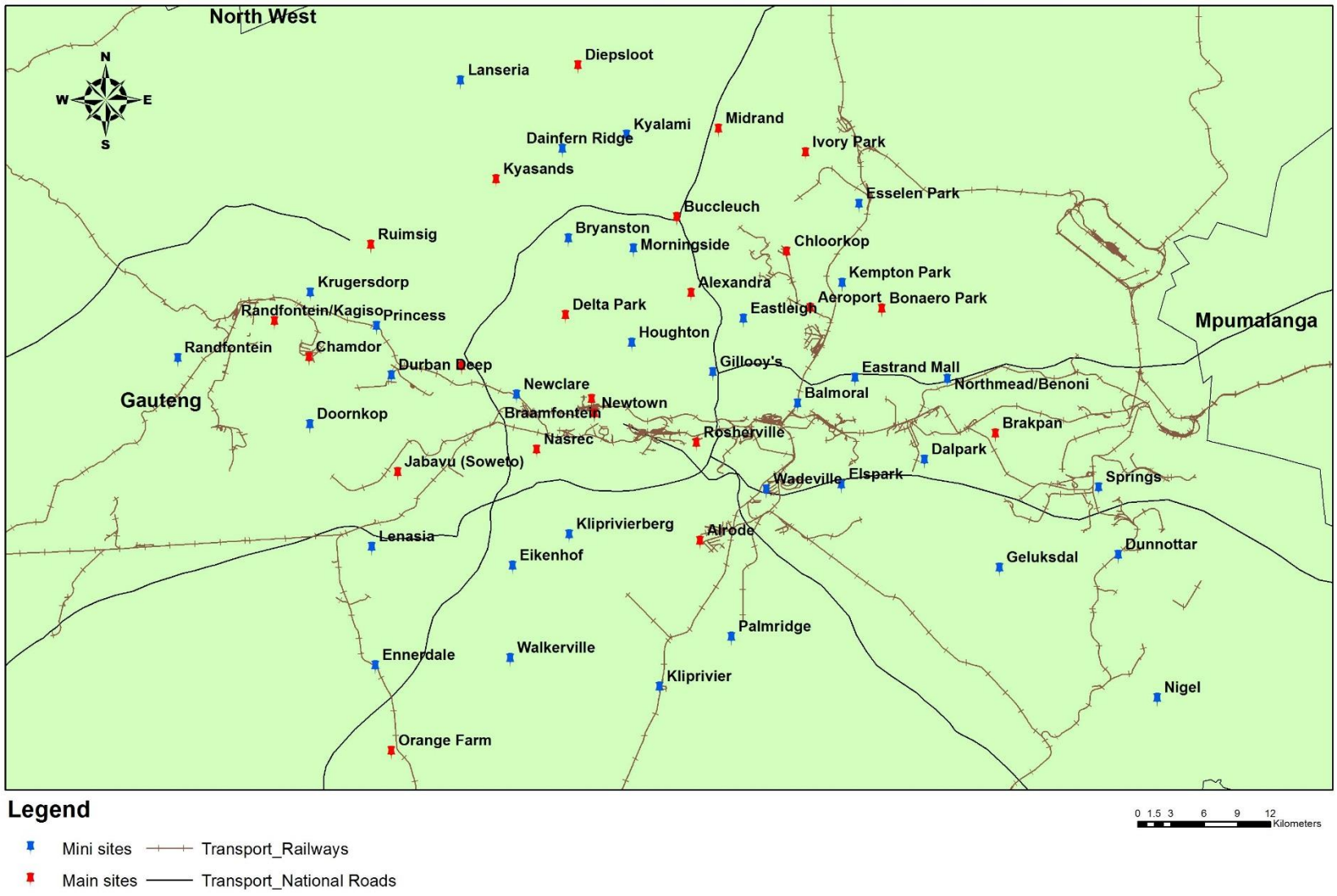


Figure 3.1 Positioning of the main and mini atmospheric corrosion monitoring sites in the GJMA. (Base map: ArcGIS).

Regarding the 35 smaller (mini) sites, the test rack dimensions were 230 x 160 mm, with a sample holding capacity of two (76 x 152 x 0.8 mm) flat steel coupons (**Figure 3.3**). The design removal interval was two panels after twelve months of exposure. Due to the taking of duplicate measurements per metal type per exposure period, the variability of the metal loss results was significantly reduced.

The exposure angle of the racks was 45° from the horizontal and the directional positioning, due north (as far as practically possible). The frames were affixed to existing structural supports at the various sites using HDPE cable ties. During installation of the 57 test racks, condition assessments of existing infrastructure near the sites were also carried out. These evaluations were done to determine the potential impact that atmospheric corrosion has on structures in the GJMA, as well as to verify whether the corrosion monitoring data obtained during the latest study, truly reflected what was happening on the ground.



Figure 3.2 Typical set-up of a main corrosion monitoring site, comprising a 21-flat coated and uncoated mild steel coupon aluminium test rack, ASTM G116 wire-on-bolt and ISO 9226:1992 open wire helix corrosion monitoring devices, attached to a steel structure at the Kagiso-Randfontein site.



Figure 3.3 Typical set-up of a mini corrosion monitoring site, comprising a flat coupon test rack, with a holding capacity of two mild steel samples.

3.2.2.2 Preparation and chemical cleaning of flat, uncoated mild steel and hot-dip galvanised steel coupons

Blank/uncoated low-carbon (mild) steel, hot-dip galvanised mild steel and coated mild steel panels, each of size 76 x 152 x 0.8 mm, were prepared before exposure. The mild steel panels used for the preparation of the blank, hot-dip galvanised and organic-coated specimens, all originated from the same source (Q-Lab Corporation). The physical and chemical properties of these flat mild steel panels (utilised for the preparation of the blank, hot-dip galvanised and organic-coated specimens), are given in **Appendix C**. Application of the galvanised coating was arranged by the HDGASA, via Orytech (Pty) Ltd. and done as per ISO 1461 procedures (International Organization for Standardization 1999). The mean zinc coating thickness, measured using an Elcometer 456 electromagnetic thickness gauge, was approximately 50 µm per side, with the elemental composition of the zinc coating presented in **Appendix C**.

Since standard low-carbon, pre-cleaned steel panels (representative of general purpose sheet metal applications) (Q-Lab Corporation 2015) were used, no descaling of the samples was required before hot-dip galvanising or coating. Therefore, experimental uncertainties due to variations in surface finishing, composition and dimensions were minimised through the use of these panels. Furthermore, holes were drilled into each

sample to enable proper identification, using a mask - before, during and after exposure at the various locations.

After marking, the uncoated samples were solvent degreased with acetone, dried, and weighed, before being sealed in plastic bags and exposure on the different racks. A calibrated analytical balance was used for weighing the samples before and after exposure, with a readability of 0.1 mg, and uncertainty of measurement of 0.4 mg (100 g load).

Two mild steel panels were retrieved per every main site, after 6, 12, 18 and 24 months of exposure, de-rusted/chemically cleaned, and re-weighed to determine the amount of metal loss due to the rusting process. In the case of the hot-dip galvanised steel specimens, however, two samples were retrieved every 12, 18 and 24 months. Following exposure, the samples were all re-weighed, chemically cleaned by the ISO 9226:1992 procedures (International Organization for Standardization 1992d) and then re-weighed again, before the corrosion rates were calculated, by converting the mass loss to corrosion rates (r_{corr} – values), using **Equations 2.20 & 2.21** (International Organization for Standardization 1992c, 2012d).

In the case of the mild steel specimens, de-rusting was done using three to four cycles of immersion in 500 ml of hydrochloric acid (ρ = 1.19 g/ml), 3.5 g of hexamethylenetetramine and distilled water to make up to 1000 ml, at a temperature of 20-25°C (International Organization for Standardization 1992c, 2012d). Regarding the hot-dip galvanised samples, these were chemically cleaned with a single one-minute immersion period in 200 g of chromium trioxide (CrO_3) and distilled water to make up to 1000 ml, at a temperature of 80 ± 2°C. Noteworthy is that the same chemical cleaning procedures (International Organization for Standardization 1992c) were utilised for de-rusting of the samples, as per the country-wide (Janse van Rensburg 2010, 2015) exposure programme. This was irrespective of the fact that an alternative procedure was subsequently introduced by the International Organization for Standardization (ISO) in 2012 (ISO 9226:2012) for the cleaning of zinc, most likely due to health, environmental and safety concerns about the use of CrO_3.

Before chemical cleaning, uncorroded specimens were immersed in the acid solutions to establish the extent of base metal losses due to the chemical cleaning procedures.

Regarding the uncoated mild steel samples, the degree of base metal loss after three ten-minute periods of immersion and cleaning procedure was about 0.04 µm/a, while concerning the hot-dip galvanised samples, following a one-minute exposure period, the extent of removal of the base metal was approximately 0.01 µm/a. Corrections were after that made for the losses in weight of the unexposed specimens.

3.2.3 Optical Surface Characterisation, Morphology and Chemical Analysis of the Mild Steel Corrosion Products Formed at the Main and Mini Sites in the GJMA

The morphologies and chemical compositions of the corrosion products formed on the flat mild steel specimens were investigated using:

i) General stereo microscopy;
ii) Attenuated total reflectance (ATR) - Fourier transform infrared (FTIR) spectroscopy;
iii) Raman micro-spectroscopy;
iv) Scanning electron microscopy (SEM) and X-ray energy dispersive spectrometry (EDS); as well as
v) pH and water-solubility salt measurements.

The purpose of this work was to establish the critical factors involved in the atmospheric corrosion processes at the different sites.

Before cleaning, stereo microscopic images (at x20 magnification) were taken of the corroded mild steel surfaces with a Motic microscope, fitted with a Moticam 2000 digital camera. Soluble salt contamination tests, using an Elcometer 137 Bresle Salt Kit were also carried out of the upper-facing (exposed) surfaces of the mild steel panels. This method involved the application of a self-adhesive rubber foam patch (Elcometer 135B - known as the 'Bresle patch'), equipped with a watertight latex pouch to the metal surface, where after 3 ml of deionised water was injected into the bag, using a 5-ml syringe (Elcometer Limited 2014). The 1250 mm^2 surface was next thoroughly washed with the deionised water, by rubbing of the latex pouch, to allow the sampling of any soluble impurities that may be present on the corroded steel surface. (A technical information sheet for the Elcometer 135B patches is provided in **Appendix D**).

Subsequently, the wash water was extracted and the conductivity thereof determined using an Elcometer 138 (Horiba) conductivity meter (with an uncertainty of measurement of 2.5%) (Elcometer Limited 2014). Before analysis, the background conductivity was measured and deducted from the readings. The conductivity measurements were then converted to soluble salt concentrations using **Equation 3.1**.

$$Water\ soluble\ salts = Conductivity\ (extracted - injected) \cdot 1.2 \qquad \textbf{Eq. 3.1}$$

where:

> $Water\text{-}soluble\ salts$ are measured in mg/m^2; and $Conductivity\ in$ µS/cm, which is multiplied with a constant of 1.2, as outlined in ISO 8502-9, entitled, "*Preparation of steel substrates before application of paints and related products - Tests for the assessment of surface cleanliness - Part 9: Field method for the conductometric determination of water-soluble salts*" (International Organization for Standardization 1998d).

Acidity or alkalinity measurements of the extracts were also performed using Hach test strips (0pH to 14pH). These tests were done to ascertain whether the solutions derived by way of the Bresle water-soluble salt test procedure were acidic or alkaline. However, the strips lacked sensitivity in providing discernible pH data for the corrosion products from the different sites, since all the results indicated a pH of 5. Consequently, scraped samples of the corrosion product were mixed with small quantities of distilled water (1:1 mix), and a Horiba pH meter was used to re-determine the pH of the corrosion product.

ATR-FTIR spectroscopy, in the frequency range of 500 cm^{-1} to 4000 cm^{-1} of the corrosion products were also done. The instrument utilised was a Thermo Scientific Nicolet™ iS™10 Fourier transform infrared spectrometer, equipped with a Smart iTR™ attenuated total reflectance sample accessory. Moreover, Raman spectroscopy analysis of select corrosion product samples was conducted to determine the different ferrous oxides formed in the rust layers. The Raman instrument used was a Horiba Scientific – LabRam HR, coupled with an Olympus BX41 confocal microscope attachment, calibrated with a silicon spectrum. An x100 lens was used to focus the laser, set at 0.4 mW to prevent overheating and to collect the scattered light. The acquisition time was set at 60 seconds.

Furthermore, scrapings of the corrosion products formed on the metal surfaces were analysed for their elemental compositions using SEM-EDS. This was done to identify

the potential corrosive species involved in the corrosion processes at the different sites. A Zeiss, high-resolution electron microscope, equipped with WinEDS hardware and software, set at an acceleration voltage of 25 kV and a take-off angle of 35.0°, was used for analyses of the samples. Since cutting and scraping of the other corroded metal surfaces would have affected the accuracy of the corrosion rate measurements, no analyses of these corrosion products were carried out.

3.2.4 ASTM G116-99 – Wire-on-bolt Corrosion Monitoring Units

Wire-on-bolt (also known as CLIMAT) test units (**Figure 3.4**), designed and fabricated as per ASTM G116 procedures (ASTM International 2004), were used to determine the seasonal fluctuations in the Atmospheric, Industrial and Marine Corrosion Indices (ACI, ICI and MCI, respectively) for the 22 primary sites. These units were fabricated from commercially pure (>99.0%), one-meter length, Type 1100 aluminium wire (0.875 ± 0.002 mm), as well as near 100 mm-long M12 nylon, copper and mild steel threaded rods (all supplied by Orytech Pty Ltd.).

The 1000 mm-long aluminium wire was wrapped around each bolt, after weighing to the nearest 0.1 mg ± 0.2. All parts were thoroughly solvent-cleaned (with acetone) before assembly, and the wire ends secured using small nylon fasteners. The units were subsequently exposed to the environment for approximately 90 days. Following exposure, the aluminium wires were removed, chemically cleaned in a boiling 2% (by weight) CrO_3 and 3.5% (phosphoric acid) solution, as per ASTM International (2003a), then rinsed, dried and re-weighed.

The Corrosion Indices (MCI, ICI and ACI), based on the mass loss of the aluminium wire and expressed as percentages, as well as normalised to a 90-day period, were subsequently calculated, using **Equation 3.2** (ASTM International 2004). Four of these devices were exposed per site during the first year of the study period.

Galvanic effect (%):

$$= \frac{mass\ loss\ per\ metre - reference\ mass\ loss\ per\ metre \times 100}{reference\ mass\ loss\ per\ metre} \qquad \textbf{Eq. 3.2}$$

where:

Initial mass = original wire mass – excess wire mass removed;

Mass loss = initial mass – final mass (after exposure); and

Mass loss/m = mass loss x original wire mass/initial mass.

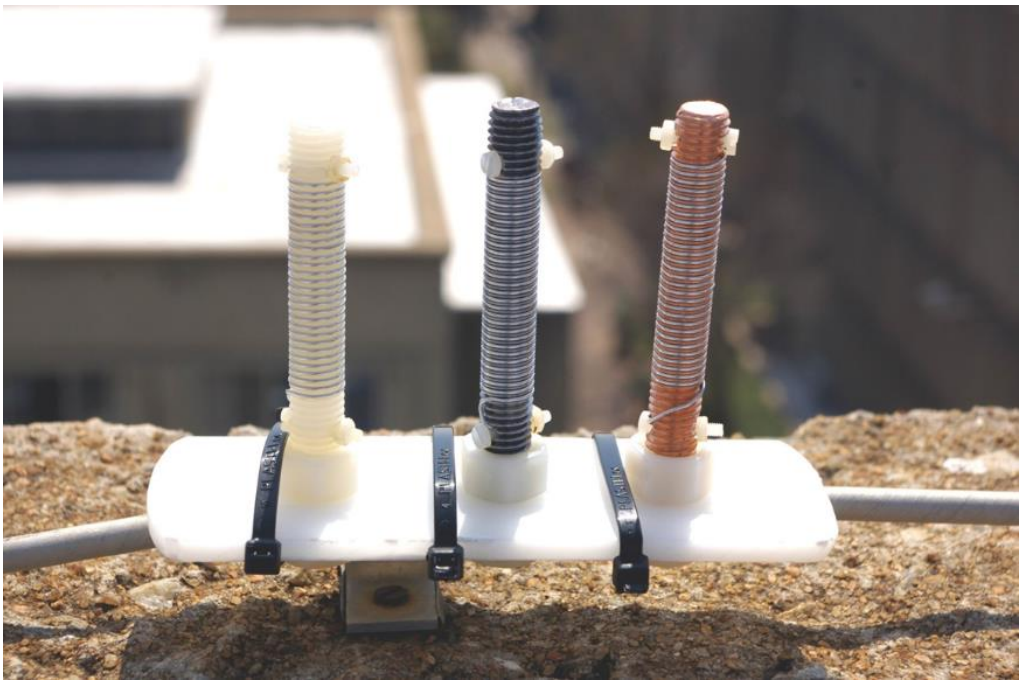


Figure 3.4 Example of a CLIMAT corrosion monitoring unit.

3.2.5 ISO 9226:1992 - Open Wire Helix (WH) Units

The ISO 9226:1992 open wire helix (WH) procedure has been withdrawn from the latest ISO 9226:2012 standard (International Organization for Standardization 2012a). However, since it was extensively used during the older atmospheric corrosion studies in South Africa (Leitch 2003, 2006; Janse van Rensburg 2010), to classify the corrosivity of atmospheres, it was included in the present study. This was to enable comparisons with previous results (Leitch 2003, 2006; Janse van Rensburg 2010), as well as to reduce costs in providing twelve-month corrosion rates (r_{corr} – values) for aluminium, copper and zinc, at the different GJMA sites.

As per ISO 9226:1992 procedures, theref ore, the units were fabricated from 100 mm-long (2 mm in diameter) aluminium, zinc and copper thermal spraying wires (**Appendix C – Tables C.3 – C5**), coiled (following solvent cleaning with acetone and weighing to the nearest 0.1 mg ± 0.2) around three 100 mm in length nylon threaded rods.

The wires, supplied by Weartech via Orytech (Pty) Ltd., were:

Zinc: > 99.9%
Copper: > 99.9%
Aluminium: > 99.0%
(See also **Figure 3.5)**.

Following assembly, the ISO 9226:1992 open wire helix units were exposed at the 22 primary sites for 12 months. After exposure, the corrosion products on the wires were chemically removed by procedures provided in ISO 9226 (International Organization for Standardization 1992b), involving the following:

Zinc: An aqueous CrO_3 acid solution at 80°C;
Copper: An aqueous H_2SO_4 solution at 40-50°C; and
Aluminium: An aqueous phosphoric acid (H_3PO_4) and H_2SO_4 solution, at a temperature of 90-95°C.



Figure 3.5 Example of an ISO 9226:1992 open wire helix corrosion monitoring unit.

The wires were subsequently re-weighed to 0.1 mg ± 0.2, and the corrosion rates (r_{corr} - values) of the wires calculated by using **Eq 3.3** (International Organization for Standardization 1992d).

$$r_{\text{corr}} = 0.25 \cdot \frac{\Delta m \cdot d}{m \cdot t} \qquad \textbf{Eq. 3.3}$$

where:

r_{corr} is the corrosion rate in μm/a (micrometres/annum);

Δm is the mass loss, in mg;

d is the wire diameter, in mm (millimetres);

t is the exposure time, in years.

3.2.6 Site Inspections, and Installation of Test Racks and Other Corrosion Monitoring Devices

Installation of the aluminium test racks, flat painted and uncoated mild steel coupons, as well as hot-dip galvanised steel panels, together with the CLIMAT and ISO 9226:1992 open wire helix units, were carried out during mid-August to late September 2013. This process involved going to the different sites, conducting corrosion and coating inspections of existing structures exposed to the surrounding atmospheres, and installation of the test racks, CLIMAT and ISO 9226:1992 open wire helix units (where applicable).

The potential sources of pollution at each site were subsequently identified (where possible), photographs were taken of infrastructure exposed to the local environment, and the GPS (global positioning satellite) coordinates captured for the various locales. The test racks were all affixed to existing structures at the different locations and positioned in such a way that they faced due north (as far as possible). Furthermore, the racks were installed at an angle of 45° with the horizontal.

3.2.7 Atmospheric Corrosivity Classification of the Environments

Classification of the corrosivity of a site was carried out using the first-year corrosion rates of the mild steel, as well as aluminium, copper and zinc wires. The classification was done using the ISO 9223:1992 and ISO 3223:2012 guidelines (International

Organization for Standardization 1992a; International Organization for Standardization 2012a), as summarised in **Table 2.2**.

3.3 Preparation, Exposure and Evaluation/Analysis of Coated Mild Steel Coupons

The painted coupons were used to examine the effects of UV light radiation and air pollution on the degradation of organic materials in the GJMA. In addition, it was considered that comparable coated samples could be an inexpensive and potential novel approach to determine the variations in sunlight radiation and local pollution, from one site to another.

3.3.1 Preparation of Coated Samples

Painted mild steel and duplex coated steel (organic coating plus galvanising) specimens were prepared for exposure at the 22 primary test sites. In this regard, the International Standards ISO 1513 – "*Paints and varnishes - Examination and preparation of test samples*" (International Organization for Standardization 2010) and ISO 1514 – "*Paints and varnishes - Standard panels for testing*" (International Organization for Standardization 2004a) were used for guidance.

Altogether, seven different coating systems were exposed, of which six were applied directly to the standard pre-cleaned mild steel plates (size 76 x 152 x 0.8 mm). The seventh (duplex) system was applied to hot-dip galvanised mild steel (also with similar dimensions and properties as used in the case of the uncoated plates). The same batches of paint were used for the preparation of the different samples, to limit application and formulation variables, which were all painted by brush. However, in the case of the powder coated samples, these were prepared by Powder-Lak (Pty) Ltd. using an electrostatic spraying technique. Subsequently, the panels were left to cure for more than seven days, before exposure.

To prevent the comparative results from being used for marketing or discrediting purposes, the disclosure of the coating product names and technical information has been excluded from the thesis. However, the generic descriptions of the different coating systems used are presented below, whereas the FTIR spectra or 'fingerprints' of the topcoats utilised are given in **Appendix E**:

- System A – two coats of a solvent-borne surface tolerant epoxy, overcoated with one coat of a water-based acrylic emulsion topcoat;
- System B – two coats of a solvent-borne surface tolerant epoxy, overcoated with one coat of a solvent-borne polysiloxane topcoat;
- System C – two coats of a solvent-borne surface tolerant epoxy, overcoated with one coat of a solvent-borne aliphatic acrylic polyurethane topcoat;
- System D – one coat water-based acrylic primer, overcoated with two coats of a water-based acrylic topcoat;
- System E – one coat water-based acrylic primer, overcoated with two coats of a water-based acrylic topcoat;
- System F – a single-layer electrostatically applied polyester powder coating; and
- System G – one coat solvent-borne alkyd primer, overcoated with two coats of a solvent-borne alkyd high-gloss enamel topcoat.

Since green is a favourite colour for the painting of fences, garage doors, gutters, roofs, etc. in the Greater Johannesburg area, it was decided to use this colour, for the top coating of all the painted samples, i.e. Brilliant Green, Grass Green (RAL 6010), Heritage Green and Leaf Green (RAL 6002) to be precise. Green also fades relatively quickly (Merchak 2012), which was considered useful from a colour change monitoring point of view. Moreover, it tends to have moderate chemical resistance (Lewis 2012), making paint formulations with green pigments potentially more suitable for the monitoring of varying sunlight radiation levels at different locations.

Following preparation and proper curing of the different coated specimens, each sample was given a specific reference code (on the reverse side) for identification purposes. The initial dry film thickness, colour and degree of gloss of each specimen were also determined as discussed below.

3.3.2 Exposure of Coated Samples

The coated samples were exposed on the aluminium test racks at the different sites for a total period of 24 months, whereafter the samples were removed, and the following parameters determined.

- Dry film thickness (DFT) – as per ISO 2808 (International Organization for Standardization 2007b) (refer also to Section 3.3.3.1);
- the degree of corrosion/rusting – as per the ISO 4628-3 pictorial rating system, ranging from Ri 0 (0%) to Ri 5 (40-50%) rust (International Organization for Standardization 2003b);
- the degree of chalking and dirt retention – by ISO 4628-6 (International Organization for Standardization 2011) (refer to Section 3.3.3.2);
- under-film creep/undercutting corrosion;
- percentage white rust (applicable to the duplex system only);
- blistering – as per the ISO 4628-2 pictorial rating scheme (International Organization for Standardization 2003a);
- flaking – by the ISO 4628-5 pictorial grading system (International Organization for Standardization 2003c);
- edge (effects) corrosion;
- colour differences – as per ISO 7724-3 (International Organization for Standardization 1984) (see also Section 3.3.3.3); and
- specular gloss - by ISO 2813 (International Organization for Standardization 2014) (refer to Section 3.3.3.4).

3.3.3. Dry Film Thickness, Chalking, Degree of Dirt Retention, Colour and Gloss Level Measurements of the Coated Samples

Dry film thickness (DFT) measurements, of the seven different coating systems, were taken before exposure (BE) at the main test sites in the GJMA. Following 24-months of exposure, the samples were removed and the average thicknesses of the surface films re-determined. Before final cleaning and measurement, the sun-exposed surfaces were analysed using ATR-FTIR spectroscopy, after which examinations were carried out to establish any signs of chalking and dirt retention by way of tape pull-off tests - like ISO 4628-6 (International Organization for Standardization 2011). This was to enable the numerical rating of this coating surface phenomenon. Subsequently, the photochemical weathering products were removed using a washing process, followed by drying of the samples, before the average dry film thicknesses (DFTs) of the sun-exposed coated surfaces were re-measured.

3.3.3.1 Dry film thickness measurements

The average dry film thickness (DFT.) of each coated sample was taken in accordance with ISO 2808 procedures (International Organization for Standardization 2007b). The readings were taken using an Elcometer 456 electro-magnetic induction dry film thickness gauge, with an accuracy of ± 2.5 µm (~1%) (Elcometer Limited 2014), calibrated by using a smooth (zero) ferrous test plate and standard 123.8 µm plastic foil (shim). Twenty DFT measurements were taken per coated panel, which was done in a matrix to improve the accuracy of the re-measurement of the painted surfaces following 24 months of exposure at the different sites. However, regarding the accuracy of any repetitive re-measurement location, the level of uncertainty of five readings in the same spot was calculated as ~1%.

3.3.3.2 Degree of chalking and dirt retention

Preceding the final thickness measurements, the level of chalking - a manifestation of the oxidation of the binder (Hare 1992) and the extent of dirt retention of each coated specimen was determined using the ISO 4628-6 tape test. In line with this standard (International Organization for Standardization 2011), 'chalking' is defined as the "*appearance of a loosely adherent fine powder on the surface of a paint coating, arising from the degradation of one or more of its constituents*". This surface phenomenon is due to sunlight exposure, which causes the disintegration of the upper surfaces of the binder, resulting in the release of pigments (Hare 1992; Mark 2007).

The test was performed before taking the final coating thickness measurements and involved the removal of disintegrated paint material and surface contaminants using pressure sensitive tape. Since the five-level pictorial rating system is subjective, the level of uncertainty is about 20%.

3.3.3.3 Colour difference measurements

Quantitative colourimetric evaluations of the small colour differences between the various paint films were determined before and after 24 months of exposure at the main GJMA sites. Colour is said to depend on three factors, namely light source, object and observer, and if any of these factors changes, so does the colour (Mark 2007).The total colour difference, ΔE^*, as recommended by the Commission Internationale de

l'Eclairage (CIE) (International Organization for Standardization 1984) for each sample was measured using an X-Rite RM200QC Imaging Spectro colourimeter, with the standard reference specimen being pure white, of which the L^*a^*b – coordinates are presented below.

	L^*	a^*	b^*
Standard (white) colour co-ordinates	100	0.0	0.0

As given above, L^* presents lightness, a^* is the red/green (chroma) coordinate, and b^* is the yellow/blue (hue) coordinate, where the total difference ΔE^*_{ab}*, is calculated by the formula $\Delta E^* = [\Delta L^{*2} + \Delta a^{*2} + \Delta b^{*2}]1/2$ (International Organization for Standardization 1984).

Important is that deltas for L^*, a^* and b^* may be positive or negative. The total difference, (ΔE^*), however, is always positive (International Organization for Standardization 1984). The original colour of each sample was measured as differences between the standard white reference and the sample colour (L^*a^*b) coordinates. Based on the five readings taken per sample, the level of accuracy of measurement was estimated at about 1%.

3.3.3.4 Gloss measurements

'Specular gloss', defined in ASTM E284 as the "*ratio of flux reflected in a specular direction to incident flux for a specific angle of incidence and source-receptor angular aperture*" (ASTM International 2013), also known as regular 'reflection', was determined for the different coated samples. The gloss unit (GU) was measured by using a calibrated Novo-Gloss Lite™ 20°/60° glossmeter, which measures gloss by "*directing a constant intensity light beam at an angle to the test surface and monitoring the reflected light at the same angle*" (Elcometer Limited 2014). Five readings were taken per sample, at an angle of incidence of 60°, of which the level of uncertainty was determined as approximately 2.5%.

Measurements were taken both before and after exposure of the coated samples at the main sites. It is important to note that specular gloss, which is a coating surface characteristic, is easily affected by sunlight and chemical pollutants in the atmosphere.

3.3.3.5 Attenuated total reflectance - Fourier-transform infrared (ATR-FTIR) spectroscopy

The identification of chemical unknowns and the molecular structures of paints and coating materials are typically carried out using infrared spectroscopy (Weldon 2012). According to Mark (2007), chemical changes start to occur in coatings before physical alterations can be observed. Therefore, in the present study, the upper surfaces of the coated flat mild steel specimens were analysed using ATR-FTIR spectroscopy. The same instrument was used for the corrosion products (Section 3.2.3).

The purpose of these tests was to determine the photochemical breakdown effects of sunlight and local pollution on the upper surfaces of the coated specimens, following 24 months of outdoor exposure in the GJMA. The weathered ATR-FTIR spectra were subsequently compared/matched to their control/reference (unexposed) 'fingerprints' of the same products and batches. These comparisons were made using the Thermo Scientific™ OMNIC™ spectroscopy (QCheck™) software programme.

ATR-FTIR analyses of the coated surfaces were carried out, before and after cleaning of the surfaces, after exposure. This was to potentially identify any weathering products or contaminants on the painted surfaces. The ATR-FTIR spectra were subsequently compared/matched to control/reference 'fingerprints' of unexposed coated surfaces of the same products and batches. This was also done using the Thermo Scientific™ OMNIC™ spectroscopy (QCheck™) software programme.

3.4 METEOROLOGICAL AND AIR QUALITY DATA SITUATION REPORTS FOR THE GJMA

Substantiating meteorological data for the study period at three main weather stations in the GJMA were obtained from the South African Weather Services (SAWS), processed into suitable formats for reference purposes. Additionally, air quality results for eight of the main test sites in the GJMA study area were obtained from the South African Air Quality Information System (SAAQIS) (DEA 2017a). These reports were used to facilitate interpretation of the corrosion results.

3.4.1 Meteorological Data

3.4.1.1 Temperature

Figures 3.6 & 3.7 present the average monthly maximum and minimum temperatures for Johannesburg, as recorded during 2013 to 2015 – derived from SAWS (2017) data.

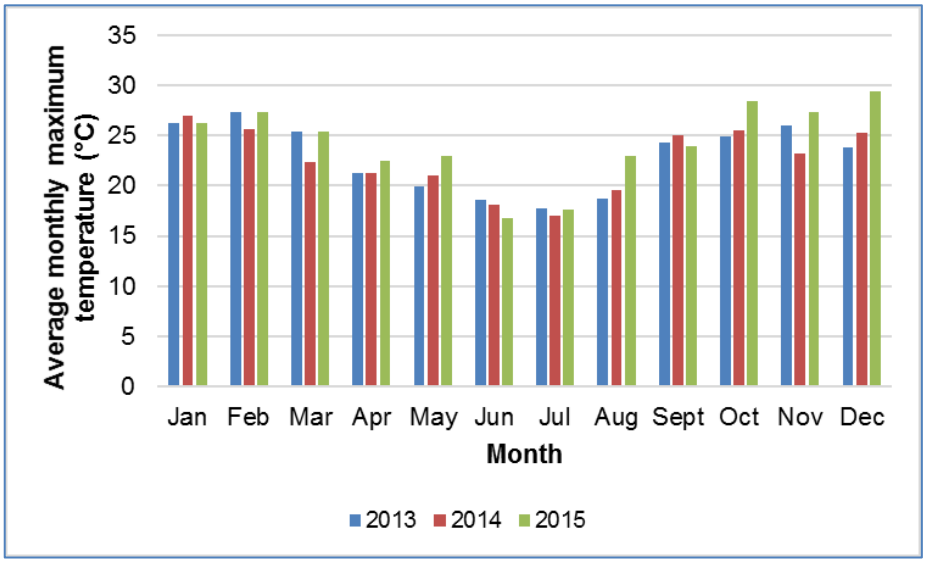


Figure 3.6 Average monthly maximum temperatures for Johannesburg during the study period 2013 to 2015, as measured at OR Tambo International Airport – Based on SAWS (2017) data.

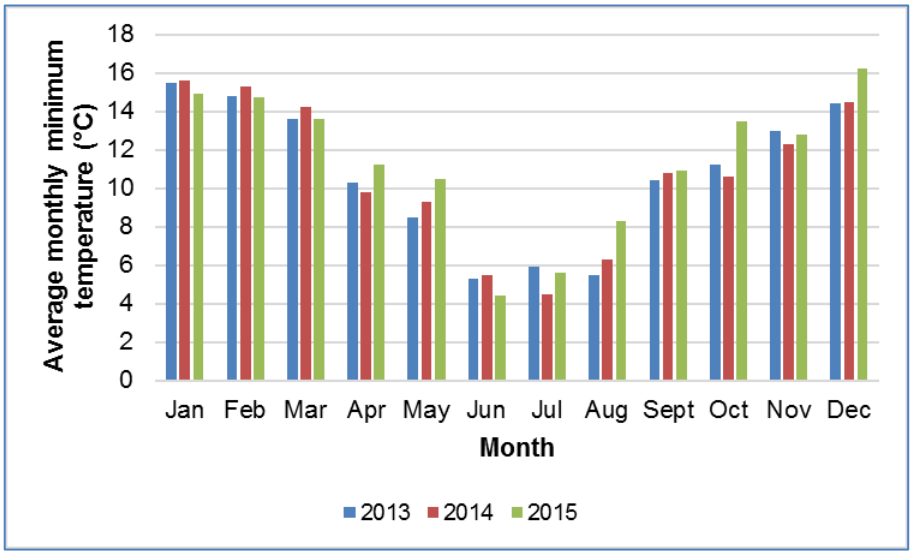


Figure 3.7 Average monthly minimum temperatures for Johannesburg during the study period 2013 to 2015, as measured at OR Tambo International Airport – Based on SAWS (2017) data.

The combined average monthly maximum and minimum temperatures for three weather stations in the GJMA area, namely at OR Tambo International Airport, the Johannesburg Botanical Gardens and Springs are given in **Figure 3.8**, while **Figure 3.9**. shows the calculated seasonal temperatures (maximum and minimum) for the GJMA, based on SAWS (2014) data.

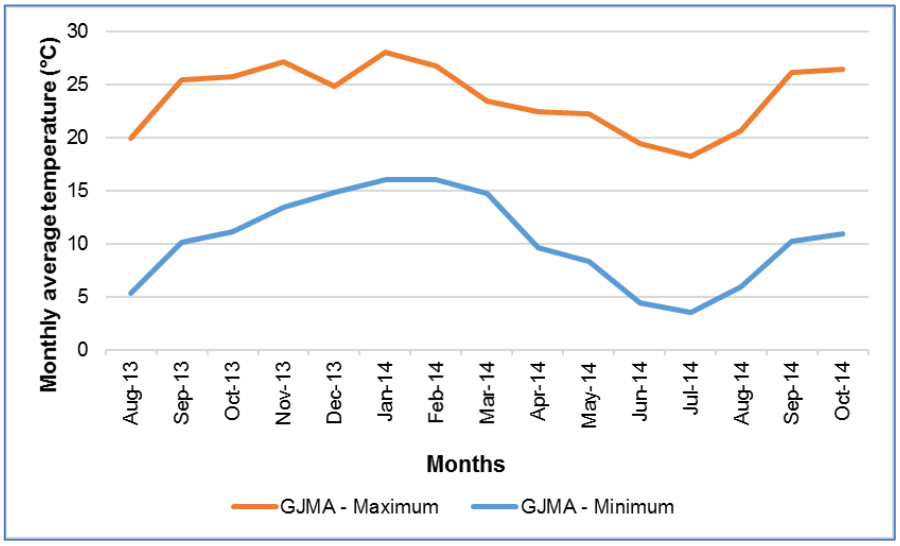
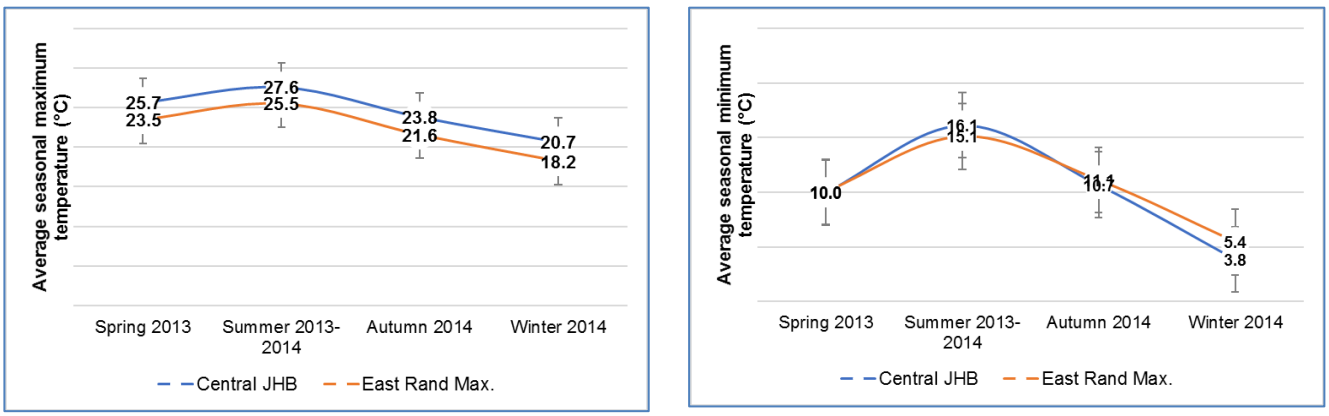


Figure 3.8 Combined average monthly maximum and minimum temperatures for three weather stations in the GJMA for the study period 2013 to 2014 – based on SAWS (2014) data.



(a) (b)

Figure 3.9 Average seasonal a) maximum and b) minimum temperatures for the GJMA during the study period, as measured at the Johannesburg Botanical Gardens and OR Tambo International Airport - based on SAWS (2014) data.

3.4.1.2 Relative humidity, rainfall and acid rain

The average monthly percentage moisture levels in the atmosphere (%RH) during the study period, measured at the Johannesburg Botanical Gardens and OR Tambo International Airport, are presented in **Figure 3.10** (SAWS 2014). **Figure 3.11** shows the changes in the %RH values from one season to the next, while **Figure 3.12** gives the average monthly RH levels for the GJMA during 2007-2016 – as measured at OR Tambo International Airport (SAWS 2017).

Figure 3.13 (SAWS 2014) presents the average monthly rainfall data for the GJMA area, also measured at the OR Tambo International Airport and the Johannesburg Botanical Gardens, while the yearly rainfall data for the GJMA area, as recorded at these locations is displayed in **Figure 3.14** (SAWS 2017). The average seasonal rainfall data measured for the central (Johannesburg Botanical Gardens) and eastern parts (OR Tambo International Airport) of the GJMA during Spring 2013 to Winter 2014, also based on the data provided by SAWS (2014) are given in **Figure 3.15.** Moreover, **Figure 3.16** (Josipovic et al. 2011) presents the total (dry plus wet) acid deposition rates in meq/m^2 per year for Gauteng and other regions of South Africa.

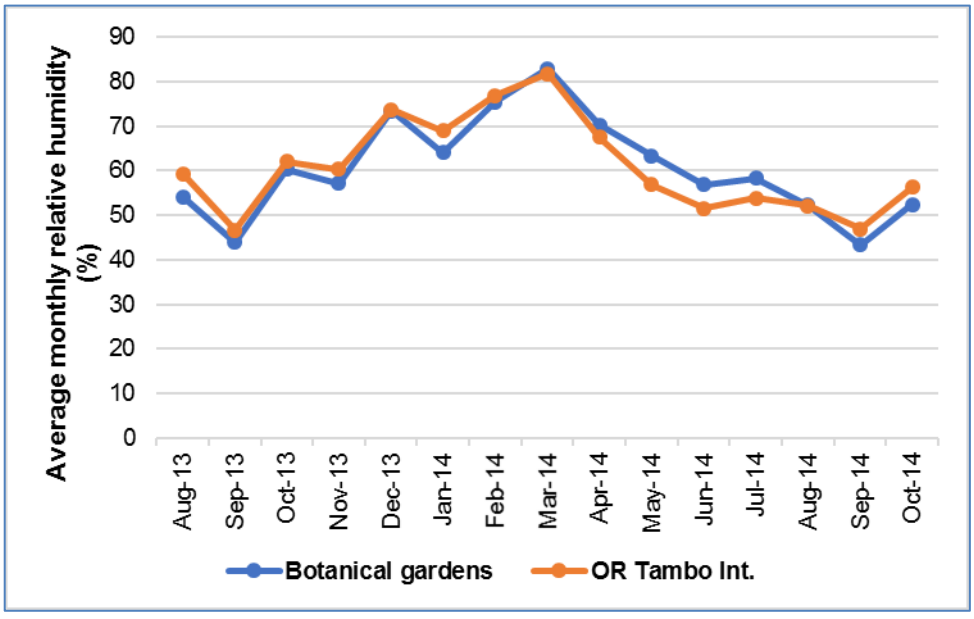


Figure 3.10 Average monthly percentage relative humidity measurements recorded during the study period at the Johannesburg Botanical Gardens (Central GJMA) and OR Tambo International Airport (East Rand) – Based on data provided by SAWS (2014).

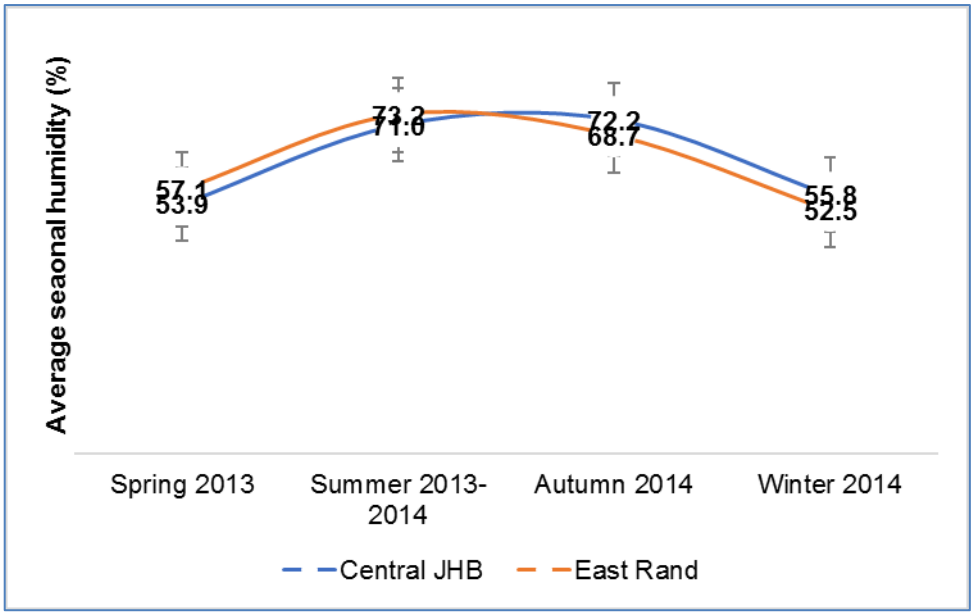


Figure 3.11 Average seasonal humidity levels for the GJMA during the study period, as measured at the Johannesburg Botanical Garden (Central GJMA) and OR Tambo International Airport (East Rand) – Based on data provided by SAWS (2014).

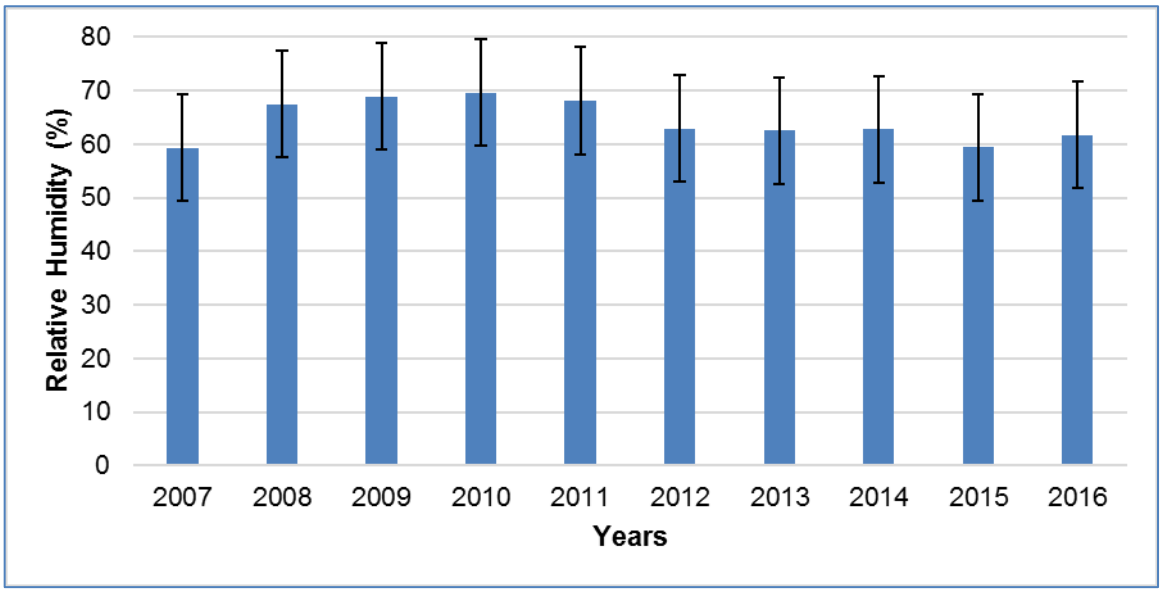
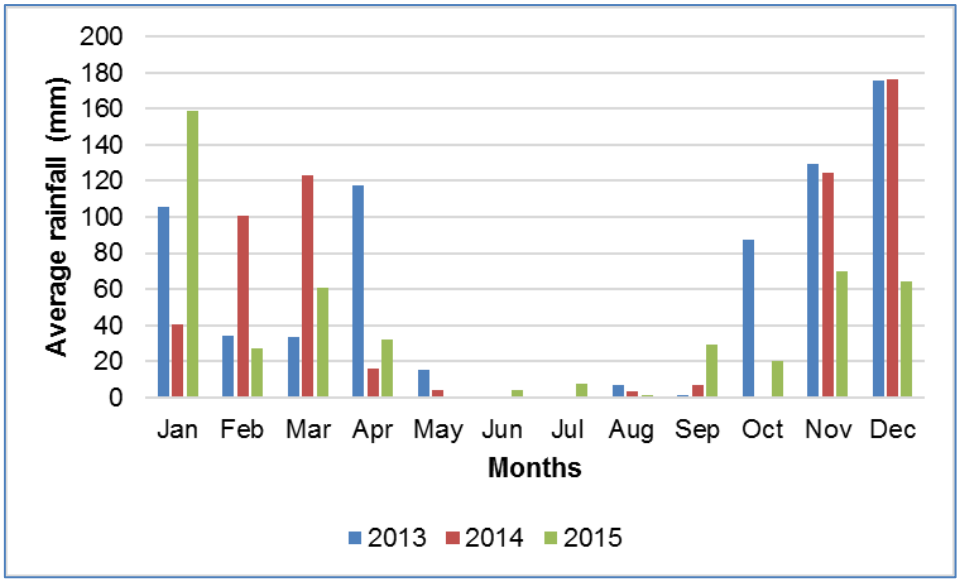
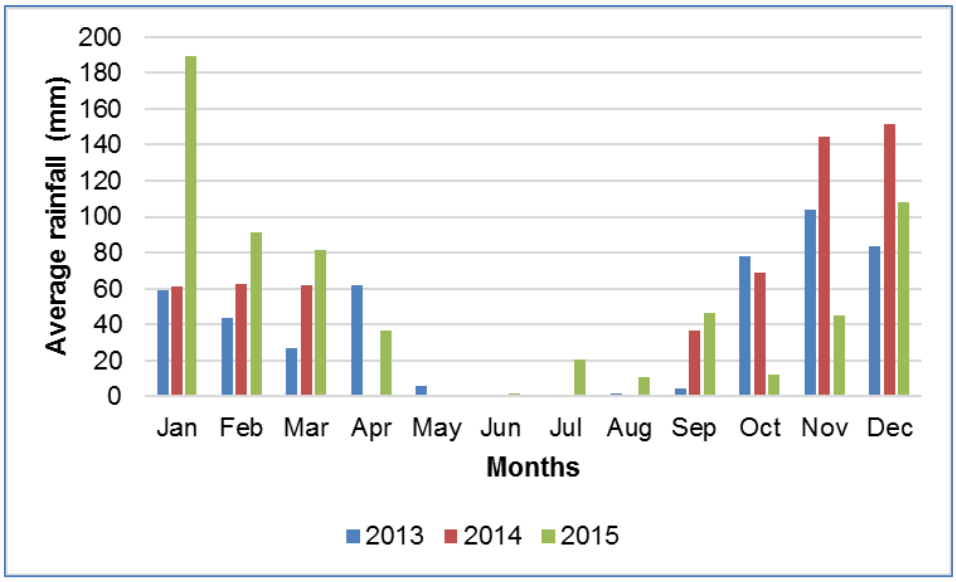


Figure 3.12 Average monthly percentage relative humidity levels for the GJMA – as measured at OR Tambo International Airport (SAWS 2017).



(a)



(b)

Figure 3.13 Average monthly rainfall data for the GJMA area, as recorded at a) OR Tambo International Airport and b) the Johannesburg Botanical Gardens – Derived from SAWS (2017) data.

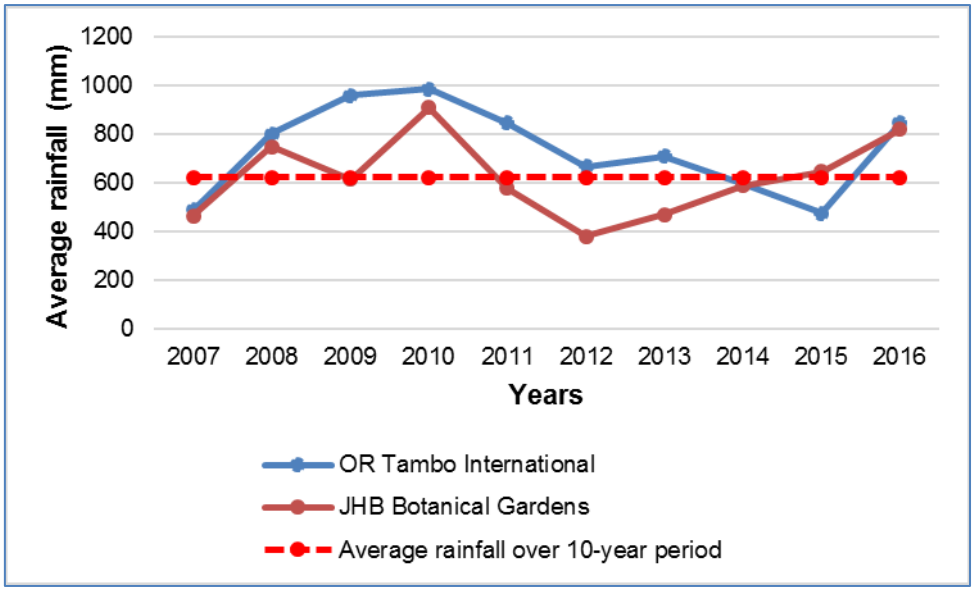


Figure 3.14 Yearly rainfall data for the GJMA area, as recorded at OR Tambo International Airport and the Johannesburg Botanical Gardens – Based on information provided by SAWS (2017).

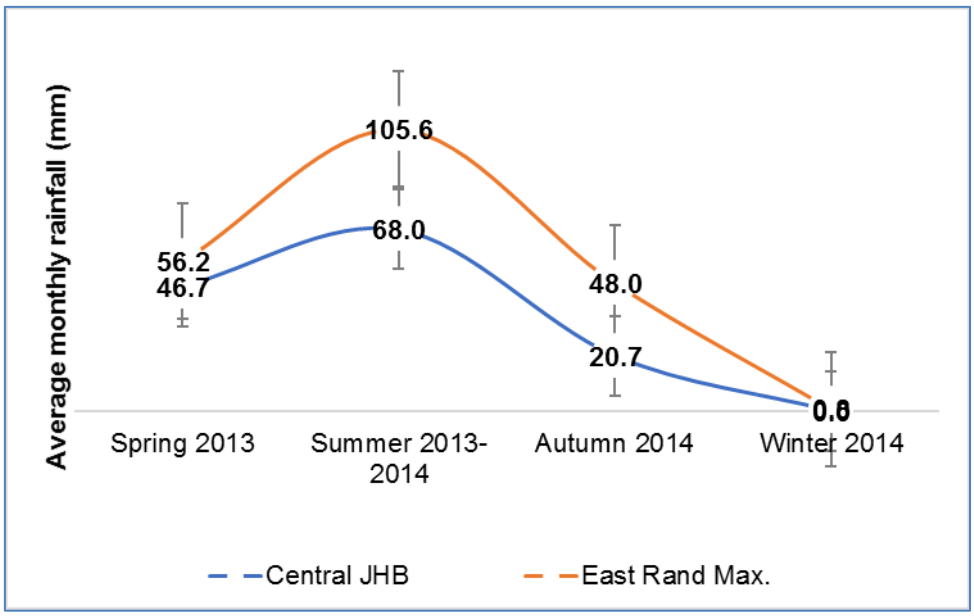


Figure 3.15 Average seasonal rainfall data measured for the central (Johannesburg Botanical Gardens) and eastern parts (OR Tambo International Airport) of the GJMA during Spring 2013 to Winter 2014 - Based on information provided by SAWS (2014).

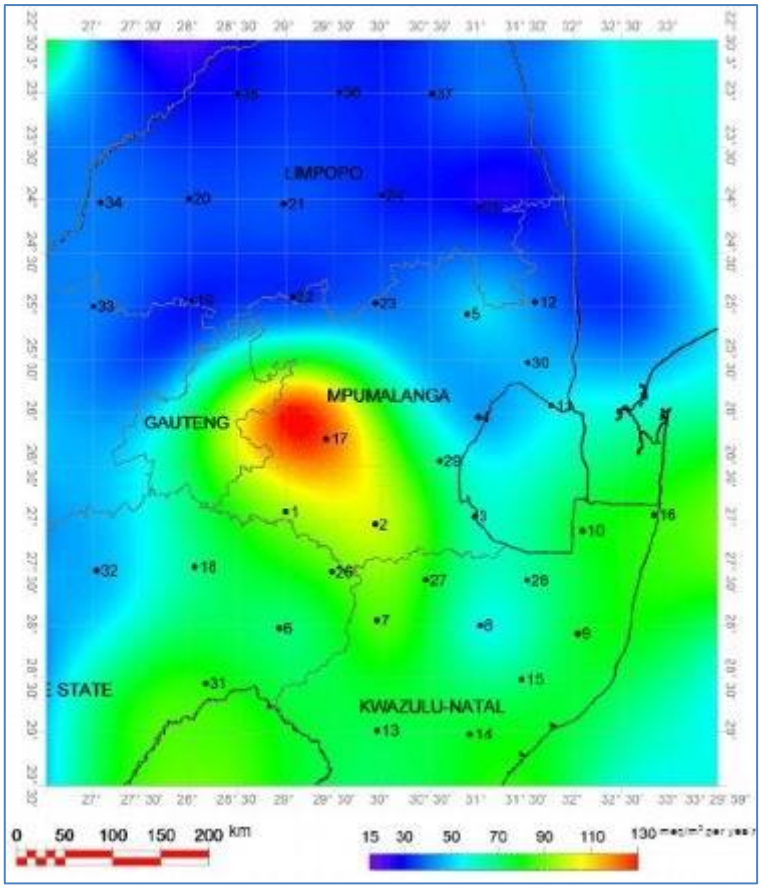


Figure 3.16 Total (dry plus wet) acid deposition rates for Gauteng and other parts of South Africa (Josipovic et al. 2011). https://journals.sajs.aosis.co.za/index.php/sajs/article/view/478/641

3.4.1.3 Wind speed and direction

Monthly wind roses for the period 2012 to 2014 are presented in **Figure 3.17** (SAWS 2014) as measured at the OR Tambo International Airport weather station. **Figure 3.18**, on the other hand (also based on SAWS 2014 measurements), gives the average seasonal wind speeds at the Johannesburg Botanical Gardens versus at OR Tambo International Airport, while wind roses for the month of July are shown in **Figures 3.19 & 3.20**.

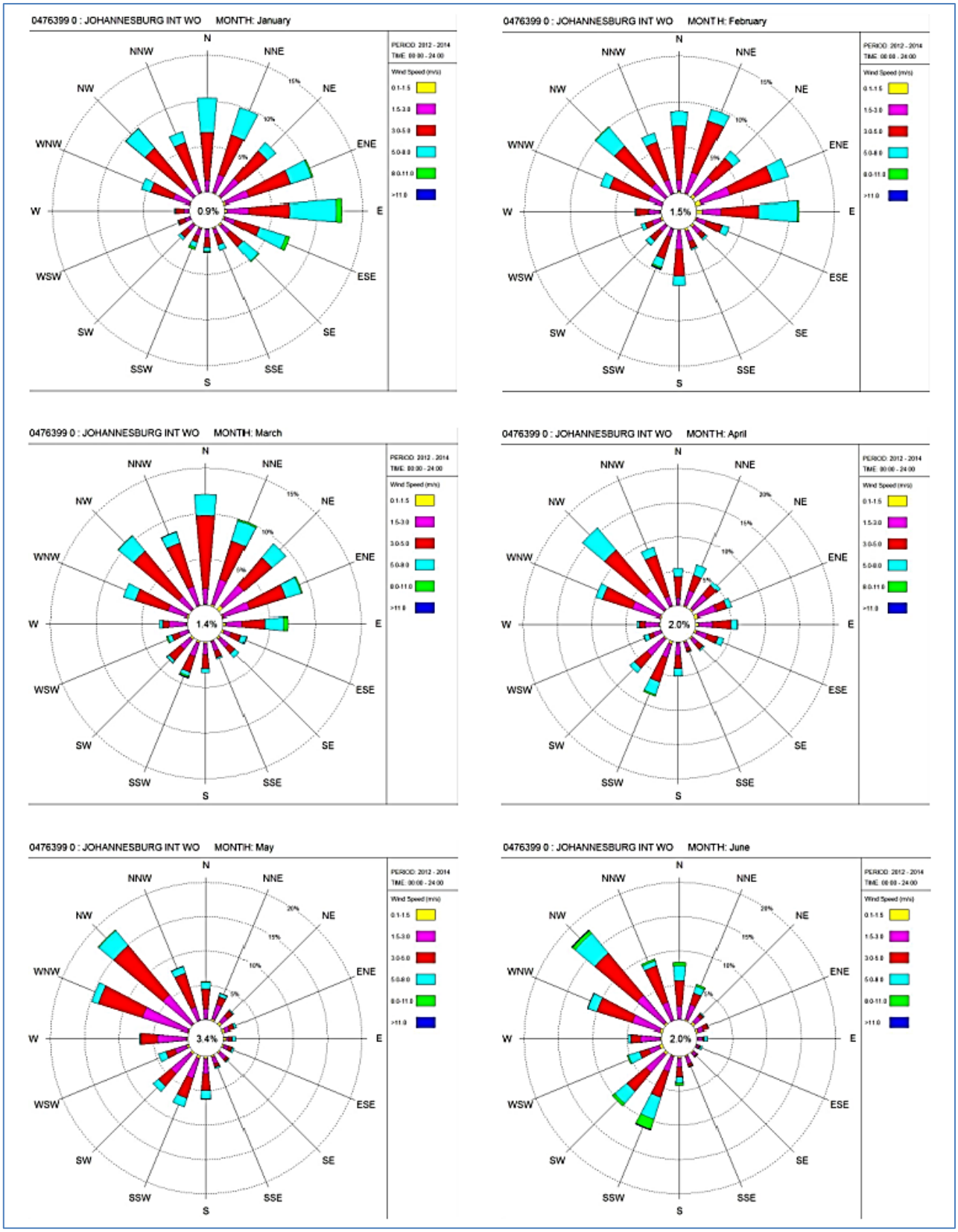


Figure 3.17 (a) Monthly wind roses for the period 2012 to 2014 – as measured at OR Tambo International Airport (SAWS 2014).

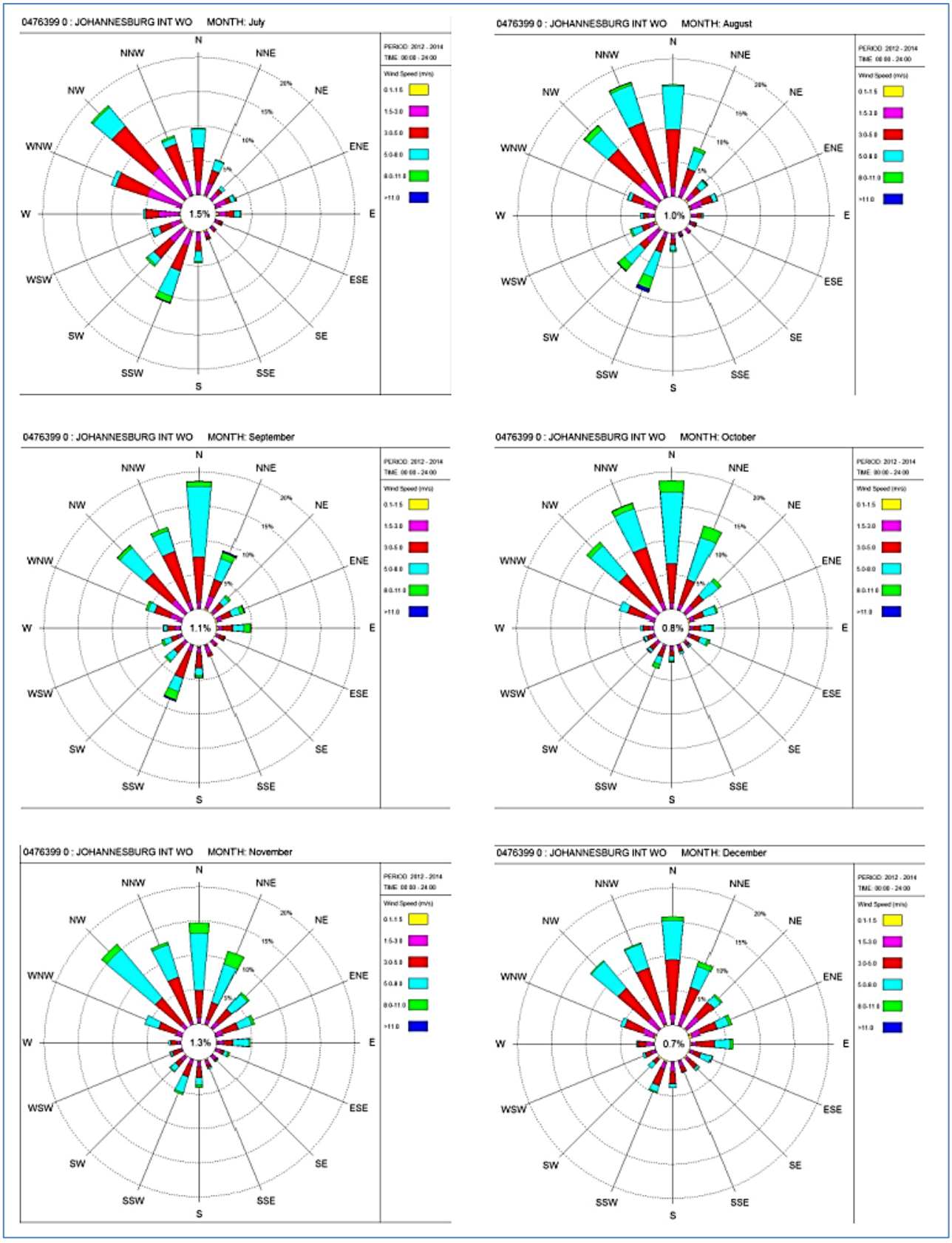


Figure 3.17 (b) Monthly wind roses for the period 2012 to 2014 – measured at OR Tambo International Airport (SAWS 2014).

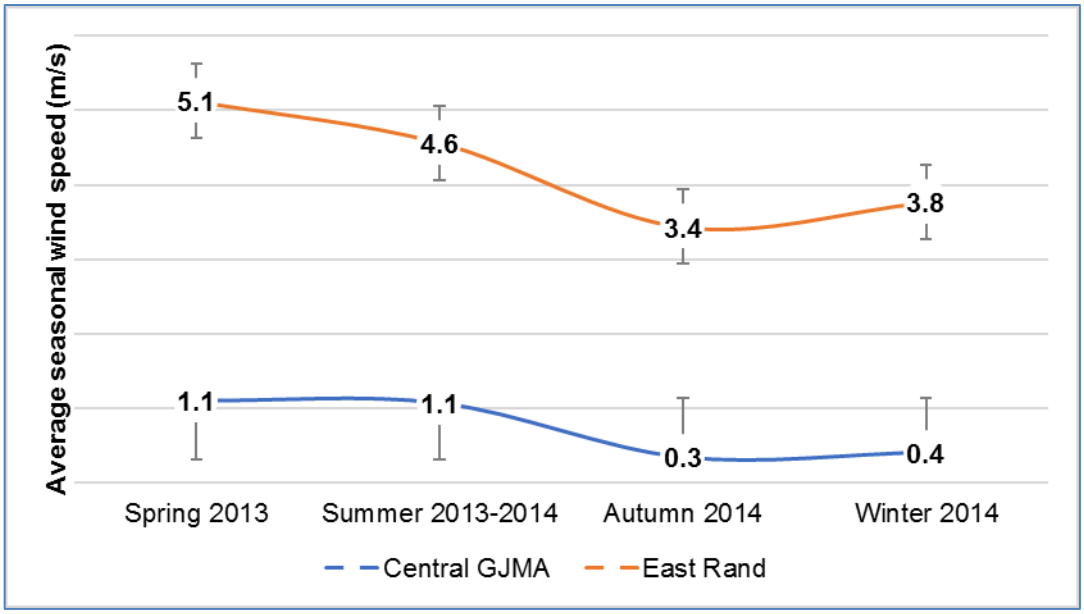


Figure 3.18 Average seasonal wind speeds at the Johannesburg Botanical Gardens (Central GJMA) versus at the OR Tambo International Airport (East Rand) – Based on SAWS (2014) data.

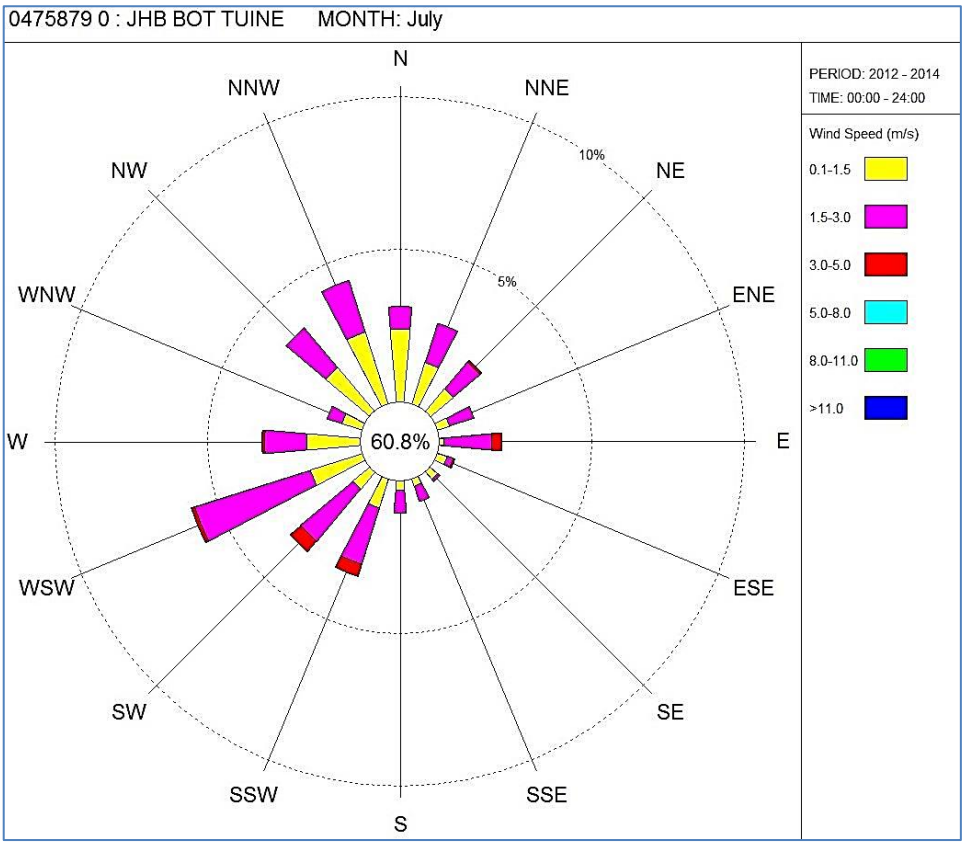


Figure 3.19 Wind roses for the month of July, as recorded by SAWS (2014), from 2012 to 2014 for the Johannesburg Botanical Gardens.

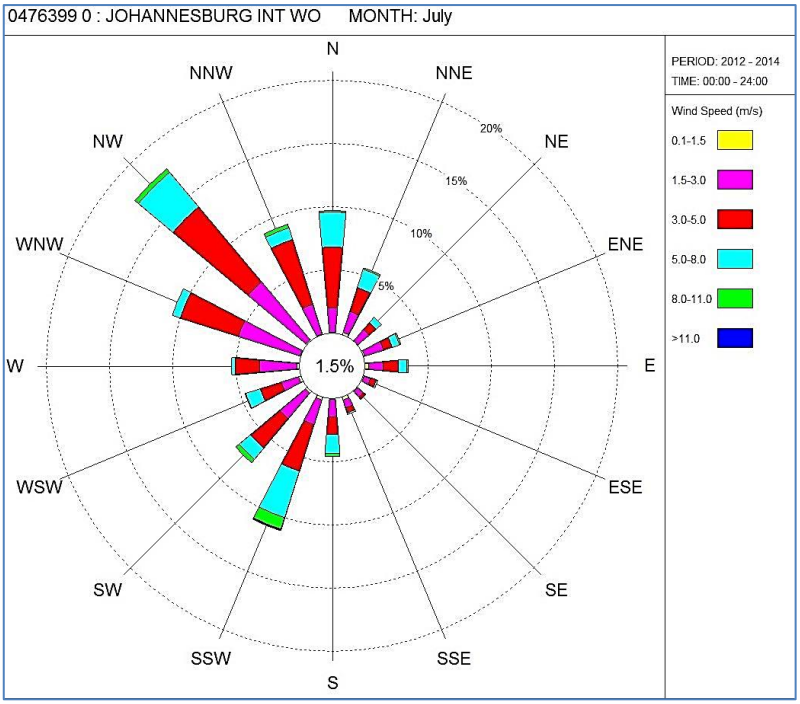


Figure 3.20 Wind roses for the month of July, as determined by SAWS (2014), from 2012 to 2014 for OR Tambo International Airport.

3.4.1.4 Ultraviolet (UV) light radiation

The average yearly and monthly sun hours and sunny days, as well as UV light indices measured for the Johannesburg area, as provided by World Weather Online (2017), are shown in **Figures 3.21 & 3.22**.

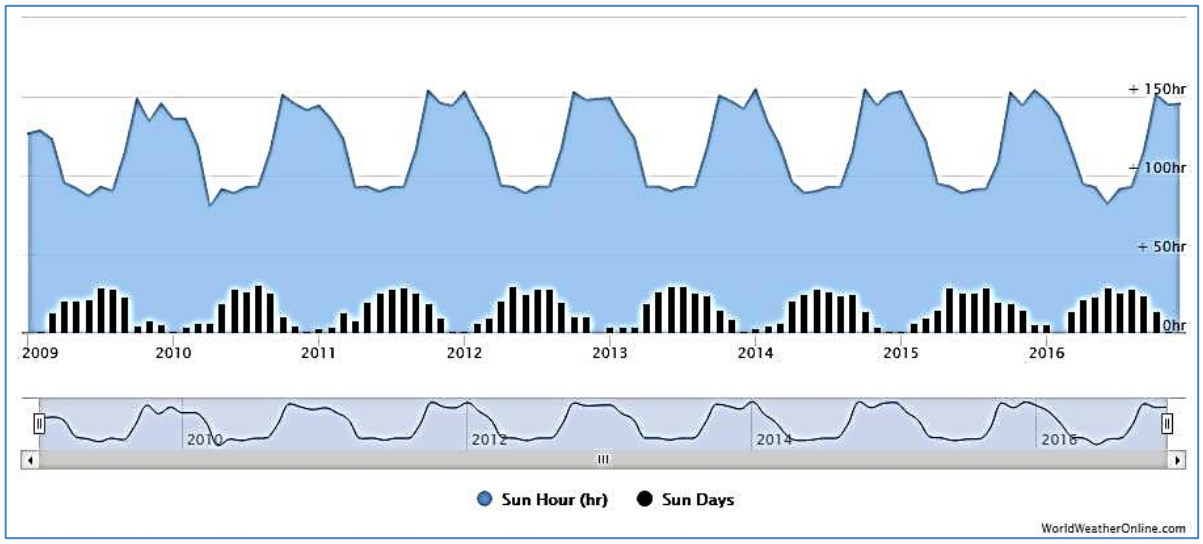


Figure 3.21 Yearly and monthly sun hours and sunny days for the Johannesburg area – Source: World Weather Online (2017). https://www.worldweatheronline.com/

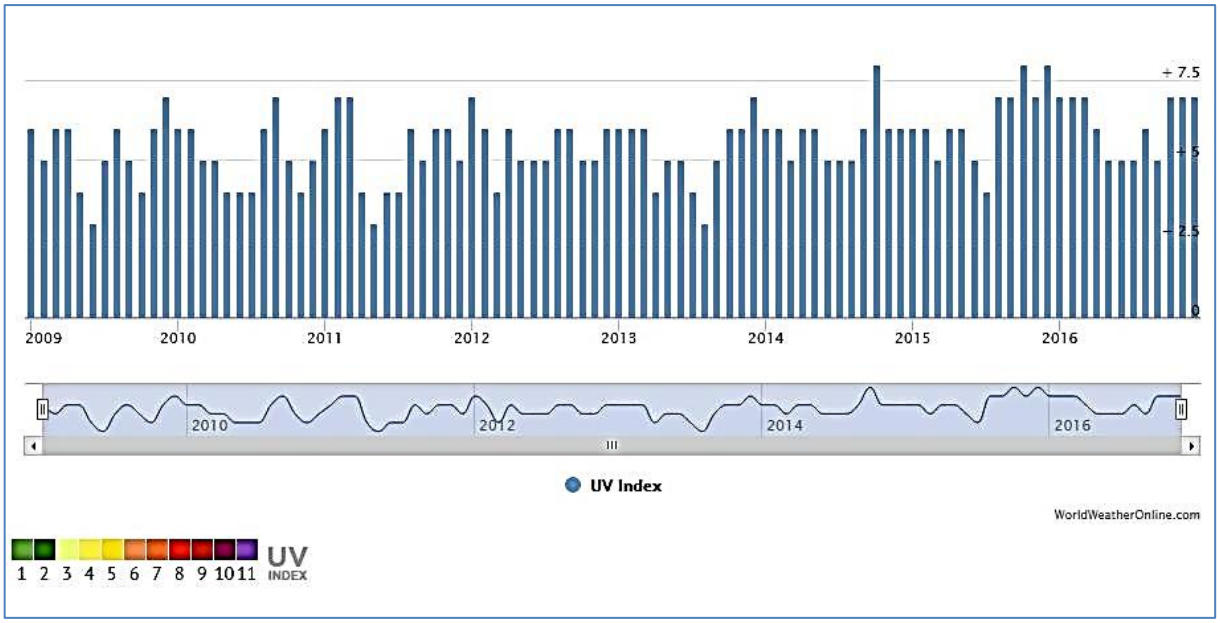


Figure 3.22 Yearly and monthly UV-index values for the Johannesburg area – Source: World Weather Online (2017). https://www.worldweatheronline.com/

3.4.2 Air Pollution Effects

Eight of the twenty-two main GJMA corrosion monitoring sites coincided with historical and current air quality monitoring stations of the City of Johannesburg Metropolitan Municipality. The air quality results from these locations are stored and managed by the South African Weather Services, via the SAAQIS system (DEA 2017a). Unfortunately, the databases for the Johannesburg sites showed significant gaps, particularly concerning the latest corrosion study period. Therefore, it was decided to instead refer to historical pollution data for these locations, which appeared more comprehensive.

A complete set of historical data for the eight air quality/corrosion monitoring sites was obtained for PM_{10} particulate (dust) matter concentrations and are presented in **Figure 3.23**. **Figure 3.24** gives the monthly levels of sulphur dioxide (SO_2) in the atmosphere at six of the locations, while NO_2 results from four main GJMA sites are presented in **Figure 3.25** (DEA 2017a).

The six-year average of global tropospheric NO_2 Vertical Column Density in 10^{15} molecule/m^2 is shown in **Figure 3.26** (Beirle et al. 2003). The data were derived by means of the Global Ozone Monitoring Experiment (GOME) on board the ESA-satellite

ERS-2 (Beirle et al. 2003). The diurnal pattern in the levels of NO_2 for the GJMA is presented in **Figure 3.27** (DEA 2017a).

Nitrogen oxide (NO) pollution data were only obtainable for three of the eight air quality/corrosion monitoring sites, as shown in **Figure 3.28** (DEA 2017a).

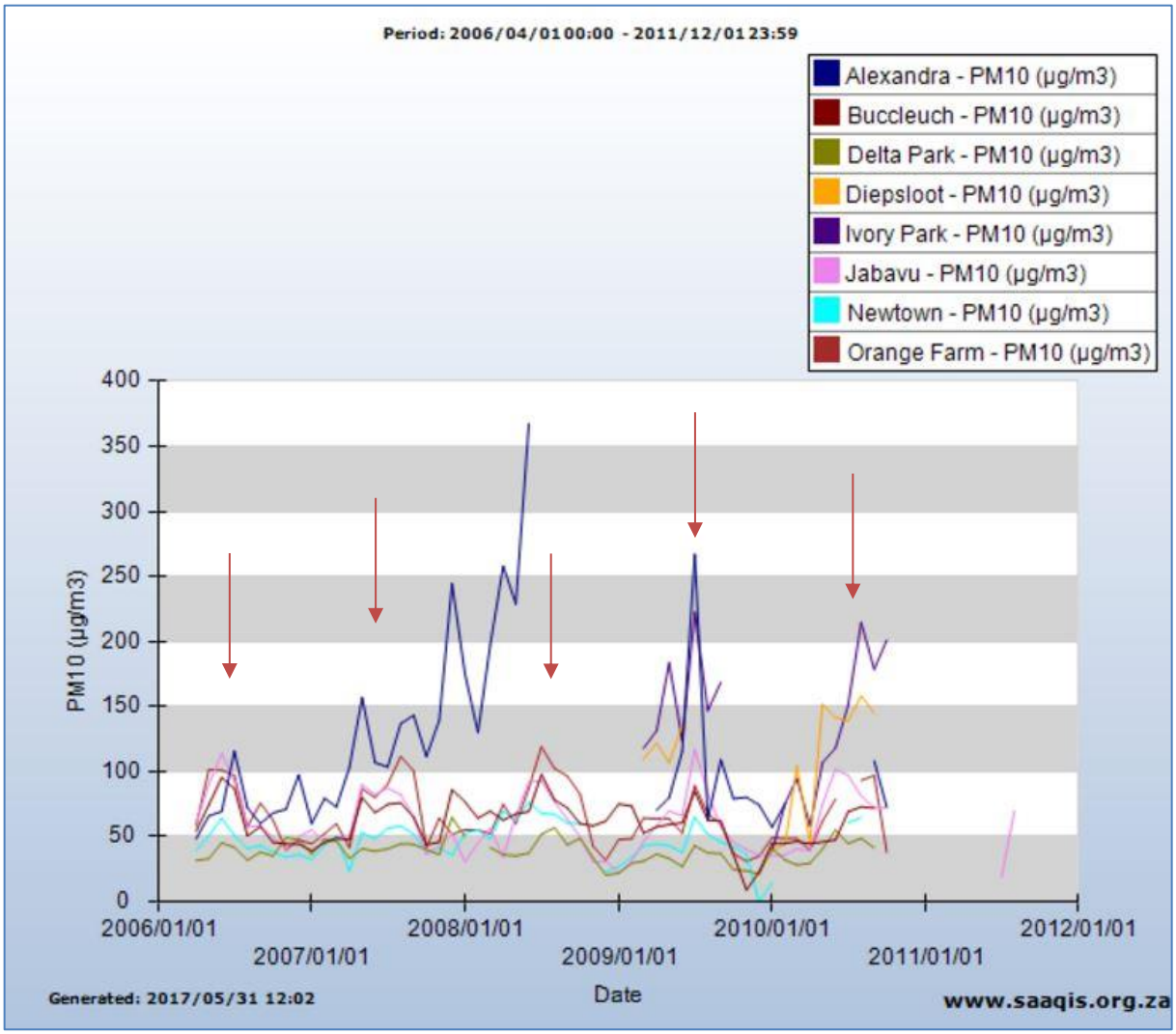


Figure 3.23 Monthly average PM_{10} particulate concentrations for eight air quality/corrosion monitoring sites in the GJMA (DEA 2017a).

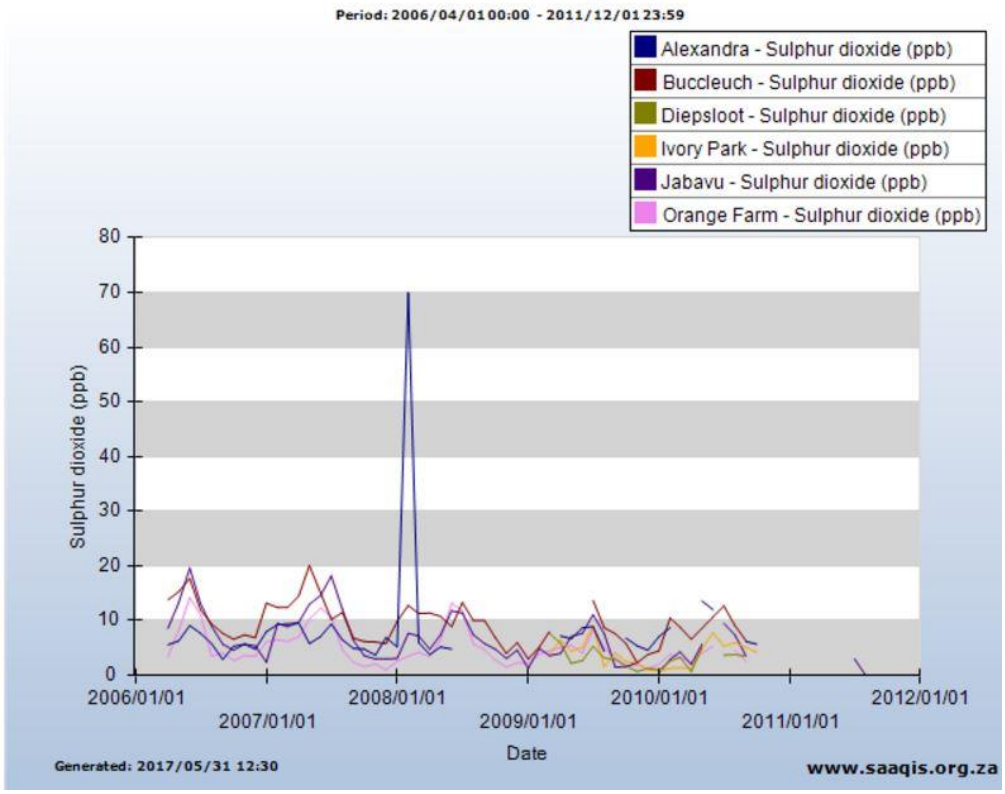


Figure 3.24 Monthly average SO_2 concentrations for six air quality/corrosion monitoring sites (DEA 2017a).

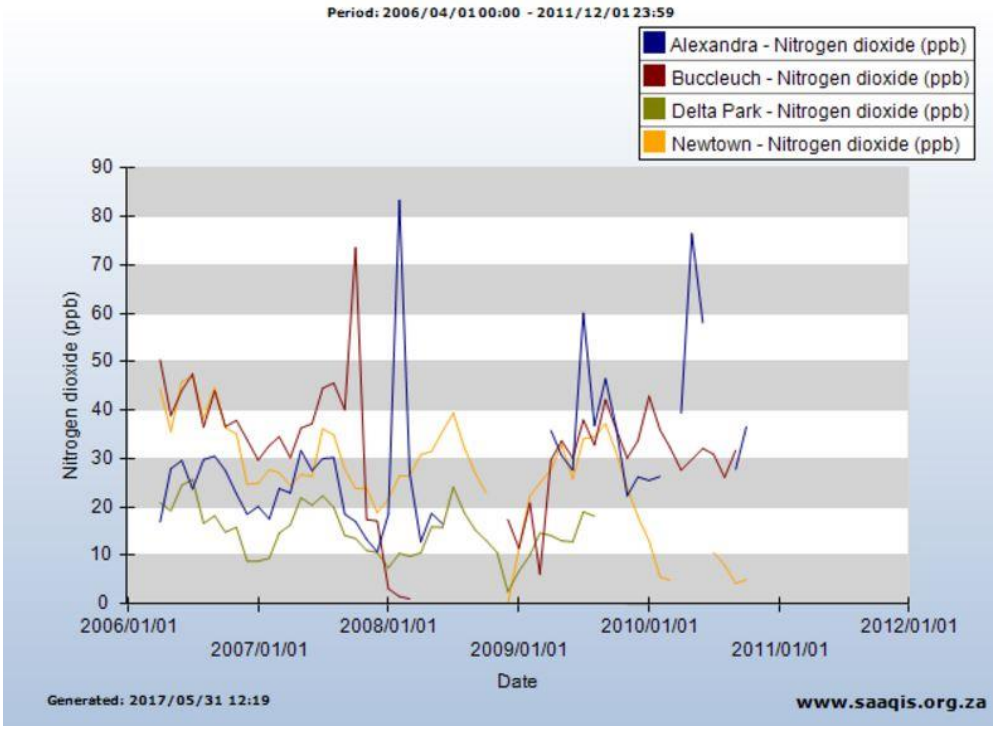


Figure 3.25 Monthly average NO_2 concentrations for some of the air quality/corrosion monitoring sites (DEA 2017a).

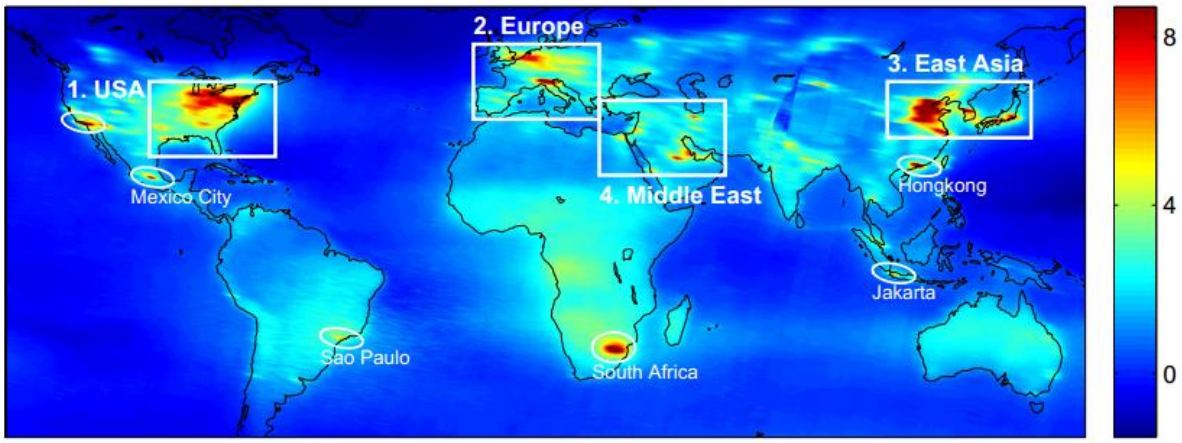


Figure 3.26 Six-year mean (1996-2001) of global tropospheric NO_2 Vertical Column Density in 10^{15} molecules/m^2 – Source: Beirle et al. (2003).

https://www.atmos-chem-phys.net/3/2225/2003/

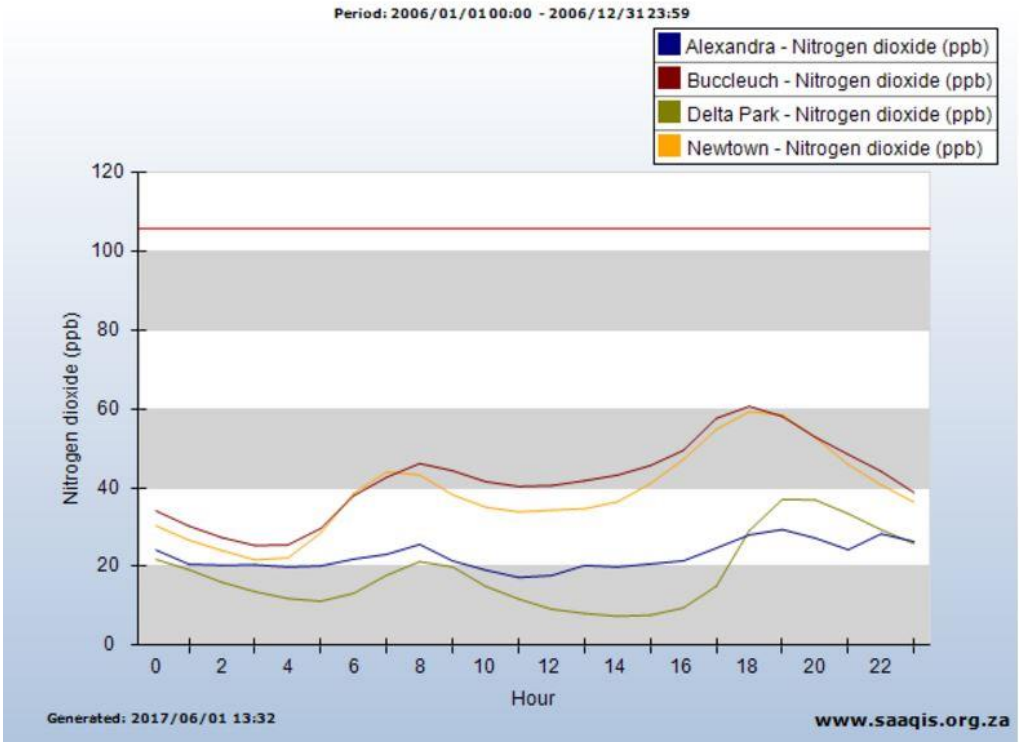


Figure 3.27 Diurnal patterns in the average NO_2 concentrations for four of the GJMA air quality/corrosion monitoring sites (DEA 2017a).

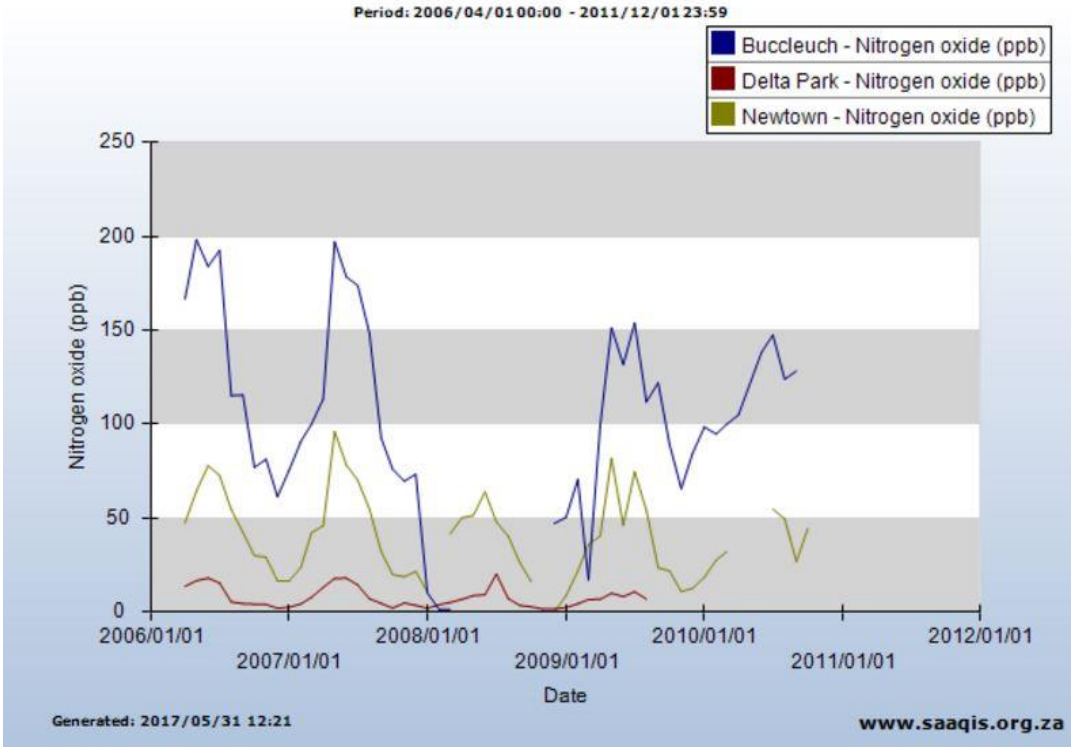


Figure 3.28 Monthly average NO concentrations for three of the eight air quality/corrosion monitoring sites (DEA 2017a).

Figure 3.29 (DEA 2017a) displays the monthly average $PM_{2.5}$ particulate (dust) matter concentrations at the Buccleuch air quality/corrosion monitoring site.

Figure 3.30 (Yale Data Driven 2016) indicates that elevated $PM_{2.5}$ levels are also a more widespread problem for the GJMA region, while **Figure 3.31** (DEA 2017a) gives the concentrations of carbon monoxide (CO) at three of the main GJMA sites.

Figure 3.32 (DEA 2017a) presents O_3 concentrations for some of the air quality/corrosion monitoring sites, with the diurnal pattern for O_3 pollution in the GJMA atmosphere given in **Figure 3.33** (DEA 2017a).

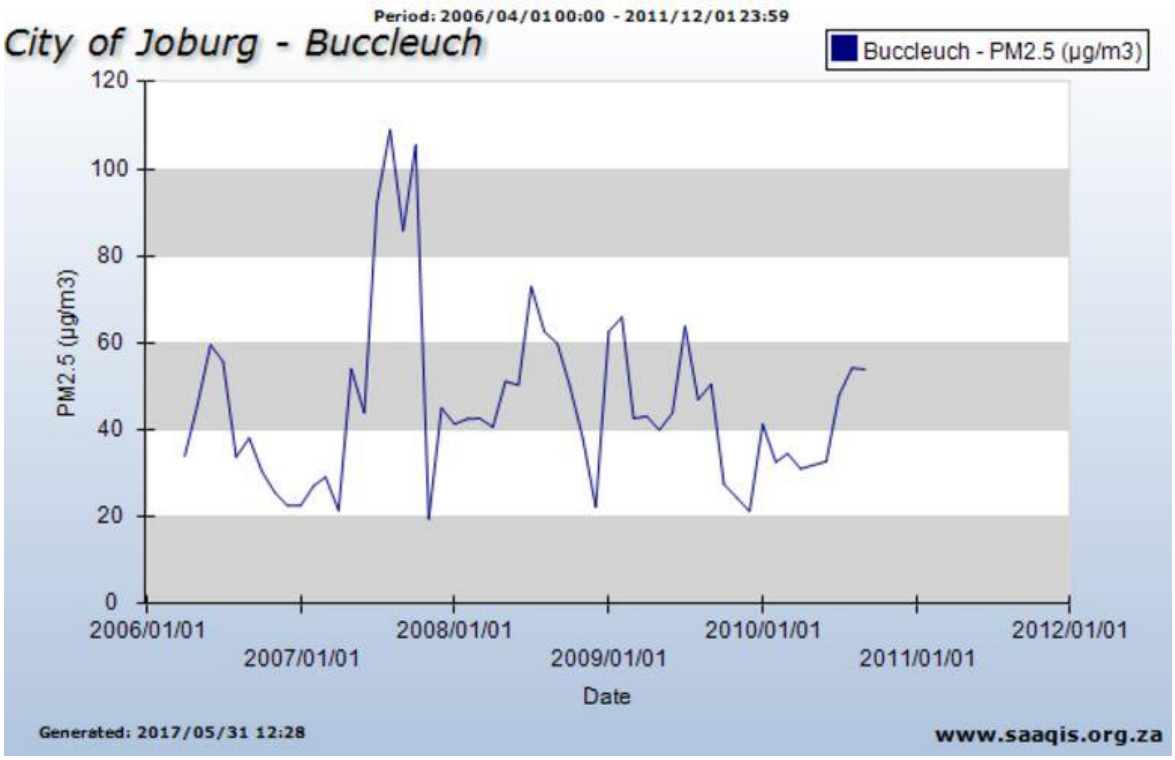


Figure 3.29 Monthly average $PM_{2.5}$ particulate concentrations for the Buccleuch air quality/corrosion monitoring site (DEA 2017a).

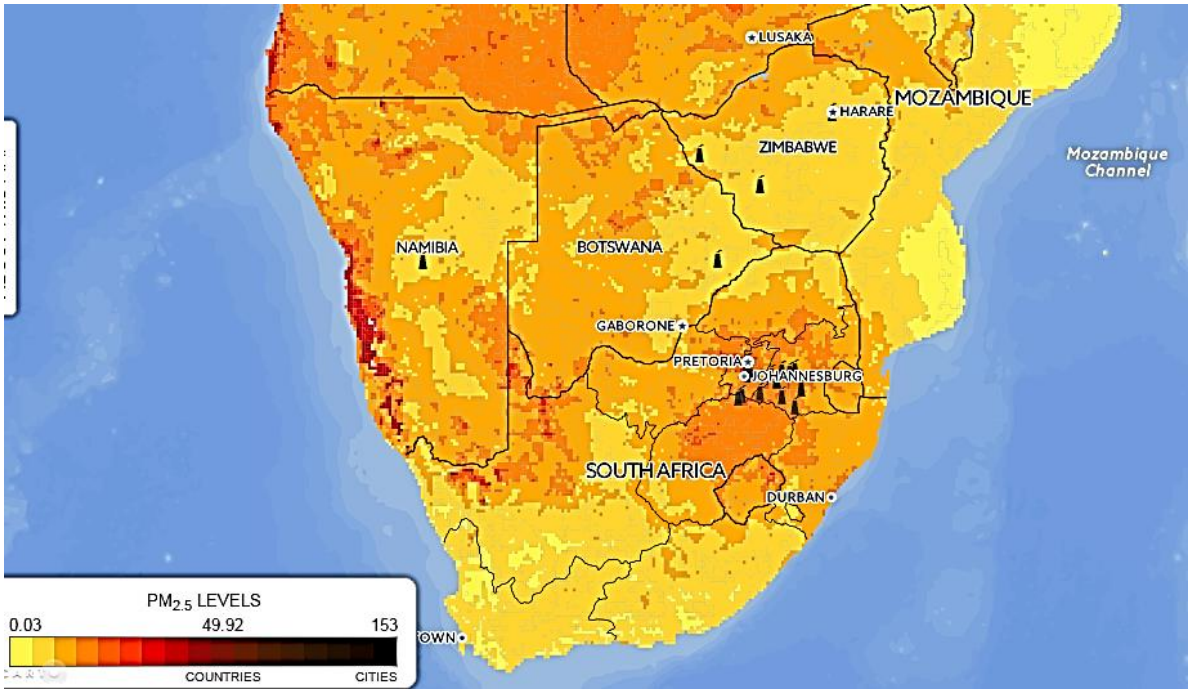


Figure 3.30 $PM_{2.5}$ satellite measurements for Southern Africa (Yale Data Driven 2016). http://visuals.datadriven.yale.edu/airmap_2016/

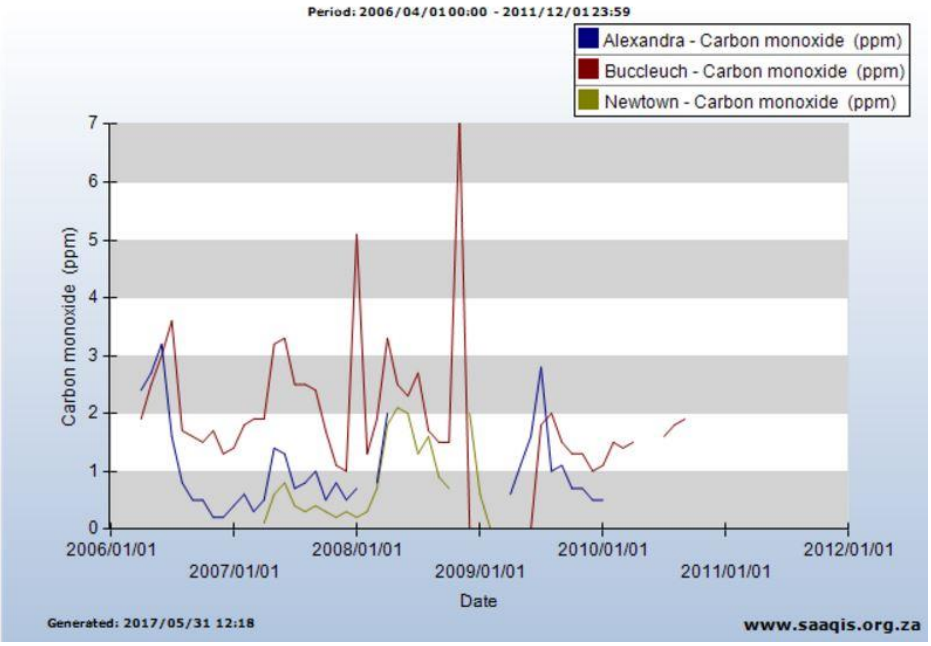


Figure 3.31 Monthly average CO concentrations for three of the air quality/corrosion monitoring GJMA sites (DEA 2017a).

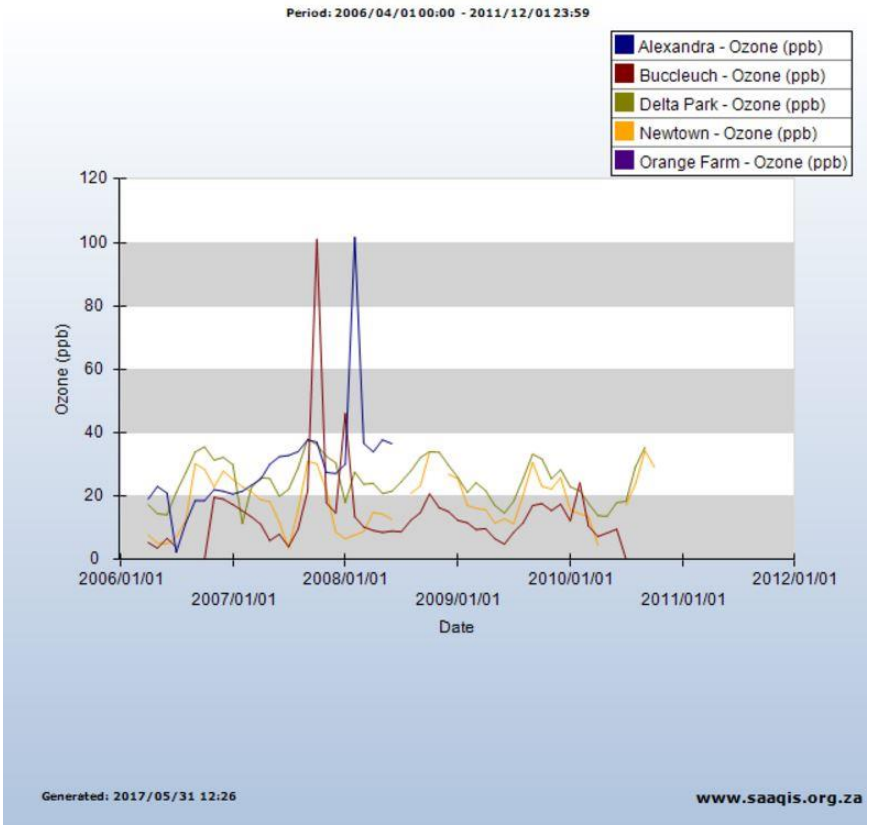


Figure 3.32 Monthly O_3 concentrations for some of the air quality/corrosion monitoring GJMA sites (DEA 2017a).

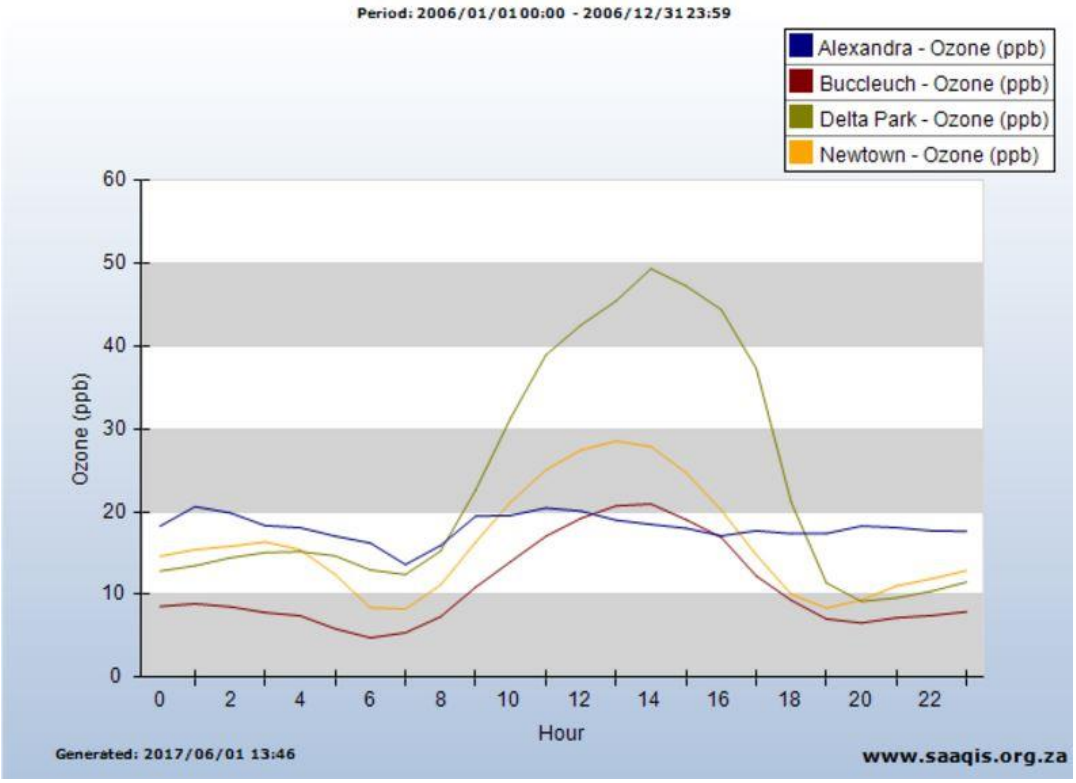


Figure 3.33 Diurnal pattern of O_3 pollution in the GJMA (DEA 2017a).

Finally, the level of visibility (generally reduced by haze - measured in km) in the GJMA is shown in **Figure 3.34** (World Weather Online 2017).

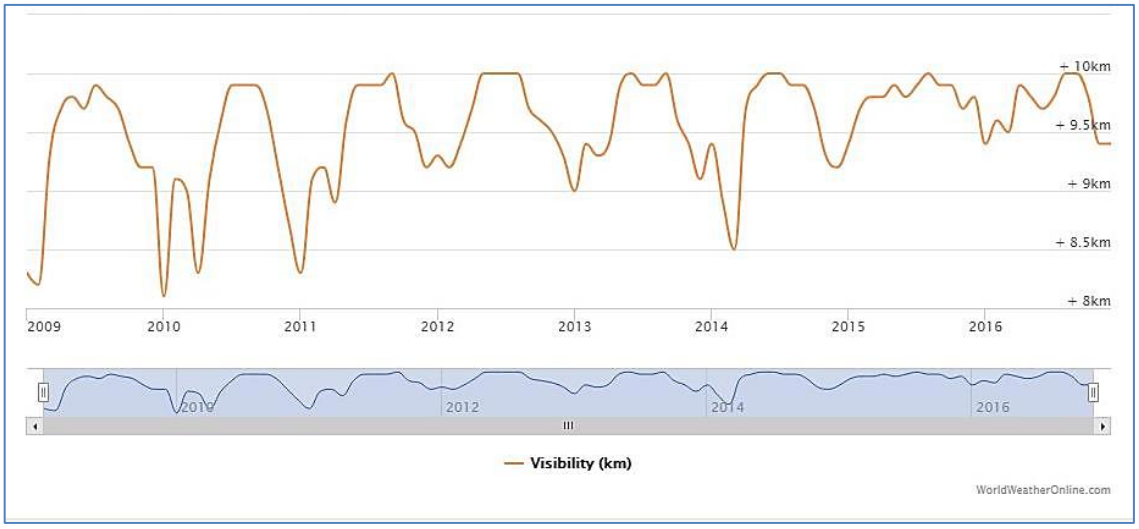


Figure 3.34 Yearly and monthly visibility data for the Johannesburg area – Source: World Weather Online (2017). https://www.worldweatheronline.com/

3.5 MAPPING PROCEDURES

The collated, as well as the latest measured corrosion data for the various South African and GJMA locations, were processed into atmospheric corrosion maps, using ESRI - ArcGIS 10.2 software - a geographical information system (GIS) developing programme. The derived maps (Chapter 6) are based on the first-year corrosion rates of mild steel, hot-dip galvanised steel, aluminium, copper and zinc, as well on the CLIMAT ICI values.

The corrosion rates per site and metal type, together with the associated GPS coordinates, tabulated in Microsoft Excel spreadsheets, were subsequently imported into the ArcGIS software programme, and layered over existing physical and rainfall base maps, using the GPS coordinates. The base maps were supplied by ESRI – ArcGIS and the South African Weather Services.

Following a display of the spatial corrosion data on the base maps, the corrosion rates at those locations without any measurements were predicted by means of the IDW (Inverse Distance Weighted) interpolation technique, with an output cell size of 0.002 and a variable radius using four points. This process assumed that the corrosion rate per metal type for an unsampled point is the weighted average of the measured values within the vicinity, and the weights are inversely related to the distances between the estimated location and the sampled sites (Lu & Wong 2008). Demarcation of the atmospheric corrosivity of South Africa's coastlines was furthermore done using Adobe Photoshop CS6 and Microsoft Paint - 2016, taking into consideration the average decreases in the corrosivity of South Africa's coastal regions, with increasing distance spans from the ocean.

In the case of the GJMA maps, the interpolated vector-data were projected over a physical map of the Johannesburg area, whereas regarding the national charts, the interpolated atmospheric corrosion data were superimposed on geographical, temperature and rainfall maps for South Africa. Keys, line scales, compasses and select conventional map symbols were included, to facilitate ease of interpretation and widespread use of the charts.

CHAPTER 4

RESULTS

4.1 ASSIMILATIONS OF EXISTING PUBLISHED AND UNPUBLISHED ATMOSPHERIC CORROSION DATA FOR SOUTH AFRICA

Based on assimilations of published and unpublished data (CSIR 1975; Callaghan 1991; Nixon 1991,1993; Gross & Nixon 1993; Janse van Rensburg 1994, 2010, 2015; Gnoinski & Ramothlola 1994; Leitch 1999, 2003, 2006; Eskom, 2010-2016) the locations where atmospheric corrosion monitoring work has been conducted in South Africa, combined with their relative altitudes, are presented in **Figure 4.1**. Recorded first-year (12-month) corrosion rates of mild (carbon) steel, galvanised steel, aluminium, copper and zinc at these sites (where available) are also presented in **Figures 4.2-4.7**.

Noteworthy is that two maps with different keys (**Figures 4.4 & 4.5**) for zinc are provided. This is to enable enhanced reflection of the corrosion rates of pure zinc at the various locations (**Figure 4.4**), as well as to allow for comparisons with the hot-dip galvanised steel data (**Figure 4.5**).

4.2 ATMOSPHERIC CORROSION OF THE GJMA

Photographs of each of the 57 GJMA sites, where mild steel, hot-dip galvanised steel, aluminium, copper, zinc and various coated mild steel coupons were exposed over a period of 24 months, are presented in **Appendix F – Figures F.1 – F.228**.

Unfortunately, some of the devices were lost (due to theft) during the study. However, this did not detract from the validity of the overall results.

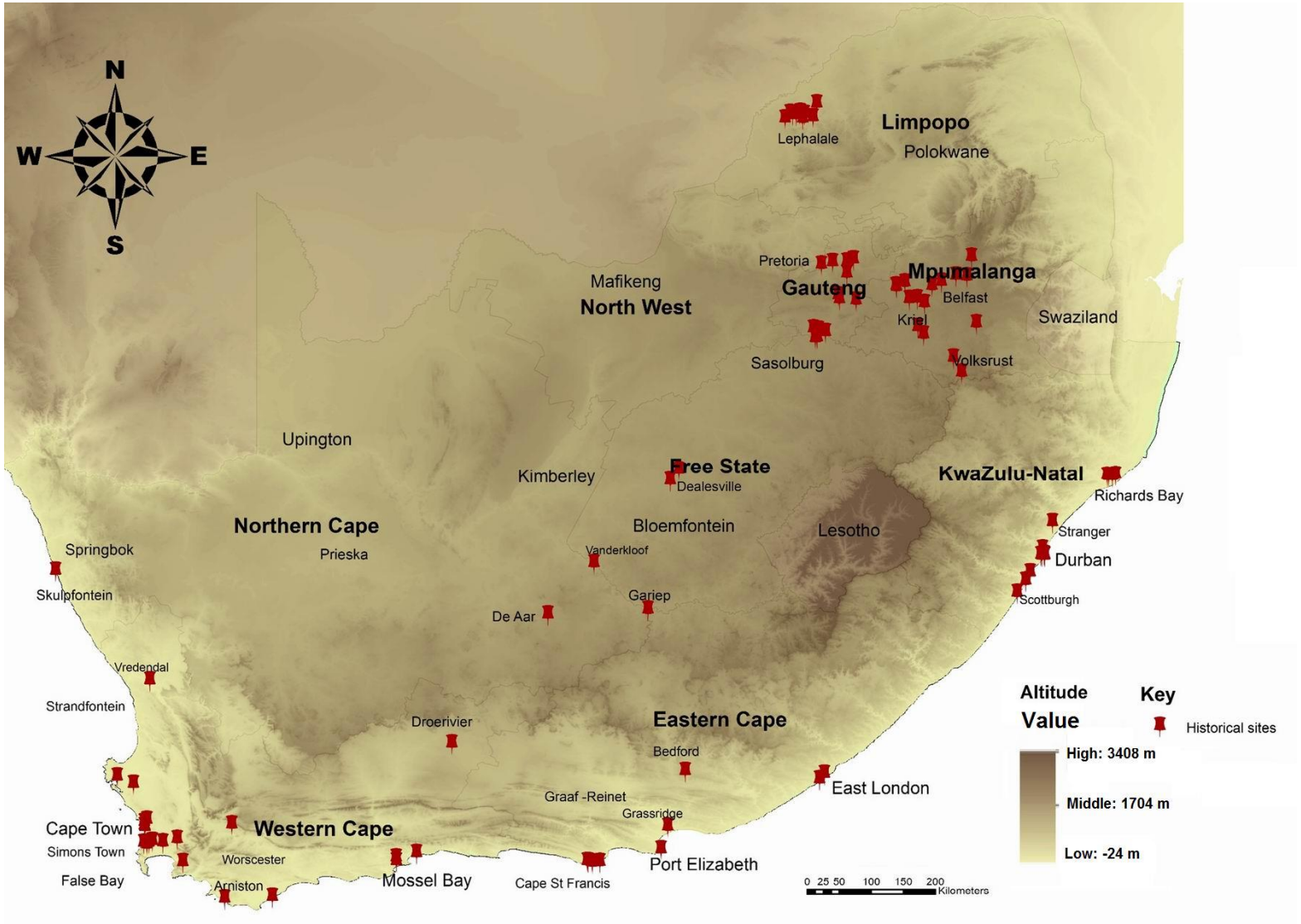


Figure 4.1 Historical atmospheric corrosion monitoring locations in South Africa – projected over an altitude map (in metres). (ArcGIS Base map).

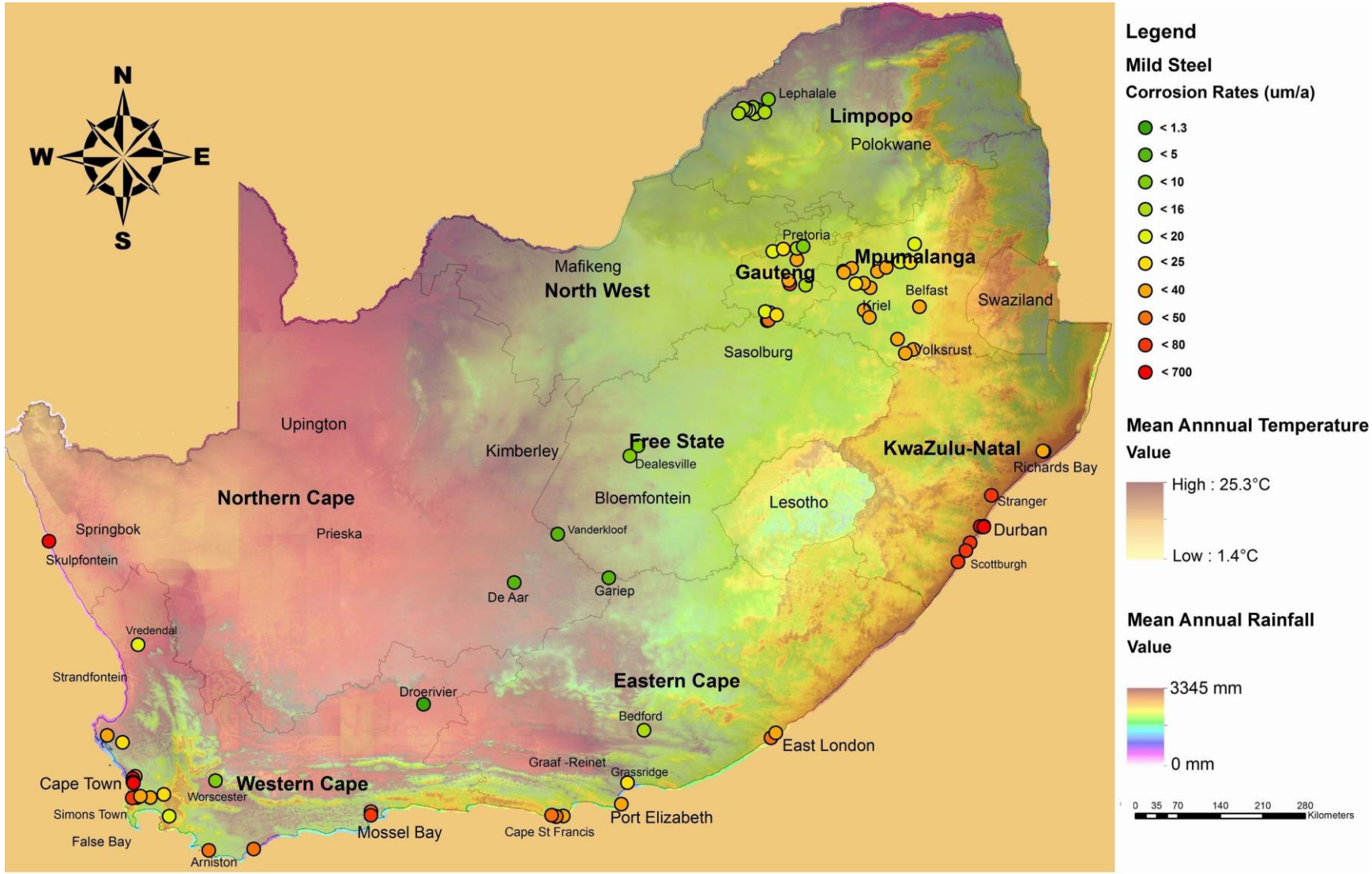


Figure 4.2 First-year (12-month) corrosion rates of mild (carbon) steel at various locations throughout South Africa (based on existing published and unpublished data). (ArcGIS Base map).

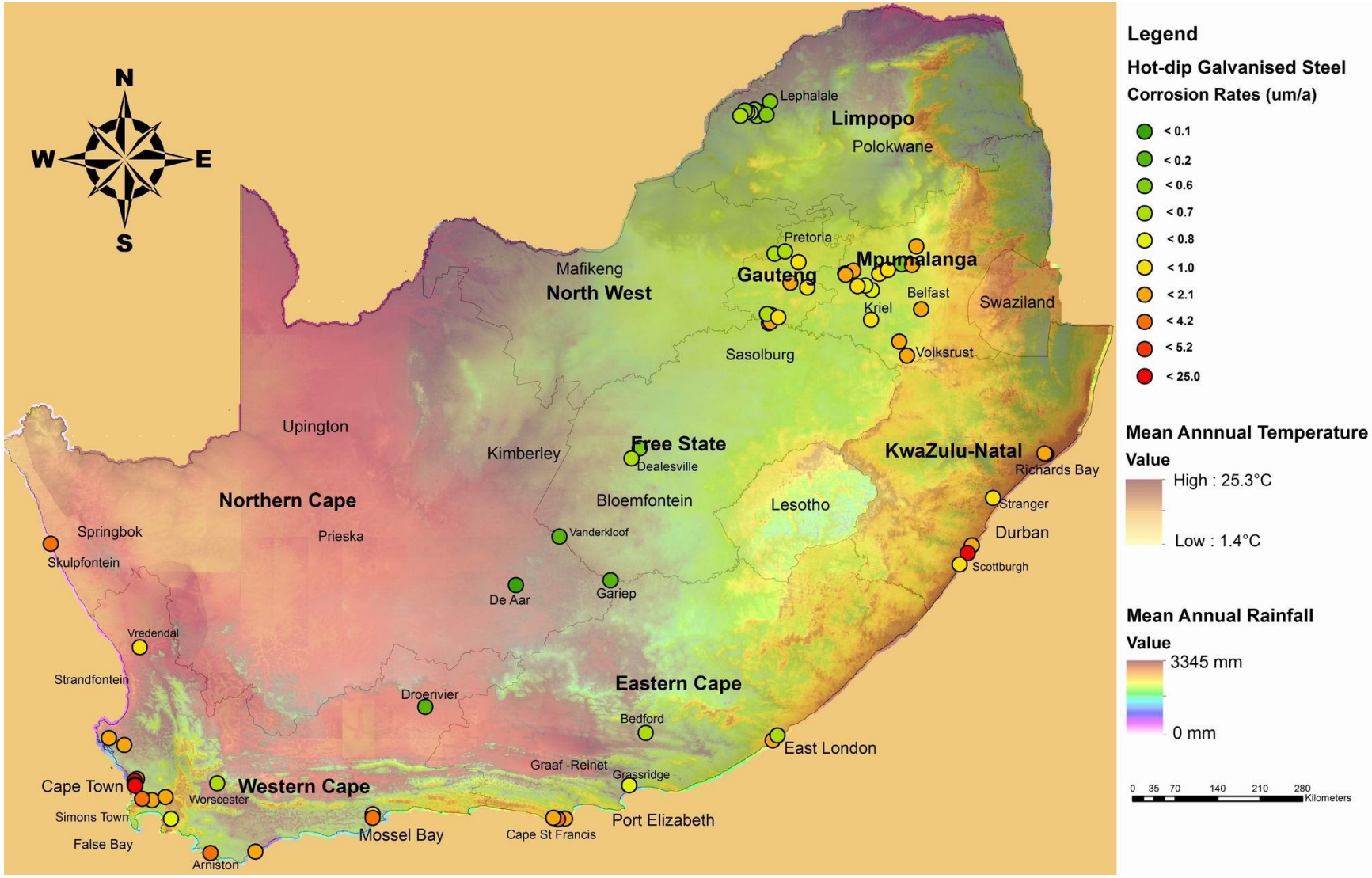


Figure 4.3 First-year (12-month) corrosion rates of hot-dip galvanised steel at different places throughout South Africa (based on existing published and unpublished data). (ArcGIS Base map).

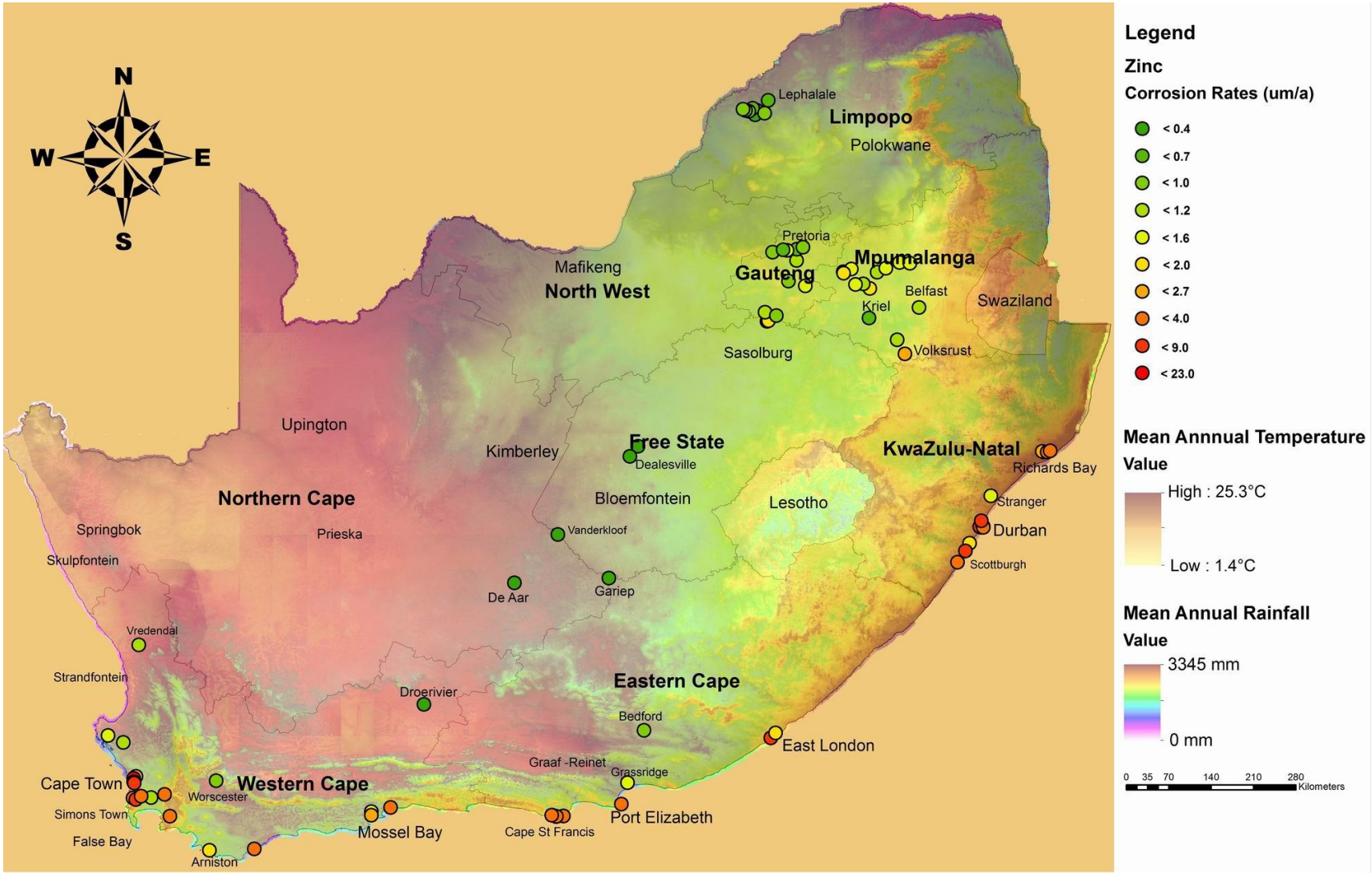


Figure 4.4 First-year (12-month) corrosion rates of pure zinc at various locations throughout South Africa (based on existing published and unpublished data). (ArcGIS Base map).

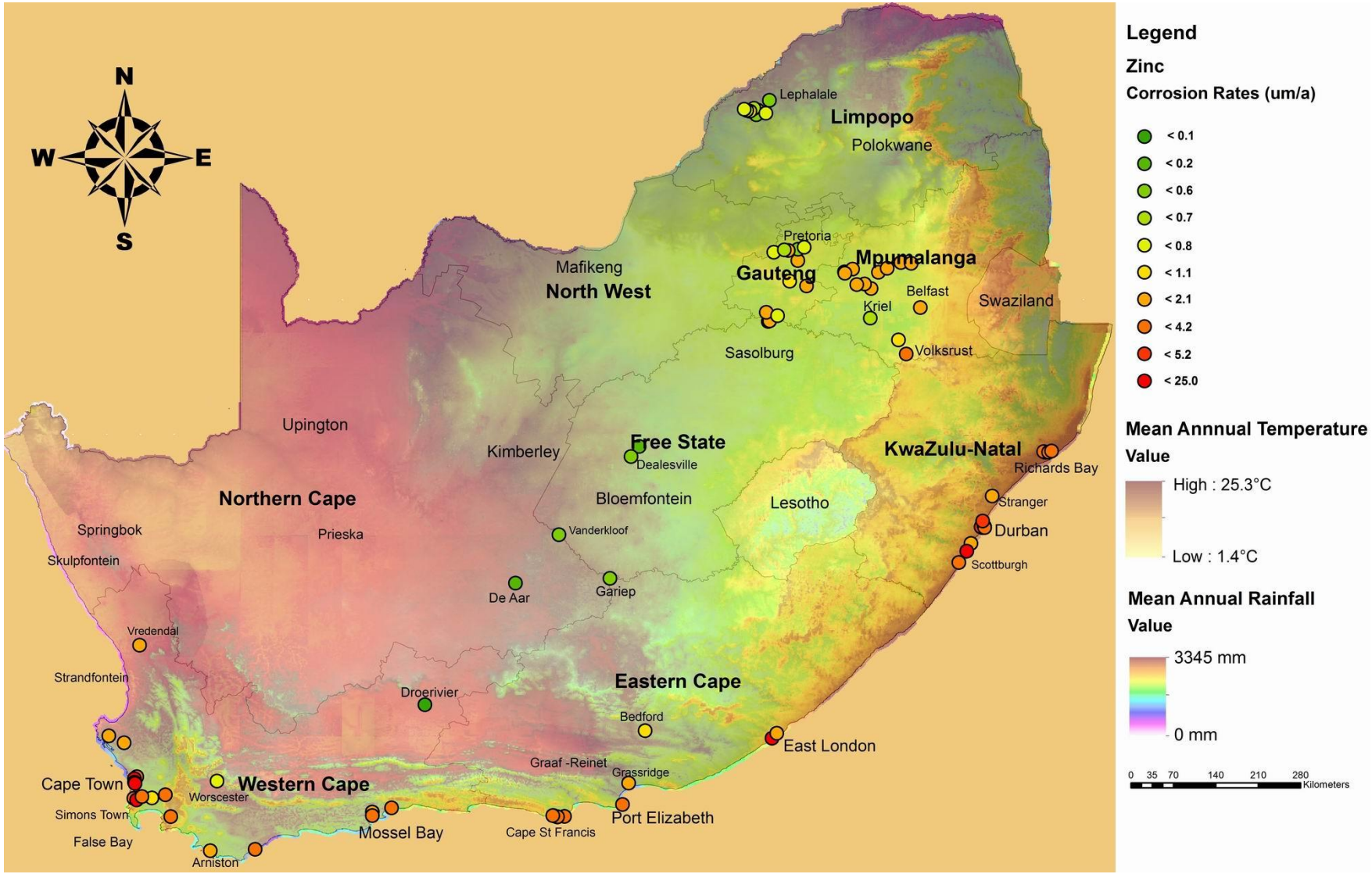


Figure 4.5 First-year (12-month) corrosion rates of pure zinc at different locations throughout South Africa (based on existing published and unpublished data) – with the same key as **Figure 4.3.** (ArcGIS Base map).

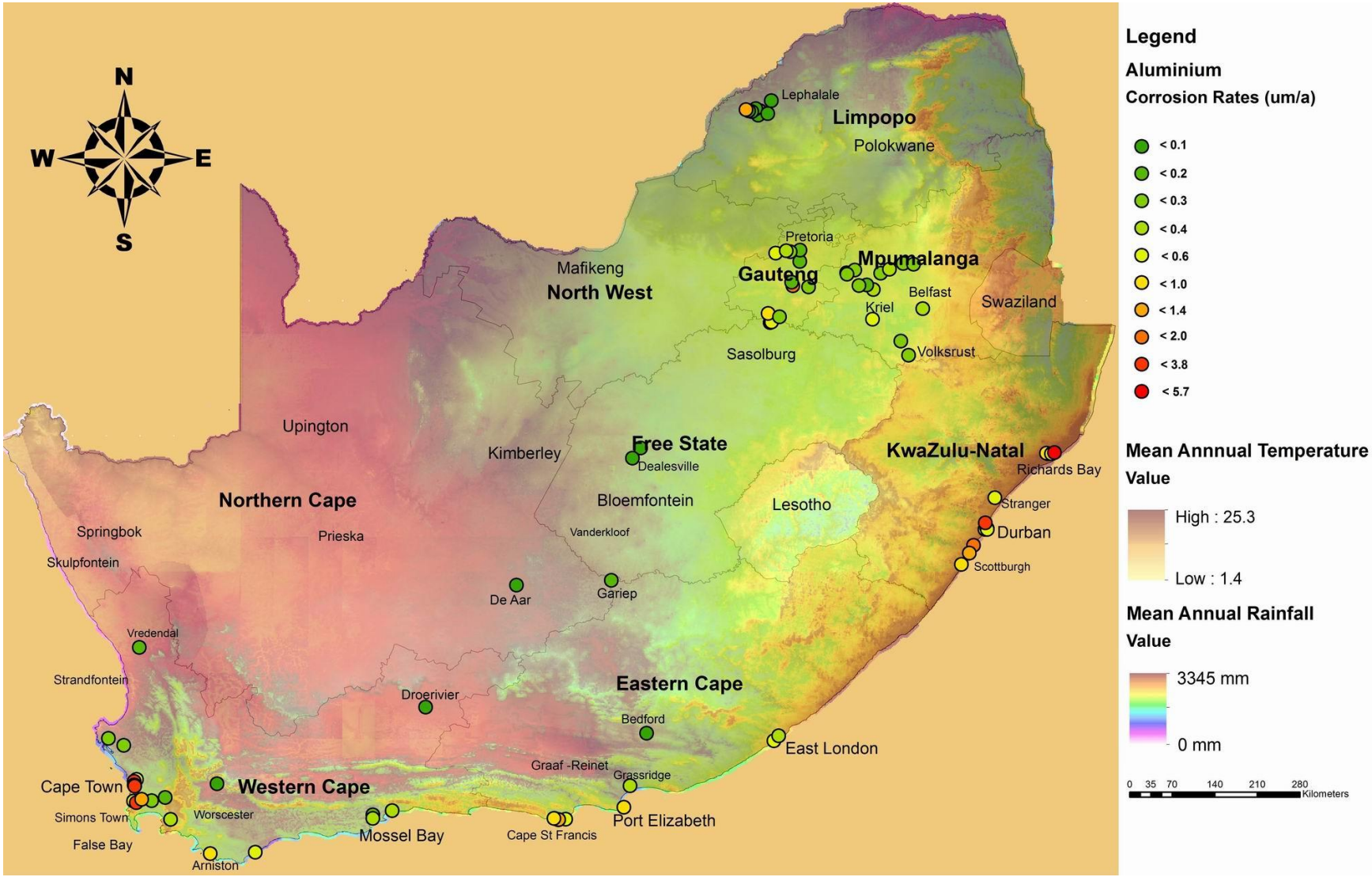


Figure 4.6 First-year (12-month) corrosion rates of pure aluminium at various locations throughout South Africa (based on existing published and unpublished data). (ArcGIS Base map).

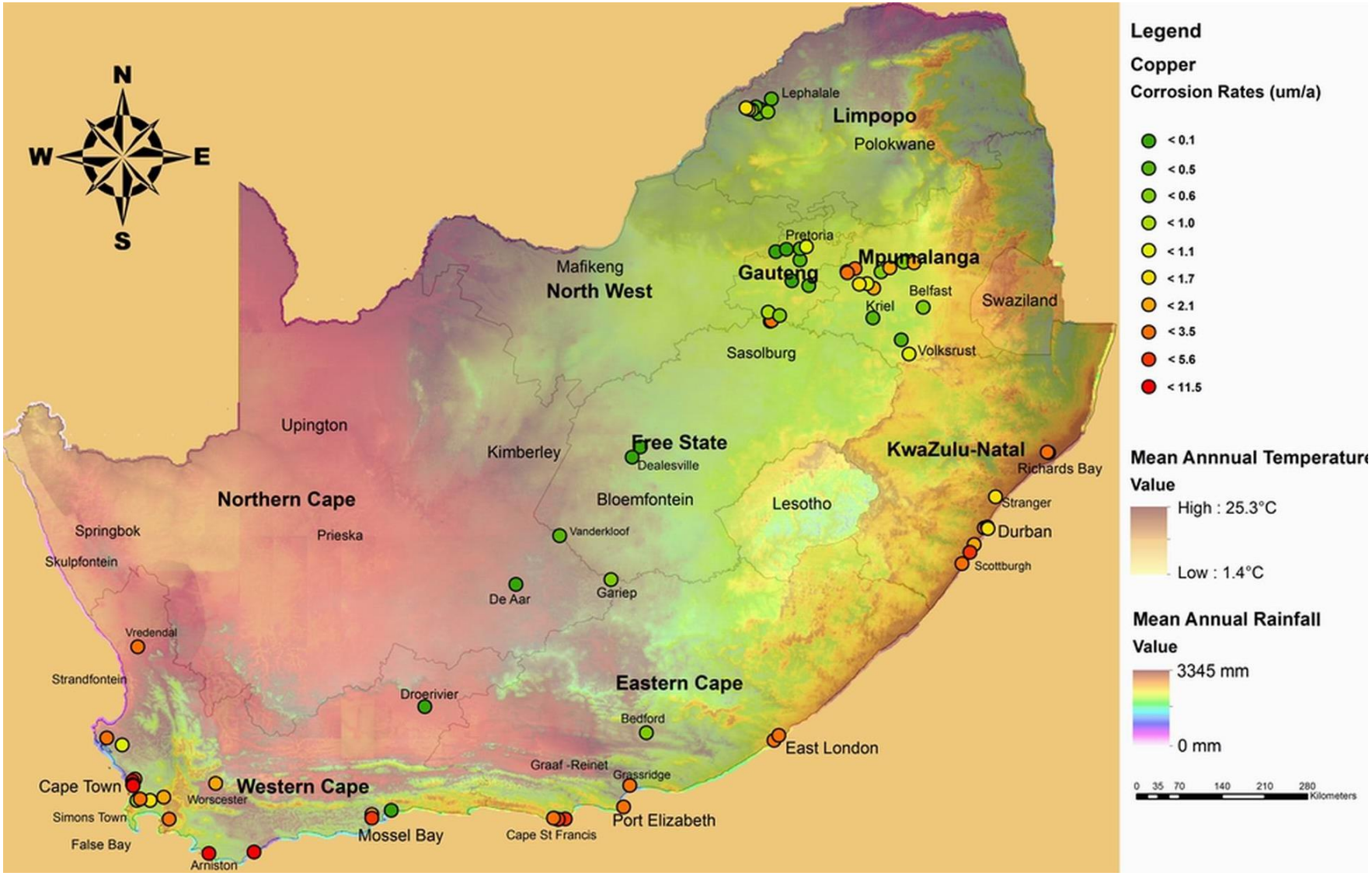


Figure 4.7 First-year (12-month) corrosion rates of pure copper at multiple locations throughout South Africa (based on existing published and unpublished data). (ArcGIS Base map).

4.2.1 Condition Assessments of Existing Infrastructure at the 57 Exposure Sites

Based on the condition assessments of existing infrastructure near the test sites, those locales that appeared more corrosive than others included:

- Kagiso-Randfontein – a mining/industrial area (**Figure 4.8**);
- Brakpan – a mining/low-income residential area (**Figure 4.9)**;
- Esselen Park – a residential/industrial/open field area;
- Ennerdale – an industrial site;
- Lenasia – a low-income residential area;
- Doornkop – a mining/low-income informal settlement area (**Figure 4.10**);
- Ivory Park – a low-income residential and unstructured settlement area;
- Rosherville – an industrial site; and
- Soweto – a low-income residential area.



(a) (b)

Figure 4.8 a) Extent of metal loss and b) pitting of steel items at the Kagiso-Randfontein site.



Figure 4.9 Atmospheric corrosion of hot-dip galvanised steel razor-wire at the Brakpan site.



Figure 4.10 Atmospheric corrosion of hot-dip galvanised steel fencing and supports at the Doornkop exposure site.

4.2.2 Corrosion Indices (CLIMAT/Wire-on-Bolt Units)

The Industrial (ICI), Marine (MCI) and Atmospheric (ACI) Corrosion Indices for the 22 main sites, measured during spring, summer, autumn and winter, i.e. August-September 2013 to August-September 2014, are given in **Figures 4.11 – 4.22,** and in further detail in **Appendix G – Table G.1**. **Table G.1** also provides the measured yearly average ICI, MCI and ACI values for the 22 main test sites in the GJMA, while **Appendix G – Figure G.1** gives a general view of the mean CLIMAT data (from one season to the next).

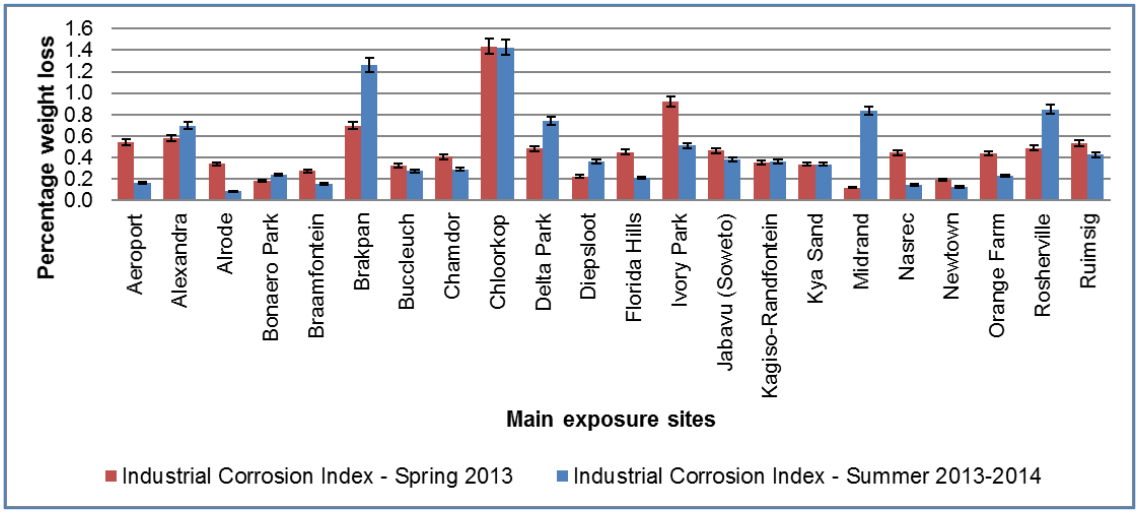


Figure 4.11 Measured Industrial Corrosion Indices (ICI values) for the 22 main sites in the GJMA during Spring 2013 and Summer 2013-2014.

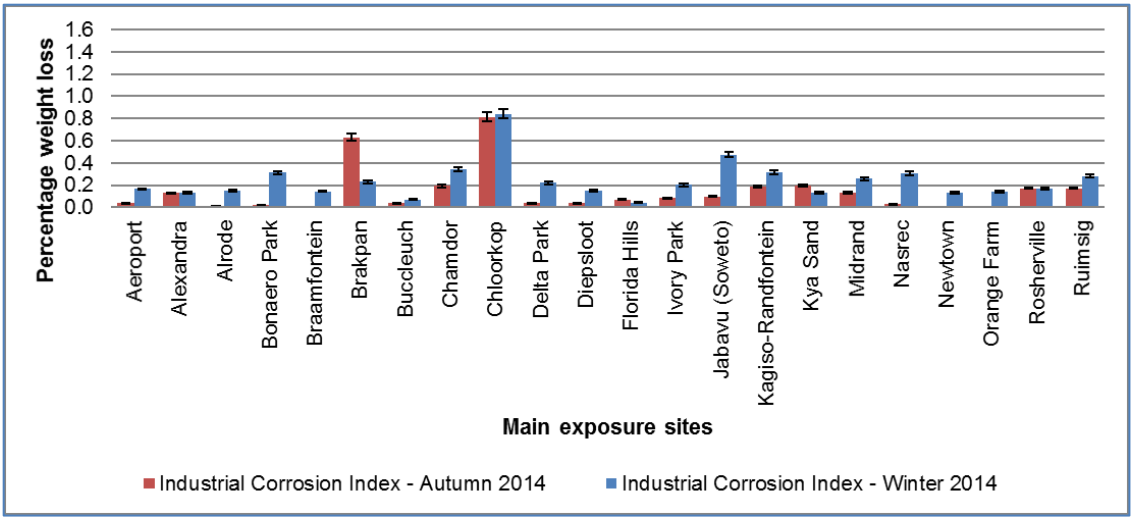


Figure 4.12 Measured Industrial Corrosion Indices (ICI values) for the main GJMA sites during Autumn 2014 and Winter 2014.

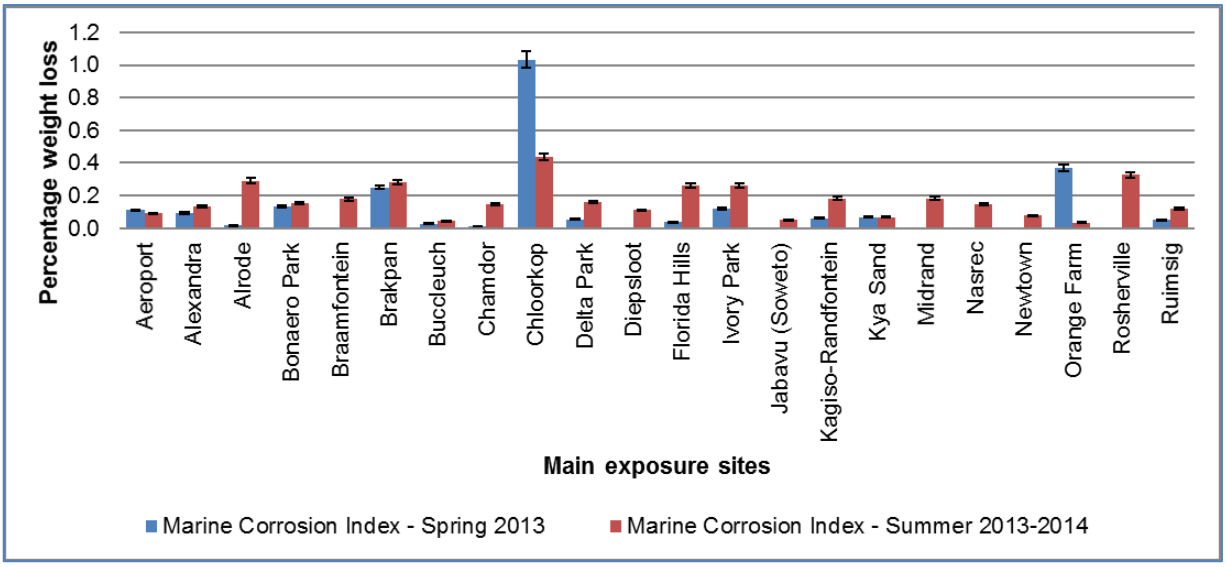


Figure 4.13 Measured Marine Corrosion Indices (MCI values) for the main GJMA sites during Spring 2013 and Summer 2013-2014.

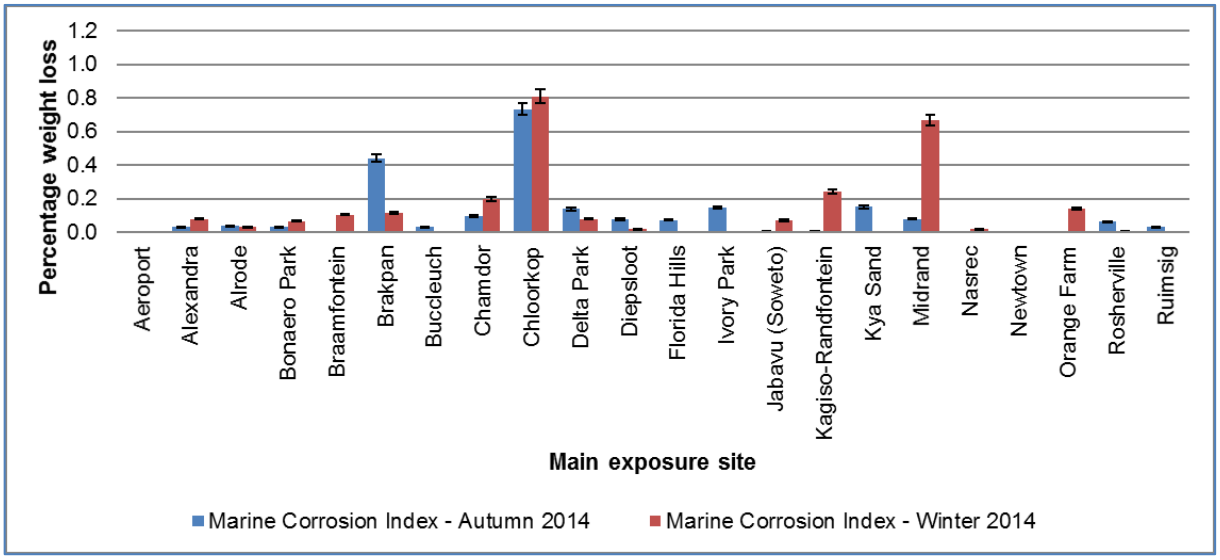


Figure 4.14 Measured Marine Corrosion Indices (MCI values) for the main GJMA sites during Autumn 2014 and Winter 2014.

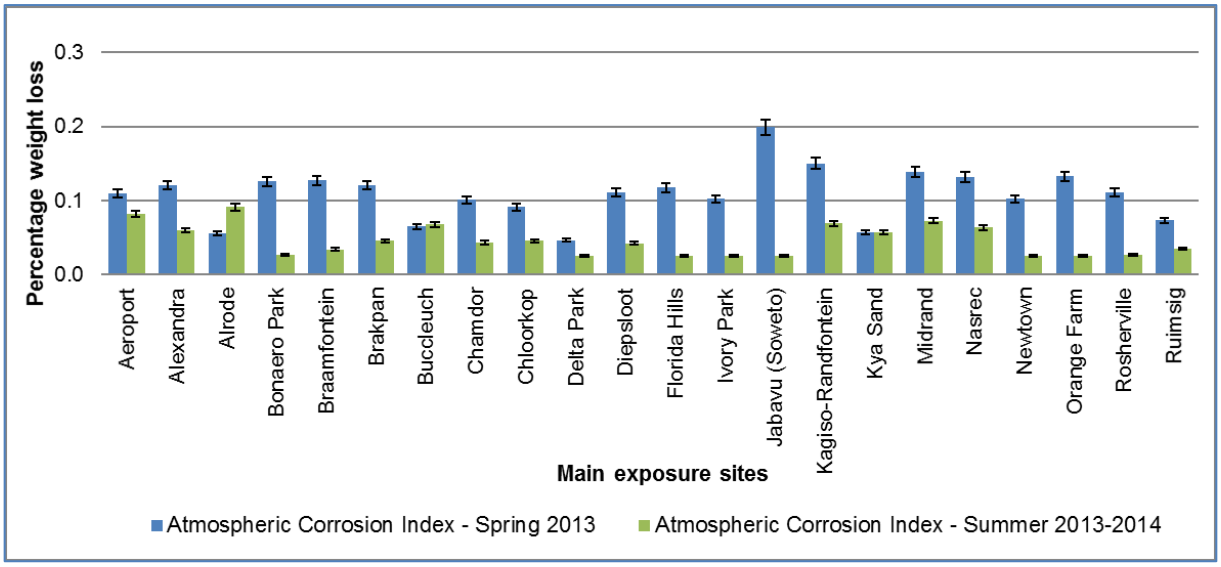


Figure 4.15 Measured Atmospheric Corrosion Indices (ACI values) at the main GJMA sites during Spring 2013 and Summer 2013-2014.

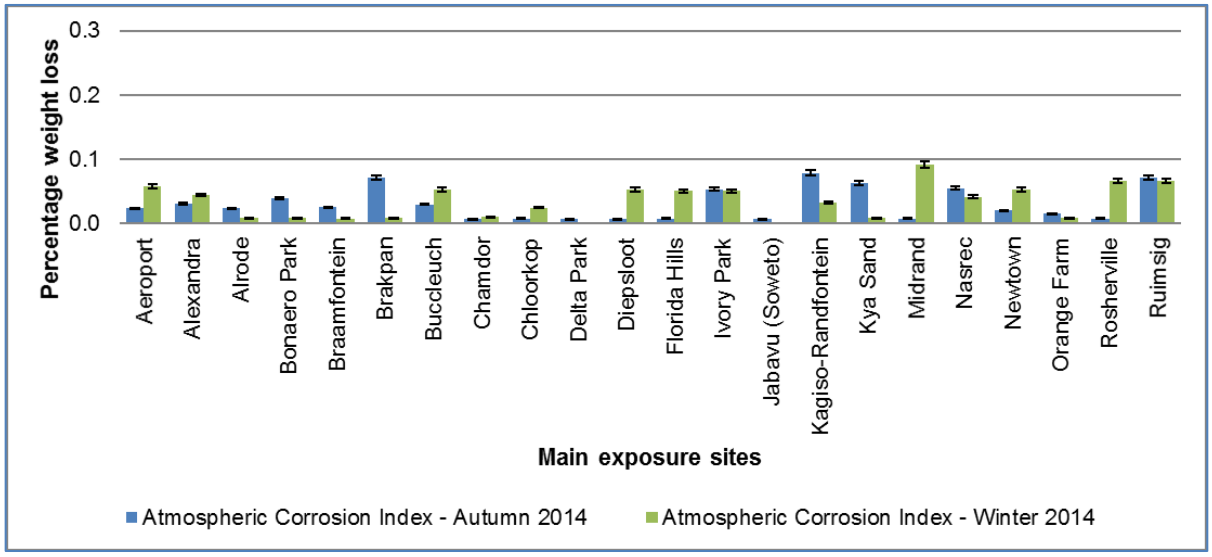


Figure 4.16 Measured Atmospheric Corrosion Indices (ACI values) at the main GJMA sites during Autumn 2014 and Winter 2014.

As shown in **Figures 4.11 & 4.12**, the highest ICI values were recorded at Chloorkop (during spring and summer), followed by Ivory Park, Brakpan, Midrand, Rosherville, Delta Park and Alexandra - also during summer (i.e. December 2013 to February 2014). These sites are all situated towards the southeasterly, easterly and northeasterly directions of the GJMA. **Figures 4.13 & 4.14**, presenting the MCI results, likewise show elevated corrosivity levels at Chloorkop, and at Midrand during winter, while

Figures 4.15 & 4.16, giving the ACI values, indicated less distinct variations between the various locations.

Figures 4.17 – 4.19 present summations (∑) of the seasonal ICI, MCI and ACI values for the different main sites, showing that Chloorkop, Brakpan and Midrand are most corrosive. Consequently, these sites were preliminarily rated as 'hotspots' in the GJMA. Additional locations which indicated higher than average ICI values included Alexandra, Ivory Park, Delta Park, and Rosherville.

The sum totals (∑) of the average seasonal ICI, MCI and ACI values for the major regions of the GJMA, i.e. the East Rand, West Rand and City of Johannesburg (CoJ), as well as the Northern and Southern Suburbs, are given in **Figures 4.20 – 4.22**. Concerning the ICI and MCI values, the East Rand sites consistently indicated the highest mean seasonal values. Conversely, the Central JHB Suburbs region displayed the lowest overall mean MCI and ACI values, particularly during spring and winter, with the differences between these indices being less distinct for the other areas.

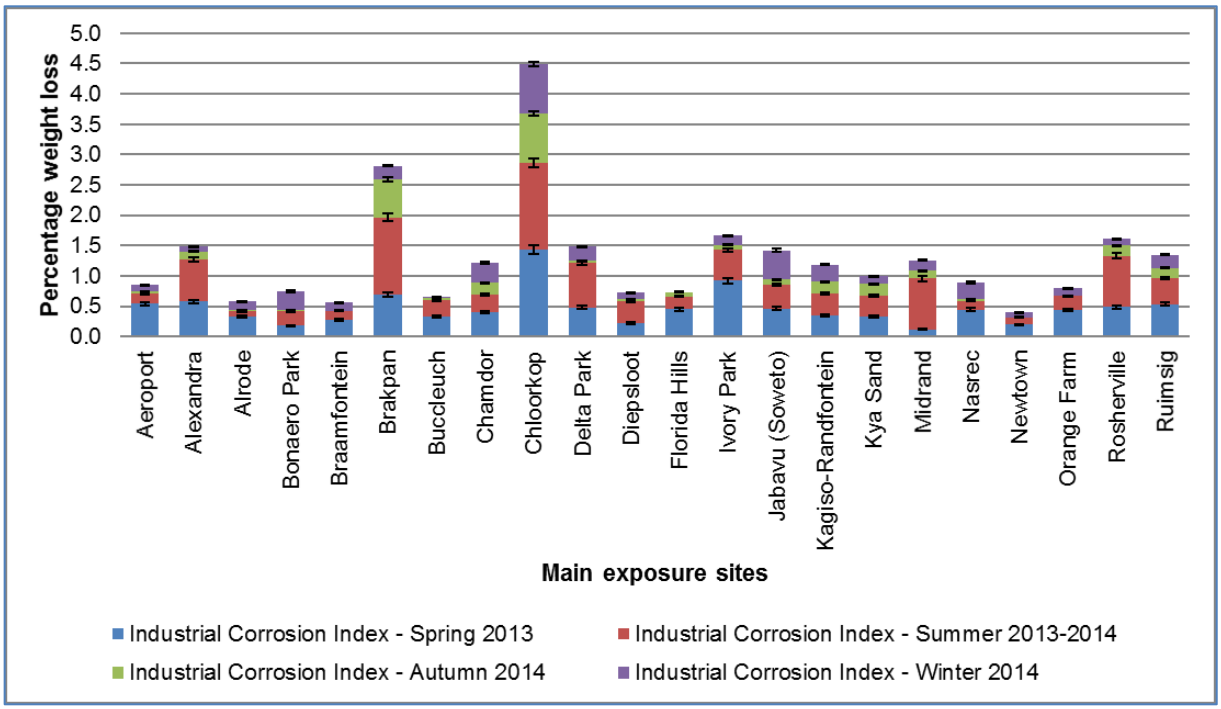


Figure 4.17 Summations (∑) of the measured seasonal Industrial Corrosion Indices (ICI values) for the main GJMA sites (Spring 2013 to Winter 2014).

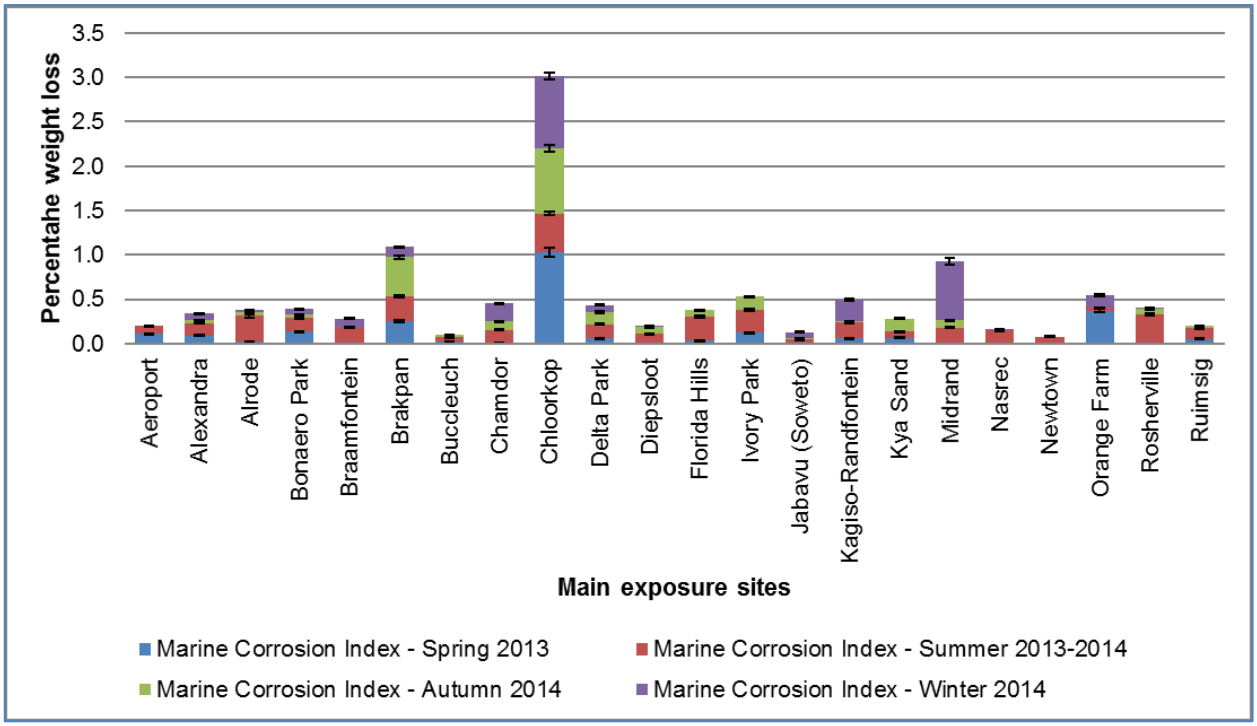


Figure 4.18 Summations (∑) of the measured seasonal Marine Corrosion Indices (MCI values) for the main GJMA sites (Spring 2013 to Winter 2014).

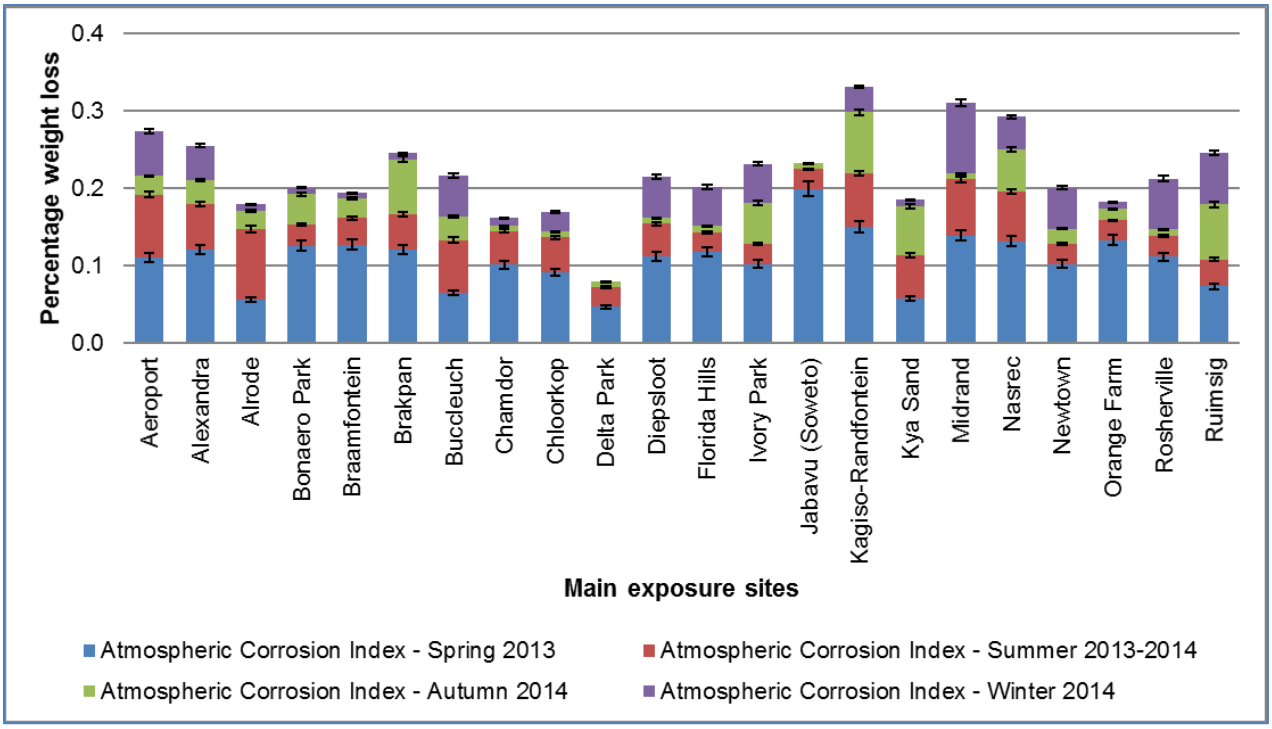


Figure 4.19 Summations (∑) of the measured Atmospheric Corrosion Indices (ACI values) for the main GJMA sites - during Spring 2013 to Winter 2014.

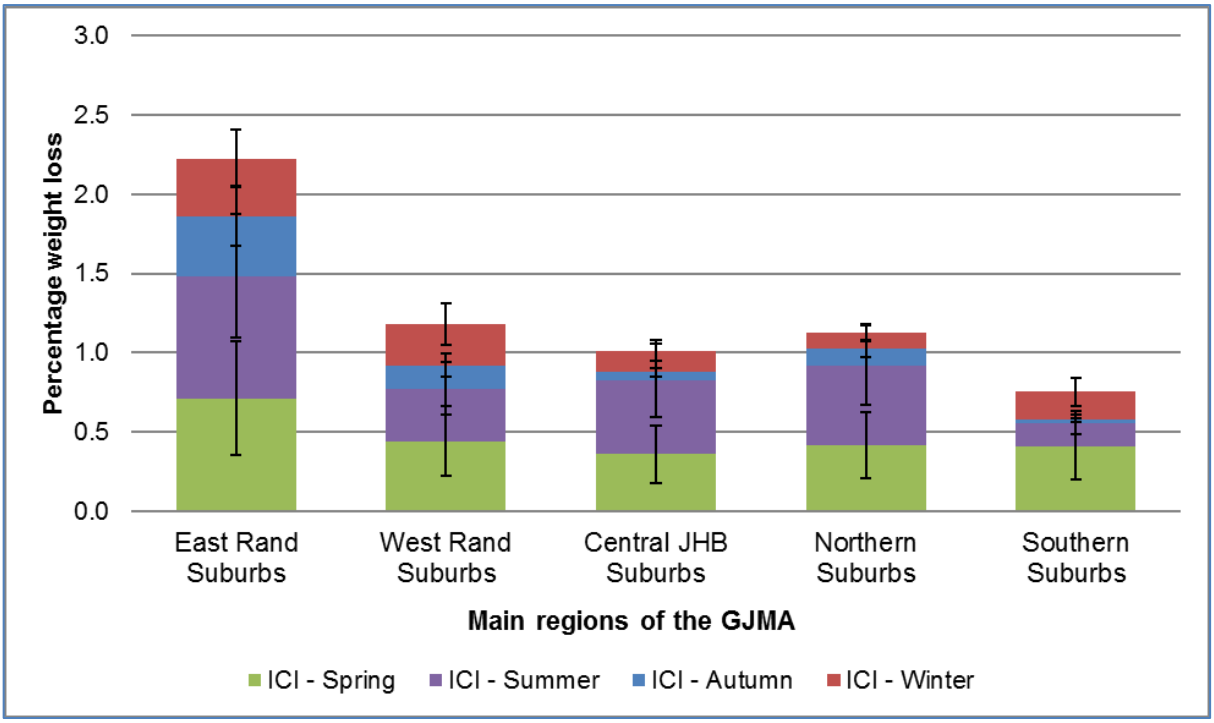


Figure 4.20 Summations of the seasonal fluctuations of the average ICI values for the major regions of the GJMA (Spring 2013 to Winter 2014).

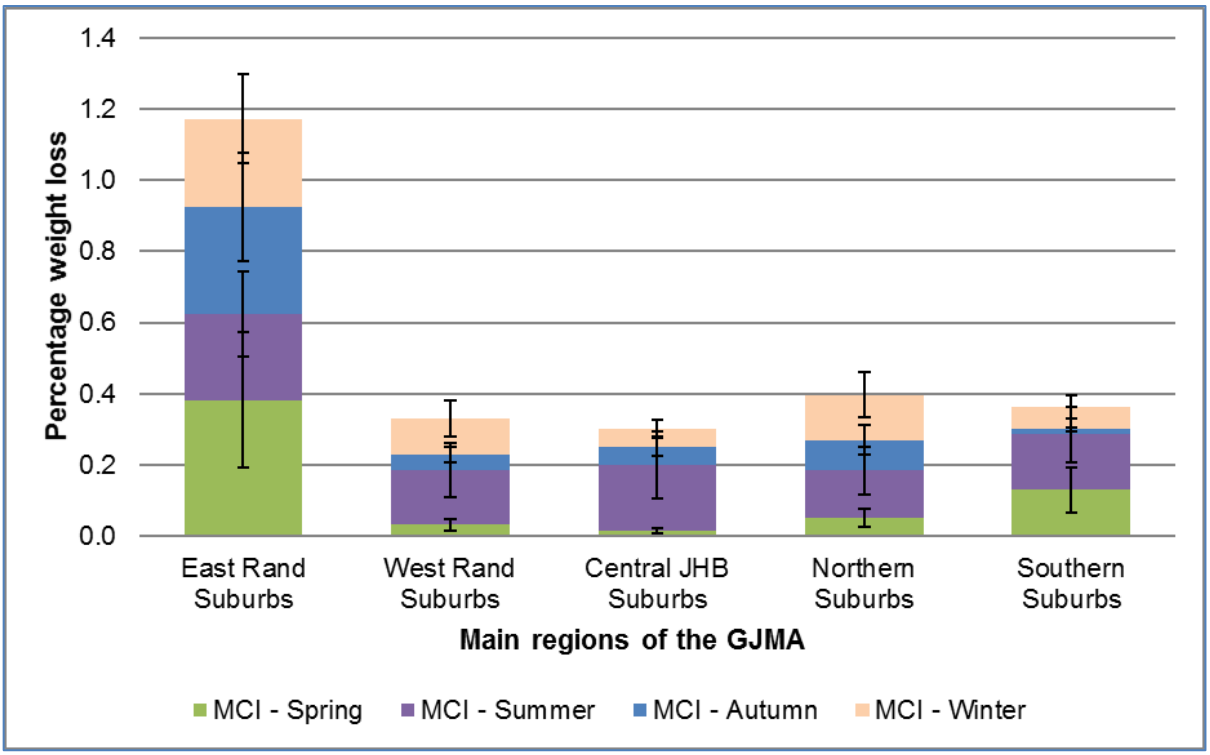


Figure 4.21 Summations of the measured average seasonal MCI values for the different major regions of the GJMA (Spring 2013 to Winter 2014).

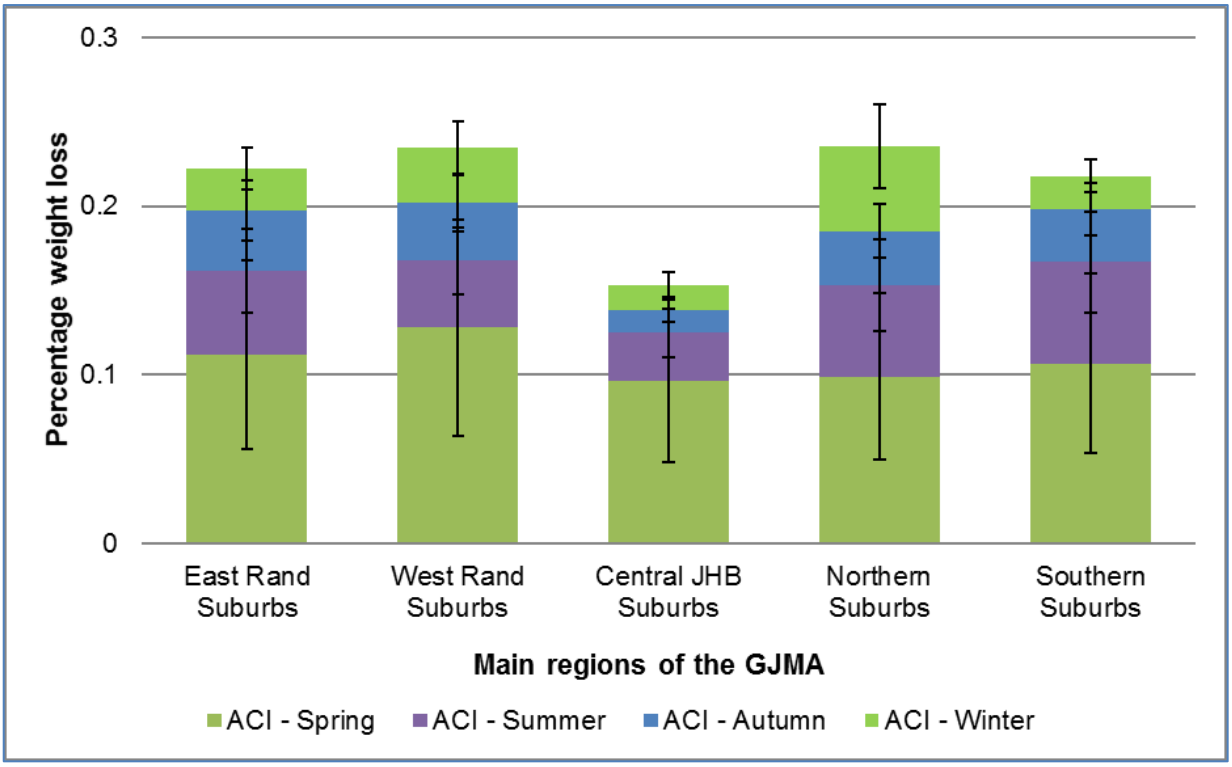


Figure 4.22 Sum totals and seasonal fluctuations of the measured average ACI values for the different major regions of the GJMA - during Spring 2013 to Winter 2014.

4.2.3 Aluminium, Zinc, and Copper Wire Helix (WH) Corrosion Rates

Figures 4.23 – 4.25 display the first-year or 12-month corrosion rates of the pure Al, Zn and Cu wire helices (Al-WH, Zn-WH & Cu-WH) at the 22 main exposure sites, whereas **Figures 4.26 – 4.28** shows the average 12-month Al-WH, Zn-WH and Cu-WH values for the different regions of the GJMA. The detailed results are given in **Appendix H – Table H.1**.

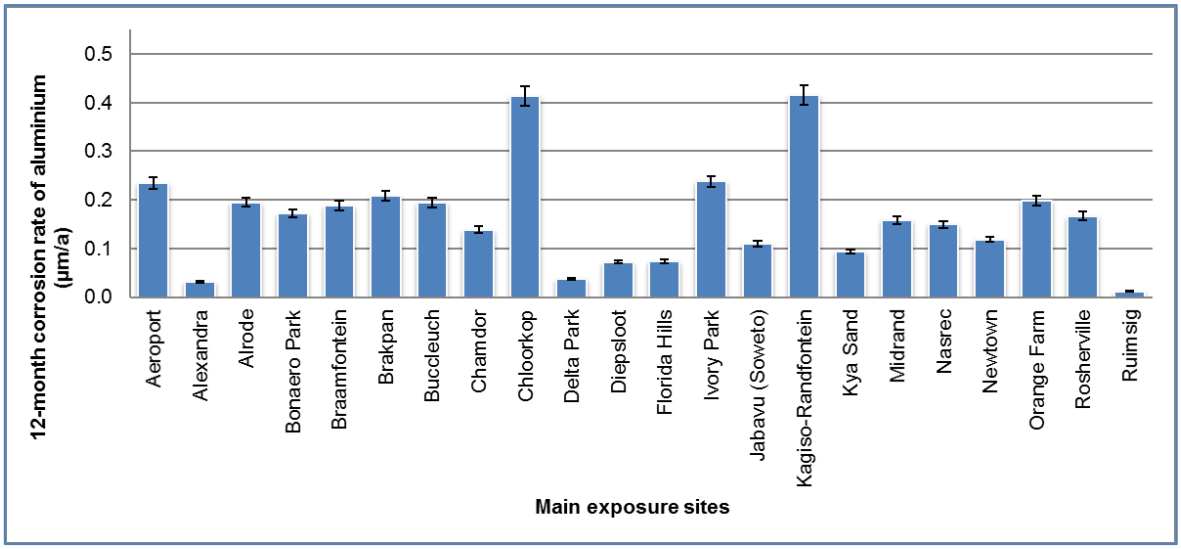


Figure 4.23 Measured 12-month aluminium wire helix corrosion rates for the 22 main sites in the GJMA.

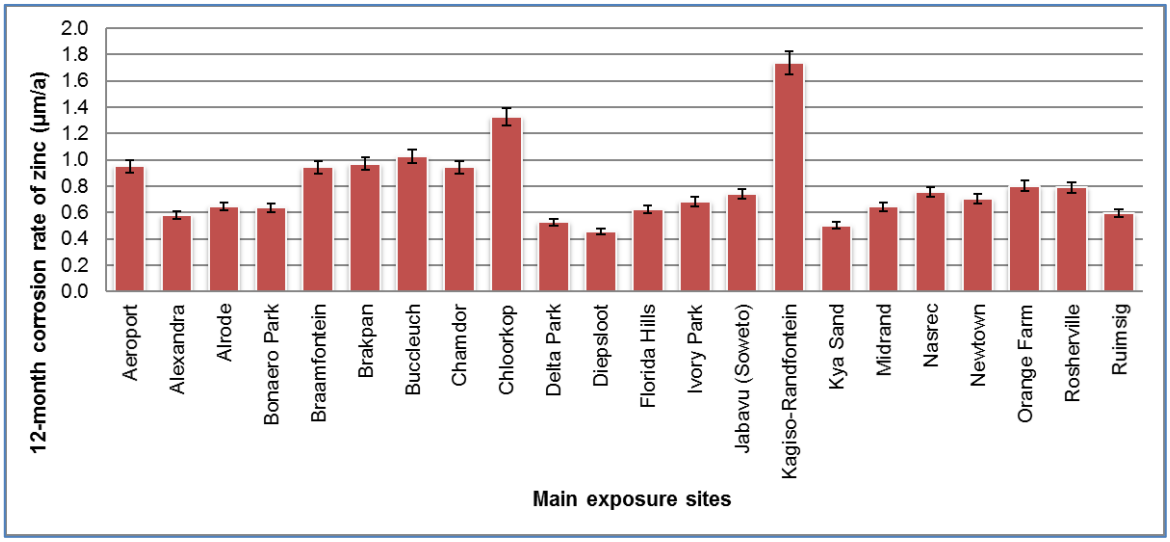


Figure 4.24 Measured 12-month zinc wire helix corrosion rates for the 22 main sites in the GJMA.

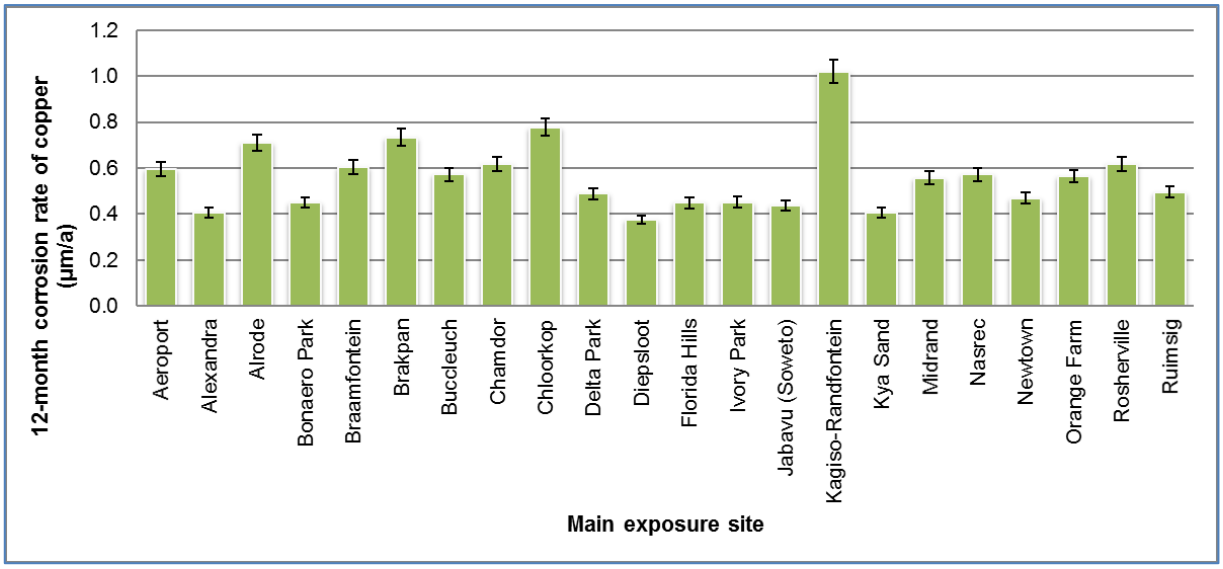


Figure 4.25 Measured 12-month copper wire helix corrosion rates for the 22 main sites in the GJMA.

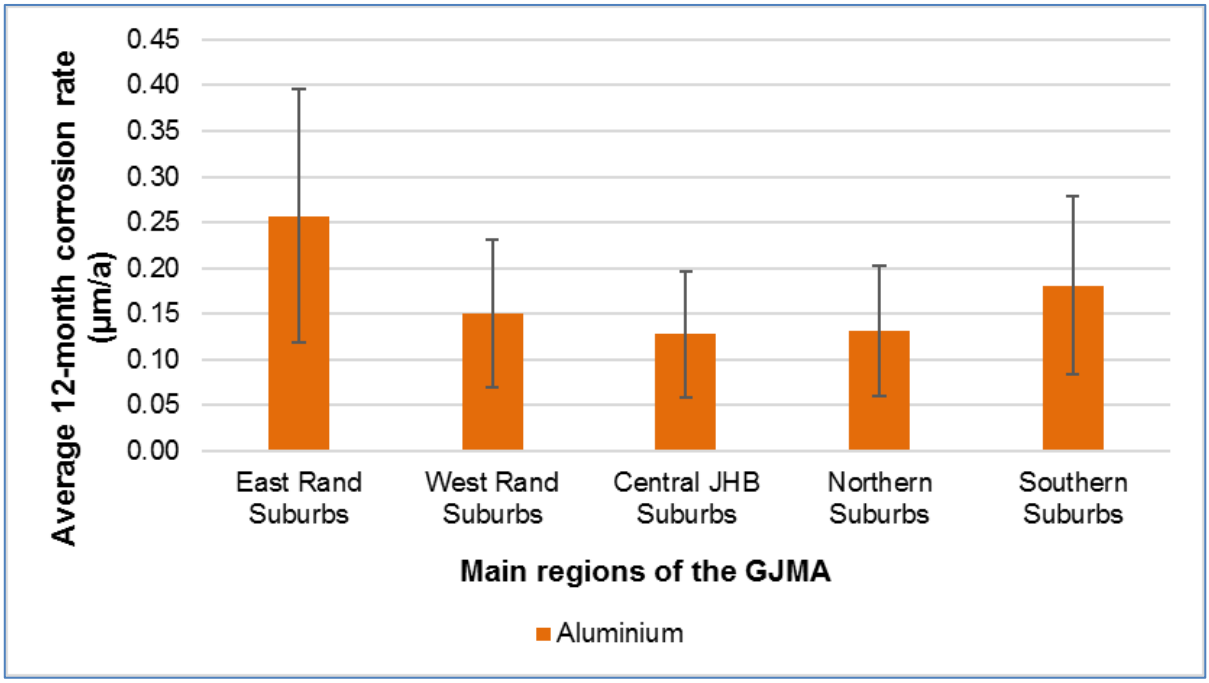


Figure 4.26 Average 12-month aluminium wire helix corrosion rates for the different regions of the GJMA.

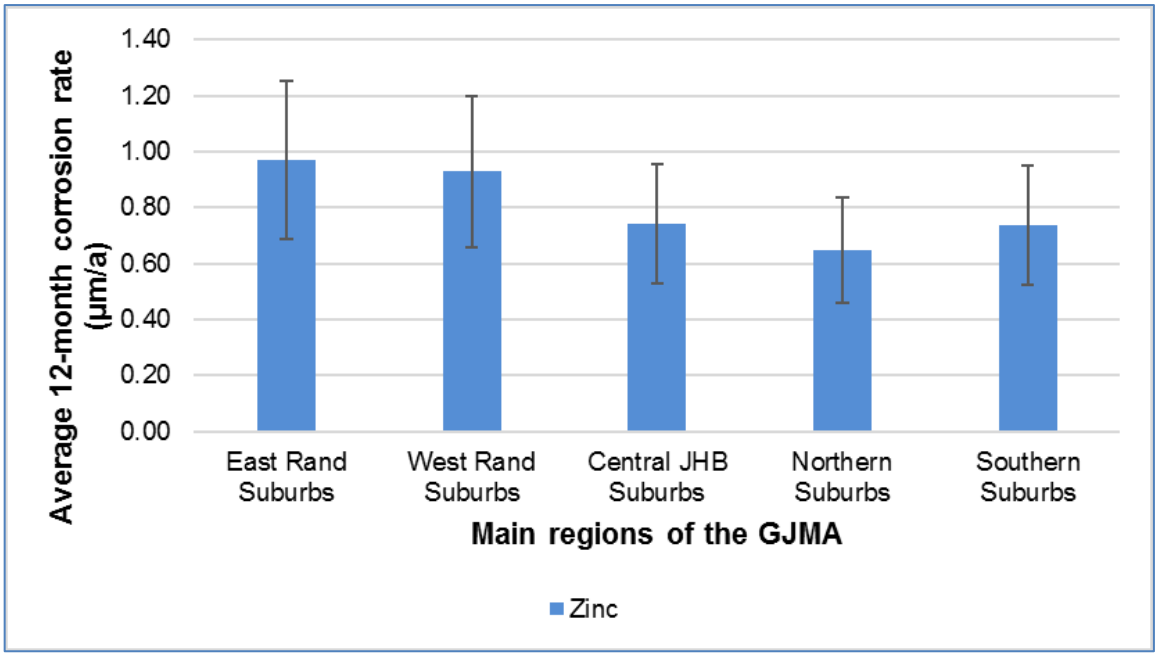


Figure 4.27 Average 12-month zinc wire helix corrosion rates for the different regions of the GJMA.

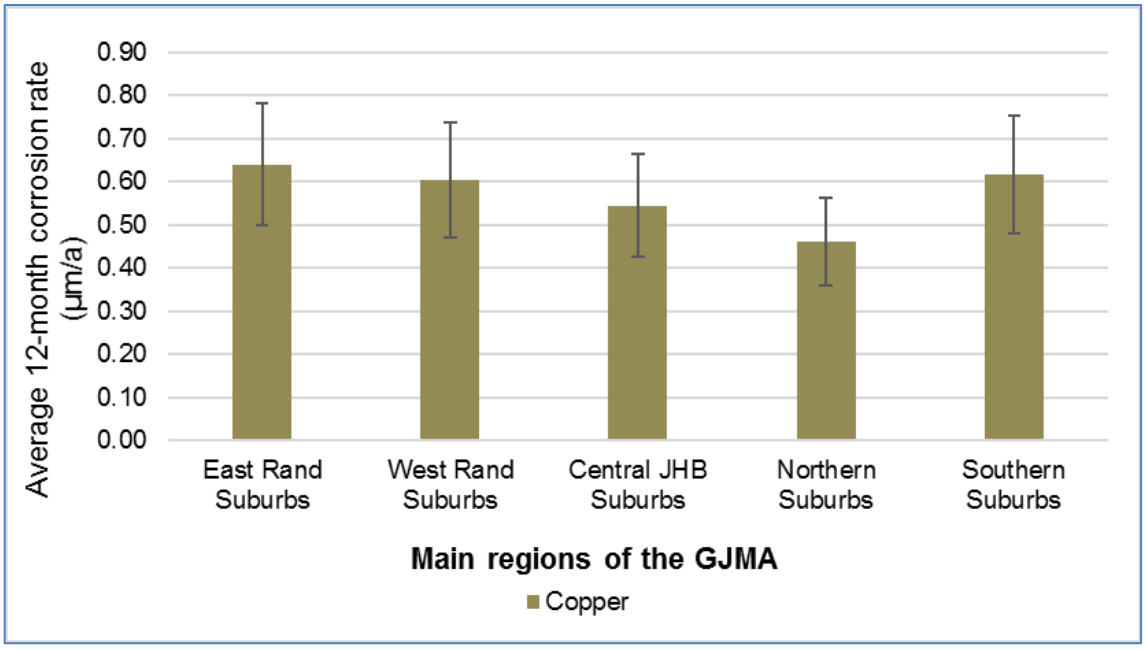


Figure 4.28 Measured 12-month copper wire helix corrosion rates for the different regions of the GJMA.

The average 12-month corrosion rates of copper at the Northern Suburbs are given in **Figure 4.29** and summations (∑) of the 12-month corrosion rates of the Al-WH, Zn-WH and Cu-WH devices for the different main sites in **Figure 4.30**.

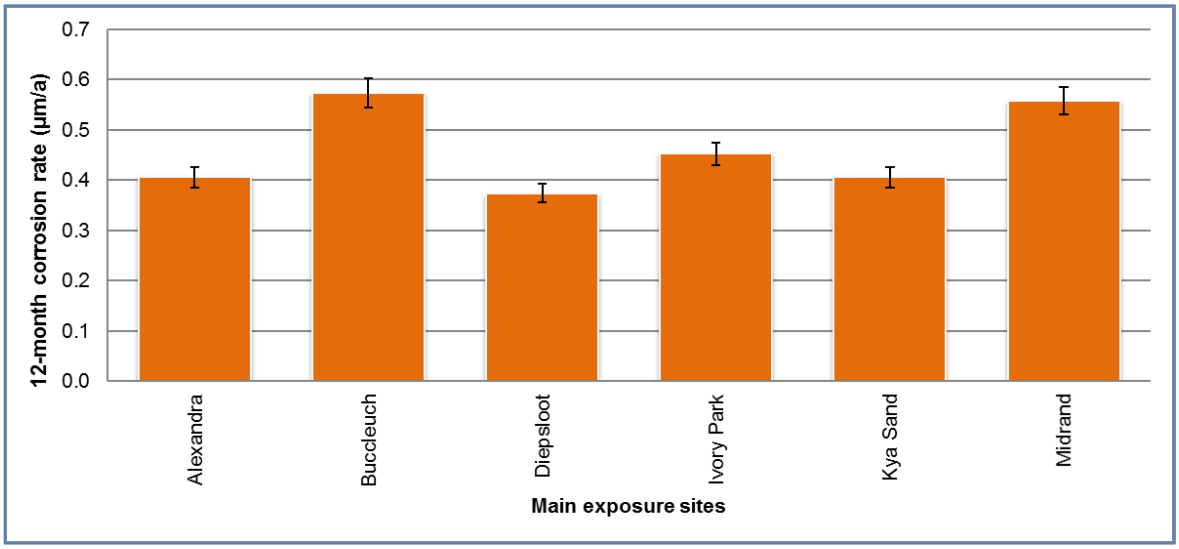


Figure 4.29 Average 12-month copper wire helix corrosion rates for the northern suburbs of the GJMA.

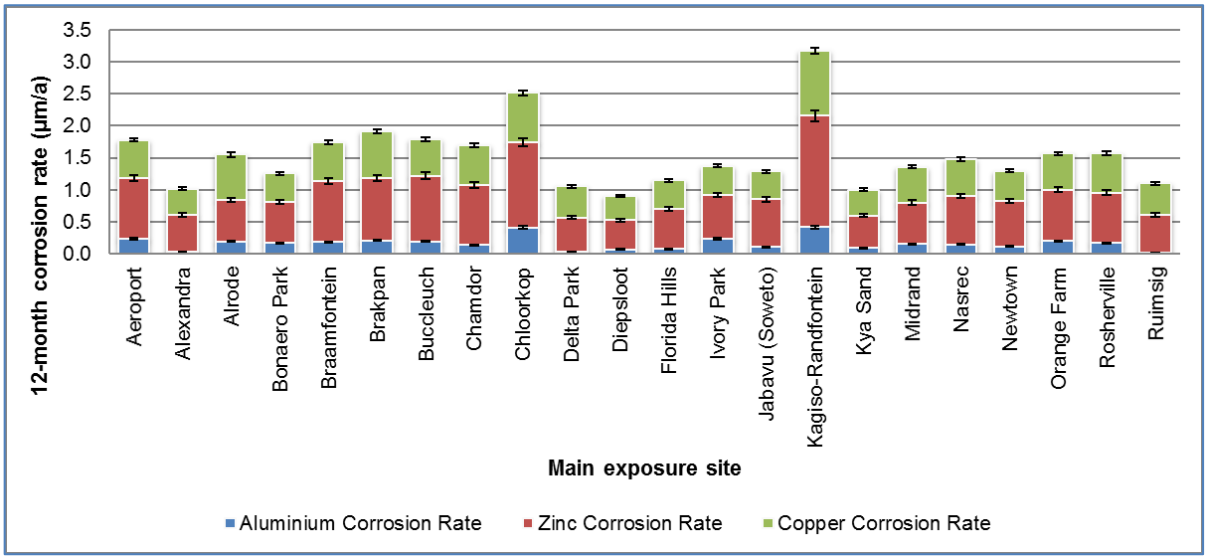


Figure 4.30 Summations (∑) of the 12-month corrosion rates of aluminium, zinc and copper for the 22 main GJMA exposure sites.

4.2.4 Flat Metal Panel Corrosion Rates

4 2.4.1 Mild steel panels (MSP) – Main sites

Figure 4.31 reflects the 6-, 12-, 18- and 24-month corrosion rates of duplicate sets of mild steel panels (MSP) for 21 of the main exposure sites. Important is that the Buccleuch exposure rack was stolen shortly after installation. Subsequently, a small two-panel test rack (like those exposed at the mini sites) was installed at Buccleuch, of which the panels were removed after 12 months of exposure. The more detailed corrosion data are given in **Appendix I – Table I.1 & Figures I.1-3**.

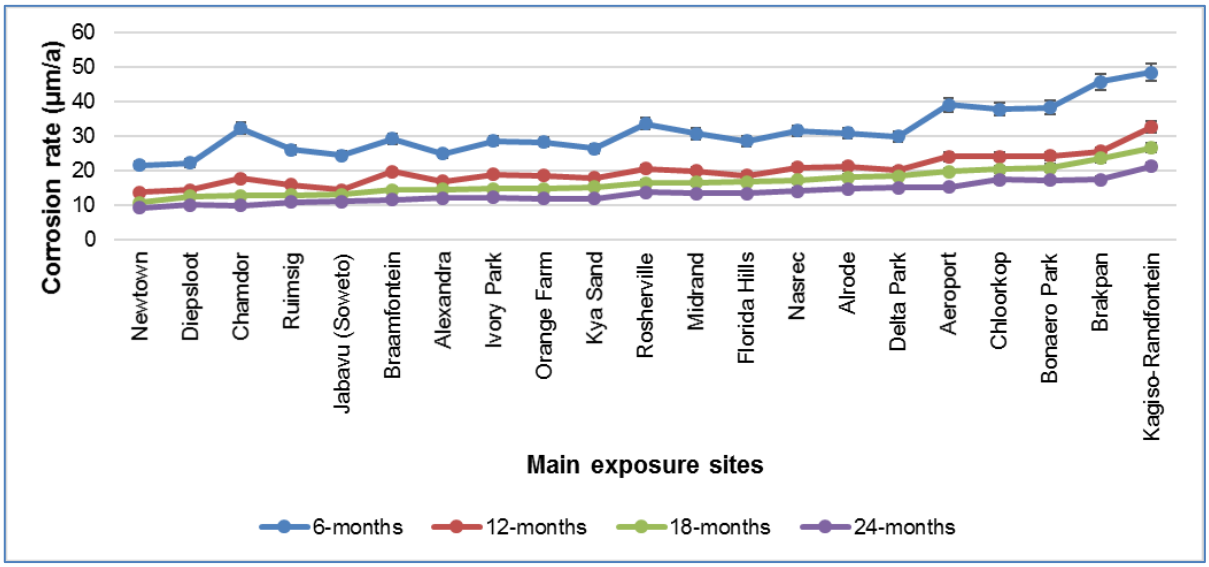


Figure 4.31 Changes in the 6-, 12-, 18- and 24-month corrosion rates of duplicate sets of mild steel panels (MSP) for 21 of the main exposure sites.

4.2.4.2 Hot-dip galvanised mild steel panels (GSP) – Main sites

As in the case of the mild steel specimens, the hot-dip galvanised samples exposed at Buccleuch were stolen shortly after installation. Consequently, no GSP data exist for this location. The results are given in **Figures 4.32-4.33**, with more detail provided in **Appendix J Table J.1 & Figure J.1**.

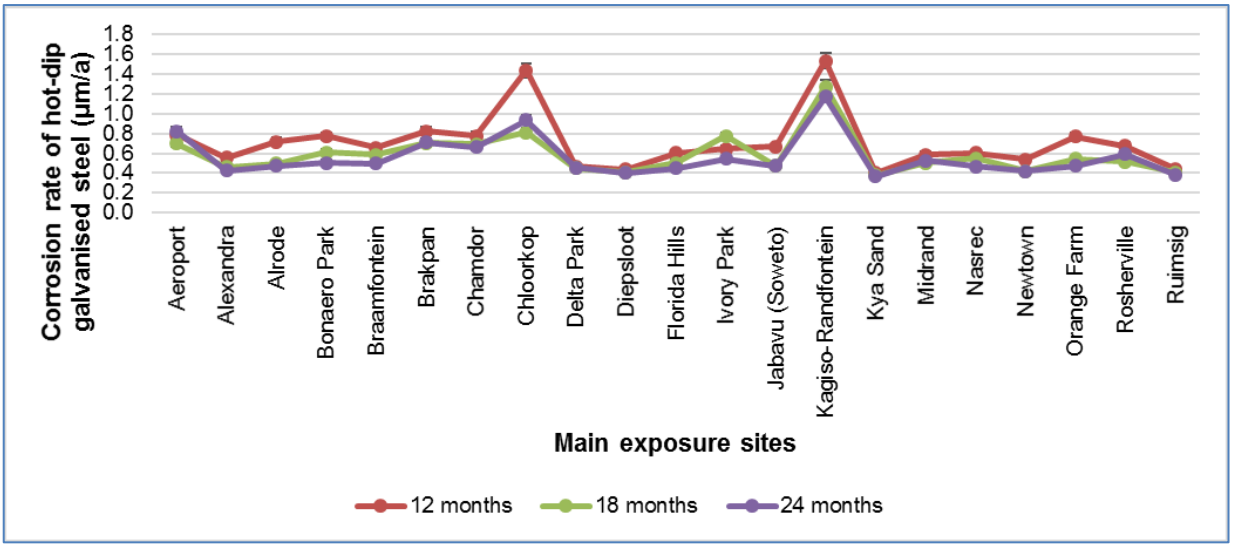


Figure 4.32 Changes in the 12-, 18- and 24-month corrosion rates of duplicate sets of hot-dip galvanised steel panels (GSP) at 21 of the main exposure sites.

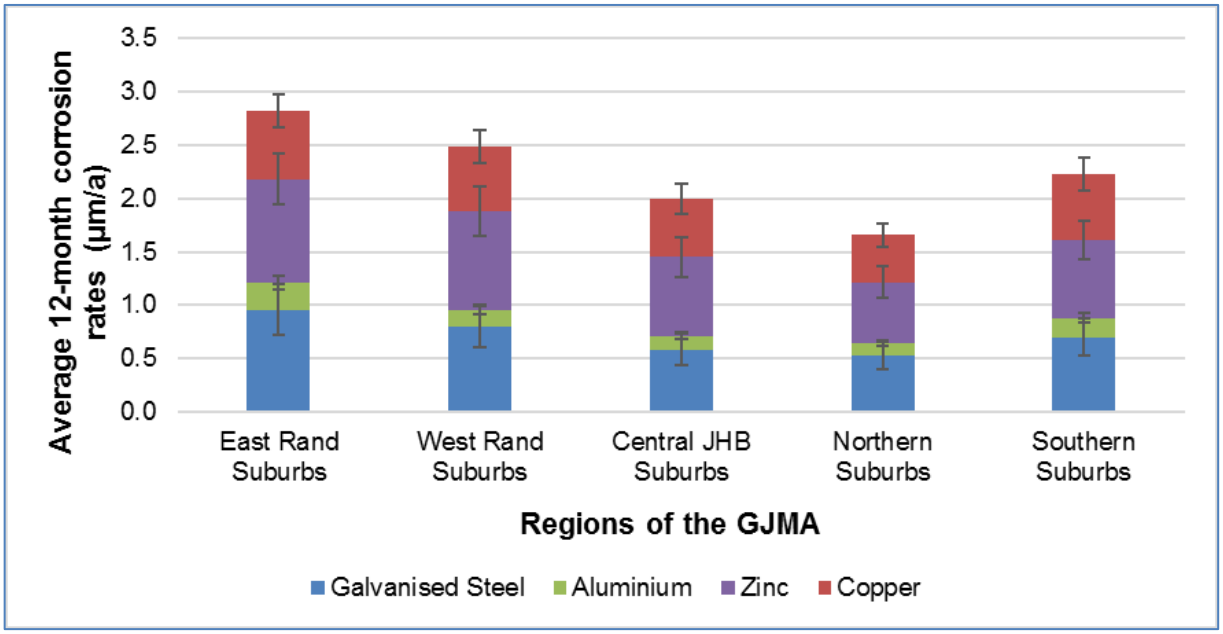


Figure 4.33 12-month average corrosion rates of galvanised steel, aluminium, zinc and copper, as measured for the different parts of the GJMA.

4.2.5 Mild Steel Panels (MSP) – Main and Mini Sites

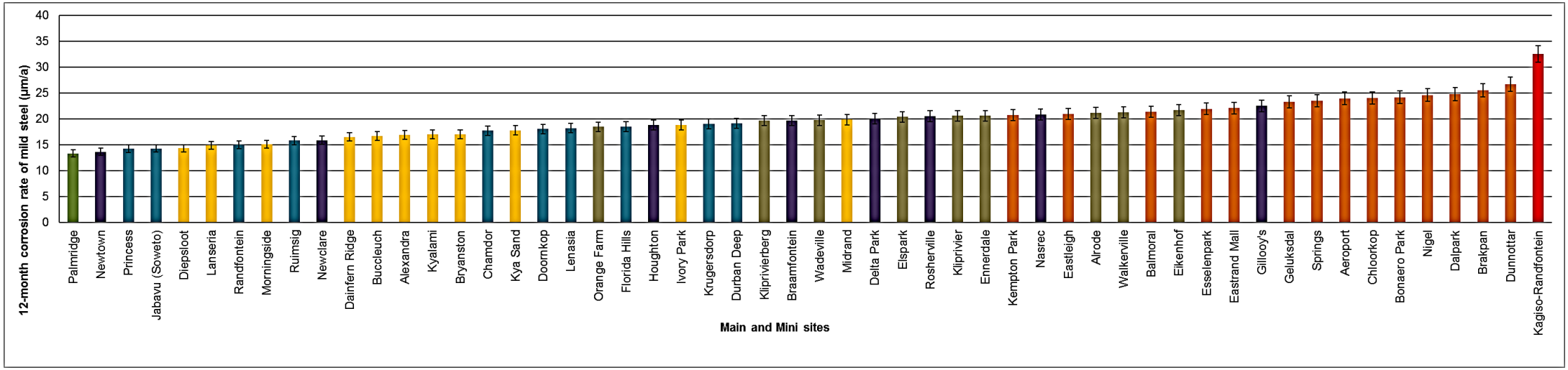
The 12-month mild steel corrosion rates of the 'mini' sites, together with the measurements for the 'main' sites, are presented in **Table 4.1** and **Figures 4.34 & 4.35**. The mild steel samples exposed at Honeydew, Rosettenville and Northmead were lost due to theft. Consequently, no 12-month corrosion data exist for these locations.

Table 4.1 Average 12-month corrosion rates of duplicate sets of mild steel specimens exposed at 22 main and 35 mini sites in the GJMA, with margin of uncertainty of about ± 5%.

GJMA exposure site	Designated environment	12-month mass loss per m^2 ($g/(m^2a)$)	12-month corrosion rate (μm)
Aeroport	Industrial/Airport	188	24
Alexandra	Township	133	17
Alrode	Industrial/Residential	166	21
Balmoral	Residential/Business	168	21
Bonaero Park	Residential	190	24
Braamfontein	Business/Inner City	155	20
Brakpan	Park/Residential/Mining	201	26
Bryanston	Park/Residential	134	17
Buccleuch	Business/Traffic	131	17
Chamdor	Industrial/Township	139	18
Chloorkop	Industrial/Business	189	24
Dainfern Ridge	Residential/Business	130	17
Dalpark	Airfield/Residential	195	25
Delta Park	Park/Residential	158	20
Diepsloot	Township	113	14
Doornkop	Industrial/Mining	142	18
Dunnottar	Field/Rural	210	27
Durban Deep	Township/Mining	150	19
Eastleigh	Business/Residential/Industrial/Traffic	165	21
Eastrand Mall	Business/Residential/Airport	174	22
Eikenhof	Field/Farming	170	22
Elspark	Residential/Business	160	20
Ennerdale	Residential/Business	162	21
Esselen Park	Residential/Industrial/Field	173	22
Florida Hills	Residential	146	19
Geluksdal	Business/Industrial/Residential	183	23
Gillooy's	Residential/Park/Traffic	177	23

Table 4.1 *Continued.*

GJMA exposure site	Designated environment	12-month mass loss per m^2 ($g/(m^2a)$)	12-month corrosion rate (μm)
Houghton	Residential	148	19
Ivory Park	Township	148	19
Jabavu (Soweto)	Township	112	14
Kagiso/Randfontein	Mining/Industrial	256	33
Kempton Park	Business/Residential	163	21
Kliprivier	Industrial	162	21
Kliprivierberg	Residential/Field	155	20
Krugersdorp	Residential/Business	150	19
Kyalami	Park/Residential	134	17
Kya Sand	Business/Industrial	140	18
Lanseria	Open Country/Airport	117	15
Lenasia	Residential/Business	143	18
Midrand	Business/Industrial	156	20
Morningside	Business/Traffic/Residential	119	15
Nasrec	Mining/Business	164	21
Newclare	Business/Traffic/Industrial/Residential	125	16
Newtown	Business	107	14
Nigel	Residential	193	25
Orange Farm	Township	145	18
Palmridge	Business/Township	105	13
Princess	Informal settlement/Business	112	14
Randfontein	Residential/Business	118	15
Rosherville	Industrial/Mining	161	21
Ruimsig	Residential	124	16
Springs	Park/Residential	185	23
Wadeville	Industrial/Business	155	20
Walkerville	Field/Farming	168	21



Colour key	Description	Average 12-month corrosion rate of steel (µm/a)
	Reduced corrosivity due to an elevation of the site above ground level	13
	Sites located to the west of the GJMA	16 (2)
	Sites located to the north of the GJMA	17 (2)
	Sites located in the centre of the GJMA	19 (3)
	Sites located to the south of the GJMA	20 (1)
	Sites located to the east of the GJMA	23 (2)
	'Hotspot'	33

Figure 4.34 Average 12-month corrosion rates of mild steel, as measured at the main and mini sites in the GJMA.

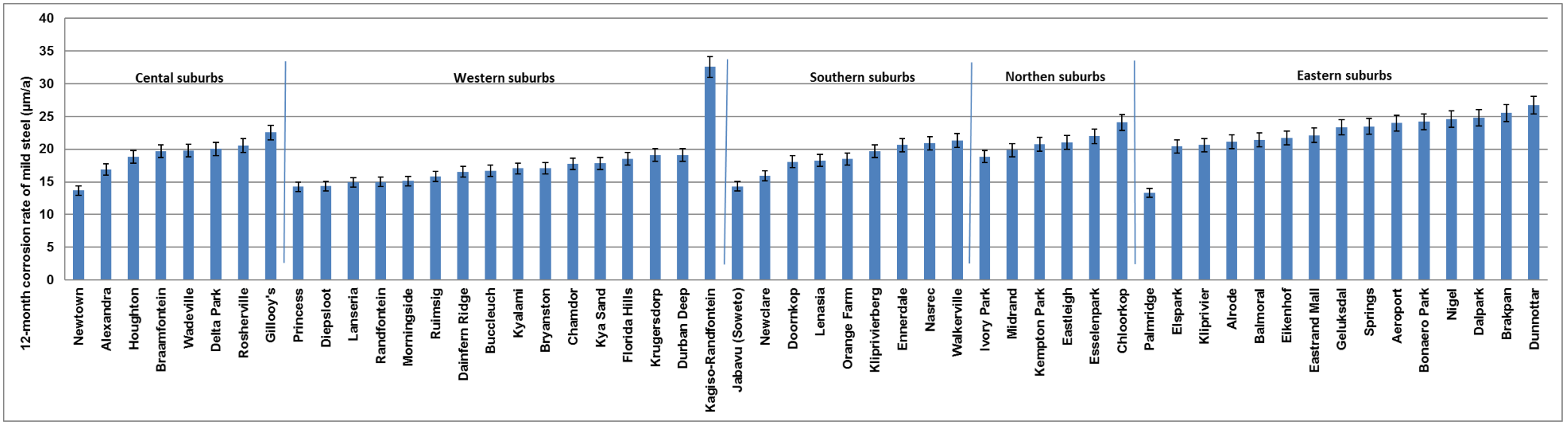


Figure 4.35 Average 12-month corrosion rates of mild steel, as measured at the main and mini sites in the different regions of the GJMA.

Figures 4.36 – 4.40 evaluate of the different sites per region (excluding the outliers).

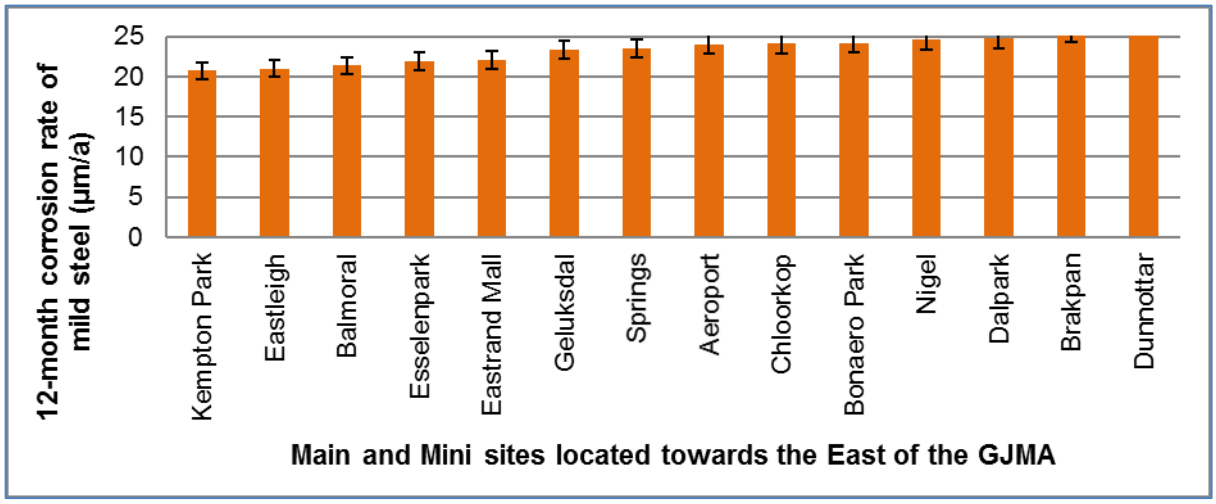


Figure 4.36 12-month corrosion rates of mild steel at the main and mini sites located in the Eastern region of the GJMA.

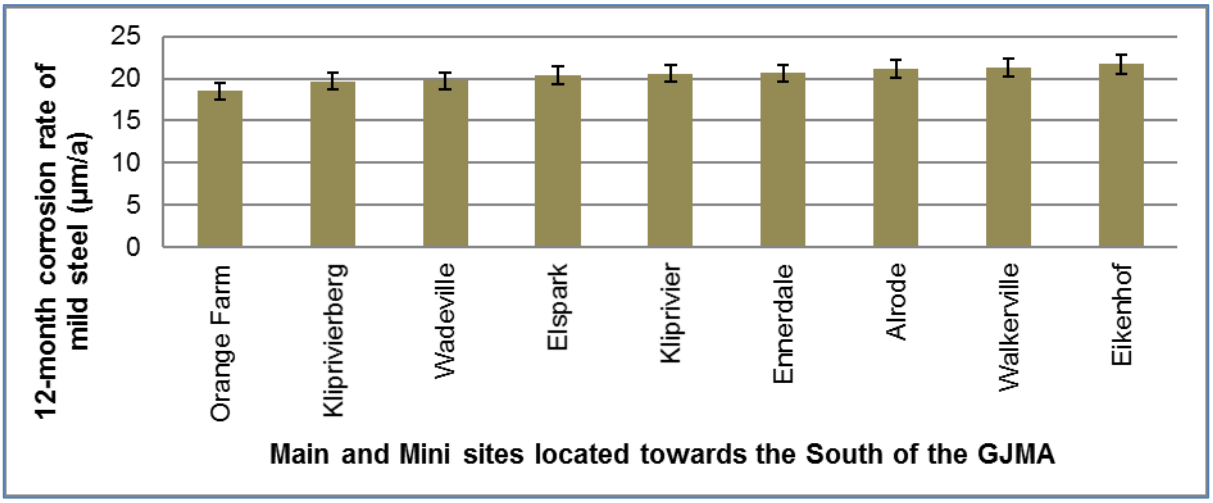


Figure 4.37 12-month corrosion rates of mild steel at the main and mini sites located in the Southern region of the GJMA.

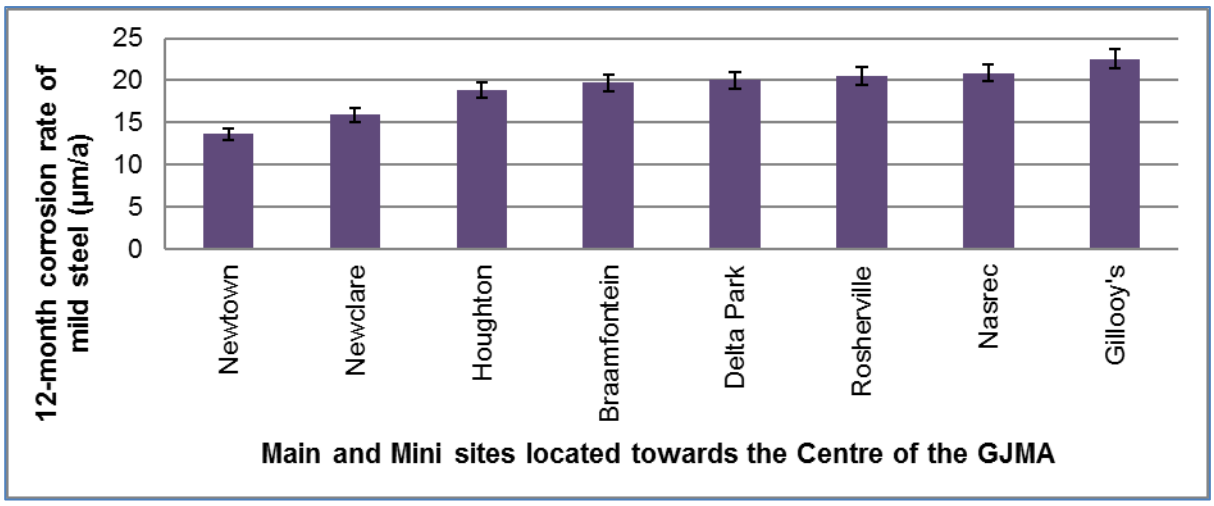


Figure 4.38 12-month corrosion rates of mild steel at the main and mini sites located in the Central part of the GJMA.

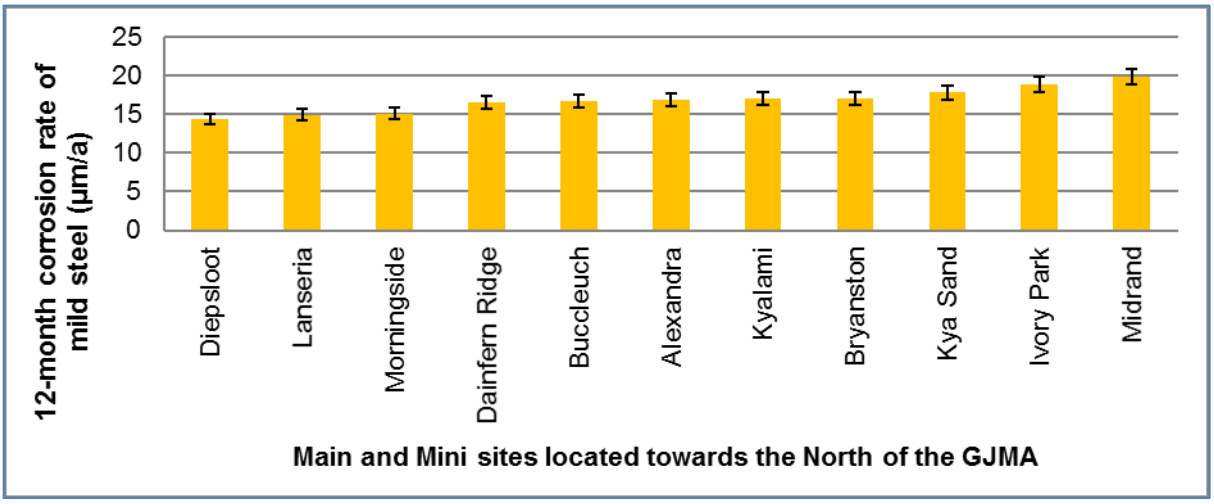


Figure 4.39 12-month corrosion rates of mild steel at the main and mini sites located in the Northern region of the GJMA.

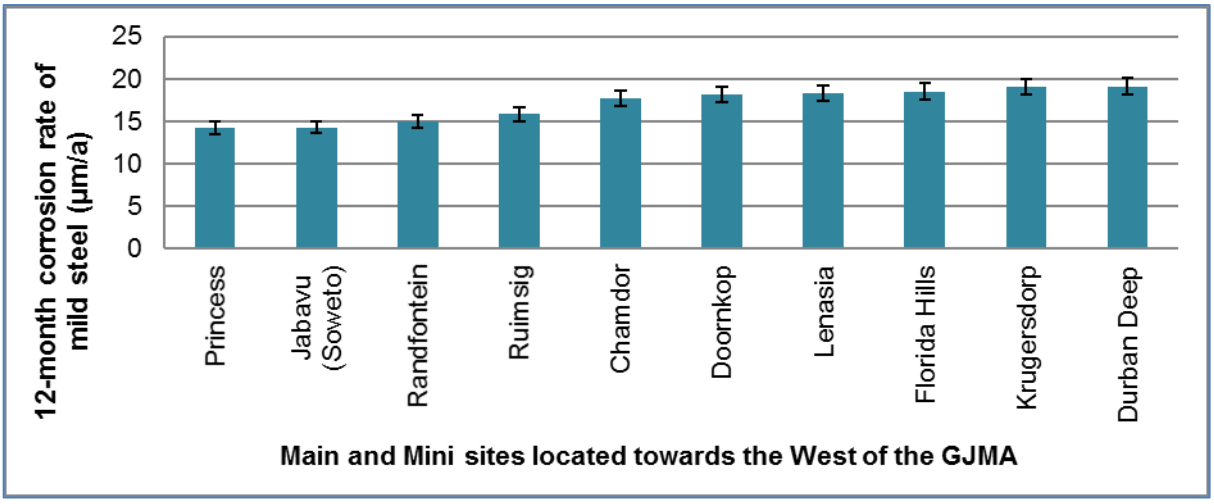


Figure 4.40 12-month corrosion rates of mild steel at the main and mini sites located in the Western part of the GJMA.

4.2.6 Optical Surface Characterisation, Morphology and Chemical Analysis of the Mild Steel Corrosion Products Formed at the Main and Mini Sites in the GJMA

4.2.6.1 Optical surface characterisation of the corrosion product

Optical micrographs of the corroded surfaces of the 12-month mild steel specimens at the respective sites are presented in **Figure 4.41**.

As examples**, Figure 4.42** provides a close-up view of the corrosion products formed on the mild steel panels at the Princess site, whereas **Figures 4.43 & 4.44** show the changes in the surface morphologies of the corrosion products of the mild steel specimens after (a) 6 months and (b) 12 months at the Kagiso-Randfontein and Florida Hills sites, respectively,

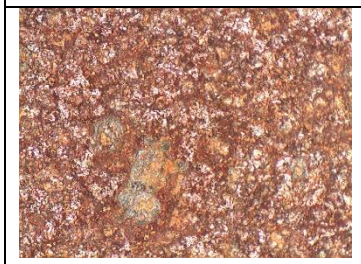
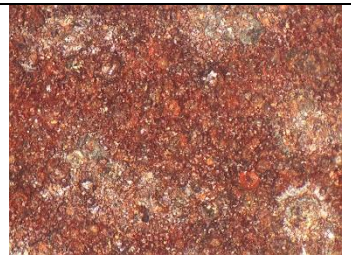
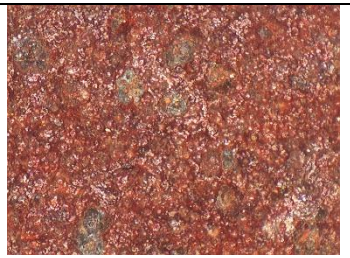
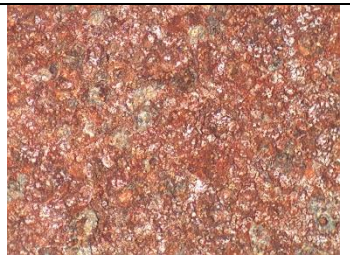
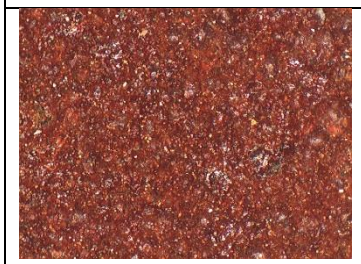
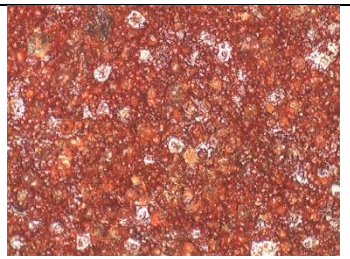
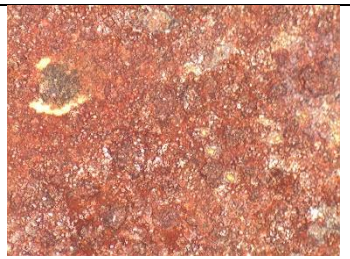
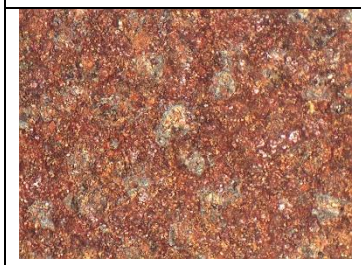
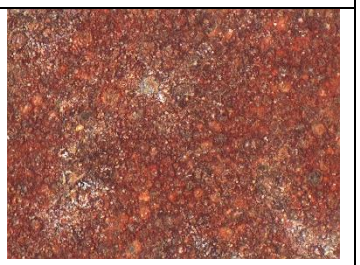
Aeroport	Alexandra	Alrode	Balmoral	Bonaero Park
				
Braamfontein	Brakpan	Bryanston	Buccleuch	Chamdor
				
Chloorkop	Dainfern Ridge	Dalpark	Delta Park	Diepsloot
				

Figure 4.41 Micrographs (x20 magnification) of the morphologies of the corrosion products formed on the 12-month flat mild steel specimens at the GJMA exposure sites.

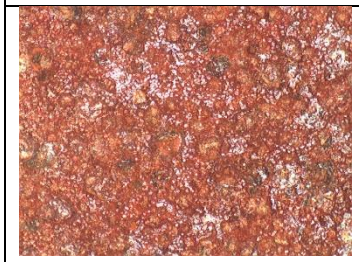
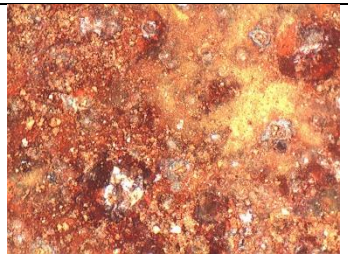
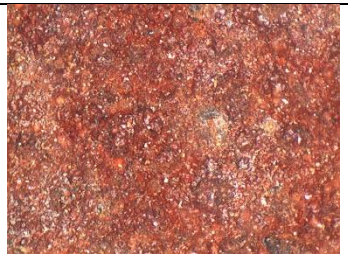
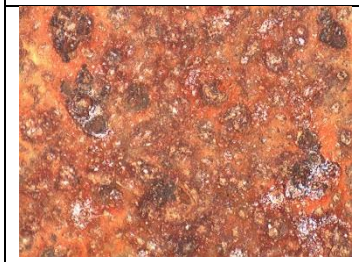
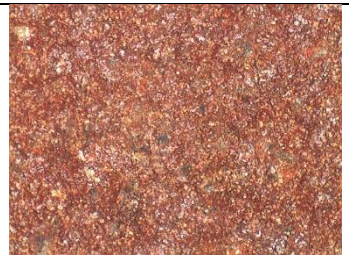
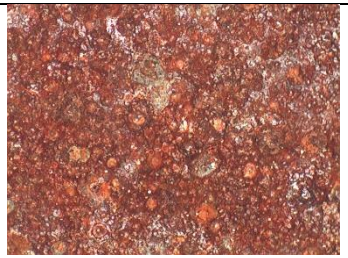
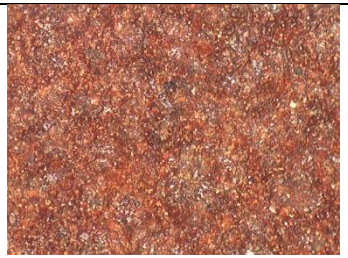
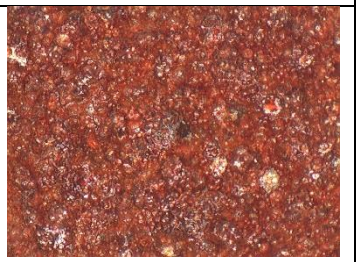
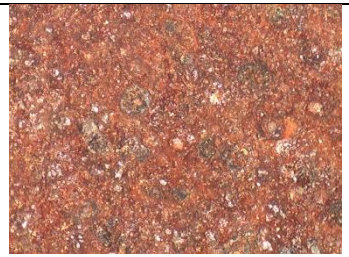
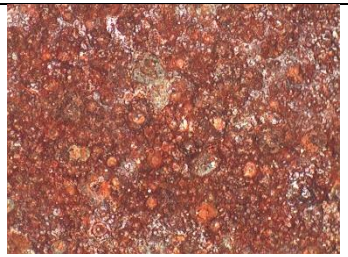
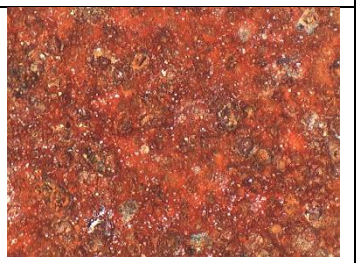
Doornkop	Dunnottar	Durban Deep	Eastleigh	Eastrand Mall
				
Eikenhof	**Elspark**	**Ennerdale**	**Esselen Park**	**Florida Hills**
				
Geluksdal	**Gillooly's**	**Houghton**	**Ivory Park**	**Jabavu (Soweto)**
				

Figure 4.41 *Continued*.

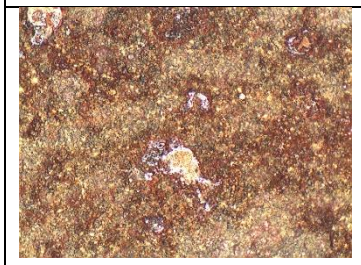
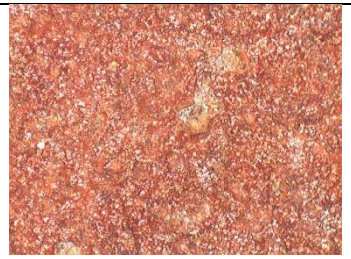
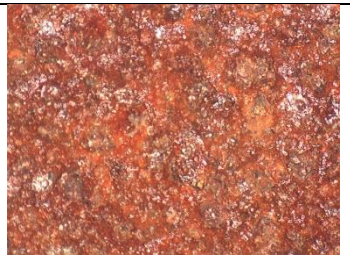
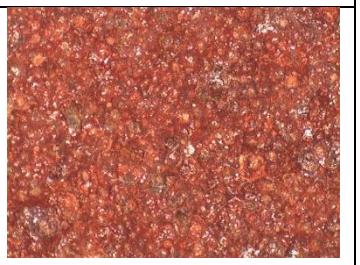
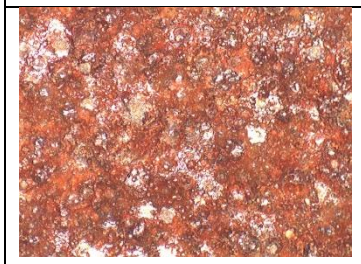
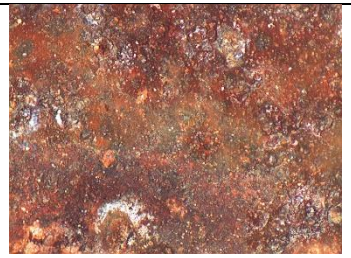
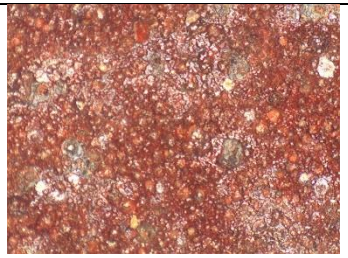
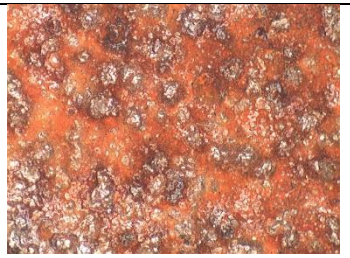
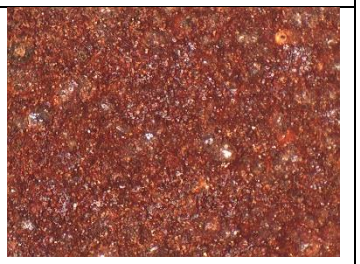
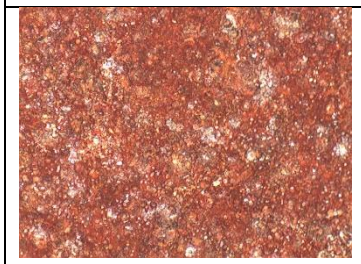
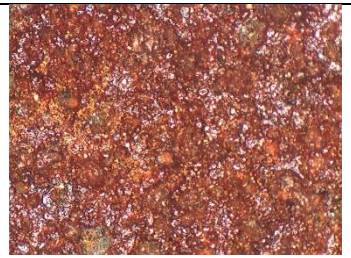
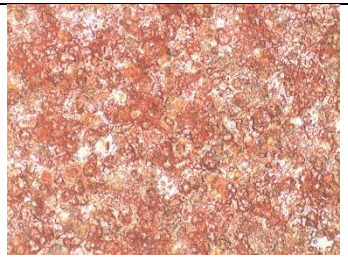
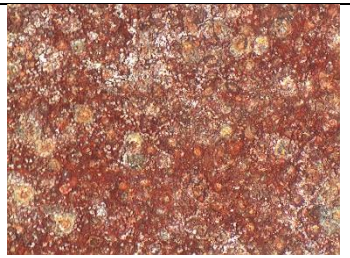
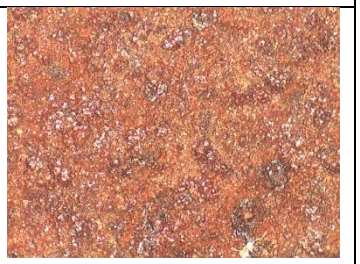
Kagiso-Randfontein	Kempton Park	Kliprivier	Kliprivierberg	Krugersdorp
				
Kyalami	Kya Sand	Lanseria	Lenasia	Midrand
				
Morningside	Nasrec	Newclare	Newtown	Nigel
				

Figure 4.41 *Continued*.

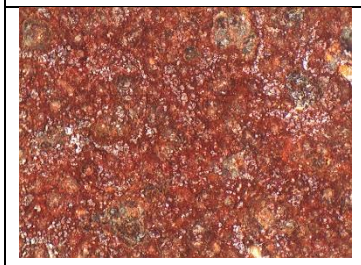
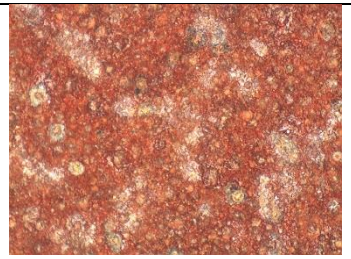
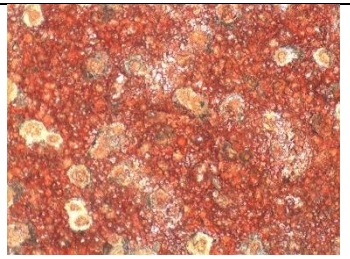
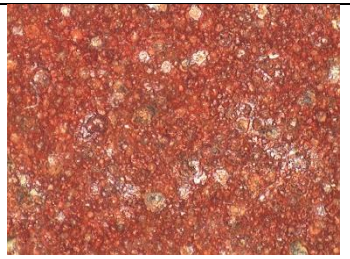
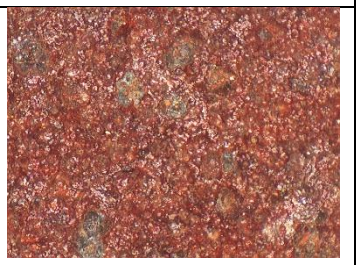
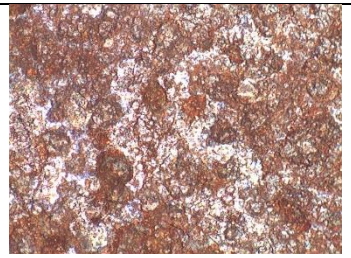
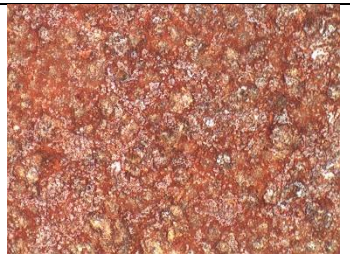
Orange Farm	Palmridge	Princess	Randfontein	Rosherville
				
Ruimsig	Springs	Wadeville	Walkerville	
				

Figure 4.41 *Continued*.

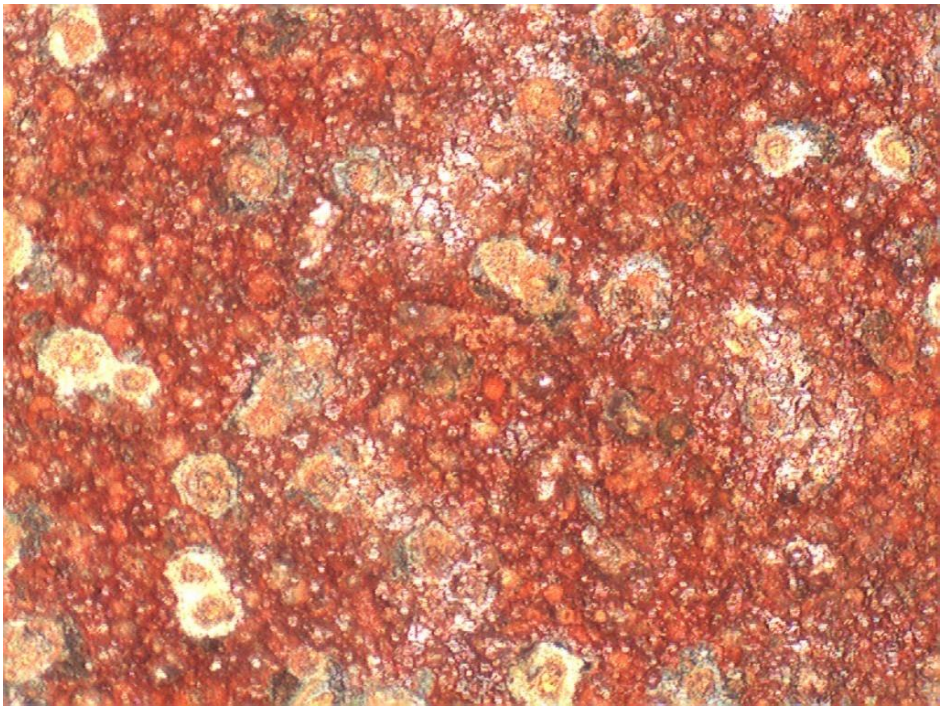
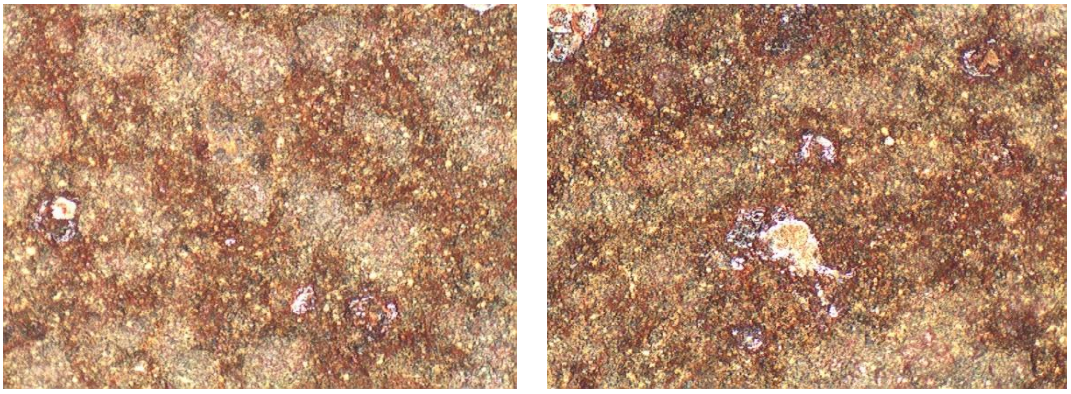
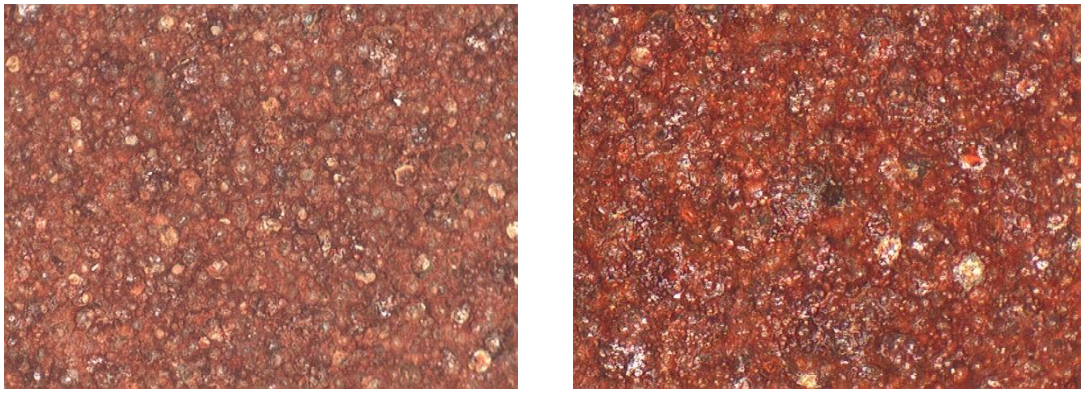


Figure 4.42 Micrograph (x20 magnification) of the corrosion product of a mild steel specimen exposed at the Princess site – Note the yellowish-white spots.



(a) (b)

Figure 4.43 Micrographs (x20 magnification) of the corrosion products of the mild steel specimens following (a) 6 months and (b) 12 months of exposure at the Kagiso-Randfontein site.



(a) (b)

Figure 4.44 Micrographs (x20 magnification) of the corrosion products of the mild steel specimens following (a) 6 months and (b) 12 months of exposure at the Florida Hills site.

4.2.6.2 Morphology of the mild steel corrosion products

Attenuated total reflectance (ATR) - Fourier transform infrared (FTIR) spectroscopy

A typical FTIR spectrum of the scraped 12-month corrosion products formed on the mild steel specimens in the GJMA is shown in **Figure 4.45**. In general, the main IR peaks identified were in the region of wavenumbers 745 cm^{-1}, 791 cm^{-1}, 1019 cm^{-1},1118 cm^{-1}, 1464 cm^{-1}, 1637 cm^{-1}, 2852 cm^{-1}, 2924 cm^{-1} and 3064 cm^{-1}. For discussion purposes, the IR spectra of the iron oxides formed at some of the sites are given in **Appendix L - Figures L.1 – L.3**

Raman Spectroscopy

Figures 4.46-4.47 & 4.49-4.51 present Raman spectra of the iron oxides, γ-FeOOH (lepidocrocite), α-FeOOH (goethite), δ-FeOOH (feroxyhyte), $Fe(OH_3)$ (ferric hydroxide), β-FeOOH (akageneite) and Fe_3O_4 (magnetite) found in the scraped 12-month corrosion products formed on the mild steel specimens exposed at selected sites in the GJMA. See also **Appendix M – Table M.1**, which present the Raman bands of the different iron oxides formed at these particular sites.

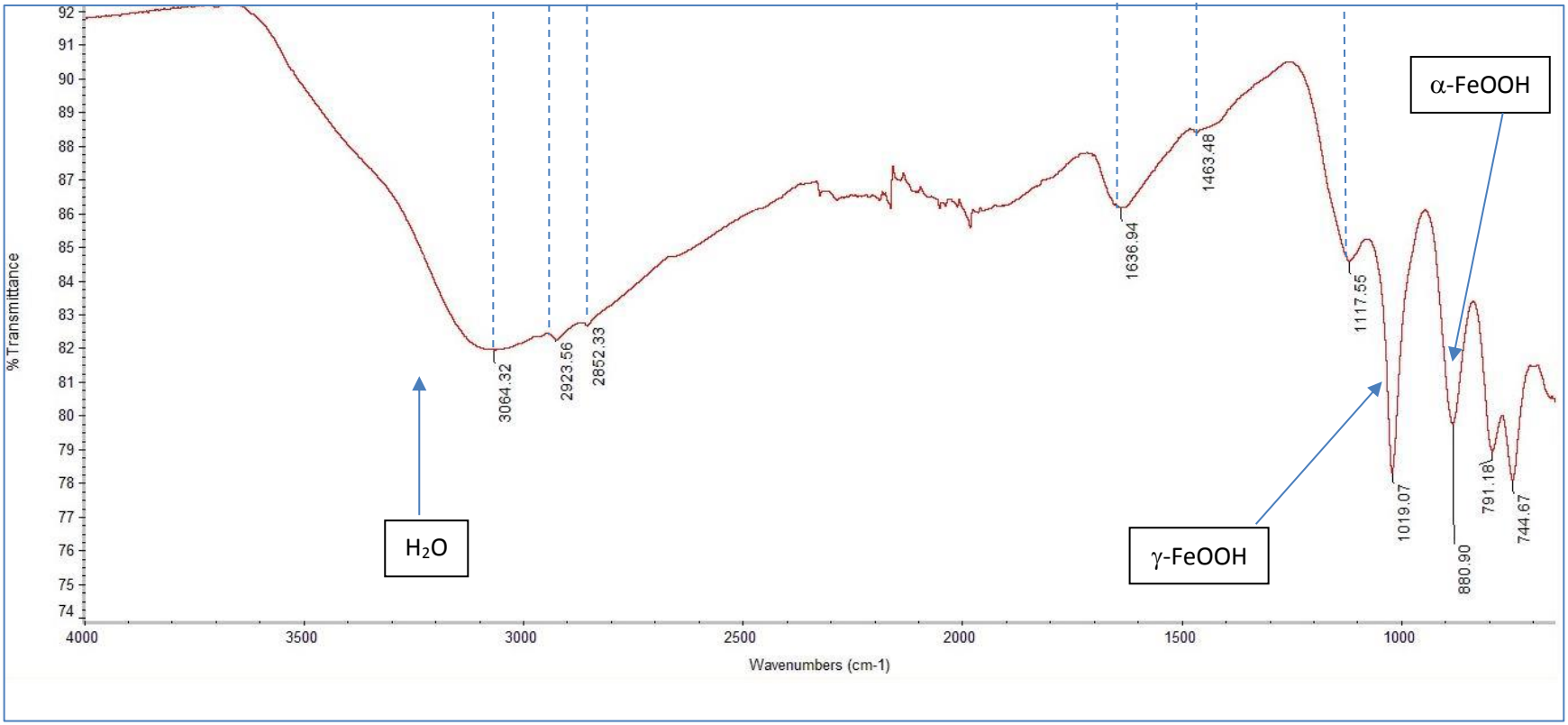


Figure 4.45 Typical FTIR spectrum of the 12-month corrosion product formed on the mild steel specimens at exposed in the GJMA. The above spectrum was taken for the mild steel samples exposed at Ruimsig.

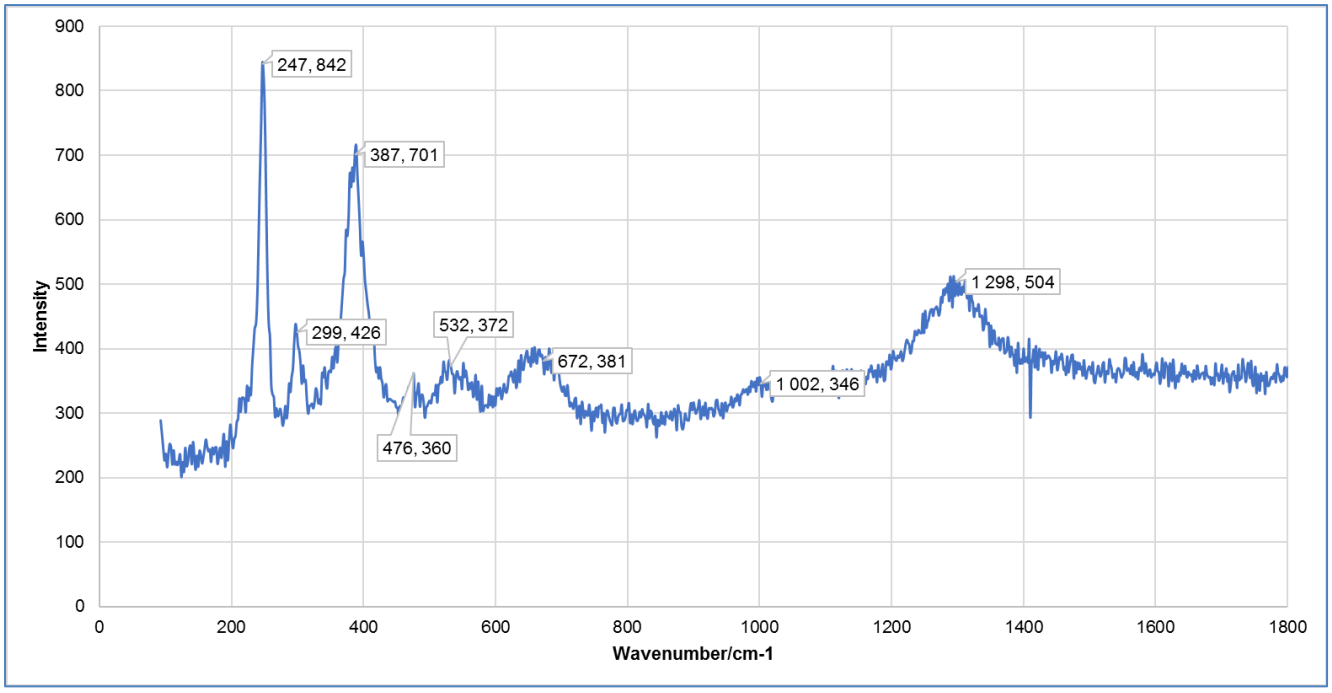


Figure 4.46 Raman spectrum of a combination of γ-FeOOH and α-FeOOH found in the corrosion product of the Alexandra site.

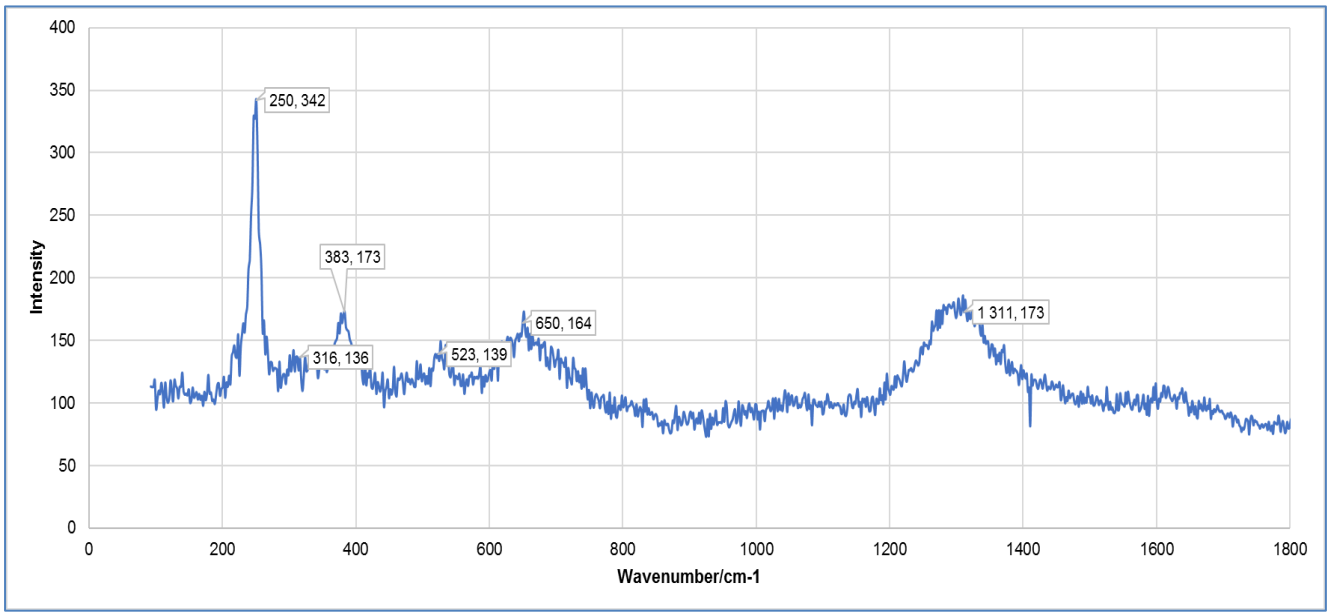


Figure 4.47 Raman spectrum of a mixture of γ-FeOOH, α-FeOOH and Fe_3O_4 found in the corrosion product of the Chloorkop site.

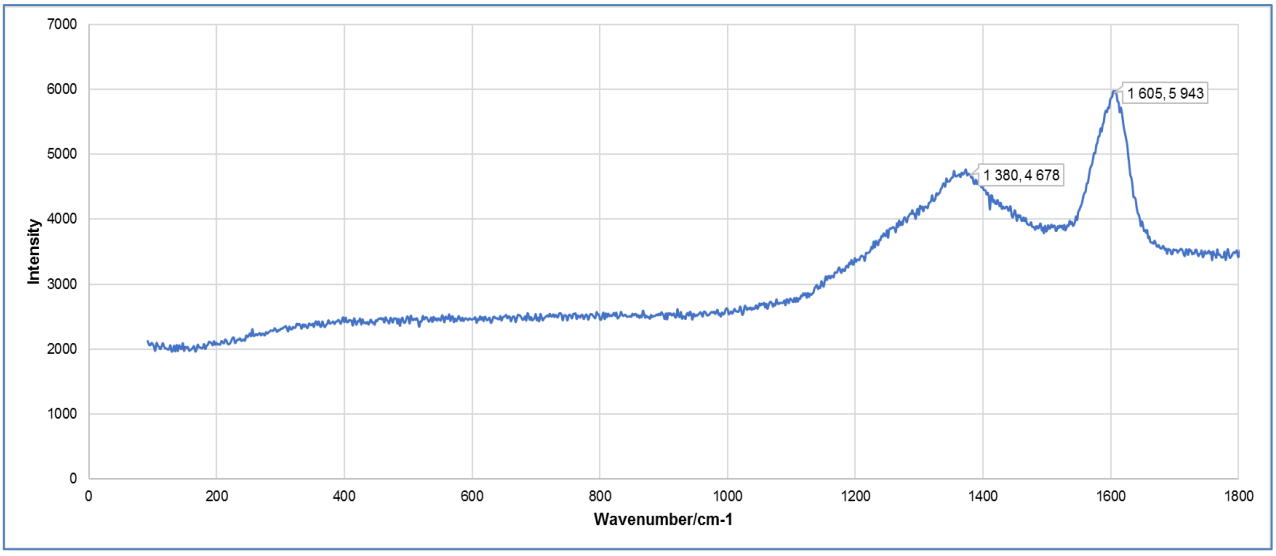


Figure 4.48 Raman spectrum of amorphous carbon found in the corrosion product of the Kagiso-Randfontein site.

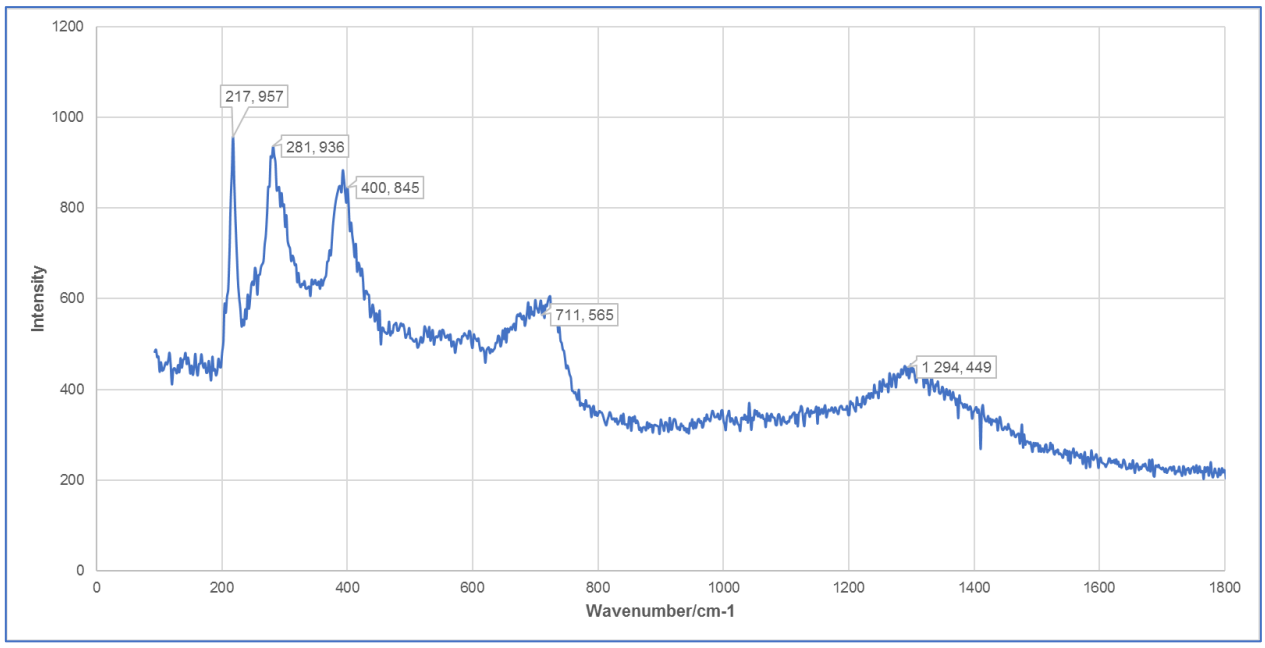


Figure 4.49 Raman spectrum of a combination of α-Fe_2O_3 and β-FeOOH found in the corrosion product of the Chloorkop site.

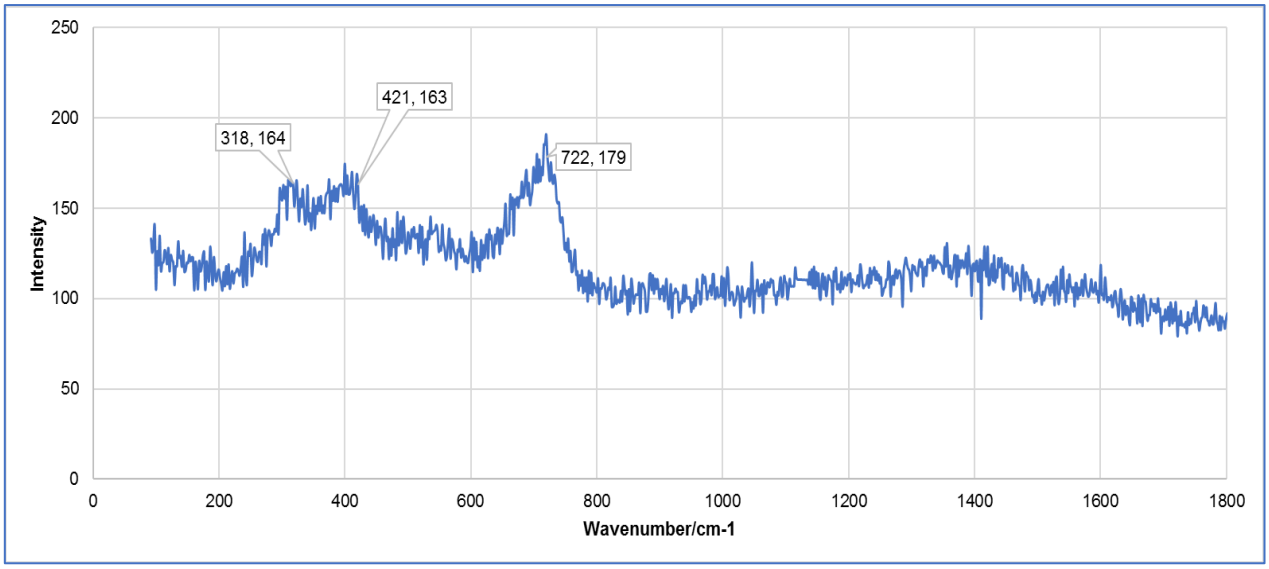


Figure 4.50 Raman spectrum of a combination of γ-FeOOH and $Fe(OH_3)$ found in the corrosion product of the Chloorkop site.

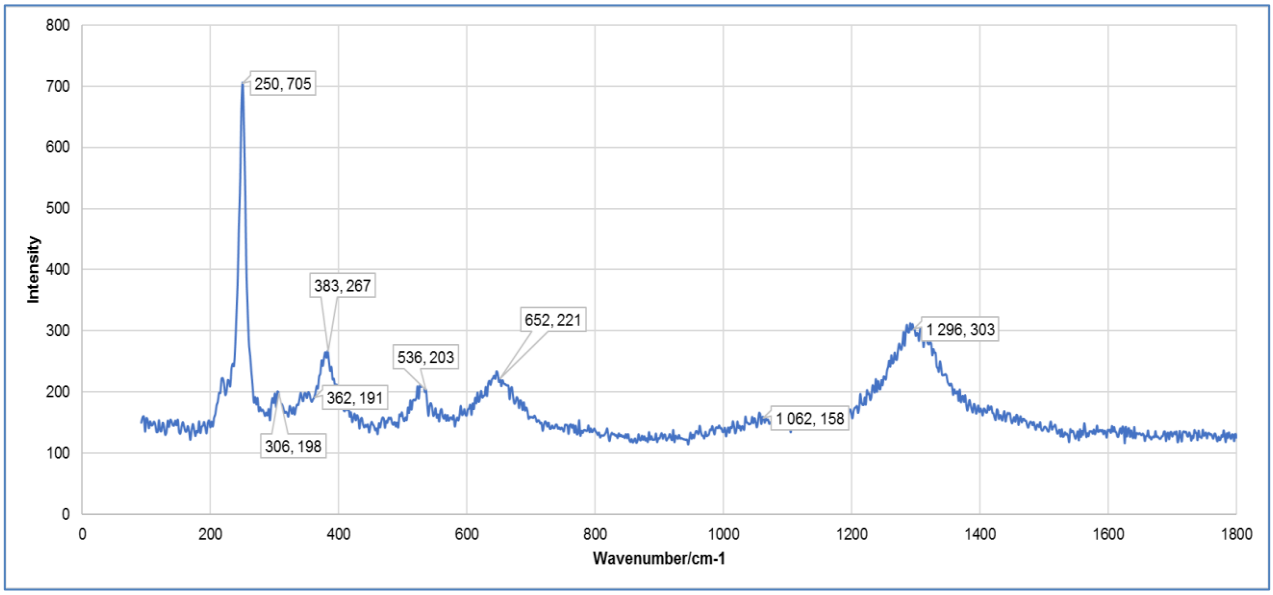


Figure 4.51 Raman spectrum of a combination of γ-FeOOH and Fe_3O_4 found in the corrosion product of the Nasrec site.

4.2.6.3 Chemical analysis of the mild steel corrosion products

Scanning electron microscopy (SEM) and energy dispersive X-ray spectroscopy (EDS) analysis

Examples of the typical SEM micrographs and EDS spectra obtained are shown in **Figures 4.52 & 4.53**, whereas **Figure 4.54** presents summations (∑) of the maximum measured concentrations for Al, Si, P, S and Cl versus the respective 12-month corrosion rates of the mild steel specimens at the different sites. The detailed results are given in **Appendix N – Table N.1**.

Water-soluble salts and pH measurements

Figure 4.55 presents the water-soluble salt concentration levels of the corrosion products of the 12- month mild steel test panels exposed at the different sites, versus their 12-month corrosion rates. The pH results obtained during the second pH test procedure are shown in **Figure 4.56**.

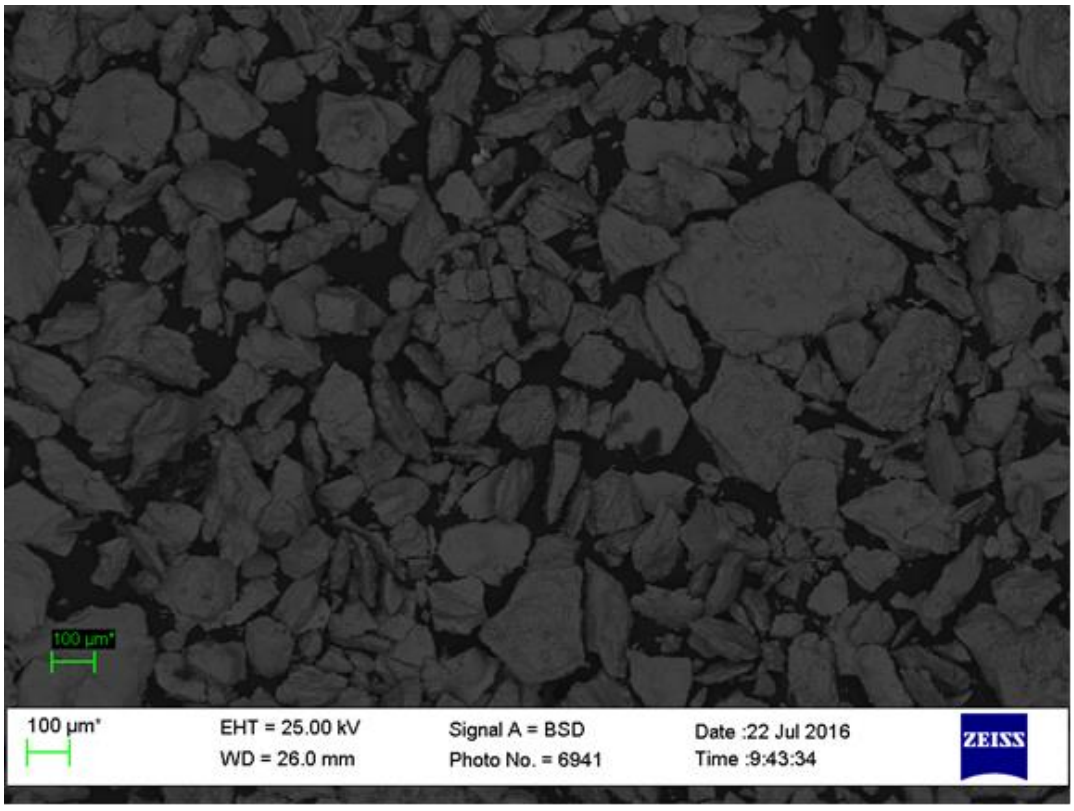


Figure 4.52 Typical scanning electron micrograph (in BSE mode) of the scraped corrosion products of the mild steel panels.

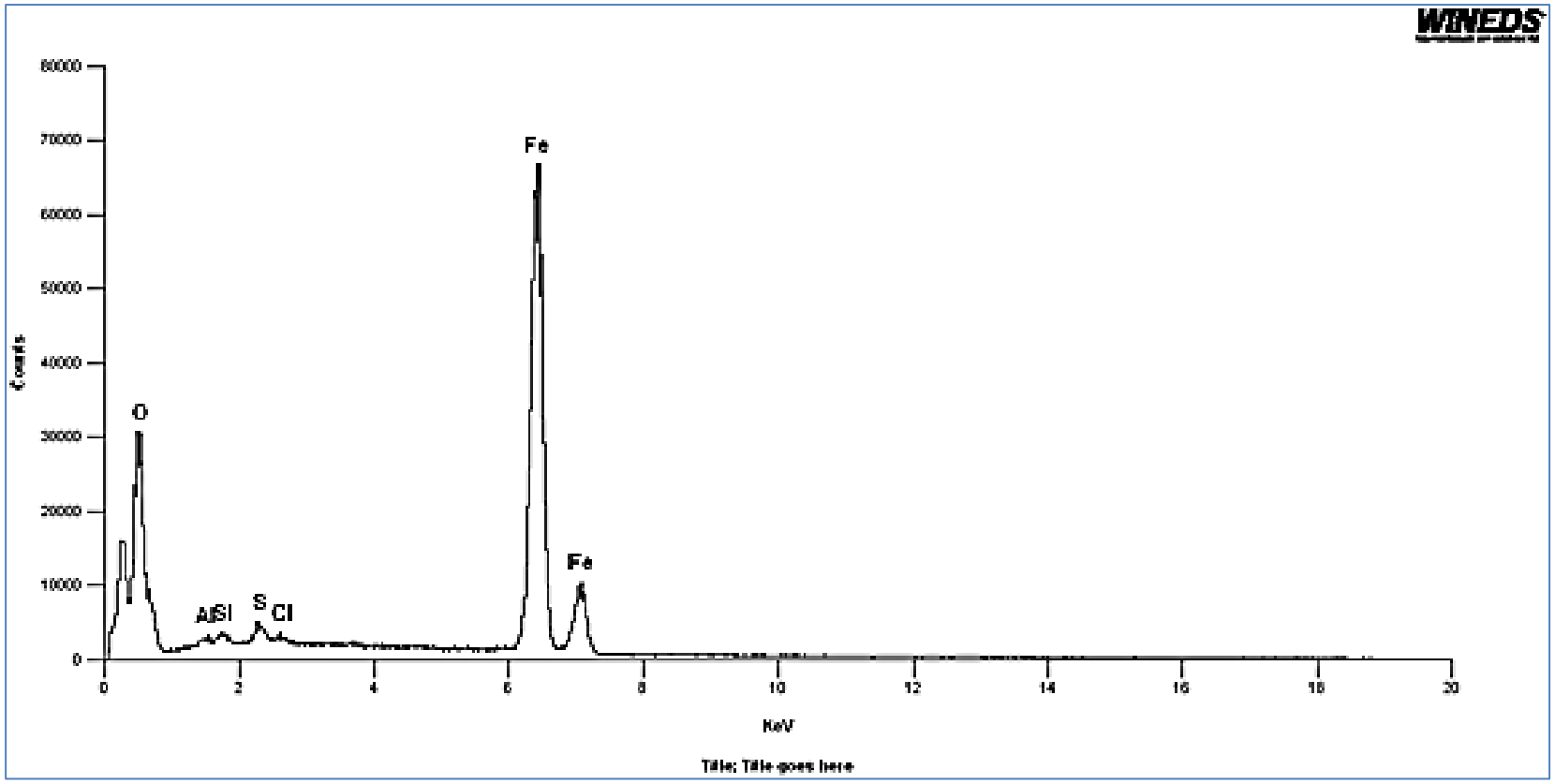


Figure 4.53 EDS spectrum indicating the elementals of the corrosion product from the mild steel panels exposed at the Chloorkop site.

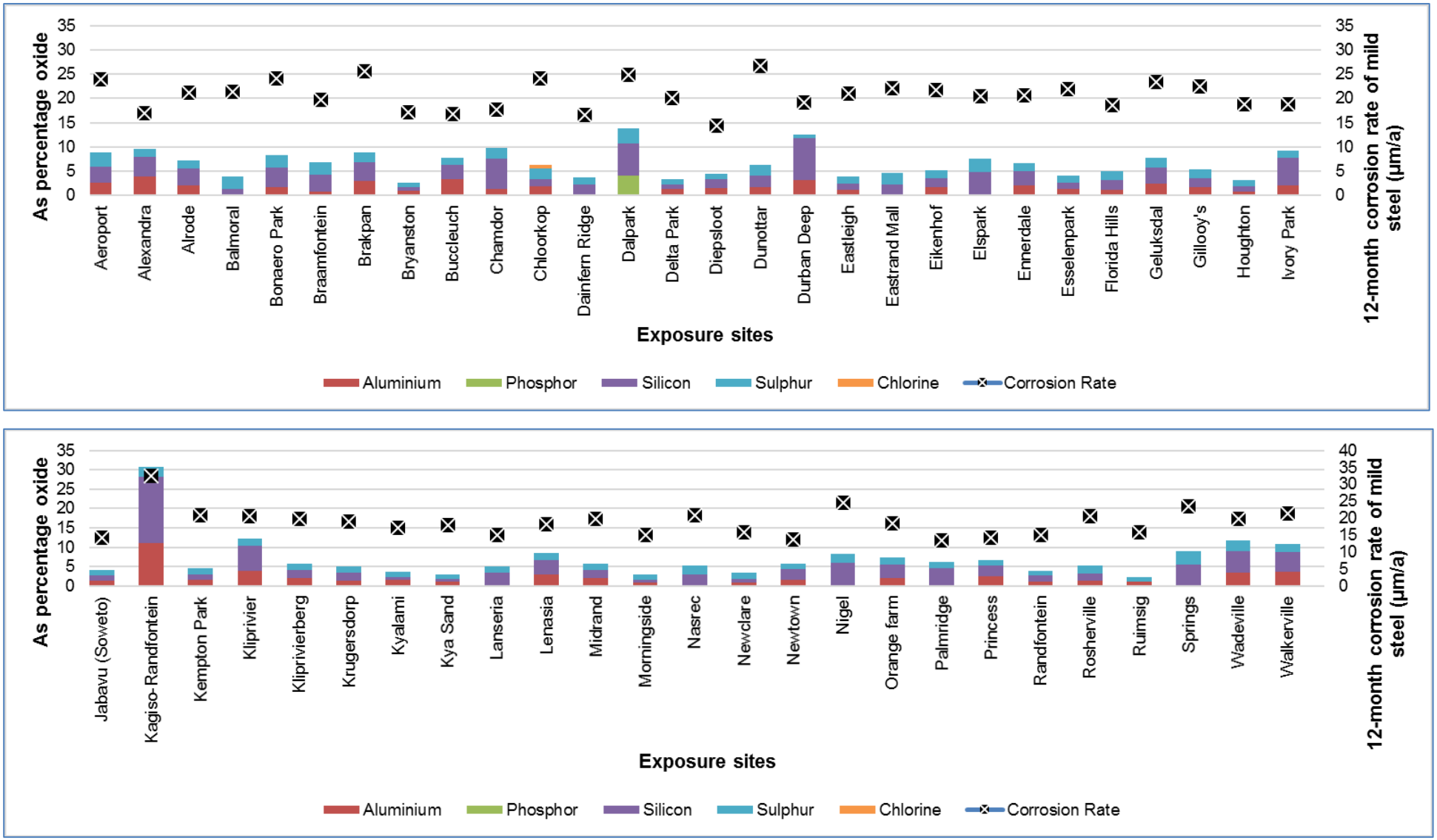


Figure 4.54 Oxide compositions of the corrosion products of the mild steel specimens exposed at the different GJMA sites, versus their respective 12-month corrosion rates.

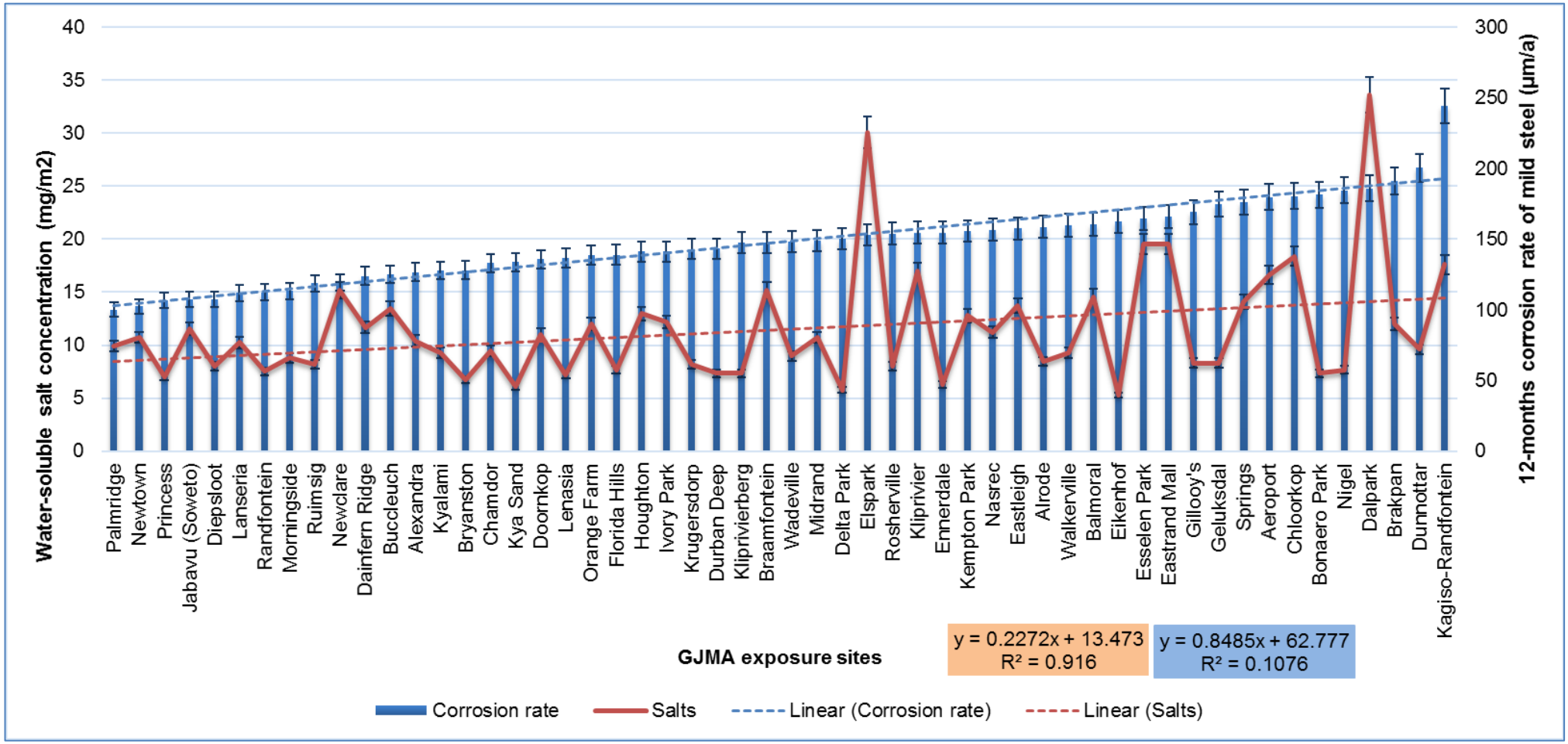


Figure 4.55 Water-soluble salt levels of the corrosion products versus the 12-month corrosion rates of the mild steel at the different GJMA sites.

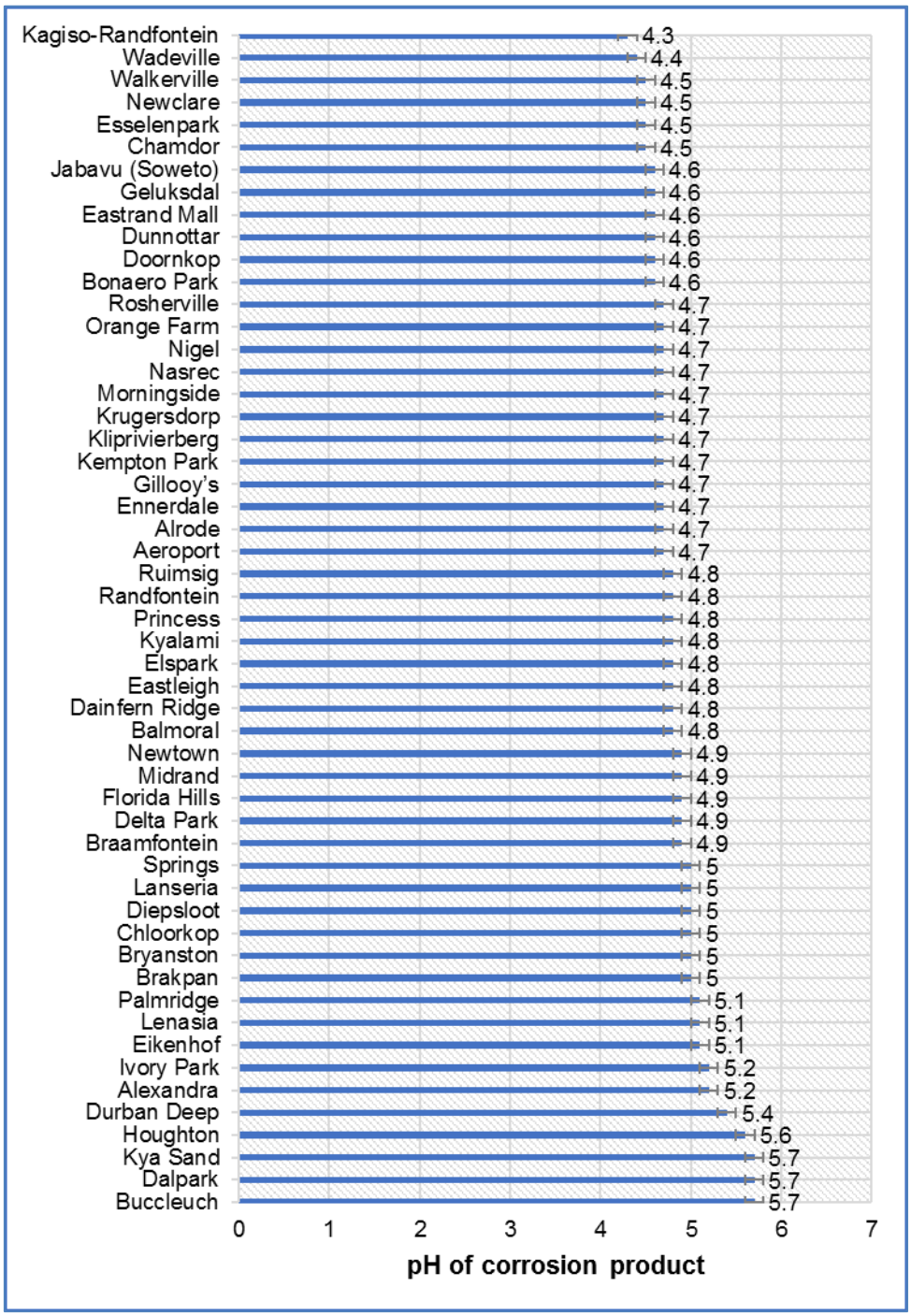


Figure 4.56 pH measurements of the mild steel corrosion products originating from the different GJMA sites.

4.3 THE EFFECTS OF THE GJMA ATMOSPHERE ON ORGANIC COATINGS

4.3.1 Degree of Corrosion of the Coated Panels

Only a few of the samples, mainly coated with System F, exhibited signs of corrosion at the steel edges following 24 months of exposure in the GJMA, while the extent of the field corrosion of all the painted panels rated Ri 0 (0% in other words), as per the ISO 4628-3 pictorial rating scheme (International Organization for Standardization 2003b). An example, **Figure 4.57** shows the conditions of the different coated panels, i.e. Systems A to G, after 24 months of exposure at the Kagiso-Randfontein site, which was identified as one of the most corrosive locales in the GJMA.

4.3.2 Changes in Average Coating Thicknesses (DFTs)

Appendix O – Tables O.1 & O2 present the before and after exposure (BE & AE) DFT measurements of the different coating systems per site. Note that no results are included for the Buccleuch locale. This was due to the samples being lost (because of theft) shortly after exposure. The sum (∑) differences of the BE and AE average thickness measurements of the various coatings are given in **Figure 4.58**, whereas **Figure 4.59** shows the average percentage changes in the mean thicknesses of the different coatings at the main GJMA sites – after 24 months of outdoor weathering. The average percentage changes in the DFTs of the various coating systems are presented in **Figure 4.60**.

Sum (∑) percentage changes in the average DFTs of Systems D to G are given in **Figure 4.61** and the percentage changes in the average DFTs of System E, after 24 months of exposure at the main GJMA sites, in **Figure 4.62**.

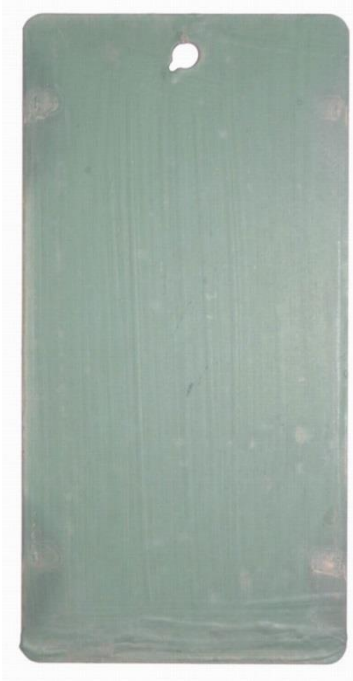
System A	System B	System C	System D
 (a)	 (b)	 (c)	 (d)
System A – two coats of a solvent-borne surface tolerant epoxy, overcoated with one coat of a water-based acrylic emulsion topcoat	System B – two coats of a solvent-borne surface tolerant epoxy, overcoated with one coat of a solvent-borne polysiloxane topcoat	System C – two coats of a solvent-borne surface tolerant epoxy, overcoated with one coat of a solvent-borne aliphatic acrylic polyurethane topcoat	System D – one coat water-based acrylic primer, overcoated with two coats of a water-based acrylic topcoat

Figure 4.57 Conditions of the coated mild steel samples (Systems A to D) after 24 months of exposure at the Kagiso-Randfontein site.

System E	System F	System G
 (e)	 (f)	 (g)
System E – one coat water-based acrylic primer, overcoated with two coats of a water-based acrylic topcoat	System F – a single-layer electrostatically applied polyester powder coating	System G – one coat solvent-borne alkyd primer, overcoated with two coats of a solvent-borne alkyd high-gloss enamel topcoat

Figure 4.57 (*Continued)* Condition of the coated mild steel samples (Systems E to G) after 24 months of exposure at the Kagiso-Randfontein site.

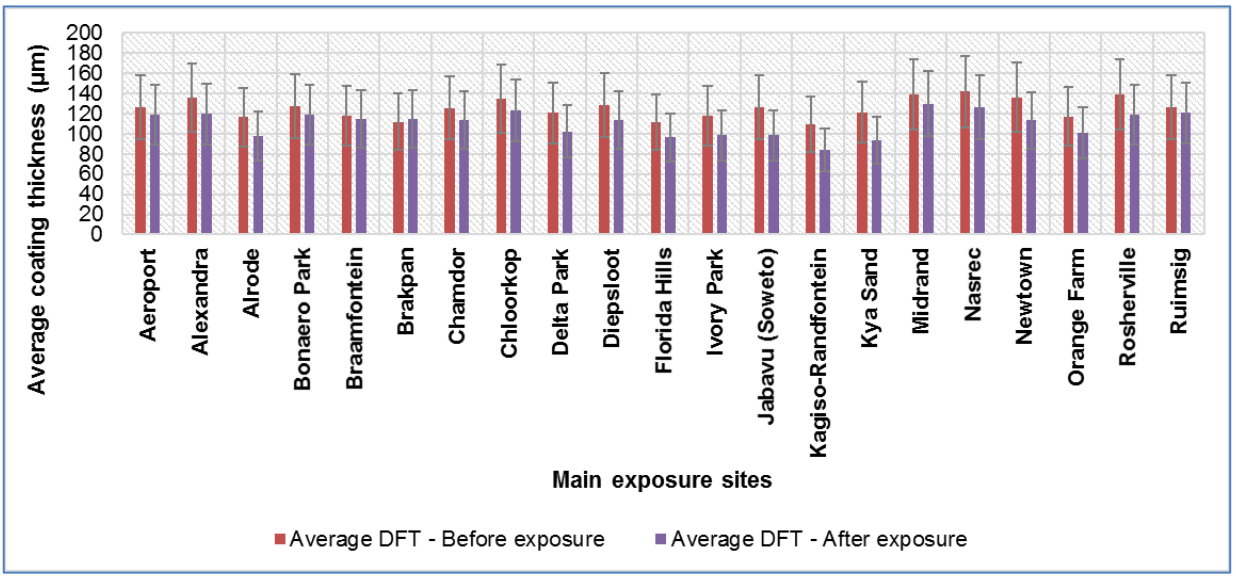


Figure 4.58 Sum (∑) differences between the average thicknesses of the various coatings before and after 24 months of exposure at the main GJMA sites.

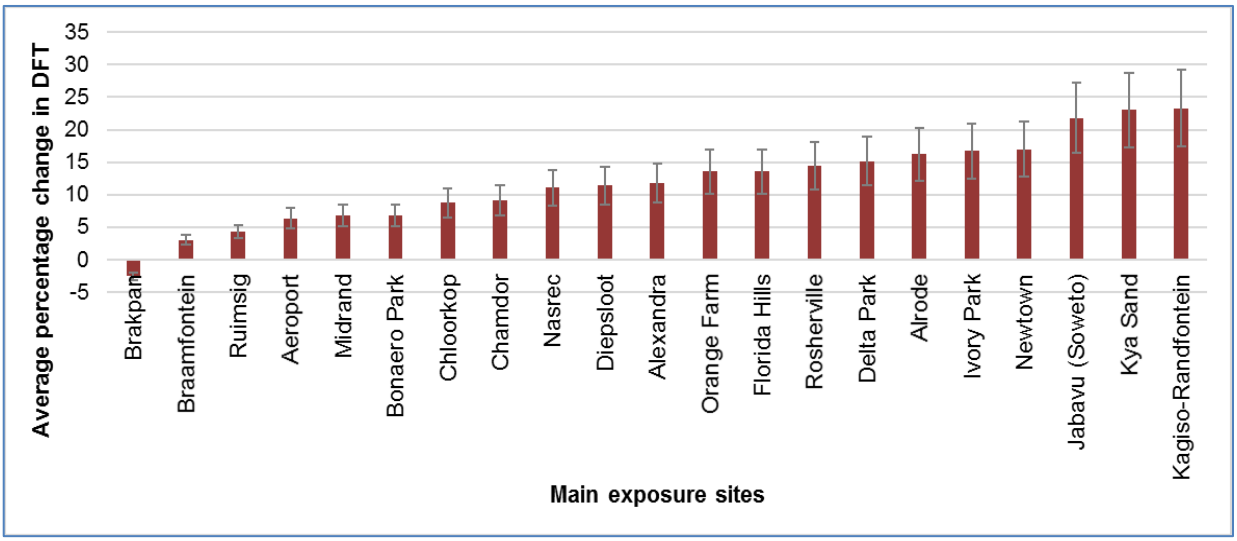


Figure 4.59 Average percentage changes in the mean thicknesses of the different coatings at the main GJMA sites – after 24 months of outdoor weathering.

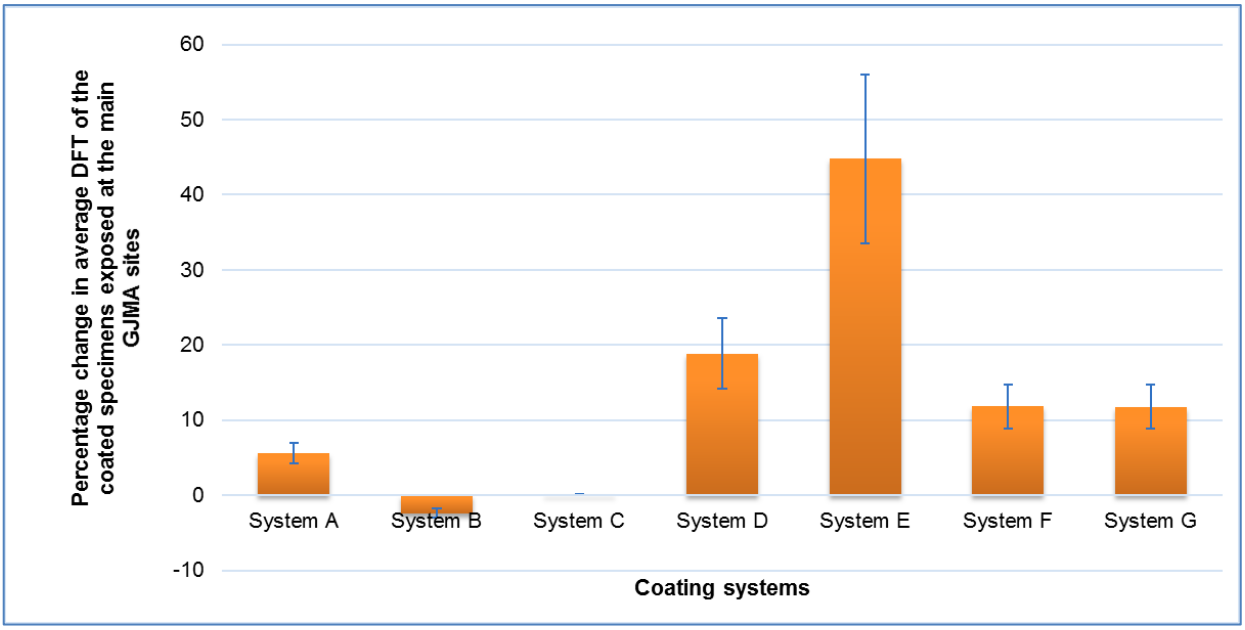


Figure 4.60 Average percentage changes in the DFTs of the various coating systems exposed at the main GJMA exposure sites over a period of 24 months.

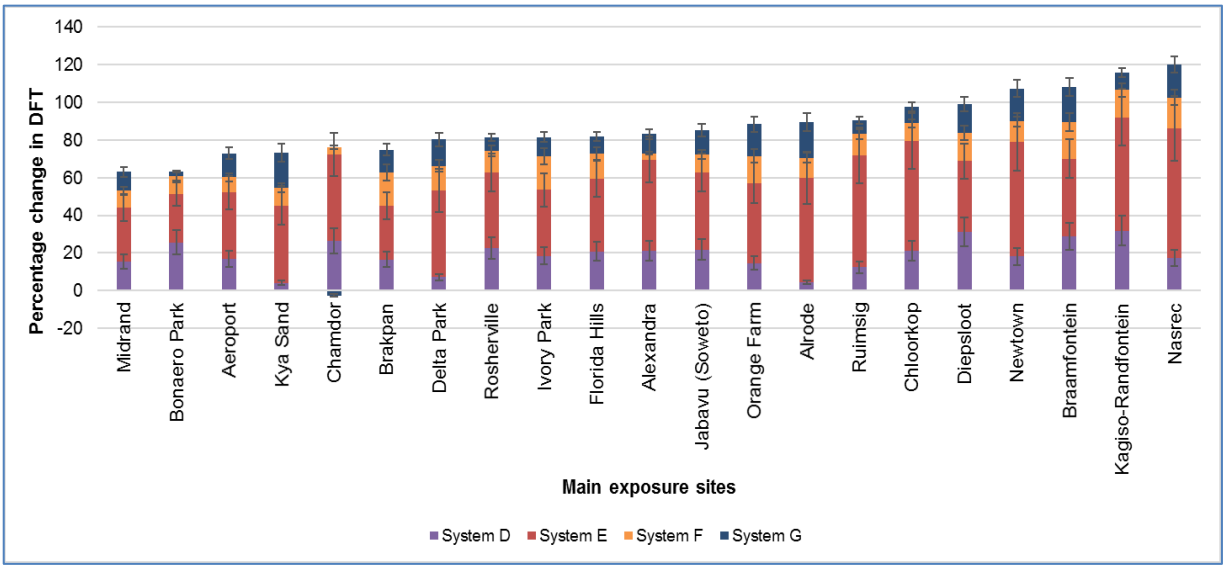


Figure 4.61 Sum (∑) percentage changes in the average DFTs of Systems D to G after 24 months of outdoor weathering at the main GJMA sites.

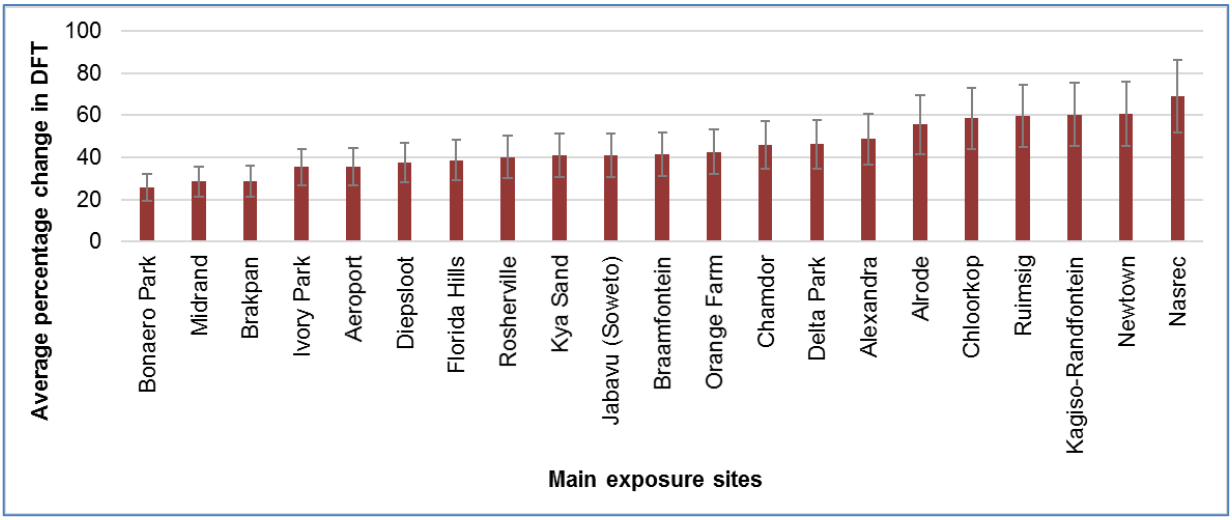


Figure 4.62 Percentage changes in the average DFTs of System E after 24 months of exposure at the main GJMA sites.

4.3.3 Degree of Chalking and Dirt Retention

Figure 4.63 presents images of the extent of chalking and dirt retention obtained by tape pull-off testing of the different coated surfaces exposed at the Braamfontein, Chloorkop, Kagiso-Randfontein and Chamdor sites, as examples. The degree of chalking and dirt retention of the mild steel specimens covered with an alkyd coating system (System G) after 24 months of exposure at Aeroport, Braamfontein and Chloorkop are given in **Figure 4.64**.

Figure 4.65, alternatively, presents the sum (∑) ratings of the degree of chalking and dirt retention of the different coatings by location, whereas the individual scores per sample per location, after 24 months of exposure, are given in **Appendix P**. The sum (∑) ratings of the degree of chalking and dirt retention of the different coating systems are displayed in **Figure 4.66**.

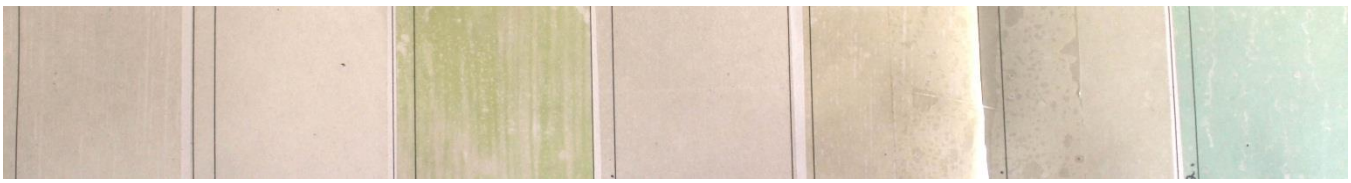
System A	System B	System C	System D	System E	System F	System G
 (a)						
 (b)						
 (c)						
 (d)						

Figure 4.63 Extent of chalking and dirt retention by tape pull-off testing of the different coated surfaces exposed at a) Braamfontein, b) Chloorkop, c) Kagiso-Randfontein and d) Chamdor.



(a) (b) (c)

Figure 4.64 Degree of chalking and dirt retention of the mild steel specimens coated with an alkyd coating system (System G) after 24 months of exposure at a) Aeroport, b) Braamfontein and c) Chloorkop.

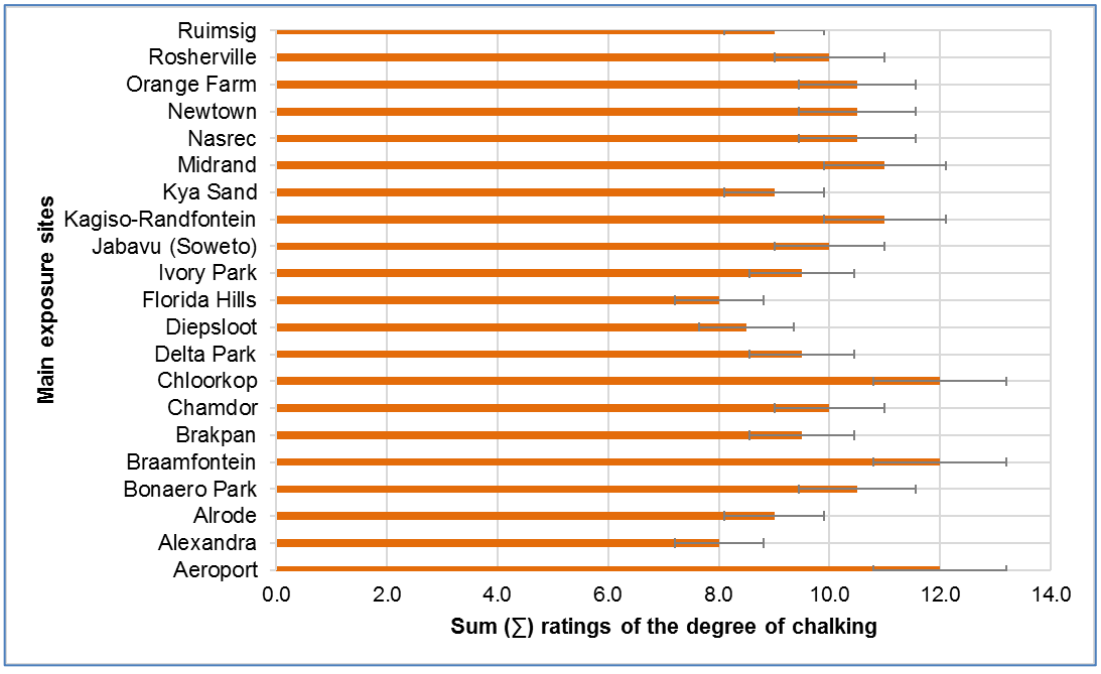


Figure 4.65 Sum (∑) ratings of the degree of chalking and dirt retention of the different coatings after 24 months of exposure at the main sites in the GJMA.

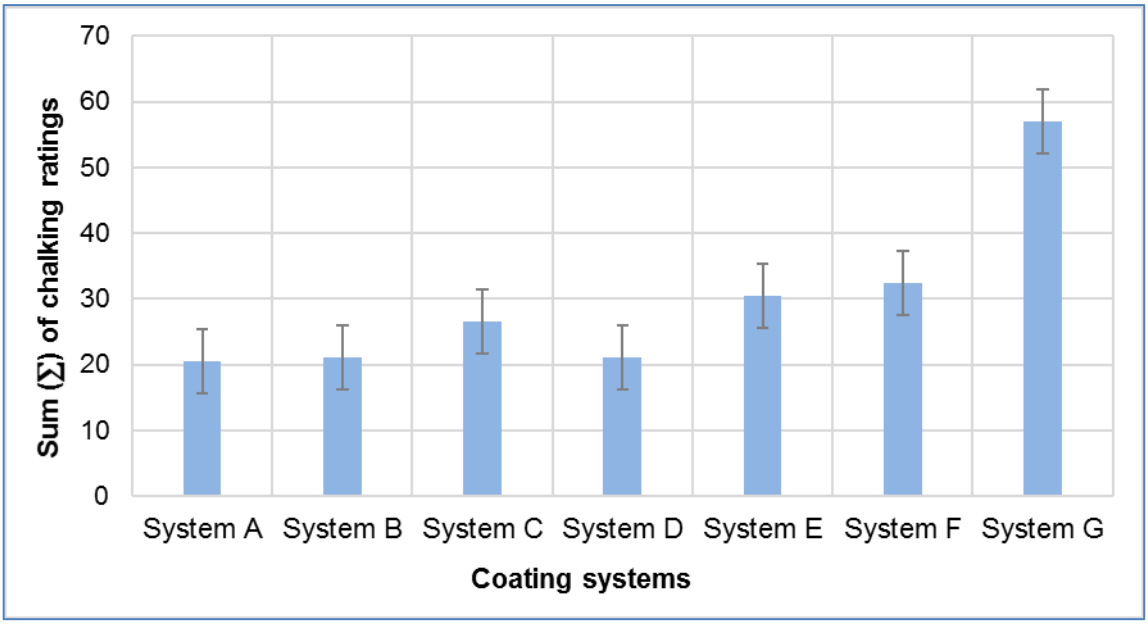


Figure 4.66 Sum (Σ) ratings of the degree of chalking and dirt retention of the different coating systems.

4.3.4 Changes in 60° Specular Gloss Levels

The before and after exposure gloss levels (GU) for the various coated samples per location are presented in **Appendix Q - Tables Q.1 & Q.2**, whereas the changed values for the main sites are given in **Appendix Q - Table Q.3**.

The variations in the gloss standards of the different samples, following 24 months of exposure at the various sites, are likewise graphically presented in **Figure 4.67**. **Figure 4.67** shows that the alkyd high gloss enamel coating (System G) exhibited the most significant percentage gloss loss, followed by System C (the epoxy-polyurethane system), while **Figure 4.68**, presents the sum (∑) gloss changes of Systems A, B, C, F and G, with System E being excluded due to a low initial gloss level.

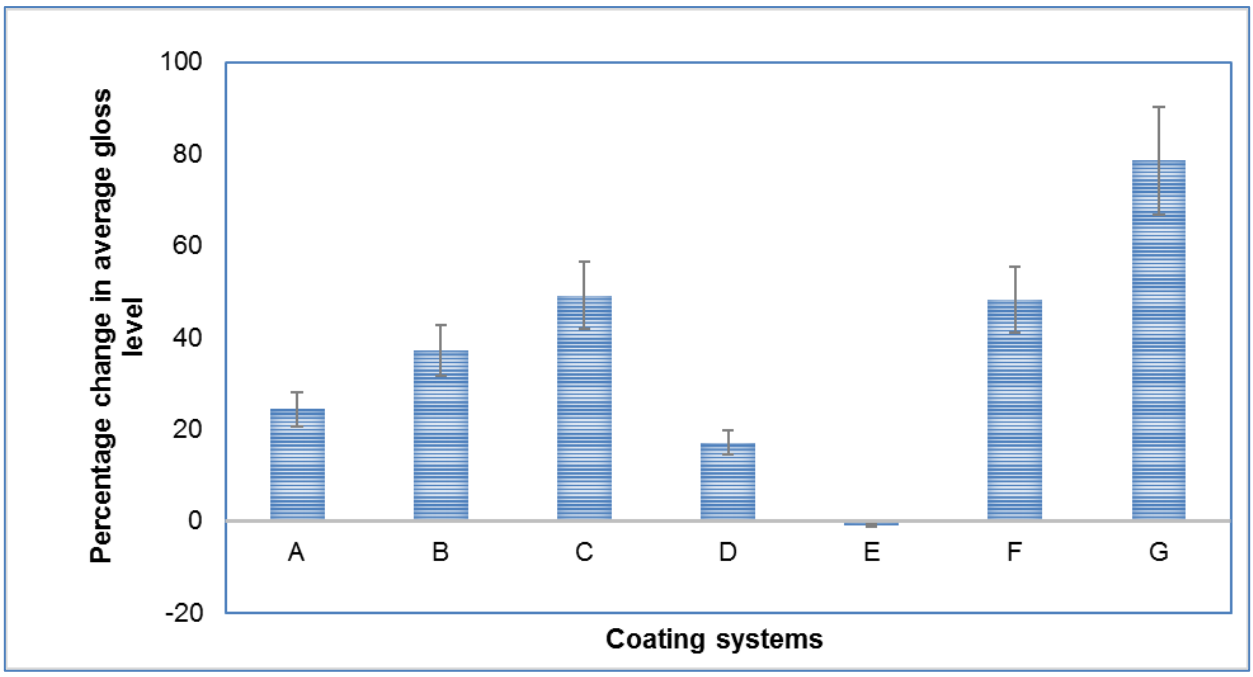


Figure 4.67 Percentage change in the average gloss levels of the different coating systems after 24 months of exposure at the main sites in the GJMA.

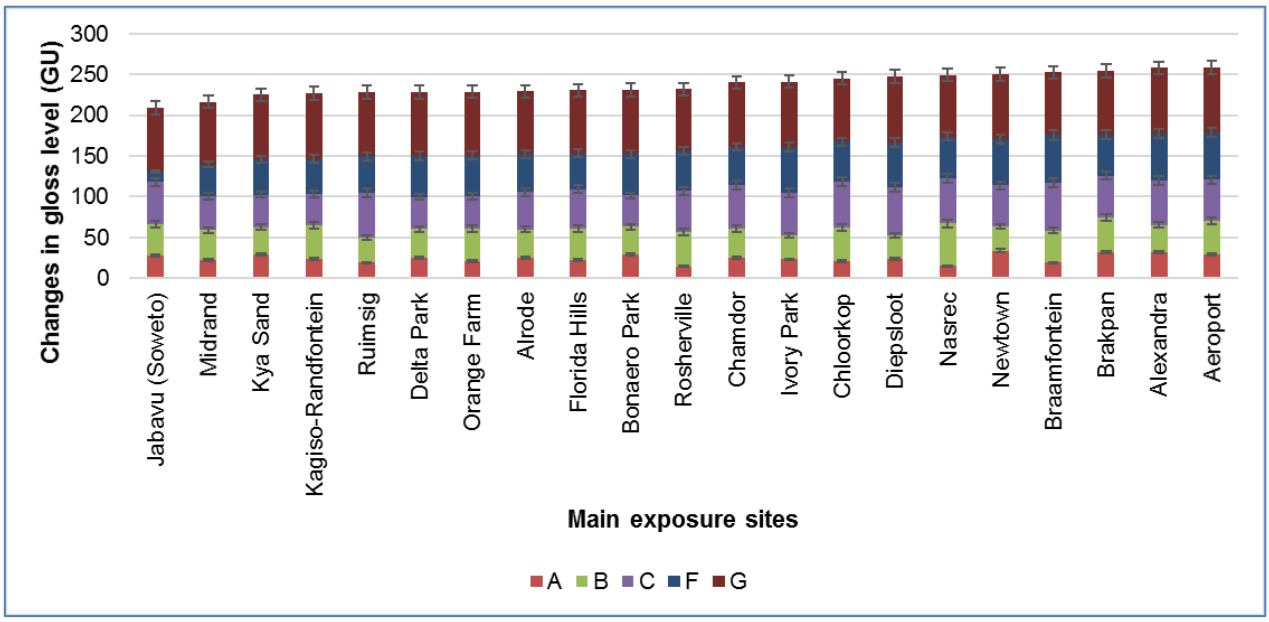


Figure 4.68 Sum (∑) changes in the average gloss levels (GU) of Coating Systems A, B, C, F and G, after 24 months of exposure at the main sites in the GJMA.

4.3.5 Changes in Colour

The differences in the total colour coordinates of the samples before and after exposure at each location are presented in **Appendix R – Tables R.1 – R.8.** Select images of some of the colour variations are also displayed in **Appendix R - Figure R.1**. **Figure 4.69**, on the other hand, presents summations (∑) of the small colour differences of the different systems at the main GJMA sites, following 24 months of outdoor weathering.

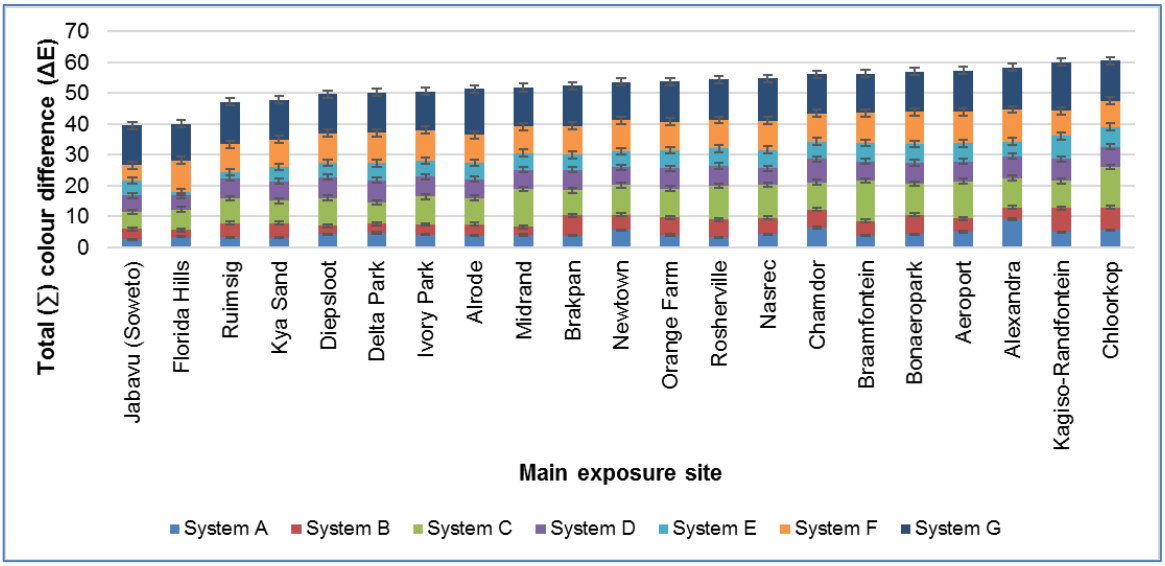


Figure 4.69 Summations (∑) of the slight colour differences (ΔE) of Systems A to G, after 24 months of exposure at the main sites in the GJMA.

4.3.6 Changes in the Chemical Structures of the Coatings

The infrared ATR-FTIR spectra or chemical 'fingerprints' of the original unexposed upper surfaces of the different multi-coat and single-layered systems are presented in **Appendix E – Figures E.1 – E.7**. Conversely, **Tables S.1 & S.2** (**Appendix S**) give the QCheck™ correlations (before and after cleaning) between the FTIR 'fingerprints' of the different coated specimens after 24 months of exposure at the main GJMA sites and their respective control spectra. These correlations are also graphically displayed in **Figure 4.70**, while **Figure 4.71** shows the QCheck™ correlations between the ATR-FTIR spectra (chemical 'fingerprints') of the different coating systems, following 24 months of exposure at the main sites and their control spectra.

For discussion purposes, the changes in the amplitudes/intensities of the peaks of the functional groups of Systems D, E and G, at Aeroport (dark blue), Jabavu (Soweto) (purple), Kagiso-Randfontein (green) and Newtown (red) are displayed in **Appendix S – Figures S.3 – S.5**.

The reduced intensities of the FTIR peaks of Systems D and E (both water-based acrylic coatings) at Aeroport (dark blue), Jabavu (Soweto) (purple), Kagiso-Randfontein (green) and Newtown (red), after 24 months of exposure at the main sites in the GJMA, are also shown in **Appendix S – Figures S.6 – S.7**. Moreover, decreased changes in the intensities of the FTIR peaks of Systems B, C and F, also at Aeroport (dark blue), Jabavu (Soweto) (purple), Kagiso-Randfontein (green) and Newtown (red) are displayed in **Appendix S – Figures S.8 – S.10**.

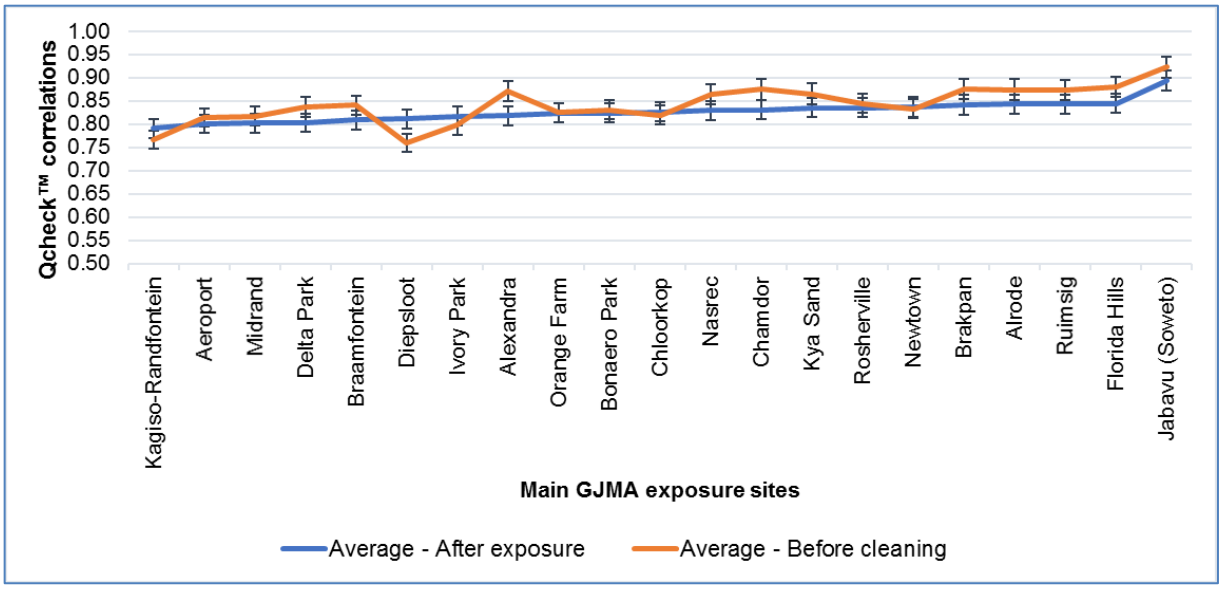


Figure 4.70 Average QCheck™ correlations of the FTIR spectra of the coated surfaces before and after cleaning with their control references – following 24 months of exposure at the main GJMA sites.

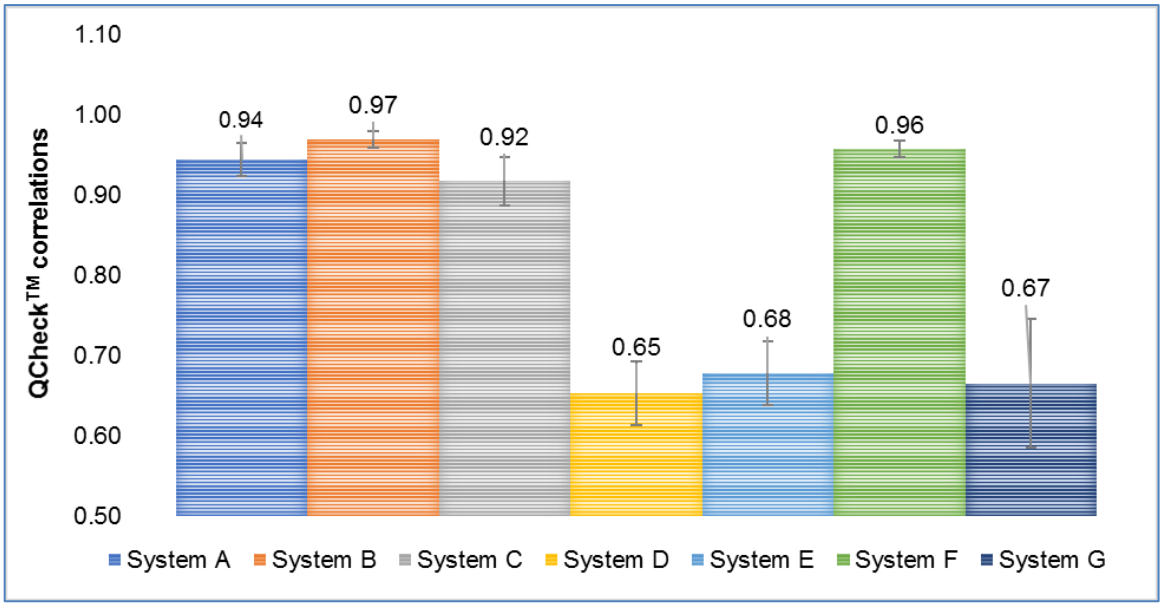


Figure 4.71 QCheck™ correlations between the ATR-FTIR spectra (chemical 'fingerprints') of the different coatings following 24 months of exposure at the main sites and their control spectra.

CHAPTER 5

DISCUSSION

5.1 ATMOSPHERIC CORROSIVITY OF SOUTH AFRICA

5.1.1 Mild (Carbon) Steel

Statistical analyses of the data presented in **Figure 4.2** showed that the average (mean) first-year corrosion rate of mild steel at the inland sites (i.e. at all corrosion monitoring spots located more than 30 km away from the ocean) was 21 ± 12 µm/a, 95% CI [18 µm/a, 23 µm/a]. The latter implies a 95% Confidence Interval (CI) that the mean is likely to fall between 18 µm/a and 23 µm/a, while the variation or dispersion of the data, also known as standard deviation (SD), is indicated by the ± value.

The minimum was about 1.3 µm/a (recorded at Droërivier in the Central Karoo) and maxima, approximately 50 µm/a in the industrial hearts of Germiston (in Gauteng) and Sasolburg (in the Free State) (Janse van Rensburg 2010). These values are outside the 5-40 µm/a range given in the old corrosion map for inland (arid, rural, urban and industrial combined) environments (Callaghan 1991). However, they are like the average values reported by Natesan et al. (2015) for mild steel exposed at inland sites in India.

In accordance with the latest revision of the ISO 9223 standard (International Organization for Standardization 2012a), the inland sites vary from *very low* (C1) to potentially *high* (C4) corrosive (**Table 2.2**). Of note is that the lowest and highest reported corrosion rates of mild steel at the inland sites are consistent with the lowest limits given in ISO 9223 for C2 and C4 corrosive environments, 1.3 µm/a and 50 µm/a, respectively. This suggests that in the desert and semi-arid (non-industrial) inland areas, the corrosivity of the environment is better rated *very low* (C1) to *low* (C2) corrosive, whereas in urban industrial locations, the atmosphere may potentially be ranked *low* (C2) to *moderate* (C3) corrosive, with a potential for *high* (C4) corrosive 'hotspots', in and around high industrial locations.

The average first-year corrosion rate of mild steel exposed within the first 150 m from the high-water mark along South Africa's coastline, was about 319 ± 112 µm/a, 95% CI [215 µm/a, 422 µm/a]. The minimum value was approximately 134 µm/a (recorded at Salisbury Island in Durban) (Callaghan 1991) and the maximum about 460 µm/a (measured close to Melkbos Strand in the Western Cape) (Janse van Rensburg 2010). This implies that the corrosivity of the atmosphere for the first 150 m from the shoreline can likely be rated *very high* (C5) to *extremely* (CX) corrosive, as per ISO 9223 (2012a).

However, as suggested by the high variation or SD of the data set, which in this case was 112 µm/a, the unpredictability of the corrosivity of the atmosphere along the coastline is substantial and depends on the surf action of the ocean, altitude, topography, temperature and onshore wind flow (speed and direction) (Callaghan 1991; Cole et al. 2003a; Janse van Rensburg 2010). As stated in Chapter 3.1, significant variations in the existing data were also likely introduced since the 12-month atmospheric corrosion rates were taken over a period of 30 years, probably changing from one year to the next (Dean et al. 2005), as well as potentially differing in terms of surface treatment and cleaning procedures.

Additionally, the corrosivity in the first 150 m from the coast is likely to be affected by the degree of landscaping of the shoreline (Janse van Rensburg 2010). Consequently, a harbour or developed coastal area, with surrounding paved or landscaped terrain, e.g. Salisbury Island (Durban), may exhibit reduced corrosivity compared to similar areas in more exposed or natural conditions. An area located on a cliff will also frequently be less corrosive than the same location positioned at a lower altitude. These findings concur with ISO 9223:2012 relating to the factors affecting the deposition rate of chlorides along coastlines (International Organization for Standardization 2012a). They are also supported by Callaghan's (1991) data, in that the corrosivity of the Durban Bluff, exposed to continuous surf action, is far higher than the Durban Bay area. Accordingly, about the former site, it was found that the high corrosivity of this CX environment can result in the penetration of 6-mm thick mild steel plate within ten years of exposure.

Alcántara et al. (2017) reported the occurrence of very high salt levels along the surf, while the salinity of the atmosphere was lower in areas with calmer waters. Cole et al. (2003a) concurred that the atmospheric corrosivity of coastlines is mostly influenced by surf action and white-caps in the ocean, which vary with changing seasons, tides and

ocean currents. Janse van Rensburg (2015, 2017) similarly found that at Duynefontein (situated next to the Western Cape coast), as well as at Fort Dauphin, located along the southern shores of Madagascar, the corrosion rate of mild steel within the first 150 m from the sea, experiencing high surf action, can be > 500 µm/a. However, this is assuming the corrosion pattern is general. If localised, pitting and crevice corrosion have been proven to cause perforation of 8 mm thick mild steel at Fort Dauphin within six years, signifying a corrosion rate of > 1 000 µm/a.

Notable is that both Durban and Fort Dauphin are exposed to South East Trade Wind during summer, travelling towards the equator (**Figure 2.6** - Maskew Miller Longman 2013). In Nigeria, around 1000 µm/a loss of mild steel has been measured within 150 m from the shoreline (Rozenfeld 1972). Correspondingly, Santana et al. (2001) reported high corrosion rates for the northern and eastern coastal regions of the Canary Isles, also due to the Trade Wind, travelling in a north-easterly direction.

Concerning those test sites that are located within 150-1000 m from the shoreline, based on the collated South African data, the average first-year (12-month) corrosion rate of mild steel measured 60 ± 22 µm/a, 95% CI [45 µm/a, 75 µm/a]. The lowest recorded value was roughly 40 µm/a (at Oyster Bay in the Eastern Cape) (Janse van Rensburg 2015) and the highest, about 122 µm/a (at Congella in Durban) (Callaghan 1991), which is justified since Oyster Bay exhibits reduced rainfall in comparison with Durban, i.e. 400-600 mm/a versus more than 1000 mm/a (My Cyberwall 2017) (**Figure 2.4**).

The approximate 80% reduction in the average corrosion rate of mild steel between the < 150 m and 150-1000 m marks, from 319 µm/a to 60 µm/a, is of note. Doyle and Goddard (CSIR 1975) reported an 80-85% decrease in the corrosivity of the environment within the first 800 m from the ocean in Durban and Port Elizabeth. Similarly, O'Donnell et al. (n.d) and Pietersen et al. (2004), found a "*rapid*" change in the corrosivity of marine atmospheres, mainly from 500-800 m onwards.

The sharp decrease in the corrosivity of the environment within the 150-1000 m zone is likely attributable to significant gravitational settling, turbulence diffusion and momentum-dominated impact of the airborne salts (Cottis et al. 2010) within the first 150 m from the sea, causing lower level of salts (chlorides) to be deposited onto

surfaces in the following 150-1000 m span. Denser and more abundant vegetation next to the coast, as may be encountered along the eastern coastline (**Figure 2.9**) (OpenStax CNX 2017), which can encourage the deposition of aerosols within a shorter distance from the ocean (Cole et al. 2004b). This drastic change in the deposition rate of salts in marine environments, particularly within the first one kilometre from the ocean, has also been demonstrated during corrosion studies in Nigeria, as shown in **Figure 5.1** (after Rozenfeld 1972). Also, the variability in the corrosivity of the 150-1000 m zone lessens by nearly 80%, with an SD descend from 112 µm/a to 22 µm/a, due to the reduced impact of sea salts and onshore wind flow at the different locations.

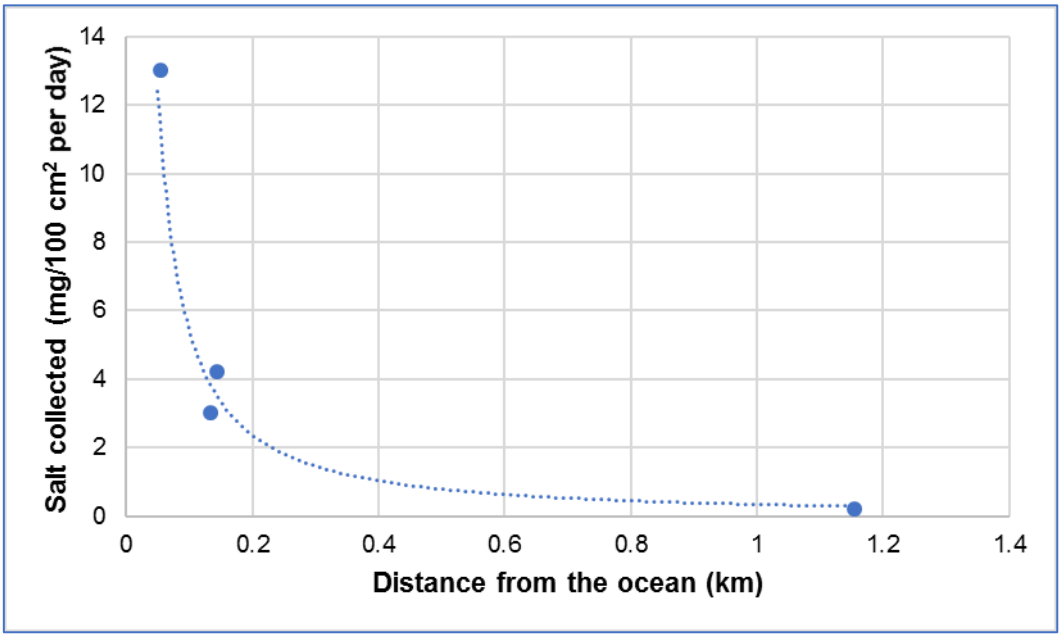


Figure 5.1 Salt deposits versus distance from the ocean (after Rozenfeld 1972).

The latest corrosion rate range for mild steel in the 150-1000 m zone, 40-122 µm/a, is significantly lower than the 100-300 µm/a span given in the Callaghan map for the intertidal to 5 km zone along South Africa's coastline. It is also much lower than the *very high* (C5) (200-300 µm/a) classification given in the HDGASA (2005) map. Based on the reported results, this section of the coastline is preferably classified mid-C4 (*high*) to mid-C5 (*very high*) corrosive.

At 1-3 km from the ocean, the average first-year (12-month) corrosion rate of mild steel measured 43 ± 14 µm/a, 95% CI [28 µm/a, 58 µm/a]. The minimum value was

approximately 28 µm/a (at Ysterplaat in Cape Town) and the maximum, around 66 µm/a (at the Durban Bayhead) (Callaghan 1991). The former locale is located to the western side of Cape Town, where it is separated from the ocean by numerous houses, industrial plants and office buildings, whereas the Durban Bayhead area is nearly encircled by the Durban Harbour, which most probably causes an increase in the local RH levels. The sea is positioned to the eastern side.

The 1-3 km zone can primarily be classified as *moderate* (C3) to *high* (C4) corrosive, regarding mild steel. In both the Callaghan (1991) and HDGASA (2005) maps, the corrosivity range of the 1-3 km region appears significantly overstated. Concerning the Callaghan map (**Figure 1.1**), the corrosion rate of mild steel in the "*Intertidal to 5 km inland mark*", is shown as 100-300 µm/a, whereas in the case of the HDGASA map, the "*Exterior: industrial with high humidity or high salinity coastal*" region is given as varying between 80 µm/a and 200 µm/a (**Figure 2.16**) (HDGASA 2005). Moreover, the predictability of the corrosivity of the environment improved by a further ± 16%, suggesting further stabilisation in the corrosivity of the environment, with increasing distance from the ocean.

The average first-year corrosion rate of mild steel recorded at all the sites located within 3-10 km from the coastline was 37 ± 13 µm/a, 95% CI [27 µm/a, 47 µm/a]. The lowest was approximately 20 µm/a at Grabouw in the Western Cape (above Sir Lowry's Pass near Gordon's Bay) (Janse van Rensburg 2010) and the highest close to 57 µm/a at Petro SA's Mossgas plant in Mossel Bay (Janse van Rensburg 2010). Important is that Grabouw is elevated about 265 m above sea level (Maps-streetview.com 2017), whereas the exposure site at Mossel Bay is located at a much lower altitude, thus being more exposed to salt-laden winds from the ocean. Hernandez et al. (2011) and Del Angel et al. (2015) concurred that altitude plays a significant role in marine corrosion.

The corrosion results of the 3-10 km zone suggest a further decrease in the average corrosivity of the atmosphere by approximately 6 µm/a (i.e. from about 43 µm/a to 37 µm/a), between the 3-10 km marks, with an additional ± 1% stabilisation of the corrosivity of the atmosphere. The 3-10 km zone is typically classified as *moderate* (C3) corrosive, which is like the corrosivity category reported by Santana et al. (2001) for coastal sites in the Canary Isles located at about 3-4 km from the sea.

Consistent with Callaghan's (1991) map, the first 5 km from the sea is treated as particularly severe, with an estimated corrosion rate of mild steel of 100-300 µm/a. Correspondingly, a Corrosion Damage Algorithm (CDA) proposed by the Michigan State University in the USA for the maintenance management of structural aircraft systems, gives the highest corrosion severity rating for areas located within 4.5 km from the ocean (Summitt & Fink 1980). Based on the latest trend, however, derived from corrosion measurements at eleven sites that all fall within the 3-10 km zone, none exhibited a corrosion rate of mild steel of > 100 µm/a.

For the 10-30 km region, the average 12-month corrosion rate of mild steel measured 35 ± 14 µm/a, 95% CI [22 µm/a, 48 µm/a], suggesting a further approximate 1% decrease in the average corrosivity of the atmosphere. This zone along the South African coastline is best classified as *moderate* (C3) corrosive. The minimum value recorded was about 16 µm/a at Vredendal (Janse van Rensburg 2010), classified as a low rainfall area in the Western Cape (**Figure 2.4**) (My Cyberwall 2017) and the highest, around 58 µm/a, at a site in Empangeni (Janse van Rensburg 2010) in KwaZulu-Natal, which is categorised as a high rainfall region (**Figure 2.4**).

The apparent slowdown in any further stabilisation of the corrosivity of the environment seems to imply that from approximately 30 km onwards, wind-borne marine salts are no longer the dominant force driving the atmospheric corrosion process. This demarcation line was also identified by Callaghan (1991). Conversely, the coefficient of variation (CV) of the average corrosion rate of mild steel remained high at nearly 40%. Congruently, studies in other countries indicated that sea salts may still affect atmospheric corrosion more than 50 km (Ballance & Duncan 1985) to 1 400 km (Thornton et al. 2010) from the ocean.

Of further importance is the emerging trend that test sites located along the eastern coast (particularly along the KwaZulu-Natal seashore) are inclined to higher corrosivity, at the same distance range from the ocean compared to sites located next to the Western and Eastern Cape ocean fronts. This tendency appears valid for the 150 m to 1000 m, 1-3 km, 3-10 km, and 10-30 km ranges from the sea. It is just below the 150 m mark that the corrosivity of the atmosphere along the Western Cape coast appears higher in comparison with the Eastern Cape and KwaZulu-Natal shorelines. This alteration in the corrosivity of the environment next to the South African coastline is

likely attributable to changing meteorological, physical and biome conditions (see **Figures 2.4 - 2.9**) (South African Tours and Travel.com 2016; Maskew Miller Longman (Pty) Ltd 2013; Evwind 2017; My Cyberwall 2017; OpenStax CNX 2017).

Concurring with Winter et al. (2013), the Northern Cape coastline, from the mouth of the Orange River to Lamberts Bay, is classified as Desert, the Western Cape coast from Lamberts Bay to the mouth of the Breë River, as Mediterranean, from the Breë River to Port Elizabeth, as Moderate Marine, whereas the northern parts of the Eastern Cape coastline, i.e. from Port Elizabeth to northern KwaZulu-Natal, is classified as sub-tropical (**Figure 5.2**) (Archive.cnx.org 2017). According to Cole et al. (2003a), in dry environments exhibiting reduced rainfall and low ground coverage, marine aerosol transport is likely to be favoured than in more humid and higher rainfall climates with forest cover.

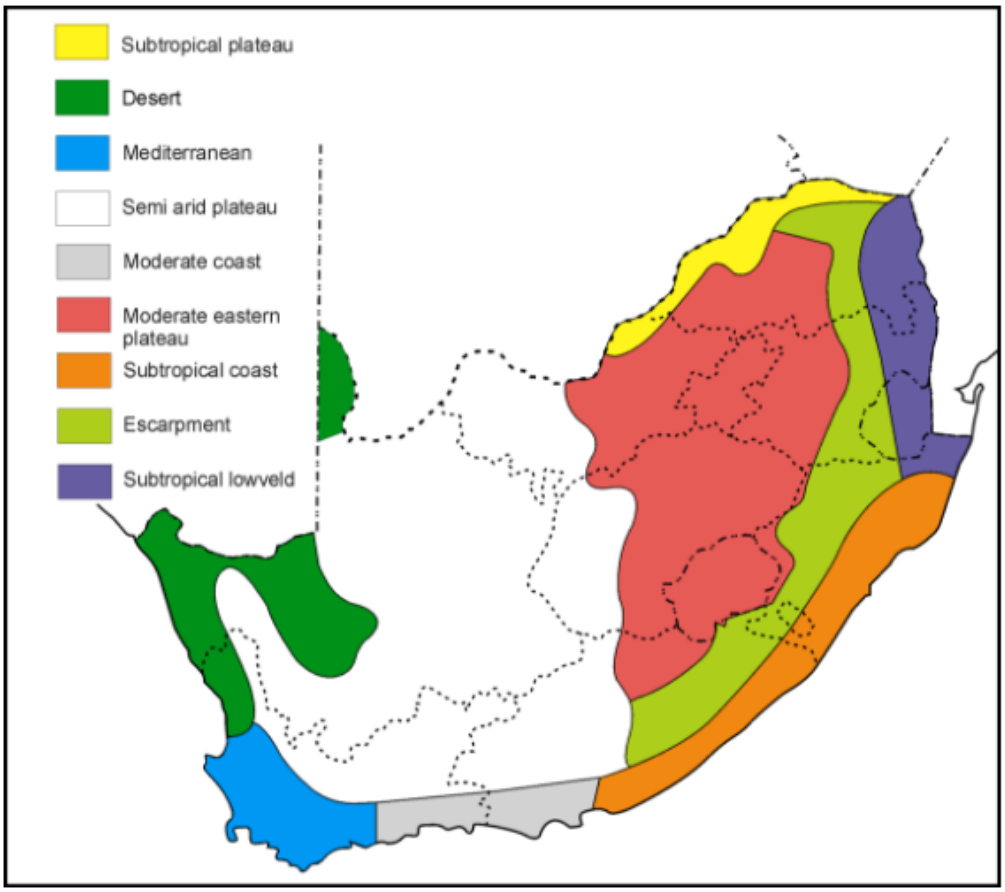


Figure 5.2 Climatic regions of South Africa – taken from Archive.cnx.org (2017) – Note the climatic variations along the coastlines.
http://archive.cnx.org/contents/d5717376-e429-4585-a1ee-98767a736cfd@1/climate-regions

Moving from the western to eastern parts of South Africa, the change in the corrosivity of the atmosphere, due to increasing temperatures, higher rainfall and RH, is partly reflected in Callaghan's (1991) and Leitch's (2006) maps. However, it is absent in the HDGASA (2005) chart.

The higher corrosion rate of mild steel below the 150 m mark (along the Western Cape shoreline) may probably be ascribed to the presence of smaller dunes and shrubbery (Wiegand 2007). 'Fynbos' offers less shielding against sea sand and spray whipped up by the high winds from the dunes and deposited onto surfaces (**Figure 2.9**) (OpenStax CNX 2017). Conversely, along the Eastern and KwaZulu-Natal coastlines, the bigger and broader leaved plants (Wiegand 2007) provide better protection against windborne salts. The presence of lingering mist banks (due to the cold Benguela current) (**Figure 2.5**) (South African Tours and Travel.com 2016), reduced rainfall (no washing effect) (**Figure 2.4**) (My Cyberwall 2017) and prevailing strong onshore winds (South-Easter primarily along the Western Cape, as well as parts of the Eastern Cape coastlines) (**Figure 2.6**) (Maskew Miller Longman (Pty) Ltd 2013), also play important roles in the corrosivity of this region (CSIR 1975; Callaghan 1991; Barnett 2006). Nixon & Janse van Rensburg (1993) reported that along the Northern and Western Cape coastlines, the highest atmospheric corrosivity is typically measured during winter, from about March to September, which corresponds with this region's rainy season. Conversely, next to the eastern coastline, the highest atmospheric corrosion rates are primarily measured during summer (Janse van Rensburg 2010).

Just below the Great South African Escarpment (**Figures 4.2 & 5.3**), the average corrosivity of the environment in the Western and Eastern Cape measured 7 ± 6 µm/a, 95% CI [0 µm/a, 20 µm/a], with a minimum of approximately 1.3 µm/a at Droërivier and a maximum of about 12 µm/a at Bedford (Janse van Rensburg 2010). Moving further inland from the low-lying zones of the Northern, Eastern, and Western Cape coastlines, above the Great South African Escarpment (onto the Central Plateau) (**Figure 5.3** - adapted from Wikipedia (2017b)), the conditions change to a desert/semi-desert plateau (the Kalahari Desert and the Karoo). In this region, the corrosion rate of mild steel measured close to 2 µm/a (at De Aar) and nearly 4 µm/a at Gariep (Janse van Rensburg 2010), averaging 3 ± 1 µm/a, 95% CI [0 µm/a, 6 µm/a]. This expanse is typically classified as *very low* (C1) to *low* (C2) corrosive, due to the arid conditions, with

the Kalahari Desert, exhibiting an average rainfall of < 200 mm/a and the Karoo, 201-400 mm/a (My Cyberwall 2017) (**Figure 2.4)**. From thereon, the corrosivity of the environment increases slightly towards the Free State, measuring roughly 7 µm/a at Dealesville (Janse van Rensburg 2010), close to Bloemfontein.

Significant is that the Kalahari, the Karoo and the Free State Province are also known for their salt pans and dry river beds (Du Toit 1926; Hanks 2009). As a result, salt-laden soil that is swept up by the wind and deposited onto metal surfaces may encourage corrosion to take place at lower RH levels (Montgomery et al. 2011; Roberge 2012; Schinderholtz & Kelly 2012). It can also increase TOW (McEwan 2004), which is of relevance when considering that the Kalahari Desert and the Karoo experience the highest percentage changes in average rainfall in South Africa, i.e. 26-50% (Winter et al. 2013). These regions also display the hottest summers and highest solar irradiation levels in the country (**Figure 2.5 & 2.7**) (South African Tours and Travel.com 2016; Evwind 2017). Consequently, the variability in the corrosivity of the environment is high. Moreover, studies conducted by Sun et al. (2009) have demonstrated that soluble salt in surface desert soil may sufficiently lower the RH at which corrosion current density suddenly increases.

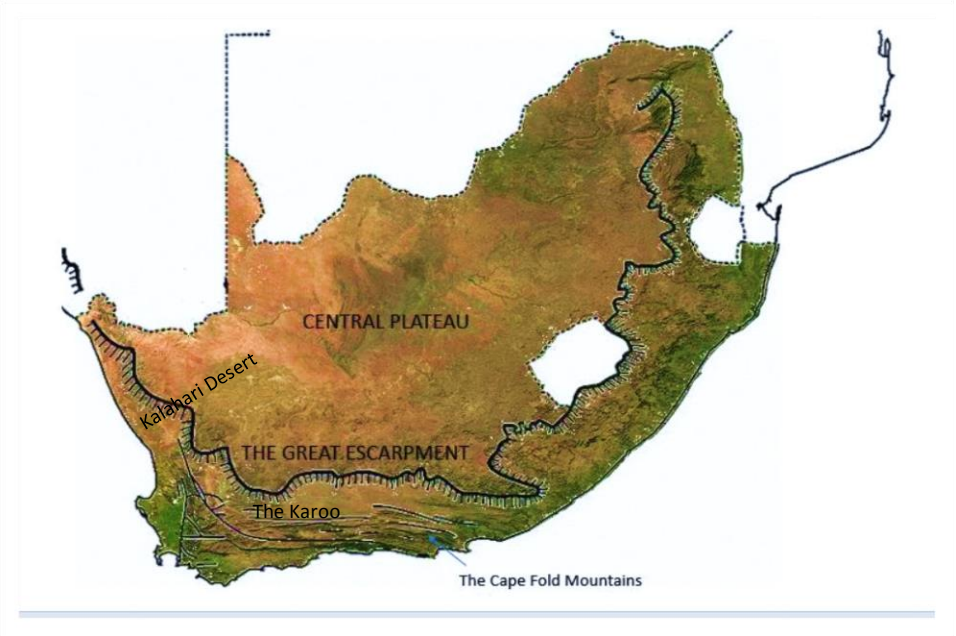


Figure 5.3 The Great Escarpment and the Central Plateau – adapted from Wikipedia (2017b). https://en.wikipedia.org/wiki/Great_Escarpment,_Southern_Africa

From the KwaZulu-Natal coastline, towards Gauteng, the change in corrosivity of the atmosphere below and above the Great Escarpment is less extreme, compared to that of the Northern, Eastern and Western Cape Provinces. This reduction is likely since the environment changes from a sub-tropical coastal to a moderate, sub-tropical rising rocky (escarpment) terrain that exhibits cold, snowy winters, with hot, rainy summers (Winter et al. 2013; Maskew Miller Longman (Pty) Ltd 2016). The diminished change may also be observed in **Figure 5.2** (Archive.cnx.org 2017), which presents the different climatic regions in South Africa.

Proceeding through the lower parts of Mpumalanga, the landscape changes to a temperate Highveld region (Maskew Miller Longman (Pty) Ltd 2016). In this section of Mpumalanga, located between KwaZulu-Natal and Gauteng, the average first-year corrosion rate of mild steel measured 29 ± 6 µm/a, 95% CI [25 µm/a, 32 µm/a], suggesting an approximate 26% reduction in the corrosivity of the environment from Empangeni (located in the lowland between the Great Escarpment and the KwaZulu-Natal coastline) towards Ogies, which is positioned on the Eastern Highveld area. This zone is classified, for the most part, as *moderate* (C3) corrosive. The maximum measured corrosion rate of mild steel was about 38 µm/a (at Secunda) (Janse van Rensburg 2015) and the minimum nearby 18 µm/a (approximately 20 km north of Belfast) (Nixon 1991). This difference may be ascribed to the fact that the Secunda and Emalahleni (Witbank) areas are some of the most polluted regions in South Africa (**Figure 5.4**) (Greenpeace Afrique 2014), due to the presence of a large petrochemical plant (Sasol Synfuels), eleven coal-fired power stations and numerous open-cast coal mines.

Shifting towards the North West, Limpopo and Gauteng Provinces, the corrosivity of the environment decreases notably. In the case of Gauteng and closely surrounding areas, rating C2 to C3, the average first-year corrosion rate of mild steel measured 25 ± 12 µm/a, 95% CI [19 µm/a, 32 µm/a], decreasing to approximately 12 ± 5 µm/a, 95% CI [9 µm/a, 16 µm/a] towards the Limpopo River (Zimbabwe) and Botswana borders.

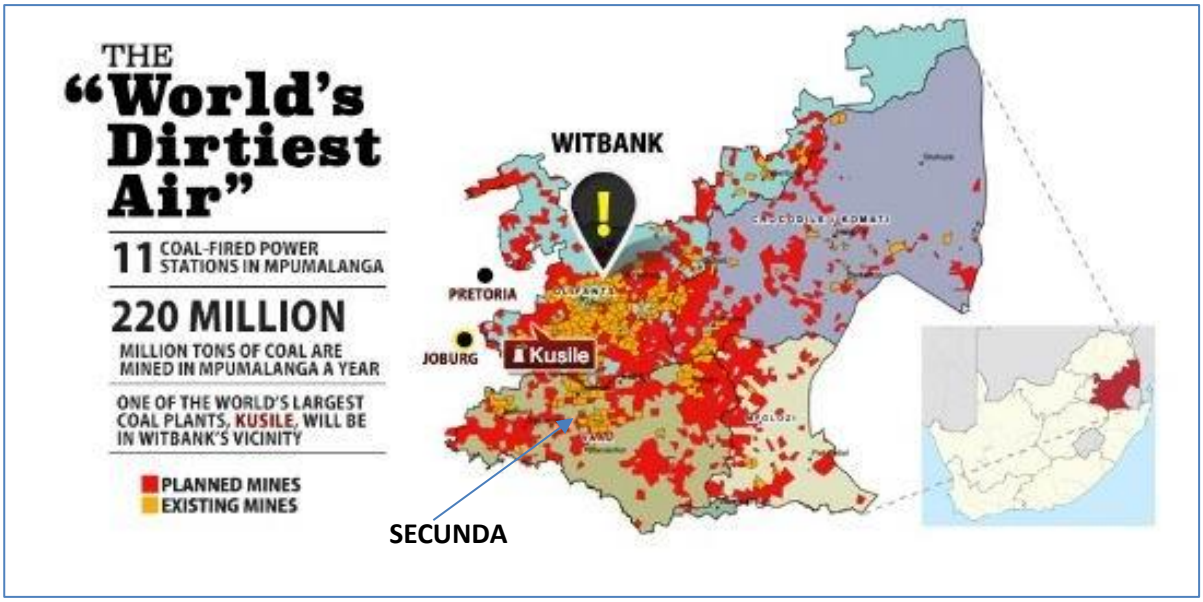


Figure 5.4 A flyer by Greenpeace showing a worldwide concern regarding the increased pollution of the Secunda and Emalahleni (Witbank) areas (Greenpeace Afrique 2014).

http://www.greenpeace.org/africa/fr/notre-action/changement-climatique/Pour-la-fin-du-charbon-en-Afrique-du-Sud/

A graphic representation of the first-year (12-month) corrosion rates of mild steel, measured at all the historical corrosion monitoring sites, versus their approximate distances from the ocean, is presented in **Figure 5.5**. Based on this plot, the macro corrosive atmosphere of South Africa stabilises meaningfully moving inland, with the corrosive effects of coastal environments being inversely related to their distance from the ocean, i.e. with an R^2 value of about 0.5 and Pearson Product Moment Correlation (PPMC) coefficient (*r*) score of around -0.4, which is significant at $P \leq 0.05$, thus rejecting the null hypothesis. See also **Equation 5.1**. Similar graphs have been reported for sea-salt transport, deposition and corrosion along other coastlines (Rozenfeld 1972; Meira et al. 2007, 2008; Corvo et al. 2008; Alcántara et al. 2015, 2017; Castaneda et al. 2018) - all displaying a significant decrease in the corrosivity of the marine environment within one to two kilometres from the ocean.

The formula for the Pearson product-moment correlation coefficient, *r*, is:

$$r = \frac{\Sigma(x-\bar{x})(y-\bar{y})}{\sqrt{\Sigma(x-\bar{x})^2\Sigma(y-\bar{y})^2}} \qquad \textbf{Eq. 5.1}$$

where: *x* and *y* mean Average (array1) and Average (array2) (Microsoft 2017).

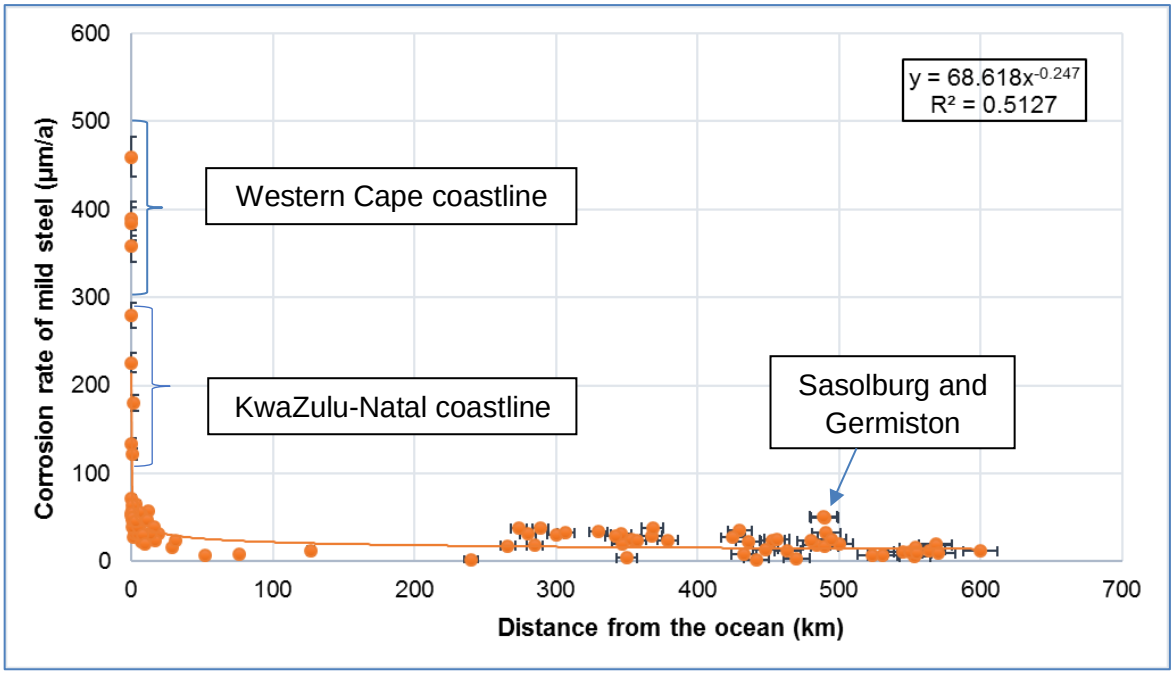


Figure 5.5 First-year (12-month) corrosion rates of mild steel, measured at numerous sites in South Africa, versus their approximate distances from the ocean.

In contrast, **Figure 5.6** gives the 12-month corrosion rates of mild steel, recorded at all the historical corrosion monitoring sites, versus their relative altitudes in metres. According to the graph, the corrosivity of South Africa's macro atmosphere is also slight to moderately negative related to altitude, with a PPMC (*r*) (**Equation 5.1**) of about -0.4. The result is significant at $P \leq 0.05$. The impact of altitude on the corrosivity of the environment is of relevance to the coastal and inland industrial areas of the country, the latter being discussed in greater detail in Section 5.2.

In the subtropical Lowveld and semi-desert Karoo regions, with altitude ranges of approximately 500 m to 1000 m, atmospheric corrosivity is notably lower. However, this phenomenon is likely due to climatic, rather than altitude variations. The differences in the 12-month corrosion rates of mild steel at some of the sites, in contrast with altitude, are also presented in **Figure 5.7**.

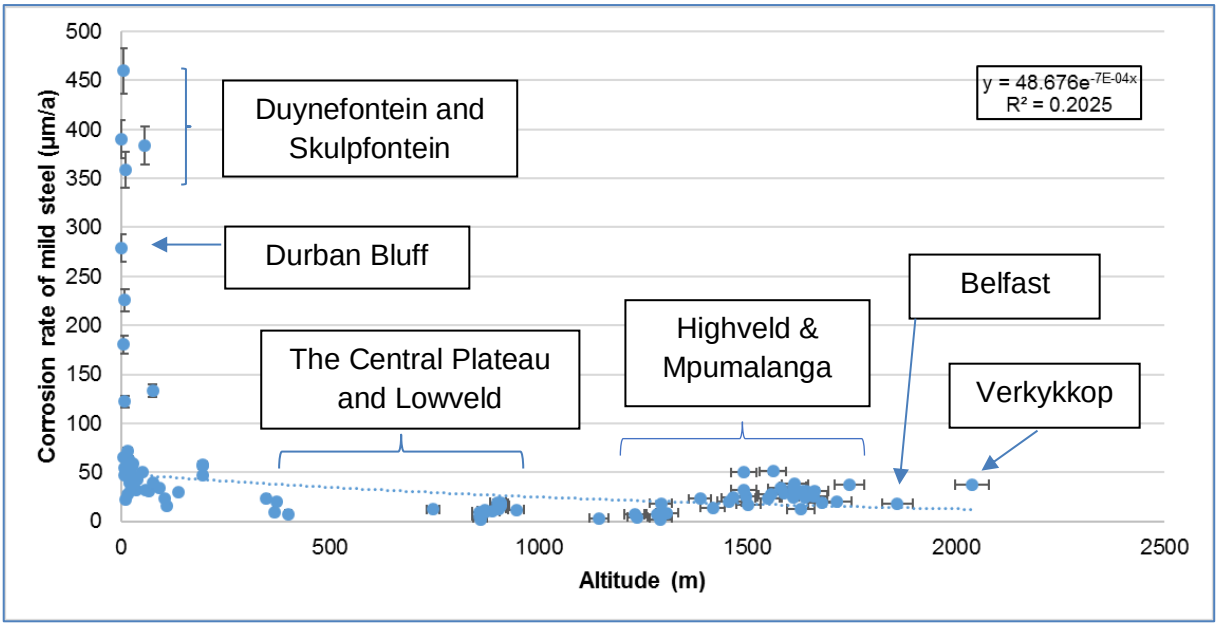


Figure 5.6 First-year (12-month) corrosion rates of mild steel, measured at numerous sites in South Africa, versus their relative altitudes (elevations above sea level).

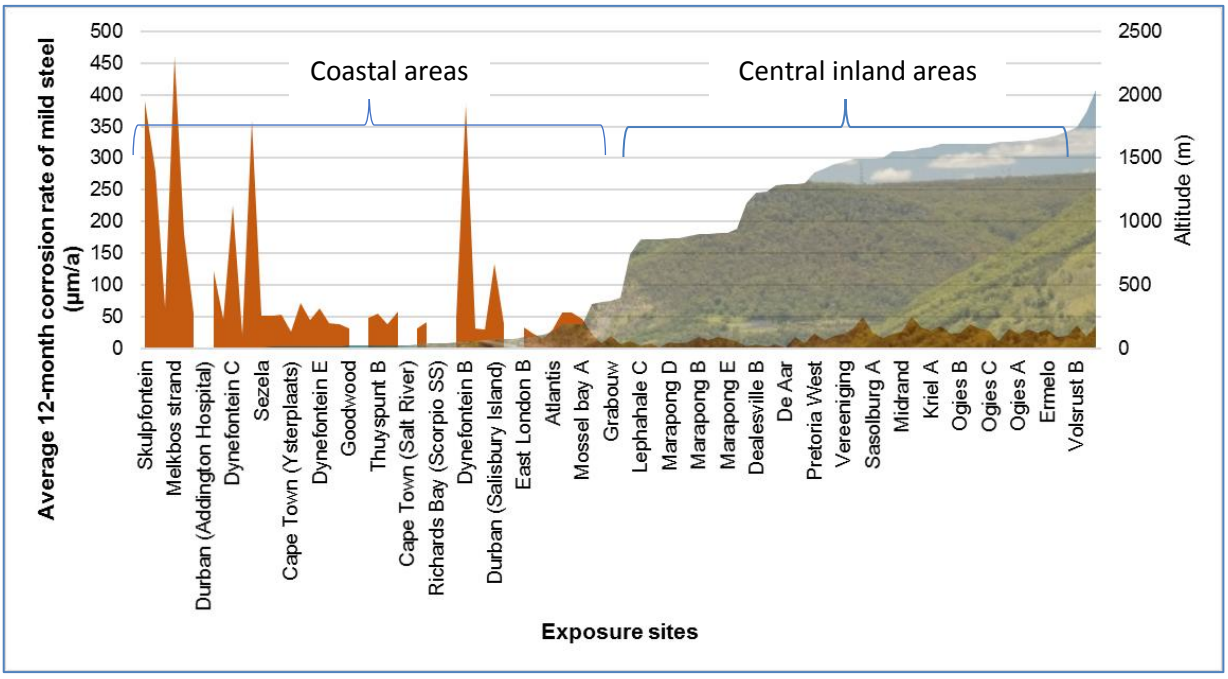


Figure 5.7 First-year (12-month) corrosion rates of mild steel, measured at numerous sites in South Africa, versus their relative altitudes (elevations above sea level).

At central inland locations (**Figure 5.7**), the results suggest that chlorides in the air no longer drive atmospheric corrosion, but rather the time of wetness (TOW), temperature, pollution (SO_x and NO_x gases), the wind, and the positioning of the metal substrate above ground level (Callaghan 1991; Brown & Masters 1982; Janse van Rensburg 2010; Montgomery et al. 2011). This may apply to regions in and around the central inland and metropolitan areas of South Africa, being:

- the City of Johannesburg Metropolitan Area;
- the City of Tshwane Metropolitan Municipality;
- the Ekurhuleni Metropolitan Municipality; and
- the Mangaung Metropolitan Municipality.

5.1.2 Hot-dip Galvanised Mild Steel

Figure 4.3 indicates that hot-dip galvanising and uncoated mild steel exhibit similar trends regarding elevated corrosion rates along the South Africa coastline, as well as in central urban and industrial areas. However, concerning the hot-dip galvanised steel corrosion rates, the differences in the coastal and inland areas are less dramatic than that of mild steel, with only a few of the locations exhibiting markedly higher corrosivity, e.g. Skulpfontein (near Kleinzee), Duynefontein (near Melkbos Strand) and Salisbury Island (in Durban). This is because the corrosion monitoring test racks at these locations were established within 150 m from the ocean. As a result, the average 12-month corrosion rate of galvanised steel at these sites measured 11 ± 8 µm/a, 95% CI [1 µm/a, 21 µm/a], which falls within the *extreme* (CX) corrosive category of ISO 9223:2012. However, the average result presents high variability and uncertainty, suggesting that the corrosivity of the environment based on the hot-dip galvanising results is best-rated upper-C5 to CX corrosive.

With regard to the aforementioned locations, the minimum value was approximately 4 µm/a at Skulpfontein (Nixon & Janse van Rensburg 1992), and the maximum, near 24 µm/a at Duynefontein (Eskom 2010-2016), implying that at the latter site, pre-galvanised Z275 sheeting (with a nominal galvanised coating thickness of nearly 19 µm) may exhibit a service life of fewer than 12 months, whereas at the Skulpfontein site, a maximum of about 5 years may be expected. Consistent with Callaghan (1991), the

expected life of galvanised sheet in severe marine environments was given as less than three years.

The corrosivity differences between Skulpfontein and Duynefontein may be attributed to the former area's low annual rainfall (< 200 mm/a), while Duynefontein exhibits average annual precipitation of about 200-400 mm/a (**Figure 2.4**) (My Cyberwall 2017), also displaying mist during summer (Janse van Rensburg 1994). Del Angel et al. (2015) correspondingly confirmed significantly higher corrosion rates of hot-dip galvanised steel within 150 m from the ocean, in Chile. Moreover, Natesan et al. (2015) reported corrosion rates for hot-dip galvanising along the shores of India of more than 20 µm/a.

Between 150-1000 m from the sea, the recorded first-year (12-month) corrosion rate of galvanising reduced to 4 ± 2 µm/a, 95% CI [2 µm/a, 6 µm/a]. The highest value (approximately 6.8 µm/a) was measured at Duynefontein (Eskom 2010-2016) and the lowest value (about 1.2 µm/a) at Oyster Bay (Janse van Rensburg 2015). This infers a nearly 63% reduction in the corrosion rate of hot-dip galvanising between the < 150 m and 150-1000 m marks, which is somewhat lower than calculated in the case of the low-carbon steel data. Nonetheless, since fewer hot-dip galvanising corrosion rate measurements were available for this distance span from the ocean, the level of uncertainty of the mean is slightly higher, i.e., 50-120% versus 33-125%.

In the 1-3 km region, the corrosion rate of hot-dip galvanised steel reduced even more to 1.2 ± 0.4 µm/a, 95% CI [0.3 µm/a, 2.1 µm/a], a further approximate 25% reduction in comparison with the 150-1000 m mark. The maximum corrosion rate was reported for a location in East London, about 1.6 µm/a, and the minimum, near 0.9 µm/a at Sezela (along the KwaZulu-Natal coastline) (Janse van Rensburg 2010). In comparison with the mild steel data, the level of uncertainty of the mean galvanising results for the 1- 3 km zone appears to be somewhat similar.

Moving further inland, into the 3-10 km zone, the change in the average corrosion rate of hot-dip galvanised steel tapers off from the Northern, Western and Eastern Cape coastlines, towards the Great South African Escarpment. The average recorded corrosion rate of galvanised mild steel in this section was only about 1.6 ± 1.0 µm/a, 95% CI [0.8 µm/a, 2.4 µm/a], and similarly for the KwaZulu-Natal coast, approximately 1.5 µm/a. These values seem to confirm that between the 1 km and 10 km marks, the

corrosion rate of hot-dip galvanising along the Northern, Western and Eastern Cape, as well as KwaZulu-Natal coastlines, appear somewhat similar and may even slightly increase in certain parts of the 3-10 km zone.

Consequently, progressing further inland, the average change in the corrosion rate of hot-dip galvanised steel is only marginal, decreasing to 1.0 ± 0.1 µm/a, 95% CI [1.0 µm/a, 1.1 µm/a], in the 10 km to 30 km zone, and 0.8 ± 0.4 µm/a, 95% CI [0.6 µm/a, 0.9 µm/a], at all sites located more than 30 km away from the ocean. This represents a mere ± 2% change between the 1-3 km and 10-30 km zones, and a meagre ± 0.5 µm/a difference between the 10-30 km and >30 km regions. The lowest corrosion rate of hot-dip galvanised steel was reported for a locale at De Aar (around 0.1 µm/a) (Janse van Rensburg 2010) in the Central Karoo, which increased to about 0.5 µm/a (Janse van Rensburg 2010) in the Free State Province, near Bloemfontein.

Concerning the Highveld (Gauteng) and Mpumalanga regions, the highest corrosion rates were recorded at Ermelo (about 1.5 µm/a), Sasolburg (approximately 1.6 µm/a), Secunda (almost 1.6 µm/a) and Germiston (around 1.4 µm/a) (Janse van Rensburg 2010). These sites are all positioned near large industrial and power generating plants, signifying an average value of approximately 1.5 µm/a, which is comparable to the mean rates measured within the 3-10 km and 10-30 km zones along the different South African coastlines.

On face value, the abovementioned data seem to correspond with Del Angel et al. (2015) results for sites in Chile and Mexico, located approximately 50-70 km from the sea. Based on their results, the average 12-month corrosion rate of hot-dip galvanising measured approximately 1.0-1.5 µm/a at distances of 50-70 km from the ocean, by the ISO 9223:2012 procedure. The corrosion rate tended to either lessen or levelled out with time. However, in coastal environments, the average 12-month corrosion rate of hot-dip galvanising varied between 1.5 µm/a and 2.4 µm/a and was disposed to a linear increase with exposure time. This observation was correspondingly made by Janse van Rensburg in 2010, at Duynefontein, and may be justified by the fact that at severe coastal areas, corrosion of the outer Zn layer rapidly takes place, followed by corrosion of the inner Zn-Fe layers, although at a reduced rate (~ 30%) (McEwan 2004). Conversely, in low to moderate corrosive environments, stable (insoluble) zinc

carbonate ($Zn_5(OH)_6(CO_3)_2$) tends to form (Schultz & Thiele 2012), providing longer-term protection of the underlying mild steel surfaces.

Figure 5.8 illustrates the extent to which the first-year (12-month) corrosion rate of hot-dip galvanised steel changes with increasing distance from the ocean, revealing a strong negative trend, about -0.4 (P ≤ 0.05), compared to uncoated mild steel. A similar PPMC of approximately -0.4 (P ≤ 0.05) was identified regarding the 12-month corrosion rate of hot-dip galvanised steel changes with increasing elevation, moving away from the sea.

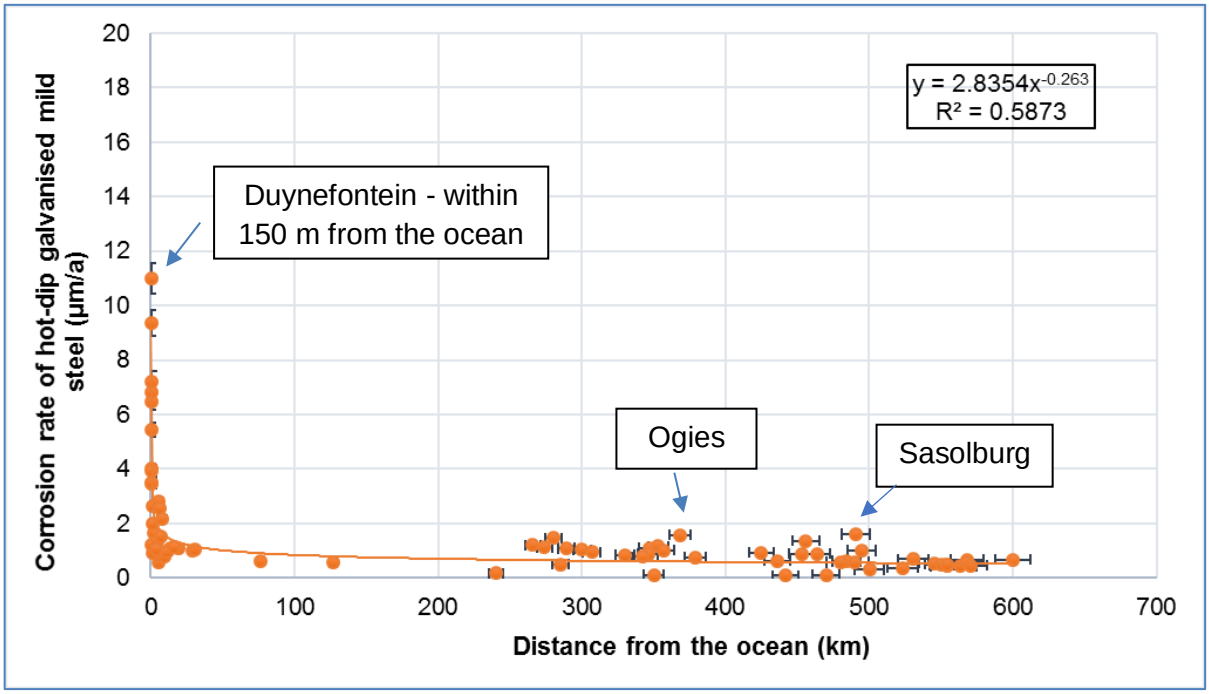


Figure 5.8 First-year (12-month) corrosion rate of hot-dip galvanised mild steel at various sites in South Africa, versus their distances from the ocean.

5.1.3 Pure Zinc

Figure 4.4 reveals that, like mild steel and hot-dip galvanised steel, the atmospheric corrosion of pure zinc along South Africa's shoreline is notably more severe than at most inland locations. The average corrosion rate of zinc, within the first 150 m from the shore, was calculated as 13 ± 8 µm/a, 95% CI [5 µm/a, 20 µm/a]. The lowest reported value was about 3 µm/a at Salisbury Island in Durban (CSIR 1975), using 99% rolled sheet samples, and the highest, approximately 18 µm/a, measured at Duynefontein (Eskom 2010-2016), next to the Western Cape coastline. Although the latter

measurement for zinc was taken using the ISO 9223:1992 zinc helix procedure, which is known to give higher readings than flat zinc panels (Knotkova et al. 2010), the Duynefontein area has been found to be one of the most corrosive locations in South Africa (Nixon 1991, 1992; Nixon & Janse van Rensburg 1993; Janse van Rensburg 1994; Northcott 1999, Janse van Rensburg 2010). Apart from being located close to the sea, studies conducted by Vosloo (2002), have shown that during winter and summer, the probability that the RH levels in the Duynefontein area will be higher than 75%, was 88% and 78%, respectively. Exceptional pollution severity, i.e. regarding "*Direct insulator pollution measurements*" and "*Directional dust deposit gauges*" were also measured within the first 500 m to 800 m from the coast.

On an average basis, the corrosion rate of zinc was approximately 16% higher than that of hot-dip galvanised steel, exposed within the same distance range from the ocean. In India, Natesan et al. (2015) also reported higher corrosion rates for hot-dip galvanising, compared to zinc, in the "*Extremely severe*" and "*Severe*" corrosivity ranges. This variation may be ascribed to the fact that pure zinc is more anodic than the inner Zn-Fe alloy layers of hot-dip galvanising, resulting in its increased depletion. Moreover, it is likely attributable to the fact that mainly open zinc wire helices (as per ISO 9226:1992 procedure) rather than flat panel specimens were used to determine the first-year corrosion rate of zinc at many of the sites (Leitch 1999, 2003, 2006; Janse van Rensburg 2010, 2015; Eskom 2010-2016).

Moving inland, between the 150 m and 1000 m marks from the sea, the average recorded corrosion rate of zinc decreased to 4.6 ± 2.2 µm/a, 95% CI [3.2 µm/a, 6.0 µm/a], demonstrating an approximate 65% reduction compared to the first 150 m, which in contrast with hot-dip galvanising, was about 15% higher. This reduction is because the atmospheric corrosion rate of zinc is influenced mainly by marine salts in the air, of which the deposition tends to significantly decrease with increasing distance from the ocean (Callaghan 1991; Cook et al. 2000, 2009; Knotkova et al. 2010). The average value for zinc, within a 150-1000 m distance span from the ocean, also corresponds somewhat with corrosion rate measurements of zinc, reported for various sites in México (Cook et al. 2000), of which the average was calculated as approximately 4.2 ± 1.5 µm/a.

Between 1 km and 3 km from the ocean, the average measured corrosion rate of zinc decreased even further, 3.7 ± 1.5 µm/a, 95% CI [2.4 µm/a, 4.9 µm/a], with a minimum of about 1.9 µm/a measured at Ysterplaat (in Cape Town) (CSIR 1975) and a maximum of approximately 5.9 µm/a along the Buffalo River in East London (Janse van Rensburg 2010). This difference may likely be ascribed to the fact that the former site is located next to South Africa's Mediterranean coastline (**Figure 5.2**), with an average rainfall figure of less than 600 mm/a, while the latter locale is positioned along SA's subtropical shoreline (**Figure 5.2**) with a mean rainfall figure of more than 1000 mm/a (Winter et al. 2013). See also **Figure 2.4** (My Cyberwall 2017).

The average corrosion rate of zinc in the 1-3 km zone is significantly higher (about three times) than the average value recorded for hot-dip galvanising within the same distance span from the ocean, confirming that hot-dip galvanising is more corrosion resistant than pure zinc, especially when moving away from the sea. This phenomenon has also been reported by Callaghan (1991), McEwan (2004), Schultz & Thiele (2012). Cook et al. (2000) arrived at an average corrosion rate of zinc of about 3.3 µm/a at their Campeche site, located about 4 km from the sea.

At distances from between 3 km and 10 km from the ocean, the average recorded corrosion rate of pure zinc decreased to 2.6 ± 0.9 µm/a, 95% CI [2.0 µm/a, 3.2 µm/a], and between 10-30 km, to about 1.8 ± 1.3 µm/a, 95% CI [0.6 µm/a, 3.1 µm/a]. In both conditions, the rates were notably higher than those recorded for hot-dip galvanising within the same distance spans from the ocean.

From 30 km onwards, at all the inland sites, the average recorded corrosion rate of zinc decreased to 1.0 ± 0.6 µm/a, 95% CI [0.8 µm/a, 1.2 µm/a]. The highest value, around 3 µm/a, was reported for Muldersvlei (near Cape Town) (Janse van Rensburg 2010), which is located approximately 30 km from the ocean, and the lowest value of about 0.2 µm/a, at Droërivier (Janse van Rensburg 2010), in the Great Karoo (Winter et al. 2013). Notwithstanding, the average corrosion rate of zinc at this distance span from the coastline was still appreciably higher, about 35% than the mean 12-month corrosion rate of hot-dip galvanising recorded at all sites located more than 30 km from the ocean.

When considering the inland corrosion data in greater detail, it is apparent that the average recorded corrosion rate of zinc in the Great Karoo was about 0.3 ± 0.1 µm/a,

95% CI [0.1 µm/a, 0.5 µm/a]. Moving towards the Free State, however, the average corrosion rate of zinc increased to 0.6 ± 0.4 µm/a, 95% CI [0.0 µm/a, 0.9 µm/a]. While in the Gauteng and Vaal Triangle areas, the reported values varied between approximately 0.5 µm/a at the CSIR's premises in Pretoria (Callaghan 1991) and roughly 1.7 µm/a at Sasolburg (Janse van Rensburg 2010) – the latter site located near the border of the Free State and Gauteng Provinces. Of note is that Sasolburg is one of the most polluted areas in South Africa (Van Tienhoven 1999), mainly due to petrochemical, steel-smelter and power generating plants in the area and exhibits spatial annual average concentrations for SO_2 and NO_2 of about 7 ± 2 ppbv and 8 ± 2 ppbv per annum, respectively. However, at a site located between Sasolburg and Vanderbijlpark, maximum daily mean concentrations of 22.6 ppb SO_2 and 130.9 ppb NO_x have been reported (Van Tienhoven 1999). The area also shows elevated levels of various hydrocarbon-based gaseous pollutants, e.g. benzene, toluene and ethylbenzene, as well as meta-, para- and ortho-benzene (Lourens et al. 2011). In the presence of elevated levels of SO_2 and smoke, hydrocarbons have been found to exhibit a potential to appreciably influence the corrosion effect of zinc in some situations (Skerry et al. 1988)

In Mpumalanga, the average reported corrosion rate of zinc was 1.4 ± 0.5 µm/a, 95% CI [1.1 µm/a, 1.7 µm/a], approximately 30% higher than galvanising, with a maximum value of about 2.7 µm/a, at a location near Volksrust (Verkykkop) (Janse van Rensburg 2010) in the highlands between Mpumalanga and KwaZulu-Natal Provinces. At this location, the average first-year corrosion rate of hot-dip galvanising measured near 1.1 µm/a, which was about 60% lower than that of zinc. The lowest corrosion rate was recorded at Standerton, which may be classified as a rural-business area.

Noteworthy is that the higher corrosivity of Verkykkop (**Figure 5.9**) may likely be ascribed to this 'koppie' (small hill) being located approximately 2 040 m above sea level (geoview.info 2017), exhibiting pronounced seasonal variations due to its elevation (Held et al. 1993). Mist and snow are also frequent in this area (Snow Report 1853 - 2016). See also **Figures 2.4 - 2.5 & 2.8** (My Cyberwall 2017; South African Tours and Travel.com 2016; Maskew Miller Longman (Pty) Ltd 2013) in this regard.

According to the reported South African corrosion results, shifting towards Limpopo, the average measured first-year (12-month) corrosion rate of zinc decreased to

0.7 ± 0.2 µm/a, 95% CI [0.6 µm/a, 0.8 µm/a], which was still 30% higher than for galvanising. The differences in the first-year corrosion rates of flat hot-dip galvanised steel specimens, as opposed to flat and open wire pure zinc units, are reflected in **Figures 4.3 & 4.5**.

Figure 5.9 reveals similar reductions in the first-year corrosion rates of zinc at the different exposure sites in South Africa, versus their distances from the ocean, as for mild steel and hot-dip galvanised steel, i.e. about -0.5 ($P \leq 0.05$). A comparable PPMC of around -0.4 ($P \leq 0.05$) was also identified regarding the changes in the 12-month corrosion rate of zinc versus an increase in elevation, moving away from the ocean.

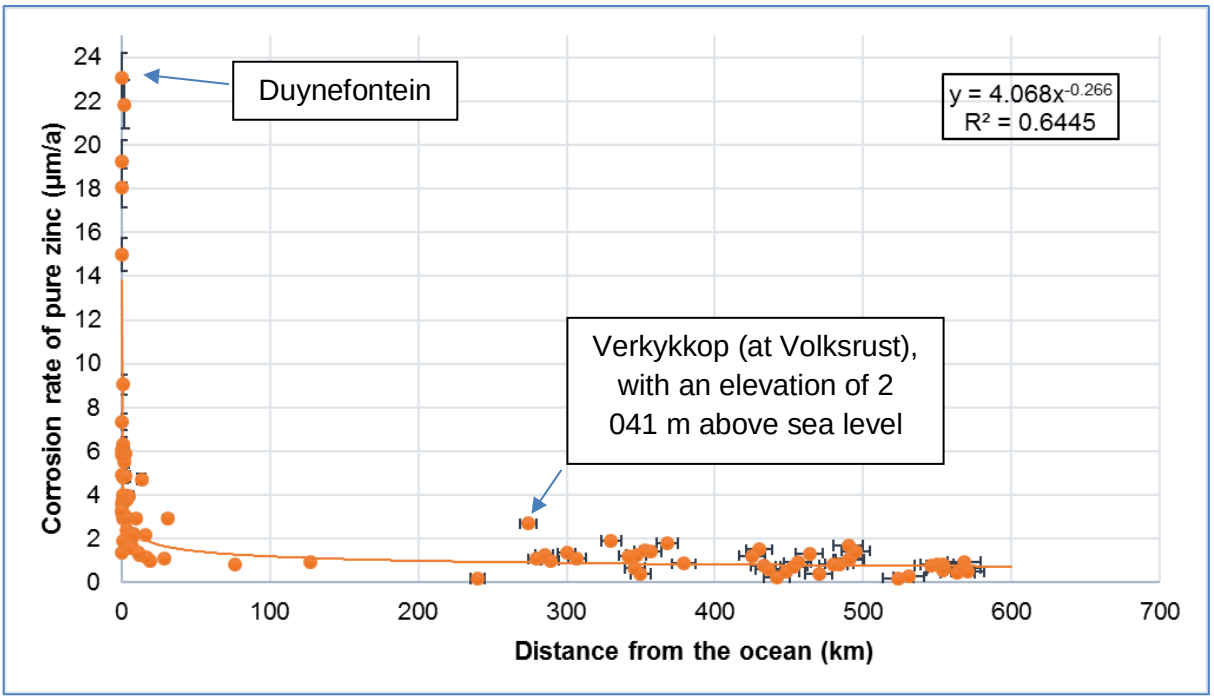


Figure 5.9 First-year (12-month) corrosion rate of zinc at exposure sites in South Africa, versus their distances from the ocean.

5.1.4 Pure Aluminium

Data relating to the first-year corrosion rates of aluminium are given in **Figure 4.6**. Statistical computations of this data are summarised in **Table 5.1**, which shows the average first-year (12-month) corrosion rates of aluminium at the 150 m, 150-1000 m, 1-3 km, 3-10 km, 10-30 km and >30 km marks along South Africa's coastline. See also **Figure 5.10**.

Table 5.1 Average first-year (12-month) corrosion rate of aluminium within varying distance spans from the ocean.

Distance from the ocean	First-year average R_{corr} (Al) value in µm/a					Approximate Ratio
	Mean	Standard deviation	95% CI of the mean	Maximum	Minimum	Max: Min
< 150 m	2.2	1.1	[1.2, 3.2]	~3.8 (Durban Bluff) (CSIR 1975)	~0.5 (Durban – Salisbury Island) (CSIR 1975)	7
150 m ≤ 1000 m	1.0	0.5	[0.7, 1.3]	~1.8 (Cape St. Francis) (Eskom 2010-2016)	~0.4 (Mossel Bay) (Janse van Rensburg 2010)	4
1 km ≤ 3 km	1.3	1.1	[0.3, 2.2]	~3.1 (Durban CTC) (Leitch 1999)	~0.40 (Cape Town – Ysterplaat) (Leitch 1999)	8
3 km ≤ 10 km	0.7	0.4	[0.1, 2.2]	~1.5 (Illovo) (Janse van Rensburg 2010)	~0.3 (Saldanha) (Leitch 2006)	18
10 km ≤ 30 km	0.4	0.2	[0.2, 0.6]	~2.0 (Germiston) (Janse van Rensburg 2010)	~0.2 (Vredendal) (Janse van Rensburg 2010)	8
> 30 km	0.3	0.4	[0.2, 0.4]	~2.0 (Germiston) (Janse van Rensburg 2010)	~0.03 (Lephalale) (Eskom 2010-2016)	67

Like mild steel, hot-dip galvanising and zinc, early corrosion results for aluminium are affirmative of the elevated corrosive levels of the conditions along South Africa's coastline, as well as at inland industrial, mining and power generating locations (Janse van Rensburg 2010). See also **Table 5.1**. Based on the reported data, the measured corrosion rate of aluminium decreased rapidly within 150 m to 1000 m from the coastline, about 55%. Moving inland, the average corrosion rate of aluminium was approximately 0.12 µm/a in the Karoo, near 0.34 µm/a in Mpumalanga, about 0.54 µm/a in Gauteng and close to 0.23 µm/a in the Limpopo regions.

The general slow corrosion rate of aluminium under atmospheric conditions may be ascribed to the formation of protective oxide layers (Graedel 1989; Lobnig et al. 1996b; Leygraf et al. 2016). However, in coastal environments, the chlorides may locally destroy this passive surface oxide, causing pitting corrosion (Leygraf et al. 2016).

The first-year corrosion rate of aluminium also confirmed an appreciable decrease in variability with increasing distance from the ocean, from approximately 1.1 µm/a to 0.4 µm/a, with *r* around -0.5 ($P \leq 0.05$), suggesting enhanced stabilisation of the environment, moving inland. A similar trend, *r* approximately -0.4 ($P \leq 0.05$), was also identified regarding the changes in the 12-month corrosion rate of aluminium versus an increase in elevation, moving away from the sea.

Regarding the 3-10 km zone, the highest value was reported for Scorpio, in Richards Bay (Leitch 1999). See also **Figure 5.10**. However, this significant outlier site ($P \leq 0.05$), detected by way of the Grubbs' test (also called the ESD method), was not included in the calculations, since the high value, around 5.7 µm/a, distorted the results.

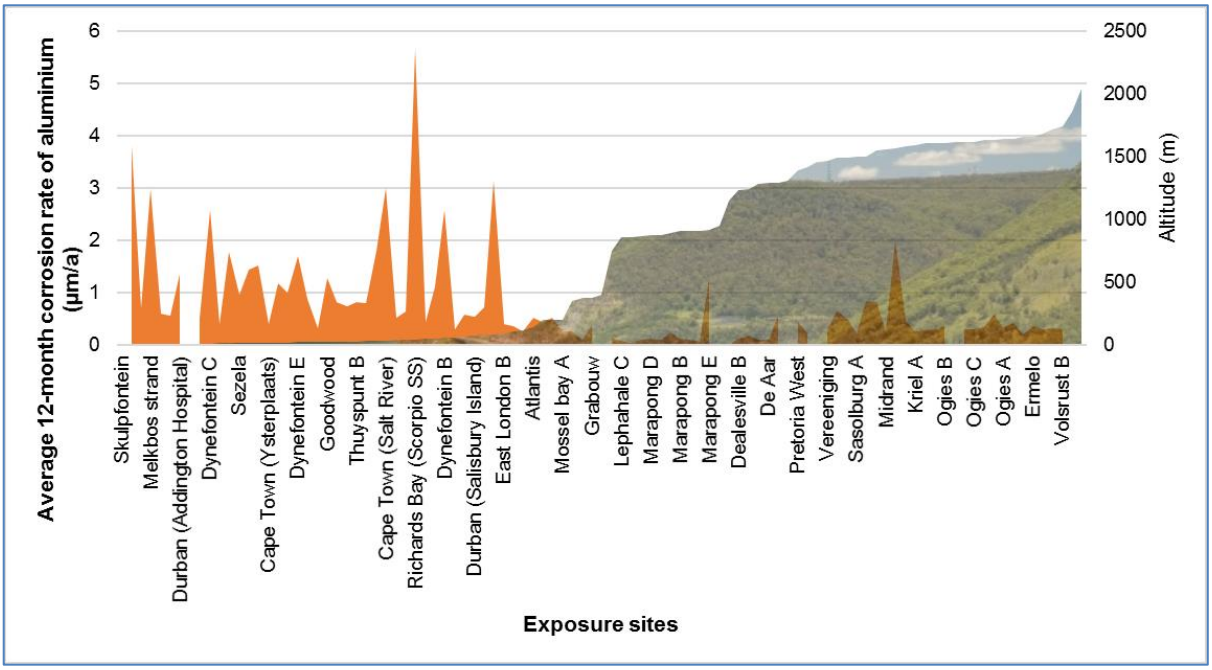


Figure 5.10 First-year (12-month) corrosion rates of aluminium, measured at numerous sites in South Africa, versus their relative altitudes (elevations above sea level).

Apart from being located approximately 7 km from the open sea and about 2.5 km from the Richards Bay Harbour (Google 2018), the Scorpio site has been shown to exhibit a maximum 10-minute average SO_2 concentration of 833 ppb, which exceeded the NEMAQA (National Environmental Management: Air Quality Act 39 of 2004), SO_2 ten-minute average standard (191 ppb), by 436% (SGS 2012). According to AFSA (2013), SO_2, together with Cl^-, can significantly enhance the atmospheric corrosion rate of aluminium.

Richards Bay is also known for its large aluminium smelter plants, as well as paper and pulp, and ilmenite production facilities. Noteworthy is that the high aluminium corrosion rate at Scorpio, is like those measured for Ponteau Martigues in France, considered a moderate marine zone (Knotkova et al. 2010). However, the corrosion rate of aluminium for the latter sites was significantly reduced when utilising flat aluminium panels.

The lowest value was measured at a rural site near Lephalale, about 0.03 µm/a, located in Limpopo Province (Eskom 2010-2016), which corresponded to the average rate for San Juan in Argentina (Knotkova et al. 2010), also measured the least in terms of aluminium of 53 sites (worldwide) during the international ISOCORRAG programme. Comparable results were correspondingly reported by Callaghan (1991) for AA3103, AA5251, AA6063 and AA6082 aluminium alloys at the CSIR's premises in Pretoria. Conversely, during the MICAT (Ibero-American) exposure programme, the lowest corrosion rate of aluminium measured 0.01 µm/a, at Arequipa (in Peru) and Trinidad (in Venezuela) (Morcillo et al. 2012). According to Morcillo et al. (2012), the 12-month corrosion rates of aluminium in the Ibero-American countries varied from close to 0 µm/a to about 5.4 µm/a, the latter value corresponding to the high value recorded at Scorpio in South Africa.

Important is that in contrast to the other metals evaluated in the current study, the corrosion of aluminium is often more localised in character, forming pits, especially in marine environments (Callaghan 1991; Morcillo et al. 2012; Melchers 2015). Callaghan (1991) also reported that at coastal sites in South Africa, after 20 years, the extent of pitting corrosion of the aluminium diminished with time, although a grey/white patina developed, while at an inland site, Pretoria, the aluminium samples still exhibited a metallic mirror-like finish. Cook et al. (2000) also reported similar corrosion rates of aluminium for several sites in México.

Significant is that although Morcillo et al. (2012) considers the concept of average penetration with time (µm/a) "*meaningless*", due to the pitting behaviour of aluminium, and should according to these scholars preferably be reported in g/(m^2·a), it was decided to present the collated South African data in µm/a, since this form was mostly used in the dated and reference studies.

5.1.5 Pure Copper

Statistical analyses of the existing first-year atmospheric corrosion data of copper at various locations in South Africa **(Figure 4.7)** are given in **Table 5.2**.

Table 5.2 Average first-year corrosion rate of copper within varying distance spans from the ocean.

Distance from the ocean	First-year average R_{corr} (Cu) value in µm/a					Approximate Ratio
	Average	Standard deviation	95% CI of the mean	Maximum	Minimum	Max: Min
< 150 m	6	4	[2.1, 10.2]	~11.5 (Melkbos Strand) (Janse van Rensburg 2010)	~1.4 ± 0.1 Durban – (Salisbury Island) (CSIR 1975)	8
150 m ≤ 1000 m	4.7	1.1	[3.8, 5.6]	~6.2 (St. Francis) (Janse van Rensburg 2010)	~3.2 (Durban – Congella) (CSIR 1975)	3
1 km ≤ 3 km	2.8	1.4	[1.0, 4.5]	~4.5 (St. Francis Bay) (Janse van Rensburg 2010)	~0.7 (Cape Town – Ysterplaat) (CSIR 1975)	6
3 km ≤ 10 km	1.9	0.6	[2.4, 3.3]	~3.7 (Mossel Bay) (Janse van Rensburg 2010)	~1.9 (Durban) (Janse van Rensburg 2010)	2
10 km ≤ 30 km	2.0	0.7	[1.3, 2.7]	~3.2 (Vredendal) (Janse van Rensburg 2010)	~1.1 (Hopefield) (Janse van Rensburg 2010)	3
> 30 km	0.86	0.81	[0.6, 1.1]	~3.5 (Sasolburg) (Janse van Rensburg 2010)	~0.6 (Marapong) (Eskom 2010-2016)	58

Variations in the 12-month corrosion rate of copper at different sites, as opposed to their relative altitudes, are also shown in **Figure 5.11**.

Comparable negative trends are recognised for copper as for mild steel, hot-dip galvanising, zinc and aluminium, i.e. with PPMC coefficients of about -0.6 ($P \leq 0.05$), between the corrosion rate of copper and an increase in distance from the sea, as well as in relation to increasing altitude moving away from the ocean. The highest corrosion rates of copper were measured along the South African coastline, decreasing to an average of 0.9 ± 0.8 µm/a, 95% CI [0.6 µm/a, 1.2 µm/a] at sites located more than 30 km from the ocean. However, as may be observed in **Figure 5.11**, the corrosion rate of copper may spike in areas exposed to industrial pollution, e.g. Sasolburg. The impact

of marine salts on the corrosion rate of copper is also evident, due to the high measurements reported at Melkbos Strand, Durban, St. Francis and Mossel Bay (**Table 5.2**).

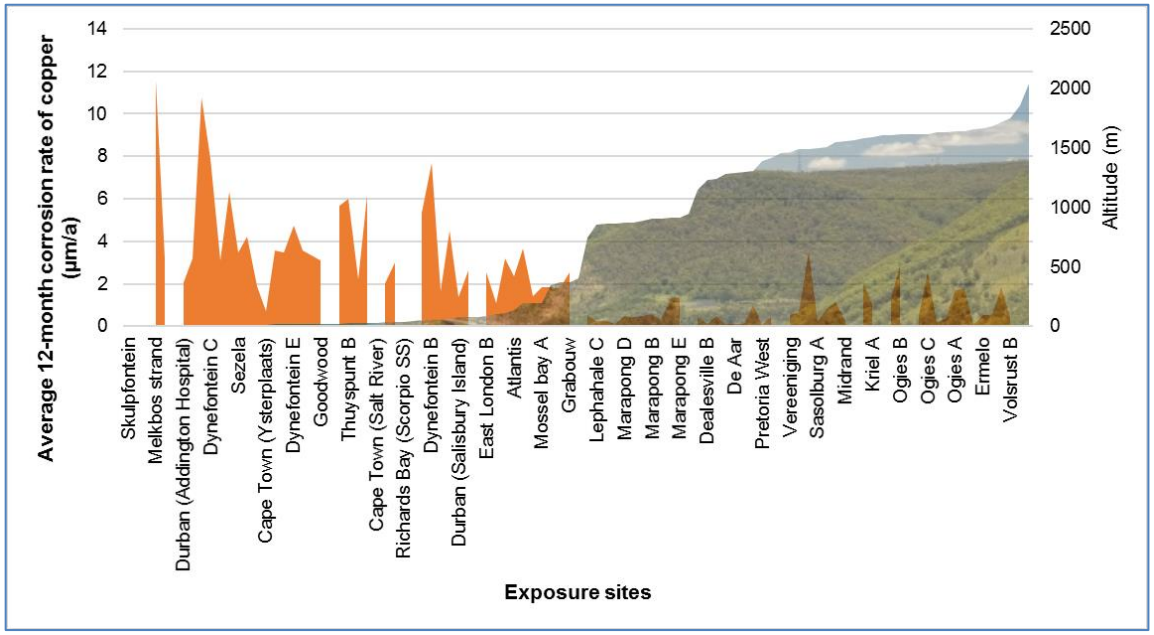


Figure 5.11 First-year (12-month) corrosion rates of copper, measured at numerous sites in South Africa, versus their relative altitudes (elevations above sea level).

The most elevated corrosion rate of aluminium in the 150-1000 m range was measured for a site in Arniston (Janse van Rensburg 2010). However, like Scorpio, due to the excessively high value reported, about 10.8 µm/a, compared to nine other sites, the result from this outlier site ($P \leq 0.05$, via the Grubbs' test) was excluded from the average calculations for this distance span from the ocean. Nonetheless, the change in the average corrosion rate of copper between the < 150 m and 150-1000 m spans from the sea was still less dramatic than in the case of the other metals.

As shown in **Figure 5.11**, other sites that displayed high corrosion rates of copper, e.g. Ogies, Kriel and Volksrust are located near large coal-fired power stations and open-cast coals mines.

5.1.6 Comparison of the Different Metal Corrosion Rates

The differences, as countrywide averages of the 12-month corrosion rates of mild steel, hot-dip galvanised steel, zinc, aluminium and copper are presented in **Figure 5.12**.

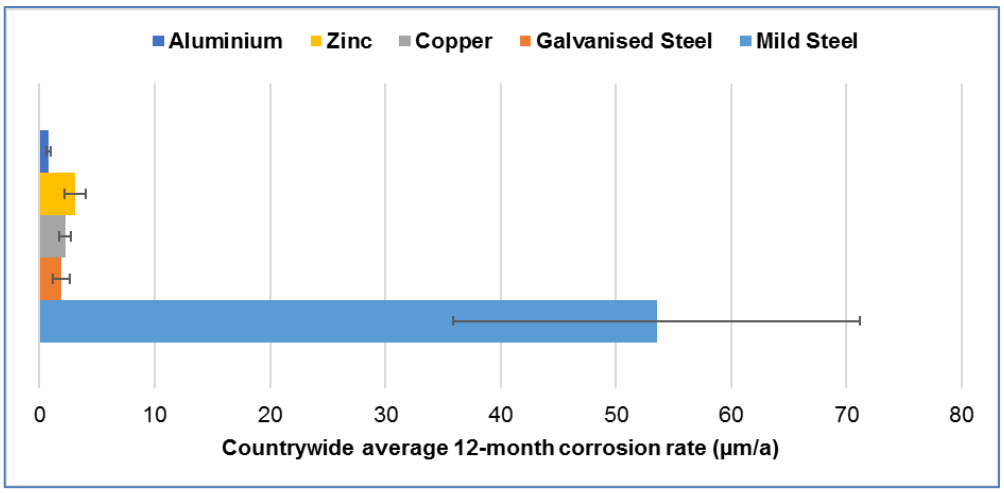


Figure 5.12 Countrywide average 12-month corrosion rates of mild steel, hot-dip galvanised mild steel, pure zinc, aluminium and copper.

As shown, the average corrosion rate of mild steel is nearly 28 times higher than for hot-dip galvanising, about 25 times more than copper, close to 17 times greater than pure zinc, and approximately 67 times more than aluminium. However, as indicated by the error bars, the CI (confidence intervals) of the mean values are high, about 30%, varying from approximately 22% (copper) to 38% (hot-dip galvanised steel).

Figure 5.13 shows that, while the five materials differ markedly regarding their average corrosion rates, all indicate a substantial decrease with increasing distance from the ocean. These ratios compare favourably with those of the ISOCORRAG programme (Knotkova et al. 2010).

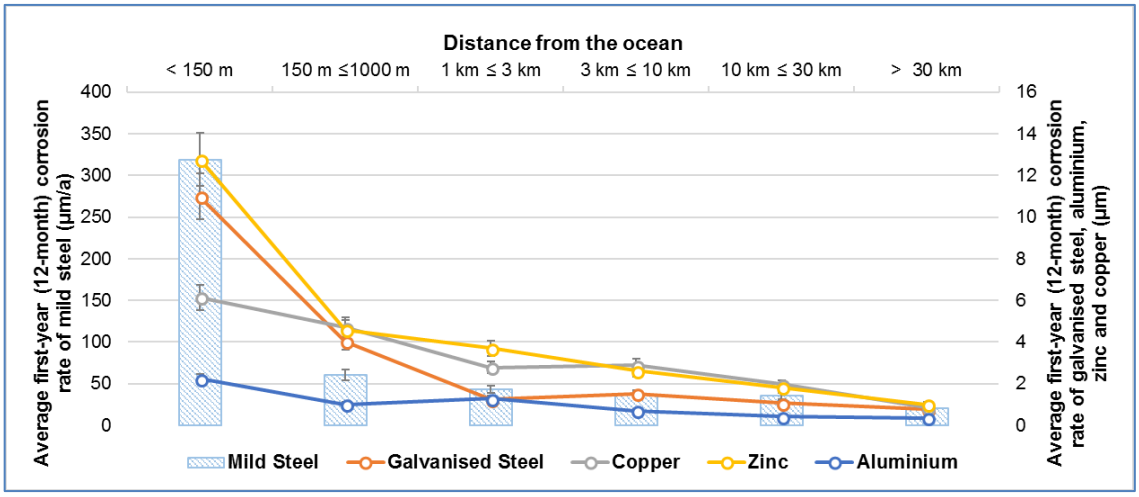


Figure 5.13 Average first-year (12-month) corrosion rates of mild steel, hot-dip galvanised steel, aluminium, zinc, and copper, at varying distance spans from the ocean.

5.1.7 Atmospheric (ACI), Industrial (ICI) and Marine (MCI) Corrosion Indices

As mentioned in Section 2.1.6.2, earlier South African studies also involved the exposure of CLIMAT (wire-on-bolt) units to different corrosive environments. This concerned mainly the Callaghan (1991), Nixon & Janse van Rensburg (1992), Gross & Nixon (1993), Leitch (1999) and Janse van Rensburg (2010) corrosion monitoring studies. Unfortunately, aside from Janse van Rensburg's and Leitch's data, as well as some unpublished Eskom results, not all the raw data could be successfully sourced.

Nonetheless, statistical analyses of available data, including summations (∑) (referred to as the Total Corrosion Index -TCI) of the ACI, ICI and MCI data for the different zones, are presented in **Table 5.3** and **Figure 5.14**. Note that 'TCI' is not a standard term in the wire-on-bolt procedure, but has been created to enable more straightforward comparison of the diverse data. Also, owing to the *very high* to *extreme* corrosivity of the 0-150 m region from the coastline, the ACI, ICI and MCI data for this zone were ignored, although it was often reported as VERY SEVERE (**Table 2.1**) (Carter 1982). The reason for this was because the results were regularly classified as invalid since the aluminium wire was either broken upon removal from the threaded bolt or wholly corroded away (Janse van Rensburg 1994, 2010, 2015). The high variability and uncertainty of the rest of the CLIMAT results are also of note.

However, **Table 5.3** and **Figure 5.14** reveal that the ACI, MCI and ICI data exhibited somewhat similar trends to those determined for the mild steel, hot-dip galvanised steel, zinc, aluminium and copper, i.e. a reduction in the corrosion indices with increasing distance from the ocean, and higher ICI values in more polluted areas. This finding concurs with studies done by Godard, Doyle, Wright and Morcillo (Doyle & Godard 1969; Doyle and Wright 1971; Doyle & Wright 1982; Morcillo et al. 2010), namely a rapid decrease in the MCI value with an increase in distance from the shore, particularly within 1-2 km from the ocean.

Table 5.3 Average ACI, ICI and MCI data for South Africa, within varying distance spans from the ocean.

Distance from the ocean	ACI			ICI		MCI		Sum (∑) (TCI)	Sum (∑)	
	$\bar{x}$ ± SD	95% CI	$\bar{x}$ ± SD	95% CI	$\bar{x}$ ± SD	95% CI	$\bar{x}$ ± SD	95% CI	Maximum	Minimum
< 150 m										
150 m ≤ 1000 m	1.0 ± 0.8	[0.0, 3.0]	8.3 ± 0.2	[6.4, 11.3]	14 ± 2.0	[8.5, 18.8]	24 ± 0.4	[23.3, 25.1]	~24.7 (Scottburgh) (Janse van Rensburg 2010)	~24.0 (Aniston) (Janse van Rensburg 2010)
1 km ≤ 3 km	0.4 ± 0.4	[0.0, 1.3]	6 ± 3	[0.0, 12.9]	9.2 ± 8.0	[0.0, 29.1]	17 ± 12	[0.0, 46.7]	~28.8 (St. Francis Bay) (Janse van Rensburg 2010)	~4.6 (East London) (Janse van Rensburg 2010)
3 km ≤ 10 km	0.3 ± 0.1	[0.2, 0.4]	6 ± 3	[3.4, 8.5]	4.7 ± 1.3	[3.7, 5.8]	12 ± 5	[7.6, 16.2]	~21.7 (Durban) (CSIR 1975)	~7.0 (Grabouw) (Janse van Rensburg 2010)
10 km ≤ 30 km	0.5 ± 0.3	[0.3, 0.8]	3.7 ± 1.4	[2.4, 5.0]	4.1 ± 2.2	[2.1, 6.1].	8 ± 3	[5.3, 11.4]	~13.9 (Empangeni) (Janse van Rensburg 2010)	~4.6 (Vredendal) (Janse van Rensburg 2010)
> 30 km	0.2 ± 0.2	[0.1, 0.2]	0.9 ± 0.7	[0.7, 1.1]	2.1 ± 5.8	[0.2, 3.8]	2.1 ± 1.6	[1.6, 2.7]	~7.4 (Muldersvlei) (Janse van Rensburg 2010)	~0.3 (Lephalale) (Janse van Rensburg 2010)

Note: $\bar{x}$ ± SD denotes average and standard deviation, CI – confidence interval and TCI - Total Corrosion Index, which is not a standard term in corrosion, but has been created to enable comparison of the diverse results.

However, from a statistical perspective, the reductions in the corrosion indices with an increase in distance from the ocean were only found to be meaningful ($P \leq 0.05$) about the ACI and TCI (PPMC) correlations, (*r*) -0.4 and -0.5, respectively. Nonetheless, the highest MCI values, often in the SEVERE (10.1-20) to VERY SEVERE (> 20) ranges (**Table 2.1**) (Carter 1982), were measured along the Northern and Western Cape coastlines, followed by the Eastern Cape and then KwaZulu-Natal regions. Areas along the coast for which the reported ICI was higher than the MCI, suggesting marine-industrial sites, included locales in Cape Town, Durban, Saldanha, East London, Mossel Bay and Richards Bay.

However, at inland areas, the elevated ICIs were reported for sites near Witbank, Hendrina, Germiston and Sasolburg, as well as close to a locale near Marapong (Lephalale), corresponding to areas known to be affected by high industrial pollution (**Figure 5.4**). In contrast to Delgado & Vera's (2013) results, on an average basis for South Africa, the highest values were typically recorded for the *aluminium-steel* galvanic couples (MCI), potentially indicating that the effects of TOW and chlorides, and then SO_2 (Carter 1982; Leitch 1994) exhibited the most significant impact on the atmospheric corrosion of South Africa. The enhanced galvanic effect of the *aluminium-steel* couple in Villahermosa (México) has also been reported by Torres-Mendoza et al. (2006).

One of the significant disadvantages of the CLIMAT test method is that it is less sensitive in distinguishing between the corrosiveness of sites located at similar distances from the ocean, or which are in somewhat comparable climatic zones. Consequently, most ICI values for the central South Africa locations measured either nil or rated NEGLIGIBLE (**Table 2.1**) (Carter 1982) (implying a percentage weight loss of less than 1%), thus preventing proper comparisons between the different places. An additional shortcoming is that the CLIMAT data only reflected the corrosiveness of an environment per specific season or three-month period. As a result, the data must be viewed with caution when considering long-term corrosion trends.

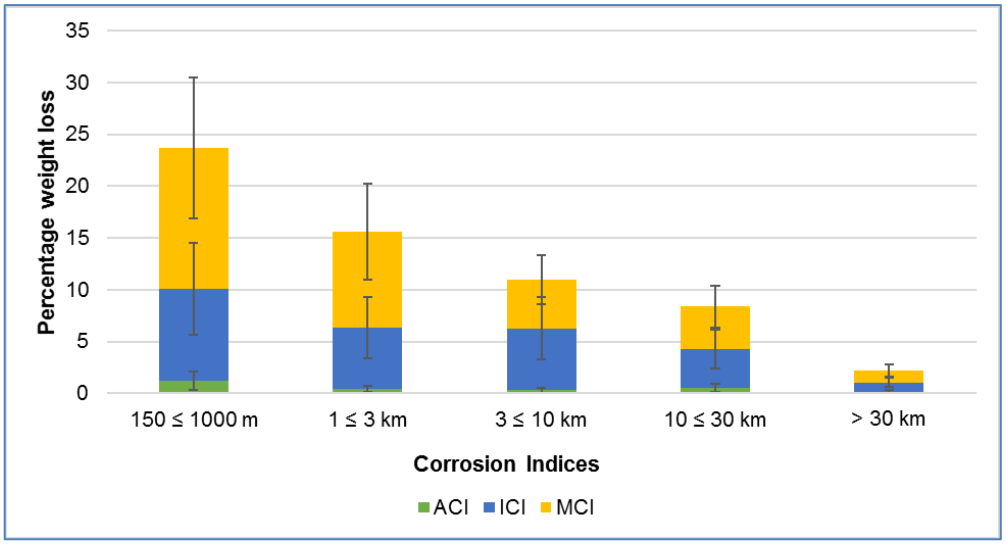


Figure 5.14 Average Atmospheric (ACI), Industrial (ICI) and Marine (MCI) corrosion indices with different distance spans from the ocean.

5.1.8 Correlations of Atmospheric Corrosion Data

The strengths of the associations (PPMC coefficients) between the different atmospheric corrosion rates and indices for South Africa are presented in **Table 5.4**.

Table 5.4 Significant (95%) rank correlations between the atmospheric corrosion data of South Africa.

Metal type	Parameter	Mild steel	HD galv.	Zinc	Aluminium	Copper	ACI	ICI	MCI	TCI
Parameter		r_{corr} (MS)	r_{corr} (HDG)	r_{corr} (Zn)	r_{corr} (Al)	r_{corr} (Cu)	Indices			
Mild steel	r_{corr} (MS)	**1.00**	**0.66**	**0.79**	**0.78**	**0.69**	-0.01	0.00	0.00	**0.88**
HD galv.	r_{corr} (HDG)		**1.00**	**0.79**	**0.78**	**0.66**	0.03	0.04	0.08	**0.86**
Zinc	r_{corr} (Zn)			**1.00**	**0.54**	**0.59**	**0.30**	**0.21**	**0.28**	**0.65**
Aluminium	r_{corr} (Al)				**1.00**	**0.74**	0.15	**0.33**	**0.35**	**0.79**
Copper	r_{corr} (Cu)					**1.00**	**0.41**	**0.22**	**0.27**	**0.82**
ACI	Indices						**1.00**	**0.41**	**0.43**	0.18
ICI								**1.00**	**0.93**	0.17
MCI									**1.00**	**0.23**
TCI										**1.00**

Note – HD denotes hot-dip galvanising, r_{corr} – 1st-year (12-month) corrosion rate, ACI – atmospheric corrosion index, ICI – industrial corrosion index, MCI – marine corrosion index and TCI – total corrosion index. The lighter shaded values indicate relationships of none or negligible significance.

Very strong positive correlations were found ($r \geq 0.7$) between the first-year (12-month) corrosion rates of the different metals exposed at the various sites throughout South Africa, between hot-dip galvanised steel and zinc, as well for mild steel and zinc. High positive relationships also existed between the first-year corrosion rates of mild steel, hot-dip galvanising, aluminium and copper, as well with the TCI values, including between the ICI and MCI results. According to Doyle & Wright (1982) and Morcillo et al. (2010), in non-industrial marine environments, both the ICI and MCI units may potentially be used to quantify the corrosivity of the environment, due to their similar responses to chlorides in the atmosphere. The very high relationship between the TCIs and the 12-month corrosion rates of mild steel is also promising since it suggests that this combined index value, is perhaps a better short-term (90-day) indicator of the corrosivity of an environment, i.e. in comparison with the singular ICI and MCI values.

Conversely, only weak ($r \geq 0.3$) to moderate ($r \geq 0.5$) correlations were determined between the corrosion rates of the different metals and the ACI, ICI and MCI values. These weaker relationships may likely be ascribed to the high variability and uncertainty of the CLIMAT data, emphasising some of the comments previously made regarding the disadvantages of the procedure. However, as shown in **Table 5.5** (adapted from Bitcon 2014), representing the conversion of helical aluminium wire CLIMAT data into equivalent corrosion rates of flat aluminium sheeting (Doyle and Wright 1982), it is apparent that the association between the ISO 9223 and CLIMAT procedure is not always consistent, adding to the weaker correlations.

Table 5.5 Aluminium corrosion rate from ISO 9223 (International Organization for Standardization 2012) and Doyle and Wright (1982).

ISO 9223 Classification for aluminium (2012)		**Doyle and Wright (1982)**		
Classification	**Corrosion rate** ($g/m^2 \cdot a$)	**Classification**	**Al/Cu CLIMAT indices range**	**Corrosion rate** ($g/m^2 \cdot a$)
C1	Negligible	**Negligible**	0 - 1	0 – 1.2
C2	≤ 0.6	**Moderate**	> 1 - 2	1.2 – 1.7
C3	0.6 to ≤ 2	**Moderately severe**	> 2 - 4	2.7 – 5.9
C4	2 to ≤ 5	**Severe**	> 4 - 7	5.9 – 10.6
C5-CX	5 to > 10	**Very Severe**	> 7	> 10.6

5.1.9 Corrosivity Rating of South Africa's Macro Atmosphere

Based on the assimilations and statistical analyses of the existing corrosion data for South Africa, a summary of the macro corrosivity of the atmosphere, regarding the latest ISO 9223 corrosivity rating scheme (International Organization for Standardization 2012a), is given in **Figure 5.15**. The expected corrosivity of the GJMA, which is located more than 30 km from the coast, is *low* C2 to *high* C4 (as per ISO 9223:2012).

Section 5.2 discusses the findings of the corrosion and coatings monitoring work carried out at the 57 inland sites, in and around the GJMA.

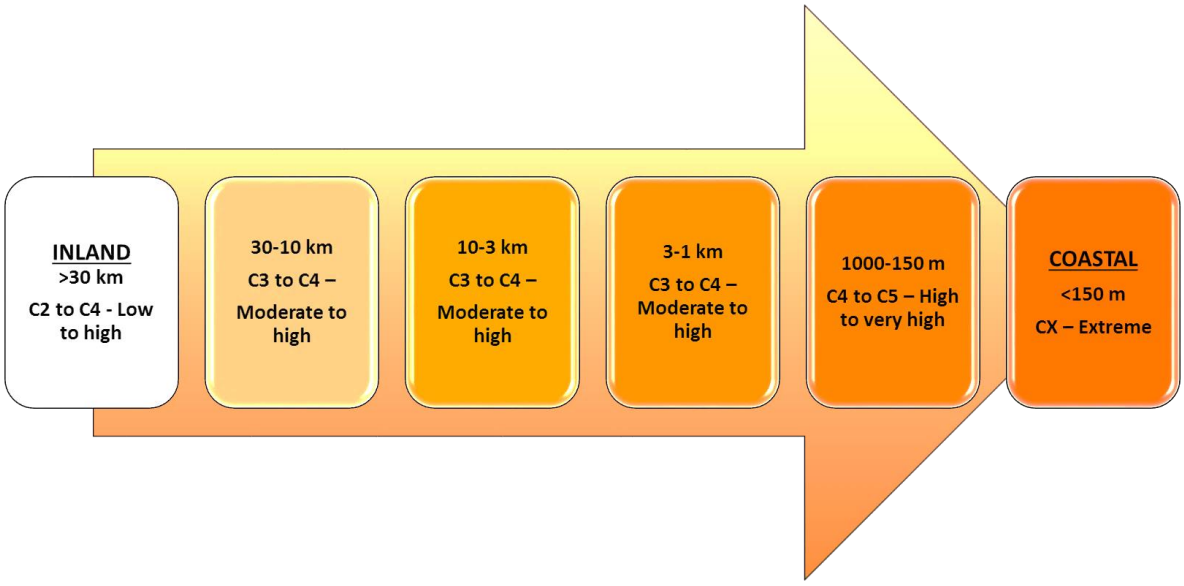


Figure 5.15 Corrosivity ratings of South Africa's macro atmosphere, based on the ISO 9223:2012 rating scheme, from inland to coastal environments.

5.2 ATMOSPHERIC CORROSIVITY OF THE GJMA

5.2.1 Industrial, Marine and Atmospheric Corrosion Indices

5.2.1.1 Industrial (ICI) corrosion indices

The ICI results (**Figures 4.11 - 4.12,** as well as **Appendix G – Table G.1**) revealed that the impact of industrial pollution on the atmosphere in the GJMA is significantly more distinct during spring and summer than in autumn and winter. This finding is statistically supported by the *t*-test, with *t*-value -7.3 and $P < 1 \times 10^{-5}$, which is significant within 95%

(P ≤ 0.05) Confidence Limit (CL)]. The increased ICI levels during spring and summer can mainly be ascribed to the higher levels of precipitation (rain) (**Figures 2.27 & 3.13)** (ClimaTemps.com 2017b; SAWS 2017) and moisture in the atmosphere during the rainy season (**Figure 3.12**) (SAWS 2017), resulting in the regular wetting of surfaces and increased TOW.

Figures 3.13 - 3.15, derived from SAWS' (2014, 2017) data, reveal that on an annual basis, the GJMA receives its rainfall primarily during September to February, causing increased TOW and elevated RH levels in the atmosphere (**Figures 3.10 – 3.12**). The average monthly RH is about 40-80% (**Figure 3.10**) (SAWS 2014), while on a yearly basis, the average RH varies from approximately 60% to 70% (**Figure 3.12**) (SAWS 2017), which is in the "*normal*" range (Vargel 2004).

The yearly rainfall figure is about 600-800 mm (Shuters-Macmillan 1996; Oxford University Press 2004) (see also **Figure 2.4**) (My Cyberwall 2017), corresponding to similar measurements for the north-eastern parts of America and northern regions of Europe (University of Wisconsin 2018). Brown & Masters (1982), Callaghan (1991), Rincon et al. (2000) and Leygraf et al. (2016) confirm that rain and RH are critical drivers of atmospheric corrosion processes. Li et al. (2013) also agree that rain plays an essential role in the initiation of the corrosion process, with moisture becoming trapped in crevices and therefore, accelerating localised areas of corrosion.

Conversely, an increase in the annual rainfall does not merely imply an increase in corrosion. For example, Chloorkop consistently exhibited the highest ICI values - for all four seasons, which can only be explained by a likelihood that this locale experienced increased levels of ground-level pollution, likely due to the emissions of caustic soda and chloralkali derivative from the industrial plants located in the area (NCP Chlorchem 2011-2017). This finding was also subsequently confirmed by chemical analysis of the mild steel corrosion product formed at this locale (**Figures 4.36 & 4.38**), displaying elevated levels of water-soluble salts and chlorides. Moreover, it showed that the ICI-couples are not only affected by moisture and sulphates present in the atmosphere, but also by chlorides (Carter 1982; Dean et al. 2000).

Throughout autumn (March to May 2014) and winter (June to August 2014), when atmospheric pollution was generally at its highest level in the GJMA (**Figures 3.23 -**

3.25, **3.28 - 3.29**, **3.30**) (DEA 2017a; Yale Data Driven 2016), the measured ICI values for Chloorkop exceeded those of the other locations. Potential changes in the wind speed and direction (**Figure 3.17**) (SAWS 2014) also became apparent during the summer months (**Figure 4.11**), when Midrand was likely more affected by airborne chlorides/salts emanating from the nearby Chloorkop (Modderfontein) area. Similarly, the ICI values of the Ivory Park during spring was likely influenced by the emissions from the Chloorkop region.

However, like Alexandra, Jabavu (Soweto) and Kagiso-Randfontein, the Ivory Park locale showed increased levels of air pollution during winter due to the burning of fossil fuel (**Figures 3.23 - 3.24**) (DEA 2017a). These suburbs are all associated with low-income residential and informal settlement areas, where the residents rely significantly on the burning of wood, coal and paraffin for heating and cooking purposes (Pretorius et al. 2015). **Figures 3.23 - 3.24**, **3.28 - 3.29 & 3.30** (DEA 2017a; Yale Data Driven 2016), show that the highest PM_{10} and $PM_{2.5}$ particulate matter, as well as SO_2, NO_2, NO, CO concentrations in the GJMA atmosphere are measured typically during the winter months, when the consumption of electricity and the use of fossil fuels, for heating and cooling purposes, increase dramatically due to the wintry weather conditions. Conversely, the high ICI values at the Brakpan and Rosherville sites were more associated with the elevated industrial activity.

Nonetheless, according to DEA (2011), emissions released via tall stacks, e.g. at Modderfontein, Rosherville and the Kelvin A & B power stations, generally allow the release of the pollutants above the stable surface layer. During night-time, the plumes are kept above the stable surface layer by temperature inversion conditions. However, during the daytime, especially during summer, convection may force the pollutants to ground level, via, so-called looping (DEA 2011), which may explain the higher ICI measurements recorded for Chloorkop, Brakpan, Midrand, Rosherville and Alexandra during summer (**Figure 4.11**).

Based on the CLIMAT atmospheric corrosivity classification system (**Table 2.1**) (Carter 1982), the average ICI for all the main sites, 0.3 ± 0.2, 95% CI [0.2, 0.4], over the first 12 months of the exposure period, rated NEGLIGIBLE. In effect, Chloorkop was the only site that ranked MODERATELY corrosive during the summer months. Throughout the rest of the year, the corrosivity of the atmosphere at this locale, as well as at all the

other sites, rated NEGLIGIBLE. Consistent with Carter (1982), the latter rating is merely given as applicable to "*rural and suburban*" areas, whereas a MODERATE ICI value (as recorded once off at the Chloorkop site), only applies to an "*urban residential area*".

The result signified that while the CLIMAT procedure is useful when it comes to the monitoring of the seasonal fluctuations of corrosive atmospheres, it is less than ideal for the overall rating or classification of corrosive environments. Similarly, Li et al. (2013) derived this conclusion. Theoretically, the limitation also elucidates why Callaghan's map reflected the same corrosivity rating for most parts of the Gauteng (Highveld) region since it relied extensively on CLIMAT results (Callaghan 1991). Dean et al. (2000) also highlighted the inability of this procedure to indicate the impact of significant weather events.

Summations (∑) of the measured seasonal Industrial Corrosion Indices (ICI values) for the main GJMA sites (Spring 2013 to Winter 2014) (**Figure 4.17**) show that from an industrial perspective, those sites that may be rated significantly more corrosive than the rest are Chloorkop, Brakpan, Ivory Park, Rosherville, Delta Park and Alexandra – all positioned from the centre to the eastern parts of the GJMA (**Figure 3.1**). However, as illustrated in **Figure 4.20**, presenting a combined seasonal ICI perspective of the different regions of the GJMA, the differences of the ICIs for the West Rand, Central JHB, Northern and Southern Suburbs of the GJMA, appear less distinct.

5.2.1.2 Marine corrosion indices (MCI)

Typically, the MCI-couple is used for the evaluation of the corrosivity of coastal environments, whereas the ICI-couple is applied to categorise the corrosivity of rural, urban and industrial atmospheres (Carter 1982). However, for the latest study, both the ICI and MCI were employed to examine the corrosivity of the GJMA, since the two galvanic couples tend to react somewhat differently to various airborne pollutants. The MCI value mainly emphasises the effect of Cl^- in the atmosphere (Carter 1982; Dean et al. 2000). This was also demonstrated by the overall South Africa MCI data (**Figure 5.14**). However, it is furthermore influenced (to a lesser extent) by moisture and SO_2 in the air (Janse van Rensburg 1994). Consequently, in contrast to the ICI results, based on the *t*-test, the statistical difference between the average MCI results for spring and summer, versus for autumn and winter was found to be statistically insignificant

(*t* is -1.3 and P = 0.2, which is insignificant within a 95% CL). See also **Appendix G – Table G.1**.

However, like the ICI data, the MCI results were elevated continuously at Chloorkop (**Figures 4.13 - 4.14**). An increased MCI was also measured at Midrand during winter, which is positioned north-west of the Chloorkop area (**Figure 3.1**), as well as at Brakpan during autumn. (See also **Figure 4.18**, presenting summations (∑) of the measured seasonal MCI values for the main GJMA sites - Spring 2013 to Winter 2014). These elevated MCIs, likely indicating the presence of Cl^- in the atmosphere (Carter 1982; Dean et al. 2000), suggested that emissions from the Chloorkop area could have been carried across into adjacent regions, because of changing wind patterns (**Figure 3.17**) (SAWS 2014).

However, the influence of air pollution from Kelvin Power Stations A & B on the corrosivity of the Brakpan area, cannot be excluded. This inference is supported by wind roses for May and July (2012 to 2014), respectively (**Figures 5.16 & 5.17)**, measured at OR Tambo International Airport (SAWS 2014).

Figures 5.16 & 5.17, based on SAWS data (2014), show that the most prominent wind direction during May 2012, 2013 and 2014 was from a north-westerly to west-north-westerly direction, which could have resulted in pollutants being carried downwind into other areas located south-east of the Chloorkop and Kelvin Power Stations. However, during July 2012, 2013 and 2014, the wind direction changed dramatically (**Figure 5.17**), stemming more from a south-south-westerly direction. During this period, the chloralkali pollutants in the air at the Chloorkop area were likely carried across into Midrand.

Overall, the average MCI values for all the sites, 0.5 ± 0.6, 95% CI [0.2, 0.8], measured during the first twelve months of exposure, rated NEGLIGIBLE regarding the CLIMAT test MCI corrosivity classification system (**Table 2.1**) (Carter 1982).

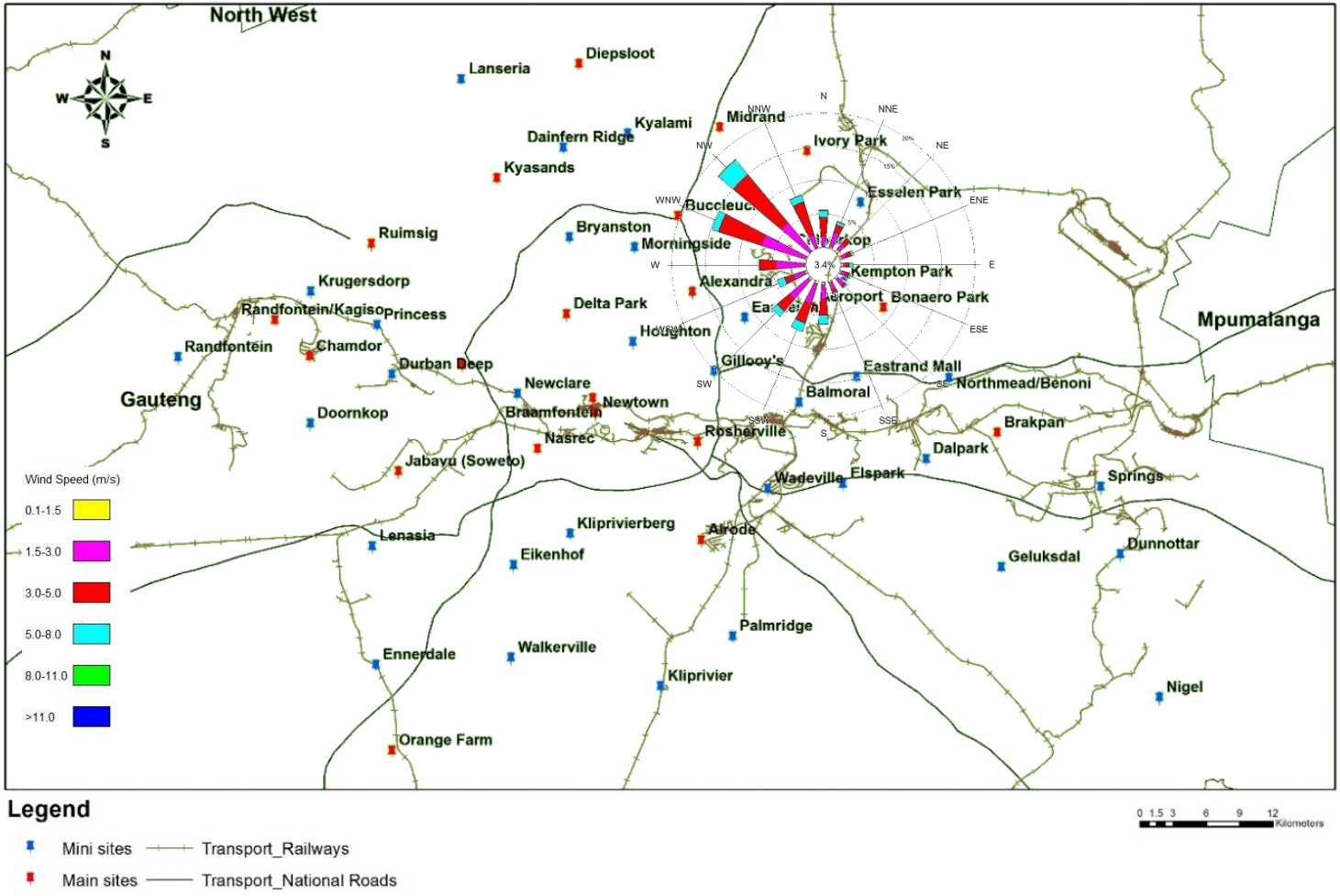


Figure 5.16 A superimposed wind rose for OR Tambo International Airport indicating the strength and predominant direction of the wind during May 2012 to 2014 - based on SAWS (2014) data. (Base map – ArcGIS).

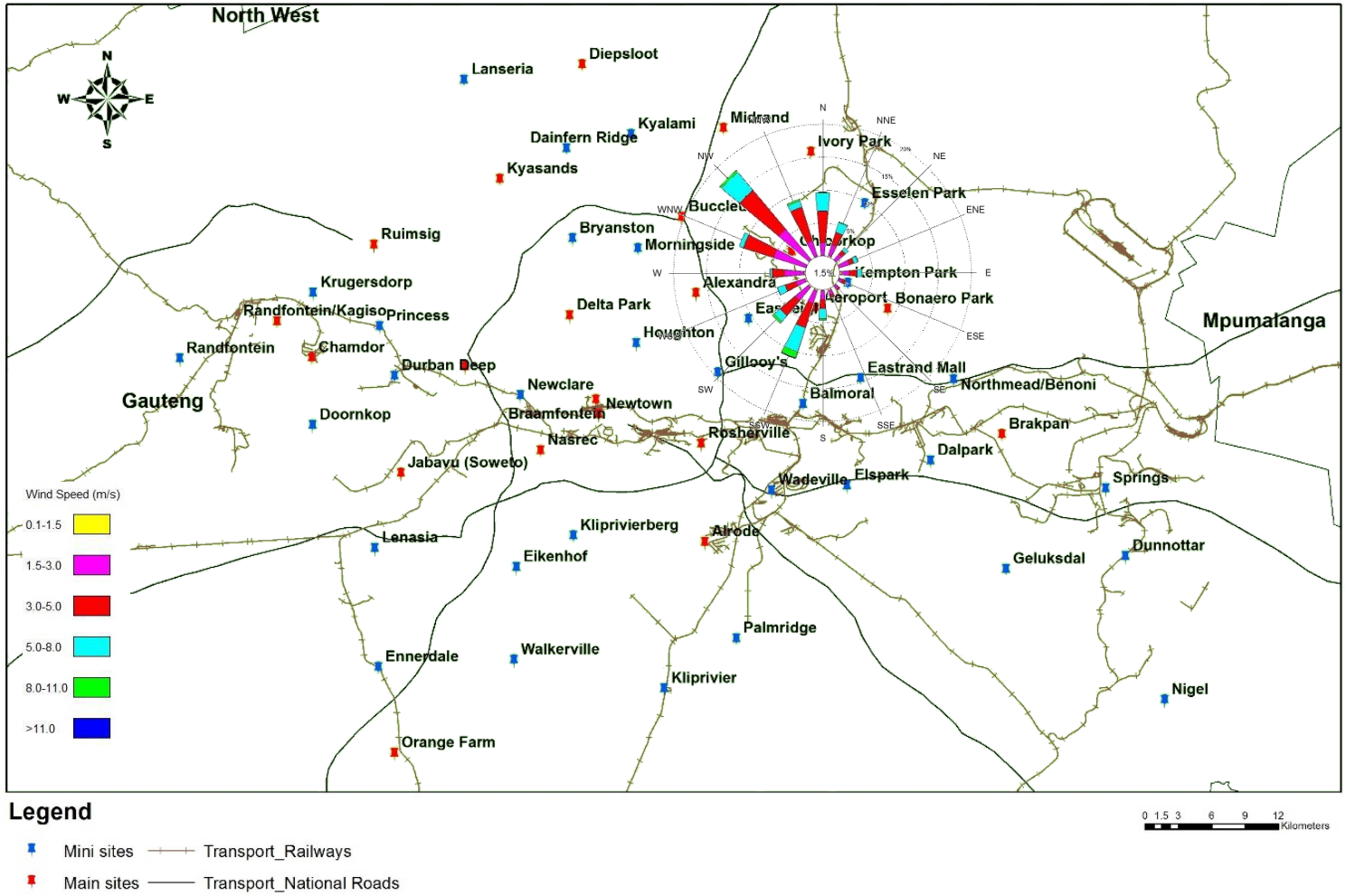


Figure 5.17 A superimposed wind rose for OR Tambo International Airport indicating the strength and predominant direction of the wind during July 2012 to 2014 - based on SAWS (2014) data. (Base map – ArcGIS).

The MCI results agreed with the ICI data that the CLIMAT test procedure is less precise for the general rating of corrosive environments, contrary to Delgado & Vera's (2013) findings. Also, it does not provide enough distinction between sites for which the corrosivity of the atmosphere may be somewhat similar, e.g. all in the NEGLIGIBLE range. Conversely, it is useful for the monitoring of seasonal fluctuations of atmospheric corrosion - also concluded by Tullmin & Roberge (2000). Considering the MCI rating scheme, the significance of a NEGLIGIBLE MCI typically applies to "*average habitable areas*" along the coast (Dean et al. 2000). The exclusive use of this procedure for the rating of inland metropolitan areas is impractical.

Regarding the sum totals of the mean seasonal MCI results for the different GJMA regions (**Figure 4.21),** the East Rand locales once again displayed the highest average MCI values. Conversely, the differences between the summations of the mean seasonal MCI values for the other three regions were less distinct.

5.2.1.3 Atmospheric corrosion indices (ACI)

The *aluminium-nylon* couple, used for measurement of the ACI (Carter 1982), primarily emphasises the effect moisture has on the corrosivity of the environment. However, it may also be affected by Cl^-, SO_2, smoke and dust particulates present in the atmosphere (Janse van Rensburg 1994), although to a much lower extent than the ICI and MCI couples.

Moreover, wire-on-bolt units are potentially more prone to the retention of water than the ISO open wire helix or flat metal panels. Therefore, the effects of increased levels of moisture (%RH) and TOW during spring and summer (September 2013 to February 2014), versus during autumn and winter (March to August 2014) on the general corrosivity of the Greater Johannesburg macro atmosphere are of importance (**Figure 4.15** versus **Figure 4.16**). Refer also to **Appendix G – Table G.1**. Based on the *t*-test, the difference in the average ACI values during the rainy versus the non-rainy seasons was found to be extremely statistically significant (t = -6.2 and $P < 1 \times 10^{-5}$, which is significant at $P \leq 0.05$). Also, the difference between the mean ACI values for spring and summer was exceptionally statistically significant (t = -6.7 and $P < 1 \times 10^{-5}$, within a 95% CL).

Consequently, at most sites, the highest ACI values were recorded during spring - explained by an increase in moisture in the air (**Figures 3.12 - 3.13**) (SAWS 2017), combined with slightly elevated pollution and dust levels in the atmosphere (**Figures 3.23 - 3.25**, **3.28 - 3.29 & 3.31**) (DEA 2017a), carried-over from wintertime and via looping (DEA 2011), due to higher ambient temperatures, as well as the lag of surface temperatures causing condensation (**Figure 5.18**) (SAWS 2014).

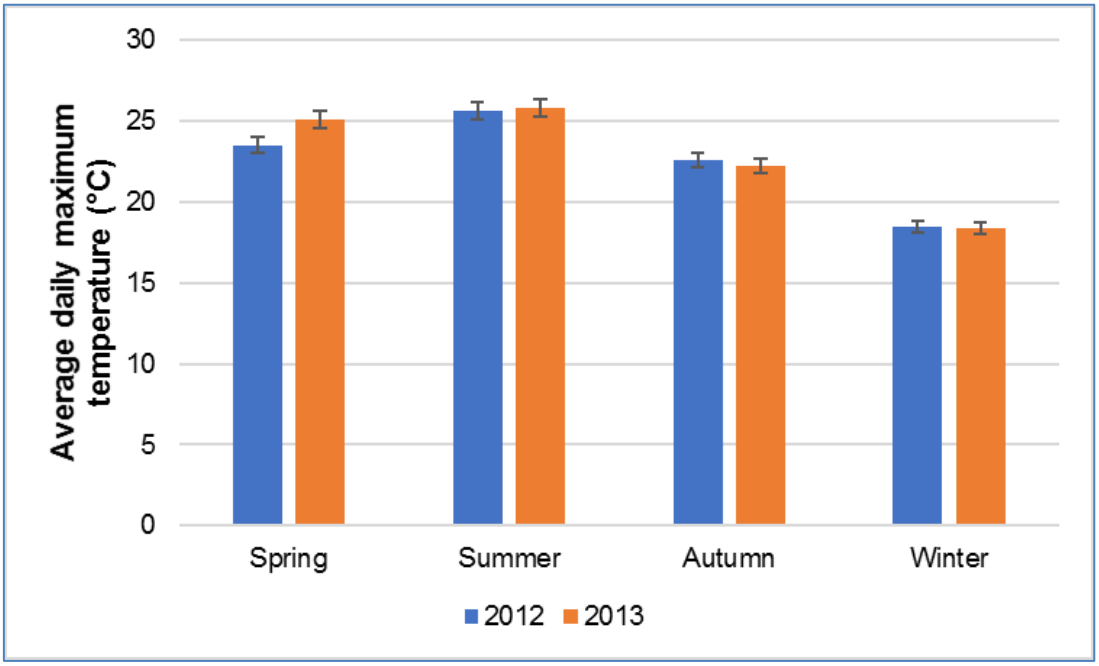


Figure 5.18 Differences in the average seasonal daily maximum temperatures during 2012 to 2014 – Based on data provided by SAWS (2014).

Conversely, in the summer months, the levels of pollution would have been reduced, surfaces better cleaned due to higher precipitation (**Figure 3.13**) (SAWS 2017), as well as wet surfaces would have dried out quicker due to higher ambient and surface temperatures (**Figure 5.18**). This disparity between spring and summer is irrespective of the fact that the highest rainfall figures are recorded during the summer months (**Figure 5.19**) (SAWS 2014).

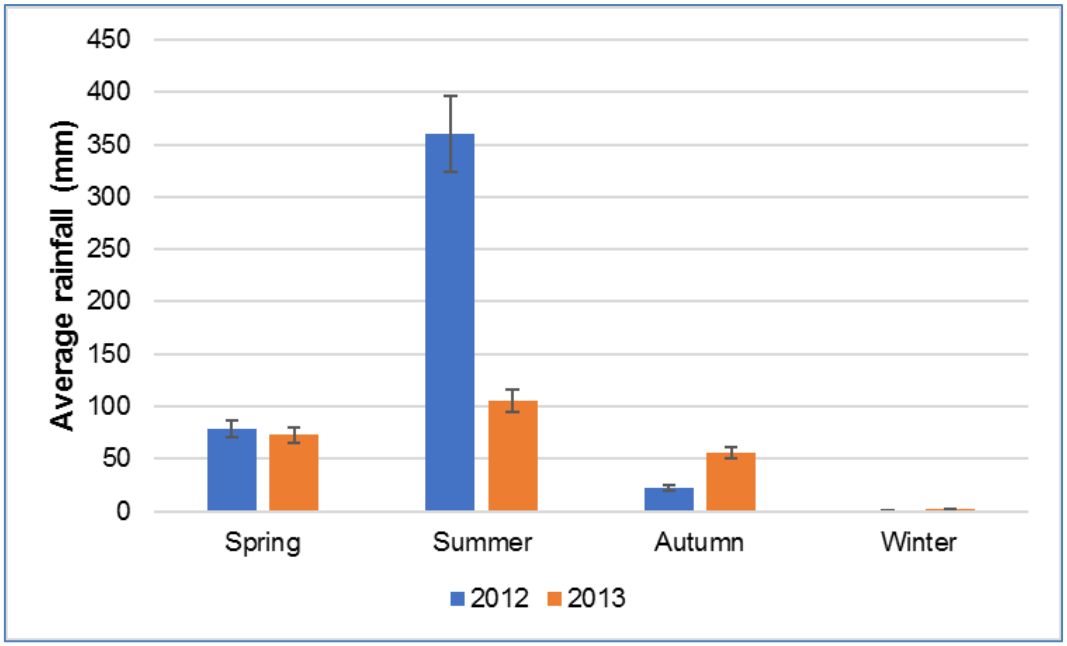


Figure 5.19 Differences in the average rainfall figures for Spring, Summer, Autumn and Winter 2012 to 2014 – Based on information provided by SAWS (2014).

The ACI values were noticeably lower during autumn and winter, due to reduced TOW. The difference between the mean and SD (standard deviation) ACI values for autumn and winter was also statistically insignificant (t = 0.4 and P is 0.7, which is not significant at P > 0.05). Moreover, the higher sum totals of the measured seasonal ACI values (**Figure 4.19**) at Aeroport, Alexandra, Brakpan, Kagiso-Randfontein, Midrand, Nasrec and Ruimsig, when compared to the other sites, was of less importance. Nonetheless, the reduced value at Delta Park may likely be since this site is in a wooded, residential area. Consequently, the impact of atmospheric-bound pollutants on the corrosivity of the surrounding environment would have been reduced, in particular, because of the lower levels of smoke and dust particulates in this area. Confirmation in this regard was provided by the SAAQIS system (DEA 2017a), which indicated reduced PM_{10} particulate, NO_2 and NO concentrations (**Figures 3.23**, **3.25 & 3.28**) for Delta Park.

Important is that the Delta Park test site, belonging to the Air Quality Monitoring Group of the City of Johannesburg Metropolitan Municipality, is used as a background monitoring station - due to its below average pollution levels. This notion is supported by the reduced PM_{10} levels for Delta Park (**Figure 5.20**) (DEA 2017a), compared to various other locations in and around Johannesburg.

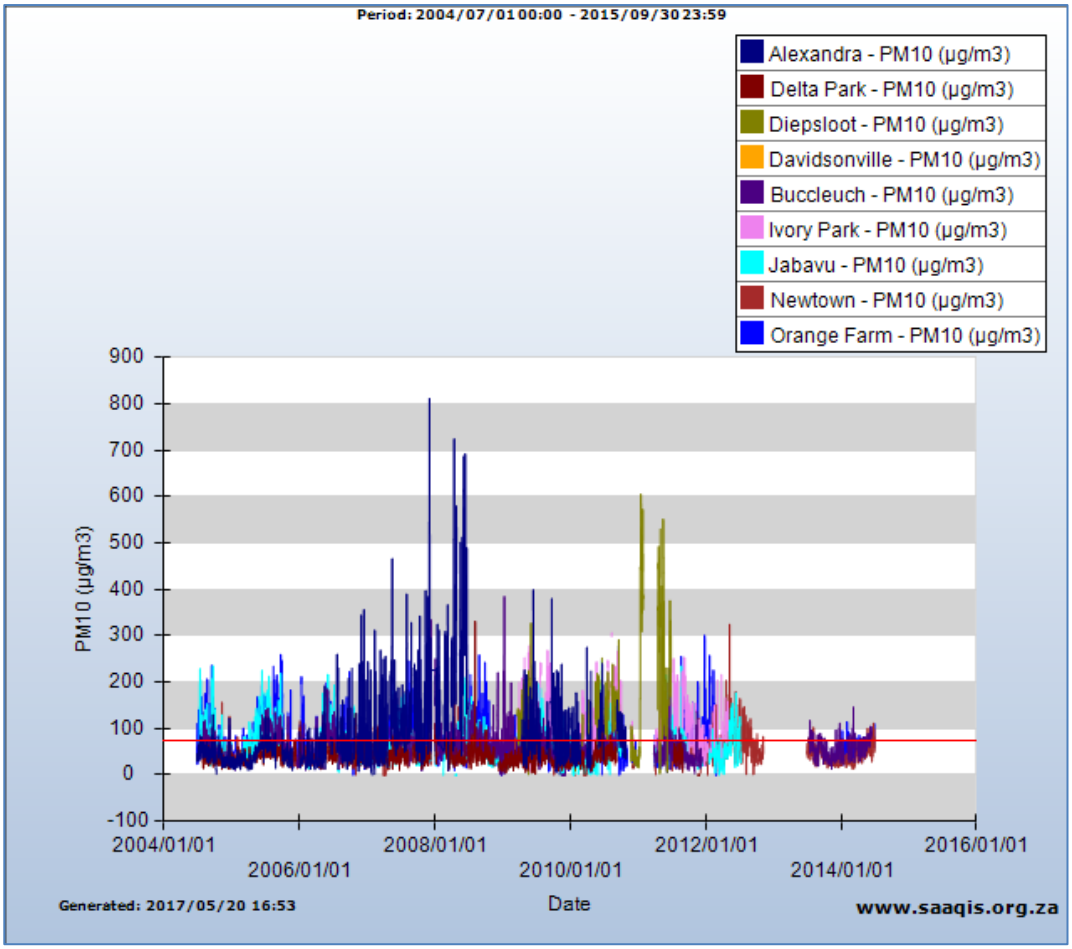


Figure 5.20 Measured PM_{10} levels for the air quality monitoring sites of the City of Johannesburg Metropolitan Municipality - during July 2004 to September 2015 (DEA 2017a).

The removal of air pollutants by leaf stomata and plant surfaces was reported by Nowak in 2002. Nowak mentioned that even though certain particles may be absorbed into the trees, some are retained on the plant surfaces, which are subsequently washed off by rain and deposited onto the ground. Consequently, vegetation merely acts as "*a temporary retention site for many atmospheric particles*". The amelioration of air pollution by vegetation has also been confirmed by researchers in Australia (Bell 1982). However, Bell (1982) also contended that the trees might merely prevent the corrosion specimens from getting wet.

Conversely, at the Kagiso-Randfontein site, the higher overall ACI value (**Figure 4.19**), was likely due to the elevated levels of dust and amorphous carbon on the surfaces, (**Figures 4.48 & 4.54**), promoting the wetting of surfaces.

Other locales that exhibited below average ACI values included Chamdor, Chloorkop, Alrode, Orange Farm, and Kya Sand. However, the mean ACI value for all the main sites (as measured during the first twelve months of the 24-month study period) was 0.05 ± 0.1, 95% CI [0.04, 0.05] or NEGLIGIBLE, based on the CLIMAT test ACI corrosivity classification system (**Table 2.1**) (Carter 1982).

The differences in the East Rand, West Rand, Northern and Southern Suburbs of the GJMA, were also of less importance (**Figure 4.22**). Conversely, the yearly ACI averages were noticeably lower for those suburbs located in and around the CoJ, which was likely attributable to the reduced pollution levels at Delta Park – skewing the results.

5.2.1.4 Summary, correlations and preliminary mapping of the CLIMAT data

Figure 5.21 provides a synopsises of the seasonal average ICI, MCI and ACI values measured at the GJMA main sites. (See also **Appendix G – Table G.1**). As revealed, the differences between the average ICI, MCI and ACI values for spring and summer, versus for autumn and winter, were statistically meaningful, as mentioned above. Conversely, the changes in the average ICI and MCI for spring vs summer was insignificant (P = 0.93, 95% CL and P = 0.17, 95% CL), including during winter and autumn (P = 0.06, 95% CL and P = 0.54, 95% CL).

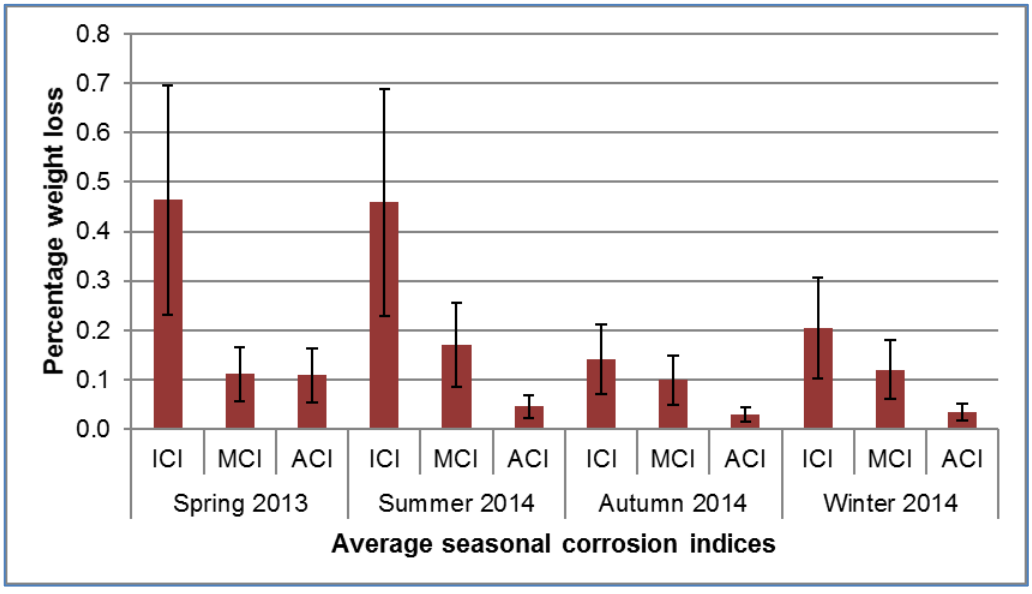


Figure 5.21 Average seasonal variations in the ICI, MCI and ACI values for the GJMA atmosphere, over the period September 2013 (spring) to September 2014 (winter).

The similarity of the average MCI results for the GJMA during spring, summer, autumn and winter also implies that this galvanic couple is less suitable for the measurement of the seasonal fluctuations of industrial (non-marine) environments. In opposition, the higher average ACI value during spring was of statistical importance ($P < 1 \times 10^{-5}$, 95% CL), not only due an increase in moisture in the air (**Figures 3.10 - 3.11**, **3.13 - 3.14**) (SAWS 2014, 2017), but also due to slightly elevated pollution levels (carried-over from wintertime) (**Figures 3.23 - 3.25**, **3.28 - 3.29. 3.31**) (DEA 2017a), as well as a potential lag of surface temperatures (**Figures 3.7 - 3.8**) (SAWS 2017) causing condensation due to a likely delayed effect. These results signified the critical roles that moisture/TOW, pollution and temperature play in atmospheric corrosion.

The strength of a linear association (PPMC) between the ICI and MCI results was very high, $r = 0.89$ ($P \leq 0.01$). However, concerning the average MCI vs ACI and ICI vs ACI data, -0.13 and -0.08, respectively, the slightly negative correlations were determined as unimportant ($P > 0.05$). These associations are also illustrated in **Figures 5.22 - 6.24**, presenting preliminary mapping of the CLIMAT data.

The high PPMC correlation between the *aluminium-copper* (ICI) and *aluminium-mild steel* (MCI) galvanic couples suggested that these units were both influenced by Cl^-, SO_2 and moisture in the GJMA atmosphere. According to studies conducted by Morcillo et al. (2010), damage functions between the *Al-Fe* (MCI) and *Al-Cu* (ICI) couples, and environmental parameters showed similar, although slightly higher, correlation of the MCI unit with Cl^- concentration, C = 0.185 + 0.065 MCI, with R – 0.93, versus for the ICI couple, C = 0.315 + 0.059 ICI (R – 0.91). Conversely, the damage function for the *aluminium-nylon* couple (ACI) was given as C = 0.097 + 0.003 ACI, with R-value 0.82. Therefore, all three indices are influenced by Cl^- in the atmosphere. However, as shown in **Figure 5.25**, the ICI and MCI galvanic-couples reacted more intensely towards corrodents in the atmosphere, compared to the ACI wire-on-bolt units. Also, worth mentioning is that the presence of Cl^- and SO_4^{2-} in soil deposits, as well as dust layers on the test surfaces, could correspondingly have triggered higher ICI and MCI results.

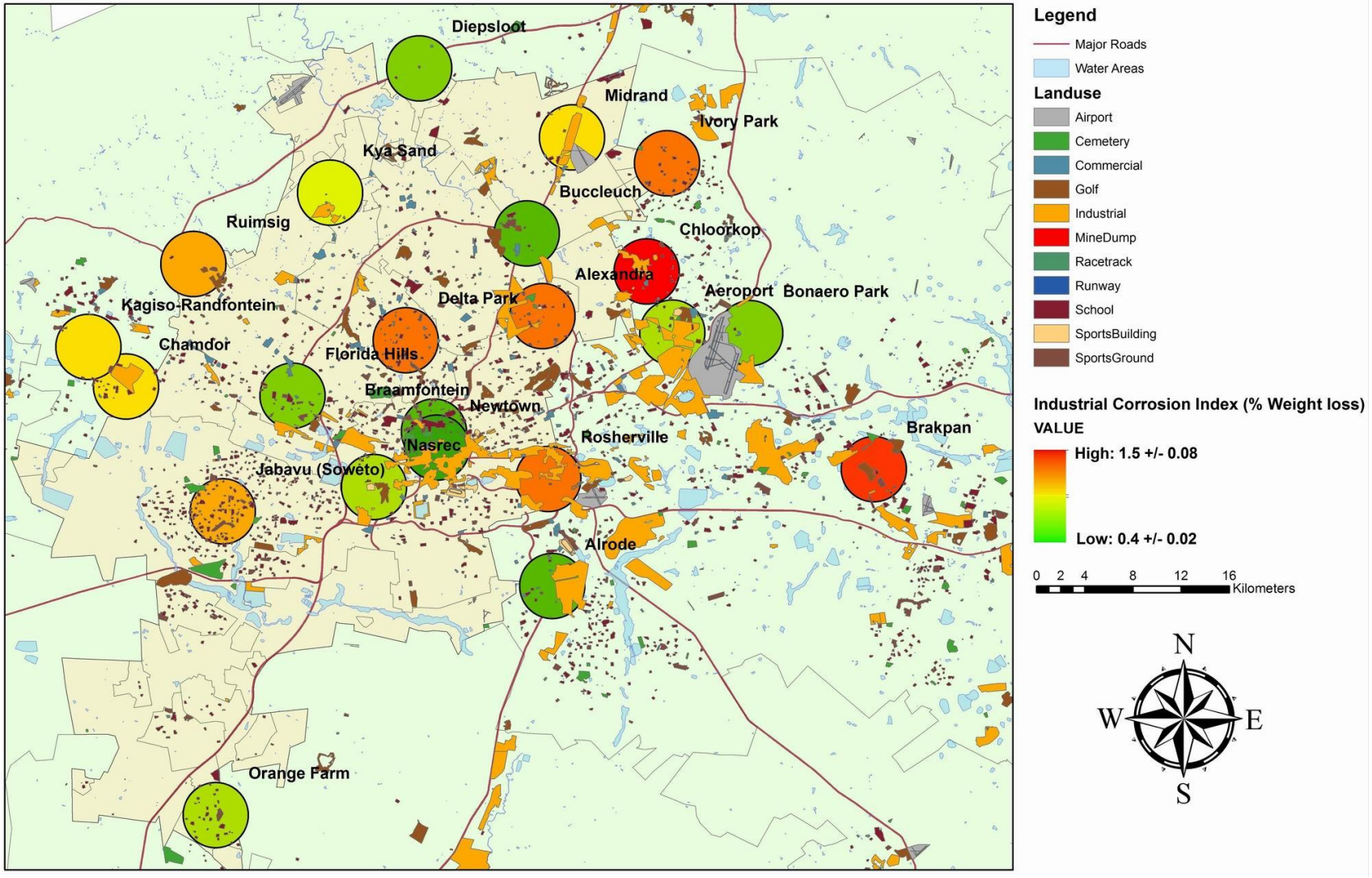


Figure 5.22 Map representation of the yearly average ICI values of the GJMA. (Base map – ArcGIS).

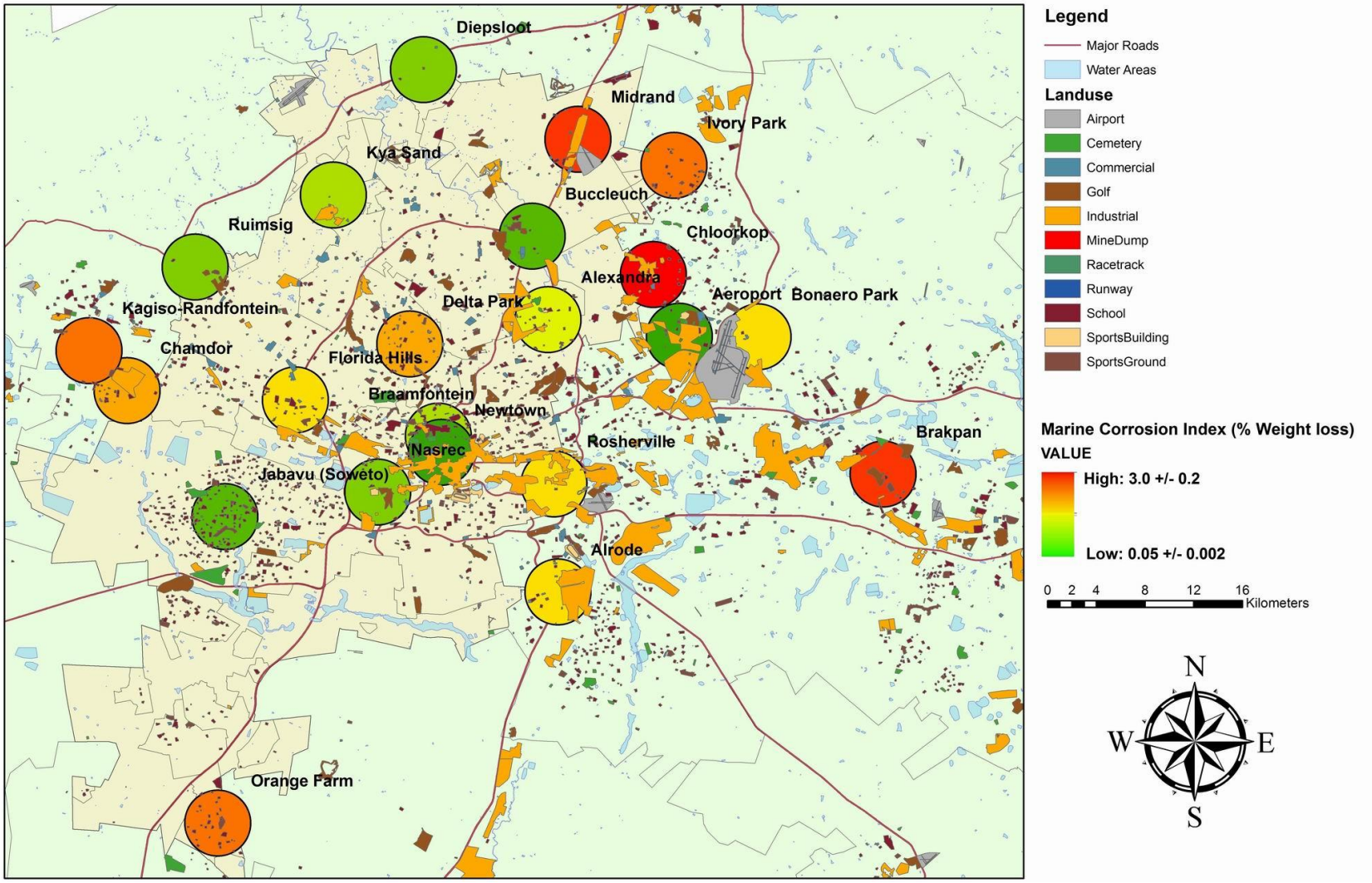


Figure 5.23 Map representation of the yearly average MCI values of the GJMA. (Base map – ArcGIS).

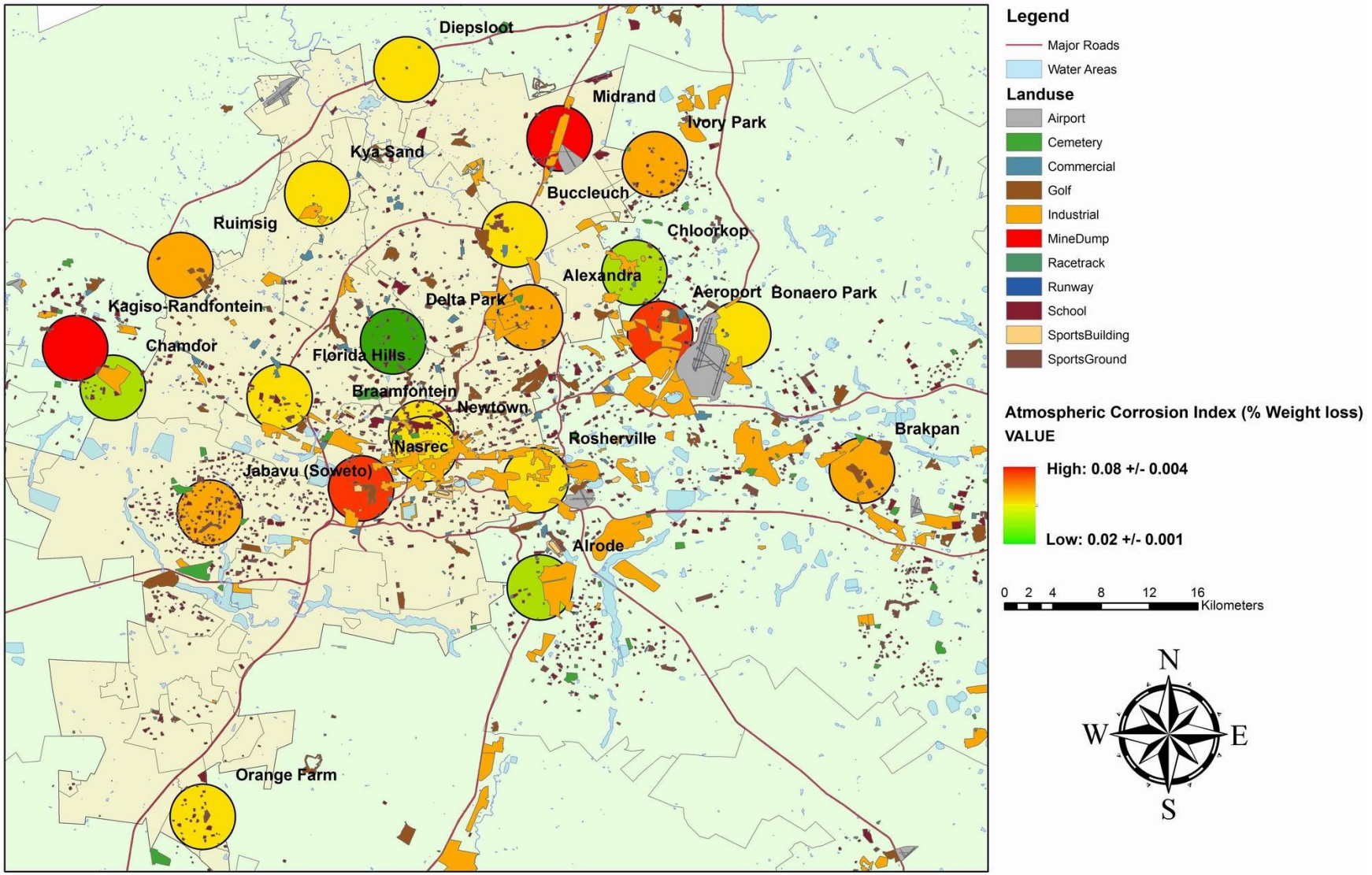


Figure 5.24 Map representation of the yearly average ACI values of the GJMA. (Base map – ArcGIS).



(a) (b) (c)

Figure 5.25 Close-up views of the (a) aluminium vs copper, (b), aluminium vs mild steel, and (c) aluminium vs nylon surfaces of the wire-on-bolt units exposed at the Brakpan site during Spring 2013 – Note that the white deposits are the corrosion products of the aluminium wires.

The *aluminium-nylon* couple was ostensibly less sensitive towards fluctuating pollution levels in the atmosphere, and imprecise when it came to providing distinctive comparisons between the different sites. Nonetheless, it remained a useful tool for measuring the changing moisture levels in the atmosphere, specifically from one season to the next.

Conversely, from a seasonal perspective, only very slight negative correlations were determined for the ACI vs ICI data for spring (r = -0.11, P > 0.05) and summer (r = - 0.09, P > 0.05), while during the winter months, this negative relationship was somewhat stronger (r = -0.35, P > 0.05), although still statically unimportant. In contrast, the correlation between the ACI and ICI data shifted towards a more positive trend during autumn (r = 0.15, P > 0.05), but was also arithmetically inconsequential. These findings potentially suggested that while precipitation and moisture in the atmosphere will undoubtedly promote the wetting of surfaces and therefore, corrosion, it also exhibits a cleaning effect, particularly during winter, when irregular rainfall may occur. Be this as it may, winter is also the period when the precipitation levels in the Greater Johannesburg are at their lowest (**Figures 3.13 & 3.14**) (SAWS 2017). Contrary to the above findings, the cleaning effect of water appears less pronounced during autumn. Montgomery et al. (2011) also described this phenomenon, namely that rain rinses away pollutants, mist deposits more pollutants, while dew reactivates surface contaminants.

5.2.2 Aluminium, Zinc, and Copper Wire Helix (WH) Corrosion Rates

5.2.2.1 Aluminium helices (Al-WH)

The mean 12-month Al-WH corrosion rate in the GJMA area measured 0.2 ± 0.1 μm/a, 95% CI [0.1 μm/a, 0.2 μm/a], which, as per Li et al. (2013), is typical for a rural to urban environment. It is also like San Juan (Argentina), Birkenes (Norway), Svanwik (Norway), El Pardo (Spain) and Stratford (United Kingdom) (Knotkova et al. 2010). Sites that exhibited higher than average values included Aeroport, Alrode, Bonaero Park, Braamfontein, Brakpan, Buccleuch, Chloorkop, Ivory Park, Kagiso-Randfontein, Orange Farm, and Rosherville (**Figure 4.23**) - all located in the north-eastern, eastern and south-eastern parts of the GJMA.

The notable higher 12-month Al-WH corrosion rates measured at Kagiso-Randfontein and Chloorkop suggested (like the CLIMAT results) (**Figures 4.18 & 4.19**) that these sites are 'hotspots' regarding the general corrosivity of the GJMA. Sites which exhibited the lowest 12-month Al-WH corrosion rates were Alexandra, Delta Park and Ruimsig - with an average rate of 0.03 ± 0.02 μm/a, 95% CI [0.0 μm/a, 0.06 μm/a]. Of the 22 main sites tested, six (27%) coincided with the *moderate* (C3) corrosivity category, while the remaining 16 (73%) locales could all be rated *low* (C2) corrosive (as per the ISO 9223:1992) (**Table 2.2**) (International Organization for Standardization (2012a).

In relationship with the yearly mean ICI, MCI and ACI data for the various locations, the dependency (PPMC coefficient) of the 12-month Al-WH corrosion rates, calculated 0.44 ($P \leq 0.05$), 0.58 ($P \leq 0.05$) and 0.26 ($P > 0.05$), respectively (**Appendix K**), which were statistically meaningful concerning the ICI and MCI results. These relationships suggested that the 12-month corrosion rates of aluminium wire correlated better with the MCI values, rather than with the ICI or ACI data, and was likely most affected by Cl^- in the atmospheres. Aside from this, the impact of other general pollutants was also evident, as shown by the weak to medium positive correlation for the Al-WH corrosion rates versus the ICI data.

According to Leitch (2006), ISO open wire helix units are more sensitive to pollution than CLIMAT units, particularly about the zinc wires. This is because open wire coils tend to catch corrodents from all directions and exhibit high mass loss sensitivity (Leitch

2006; Knotkova et al. 2010). Nevertheless, like CLIMAT units, WH devices are affected by TOW, SO_2 and salinity (Cl^-). They furthermore provide indications about the corrosivity of different environments due to these factors. During the ISOCORRAG programme (Knotkova et al. 2010), it was found that the corrosion rate of the zinc wire helix was more accelerated by SO_2, the copper wire more by Cl^-, while the aluminium wire was mostly affected by Cl^- and SO_2 in the atmosphere.

Figure 4.26 shows the average 12-month Al-WH values for the different regions of the GJMA. As indicated, the highest mean value was measured on the East Rand (especially at Chloorkop), followed by the Southern Suburbs. In the West Rand, however, Kagiso-Randfontein displayed the highest 12-month result. In the case of the Chloorkop site, the presence of Cl^- was detected on the metal surfaces, whereas pertaining to the Kagiso-Randfontein locale, the increased value was associated with the presence of mine dust (likely crystalline silica dust) (Azue 1999) on the metal surfaces (**Figure 4.38**).

Following Annegarn et al. (1987), regarding the composition and size of individual particles from a gold mine atmosphere in South Africa, silicon-rich particles were found to be the most abundant overall, while chlorine-rich particles dominated (up to 80%) in the range 0.2–1.0 µm. However, studies conducted by Malatse & Ndlovu (2015) have revealed no Cl^- in the gold mine tailings from the Witwatersrand, but typically contain high levels of Si and Al, about 78% and 10%, respectively. The Kagiso-Randfontein site was also located near an active brick manufacturing facility, which would have added to the production of dust and ash (Malatse & Ndlovu 2015). According to DEA (2011), brick manufacturing is listed as a major contributor to PM_{10} and SO_2 pollution in the Highveld.

5.2.2.2 Zinc Helices (Zn-WH)

The average 12-month Zn-WH-rate for the GJMA area measured 0.8 ± 0.3 µm/a, 95% CI [0.6 µm/a, 0.9 µm/a], which was lower than reported for many other urban environments (Li et al. 2013). However, it was like San Juan (Argentina) and Judgeford (New Zealand) (Knotkova et al. 2010). Sites exhibiting higher than average 12-month Zn-WH corrosion rates, included Aeroport, Braamfontein, Brakpan, Buccleuch, Chamdor, Chloorkop, and Kagiso-Randfontein (**Figure 4.24**).

Like the aluminium results, the 12-month corrosion rates of the Zn-WH units at the Chloorkop and Kagiso-Randfontein sites were elevated in comparison with the other locales. This outcome substantiated the conclusion that these locations were potential 'hotspots', with higher levels of corrodents present in the atmosphere. Sites that indicated low 12-month Zn-WH corrosion rates involved Delta Park, Diepsloot, and Kya Sand, which is likely due to reduced SO_2 and water-soluble salts levels in the atmosphere (**Figure 3.24** (DEA 2017a) and **Figures 4.36 & 4.38**). These sites are located north and north-west of Johannesburg's CBD. Of the 22 main sites tested, twelve (54%) fell into the *moderate* (C3) corrosive category, while the remaining ten locales (46%), rated *low* (C2) corrosive (**Table 2.2** - International Organization for Standardization 2012a).

The findings mentioned above differ somewhat from those derived by Leitch (1999, 2003, 2006) during his analyses of atmospheric corrosion data for the Highveld region. As stated by this scholar, the Highveld area rated "*surprisingly high*", "*C3 overall but with a rating of C4 at specific centres of industrial or chemical plant activity*", for example, the Highveld urban and industrial areas. However, based on the latest data, which represent 22 sites and consequently, a far higher level of certainty, it is evident that Leitch's rating for the region was too high, although it was still an improvement on the values given by Callaghan (1991).

Compared to the yearly mean ICI, MCI and ACI values for the different sites, the PPMC coefficients (*r*) of the 12-month corrosion rates of the zinc wire measured 0.37 ($P \leq 0.10$), 0.41 ($P \leq 0.10$) and 0.32 ($P > 0.10$), respectively (**Appendix K**). However, the relationships were only found to be statistically meaningful for the ICI and MCI data, within a 90% CL. Apart from the ACI vs Al-WH relationship, the ICI vs Zn-WH and MCI vs Zn-WH values were also slightly reduced compared to the ICI vs Al-WH, and MCI vs Al-WH data.

From a regional viewpoint (**Figure 4.27**), the most elevated 12-month Zn-WH corrosion rates were determined at Chloorkop (East Rand) and Kagiso-Randfontein (West Rand), associated with increased industrial and mining activity in these areas.

5.2.2.3 Copper Helices (Cu-WH)

The average 12-month corrosion rate of copper wire in the GJMA area measured 0.6 ± 0.2 μm/a, 95% CI [0.5 μm/a, 0.6μm/a], which was like the zinc values, lower than typically reported for urban and industrial areas (Li et al. 2013). However, it corresponded to copper wire helix measurements taken at Iguazu, a rural area with a high waterfall in Argentina (Knotkova et al. 2010). Nevertheless, the average corrosion rate of the copper wire was still about four times higher than that of the Al-WH wires.

Kagiso-Randfontein, followed by Chloorkop, Brakpan and Alrode displayed the highest 12-month corrosion rates of copper (**Figure 4.25**). Of importance was the increased corrosion rate of copper at the Kagiso-Randfontein site, when compared to the Chloorkop locale, justified by the presence of significant levels of dust (gold mine tailings) on the former locale surfaces (**Figure 4.38**), promoting TOW and exhibiting not only reduced pH (**Figure 4.37**), but also higher levels of sulphur-bearing corrodents (**Figure 4.38**).

Furthermore, the high disparity relating to the 12-month corrosion rates of copper wire at the Kagiso-Randfontein versus the Chloorkop, Alrode and Brakpan sites signified that the copper wire helices were less affected by Cl^- in the atmosphere than the aluminium and zinc wire coils. While this result opposed Knotkova et al.'s (2010) findings that Cl^- accelerate the corrosion rate of the copper wire helix more, it agreed with the latest CLIMAT ICI data, as well as with other researchers (Leygraf 2016) that copper tends to react more with sulphur-based pollutants.

In keeping with Leygraf et al. (2016), the sensitivity of aluminium, zinc and copper to corrosive atmospheric species are given in **Table 5.6**, showing that copper tends to be more susceptible to sulphur-borne corrodents. Yibas et al. (2010) report that FeS_2 (pyrite) in the gold mine tailings of the Witwatersrand can react with H_2O and O_2, to produce H_2SO_4 and $FeSO_4$ (iron sulphate).

Sites with the lowest 12-month corrosion rates of copper wire were Alexandra, Diepsloot and Kya Sand. Of all the 22 main sites tested, 36% (eight) fell into the *moderate* (C3) corrosive category, while the remaining 14 locales (64%) rated *low* (C2) corrosive (as per ISO 9223 - International Organization for Standardization 1992a). This finding again reinforced the earlier deduction that the rankings by Leitch (1999, 2003, 2006) and

Callaghan (1991) for the corrosivity of the Highveld region, were somewhat inflated. The PPMC coefficients of the 12-month corrosion rates of copper wire versus the mean ICI, MCI and ACI values for the different sites, were 0.36 ($P > 0.10$), 0.43 ($P \leq 0.10$) and 0.28 ($P > 0.10$), respectively (**Appendix K**), which were somewhat reduced compared to the relationships determined for the Al-WH and Zn-WH, vs the CLIMAT ICI and MCI data.

Table 5.6 Sensitivities of iron, aluminium, zinc and copper to corrosive atmospheric species (after Leygraf et al. 2016).

Corrosive species	Aluminium	Zinc	Copper	Iron
CO_2/CO_3^{2-}	-	M	-	M
NH_3/NH_4^+	L	L	M	L
NO_2/NO_3^-	L	M	M	M
H_2S	L	L	H	L
SO_2/SO_4^{2-}	M	H	H	H
HCl/Cl^-	H	M	M	H
$RCOOH/COOH^-$	L	M	M	M
O_3	N	M	M	M

Note: L denotes low, M – medium and H – high.

Regionally speaking (**Figure 4.28**), the highest 12-month corrosion rates of copper wire were measured on the East Rand (at Chloorkop and Brakpan), as well as in the southern parts of the GJMA, at Alrode. Conversely, while the Northern Suburbs exhibited the lowest 12-month corrosion rates of copper wire overall, Buccleuch, Midrand, and Ivory Park indicated slightly higher values compared to the other sites, also located in the North (**Figure 4.29**). Worth noting is that the former areas are all positioned near one another (**Figure 3.1**) and likely influenced by chloride emissions from the Chloorkop area.

5.2.2.4 Statistical analyses and preliminary mapping of the Al-WH, Zn-WH and Cu-WH data

Figure 4.30 presents summations ($\sum$) of the average 12-month corrosion rates of the WH (aluminium, zinc and copper wire) units. By and large, the wire helices results (aluminium, zinc and copper combined) indicated that Kagiso-Randfontein, Chloorkop, Brakpan, Aeroport, Alrode, Braamfontein, Buccleuch, Chamdor and Rosherville were

potentially more corrosive than the other sites. This was because these locales are associated with increased industrial, mining and vehicle-related activity in the GJMA.

PPMC coefficients for the Al-WH vs Zn-WH, Al-WH vs Cu-WH, and Zn-WH vs Cu-WH data for the different areas measured 0.87 ($P \leq 0.01$), 0.81 ($P \leq 0.01$) and 0.88 ($P \leq 0.01$), respectively (**Appendix K**). As shown, these relationships were statistically meaningful within a 99% CL and are also illustrated in **Figures 5.26 - 5.28**.

The high correlations supported International Organization for Standardization's (1992a) original approval that each of the aluminium, zinc or copper helix corrosion rates could be used to assign the ISO 9223:1992 corrosivity category (like **Table 2.2**, however, excluding the Extreme CX category). However, the results also revealed that the rankings per site, based on the 12-month corrosion rates of the different open wire helices, do not always coincide. Consequently, Leitch (2003) admitted being somewhat biased regarding the zinc results, which clarified why he classified the corrosivity of the GJMA as C3 corrosive since the Zn-WH units would have measured higher corrosion rates.

During the ISOCORRAG study, which included comparisons of the atmospheric corrosion rates of the metal plate and open wire helix specimens (Knotkova et al. 2010), it was found that the open wire helices exhibited significantly higher corrosion rates than flat metallic panels. Knotkova et al. (2010) ascribed this difference to the fact that the helices are more effectual at accumulating gaseous and particulate pollutants.

Moreover, smaller diameter wires were found to exhibit higher corrosion rates than larger diameter wires. Consequently, the ISOCORRAG Working Group decided to exclude the open wire helix specimen procedure from the ISO 9226:2012 revised standard (International Organization for Standardization 2012d).

The withdrawal of these procedures was unfortunate, since as Leitch (2003) adequately puts it, "*the ISO unit is akin to a guerrilla fighter when compared to fixed long-term corrosion test racks. It is a short-term exposure, relatively cheap to make, easy to place at a site, and relatively easy to camouflage or hide from theft*". The latter benefit is particularly of relevance in South Africa.

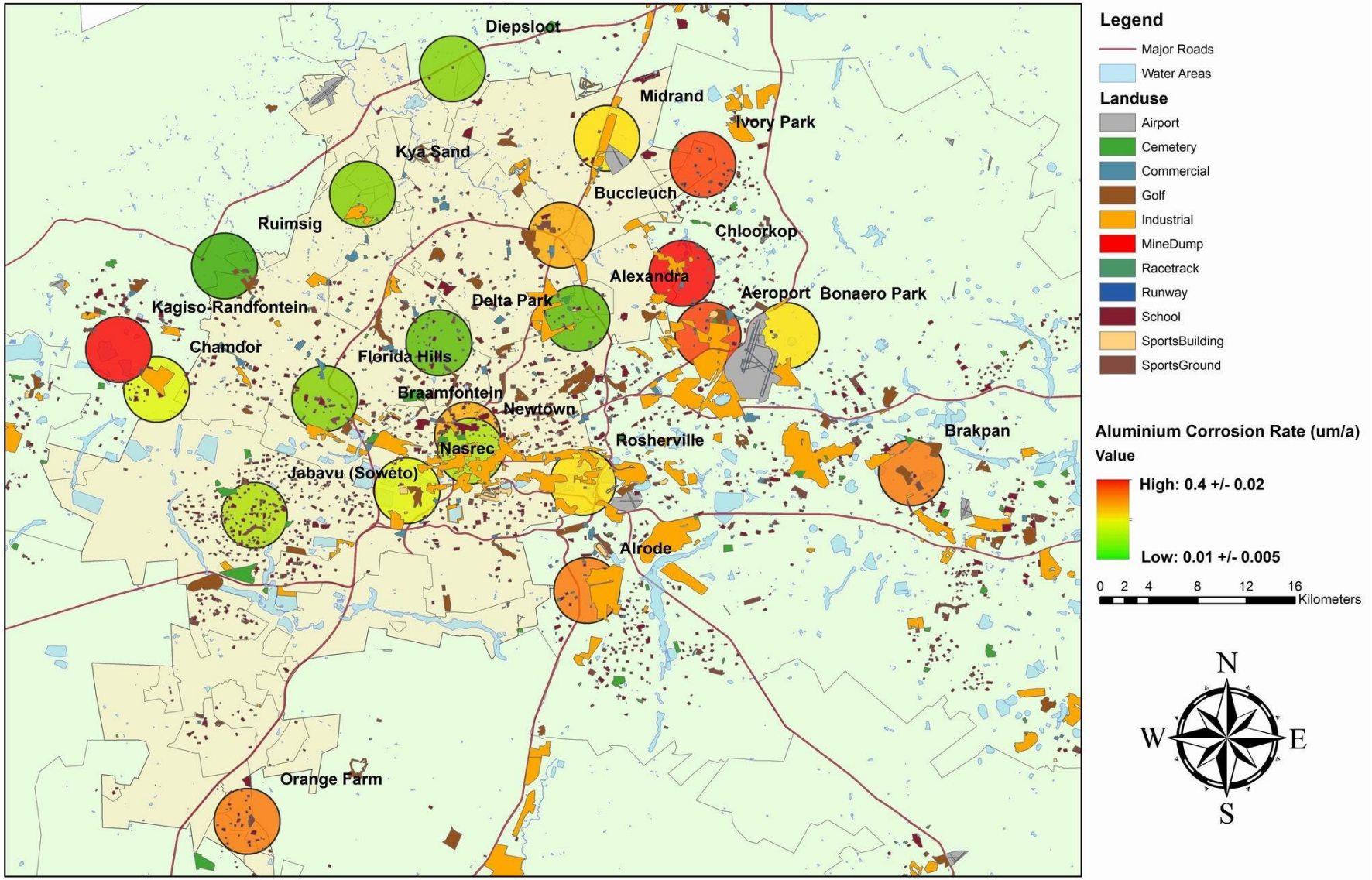


Figure 5.26 Map representation of the 12-month corrosion rates of aluminium helices in the GJMA. (Base map – ArcGIS).

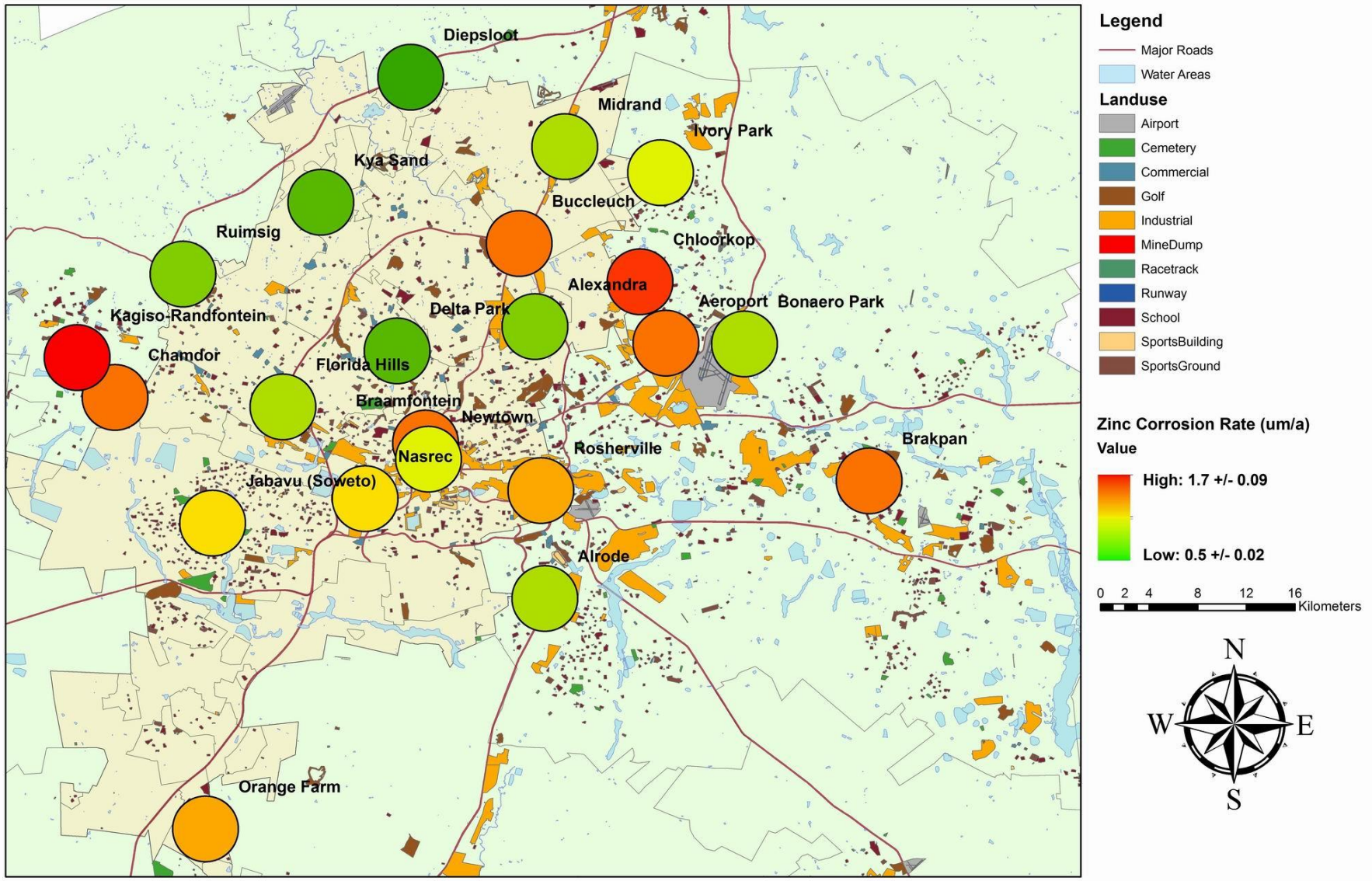


Figure 5.27 Map representation of the 12-month corrosion rates of zinc helices in the GJMA. (Base map – ArcGIS).

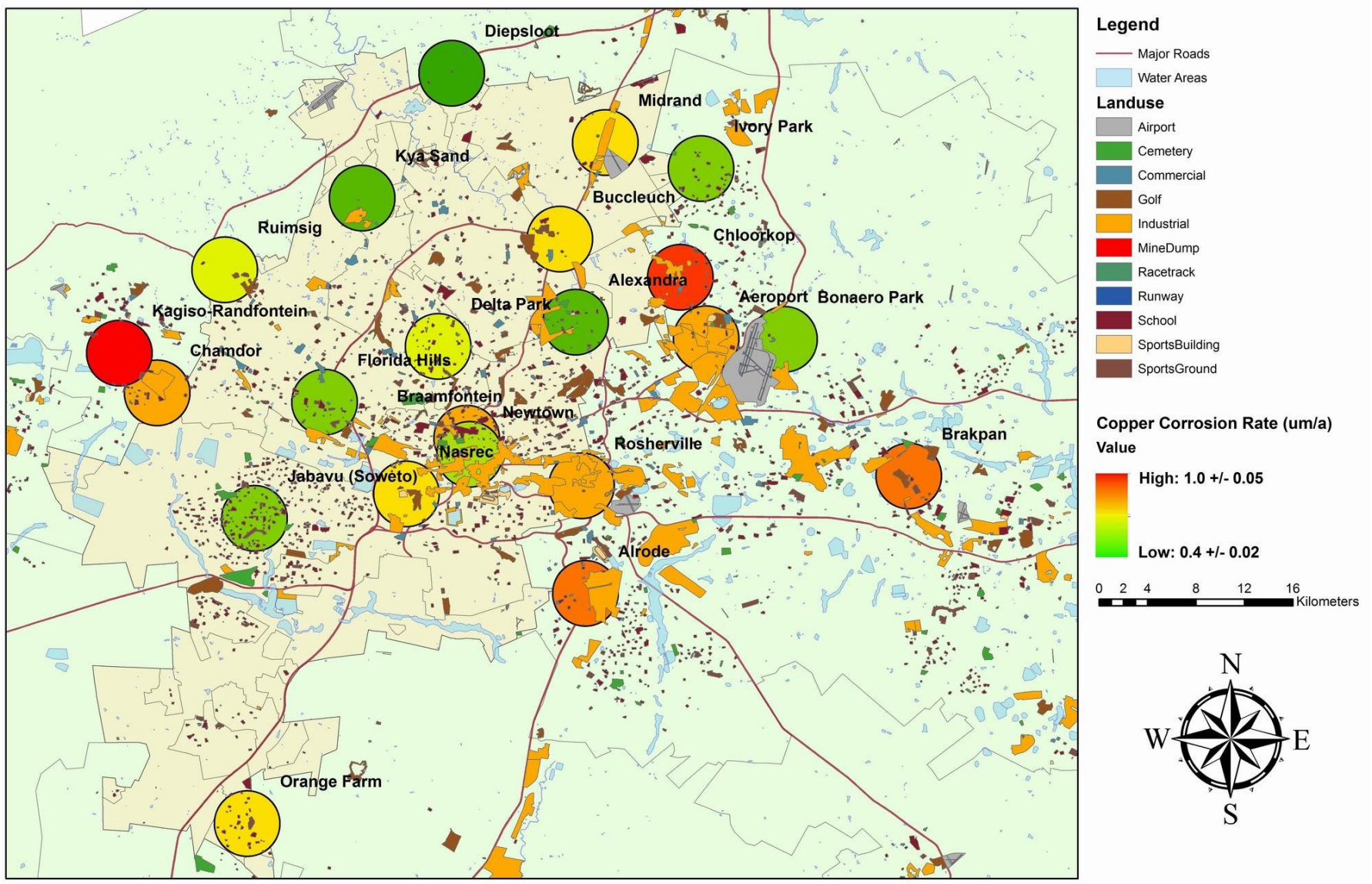


Figure 5.28 Map representation of the 12-month corrosion rates of copper helices in the GJMA. (Base map – ArcGIS).

5.2.3 Mild Steel (MSP) Corrosion Rates – Main Sites

Noteworthy is the similarity of the corrosion rates of each duplicate set of mild steel samples (**Appendix I - Figure I.1**), differing by about 4-5% or 1-4 μm/a, 95% CI [2.5 μm/a, 5.0 μm/a] on average - confirming a high degree of certainty for the measured corrosion rates of the mild steel specimens at the different sites. This value coincided with Knotkova et al.'s (2010) reported margin of uncertainty for the measurement of the 12-month corrosion rate of carbon steel at 53 countries using the ISO 9226 flat metal procedure (International Organization for Standardization 1992d). The average 6-month corrosion rate (Spring 2013 and Summer 2014) of mild steel in the study area, measured 31 ± 7 μm/a, 95% CI [28 μm/a, 35 μm/a]. The highest rates were measured at Kagiso-Randfontein, Brakpan, Bonaero Park, Aeroport and Chloorkop, whereas the lowest values were determined at Newtown, Diepsloot and Alexandra.

Of interest is that two of the sites are near OR Tambo International Airport, signifying a potential influence of the airport on the corrosivity of the GJMA. The possibility of airports as local corrosion 'hotspots' have been mentioned by Bell in 1982, as well as queried by Leitch in 2000, in an open internet discussion. In answer to John Leitch's enquiry, Robert Baboian (2000) confirmed that they had carried out corrosion studies of motor vehicles at parking lots near an airport in Montreal, over several years. During this investigation, it was found that at a new car dealership, which was located at the end of the runway, the metallic trims of the vehicles, comprising Type 434 stainless and chrome plated steel, showed signs of pitting and crevice corrosion after a brief time in the lot. The corrosion was attributed to emissions from the aircraft jet engines.

Although the attribution of Aeroport's and Bonearo Park's elevated corrosivities to the nearby airport activities may appear speculative, studies have shown that the combustion of aviation fuel, mostly kerosene, produces NO_x, CO and SO_x, hydrocarbons and particulates. The greenhouse gas CO_2 is also produced. Furthermore, fuel dumping often occurs near airports, which is a source of VOC (Aviation Environment Federation (UK) 2000-2018).

Moreover, in the present study, the presence of oil-like stains was found on the mild steel panels exposed at two of the sites near the airport, Aeroport and Eastrand Mall, the latter 'mini' site positioned within 500 m from the OR Tambo International Airport

(**Figure 5.29**). Also, the Aeroport and Bonaero Park locales showed higher gloss and colour changes compared to the other GJMA sites (**Figures 4.52 & 4.53**). However, further investigations are required in this regard.

Excluding the Buccleuch locale, the 6-month corrosion rates of mild steel exhibited weak PPMC coefficients, 0.33 ($P > 0.10$), 0.39 ($P \leq 0.10$) and 0.20 ($P > 0.10$) with the average CLIMAT ICI, MCI and ACI values (for Spring 2013 to Summer 2013-2014), respectively. However, the only correlation that was meaningful within a 90% CL was the MCI data vs the 6-month MSP values. Conversely, the correlations between the Al-WH, Zn-WH and Cu-WH, versus the MSP values, were much stronger, 0.72 ($P \leq 0.05$), 0.75 ($P \leq 0.05$) and 0.80 ($P \leq 0.05$), respectively (**Appendix K**). These higher associations implied that the WH data compared more favourably with the MSP corrosion rates and affirmed that CLIMAT test data should preferably be used as guidance only and to evaluate seasonal corrosivity fluctuations.



(a) (b)

Figure 5.29 The Eastrand Mall site located next to OR Tambo International Airport. Note the presence of the low-flying aircraft and the oil-like stains on the mild steel panel surface.

The slightly weaker relationship between the Al-WH (12-month) and MSP (6-month) corrosion rates, may be attributable to the fact that aluminium tends to experience localised corrosion attack (Callaghan 1991; Morcillo et al. 2012; Melchers 2015), rather than uniform corrosion, although the latter scenario is used for calculation of the corrosion rate (Knotkova et al. 2010).

Table 4.1 & Figure 4.31 show that between six and twelve months of exposure, the corrosion rate of mild steel at the main GJMA sites decreased by about 36 ± 4% on average, resulting in a mean 12-month value for steel of 20 ± 4 μm/a, 95% CI [18 μm/a, 22 μm/a]. This yielded an overall C2 (*low*) corrosivity rating (**Table 2.2** – International Organization for Standardization 2012a), although to the upper end of this category. The highest variances between the 6-month and 12-month corrosion rates were measured for Brakpan, Chamdor and Jabavu (Soweto), about 44%, 45% and 42%, respectively. Conversely, the lowest differences were recorded for Alexandra and Alrode, approximately 32%.

Ignoring Buccleuch, the PPMC coefficient between the 6-month (spring and summer) and 12-month (spring, summer, autumn and winter) results for the main sites, was 0.96 ($P \leq 0.05$) (**Appendix K**). This very high correlation suggested that a function could be derived (**Equation 5.2**), also shown in **Figure 5.30 (a)**, for the extrapolation of short-term 6-month corrosion monitoring results, to 12-month data - thus enabling the corrosivity rating of other locations in the GJMA.

$$y = 0.5907x + 1.4223 \text{ with } R^2 = 0.91 \qquad \textbf{Eq. 5.2}$$

where:

y is the extrapolated 12-month (r_{corr}) corrosion rate of steel in μm/a; and

x is the measured 6-month corrosion rate of steel in μm/a.

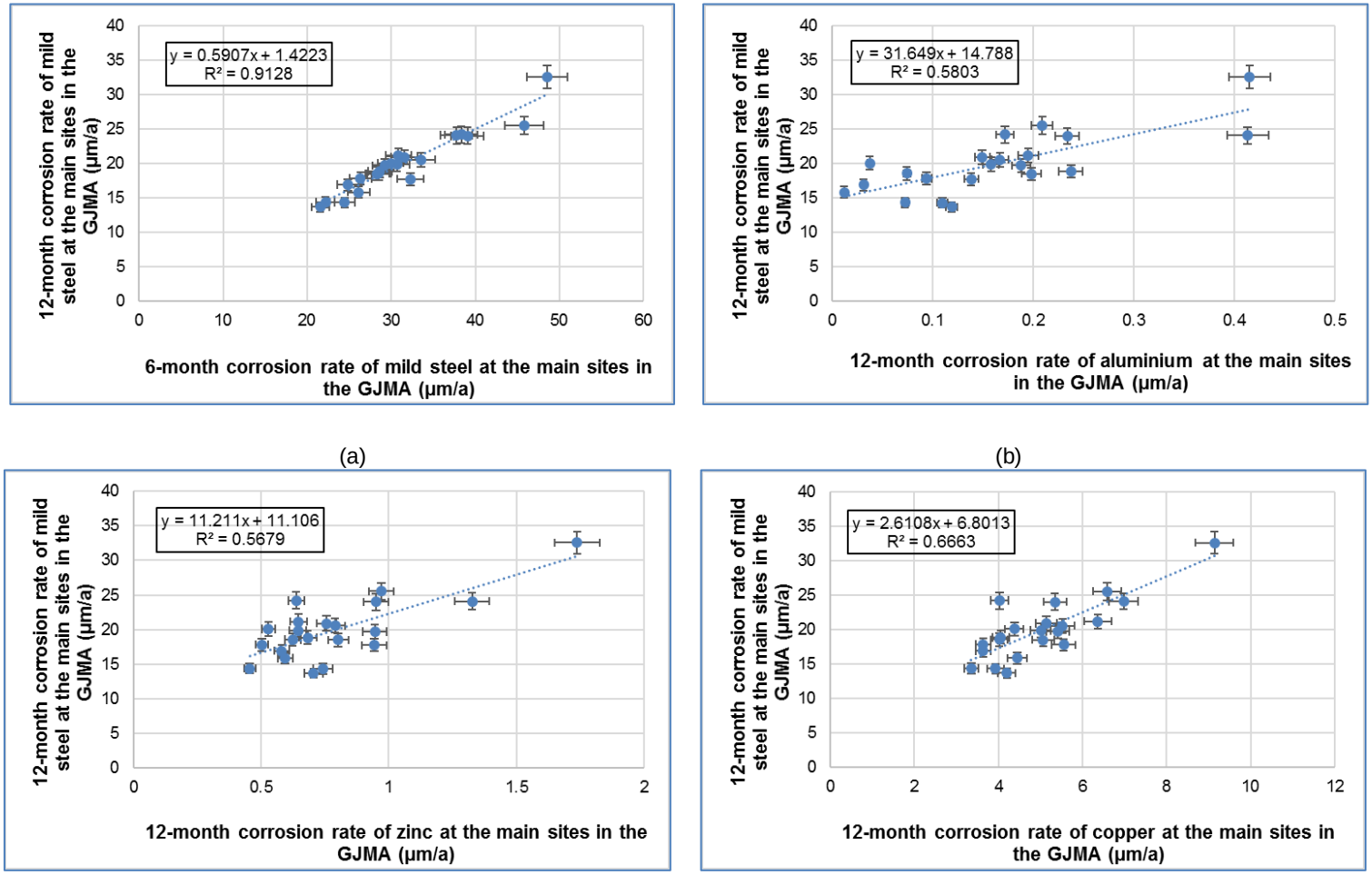


Figure 5.30 Linear regressions of (a) 6- versus 12-month corrosion rates of mild steel, and 12-month corrosion rates of mild steel versus the 12-month corrosion rates of (b) aluminium, (c) zinc and (d) copper, as measured at the main sites in the GJMA.

However, it is essential to keep in mind that the equation will only be applicable for the extrapolation of 6-month corrosion rates of mild steel, measured from the beginning of spring to the end of summer in the GJMA, to 12-month data. Nonetheless, the shortening of any atmospheric corrosion monitoring period allows for significant cost and time-saving benefits.

Omitting Buccleuch, the r_{corr}-values of mild steel at the different sites exhibited weak PPMC coefficients with the mean ICI, MCI and ACI values, 0.31 ($P > 0.10$), 0.35 ($P > 0.10$) and 0.33 ($P > 0.10$), respectively (**Appendix K**). However, these relationships were found to be statistically insignificant. Conversely, the PPMC coefficients for the Al-WH, Zn-WH and Cu-WH, versus the 12-month MSP values, were 0.76 (R^2 - 0.58), 0.75 (R^2 - 0.57) and 0.82 (R^2 - 0.67), respectively (**Appendix K** and **Figure 5.30 b-d**). These associations were slightly better than those relations measured on the same basis for the 6-month MSP results and significant within a 95% CL - affirmative that the WH data compared better with the MSP corrosion rates. Linear regressions of the 12-month corrosion rates of mild steel versus the 12-month-values of aluminium, zinc and copper are presented in **Figure 5.30 (b-d)**.

The close agreement of the Cu-WH with the 6- and 12-month MSP corrosion rates, signify that open wire copper coils may be more reliable regarding the prediction of the short-term corrosion rates of mild steel, compared to aluminium and zinc wires.

However, the use of metal plate specimens for atmospheric corrosion monitoring is still favoured, due to larger test surfaces. Also, worth pointing out is that the thesis presents the first published data for copper helices in South Africa. Moreover, the results were used to estimate the residual life of bronze statues in South Africa - published separately from this thesis (**Appendix T**).

Regarding the 12-month mild steel corrosion data (**Table 4.1**), only Brakpan and Kagiso-Randfontein rated *moderately* (C3) corrosive (**Table 2.2** - International Organization for Standardization 2012a), while all the other sites ranked *low* (C2) corrosive (mid to upper end of this corrosivity category). As stated above, both locales are situated near old gold mine tailing dumps, found to impact on the corrosivity of the GJMA. Other sites that ranked slightly below the C3 corrosive mark were Chloorkop, Bonaero Park and Aeroport - all located on the East Rand, with the latter two areas

situated near Kelvin A and B Power Stations, in addition to being near OR Tambo International Airport.

A separate corrosion study correspondingly confirmed the *moderate* (C3) corrosivity rating of the OR Tambo/Kelvin area. This study conducted by the author (on behalf of a client) in Tunney (an industrial area just south of the Kelvin Power Stations) indicated a 12-month corrosion rate of mild steel of about 27 μm/a (Janse van Rensburg 2015).

Following 18 months of exposure, the mean corrosion rate of mild steel in the GJMA measured 17 ± 4 μm/a, 95% CI [15 μm/a, 18 μm/a] (**Figure 4.32 & Appendix I**), representing a further 17 ± 6% decrease in the overall corrosion rate of this metal. Among the 12- and 18-month corrosion rates, the highest variances were determined for the Braamfontein and Rosherville sites, about 27% and 29%, respectively. Conversely, the lowest differences were recorded at Brakpan, Delta Park and Jabavu (Soweto), approximately 8-9%.

Moreover, it is evident that the Kagiso-Randfontein locale (a West Rand 'hotspot') exhibited the highest corrosion rate of mild steel, nearly 27 μm/a, followed by Brakpan (an East Rand site) at about 24 μm/a.

Of greater significance, however, was the similarity of the average corrosion rates of mild steel after 18 months of exposure at Bonaero Park, Aeroport and Chloorkop, 20 ± 0.5 μm/a, 95% CI [20 μm/a, 21 μm/a], respectively, potentially implying that these sites exhibit similar long-term corrosion trends.

The PPMC coefficient of the 12- vs the 18-month corrosion rates of mild steel at the main sites, was 0.99 ($P \leq 0.01$) (**Appendix K**), revealing that the seasonal and yearly variations in the corrosion rates of steel between the different locations stabilised considerably with time. Linear regressions of the 6- and 18-month, as well as 12- and 18-month corrosion rates of mild steel, given in **Figures 5.31 & 5.32**, signify that extrapolations of the short-term corrosion monitoring results of mild steel, for example 6- 8 months (**Equation 6.2**), and 12-18 months (**Equation 6.3**), are possible, as indicated below:

From 6 to 18 months:

$$y = 0.5102x + 0.6319 \text{ with } R^2 = 0.86 \quad \textbf{Eq. 5.3}$$

where:

y is the extrapolated 18-month corrosion rate of mild steel in μm/a; and

x is the measured 6-month corrosion rate of mild steel in μm/a.

From 12 to 18 months:

$$y = 0.856x - 0.4402 \text{ with } R^2 = 0.92 \quad \textbf{Eq. 5.4}$$

where:

y is the extrapolated 18-month corrosion rate of mild steel in μm/a; and

x is the measured 12-month corrosion rate of mild steel in μm/an.

The 18-month corrosion rates of mild steel at the different sites exhibited weak correlations with the mean ICI, MCI and ACI values measured at the same locations, *r* = 0.36 (P > 0.10), 0.37 (P ≤ 0.10) and 0.28 (P > 0.10), respectively (**Appendix K**). Conversely, the relationships between the Al-WH, Zn-WH and Cu-WH, and the MSP 18-month data, were moderate to strong, 0.65 (P ≤ 0.05), 0.63 (P ≤ 0.05) and 0.72 (P ≤ 0.05), respectively (**Appendix K**), which was lower than the relationships measured on the same basis for the 12-month MSP corrosion results. Again, it confirmed that copper wire helices are seemingly more precise in determining the corrosivity of urban/industrial areas than aluminium or zinc wire coils.

After 24 months of exposure, the mean corrosion rate of mild steel in the GJMA decreased to 14 ± 3 μm/a, 95% CI [12 μm/a, 15 μm/a] (**Figure 4.32**), representing an additional 19 ± 3% reduction. Between the 18- and 24-month corrosion rates, the highest changes were measured at Aeroport and Brakpan, about 23% and 26%, respectively. These changes are due to the formation of protective oxide layers on the metal surfaces, which tends to be more stable and passivating in nature, particularly during periods of low RH and atmospheric pollution (Leygraf et al. 2016).

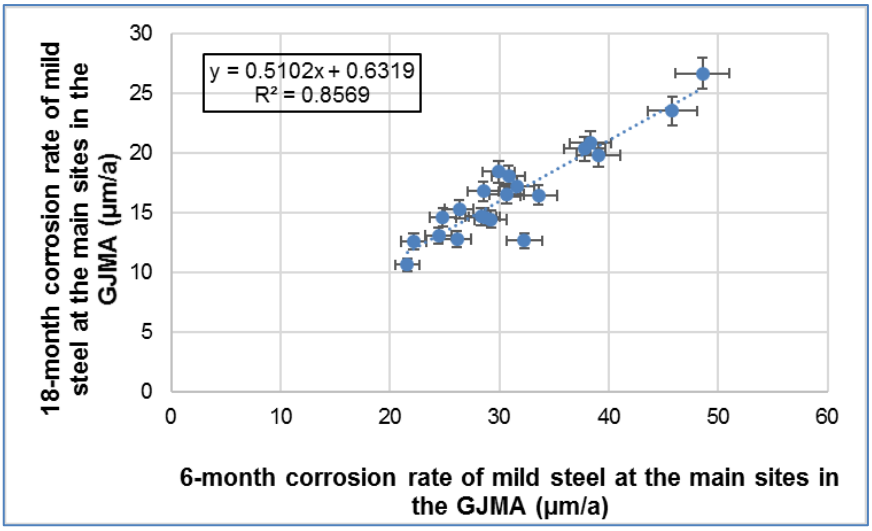


Figure 5.31 Measured linear relationship between the 6- and 18-month corrosion rates of mild steel at the main sites in the GJMA.

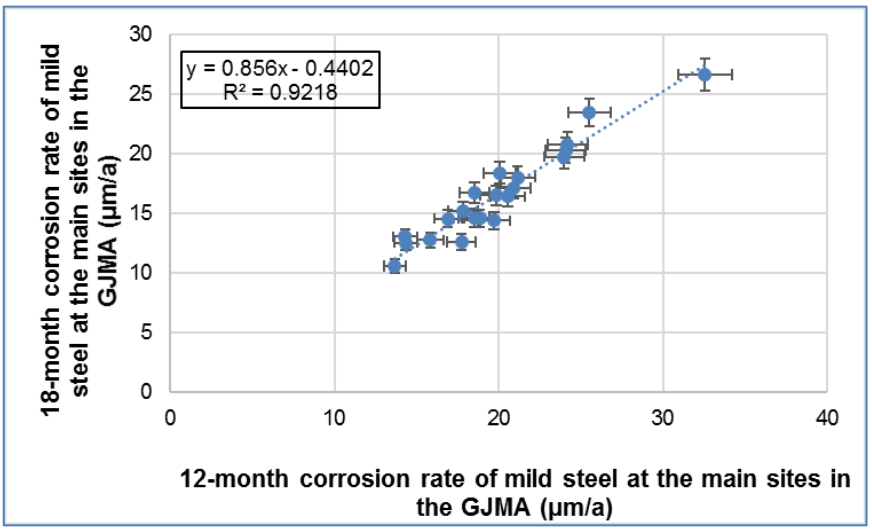


Figure 5.32 Measured linear relationship between the 12- and 18-month corrosion rates of mild steel at the main locations in the GJMA.

The results again confirmed that the Kagiso-Randfontein site exhibited the highest corrosion rate of steel, about 21 µm/a, followed by Brakpan, Chloorkop, Bonaero Park, and Aeroport. Important to note is that the corrosivity of the atmosphere at Kagiso-Randfontein was approximately three times higher than measured in the Johannesburg CBD, e.g. at Newtown, the last result demonstrating the shielding effects that buildings have on the corrosivity of an environment (see also **Appendix B**). Conversely, the Braamfontein locale displayed an approximate 21% higher corrosion rate of mild steel

than Newtown, even though these two sites are situated close to each other. Therefore, the difference is attributed to the reality that the former site is located at an elevated position, where it is more exposed to Johannesburg's urban atmosphere.

The PPMC coefficient of the 18-month vs the 24-month corrosion data of mild steel was closer to 1 ($P \leq 0.01$) (near 100% in other words), compared to the relationship between the 12- and 18-month results (**Appendix K**). This result implied even further stabilisation of the corrosion trends of the different sites, with increased exposure time. Linear regressions of the 12- and 24-month (**Equation 5.5**), as well as 18- and 24-month (**Equation 5.6)** corrosion rates of mild steel, are shown in **Figures 5.33 & 5.34**.

12- versus 24 months:

$$y = 0.5609x + 0.4663 \text{ with } R^2 = 0.90 \qquad \textbf{Eq. 5.5}$$

where:

y is the 24-month corrosion rate of mild steel in μm/a; and

x is the 12-month corrosion rate of mild steel in μm/a.

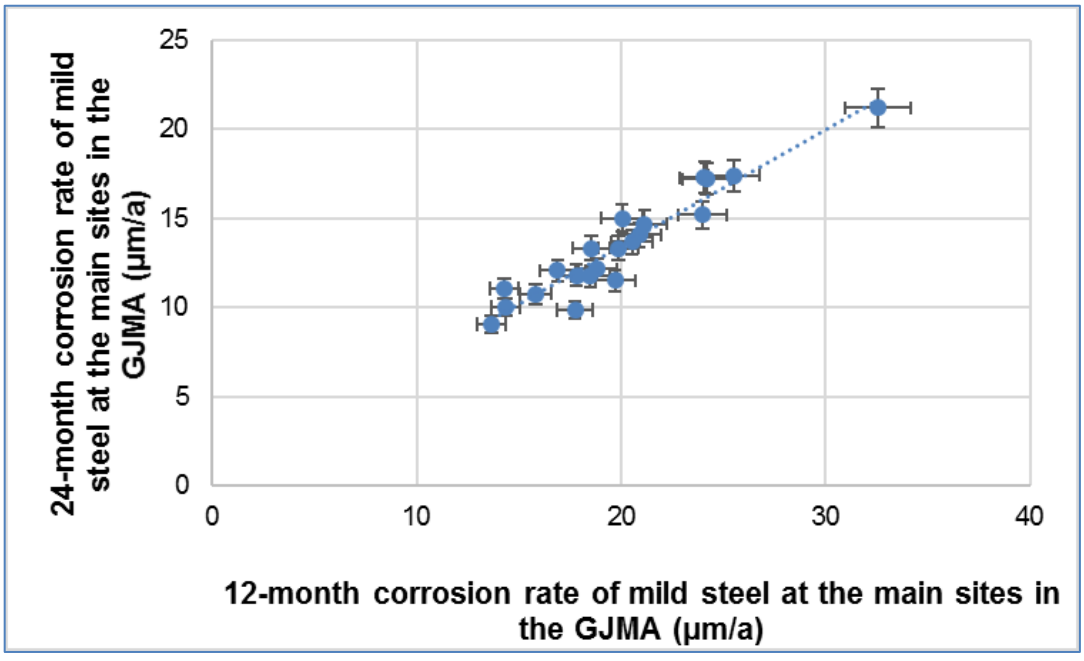


Figure 5.33 Linear regression of the measured 12- and 24-month corrosion rates of mild steel at the main sites in the GJMA.

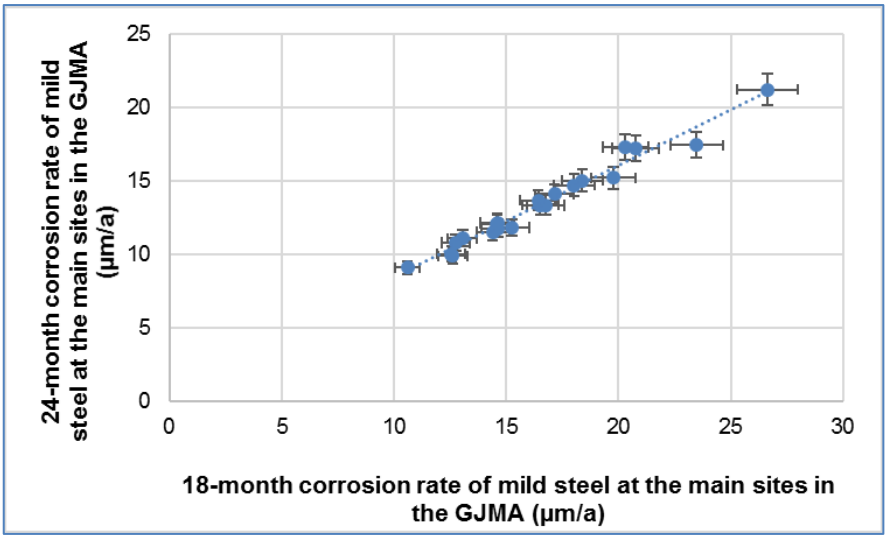


Figure 5.34 Linear regression of the measured 18- and 24-month corrosion rates at the main sites in the GJMA.

18- versus 24 months:

$$y = 0.7575x + 0.5801 \text{ with } R^2 = 0.97 \qquad \textbf{Eq. 5.6}$$

where:

y is the 24-month corrosion rate of mild steel in µm/a; and

x is the 18-month corrosion rate of mild steel in µm/a.

The PPMC correlations between the 12-month Al-WH, Zn-WH and Cu-WH, versus the 24-month MSP data, were 0.68 ($P \leq 0.05$), 0.64 ($P \leq 0.05$) and 0.72 ($P \leq 0.05$), respectively. These relationships were reasonably like those correlations measured on the same basis for the 18-month MSP results. The higher correlation for copper is again indicating that this metal type is a better indicator of the corrosion of mild steel in urban/industrial environments than aluminium or zinc.

To enable further extrapolations of the results, regression analysis of the average corrosion rates of mild steel at the different sites, after 6, 12, 18 and 24 months of exposure in the GJMA, is presented in **Figure 5.35**. According to **Equation 5.7**, the expected corrosion rate of steel after five years in the GJMA is approximately 8 µm/a, and after ten years, about 5 µm/a. Due to the build-up of protective oxide films on the metal surfaces, which tends to be passivating in nature (Leygraf et al. 2016), the

projected values present a substantial decline in the corrosion rate of steel, with an increase in exposure time. However, as may be observed, the regression analysis is only based on four data points, influencing the accuracy of the result.

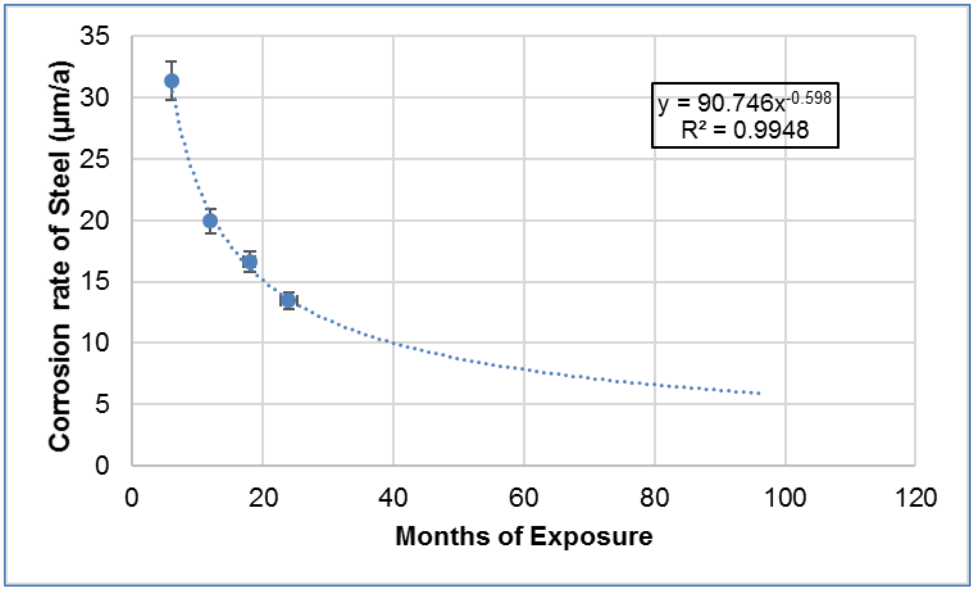


Figure 5.35 Regression analysis of the average measured 6-, 12-, 18- and 24-month corrosion rates of mild steel at the main sites in the GJMA.

Long-term corrosion trend of mild steel in the GJMA

$$y = 90.746x^{-0.598} \quad \text{with } R^2 = 0.9948 \qquad \textbf{Eq. 5.7}$$

where:

y is the projected corrosion rate of mild steel in µm/a; and

x is the exposure period in µm/a.

Worth noting is that the estimated values agree with the average 10-year and steady-state corrosion rates given in ISO 9224:2012 for mild steel exposed to *moderate* (C3) corrosive environments, $5 < r_{av} \leq 12$ and $1.5 < r_{lin} \leq 6$, respectively (International Organization for Standardization 2012b). However, these values are significantly lower than the range given in the Callaghan map for the urban (inland) environments, which is 15 µm/a to 40 µm/a (Callaghan 1991), suggesting that the map was likely based on the short-term corrosion rates of mild steel.

The estimated 10-year rate is of similar scale than the actual 10-year results reported by Callaghan (1991) for carbon steel exposed in the Highveld and Vaal Triangle regions. According to Callahan's data, the 10-year corrosion rate of carbon steel at the CSIR in Pretoria measured approximately 4 μm/a. In Secunda, the 10-year corrosion rate of carbon steel was reported as about 15 μm/a, while at Sasolburg, the long-term corrosion rate of mild steel was cited as also around 15 μm/a. These results present a potential range of 4 μm/a to about 15 μm/a for the Highveld region.

5.2.4 Hot-dip Galvanised Mild Steel (GSP) Corrosion Rates – Main Sites

The average 12-month value of hot-dip galvanised steel in the GJMA was 0.7 ± 0.3 μm/a, 95% CI [0.6 μm/a, 0.8 μm/a], varying between 0.4 μm/a (Kya Sand) and 1.5 μm/a (Kagiso-Randfontein) (**Figure 4.32**). See also **Appendix J**. Chloorkop likewise exhibited a high 12-month value for galvanised steel, as did most of the other industrial locations.

The average variation between each duplicate set of hot-dip galvanised panels per exposure period was about 0.1 μm/a (67%) - lower than for the matching sets of mild steel panels. Apart from the Kagiso-Randfontein and Brakpan locales, already ranking as *medium* (C3) corrosive (**Table 2.2** – International Organization for Standardization 2012a), based on their respective r_{corr}-values for mild steel, two additional sites found to belong to this corrosivity category were Aeroport and Chloorkop. The remaining sites were all classified as *low* (C2) corrosive.

PPMC coefficients of the 12-month corrosion rates of hot-dip galvanised steel versus the average ICI, MCI, and ACI values measured for the different sites, excluding Buccleuch, were 0.52 ($P \leq 0.05$), 0.62 ($P \leq 0.05$) and 0.24 ($P > 0.05$), respectively (**Appendix K**). Concerning the GSP vs ICI and MCI relationships, these were significantly higher than the correlations determined on the same basis for the 12-month corrosion rates of uncoated steel. This suggested that CLIMAT devices are better indicators of the impact of atmospheric pollutants on the 12-month corrosion rate of hot-dip galvanised steel, than of uncoated carbon steel. However, contrary to uncoated steel, the correlation between the 12-month corrosion rates of hot-dip galvanised steel and the average measured CLIMAT ACI values was reduced even further, inferring that

moisture singularly has a decreased effect on the corrosion of hot-dip galvanised steel components in the GJMA.

Conversely, the relationships between the 12-month corrosion rates of aluminium, zinc and copper wire, and the GSP rates were considerably stronger, 0.91 (R^2 - 0.84), 0.94 (R^2 - 0.88) and 0.85 (R^2 - 0.72), correspondingly (**Appendix K & Figure 5.36 a-c**). These PPMC correlations were established as being significant within a 99% CL and are presented in **Equations 5.8 – 5.10**.

12- month corrosion rate of hot-dip galvanised steel vs 12-month corrosion rate of aluminium wire

$$y = 2.4582x + 0.3083 \text{ with } R^2 = 0.84 \qquad \textbf{Eq. 5.8}$$

where:

y is the 12-month corrosion rate of hot-dip galvanised mild steel in μm/a; and

x is the 12-month corrosion rate of aluminium wire in μm/a.

12- month corrosion rate of hot-dip galvanised steel vs 12-month corrosion rate of zinc wire

$$y = 0.9015x - 0.002 \text{ with } R^2 = 0.88 \qquad \textbf{Eq. 5.9}$$

where:

y is the 12-month corrosion rate of hot-dip galvanised mild steel in μm/a; and

x is the 12-month corrosion rate of zinc wire in μm/a.

12-month corrosion rate of hot-dip galvanised steel vs 12-month corrosion rate of copper wire

$$y = 1.579x - 01784 \text{ with } R^2 = 0.72 \qquad \textbf{Eq. 5.10}$$

where:

y is the 12-month corrosion rate of hot-dip galvanised mild steel in μm/a; and

x is the 12-month corrosion rate of copper wire in μm/a.

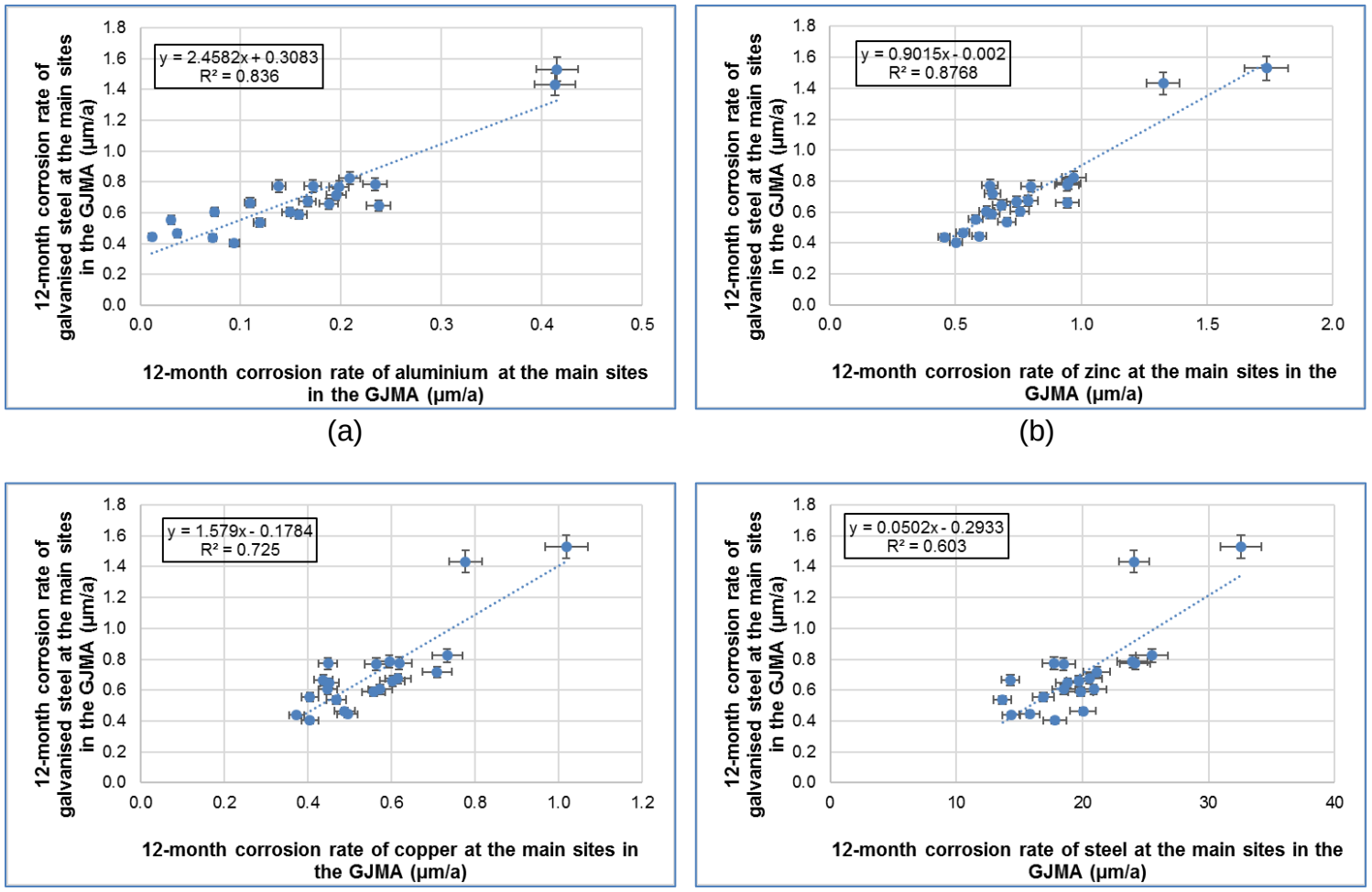


Figure 5.36 Linear regressions of the 12-month corrosion rates of hot-dip galvanised steel versus the 12-month corrosion rates of (a) aluminium, (b) zinc, and (c) copper, as well as (d) uncoated mild steel, as measured at the main sites in the GJMA.

The above heightened correlations implied that the Al-WH and Zn-WH data compared favourably with the 12-month GSP corrosion rates – affirming the benefit of using open wire helices as "*guerrilla fighters*" (Leitch 2003) for the atmospheric corrosion monitoring of environments.

Conversely, the correlation coefficient of the GSP vs the MSP data was only 0.77 (R^2 – 0.60, P ≤ 0.01), which is presented in **Equation 5.11** and **Figure 5.36 d**.

12- month corrosion rate of hot-dip galvanised steel vs 12-month corrosion rate of mild steel

$$y = 0.0502x - 0.2933 \text{ with } R^2 = 0.60 \qquad \textbf{Eq. 5.11}$$

where:

y is the 12-month corrosion rate of hot-dip galvanised mild steel in μm/a; and

x is the 12-month corrosion rate of uncoated mild steel in μm/a.

After 18 months of exposure, the average corrosion rate of the hot-dip galvanised steel specimens at the different sites calculated 0.6 ± 0.2 μm/a, 95% CI [0.5 μm/a, 0.7 μm/a], representing an approximate 14% reduction from the 12-month results, likely because of the formation of zinc carbonate on the metal surfaces (Schultz & Thiele 2012). The PPMC coefficients between the 12- and 18-month corrosion rates of hot-dip galvanised steel (**Figure 5.37**), was 0.88 (P ≤ 0.01) or R^2 – 0.78 (see also **Equation 5.12** and **Appendix K**).

The highest 18-month GSP corrosion rates were measured at Kagiso-Randfontein, Chloorkop and Brakpan. Other locales indicating a rise in the 18-month corrosion rates of hot-dip galvanised steel included Aeroport, Bonaero Park, and Chamdor.

18- versus 12-month corrosion rates of hot-dip galvanised steel

$$y = 0.6211x + 0.1433 \text{ with } R^2 = 0.78 \qquad \textbf{E.q. 5.12}$$

where:

y is the 18-month corrosion rate of hot-dip galvanised mild steel in μm/a; and

x is the 12-month corrosion rate of hot-dip galvanised mild steel in μm/a.

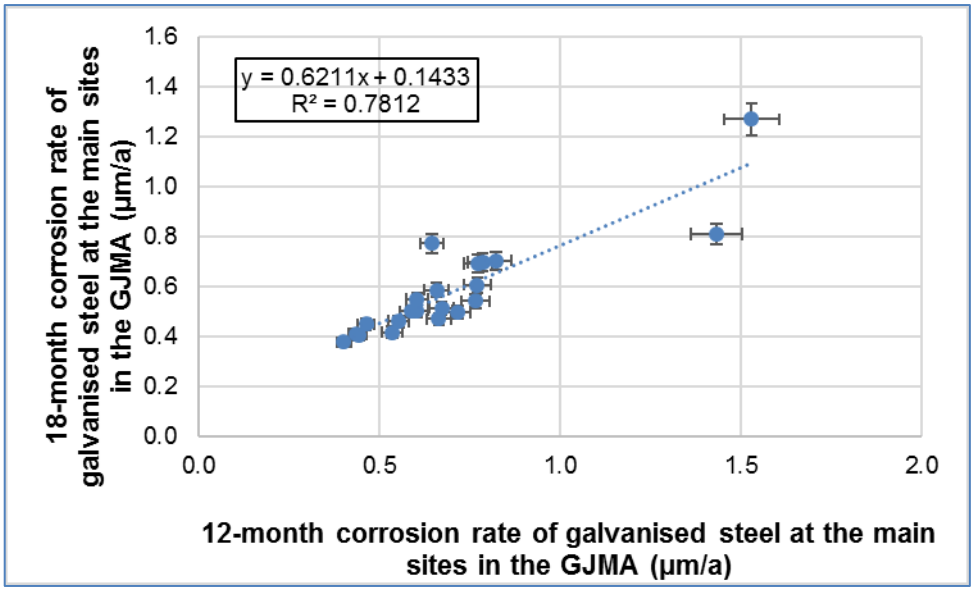


Figure 5.37 Linear regression of the 18-month versus the 12-month corrosion rates of hot-dip galvanised steel, as measured at the main sites in the GJMA.

As expected, the correlations between the 18-month corrosion rates of the galvanised steel specimens and the CLIMAT ICI, MCI and ACI values decreased to 0.33 ($P > 0.10$), 0.35 ($P > 0.10$) and 0.38 ($P > 0.10$), respectively (**Appendix K**). Similarly, the relationships between the 18-month corrosion rates of galvanised steel and the r_{corr} Al- WH, r_{corr} Zn-WH and r_{corr} Cu-WH data, lessened to 0.85 ($P \leq 0.01$), 0.91 ($P \leq 0.01$) and 0.81 ($P \leq 0.01$), correspondingly (**Appendix K**), although it was still strong within a 99% CL.

Following 24 months of exposure, the corrosion rates of the hot-dip galvanised steel plate specimens revealed only minor further stabilisation, compared to the 18-month data, 0.6 ± 0.2 µm/a, 95% CI [0.5 µm/a, 0.6 µm/a], demonstrated in **Figure 4.32**. Based on the results, the PPMC coefficients for the 12- and 24 months, as well between the 18- and 24-month corrosion rates of the hot-dip galvanised specimens exposed in the GJMA, calculated 0.92 ($P \leq 0.01$), in both circumstances (**Appendix K**). As a result, it was submitted that the short-term exposure results of hot-dip galvanised steel could be used to predict the 10-year and steady-state corrosion rates of the same material. This finding also confirmed the accuracy and value of the ISO 9223:2012 and ISO 9224:2012 short- and long-term corrosivity rating schemes (International Organization for Standardization 2012a, 2012b).

Regression of the average 12-, 18- and 24-month corrosion rates of galvanised steel, as measured at the main sites in the GJMA, is shown in **Figure 5.38**. It is important to note that since the graph only comprises three points, it is likely that the long-term trend is less accurate than indicated, R^2-value of 0.94. Nonetheless, according to the function derived (**Equation 5.13**), the average corrosion rate of hot-dip galvanised steel after five years of exposure in the GJMA is expected to be about 0.4 μm/a, and after ten years, approximately 0.3 μm/a. These projected values suggest only a modest decline in the corrosion rate of hot-dip galvanised steel with an increase in exposure time, potentially indicating the formation of stable zinc carbonate layers on the test surfaces. Agreeing with Schultz & Thiele (2012), providing these protective layers are maintained, zinc will exhibit low corrosion rates. However, in the absence of oxygen and carbon dioxide, or when zinc is exposed to low or high pH or other aggressive environments, corrosion will be rapid. This may be of relevance in those areas exposed to acid rain.

Long-term corrosion trend of hot-dip galvanised mild steel in the GJMA

$$y = 1.6687x^{-0351} \quad \text{with } R^2 = 0.94 \qquad \textbf{Eq. 5.13}$$

where:

y is the projected corrosion rate of hot-dip galvanised steel in μm/a; and

x is the exposure period in μm/a.

Worth noting is that these projected values fall within the average 10-year and steady-state ranges given in ISO 9224:2012 for the corrosion rate of zinc exposed to *low* (C2) corrosive environments, $0.1 < r_{av} \leq 0.5$ and $0.05 < r_{lin} \leq 0.5$, respectively (International Organization for Standardization 2012b).

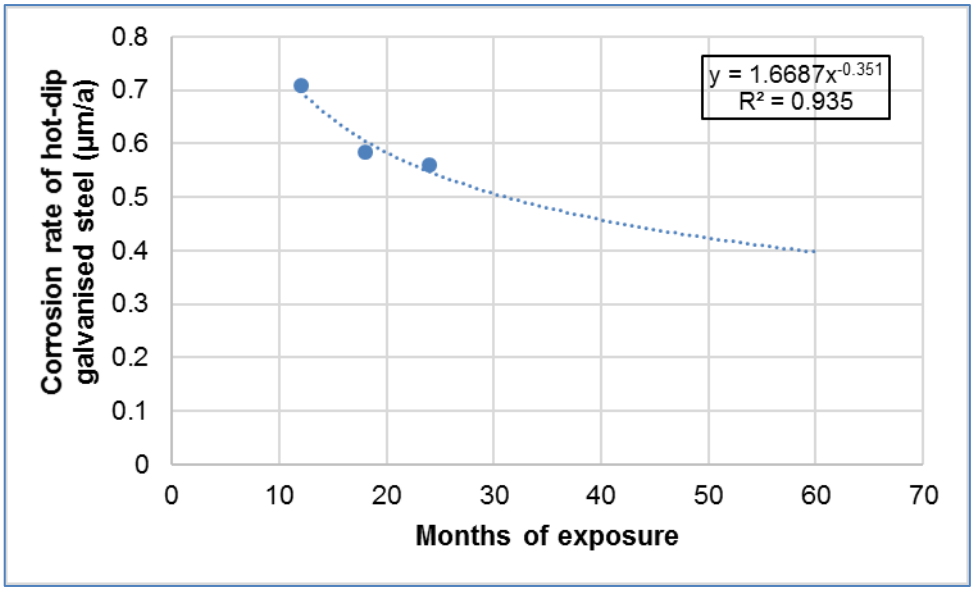


Figure 5.38 Regression analysis of the average 12-, 18- and 24-month corrosion rates of galvanised steel, as measured at the main sites in the GJMA.

Moreover, compared to Callaghan's (1991) 5- and 10-year corrosion rates of zinc, the derived data appeared similar than those measured at the CSIR's premises (in Pretoria), which were about 0.3 µm/a for both periods. The slowdown or increased consistency of the long-term corrosion rate of hot-dip galvanising is likewise reflected in Callaghan's results for zinc in the Highveld region. Nonetheless, the expected service life of Z275 coated mass galvanised sheeting, with a nominal thickness of 19 micrometres (ArcelorMittal South Africa 2017), is given in the Callaghan map as 5- 15 years for central industrial areas. This implies a corrosion rate of approximately 1.3-3.8 µm/a for zinc, which is significantly overstated, again inferring that Callaghan's map was likely based on short-term corrosion results. Based on the latest results, the projected service life of Z275 galvanised sheeting in the GJMA is estimated as being in the order of 13-48 years, assuming uniform corrosion of the pure zinc and zinc-iron alloy inner layers.

From a regional perspective, similar corrosion patterns were identified for hot-dip galvanising, compared to those for uncoated mild steel, aluminium, zinc and copper, namely that the corrosion rates were highest on the East Rand, followed by the West Rand and Southern Suburbs of the GJMA (**Figure 4.33**). Consequently, very high PPMC coefficients were determined for the average corrosion rates of galvanised steel

and those of the pure zinc wires, as well as opposed to the uncoated mild steel data, 0.94 (P ≤ 0.01) and 0.93 (P ≤ 0.01), respectively. Conversely, the regional rankings were somewhat different compared to the CLIMAT ICI, MCI and ACI data, although the correlations were still high, 0.71 (P ≤ 0.01) and 0.72 (P ≤ 0.01) for the ICI and MCI data, respectively.

Figure 4.33 shows the regional patterns of the average 12-month corrosion rates of hot-dip galvanising, compared to those for uncoated mild steel, aluminium, zinc and copper. Noteworthy is that when the Kagiso-Randfontein 'hotspot' is taken out of the equation, the corrosivity ranking of the different regions changes to the East Rand and Southern Suburbs being most corrosive, followed by the City of Joburg, West Rand and then Northern Suburbs - the last three regions being of similar rating.

5.2.5 Mild Steel (MSP) Corrosion Rates – Main and Mini Sites Combined

Concerning the combined average 12-month corrosion rate of uncoated mild steel at the main and mini sites in the GJMA, the average measured value was 20 ± 4 μm/a, 95% CI [19 μm/a, 21 μm/a], varying between about 13 μm/a at Palmridge, and approximately 33 μm/a at Kagiso-Randfontein (**Table 4.1** and **Figure 4.34**).

The difference between each duplicate set of mild steel samples for the different sites per 12-month period, was 0.7 ± 0.5 μm/a, 95% CI [0.6 μm/a, 0.8 μm/a], signifying an average correspondence of about 96%. The margin of error was likely caused by the additional removal of base metal during the corrosion product sampling process, via the scraping procedure, as well as during the Bresle latex pouch removal method, and subsequent weighing stage. See Sections 3.2.2.2 and 3.2.2.3 in this regard. However, the development of varying protective iron oxide layers on the metal surfaces cannot be excluded (Morcillo et al. 2010). However, this is unlikely to be of relevance when duplicate specimens are exposed per site per exposure period. Nonetheless, the level of certainty of the corrosion rate measurements for each duplicate set of mild steel specimens per site was calculated as approximately 96%, CI [95%, 97%], which was slightly lower than the value reported by Knotkova et al. (2010) for flat mild steel coupons, as per the ISO 9226 procedure, given as ± 2%. However, relating to the ISOCORRAG programme, the measurements were taken in triplicate form.

Considering all the GJMA sites, excluding the Kagiso-Randfontein locale, those areas that exhibited the highest corrosion rates of mild steel were Dunnottar, Brakpan, Dalpark, Nigel, and Bonaero Park. These were all more corrosive than the Chloorkop site (**Figure 4.34**), located on the eastern side of the GJMA. In contrast, the lowest corrosion rates of mild steel (excluding the Palmridge locale) were measured at Newtown, Princess and Jabavu (Soweto). Of note is that Newtown is classified as an urban/business environment (**Appendix B – Table B.1**), whereas Princess and Jabavu (Soweto), are categorised as low-income residential areas. The reduced corrosion rates of these sites of mild steel hinted that heavy industrial and mining activities play more important roles regarding the general corrosivity of the GJMA atmosphere, compared to regular business and household doings, even when it comes to informal settlement areas.

Outlier sites

Both the Kagiso-Randfontein and Palmridge test locales were identified as outliers, regarding the general corrosivity of the GJMA. This finding is visible in the map representation of the 12-month corrosion rates of mild steel at the main and mini sites in the GJMA (**Figure 5.39**) and attributable to the following:

- The Palmridge test site is elevated approximately 40 m above ground level (**Appendix B - Table B.1**), on top of the local Magistrate's Court building, which is surrounded by low-income residential and informal settlement areas. This area is also positioned between Rosherville, Walkerville, Geluksdal, Kliprivier and Eikenhof, of which the average 12-month corrosion rate of mild steel measured about 22 µm/a. The fact that the average r_{corr}-value of mild steel at the Palmridge test locale measured only about 13 µm/a, strongly suggested that the level of pollution of the surrounding environment was somewhat reduced, due to the elevation of the test rack. Accordingly, the corrosivity of the encircling atmosphere declined by as much as 38%, due to the 40 m rise in height above ground level.



Figure 5.39 Map representation of the 12-month corrosion rates of mild steel at the main and mini sites in the GJMA - revealing two outlier locales. (Base map – ArcGIS).

- The Kagiso-Randfontein site, on the other hand, has been identified as a 'hotspot' regarding general atmospheric corrosion in the GJMA. This is due to the ongoing mining and brick manufacturing activities in the immediate area. See also **Appendix B - Table B.1**. These operations impacted significantly on the corrosion rates of the different metals, particularly in contrast with the Palmridge site. However, as was established by the Grubbs' test, while Kagiso-Randfontein was indicated as a significant outlier within a 95% CL, within a 99% CL, it was statistically viewed as a less important outlier, but simply furthest from the other rates.

Nonetheless, the outlier data are useful in the sense that they indicated the impact of extremes, e.g. altitude, and localised pockets of mining and industrial activities, on the general corrosivity of the Greater Johannesburg area.

Changing altitude

It is important to mention that increasing height above ground level does not necessarily equate to a reduction in the corrosivity of the surrounding environment. In this regard, the higher corrosivity of the Braamfontein site, versus the Newtown locale, may potentially be linked to the fact that the former area is located far above the ground (**Appendix B - Table B.1**), where it is more exposed to the general urban atmosphere of Johannesburg's CBD. This phenomenon is also often found in coastal regions, where due to the elevation of structures on roofs, it may be subjected more to the onshore salt-laden wind, e.g. the Addington Hospital in Durban (CSIR 1975).

Other factors that influence the corrosivity of elevated places are:

i) the extent of ground-level pollution in the surrounding area;
ii) the prevailing wind speed and direction;
iii) the shielding effects caused by other buildings or structures, as well as
iv) the impact of the surrounding infrastructure (Janse van Rensburg 2010).

Similar observations have also been made by Ríos-Rojas et al. (2015) about the atmospheric corrosivity of several sites in Bogota, a vast metropolis positioned at about 2600 m above sea level.

Notwithstanding the above, regarding all the GJMA exposure sites, changing altitude appears to have a slight bearing on the general corrosivity of the environment. This conclusion is drawn since the average 12-month corrosion rate of mild steel at sites exhibiting higher elevations above sea level, namely Braamfontein, Florida Hills, Durban Deep, Krugersdorp, Princess, and Kliprivierberg, measured approximately 18 μm/a. These areas are all located on a protruding rocky ridge in the region (the Witwatersrand), with an average altitude of about 1.9 km. (See also **Appendix B, Table B.1**, which shows the relative altitudes for the various sites). In contrast, the mean 12- month corrosion rate of mild steel at sites at lower altitudes, near 1.4 km on average, measured merely ~ 16 μm/a, e.g. at Dainfern Ridge, Diepsloot, Kya Sand and Lanseria, which are all situated in more north-westerly directions of the GJMA.

As displayed in **Figure 2.26,** adapted from City of Johannesburg (2003), the highest rainfall in the Greater Johannesburg area also often corresponds with the rocky ridge that runs east-west across the area. Nonetheless, the slight difference may also be linked to the fact that these elevated places are mainly located towards Johannesburg's and Roodepoort's business centres (**Figure 2.20**) (Google Inc. 2016b), with increased transport activities, whereas the lower altitude sites are mostly positioned in rural to semi-rural environments.

Regional Perspective

From a regional point of view, like the CLIMAT and ISO open wire helix unit data (**Figures 4.20 - 4.22**, **4.26 - 4.28**), the results confirmed that the eastern and southern parts of the GJMA appear to be more corrosive than the central, northern and western regions. The average corrosivity of the Central JHB Suburbs is, however, nearer to that of the southern region.

Figure 4.36 shows that regarding those sites that are positioned towards the east of the GJMA, the Dunnottar locale, followed by the Brakpan area, they are not only most corrosive but, regarding their respective 12-month corrosion rates of mild steel, also the only two sites that may be rated *medium* (C3) corrosive. In contrast, all the other sites fall within the *low* (C2) corrosivity range (**Table 2.2**. - International Organization for Standardization 2012a).

Nonetheless, many of the East Rand sites bordered on the *medium* (C3) corrosive category, with a 12-month corrosion rate of mild steel varying between 25 μm/a and 50 μm/a. Therefore, each ISO 9223:2012 corrosivity category was divided into additional levels, namely, Lower, Mid, and Upper, except for the C1 and CX groupings. This was to facilitate better interpretation of the results. The revised corrosivity classification system is given in **Table 5.7**.

As per the modified rating system, the corrosivity of the Dunnottar and Brakpan locales rated Lower-C3 corrosive, whereas the corrosivity of the other East Rand sites, ranked Upper-C2 corrosive. On average, however, the 12-month corrosion rate of mild steel for this region measured 23 ± 2 μm/a, 95% CI [22 μm/a, 24μm/a] or Upper-C2 corrosive (*low* to *medium*).

Concerning the area with the second highest average 12-month corrosion rate of mild steel, namely, the Southern Suburbs (**Figure 4.37**), Eikenhof displayed the highest corrosivity (Upper-C2), and Orange Farm the lowest (Mid-C2). The similarity of the corrosivity of the Elspark, Kliprivier and Ennerdale sites, is of note. Overall, the average 12-month corrosion rate of steel measured 20 ± 1 μm/a, 95% CI [20 μm/a, 21μm/a], or Upper- 2 (*low* to *medium*) corrosive.

The central region of the GJMA study area indicated the third highest average 12- month corrosion rate of mild steel, 19 ± 3 μm/a, 95% CI [17 μm/a, 21 μm/a] (**Figure 4.38**) and rated Mid-C2 corrosive. Gilloolys, the most easterly locale for this region, showed the highest 12-month corrosion rate of steel, about 22 μm/a, which falls within the Upper-C2 corrosivity range. Conversely, Newtown, located in Johannesburg's CBD, displayed the lowest value for this region, approximately 14 μm/a. Both the Gilloolys and Newtown sites are located along heavy traffic routes, potentially suggesting that the impact of traffic pollution on the corrosivity of the atmosphere, by way of soot, NO_x and CO emissions (**Figures 3.25**, **3.27 & 3.31**) (DEA 2017a), was small. A similar finding was made by Bell (1982), during the corrosion monitoring of the main roads in Melbourne (Australia).

Table 5.7 Revised corrosivity categories of the atmosphere - adapted from International Organization for Standardization (2012a).

Corrosivity category		Corrosion rates of metals			
		12-month rate - Steel (μm/a)	12-month rate - Aluminium (μm/a)	12-month rate - Zinc (μm/a)	12-month rate - Copper (μm/a)
C1	Very low	ISO 9223:2012 values divided into further categories. NOT PUBLICLY AVAILABLE			
Lower-C2	Very Low to Low				
Mid-C2	Low				
Upper-C2	Low to Medium				
Lower-C3	Low to Medium				
Mid-C3	Medium				
Upper-C3	Medium to High				
Lower-C4	Medium to High				
Mid-C4	High				
Upper-C4	High to Very High				
Lower-C5	High to Very High				
Mid-C5	Very High				
Upper-C5	Very High to Extreme				
CX	Extreme				

The average 12-month corrosion rate of steel in the Northern Suburbs measured 17 ± 2 μm/a, 95% CI [16 μm/a, 18 μm/a], with the more north-westerly sites, Diepsloot and Lanseria, displaying the lowest corrosion rates, while the north-easterly locales, Midrand and Ivory Park, exhibited the highest values (**Figure 4.39**). Overall, the corrosivity classification for this region is Mid-C2 (*low*) corrosive (**Table 5.7** - adapted from International Organization for Standardization 2012a).

Generally, the West Rand region demonstrated the lowest average 12-month corrosion rate of mild steel, 16 ± 2 μm/a, 95% CI [15 μm/a, 17 μm/a]. This excluded the Kagiso-Randfontein locale, which is a local 'hotspot'. The general corrosivity of this region is ranked Mid-C2 (*low*) corrosive.

Concerning the individual sites of the West Rand area (**Figure 4.40**), the Durban Deep test location, positioned at the Durban Deep Gold Mine's golf course, exhibited the highest 12-month corrosion rate, whereas the lowest value was measured at Princess, located next to a large informal settlement area. These results signified again that the mining activities in the GJMA area play a crucial role regarding the corrosivity of the region.

Comparisons with Callaghan's (1991) and Leitch's (2006) corrosion maps

The above data confirmed that Callaghan's (1991) corrosivity ratings for the *Inland Industrial* zone of South Africa (covering most parts of the GJMA) was excessive. Moreover, the latest results supported the assumption that the Callaghan map was based on 12-month exposure data, instead of 10-year corrosion results, as is commonly alleged.

The maximum corrosion rate of mild steel for the *Inland Industrial* region (the Vaal Triangle and Highveld areas) given in the old map is about 40 μm/a (Callaghan 1991). This perceptibly only applies to the local pockets of industrial corrosion initially measured at Iscor in Pretoria (nowadays known as ArcelorMittal), Sasol (in Secunda) and Sasolburg in the Free State.

Leith (2006) estimated that the corrosivity of the industrial areas of the Highveld (GJMA) area ranged between *medium* (C3) and *high* (C4) corrosive, the latter applying to unusually heavy industrial locations. Even though these ratings compared better with the latest corrosion results, it was perceptible that for the most part, the macro atmosphere should preferably be rated Upper-C2 (*low* to *medium*) corrosive (**Table 5.7** - adapted from International Organization for Standardization 2012a), with isolated pockets of increased corrosivity (Lower-C3 to Lower-C4) being likely in and around mines (active or historical), power stations and heavy industrial installations, e.g. at Chloorkop and Germiston.

5.2.6 Visual Condition Assessments of Existing Infrastructure vs Measured Corrosion Rates

The visual inspection results (**Figures 4.7 - 4.10** and **Appendix F**) suggested that at industrial, mining, low-income residential and informal settlement areas, the existing infrastructure exhibited notable corrosion and coating problems, compared to structures located in more upmarket residential, rural and business districts. These contrasting results implied either reduced upkeep of the former areas or that these sectors were in locations exhibiting higher levels of atmospheric corrosion.

As mentioned in Section 4.2.1, several sites were initially found that showed advanced signs of the corrosion of the surrounding infrastructure. This was postulated as perhaps

due to the higher corrosivity of the environment. However, as shown in **Table 5.8**, the apparent (visual) corrosivity ratings of sites may be misleading. According to the corrosion rate measurements of mild steel in the GJMA, it was found that the extent of corrosion of infrastructure at the Kagiso-Randfontein, Esselen Park, Ennerdale and Rosherville sites, accurately depicted the higher corrosivity of these locations. However, at Lenasia, Doornkop and Brakpan, the corrosivity ratings (based on the visual condition assessments) were less precise. Accordingly, the corrosion of structures at these locations was likely due to poor upkeep, or the utilisation of improper and/or inferior corrosion protection procedures.

Table 5.8 Comparisons between the measured 12-month corrosion rates of mild steel, with a margin of error of about 5%, versus the visual condition assessments of select sites in GJMA.

Site	Environmental classification	12-month corrosion rate of mild steel (µm/a),	Percentage corrosivity above the average background level measured for the GJMA
Kagiso-Randfontein	Mining/industrial	33	65%
Esselen Park	Residential/industrial/field	22	11%
Ennerdale	Industrial	21	5%
Lenasia	Low-income residential	18	-8%
Doornkop	Mining/low-income/informal settlement	18	-8%
Brakpan	Mining/low-income residential	19	-5%
Ivory Park	Low-income residential settlements	19	-5%
Rosherville	Industrial	21	4%
Jabavu (Soweto)	Low-income residential area	14	-28%

5.2.7 Optical Surface Characterisation, Morphology and Chemical Analysis of the Mild Steel Corrosion Products Formed at the Main and Mini Sites in the GJMA

5.2.7.1 Optical surface characterisation of the mild steel corrosion product

The corrosion products formed were not only different, but depended on the area and conditions of exposure (**Figure 4.41**). This finding substantiates studies done by Morcillo et al. (2011), Li et al. (2013) and Alcantara et al. (2015) pertaining to the variations in the surface morphologies of mild steel corrosion products at different exposure sites. The changes are also confirmed by Leygraf et al. (2016). According to Syed (2006), Parekh et al. (2012) and Li et al. (2013), the initial corrosion layers that

are formed also can be significantly influenced by the starting time of the exposure programme, which in the case of the latest study was at the beginning of the rainy season for the GJMA, August-September 2013.

The results showed that the colour shades, particle-like morphologies and surface consistencies of the corrosion products formed on each duplicated set of mild steel panels, exposed per site per period, were similar. However, they changed slightly from one exposure period to the next, as indicated in **Figures 4.42 & 4.43**.

Sites located in and around townships and informal settlement areas exhibited yellowish-white spots, e.g. Alexandra, Diepsloot, Palmridge (Katlehong) and Princess (**Figure 4.41**). Conversely, in more upmarket residential areas, namely Ruimsig, Florida Hills, and Bryanston, the corrosion products of mild steel were a darker reddish-brown colour, with little (if any) yellow-white spots present. In this regard, Janse van Rensburg (2010) identified similar white-greyish flecks in the corrosion product of mild steel exposed at various coal-fired power stations in the Mpumalanga area, which were attributed to fly-ash deposition.

Of note is that the colour shade of the corrosion product of the mild steel specimens exposed at the Kagiso-Randfontein locale was different from all the other sites. The yellowish colour (**Figures 4.41 & 4.43**) was likely attributable to the presence of fine tailings from a nearby gold mine dump (**Figure 5.40**). This was subsequently confirmed by SEM-EDS analysis, revealing elevated levels of Si and Al (likely aluminosilicate glass) in the corrosion product (Section 5.2.8.2). It was also supported by the FTIR and Raman spectroscopy results (Section 5.2.8.2), namely that quartz was present in the corrosion product.



Figure 5.40 The gold mine tailings dump located next to the Kagiso-Randfontein site.

5.2.7.2 Morphology of the mild steel corrosion product

Attenuated total reflectance (ATR) - Fourier transform infrared (FTIR) spectroscopy analysis

The formation of rust on carbon steel is complex and may vary over the surface. It also changes with time and environmental exposure conditions (Misawa et al. 1974; Stratmann et al. 1987; Leygraf et al. 2016). Balasubramaniam et al. (2003) and Morcillo et al. (2011) state that most iron corrosion products display a wide range of crystal structures, therefore, it is often problematic to designate a single morphology to a specific corrosion product. This problem was also encountered in to the latest corrosion monitoring study of the GJMA.

At most of the locations (**Appendix L - Figure L.1-L3**), the reddish-brown colour of the rust (see also **Figure 4.41**) was attributable to the presence of lepidocrocite (γ-FeOOH) (**Figure 4.45**), the primary or first crystalline structure of rust (Hiller 1966; Misawa et al. 1974; Stratmann et al. 1987; Freudenberger et al. 2009; Alcántara et al. 2015; Morcillo et al. 2015; Leygraf et al 2016) in open atmospheres. As acknowledged by Leygraf et al. (2016), γ-FeOOH and the amorphous phase are abundant in rust layers of only a few years old. However, with time the amorphous phase starts to dominate, finally, after

decades, changing into α-FeOOH (goethite), exhibiting an order of magnitude lower solubility than γ-FeOOH. Under outdoor conditions, these changes are governed by wetting-and-drying cyclic transitions (Stratmann et al. 1987; Stratmann 1990).

In infrared spectroscopy, the presence of lepidocrocite (γ-FeOOH) is shown by a characteristic sharp peak at wavenumber 1020 cm^{-1} (Raman et al. 1991; Balasubramaniam & Ramesh Kumar 2000) or in the case of the current study, at 1019 cm^{-1} (**Figure 4.45**). See also **Appendix L – Figure L.1**. Following Raman et al.'s (1991) study of atmospheric rust systems, highly crystallised γ-FeOOH shows infrared OH absorption peaks at around 3100-3150 cm^{-1} (OH stretching), as well as at near 1150 cm^{-1}, 1020 cm^{-1}, and 750 cm^{-1} for OH bending. Concerning poorly crystallised corrosion products, however, these peaks display a reduction in amplitude.

At the Lenasia, Buccleuch, Kya Sand and Walkerville sites, the typical γ-FeOOH peak of the corrosion products at wavenumber 1020 cm^{-1} lacked intensity and changed in shape (**Appendix L - Figure L.2**). Consequently, dual asymmetrical peaks (**Appendix L - Figure L.3**) were present between wavenumbers 980 cm^{-1} to 1020 cm^{-1}, rather than a single sharp peak. This suggested either the presence of contaminants on the metal surfaces or that γ-FeOOH was no longer the primary crystallised form of the corrosion product. Conversely, in the case of Kagiso-Randfontein (**Appendix L - Figure L.2**), the 1020 cm^{-1} peak also appeared slightly broader, which was likely due to an overlapping Si-O (quartz) stretching peak in this region (Raman et al. 1991). This indicated the presence of mine sand on the metal surfaces – potentially explaining the yellowish-brown colour of the corrosion product. (Also refer to **Figures 4.41 & 4.43**).

At most sites, the existence of goethite (α-FeOOH), in combination with lepidocrocite (γ- FeOOH) was somewhat likely. According to Morcillo et al. (2010), black spots are due to the formation of magnetite (Fe_3O_4) and the green-blue-greyish colours, because of the development of Fe (II/III) hydroxy salts. Raman et al. (1991) state that in the case of α-FeOOH, two peaks in the region of 880 $cm^{-1}$and 790 cm^{-1} typically give rise to a definite "W" shape (**Figure L.1**). Conversely, concerning δ-FeOOH (feroxyhyte), the peaks appear more wave-like (with diminished intensity) in shape, which might apply to the Kagiso-Randfontein locale (**Figure L.2**).

Moreover, regarding the infrared spectra of the outlier sites (**Figure L.2**), much stronger peaks could be observed in the 1500 cm^{-1} to 1700 cm^{-1} range. These were likely due to an increase in OH^- bonds, whereas the additional peaks between 1250-1400 cm^{-1} might potentially be associated with the salts of bird droppings.

Raman spectroscopy analysis

Given the said uncertainties, Raman micro-spectroscopy analyses of the corrosion products of select samples were carried out to enable further identification of the different iron oxides formed on the mild steel specimens. Typically, the corrosion products analysed showed different coloured particles, reddish-brown, yellow and black. The Raman spectral bands for various coloured regions of the corrosion products from specific sites are given in **Appendix M - Table M.1**.

Concerning the most prevalent reddish-brown areas (**Figure 4.41**), the Raman spectra indicated the primary peaks for γ-FeOOH - according to Thibeau & Heidersbach (1978), Keiser & Brown (1982), Williams et al. (1995), de Faria et al. (1997), Antunesa et al. (2003) and Morcillo et al. (2016), distinguishable with a strong peak near 245-257 cm^{-1}, the second highest at around 373-393 cm^{-1}, and less significant bands close to 493 cm^{-1} (shoulder), 522-530 cm^{-1}, 650-655 cm^{-1} (shoulder) and 1303-1310 cm^{-1}. This finding also agreed with the FTIR results, namely that γ-FeOOH was the main iron oxide form present in the rust layers of mild steel after 12 months of exposure in the GJMA. The outcome similarly coincided with the findings of Antunesa et al. (2003) and Morcillo et al. (2011), showing that the main iron oxide often identified in the rust layers of mild steel exposed to rural and urban environments is γ-FeOOH. (See also **Figures 4.46 & 4.47 & 4.51)**.

Pertaining to the yellow coloured areas (**Figure 4.41**), although less prevalent than the reddish areas, the Raman spectra matched a mixture of the γ-FeOOH and α-FeOOH bands - the latter crystal form's strongest peak typically given at around 380-397 cm^{-1}, with other representative peaks near 241-250 cm^{-1}, 292-307 cm^{-1}, 474-480 cm^{-1} and 549-554 cm^{-1} (Thibeau & Heidersbach 1978; Keiser & Brown 1982; Nauer et al. 1985; England et al. 1986; Williams et al. 1995; Antunesa et al. 2003; Li & Hihara 2015; Morcillo et al. 2016). Like lepidocrocite, goethite (α-FeOOH), often coinciding with γ- FeOOH (Morcillo et al. 2016), was found to be present in all the corrosion products

analysed using Raman micro-spectroscopy (**Appendix M - Table M.1**). This finding agreed with those of Misawa et al. (1974) and Morcillo et al. (2012), namely that while in a rural (unpolluted) atmospheres, γ-FeOOH is dominant, in SO_2 polluted environments, e.g. at Alexandra (**Figure 4.46**), higher amounts of α-FeOOH may be detected. Morcillo et al. (2016) affirm that the coexistence of γ-FeOOH and α-FeOOH is logical, considering the conversion that takes place between these two phases (Section 2.1.3.2)

Morcillo et al. (2012) further state that in SO_2 polluted atmospheres, the SO_2 is adsorbed in the rust layer and oxidised to sulphate (SO_4^{2-}), which collects in the corrosion cells at the anodes, creating SO_4^{2-} nests, described for the first time by Schwarz in 1965. Once the surface is moistened, these SO_4^{2-} nests, together with the surrounding areas form corrosion cells, of which the electrolyte is often highly concentrated, with low water activity. The anodes are situated inside these sulphate nests. Conversely, it is understood that below a certain pH level in polluted atmospheres, SO_2 can behave as an oxidising agent and significantly accelerate the cathodic process (Alcántara et al. 2017).

Occasional black oxides or particles were found to correspond to either amorphous carbon, with characteristic peaks near 1380 cm^{-1} and 1600 cm^{-1} (**Figure 4.48**) (Bokobza et al. 2013) or magnetite (Fe_3O_4) (**Figures 4.47 & 4.51**), with the main Raman band close to 686 cm^{-1}. According to Thibeau & Heidersbach (1978), Nauer et al. (1985), England et al. (1986), Williams et al. (1995) and Larroumet et al. (2007), the primary peak of magnetite is located around 662-670 cm^{-1}, with a less distinct peak at 535-550 cm^{-1}, which was found to be present in the corrosion products of Chloorkop (**Figure 4.47**), as well of Aeroport, Alexandra, Lenasia and Nasrec (**Appendix M – Table M.1**). This rust phase is usually found at the steel/rust interface, where the O_2 concentrations are depleted (Misawa et al. 1974; Francis 1987).

At the Chloorkop site, β-FeOOH (akageneite) (**Figure 4.49**) and $Fe(OH_3)$ (ferric hydroxide) **(Figure 4.50**) were also detected in the corrosion product. As per Nauer et al. (1985), the typical Raman peaks for β-FeOOH are typically positioned near wavenumbers 415 cm^{-1} and 715 cm^{-1}, which are also known to develop in polluted chloride environments, often in association with Fe_3O_4 (Morcillo et al. 2012; Alcántara et al. 2017), while the hydroxide $Fe(OH_3)$ (Bernalite) exhibits characteristic peaks near

303 cm^{-1}, 387 cm^{-1} and 698 cm^{-1} (Williams et al. 1995) . The presence of β-FeOOH in the corrosion product of steel from the Chloorkop site was significant, as it indicated the influence of chlorides in the local atmospheric corrosion processes. This finding was also reinforced by the EDS results (**Figure 4.54**), which showed the presence of chlorides in the corrosion product of the mild steel specimens exposed at Chloorkop.

At Kagiso-Randfontein, the main constituents of the corrosion product were established as γ-FeOOH, α-FeOOH, quartz and amorphous carbon. This finding agreed with the EDS (**Figure 4.54**) and FTIR results (**Figure L.2 – Appendix L**), namely that the alternative colour of the corrosion product from this site (**Figures 4.41 & 4.43**) was likely due to the presence of mine sand on the surfaces. Conversely, the amorphous carbon probably originated from the poor combustion of coal, from the nearby brick manufacturing facility and 'township' area. Yocom (2012) states that carbonaceous airborne materials, resulting from the incomplete combustion of fossil fuel, e.g. coal and oil, are sticky and acidic. Therefore, their corrosiveness is likely to endure over long periods when they are not removed by rain and will increase with a rise in RH. Consequently, the presence of carbon in the Kagiso-Randfontein mild steel corrosion product may have assisted in the reduction of its pH value (**Figure 4.56**).

5.2.7.3 Chemical analysis of the mild steel corrosion product

Scanning electron microscopy (SEM) and energy dispersive X-ray spectroscopy (EDS) analysis

Carbon (C), oxygen (O), aluminium (Al), silicon (Si), phosphorus (P), sulphur (S), chlorine (Cl), potassium (K), calcium (Ca) and iron (Fe) were present in the corrosion products (**Figure 4.54**). Since the electrical conductivity of the corrosion product was enhanced with a thin layer of carbon (using a sputter-coat technique) before EDS analysis, the carbon results were ignored. Conversely, the presence of K and Ca was linked to the occurrence of bird droppings on the corroded surfaces and O, considered the primary driver of the atmospheric corrosion process (Fontana 1987; McEwan 2004; Leygraf et al. 2016). Refer also to **Appendix N**.

Huang & Lavenberg (2011) states that while K and Ca are the major cations in bird faeces (Chapter 2 - Section 2.1.4.6), the main chemical constituents of bird's droppings are mostly organic and due to the acidic character, may increase localised corrosion

and deterioration. However, as the corrosion product needed to be removed without any damage to the base metal, the potential for localised forms of corrosion caused by the presence of bird droppings was not considered in the latest study.

Figure 4.54 presents summations (∑) of the maximum concentrations measured for Al, Si, P, S and Cl versus the respective 12-month corrosion rates of the mild steel specimens at the different sites. While Al and Si are not seen as corrosive as such, the occurrence of these elements signified the likely presence of dust, ash and other particulate matter on the metal surfaces, which are known to be hygroscopic, thus promoting increased TOW (Leitch 1994; McEwan 2004; Kusmierek & Chrzescijanska 2015).

The PPMC coefficient for the summations (∑) of Al, Si, P, S and Cl and the 12-month corrosion rates of the mild steel specimens was 0.58 (with $P = 1 \times 10^{-5}$ and significant at $P \leq 0.05$). When Al and Si were taken out of the equation, the relationship (*r*) between these two parameters reduced to 0.51 ($P = 9.6 \times 10^{-5}$ and significant at $P \leq 0.05$), highlighting the important role that Al- and Si-bearing dust, and particulate matter, play in the atmospheric corrosion of mild steel in the Highveld region. As per **Figure 3.23** (DEA 2017a), elevated levels of PM_{10} particulate concentrations are typically encountered in the GJMA during the winter periods, due to the burning of fossil fuel, for domestic heating and electricity production purposes.

Overall, sulphur-bearing corrodents and particulate matter appeared to be the primary pollution drivers of the atmospheric corrosion processes of mild steel in the GJMA. This finding agrees with most urban and industrial environments (Tullmin & Roberge 2000). As shown in **Figure 4.54**, sulphur was detected in all the corrosion products, with the highest concentration of sulphur (expressed as percentage SO_2) measured at the Springs, Dalpark and Aeroport sites. This increase could also be associated with bird droppings on the test surfaces (Huang & Lavenberg 2011). However, since two of these areas are located near airfields, Dalpark and Aeroport, the increase might also have been caused by the combustion of aviation fuel - the latter, like diesel fuel, known to contain elevated levels of sulphur (up to 3 000 ppm) (Miller et al. 2010).

Miller et al. (2010) state that the current average sulphur contents of aviation fuel in the United Kingdom and America are approximately 600 ppm. It is said that the formation

of SO_2, via the combustion of aviation fuel, is a rapid process. The conversion of SO_2 to SO_3 already starts in the aircraft engine, although, due to the unstable nature of SO_3, is quickly converted to H_2SO_4. It is further affirmed that aircraft emissions contain non-volatile, organic-volatile and organic-sulphate components.

Elevated levels of phosphorus were also detected in the corrosion product of the mild steel panels exposed at the Dalpark site (**Figure 4.54**), located at the Benoni-Brakpan Airfield. While these elevated P levels were likely attributable to bird droppings on the corroded test specimens, it could also have been due to particle emissions from the aircraft engines, since additives used in aviation fuels often contain phosphorous-based compounds (Anthanassiadis 1969).

Of note is that in 2010, the author identified phosphorous in the corrosion product of mild steel exposed at Stikland, a suburb of the City of Cape Town in the Western Cape. Since no bird faeces were present on the corroded steel surfaces, this was linked to the spraying of fertilisers over the vineyards, using low-flying aircraft (Janse van Rensburg 2010).

Chloorkop was the only site that displayed detectable levels of chlorine in the corrosion product of the mild steel panels (**Figures 4.53 & 4.54**). However, the presence of minute concentrations of chlorine in the other samples could not be excluded, since EDS analysis is less precise for to the detection of trace elements. Also, the EDS measurements were taken of a combined scraped sample of the corrosion products of the duplicate set of panels, rather than of individual particles or specific corroded areas, which would have lowered the trace element detection levels. However, this was to ensure that the analysis of selective particulates did not skew the overall results and because the test panels could not be cut (for SEM or EDS work) to consider variability across the surfaces of the individual samples.

The high aluminium concentrations measured in the corrosion products of the mild steel panels exposed at the mining and township sites, Alexandra, Buccleuch, Brakpan, Durban Deep and Kagiso-Randfontein, were of further interest. These elevated levels were likely due to the presence of sand and ash, which could explain the yellowish-white spots observed on the metal surfaces. Notable is that Alexandra displays some of the highest PM_{10} levels in the GJMA area (**Figure 3.23**) (DEA 2017a). Moreover, the

industrial, mining and township locales tended to exhibit higher Si concentrations in the corrosion products - likely since Si, and Al (aluminosilicate glass) are significant components from airborne ash originating from the burning of coal (Rivera et al. 2015).

Water-soluble salts in the mild steel corrosion product

The formation of the different forms of rust depends on their solubility (Morcillo et al. 2011). In order to investigate this hypothesis, the pH and water-solubility of the salts in the corrosion products formed on the mild steel panels were analysed (**Figure 4.55**). Regarding the Bresle test, Dalpark and Elspark, both located to the east of Germiston, exhibited the highest levels of water-soluble salts in the mild steel corrosion products. Conversely, the lowest values were recorded at Eikenhof and Delta Park.

While somewhat difficult to discern, **Figure 4.55** reveals a slight positive linear trend ($R^2 = 0.11$) regarding the corrosion rates versus the concentrations of water-soluble salts in the corrosion products of the mild steel specimens. The PPMC coefficient for these two parameters was calculated as 0.33, although statistically insignificant within a 90% CL. Therefore, to substantiate this relationship further, regression analysis of the average corrosion rates of mild steel at the different sites, with every 20 mg/m^2 rise in the concentration of water-soluble salts in the corrosion product, was conducted (**Figure 5.41**). The results revealed a substantial linear correlation ($R^2 = 0.84$ and $r = 0.92$, significant within the 99% CL). Based on the function derived (**Equation 5.14**), the average corrosion rate of mild steel in the GJMA increased by approximately 9 μm/a, with every 20 mg/m^2 rise in the soluble salt concentration of the corrosion product.

$$y = 0.15x + 5.77 \text{ with } R^2 = 0.84 \qquad \textbf{Eq. 5.14}$$

where:

y is the average 12-month corrosion rate of mild steel in μm/a; and

x is the average water-soluble salt concentration level in mg/m^2.

Important to mention is that the Bresle water-soluble salt test procedure was introduced into the corrosion protection industry in 1995, as ISO 8502-6 and ISO 8502-9 standards (International Organization for Standardization 2006, 1998d). This method was developed to assist in the prevention of coating failures, which may occur due to the

presence of chlorides and sulphates on metal surfaces before painting. Since salts are hygroscopic, moisture may be attracted to the metal substrate, thereby creating an electrolytic cell and causing corrosion and coating failure. Moreover, salts may encourage the wetting of surfaces below the CRH values (Alcantara et al. 2015; Cottis et al. 2010; Leygraf et al. 2016).

The high correlation between the water-soluble salts levels of the rusted surfaces and their measured 12-month corrosion rates suggested that potentially a new procedure could be developed for the rapid classification of corrosive environments. Alternatively, it could be used as an indicator of the corrosivity of environments, in combination with existing atmospheric corrosion models, e.g. ISO 9223:2012 and ISO 9226:2012 (International Organization for Standardization 2012a, 2012d). However, further work is still needed in this regard.

To test this preliminary finding, the water-soluble salt concentrations of corroded steel surfaces exposed to a known C5 to CX corrosive environment were determined. The results showed that the levels of soluble salts (assuming chlorides in this case) measured 180 mg/m^2 to 360 mg/m^2, potentially suggesting a 12-month corrosion rate of mild steel of about 80-161 μm/a. This finding was intriguing since it was within the guideline values given in ISO 9223 (International Organization for Standardisation 2012a) for the corrosion rate of mild steel in a *very high* C5 corrosive environment, thereby, suggesting some validity to this result.

The trends between the water-soluble salt concentration levels of the corrosion products of the mild steel samples were also compared to the 12-month corrosion rates of the hot-galvanised steel, aluminium, zinc and copper specimens, exposed at the main sites. The results revealed strong (with $P \leq 0.01$) PPMC coefficients with the hot-dip galvanised steel, zinc and aluminium data (**Table 5.9**), which suggested that water-soluble salts present in the GJMA atmosphere were more likely to affect the passivating films of hot-dip galvanising, zinc and aluminium, than of steel and copper. Hypothetically, this result also gave some explanation to the higher correlation between the mild steel and the copper corrosion rates, compared to the mild steel versus the aluminium, zinc or hot-dip galvanising values (**Appendix K**).

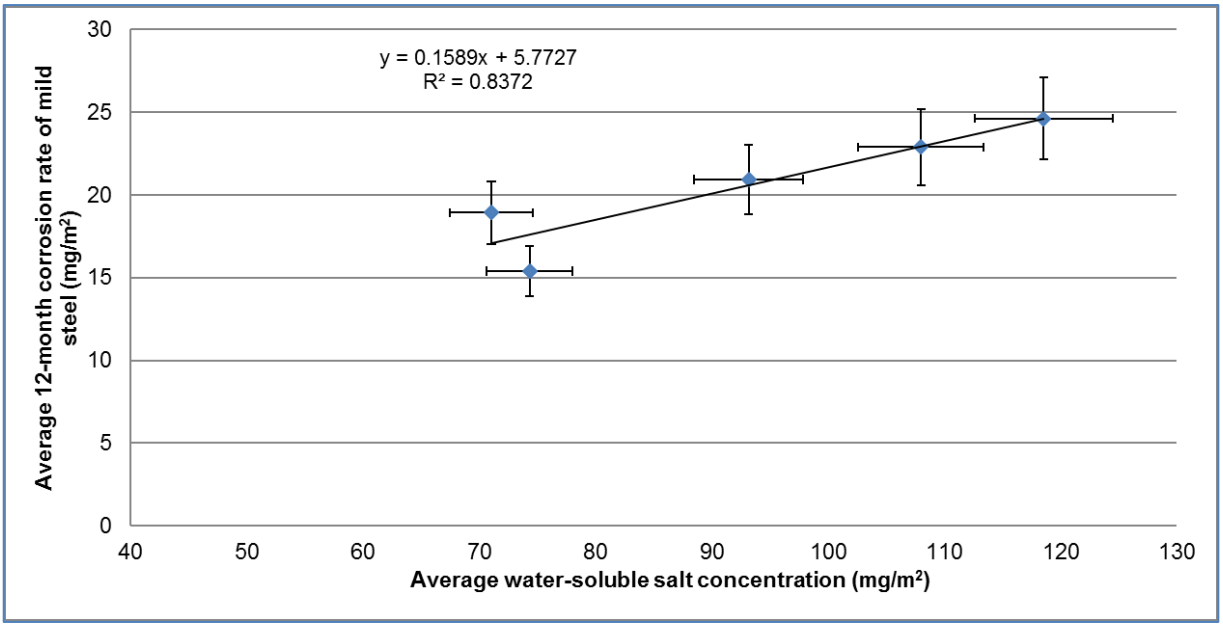


Figure 5.41 Linear regression analysis of the average 12-month corrosion rate of mild steel at the various GJMA sites, versus 20 mg/m^2 rises in the concentration of water-soluble salts in the corrosion products.

Table 5.9 Significant PPMC coefficients between the water-soluble salt levels of the corroded mild steel surfaces and the average 12-month corrosion rates of the different metals, as well as the CLIMAT indices, derived from the different corrosion monitoring procedures.

Corrosion data vs water-soluble salt concentrations of the mild steel corrosion product	Pearson correlation (*r*)	P value for Pearson (*r*)
ICI	0.40	≤ 0.10
MCI	0.45	≤ 0.05
ACI	0.42	≤ 0.10
12-month corrosion rates of mild steel	0.52	≤ 0.05
12-month corrosion rates of hot-dip galvanised mild steel	0.76	≤ 0.01
12-month corrosion rates of aluminium	0.80	≤ 0.01
12-month corrosion rates of zinc	0.82	≤ 0.01
12-month corrosion rates of copper	0.64	≤ 0.01

It is important to reiterate that both aluminium and zinc exhibit amphoteric behaviour (McEwan 2004; Schultz & Thiele 2012). These metals are also strongly affected by salts in the atmosphere (Leygraf et al. 2016), in comparison with other influencing factors, such as moisture and SO_2.

The measured 6- and 12-month water-soluble salt concentrations of the corroded mild steel specimens versus the 12-month corrosion rate of pure zinc at the East Rand and West Rand sites, are also given in **Figures 5.42. & 5.43**, respectively. The same trends may be observed, namely a substantial escalation in the water-soluble salt levels on the metal surfaces, with an increase in exposure time, particularly pertaining to the West Rand locales.

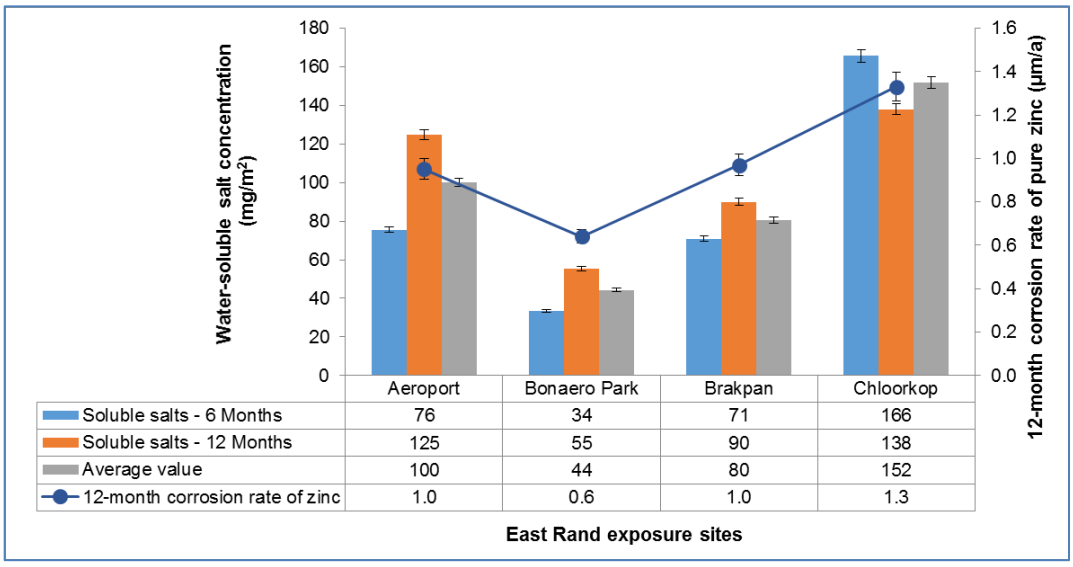


Figure 5.42 Measured 6- and 12-month water-soluble salt concentrations of the corroded mild steel specimens versus the 12-month corrosion rate of pure zinc at the East Rand sites.

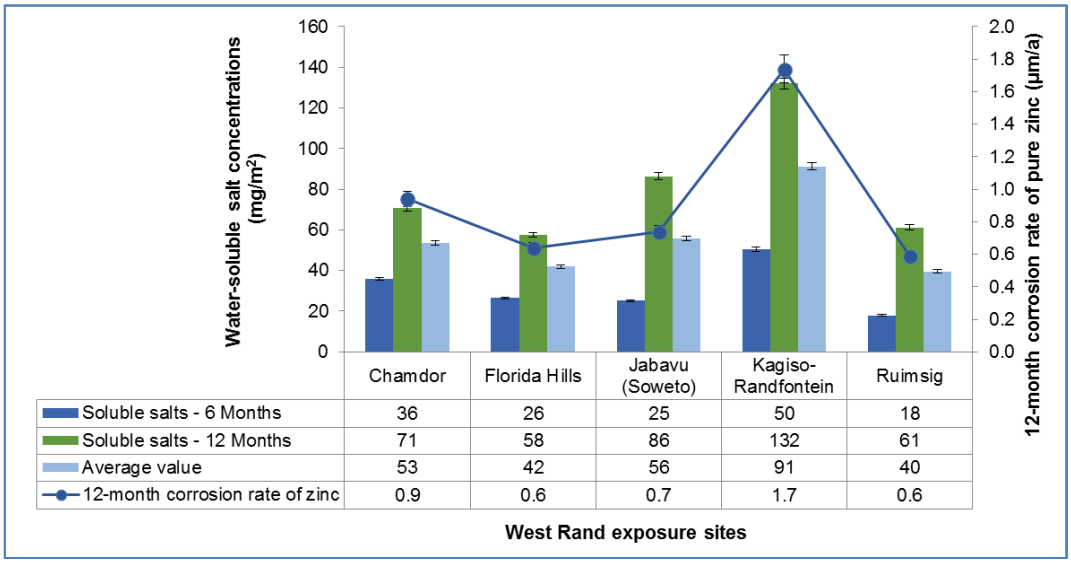


Figure 5.43 Measured 6- and 12-month water-soluble salt concentrations of the corroded mild steel specimens versus the 12-month corrosion rate of pure zinc at the West Rand sites.

Generally, as the concentration of water-soluble salts increased on the metal surfaces, so too did the corrosion rate of zinc. The higher concentrations of water-soluble salts on the test surfaces at Chloorkop and Kagiso-Randfontein also impacted significantly on the corrosion rate of zinc. Moreover, those sites located in residential areas, e.g. Bonaero Park, Florida Hills and Ruimsig exhibited significantly lower salt levels compared to the industrial, mining and township locales.

pH Measurements of the mild steel corrosion product

The pH of the mild steel corrosion products of the main and mini sites of the GJMA averaged at pH4.9 ± 0.3, 95% CI [pH4.8, pH4.9] (**Figure 4.56**). The Kagiso-Randfontein site, identified as a 'hotspot' regarding atmospheric corrosion in the GJMA, exhibited the lowest pH value, pH4.3, whereas reduced readings were also recorded for the Wadeville, Esselenpark, Walkerville, Newclare and Chamdor sites, which, apart from the Walkerville location, are all classified as industrial areas.

Misawa et al. (1974), as reported by Morcillo et al. (2011), confirmed that the pH of the electrolyte plays a vital role in the compositions of rust layers. Firstly, atmospheric oxidised ferrous ions dissolve into a neutral or slightly acidic thin moisture layer on the steel surface, resulting in the precipitation of lepidocrocite (γ-FeOOH). However, in SO_2 polluted environments, which lower the pH of rainwater, the γ-FeOOH will be inclined to dissolve, causing the precipitation of amorphous ferric oxyhydroxide upon drying. The latter is then converted to goethite (α-FeOOH), using OH^- (hydroxyl ions) supplied by the rain (**Equation 2.5**) (Misawa et al. 1974; Morcillo et al. 2011).

Linear regression analysis of the pH data versus the measured average corrosion rates of the mild steel panels, of the various locations, indicated a slight negative correlation, *r*-value of about -0.22 (R^2 = 0.05). However, this result was established as not statistically meaningful within the 90% CL. Nonetheless, the slightly negative value hinted at the possibility that although acidity may play a role in the corrosion of mild steel exposed to the GJMA atmosphere, in the pH4.3 to the pH5.7 range, it is a less critical influencing factor of the corrosion rate of this metal (**Figure 5.44**).

Considering only the main sites, the relationships between the pH values of the corrosion products versus the 12-month corrosion rates of mild steel, hot-dip galvanised

steel, aluminium, zinc and copper, as well as in opposition to the ICI, MCI and ACI values, appeared somewhat stronger (**Table 5.10**). The results showed increased negative correlations between the pH values of the corrosion products versus the 12-month corrosion rates of hot-dip galvanised steel, zinc, and copper - potentially indicating that these metals were somewhat affected by atmospheric and surface acidic variations in the pH4.3 to pH5.7 range, compared to mild steel and aluminium. Notable is that zinc (and for that matter also hot-dip galvanising), is said to be less sensitive in a pH range of 6.0 to12.5 (McEwan 2004). However, at an average pH of about 4.7 - the mean pH measured for the GJMA sites, it is evident that the corrosion rates of the zinc and copper specimens were increased.

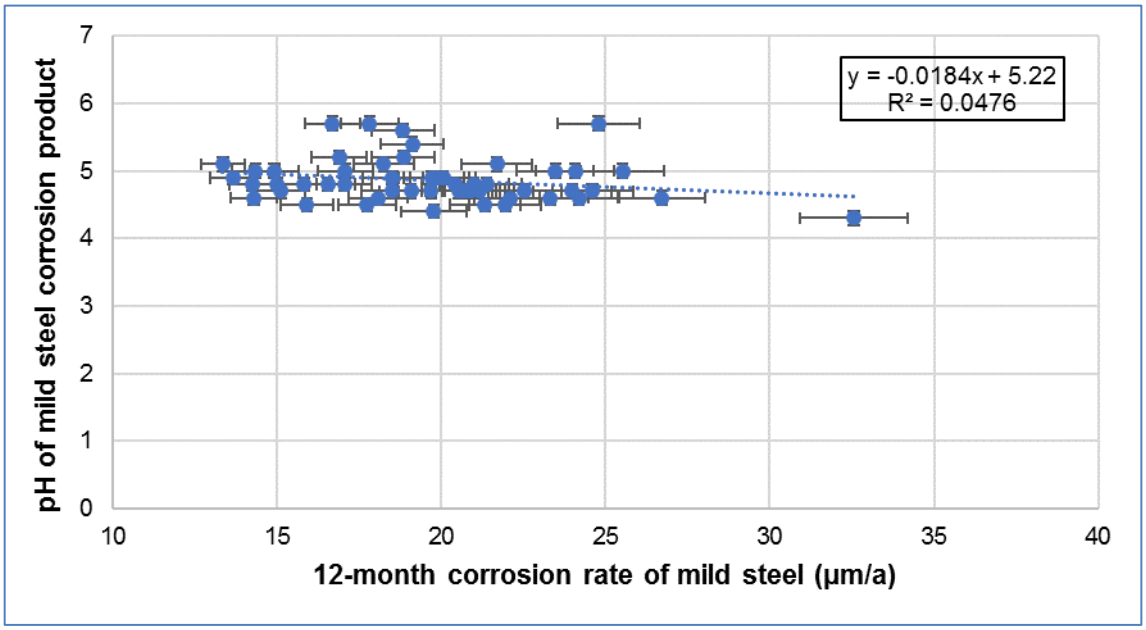


Figure 5.44 Linear regression analysis of the pH values of the corrosion products versus the 12-month corrosion rates of mild steel, as recorded at the different GJMA main and mini sites.

Like aluminium and zinc, copper oxides also exhibit amphoteric behaviour at anodic potentials (Lindstrom et al. 2007) and dissolve to form Cu^{2+} at low pH, Cu_2O and CuO at neutral to weakly alkaline pH, as well as dissolve at high pH to form soluble hydroxide complexes. This link between the latest present corrosion data and the pH values of the mild steel corrosion products may provide some explanation for the apparent relationship identified in Section 5.2.4 between these two metals, with a PPMC of 0.80 ($p \leq 0.05$) for the corrosion rates of the Cu-WH, versus the MSP values (**Appendix K**).

This strong connection was in opposition to the mild steel versus the aluminium or zinc results.

Table 5.10 PPMC coefficients between the pH values of the corrosion products of the mild steel specimens versus the 12-month corrosion rates of mild steel, hot-dip galvanised steel, aluminium, zinc and copper, as well as opposed to the ICI, MCI and ACI values.

Corrosion data vs pH of the mild steel corrosion products	Pearson correlation (*r*)	P value for Pearson
ICI	0.17	> 0.10
MCI	0.13	> 0.10
ACI	-0.21	> 0.10
12-month corrosion rate of mild steel	-0.37	≤ 0.10
12-month corrosion rate of hot-dip galvanised mild steel	**-0.45**	**≤ 0.05**
12-month corrosion rate of aluminium	-0.31	> 0.10
12-month corrosion rate of zinc	**-0.48**	**≤ 0.05**
12-month corrosion rate of copper	**-0.51**	**≤ 0.05**

Moreover, the link hinted at the possibility that the effect of varying pH of surface electrolytes on the corrosion of copper and mild steel is somewhat comparable under similar exposure conditions, with more limited pH regions of solubility of their protective corrosion products at anodic potentials, compared to zinc and aluminium. This finding is also supported by Pourbaix diagrams for these metals at 25°C, as presented in **Figure 5.45** (McEwan 2004), indicating that both aluminium and zinc have greater pH ranges of soluble corrosion products at given anodic potentials, compared to iron and copper.

Table 5.10 also shows a weak negative relationship between the pH measurements of the mild steel corrosion products and the recorded ACI values for the different sites. This finding alluded to the possibility that the *aluminium-nylon* wire-on-bolt (ACI) unit was most sensitive to changes in the pH4.3 to pH5.7 range, compared to the *aluminium-copper* (ICI) and *aluminium-steel* (MCI) CLIMAT galvanic couples. The corrosion of the last-mentioned units was somewhat retarded (although weakly) by a decrease in acidic pH of the surface electrolyte. This phenomenon can also be explained by the Pourbiax diagram for aluminium at 25°C (McEwan 2004), which indicates that at high cathodic

potentials, a slight increase in acidic pH, between pH4 to pH6, can result in a small decrease in the cathodic potential.

The result that the galvanic corrosion rate of the wire-on-bolt units may decrease slightly, with a small rise in acidic pH, is significant. This is since it provides potential rationalisation as to why the PPMC coefficients between the ICI, MCI and ACI values for the GJMA sites, when compared to their mild steel corrosion rates, were markedly weaker than in the case of the ISO open wire aluminium, zinc and copper helices (**Appendix K**). The impact of acidic pH in the range of 4.3 to 5.7, was less noticeable regarding the galvanic corrosion created with the wire-on-bolt CLIMAT units.

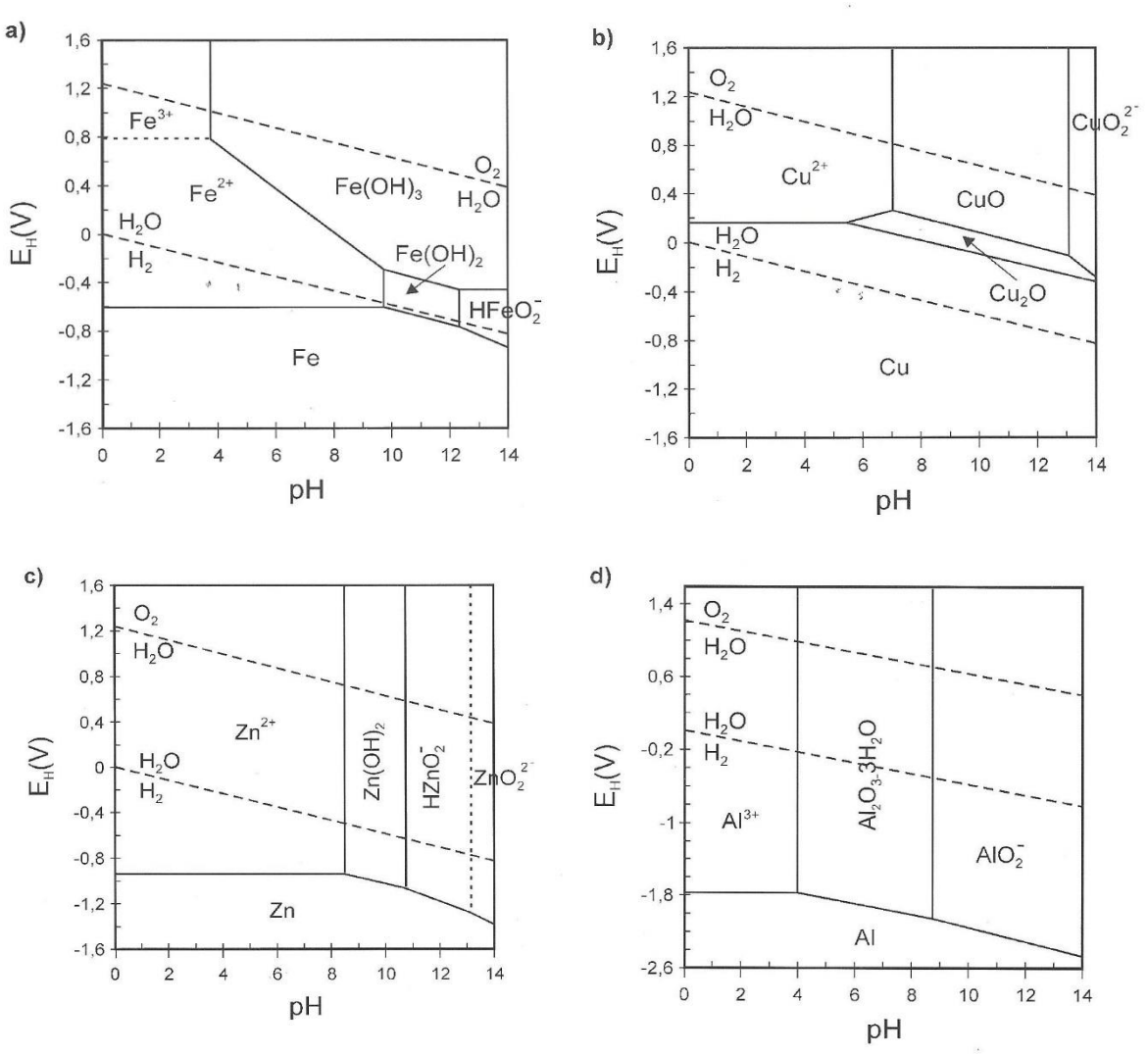


Figure 5.45 Pourbaix diagrams for a) iron, b) copper, c) zinc, and d) aluminium at 25°C (McEwan 2004).

5.3 EFFECTS OF THE GJMA'S ATMOSPHERE ON ORGANIC COATINGS

As stated in Chapter 2, many scholars view 'corrosion' as also applicable to the degradation of non-metallic materials, due to environmental effects (Uhlig 1963; Fontana 1987; Roberge 2012). Given that these materials are often used to protect metal surfaces from corrosion, the effects of atmospheric environments on them are also of relevance, and like metals, will vary in natural C1 to CX corrosive atmospheres (International Organization for Standardization 2007a). However, the extent of the environmental degradation will also be influenced by air pollution, caused by human activity, particularly in urban and industrial environments. Li et al. (2013) state that SO_2 may cause damage to stone, concrete, metal and organic coatings.

Yocom (2012) reports that motor vehicle coatings are good indicators of corrosive or damaging atmospheres since the owners tend to notice damage to their vehicles quickly, which is then frequently brought to the attention of those in charge of air pollution. The appearance of coatings is typically evaluated by monitoring changes in colour and gloss, following exposure to various indoor and outdoor weathering conditions, and relating these performance parameters to corresponding changes in the chemical and physical properties of the coatings (Keene et al. 2004). Regarding the present study, the impact of the corrosiveness of the GJMA's atmosphere was evaluated by monitoring the changes in coating thickness, gloss, colour, the degree of chalking, dirt retention and modifications of the general corrosion protection properties of the materials. A further objective of the current work was to verify whether water-based and powder coatings (non-VOC emission coatings) are suitable for the corrosion protection of mild steel and other metal surfaces in the GJMA, as an alternative to less user- and environmentally-friendly solvent-borne materials.

The results showed that the degree of corrosion of the different coated specimens exposed at the main sites was not important after 24 months of exposure, regarding ISO 4628-3 (International Organization for Standardization 2003b). Nonetheless, measurable changes were found concerning the average DFT, gloss level, colour, chemical structure, as well as the degrees of chalking and dirt retention of the coatings (**Figure 4.57**).

5.3.1 Dry Film Thickness (DFT) Changes

Table O.1 (**Appendix O**) reveals that following 24 months of exposure in the GJMA atmosphere, the polyester powder coating (System F) and a water-based acrylic coating system (System D) typically exhibited the lowest average DFTs, followed by Systems G, E and A. Apart from System A, these are all 'single-component' coatings, typically viewed as less suitable for more corrosive environments, especially in the ISO 9223:2012 *high* C4 to *extreme* CX ranges (International Organization for Standardization 2018a; 2012a). This is mainly because of their reduced film-build (Nelson 2012; Friel & Nungesser 2012) and higher moisture vapour permeability characteristics (Mark 2007). Consistent with ISO 12944 - Part 5 (International Organization for Standardization 2018a), the expected durability of these systems in *low* C2 to *moderate* C3 corrosive environments is about 5-15 years, although in *high* C4 to *extreme* CX conditions, it is given as less than five years. Nonetheless, from an application, consumer and environmental point of view, these systems are more user- and environmentally-friendly compared to two-part solvent-borne materials (McEwan 2004). Therefore, their potential use in less corrosive areas is pertinent.

Concerning the different coating systems, the percentage variability in their initial average thicknesses ranged from about 9-27% (**Appendix L - Table L.1**), depending on the modes of application, such as whether the coating was applied by brush or spray technique, as well as its general levelling (flow-out) properties. However, following 24 months of the exposure in the GJMA, the variability in the average DFTs of the different coating systems increased slightly to approximately 11-32%, although, the initial connections between these were still relevant, $r \sim 0.87$ ($P \leq 0.05$). This inferred that the slight changes were likely associated with the uncertainty of re-measurement of the average DFTs (Section 3.3.3.1), rather than because of exposure to the GJMA's atmosphere. However, the other coating parameters still necessitated consideration.

The Brakpan locale was the only site that exhibited an overall increase in average coating thickness (**Figures 4.58 & 4.59)**. While curious at first, this finding was subsequently linked to reduced UV light exposure at this site (**Appendix S – Tables S.1 & S.2**). Conversely, Kagiso-Randfontein, Kya Sand and Jabavu (Soweto) displayed the highest overall changes regarding their average coating thicknesses, whereas in addition to Brakpan, minimal variations were also recorded for Braamfontein and

Ruimsig (**Figure 5.59**). Systems D, E, F and G consistently showed a decrease in average thickness at all the main GJMA sites (**Table O.2 – Appendix O**). Conversely, some of the samples coated with Systems A (epoxy-acrylic), B (epoxy-polysiloxane) and C (epoxy-polyurethane) revealed slightly positive variations. In this regard, it is of note that polysiloxanes and polyurethanes exhibit better resistance to UV light radiation than other organic topcoats (Mowrer 2003). For example, polysiloxanes (System B) display a much higher resistance to temperature, UV light degradation and oxidation, also when compared with polyurethanes (Mowrer 2003) - justifying the adverse average DFT change of System B after 24 months of outdoor weathering (**Figure 4.60**).

System E (a three-coat water-based acrylic emulsion paint) presented the most substantial change in average coating thickness (**Figure 4.60**), followed by System D (another water-based acrylic system), and then Systems F and G. Of importance are that the latter two systems (polyester powder and alkyd systems) displayed similar variations in average DFT, following 24 months of outdoor exposure. Accordingly, these two coatings showed a connection between their respective average DFT changes from one site to the other (**Figure 4.60**), even if modest. This relationship was justified since alkyds are complex oil-modified polyesters (Nelson 2012; Encyclopaedia Britannica 2016), implying that Systems F and G are chemically related. Nevertheless, the results corroborated the understanding that some coatings exhibit better resistance to UV light degradation than others, e.g. the polysiloxane and polyurethane coatings. Consequently, the results were successively interpreted per system type, rather than collectively.

Linear correlations (PPMC) between the changes in the DFTs of the different coating systems at the main sites (**Table 5.11**) confirmed insignificant ($P > 0.10$) to weak ($P \leq 0.10$) positive trends between the percentage changes in the DFTs of Systems A and E, A and F, A and G, B and C, B and G, as well as F and G. Conversely, meaningless to moderate negative trends were established between Systems B and E, C and F, including D and G. As a result, the responses of Systems A, E, F and G to outdoor weathering (at the different GJMA exposure sites) were comparable to some degree. Contrarywise, the reactions of Systems B, C and D appeared more alike. Their colour was also similar, namely Leaf Green (RAL 6002).

The higher durability of Systems A, B and C to long-term outdoor weathering was evident (**Figure 4.60**). These three systems were thus viewed as poor indicators of the effects of UV light radiation at the different sites, based on their DFT changes. As a result, considering only the DFT changes in Systems D to G (**Figure 4.61**), Nasrec, Kagiso-Randfontein, Braamfontein and Newtown appeared most influenced by direct sunlight exposure and pollution. In this regard, it is notable that Nasrec and Kagiso-Randfontein are both situated near old gold mine tailing dumps (**Figure 2.20 & 2.23**) (Google Inc. 2016a, 2017a), whereas the Braamfontein locale, exhibits the highest elevation above ground and sea levels (**Appendix B – Table B.1**). As in the case of the Braamfontein area, Newtown is positioned in Johannesburg's CBD (**Appendix F**). However, the implications of these findings were uncertain, and possibly even coincidental, especially before considering the other coating parameter responses. Moreover, it was likely that the DFT changes were associated with the shrinkage of the coatings (Laudone et al. 2003, Tator 2015), rather than due to atmospheric pollution.

Table 5.11 PPMC coefficients between the changes in the average DFTs of the various coating systems after 24 months of outdoor weathering at the main GJMA sites.

	System	**A**	**B**	**C**	**D**	**E**	F	G
		r-value	*r*-value	*r*-value	*r*-value	*r*-value	*r*-value	*r*-value
Changes in average DFT	**A**	1	0.10	-0.11	-0.11	0.29	0.36	0.37
	B		1	0.37	-0.18	-0.34	0.10	0.35
	C			1	-0.08	-0.11	-0.34	-0.18
	D				1	-0.10	0.11	-0.42
	E					1	-0.03	0.22
	F						1	0.45
	G							1

Note: – *r*-value – Pearson product-moment correlation (PPMC) coefficient.

5.3.2 Degree of Chalking and Dirt Retention

The highest levels of chalking and dirt retention (the latter potentially being an indicator of the roughening of surfaces due to photochemical breakdown) were measured for the Aeroport, Braamfontein and Chloorkop sites (**Figures 4.64 & 4.65**) - all with a sum (∑) value of 12 ± 2 **(Figure 4.65)**. These were trailed by the Midrand and Kagiso-Randfontein locales, with a total of 11 ± 2. The least chalking and dirt retention were

recorded at the Alexandra and Florida Hills locales, potentially indicating lower levels of solar radiation at these specific sites.

Important is that the chalking and dirt retention results correlated only slightly negative with the sum (∑) average DFT changes of the coating systems at the various sites, with the PPMC equal to -0.22 and $P > 0.10$. This statistically meaningless relationship sustained that the average DFT variations were unlikely to be caused by the chalking and dirt retention processes, but instead by the shrinkage of the paint layers or possibly owing to the further volatilisation of organic components (Hare 1992) - once exposed to sunlight and higher surface temperature. However, concerning the epoxy-polysiloxane coating system (System B), the linear trend between the average DFT changes of the coated specimens and their gloss level variations was stronger, with a PPMC value of -0.38 and $P \leq 0.10$ (within a 90% CL), hinting that these DFT changes might at least partially be associated with sunlight exposure.

While System G (the alkyd system) displayed the highest degree of chalking (**Figures 4.64 & 4.66**), System E exhibited greater film loss, likely caused by shrinkage (**Figure 4.60**). The latter system also appeared more affected by dirt retention, common in many exterior-quality acrylic emulsion paints. Mark (2007) mentions that acrylic coatings are particularly vulnerable to the retention of soot and dirt at warmer temperatures, which are difficult to remove by rain. While soiling of the coated surfaces does not necessarily cause deterioration directly, the removal of it does, e.g. the removal of sooty layers by way of abrasive blast-cleaning from buildings (Yocom 2012)

5.3.3 Changes in the 60° Specular Gloss Levels

The initial percentage variability in the specular gloss levels of the different coating systems ranged between 1% and 13% (**Appendix Q – Table Q.1**), depending on the modes of application and generic coating formulations. The polyester powder coating (System F) also exhibited the lowest percentage variation in gloss level, approximately 1%, since an electrostatic spray process was used for the application. Moreover, Systems G, F and C (in that order) displayed the highest initial gloss levels.

After 24 months of exposure in the GJMA, the alkyd high gloss enamel coating (System G) presented the highest percentage gloss change, followed by System C (the epoxy-polyurethane system) (**Figure 4.67**). This finding corresponded, to some degree,

with the chalking and dirt retention results, revealing that System G was most affected by chalking and gloss level changes.

Systems D and E also exhibited lower initial gloss levels (**Appendix Q – Table Q.1**). Therefore, these systems were found to be less responsive in reflecting the levels of UV light radiation at the different locales. Worth mentioning is that the formation of loose chalky layers and dust on coated surfaces may partially protect surfaces from sunlight exposure (Hare 1992). Therefore, this impact also required consideration.

The gloss level changes were based on more quantitative data, compared to the chalking and dirt retention results. Accordingly, evaluation of the solar radiation levels at the different sites, based on their gloss changes, appeared more relevant. Consistent with **Figure 4.68**, based on summations (∑) of the variations in the average gloss levels (GU) of Coating Systems A, B, C, F and G, Aeroport, Alexandra, Brakpan and Braamfontein were more affected by UV light radiation and pollution. Conversely, Jabavu (Soweto), Midrand and Ruimsig were the least influenced.

The strongest linear correlations, modest ($r > 5$) to high ($r > 7$), within a 95% CL, were recorded for the gloss changes of Systems B and E versus the 12-month corrosion rates of mild steel, galvanised steel, aluminium, zinc and copper (**Table 5.12**).

Table 5.12 PPMC coefficients between the changes in the average gloss levels of the coating systems after 24 months of exposure, and the 12-month corrosion rates of mild steel, galvanised steel, aluminium, zinc and copper at the different sites.

Coating system		R_{corr} (MS) steel	R_{corr} (Galv) steel	R_{corr} (Al)	R_{corr} (Zn)	R_{corr} (Cu)
		***r*-value**	***r*-value**	***r*-value**	***r*-value**	***r*-value**
Changes in gloss level	**A**	-0.06	-0.09	-0.14	-0.13	-0.20
	B	**0.50**	**0.40**	**0.40**	**0.47**	**0.50**
	C	-0.38	-0.11	-0.11	-0.02	-0.13
	D	-0.19	-0.00	0.04	-0.11	-0.18
	E	**0.60**	**0.71**	**0.73**	**0.69**	**0.62**
	F	0.13	-0.06	0.06	-0.04	-0.01
	G	-0.05	0.13	0.06	0.12	-0.11

Note: R_{corr} denotes 12-month corrosion rate, MS – mild steel, Galv. – hot-dip galvanising, Al – aluminium, Zn – zinc, Cu – copper and *r*-value – PPMC. Also, values of +/- 0.41 indicate statistical importance within a 95% CL.

The high correlations implied that the changes in the average gloss levels of these two systems were more impacted by the corrosive conditions of the atmosphere, than by sunlight radiation. Also, the result supported the rhetoric that polysiloxanes are more resistant to UV light radiation, whereas solution-acrylics tend to absorb lower levels of UV light (Friel & Nungesser 2012).

5.3.4 Changes in Colour

Generally, the coated samples at Chloorkop and Kagiso-Randfontein displayed the highest colour changes after 24 months of outdoor weathering, followed by the Alexandra, Aeroport and Bonaero Park locales (**Figure 4.69**). The least overall changes were recorded for the Jabavu (Soweto) and Florida Hills sites. Refer also to **Appendix R – Figure R.1**). This finding implied that the Chloorkop and Kagiso-Randfontein were likely most influenced by photochemical impact (UV light radiation and pollution), compared to the other sites.

Important to note is that medium to strong correlations existed between the measured total colour differences (ΔE) and summations of the degree of chalking and gloss loss of the coated surfaces (at the different sites), with PPMC coefficients of 0.63 ($P \leq 0.01$) and 0.50 ($P \leq 0.05$), respectively. Conversely, the linear correlation between the colour changes and DFT losses was only weakly negative, -0.28, statistically insignificant within a 90% confidence limit. Therefore, as mentioned above, the DFT measurements were less precise in reflecting the levels of solar irradiance at the different sites.

In general, in comparison with the corrosiveness of the environment, based on the 12-month corrosion rates of mild steel, galvanised steel, aluminium, zinc and copper, medium to strong linear correlations (within a 95% CL) were calculated regarding the total colour differences (ΔE) of the coated samples exposed at the sites. This was particularly valid for Systems B (polysiloxane), E (water-based acrylic) and G (alkyd high-gloss enamel) (**Table 5.13**), which showed the likelihood that the overall corrosiveness of the environment strongly influenced the slight colour changes of these coating systems, particularly concerning the green-pigmented polysiloxane coating. Nonetheless, the latter coating exhibited the best overall resistance to UV light radiation.

Table 5.13 PPMC coefficients between the total colour differences (ΔE) of the coating systems after 24 months, and the 12-month corrosion rates of mild steel, galvanised steel, aluminium, zinc and copper at the various locales.

Coating system		R_{corr} (MS) steel	R_{corr} (Galv) steel	R_{corr} (Al)	R_{corr} (Zn)	R_{corr} (Cu)
		r-value	*r*-value	*r*-value	*r*-value	*r*-value
Colour difference (ΔE)	**A**	0.03	0.18	0.02	0.15	0.04
	B	**0.63**	**0.74**	**0.67**	**0.76**	**0.70**
	C	0.28	0.30	0.46	0.31	0.29
	D	0.28	0.25	0.18	0.24	0.26
	E	**0.53**	**0.55**	**0.65**	**0.54**	**0.52**
	F	0.04	-0.26	-0.19	-0.26	-0.21
	G	**0.60**	**0.49**	**0.40**	**0.50**	**0.69**

Note: R_{corr} denotes 12-month corrosion rate, MS – mild steel, Galv. – hot-dip galvanising, Al – aluminium, Zn – zinc, Cu – copper and *r*-value – Pearson product-moment correlation coefficient. Also, values of +/- 0.41 indicate statistical importance within a 95% CL.

5.3.5 Changes in Chemical Structure

The highest average FTIR spectral QCheck™ correlations of the coated surfaces before and after cleaning, following 24 months of exposure at the main GJMA sites, versus their initial (control) spectra, were established for the Jabavu (Soweto), Florida Hills, and Ruimsig locations (**Figure 4.70**). Conversely, the lowest correlations were calculated for the Kagiso-Randfontein, Aeroport, Midrand and Delta Park sites, potentially indicating that the former sites displayed the least photochemical breakdown of the coated surfaces, compared to the latter areas (see also **Appendix S - Tables S.1 & S.2)**.

Of importance were the slight differences in the correlations before and after cleaning of the coated coupons, likely caused by the accumulation of weathering products (chalking compounds) and dust deposits on the surfaces (**Figure 4.70**). Also, noteworthy was the apparent higher average correlation for the Jabavu (Soweto) versus the other sites (**Appendix S - Tables S.1 & S.2**, as well as **Figure 4.70**) - potentially suggesting that this locale experienced abnormally reduced UV light radiation compared to the other areas. This was likely caused by the shadowing effects of a water tank and structural steelwork to which the test rack was attached. Therefore, the results were viewed as being less representative of the actual solar irradiance level of this area.

Those systems that showed the highest variations from their control spectra, following 24 months of exposure at the main GJMA sites, were Systems D (water-based acrylic), E (water-based acrylic) and G (alkyd high gloss enamel) (in that order). The least changes were recorded for Systems B (epoxy-polysiloxane), A (epoxy-acrylic) and F (polyester powder coating). See also **Figure 4.71** in this regard.

PPMC coefficients for the after exposure 'fingerprint' matches with the unexposed control FTIR spectra, compared to the levels of chalking, loss of gloss and total colour differences, as well as the 12-month corrosion rates of mild steel, galvanised steel, aluminium, zinc and copper, at the various locations, are presented in **Table 5.14**.

Table 5.14 PPMC coefficients for the FTIR (chemical 'fingerprint') matches of the control versus the after-exposure spectra, with the DFT, gloss, chalking and colour (ΔE) differences of the coating systems after 24 months of exposure, as well as in comparison with the 12-month corrosion rates of mild steel, galvanised steel, aluminium, zinc and copper at the different locales.

Coating system	DFT change	Degree of Chalking	Loss of gloss	Colour change	R_{corr} (MS) steel	R_{corr} (Galv) steel	R_{corr} (Al)	R_{corr} (Zn)	R_{corr} (Cu)
	***r*-value**	***r*-value**	***r*-value**	***r*-value**	***r*-value**	***r*-value**	***r*-value**	***r*-value**	***r*-value**
A	0.12	-0.05	-0.03	-0.26	0.13	0.28	0.20	0.29	**0.35**
B	-0.02	-0.17	-0.11	-0.25	**-0.40**	-0.27	-0.20	-0.30	**-0.37**
C	0.42	**-0.55**	**-0.54**	**-0.42**	-0.11	0.03	-0.15	-0.09	-0.01
D	-0.11	**-0.45**	**-0.39**	**-0.59**	**-0.74**	**-0.74**	**-0.63**	**-0.77**	**-0.75**
E	0.04	**-0.64**	**-0.57**	**-0.73**	**-0.71**	**-0.65**	**-0.65**	**-0.70**	**-0.66**
F	0.15	0.30	0.34	-0.31	0.19	0.31	0.38	0.32	0.31
G	0.15	0.17	0.21	-0.23	-0.08	0.23	0.08	0.24	0.15

Note: R_{corr} denotes 12-month corrosion rate, MS – mild steel, Galv. – hot-dip galvanising, Al – aluminium, Zn – zinc, Cu – copper and *r*-value – Pearson product-moment correlation coefficient. Also, values of +/- 0.41 indicate statistical importance within a 95% CL.

The chemical 'fingerprints' of Systems D and E displayed medium to strong negative correlations ($P \leq 0.05$) with their respective chalking, loss of gloss, and colour variation data. This inferred that the latter changes (due to sunlight exposure), produced lower correlations between the chemical 'fingerprints' of Systems D and E, and their control spectra. Understandably, the latter was a symptom of increased photochemical ageing of the sun-exposed surfaces of the coated samples – most likely caused by the breakdown of the molecular structure of the binder, i.e. acrylic polymers. This

breakdown is illustrated by the changes in the FTIR spectra of Systems D and E at selected sites (**Appendix S - Figures S.1 & S.2**) – indicated by the decreased amplitudes/intensities of the peaks in the wavenumber region of 500 cm^{-1} to 1800 cm^{-1}. Important is that concerning some of the FTIR spectra, only select regions of the infrared frequency range are given. This is to highlight the differences between the various sites.

Regarding System C (polyurethane), although the trend was somewhat reduced in comparison with Systems D and E (**Figure 5.46**), the changes of the exposed surfaces were seemingly more related to photo-oxidative ageing rather than the general corrosivity of the environment (**Table 5.14 & Figures 4.71 & 5.46**). Of further note is that the negative correlations between the FTIR QCheck™ matches of the control versus the exposed surfaces of Systems A (epoxy-acrylic) and B (epoxy-polysiloxane), with their changes in coating thicknesses, colours, degrees of chalking, and loss of gloss levels, somewhat reduced. This was in comparison with Systems C, D and F, potentially suggesting that the chemical changes in the coatings were less influenced by solar radiation (**Table 5.14 & Figures 4.71 & 5.46**). The chemical changes in the epoxy-polysiloxane coating system were more influenced by variations in the corrosivity of the environment, e.g. moisture and pollution levels, than in the case of System A. The same applies for Systems F and G (**Table 5.14**).

About the different 12-month corrosion rates of mild steel, galvanised mild steel, aluminium, zinc and copper at the main sites, the highest negative correlations, with ($P \leq 0.01$) were recorded for Systems D, and E (**Table 5.14**) See also **Figure 5.46** in this regard. This finding suggested that the upper-facing surfaces of these two systems were also significantly affected by the varying corrosive levels of the atmosphere. By contrast, the molecular breakdown of the upper-facing surfaces of Systems, A, F and G appeared less influenced by the corrosivity of an environment.

Based on the results, Kagiso-Randfontein and Aeroport were most influenced by UV light radiation, combined with pollution in the atmosphere, whereas the Jabavu (Soweto) and Florida Hills locales were least affected. However, the Jabavu (Soweto) results were considered less representative of the real solar irradiance level of this locale.

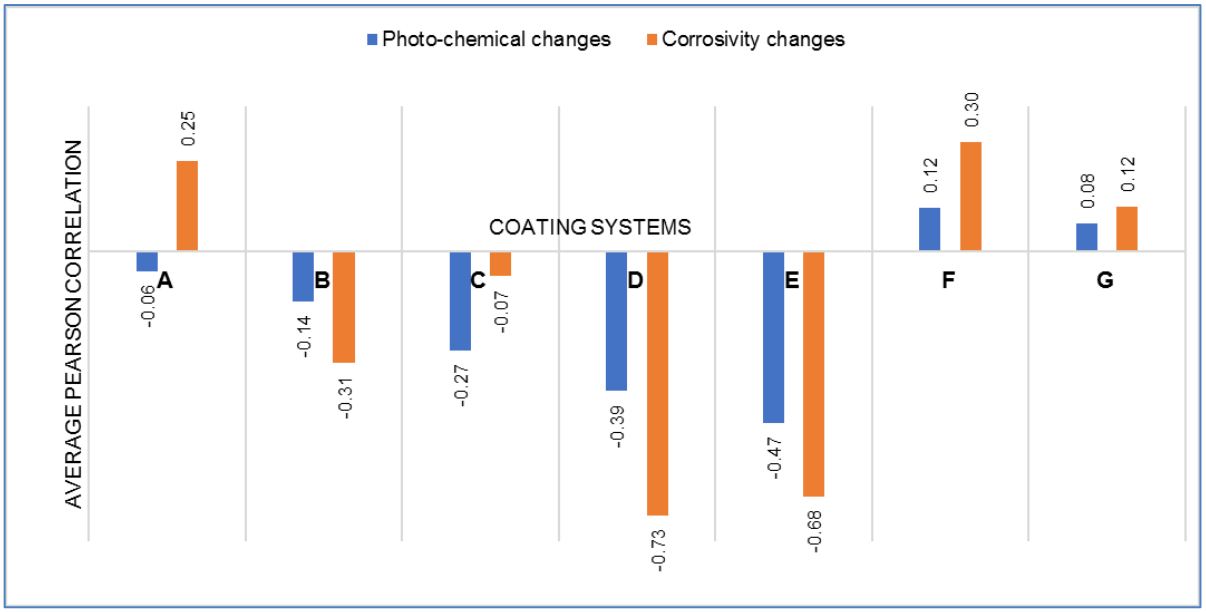


Figure 5.46 Average PPMC coefficients between the FTIR spectra of the different coatings after exposure in the GJMA environment and their respective control spectra, as well as opposed to the changes in the corrosivity of the local environments. Values of +/- 0.41 indicate statistical importance within a 95% CL.

As stated above, the Brakpan site displayed an overall increase in the sum (∑) average DFTs of the coatings after 24 months of exposure. This finding was finally explained by the fact that the Brakpan locale exhibited one of the lowest solar irradiation levels of all the main GJMA sites. Therefore, the extent of shrinkage of the coating due to sunlight and elevated temperature exposure, may well have been reduced. Additional swelling (due to the uptake of moisture) also could not be excluded, mainly since the Brakpan site is in a well-established bowling field, with the lawn being watered on a regular basis.

Noteworthy is that at the Aeroport site, premature corrosion problems were reported for coated galvanised profiled sheeting within only eight years of exposure, although anticipated to last for more than two decades (Janse van Rensburg 2015). The corrosiveness of the atmosphere resulted in the increased breakdown of the organic materials, due to pollution from the nearby industries, as well as from the Kelvin A and B Power Stations. Also, the area is positioned in the vicinity of South Africa's largest airport, OR Tambo International.

Worth noting is that the dumping of aviation fuel before landing, causing a mist containing mostly of kerosene to fall on houses, vehicles and other structures, has been

reported to be a cause of concern (Airliners.net 2004; Adams 2014). Seeing that hydrocarbon fuels are known to attack certain generic types of coatings, it is not improbable that the dumping of fuel in this area of the GJMA may accelerate the photochemical degradation of organic coatings. The impact of Kelvin Power Stations A and B (the only remaining operating coal-fired power stations in the GJMA) on the organic coated surfaces is also of vital importance.

According to the Airshed (2008), as summarised in the "*Highveld priority area air quality management plan*" (DEA 2011), the OR Tambo International Airport and supporting services areas contribute to local pollution. It is estimated that the emissions from aircraft exhaust add 1941 tons of CO, 1092 tons of NO_x, 85.4 tons of SO_2, 295 tons of hydrocarbon, 5.6 tons of benzene, 5.2 tons of 1,3 butadiene and 1.8 tons PM_{10} to the surrounding atmosphere.

5.4 PHYSICAL, METEOROLOGICAL AND POLLUTION EFFECTS ON THE CORROSIVITY OF THE GJMA

5.4.1 Physical Effects

5.4.1.1 Topography and relief

The topography and relief of the GJMA have a substantial effect on the corrosivity of the environment. This was evident from the higher corrosion rates measured for suburbs located at higher altitude (e.g. at sites situated along the high ridge between Mogale City and Edenvale) (**Figure 2.26** - adapted from City of Johannesburg (2003) and **Figure 5.39**). However, it was also due to increased elevations above ground level, namely, the upper locales of buildings in the various CBD areas (e.g. the Braamfontein-Wits area, which is also located on the rocky ridge) (Section 5.2.6). The opposite is typically a reality in densely populated low-income areas, or in and around high industrial and traffic zones, where due to the combustion and/or burning of fossil fuel, or other sources of pollution, ground-level pollution generally decreases with an increase in elevation above ground level (e.g. at Palmridge, which is located next to Katlehong) (Section 5.2.6).

In this regard, **Figure 5.47**, adapted from Piketh et al. (2007), aptly presents the atmospheric pollution processes in an urban environment, showing that the concentrations of air fumes decrease with altitude and distance from the sources of pollution.

Of importance is that between the parallel ridges of the GJMA, pollution gets trapped due to winter inversion conditions (Gauteng Provincial Government 2017). It is also said that the northwards- and southwards-flowing basins create similar lowland areas, relative to the general topography of the GJMA, which serves as routes for the drainage of chilly air during winter (Gauteng Provincial Government 2017).

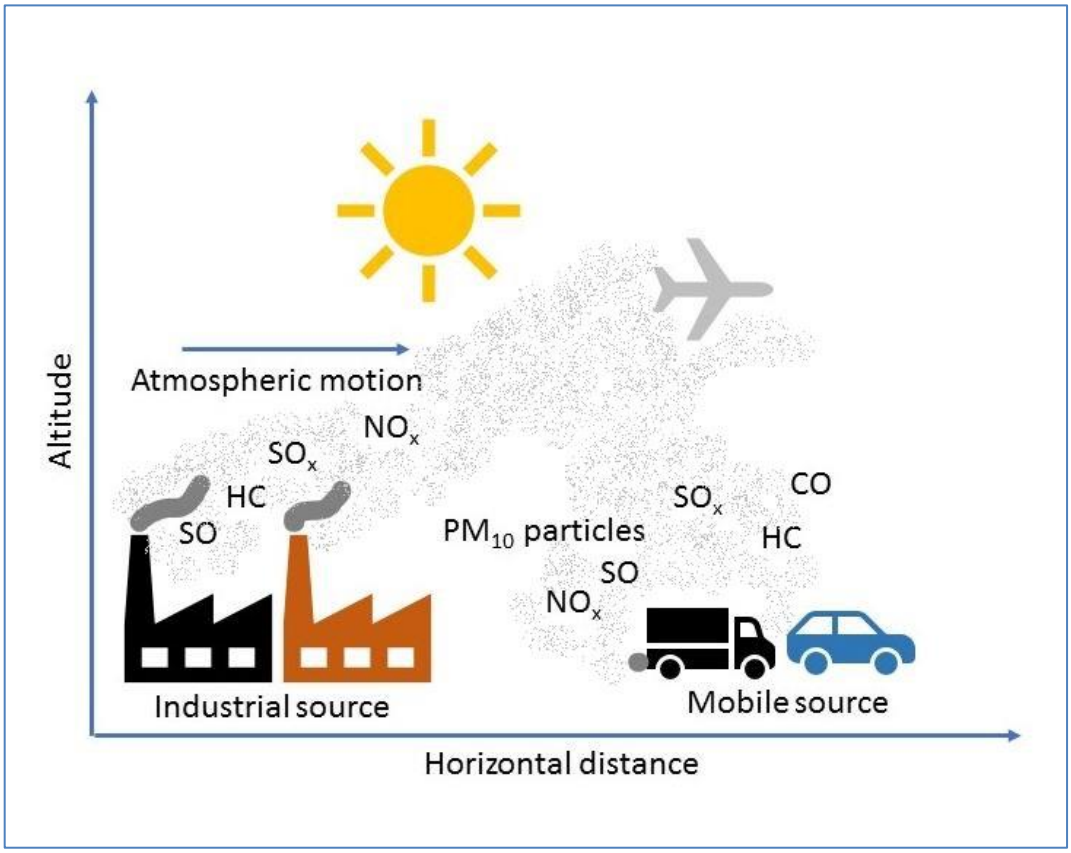


Figure 5.47 Illustration showing that the concentrations of air fumes decrease with an increase in altitude and distance from the sources of pollution – Adapted from Piketh et al. (2007).

Towards the south and eastern parts of the GJMA, the area changes into an open valley, which hosts numerous industrial and business installations, at Aeroport, Alrode, Kelvin, Isando, Modderfontein and Germiston. In comparison with the northward, central

and westward suburbs of the GJMA, these areas appear to be most affected by atmospheric corrosion (**Figures 5.22 - 5.24**, **5.26 - 5.28 & 5.39**).

5.4.1.2 Shading and vegetation

Figures 3.23 - 3.25 (DEA 2017a) and **Figures 4.19**, **4.23**, **4.30**, **4.32**, **4.54 & 4.70** support the understanding that the presence of trees and other vegetation in the GJMA generally reduces the impact of atmospheric pollution, e.g. at Delta Park (**Figure 5.48**). This appears to be particularly relevant in the more prosperous suburbs of Johannesburg, e.g. Houghton, Delta Park, Saxonwold and Northcliff, where the financial means not only exist for the procurement and planting of new trees, but also for the long-term preservation of established wooded areas. These wooded suburbs are mainly located towards the northern and north-western regions of the Johannesburg CBD. Conversely, the presence of trees and vegetation may also increase TOW, due to the shielding effects created by sunlight exposure. This is mainly relevant concerning metal surfaces positioned close to the ground, which was also found to have an impact at the Jabavu (Soweto) test location (**Figures 4.68 - 4.70**). The results at this site showed reduced UV light degradation of the coated specimens due to shielding/shading effects (Section 5.3.5).



Figure 5.48 Shielding and shading effects at Delta Park.

5.4.1.3 Waterbodies

Only one site was positioned near a large water body, namely Bonearo Park, which is a residential area next to the Blaauwpan Lake (**Figure 5.49**). An interesting observation is that this locale showed a slight increase in the corrosivity of the environment, with $P \leq 0.05$, when compared to other nearby areas, e.g. East Rand Mall, Kempton Park CBD, and the Northmead sites (**Figure 5.39**), which possibly could be explained by the proximity of the lake that gives rise to higher humidity levels in the vicinity. According to Gregory & Smith (1967), it is likely that similar influences occur around all water bodies, with the magnitude determined by the size of the lake or water reservoir.

The Bonaero Park and East Rand Mall test sites are also positioned on opposite sides of the OR Tambo International Airport, where large aircraft are often spotted flying directly over these locations. See **Figure 5.29** and Section 5.2.8.3.



Figure 5.49 Blaauwpan Lake located next to the Bonaero Park corrosion monitoring locale, causing a spike in backdrop humidity levels.

5.4.2 Meteorological Effects

The effects of the climatic factors on the corrosivity of the GJMA are diverse and likely triggered by a thin film of moisture on the metal surface (Payne 1961; Uhlig 1963; Fontana 1987; Tullmin & Roberge 2000; Roberge 2012; Cole 2017; Leygraf et al. 2016). The influences are also determined by the composition and morphology of the corrosion products formed on the metals' surfaces, its solubility in the electrolyte, and the development of passive oxide films (Fontana 1987; Tullmin & Roberge 2000), as well as variations in the meteorological conditions of the environment (Grøntoft 2011; Li et al. 2013; Leygraf et al. 2016).

5.4.2.1 Temperature

Figures 3.6 & 3.7 present the average monthly maximum and minimum temperatures for Johannesburg, as recorded during 2013 to 2015 - based on SAWS' (2017) statistics. As per the data, the mean monthly maximum temperatures for the area measured 22.9°C, 95% CI [20.7°C, 25.1°C], 22.6°C, 95% CI [20.6°C, 24.6°C] and 24.2°C, 95% CI [21.7°C, 26.7°C], for 2013, 2014 and 2015, respectively, whereas the corresponding average monthly minimum temperatures were 10.7°C, 95% CI [8.3°C, 13.1°C], 10.7°C, 95% CI [8.3°C, 13.1°C] and 11.4°C, 95% CI [9.1°C, 13.8°C]. The effect of an abnormally dry year in 2015, causing higher average maximum and minimum temperatures, is also observable in the results. It is therefore likely that the corrosion measurements taken during this period would have been influenced by the drier conditions, particularly relating to the 24-month mild steel and galvanised steel corrosion rates.

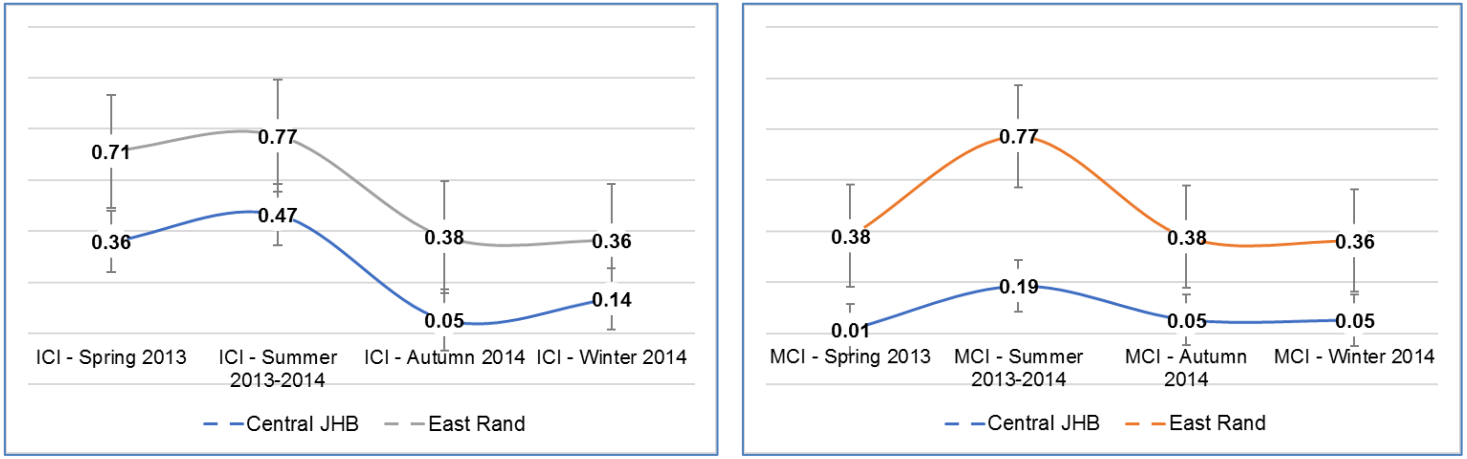
Figure 3.8 (based on SAWS (2014) data) presents the combined average monthly maximum and minimum temperatures for three weather stations in the GJMA area, namely at OR Tambo International Airport, the Johannesburg Botanical Gardens and Springs. As shown, the average diurnal temperature fluctuation in the GJMA during the study period was about 14°C (M = 13.7°C, 95% CI [12.1°C, 15.3°C], which, due to the temperature lag of materials, compared to ambient air (during night times), often encourages condensation of moisture on metal surfaces (Dean & Reiser 2002; McEwan 2004; Roberge 2012). The latter is a particularly frequent occurrence during

winter in the southern areas of the GJMA, due to the dry, cold and windless conditions (Gauteng Department of Agriculture and Rural Development 2011).

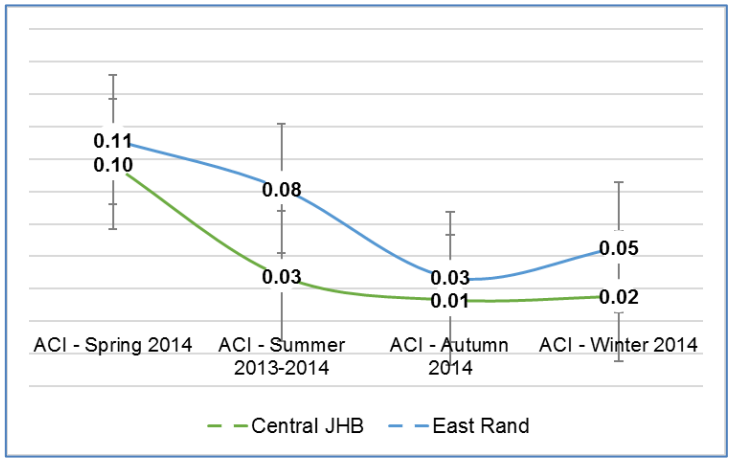
The average seasonal maximum and minimum temperatures of the OR Tambo International Airport and Johannesburg Botanical Gardens Weather Stations were compared with the collective measured seasonal ICI, MCI and ACI result for two regions for the GJMA. **Figure 5.50a** shows that the seasonal ICI fluctuations for the Central JHB and the East Rand Suburbs, where the weather stations mentioned above are located, related somewhat with the average cyclic maximum temperatures (**Figure 3.9a**) (based on SAWS (2014) data). However, the established PPMC coefficients of 0.81 and 0.89, for the Central JHB and the East Rand Suburbs, respectively, were found to be statistically insignificant within a 90% CL. This was possibly due to the limited period of analysis, which only covered four seasons (12 months). Similarly, while moderate to high correlations were found between the maximum seasonal temperatures and MCI data (**Figures 5.50b & Figure 3.9a**), these were statistically meaningless, as well as concerning the ACI results (**Figure 5.50c** and **Figure 3.9**) (SAWS 2014).

These findings hinted that while atmospheric corrosion in the GJMA may be influenced by daily and seasonal temperature fluctuations, mainly when elevated, the associations mentioned above are instead due to the link between increased temperatures and the rainy seasons of the year, during spring and summer. However, since RH is a function of temperature, it will also affect the amount of moisture that will be present in the air (Castillo 2011). Moreover, it is also a function of the deliquescence of deposited salts (Schindelholz et al. 2014) and will influence the residence time of the film electrolyte (TOW) (Schinderholtz & Kelly 2012).

However, concerning the Delta Park site, which is positioned within one kilometre from the Johannesburg Botanical Gardens, a PPMC of -0.92 was obtained between the seasonal, diurnal temperature fluctuations and the MCI results, statistically meaningful within a 90% CL. This finding suggested that at this location, an increase in the diurnal temperature variation inhibited rather than encouraged the corrosion rates.



(a) (b)



(c)

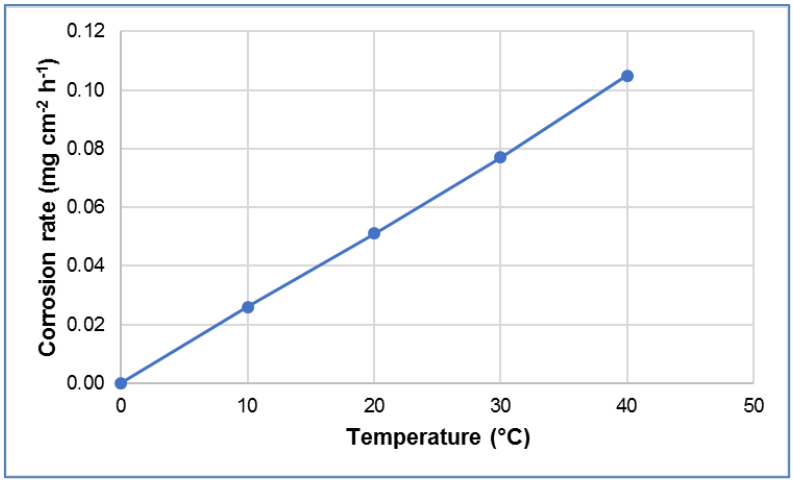
Figure 5.50 Average seasonal corrosion indices (as percentage weight loss) for the GJMA measured during the period August/September 2013 to August/September 2014: a) ICI, b) MCI and c) ACI.

Linarca & Geert (2002) report that the temperatures measured at street level in a major urban area, such as Johannesburg, can be several degrees higher than those in the surrounding valleys. However, trees and vegetation will cool the air by evapotranspiration (Tahir & Yousif 2013). During night-time, though, the reverse is relevant, that is the trees and vegetation will reduce the loss of heat from urban surfaces, consequently providing a canopy between the colder night air and the warm surface materials (Holewinski & Zeigler 1979), while the street surfaces will rapidly lose heat. In urban areas, this difference may be up to 5°C to 8°C (Federer 1971).

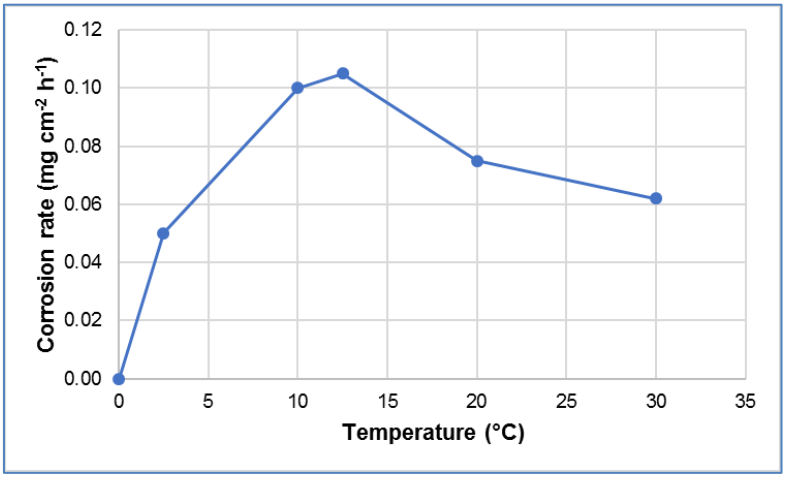
Temperature is also influenced by latitude, implying that the southern parts of the GJMA tend to be colder than the northern areas, particularly during summer. This finding supports the general understanding that temperature is undoubtedly a significant player when it comes to varying meteorological conditions (Dean & Reiser 2002; Roberge 2012; Leygraf at al. 2016). It is especially true regarding the percentage of moisture in the atmosphere (RH). the solubility of pollutants in wet films on metal surfaces, the drying time of surfaces, acceleration of electrochemical corrosion rates, the formation of wind and various other phenomena.

Leygraf et al. (2016) states that under permanent surface wetting conditions, such as encountered during precipitation, the overall effect of higher temperatures is likely to increase corrosion rates (**Figure 5.51a**) (reproduced from Leygraf et al. 2016). However, during fluctuating wetting conditions, the corrosion rate tends to increase with rising temperature up to a certain point but then decreases (**Figure 5.51b**).

This limited influence of the chlorides is possibly due to the higher desorption rates of the liquid film, consequently limiting the time for the surface to be wetted. It is mentioned further that higher temperatures also decrease the solubility of gases such as oxygen, which is known to play a crucial role in many atmospheric corrosion oxidising processes.



(a)



(b)

Figure 5.51 The effect of air temperature on the atmospheric corrosion rate of carbon steel: a) during rain and b) at drying out of a film of moisture during a constant RH of 75%. Reproduced from Leygraf et al. (2016).

5.4.2.2 Humidity

Figure 3.10 (SAWS 2014) shows that the variations in the average monthly RH levels in the atmosphere were less distinct in comparison with the maximum and minimum temperatures (**Figure 3.8**, also based on SAWS (2014) data), with the mean values for the period measuring 61.0%, 95% CI [53.9%, 68.1%] and 60.6%, 95% CI [53.4%, 67.7%] for the Botanical Gardens and OR Tambo sites, respectively.

The seasonal relationships between the two weather stations are indicated in **Figure 3.11** (SAWS 2014). As suggested, during autumn and winter, the percentage of

moisture in the atmosphere at the Botanical Gardens was slightly higher than at OR Tambo International Airport. This was likely due to the presence of trees and other plant life at the former location, causing a rise in local humidity levels. Sterling (2004) states that up to 99% of the water absorbed by trees via their roots are lost via transpiration through plant leaves. Holewinski & Zeigler (1979) also confirm that large groups of trees, e.g. found in parks, can lower summer air temperatures and increase humidity over large areas. In this regard, Kramer and Kozlowski (1960) found that a single tree can transpire approximately 300 litres of water per day, providing soil moisture levels are sufficiently high. However, since the former weather station is located at the Botanical Gardens, the possibility of additional watering of the area cannot be excluded.

Figure 5.52 shows that the changes in the %RH values from one season to the next, corresponded in a strongly positive manner with the variations in the MCI data, followed by the ICI results for the East Rand locales. Conversely, concerning the ACI data for the Central JHB and East Rand regions, negative correlations were determined. Nevertheless, the correlations were statistically meaningless ($P > 0.10$) within a 90% CL, likely due to the limited period of testing. The results did suggest, however, that %RH was not the sole driving force behind the atmospheric corrosion processes and that the CRH is not constant for all metals, surface contaminants or environments, but varies depending on the type of the material, affinity of the corrosion product and other surface deposits to absorb moisture, as well as the presence of atmospheric pollutants (Brown and Masters 1982; Tullmin & Roberge 2000; Li et al. 2013), e.g. sulphur dioxide and chlorides. Therefore, the reaction of the ICI *aluminium-copper* wire-on-bolt, versus the MCI *aluminium-steel* galvanic couples might have been different.

An additional point to draw attention to is that the Chloorkop site, which falls within the East Rand region, was the only locale that yielded chlorides in the mild steel corrosion product (**Figure 4.54**). Since chloride is known to affect the corrosion rates of metals, due to its deliquescence nature (Montgomery et al. 2011; Roberge 2012; Schinderholtz & Kelly 2012), it is likely that the galvanic corrosion of the ICI couples for this area/region could have been encouraged to take place at lower RH, therefore, resulting in higher correlations between the %RH and ICI values.

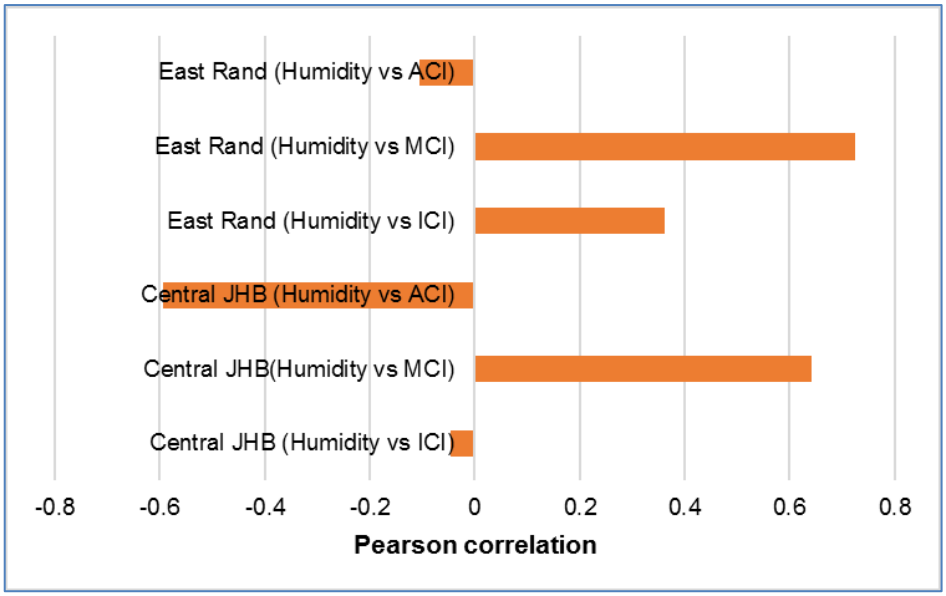


Figure 5.52 PPMC coefficients between the average seasonal changes in %RH versus variations of the CLIMAT corrosion indices.

5.4.2.3 Rainfall

Figures 3.14 (based on SAWS' (2017) measurements for the yearly rainfall at OR Tambo International Airport and the Johannesburg Botanical Gardens), reflects the 2011 to mid-2015 El Niño event, resulting in one of South Africa's worst drought periods (News24 2015). See also **Figure 3.12** (SAWS 2017). Comparable with the increased temperatures and lower RH effects associated with these events (Botkin & Keller 2010), the reduced rainfall during this period would have had consequences on the corrosion rate measurements taken during the current study. However, as also indicated, the effect of the drought on the interior regions of the GJMA during 2014-2015 would have been reduced.

Figures 3.13 & 3.15 (SAWS 2014, 2017) show that the GJMA receives most of its rain during spring and summer, particularly during the latter season, whereas during winter, rainfall is almost non-existent. Comparisons of the seasonal variations of the rainfall data versus the average cyclic changes in the ICI, MCI and ACI values for the Central and East Rand areas (**Figure 5.53**) revealed high correlations, 0.82 and 0.89 for the ICI values of the former and latter locales, respectively. In the case of the MCI data, the seasonal variations also corresponded with the rainfall results, with correlations of 0.61

and 0.84 for the central and eastern regions, respectively. Moreover, the cyclic fluctuations in the ACI data agreed moderately with the rainfall figures.

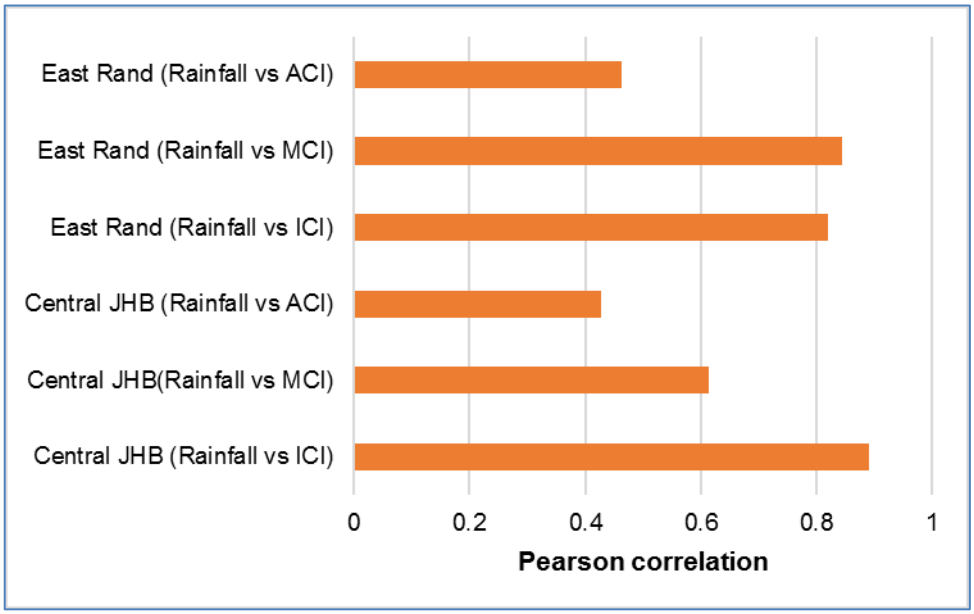


Figure 5.53 PPMC coefficients for the mean seasonal rainfall values versus the CLIMAT indices for the central and eastern parts of the GJMA.

However, due to the limited period of measurement, i.e. only four seasons, these correlations were established as statistically insignificant ($P > 0.10$). Nonetheless, these findings suggested that the average rainfall per area plays a vital role in the corrosivity of the GJMA, in comparison with the average RH values for the various locations (**Figure 5.52**). This finding also concurred with work done by Li et al. (2013), in New Zealand, in that the annual rainfall correlated to some degree with the atmospheric corrosion rate of mild steel. Moreover, Leygraf et al. (2016) state that the shape of a surface is essential when it comes to the retention of atmospheric water. Consequently, the wire-on-bolt units would likely have been more prone to the retention of moisture, than for example the open wire helix or flat metal panel devices. Similar observations have also been made by Cole et al. (2007, 2011). Noteworthy is that rain also rinses away pollutants and may even dissolve corrosion products, thus exposing fresh metal surfaces to corrosion Li et al. (2013).

5.4.2.4 Wind speed and direction

The speed and direction of the wind are important in atmospheric corrosion, particularly in polluted environments (Morcillo et al. 2000; Cottis et al. 2010; Roberge 2012). **Figure 3.17** (SAWS 2014) shows that the main wind direction at the OR Tambo International Airport weather station is from north, north-northwest to the north-west, with maximum speeds of up to approximately 11 m/s being reached during June to August. Additionally, it is evident that during winter, fierce winds may originate from southwest to south-south-westerly directions. However, on an average seasonal basis, **Figure 3.18** (based on SAWS (2014) measurements) indicates that the highest mean wind speeds are generally recorded during spring, followed by summer. This is likely related to the severe thunderstorms that occur during this time of the year.

To allow for comparisons with the latest ICI, MCI and ACI data for the GJMA, **Figure 3.18** (SAWS 2014) further reveals the measured average seasonal wind speeds (in m/s) for the Central and East Rand regions, for the period August-September 2013 to August-September 2014. According to the data, the winds at the East Rand locations, as measured at OR Tambo International Airport, are significantly stronger than the winds at the Central GJMA region (as measured at the Johannesburg Botanical Gardens). However, from a cyclic variability perspective, the same trends can be observed; namely, higher wind speeds during spring and summer, followed by a reduction during autumn and then an escalation during winter.

These cyclic trends correspond strongly with the seasonal ICI values measured for the two regions, with PPMC coefficients of 0.96 and 0.89 for the central and eastern parts, respectively (**Figure 5.54**), the former being statistically significant within a 95% CL. Moreover, the correlation coefficient for the seasonal changes in the wind speed versus those for of the average cyclic ACI values (as measured for the East Rand area), was about 1, or $r = 0.999$ to be exact, which was statistically meaningful ($P \leq 0.01$) within a 99% CL. A strong positive correlation was also determined for the variations in the ACI data versus those in the wind speed for the central region, although not statistically significant at the 10% level, while the lowest correspondences were established for the MCI results.

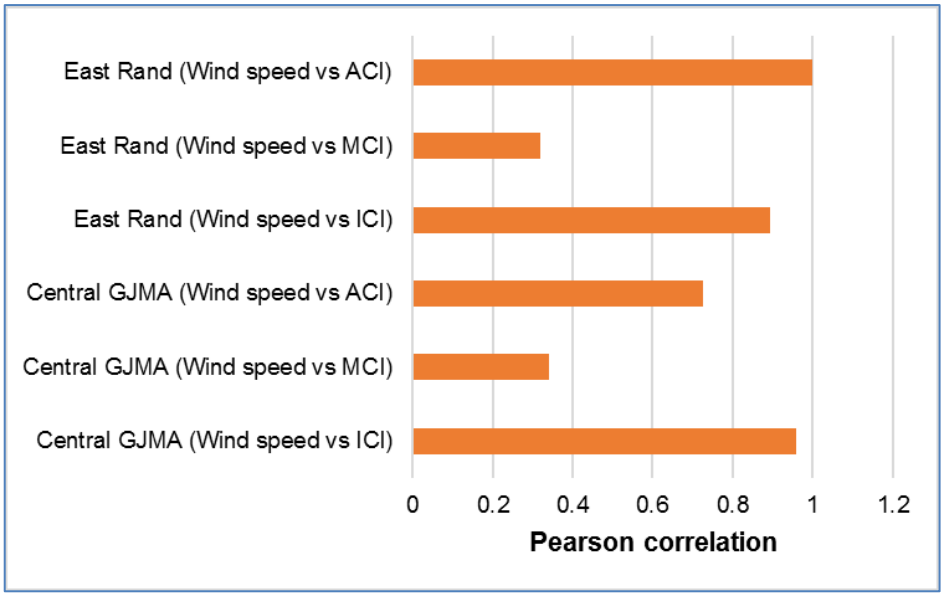


Figure 5.54 PPMC coefficients between the average seasonal wind speeds and the cyclic CLIMAT corrosion indices for the central and eastern regions of the GJMA.

The high correlations between the changes in seasonal wind speed and the cyclic CLIMAT data strongly suggest that the wind significantly influences the atmospheric corrosion patterns of the GJMA, particularly concerning its impact on the industrial (ICI) and general atmospheric (ACI) conditions. The lower correspondence with the seasonal MCI data may likely be attributed to the fact that chlorides mostly influence the *aluminium-steel* wire-on-bolt galvanic couples, which was only of real concern at Chloorkop, as well as due to the limited period of measurement. Conversely, the ICI-couples are significantly influenced by moisture, sulphates and then chlorides in the atmosphere (Carter 1982; Leitch 1994).

The significant difference ($P \leq 0.05$) in the average wind speed of the Johannesburg Botanical Gardens and at the OR Tambo International Airport may likely be attributed to elevation (Kruger et al. 2013) and landscape differences. The former weather station is located on the Melville 'Koppies' (hills) near Emmarentia, whereas the latter is located on the open planes of Kempton Park (East Rand). Although, the potential shielding effects of trees in the case of the Botanical Gardens is also a possibility. Refer also to **Appendix B – Table B.1**.

5.4.2.5 Overall impact of meteorological conditions

A graphical synopsis of the relations of the seasonal changes in the meteorological conditions versus the cyclic ICI, MCI and ACI data is given in **Figure 5.55**. This excludes any pollution variables. As shown, the wind appears to be an essential determinant when it comes to the corrosivity of the GJMA. In this regard, **Figures 3.19 & 3.20** (SAWS 2014) show that during wintertime, when the GJMA is known to exhibit high pollution levels, the main wind direction at the East Rand and Central GJMA regions varies. Consequently, it is assumed that the effects of air pollution at the various GJMA exposure sites will also be different.

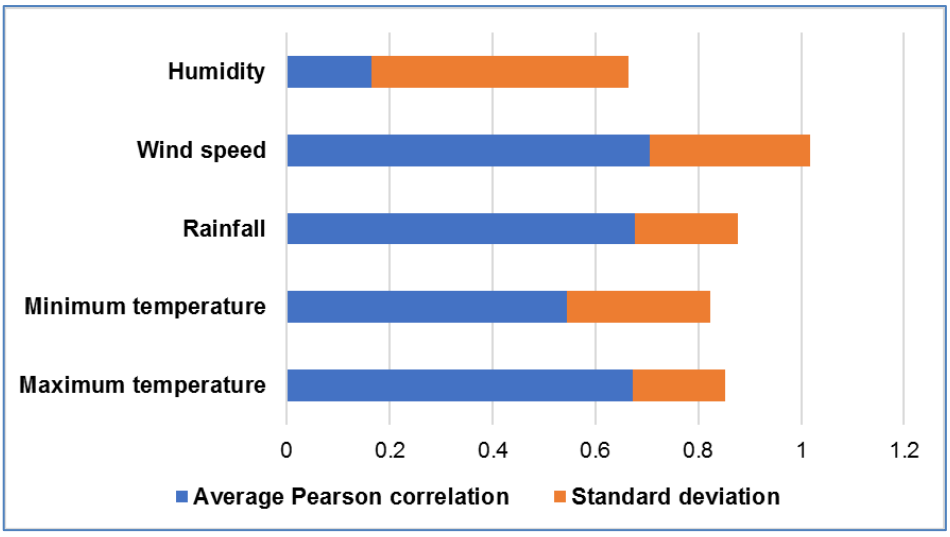


Figure 5.55 Average PPMC coefficients and standard deviations for the meteorological parameters and the atmospheric corrosivity measurements of the GJMA – excluding any pollution effects.

The apparent reduced RH effect on the corrosivity of the GJMA, in comparison with the other parameters, may likely be attributed to the fact that for most of the year, as well as within 24-hour cycles (**Figure 2.24**) (Callaghan 1991; McEwan2004), the RH of GJMA is below the "*primary critical relative humidity*" for most clean metal surfaces, for significant corrosion to take place, stated by Li et al. (2013) as approximately 66%. However, the uncertainty of the average correlation for RH with the corrosion data is high. Also, considering the limited duration of the present study, further investigation is warranted. Moreover, the graph is based on PPMC coefficients that are not always statistically meaningful, due to the limited study period.

5.4.2.6 Ultraviolet (UV) light radiation

No solar irradiation data for the exposure sites were available. Nonetheless, **Table 2.5** - adapted from ClimaTemps.com (2017b) and **Figures 3.21 & 3.22** (World Weather Online 2017) show that the GJMA experiences the highest number of monthly sun hours during the spring equinox (23 September) and summer solstice (22 December), whereas the highest number of sunny days are endured during the autumn equinox (21 March) and winter solstice (21 June) (Oxford University Press 2016). Yearly and monthly UV-indices for the region are also presented in **Figure 3.22** (World Weather Online 2017), showing that on an average basis, the highest UV light radiation levels are experienced during summer, measuring typically from about 5.5-7.0 (based on the 0-11 UV-index scale). The lowest values are recorded during the winter solstice.

In comparison with the seasonal ICI, MCI and ACI data for the GJMA (also refer to **Figure 3.9** (SAWS 2014)), it is apparent that the impact of the sun may be two-fold, namely: i) because of solar heating of surfaces during spring and summer, TOW may be reduced due to an increase in evaporation rates, and ii) during autumn and winter, the cloudless sunny days may promote photochemical pollutants in the atmosphere, e.g. ozone may be produced by the photolysis of nitrogen dioxide (NO_2) and SO_2 by the photolysis of carbonyl sulphide (OCS) (Cottis et al. 2010).

Due to the rise in surface temperature, it is likely that the seasonal impact of sunlight on the corrosivity of the GJMA follows the cyclic maximum and minimum temperatures for the region (**Figures 3.6 - 3.8**) (SAWS 2014, 2017). Conversely, based on the results of the organic coated steel specimens exposed at the different main sites (Section 5.3), it is apparent that several other factors also play a role regarding the effects of solar radiation, namely, shielding/shading effects (**Figure 4.70**), the number of sun hours and sun days experienced per annum (**Figure 3.21**) (World Weather Online 2017), as well as the colour and generic composition of the exposed material (**Figure 4.69**). Moreover, the impact of the UV light will be influenced by local humidity and pollution levels (**Figures 3.23 - 3.34**) (DEA 2017a).

As such, those sites which appeared most affected by UV light radiation were, Kagiso-Randfontein (West Rand), Aeroport (East Rand) and Chloorkop (East Rand)

(**Figure 4.69**), which have been shown to exhibit higher corrosivity than the average GJMA site (**Figure 4.23 - 4.25**, **4.34**).

5.4.3 Air Pollution Effects

Eight of the twenty-two main GJMA corrosion monitoring sites coincided with historical and current air quality monitoring stations of the City of Johannesburg Metropolitan Municipality. The air quality results from these locations are stored and managed by the SAWS, via the SAAQIS system (DEA 2017a). Unfortunately, the databases for the Johannesburg sites showed significant gaps, particularly concerning the latest corrosion study period. Therefore, it was decided to instead refer to historical pollution data for these locations, which appeared more comprehensive.

From a corrosion perspective, **Figure 5.56** presents the 12-month corrosion rates of mild steel at the eight-air quality/corrosion monitoring sites, as determined during the study period. It is worth noting that Delta Park, which is used by the City of Johannesburg as a baseline locale regarding air quality monitoring, exhibited the highest average 12-month corrosion rate of mild steel. This was made possible by the fact that the site is a wooded area, where the shielding and shading effects of the trees likely caused a rise in TOW, resulting in increased mild steel corrosion rates. This occurrence was also potentially signified by the elevated ICI and MCI data measured at Delta Park during spring and summer (**Figure 5.57**), as was similarly the case for most of the other locations. Moreover, it was likely that Delta Park experienced less wind (**Figure 3.18**) (SAWS 2014), causing surfaces to remain wet for more extended periods.

Based on the average ICI data, however, the highest values were recorded at Ivory Park, during spring, followed by Alexandra and Delta Park during summer, whereas concerning the MCI values, Delta Park was rated most aggressive during summertime, followed by Alexandra and Ivory Park.

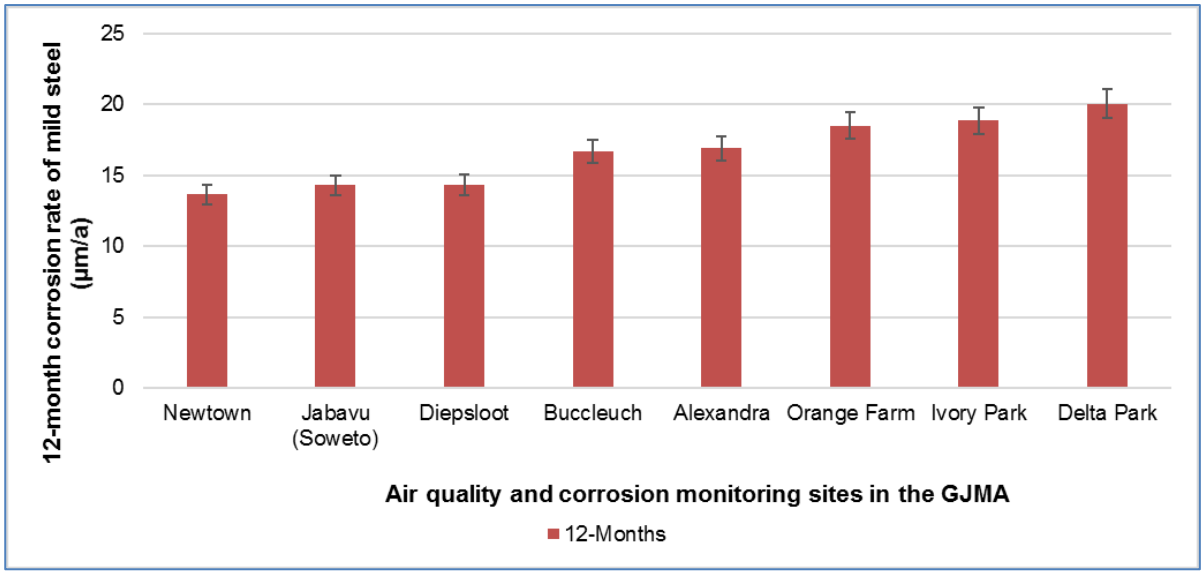


Figure 5.56 Measured 12-month corrosion rates of mild steel at the different air quality/corrosion monitoring sites of the GJMA.

As per **Figure 5.58**, which presents the 12-month corrosion rates of the aluminium, zinc and copper open wire helices, Buccleuch ranked most corrosive overall, followed by Orange Farm and Ivory Park. However, considering the zinc data only, the Jabavu (Soweto) site superseded the Ivory Park location. Ivory Park was also rated most corrosive regarding the aluminium results, followed by Buccleuch and Orange Farm, which corresponded closely, while the corrosivities of the latter two locales were also similar regarding the copper data. The corrosivity of the air quality/corrosion monitoring sites is influenced by several factors, such as the type of corrosion measuring device, metallic substrate, area of exposure, humidity/rainfall levels, and pollution.

A rating scheme was devised, ranging from 0 to 8 (indicating lowest to highest average measurements) to ensure more reliable comparisons of the various corrosion results. Based on the summations (∑) of the mild steel, aluminium, zinc and copper corrosion rankings, the atmospheric corrosivity of the different sites were ranked, as shown in **Figure 5.59**.

Since the GJMA air quality data were only available in graphic format, obtained using the SAAQIS system, a similar rating scheme was implemented for interpretation of these graphs.

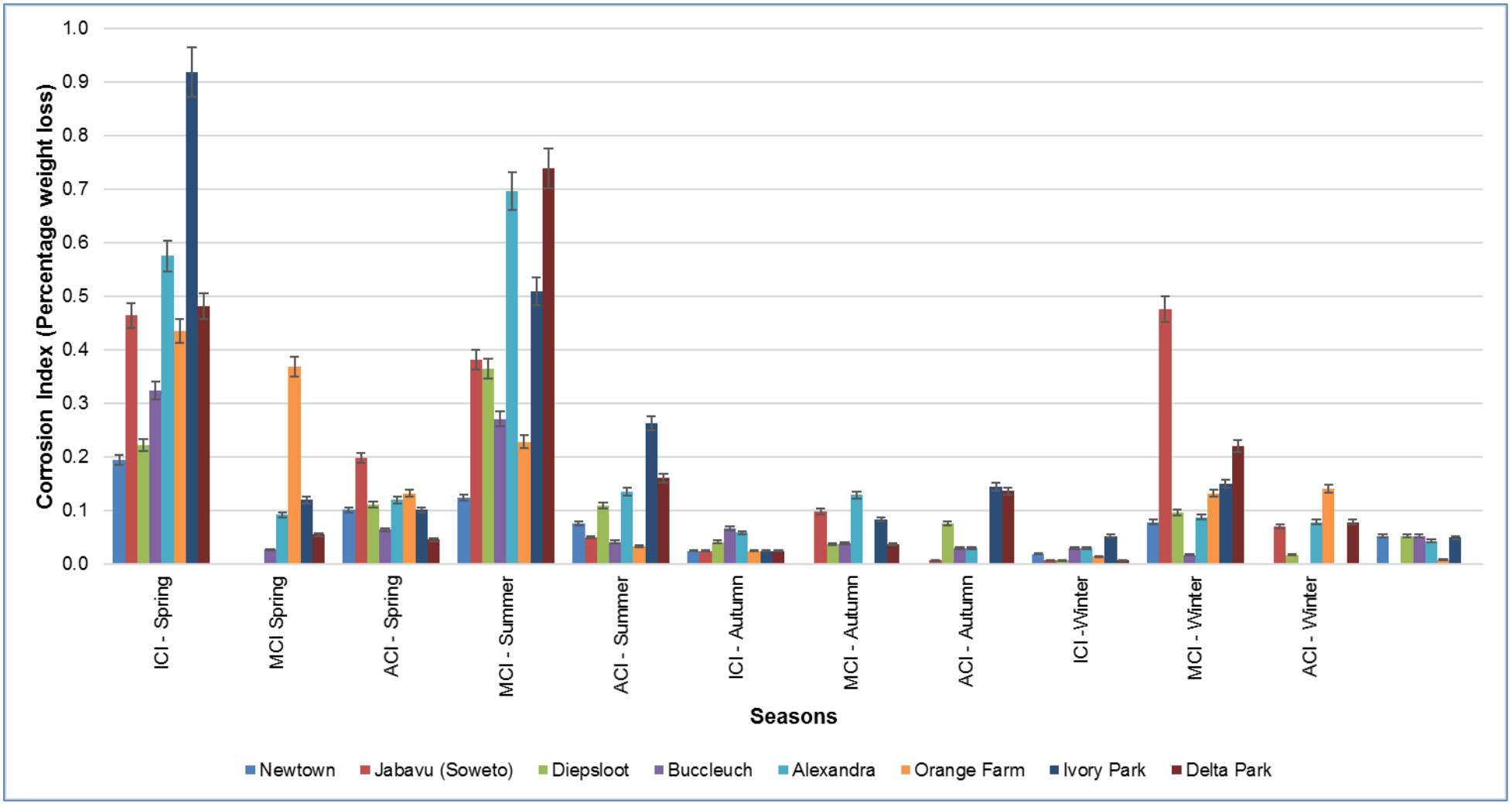


Figure 5.57 Measured average ICI, MCI and ACI values for the various air quality/corrosion monitoring sites of the GJMA.

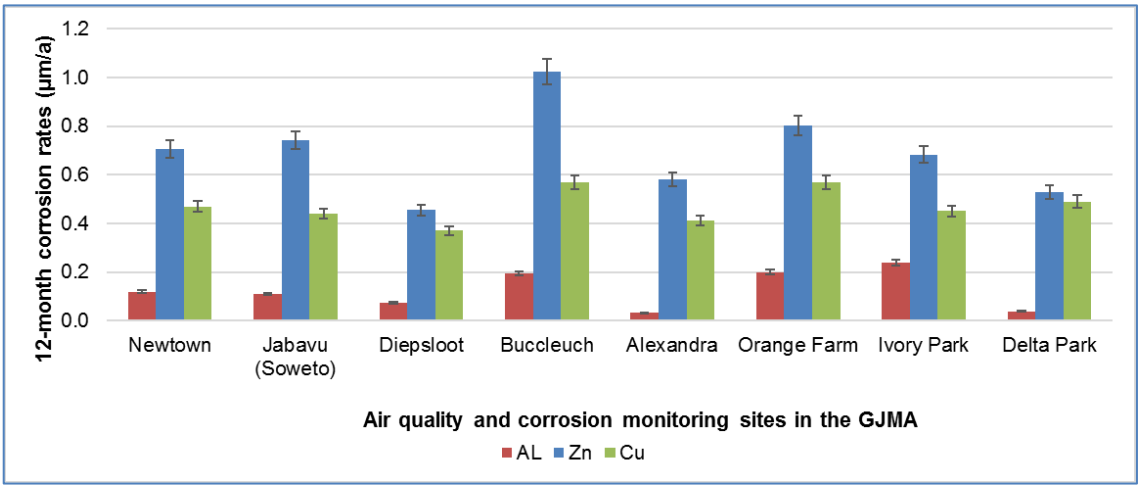


Figure 5.58 Measured 12-month corrosion rates of aluminium, zinc and copper at the different air quality/corrosion monitoring sites of the GJMA.



Figure 5.59 Overall corrosivity rating of the various air quality/corrosion monitoring sites – based on the rankings of their 12-month corrosion rates of mild steel, aluminium, zinc and copper.

5.4.3.1 PM_{10} Particulate/dust matter

Particulate matter/dust, that may be carried by the wind for long distances from their source, play an essential role in the wetting of surfaces (McEwan 2004; Sica et al. 2007). However, when alkaline-based (e.g. sodium-, potassium- and calcium-based), the dust may neutralise atmospheric acidity (Encyclopedia.Com 2008a), consequently limiting corrosion rates.

A complete set of historical data for the eight-air quality/corrosion monitoring sites was obtained for PM_{10} particulate (dust) matter concentrations. As may be seen in **Figure 3.23** (DEA 2017a), the PM_{10} particulate matter levels in the GJMA typically vary between 30 µg/m^3 to 100 µg/m^3, spiking to approximately 250 µg/m^3 during wintertime due to the burning of fossil fuels. According to the Gauteng Department of Agriculture and Rural Development (2011), the spikes in the 2008 and 2009 data were attributable

to large-scale power outages experienced throughout this period, during which most households were forced to make use of coal, wood and paraffin. **Figure 3.23** also suggests that Alexandra exhibited the highest PM_{10} particulate matter concentrations, followed by Ivory Park and then Diepsloot, all classified as low-income 'townships' and informal settlement areas. The entire ranking order is presented in **Figure 5.60**.



Figure 5.60 Ranking order of the different air quality/corrosion monitoring sites based on their average PM_{10} particulate matter concentrations.

Based on PPMC coefficients of the ranking order of the PM_{10} data versus the different corrosivity ratings (**Figure 5.61**), the sequence of the PM_{10} results corresponded most with the ICI data for autumn, followed by spring, and then the ACI data for autumn. However, these correlations were established as statistically insignificant within a 90% CL.

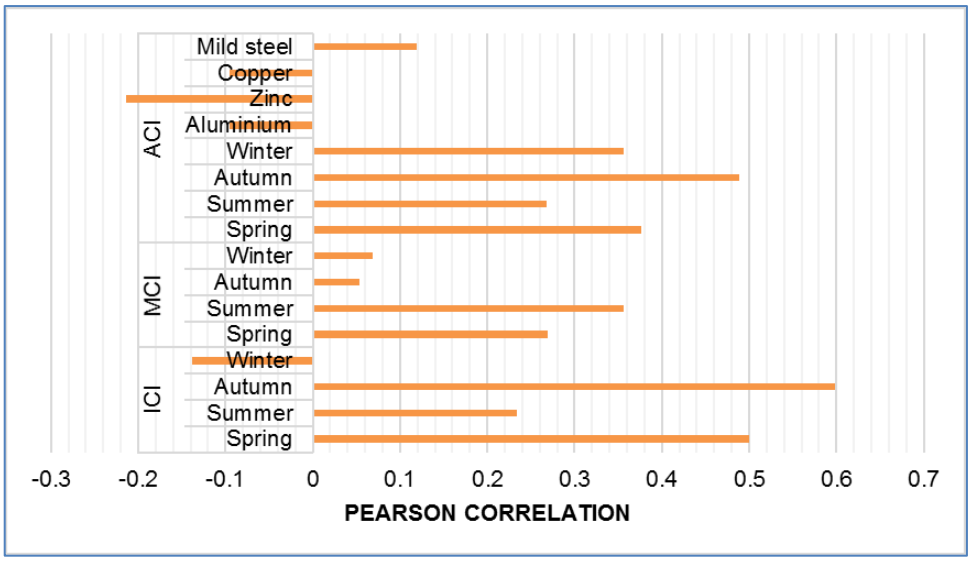


Figure 5.61 PPMC coefficients between the rankings for PM_{10} particulate matter concentration and the different corrosion monitoring results at the various sites.

While not statistically significant, the outcome above suggested that the galvanic-wire-on-bolt-couples were, at least partially, affected by the levels of PM_{10} particulate matter in the atmosphere. This was likely due to the particulate matter being trapped in the

crevices between the wire and bolt surfaces, where it promoted wetting, which increased TOW and corrosion.

Regarding the open helix wire surfaces, which exhibited no crevices, the wind likely caused drying of the surfaces, resulting in more negative trends. As for the flat mild steel panels, the 45° angle of the surfaces likely allowed for the partial collection of the particulate matter, causing increased wetting and corrosion of the surfaces.

5.4.3.2 Sulphur dioxide (SO_2)

SO_2 is a precursor to acid rain (Botkin & Keller 2010; Roberge 2012) and mainly produced by the burning of fossil fuels (Botkin & Keller 2010; Leygraf et al. 2016). The presence of SO_2 may also cause a decrease in the CRH for corrosion initiation (Li et al. 2013). Therefore, it plays a significant role in atmospheric corrosion in urban and industrial atmospheres (McEwan 2004; Syed 2006; Roberge 2012; Leygraf et al. 2016).

The monthly concentrations of SO_2 in the atmosphere at six of the locations are presented in **Figure 3.24** (DEA 2017a). Ignoring the 2008 peak for Alexandra, which was caused by power outages (Gauteng Department of Agriculture and Rural Development 2011), the results suggest that the average SO_2 levels in the GJMA vary from 2.5 ppb to 7.5 ppb during summertime and 5 ppb to 20 ppb during winter. The ranking order of the sites based on their apparent SO_2 levels is presented in **Figure 5.62**. The yearly average, about 10 ppm, is like the estimated average value given in **Table 2.6**, derived from Zunckel et al. (2005), Tidblad et al. (2007) and Lourens (2012). However, it is much higher than Vargel's (2004) SO_2 concentration for a typical urban atmosphere.



Figure 5.62 Ranking order of the different air quality/corrosion monitoring sites (excluding the Delta Park and Newtown locales) based on their average SO_2 concentrations.

Worth noting is the strong PPMC coefficient between the ranking order of the 12- month zinc corrosion data of the different sites and their respective SO_2 results, 0.91, which was established as having statistical significance within a 95% CL. This finding indicated

that SO_2 is a major player regarding the corrosion rate of zinc in the GJMA, as well as of hot-dip galvanised steel. However, since the zinc-coated panels at Buccleuch were stolen shortly after installation, the galvanised steel results were not considered.

Concerning the copper data grading, a PPMC coefficient of 0.71 was determined, which hinted at the possibility that the copper open wire helices being more suited for detection of SO_2 pollution than aluminium, the latter merely indicating a correspondence of 0.27. However, both these correlations were established as statistically insignificant, including the matches between the SO_2 ranking and the 12-month corrosion rates of mild steel at the different sites, as well as their respective ICI and MCI data, which were -0.26, -0.37 and -0.39, respectively.

However, the above correlations do not distract from the reality that significant amounts of sulphur were detected in the corrosion products from all the GJMA sites (**Table 4.54**).

5.4.3.3 Nitrogen dioxide (NO_2)

In the GJMA area, the reddish colour of smog (Roberge 2012), often seen during the afternoons, may be attributed to NO_2 (Kerrod 1983; Roberge 2012). NO_2 is also a precursor to HNO_3 (Arroyave et al. 2002; Botkin & Keller 2010), and extremely soluble in water (Leygraf et al. 2016). Roberge (2012) mentions that in modern cities, 50% of the haze or smog may be ascribed to a combination of H_2SO_4 and HNO_3.

The NO_2 levels in the GJMA, likely released from the combustion of fossil fuels (Syed 2006; Botkin & Keller 2010; Leygraf et al. 2016; DEA 2011), ranges between 10 ppb and 35 ppb during summer, and from 20 ppb to 50 ppb during winter, with those sections located to the north of the GJMA, e.g. Alexandra and Buccleuch, showing sharp rises in NO_2 pollution during power outages **(Figure 3.25**) (DEA 2017a). These values are of similar range than those reported by Zunckel et al. (2005) and Tidblad et al. (2007) (**Table 2.6**).

Figure 5.39 supports the NO_2 results, namely that the north-eastern parts of the GJMA are more corrosive than the central region, e.g. Buccleuch appears to be the most polluted, followed by Newtown, Alexandra and then Delta Park.

The six-year average of global tropospheric NO_2 Vertical Column Density in 10^{15} molecule/m^2 is shown in **Figure 3.26** (Beirle et al. 2003), revealing that the eastern GJMA and Mpumalanga regions are some of the worst NO_2 polluted areas in the world. The data were derived using the Global Ozone Monitoring Experiment (GOME) on board the ESA-satellite ERS-2 (Beirle et al. 2003).

The diurnal pattern in the levels of NO_2 for the GJMA is presented in **Figure 3.27** (DEA 2017a). As indicated, elevated NO_2 concentrations are frequently recorded at sunrise and sunset when traffic activity and domestic energy usage levels are at their highest. Of note is that both Buccleuch and Newtown are located near busy traffic areas, potentially hinting that motor vehicle emissions influence pollution levels in the GJMA. According to the Gauteng Department of Agriculture and Rural Development (2011), it has been estimated that approximately 60-70% of atmospheric NO_x in the Gauteng area is due to motor vehicle emissions, although Beirle et al. (2003) contend that the general figure is closer to 50%, which reduces typically during weekends.

5.4.3.4 Nitrogen oxide (NO)

Most NO_x is emitted as nitrogen oxide (NO), which under the influence of sunlight, moisture and catalysts, can be quickly oxidised to NO_2 (Li et al. 2013). Regarding the GJMA, NO pollution data were only obtainable for three of the eight air quality/corrosion monitoring sites, as shown in **Figure 3.28** (DEA 2017a). According to these results, the levels of NO in the GJMA atmosphere vary from below 5 ppb to near 60 ppb during summer, and between about 100 ppb to 200 ppb during winter. These values concur with those derived by Zunckel et al. (2005), indicating an average of approximately 48 ppb for the Gauteng/Greater Johannesburg area.

Buccleuch showed increased values of NO, in comparison with the Newtown and Delta Park locales, which also coincided with the corrosion results for the GJMA, demonstrating the same ranking for these sites (**Figure 5.59**) regarding their overall corrosion data. Of note is that the Buccleuch air quality/corrosion monitoring site is situated in the middle of the intersection at the ‘Buccleuch’ interchange between the N1 and N3 highways.

5.4.3.5 $PM_{2.5}$ particulate (dust) matter

Figure 3.29 (DEA 2017a) displays the monthly average $PM_{2.5}$ particulate (dust) matter concentrations at the Buccleuch air quality/corrosion monitoring site. As indicated, the average $PM_{2.5}$ value for the area varies between 20 µg/m^3 and 40 µg/m^3, during spring and summer, and can reach a mean maximum of more than 100 µg/m^3, during winter. The sharp peaks caused by the 2008 power outages are also shown. According to the corrosion data of the eight air quality monitoring sites, this site was rated second highest overall regarding its corrosivity. Important to observe is that increased $PM_{2.5}$ levels are associated with vehicle tailpipe emissions (Gauteng Department of Agriculture and Rural Development 2011). **Figure 3.30** (Yale Data Driven 2016) indicates that elevated $PM_{2.5}$ levels are also a more widespread problem concerning the GJMA region.

5.4.3.6 Carbon monoxide (CO)

Figure 3.31 (DEA 2017a) gives historical concentrations of carbon monoxide (CO) at three of the main GJMA sites, which may form carbonic acid and therefore, encourage corrosion (Guttman 1982). As shown by the 2006 to 2011 results, Buccleuch appears most affected by CO pollution in the atmosphere, compared to Alexandra and Newtown. This is likely since the former site is positioned in the middle of the intersection of the N1 and N3 highways, some of the busiest roads in South Africa (Manana 2011). The peaks during the 2008 and 2009 power outages are also evident.

Like most of the earlier discussed air pollutants, elevated CO levels may be ascribed to vehicle emissions and the burning of fossil fuel (Botkin & Keller 2010; Leygraf et al. 2016). The latter was particularly evident during 2008 and 2009 when most households made use of fossil fuel for heating and cooking purposes. The results showed once more that the northern and eastern suburbs are most affected by pollution. This trend was also reflected in the corrosion data.

5.4.3.7 Ozone (O_3)

The City of Johannesburg (2003), Tidblad et al. (2007) and Lourens (2012) give the average concentration of O_3 for Gauteng/Greater Johannesburg and its surrounding areas as varying between 35-70 ppb. However, as shown in **Figure 3.32** (DEA 2017a),

the O_3 concentrations for five of the air quality/corrosion monitoring sites in the GJMA were much lower, mostly below about 40 ppb.

Nonetheless, tropospheric ozone (O_3) is of concern when it comes to the long-term durability of organic materials (Druzik 1985). Elevated levels are said to result from complex reactions between various pollutants, and are problematic in areas where photochemical smog develops (Leygraf et al. 2016). However, increased levels of O_3 may also come about due to the burning of fuels, via NO_x emissions (California Environmental Protection Agency 2015).

Figure 3.32 shows that the highest levels of ground-level ozone are measured during spring. Piketh et al. (2007) concur with this finding. It is furthermore suggested that of the five sites listed, the Alexandra locale is most affected by elevated levels of O_3, followed by the Delta Park region. This is because O_3 is produced as a secondary pollutant on bright, sunny days in areas that typically exhibit high NO_2 pollution (Botkin & Keller 2010).

The diurnal pattern for O_3 pollution in the GJMA atmosphere is given in **Figure 3.33** (DEA 2017a). As shown, during the daytime, the levels of O_3 at Delta Park surpass that of the Alexandra site, most likely due to the oxygen-rich environment created by the trees. The latter phenomenon also explains why the Delta Park site exhibited the highest 12-month corrosion rate of mild steel of all the air quality/corrosion monitoring locales (**Figure 5.56**). O_3 could have been a driving force, which is highly active (Botkin & Keller 2010) and a strong oxidant (Leygraf et al. 2016) that can encourage the corrosion of steel (California Environmental Protection Agency 2015). The high oxygen-rich environment during daytime will also promote most corrosion processes.

At the other locations, due to the lack of a significant number of trees, it is assumed that O_3 is created by the photolysis of NO_2 by sunlight, forming nitric oxide (NO) and atomic oxygen O, followed by the rapid reaction of atomic oxygen with molecular oxygen to form ozone (Druzik 1985).

Considering the results of the polymeric coated specimens, the changes in the ΔL^*- value (which represents lightness or fading) in terms of the CIE L^*a^*b – colour space coordinates, indicated the highest sum ($\sum$) positive change regarding the different coatings at the Alexandra site (**Figure 5.63**). This suggested that the green-coated

samples exposed at this location were more affected by fading, and potentially O_3 bleaching, compared to the samples at Delta Park and Newtown, for which the ΔL^* values were somewhat comparable. However, the impact of shading effects could not be excluded. Unfortunately, no conclusions were drawn from the Buccleuch site, due to the theft of the organic coated samples.

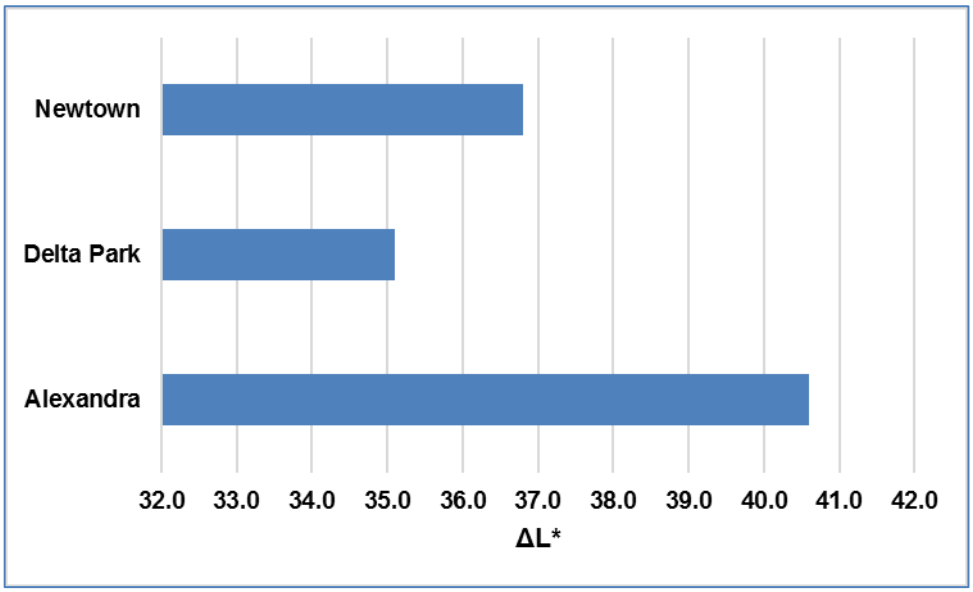


Figure 5.63 Sum changes in the *ΔL**- value (which represents lightness or fading) regarding the CIE *L*a*b* – colour space coordinates.

5.4.3.8 Visibility (haze) and El Niño event

Figure 4.34 (World Weather Online. Com 2017) shows that the level of visibility (generally reduced by haze - measured in km) in the GJMA has been steadily improving in recent years. According to the Environmental Protection Agency (2017), haze is caused by sunlight being absorbed and scattered by small pollution particles in the atmosphere. This, in turn, reduces the colour and clarity of the landscape, as well as other visible things, particularly during humid conditions.

Although the improved level of visibility may partially be attributed to the fact that more households are making use of electricity in the GJMA, rather than using fossil fuel for heating and cooking purposes, it is more likely due to a reduction in the humidity levels in the atmosphere (**Figure 3.12**) (SAWS 2017). The latter was caused by the recent El Niño weather pattern, which reportedly occurs every seven years (Botkin & Keller 2010). As the latest corrosion study was conducted during 2013 to 2015, in other words during

the ‘peak’ of the latest El Niño event, it is likely that the corrosion measurements made would have been somewhat reduced than those recorded during non-El Niño conditions. In this regard, Botkin & Keller (2010), as well as Cole & Paterson (2010), contemplate that El Niño and La Nina events are likely to become more common in the future. Moreover, due to global climate change effects, weather models for the GJMA have shown that the area is liable to become warmer and more humid by 2056-2065 (City of Johannesburg 2012). Leygraf et al. (2016) also confirm that the average CO_2 level in the atmosphere is increasing each year by approximately 0.5%. Consequently, it is anticipated that future potential changes in RH, UV light radiation levels, TOW, wind patterns, pollution, or dramatic meteorological events, will ultimately have an impact on the corrosivity of the GJMA.

5.4.3.9 Acid Rain

The total (dry plus wet) acid deposition rates in meq/m^2 per year for Gauteng and other regions of South Africa is given in **Figure 3.16** (Josipovic et al. 2011). As shown in the interpolated map (derived from the two-year mean results for 37 sites), the eastern parts of Gauteng (including the GJMA), exhibit increased signs of acid deposition, especially moving towards the Eastern Highveld region. This trend was also found concerning the measured corrosion rates for the GJMA (**Figures 5.26 - 5.28 & 5.39**), particularly regarding those for mild steel and copper.

Important is that the highlighted area, see also **Figure 5.4** (Greenpeace Afrique 2014), houses ten coal-fired power stations, several smelters, open-cast coal mines, including a sizeable synthetic fuel production plant. The impact of this industrialised Eastern Highveld region on the atmospheric corrosivity of the GJMA is also clearly discernible in the different preliminary corrosion maps (**Figures 5.26 - 5.28 & 5.39**). This finding is contrary to DEA’s (2017b) statement that “*acid rain over South Africa is not as serious an issue as previously thought*”. Considering that Kusile Power Station is still in its construction stage and that once all six 800 MW units have been fully commissioned, it will be the fourth largest coal-fired power station in the world (Eskom 2017), it is likely that the atmospheric corrosivity of the eastern part of GJMA and the Highveld will increase even further.

CHAPTER 6

ATMOSPHERIC CORROSION MAPS FOR SOUTH AFRICA AND THE GJMA

6.1 INTRODUCTION

Chapter 10 presents, for the first time, medium-scale vector-based atmospheric corrosion maps for a metropolitan area (the GJMA) in South Africa (SA) (**Figures 6.1 - 6.6**), derived from:

- the yearly average Industrial Corrosion Indices of the main sites in the GJMA (**Figure 5.22 & Appendix G – Table G.1**);
- the 12-month corrosion rates of mild steel exposed at the main and mini sites in the GJMA (**Table 4.1 & Figure 5.39**);
- the 12-month corrosion rates of hot-dip galvanised mild steel exposed at the main sites in the GJMA (**Appendix J – Table J.1**)
- the 12-month corrosion rates of pure aluminium exposed at the main sites in the GJMA (**Figure 5.26 & Appendix H – Table H.1**);
- the 12-month corrosion rates of pure zinc exposed at the main sites in the GJMA (**Figure 5.27 & Appendix H – Table H.1**); and
- the 12-month corrosion rates of pure copper exposed at the main sites in the GJMA (**Figure 5.28 & Appendix H – Table H.1**).

The maps, mentioned above, have been merged with small-scale national corrosion maps for SA (**Figures 6.7 – 6.12**), based on the results presented in **Figures 4.1 - 4.7 & Figure 5.15**, using the procedures described in Section 3.5. As a result, the new proposed corrosion maps for SA have been derived from the latest and historical (published and unpublished) corrosion monitoring results, as discussed in Sections 5.1 to 5.4.

A chart has also been developed for SA's macro atmosphere (**Figure 6.8**), based on the ISO 9223:2012 corrosivity rating scheme (**Table 2.2)** pertaining to mild steel. Lastly,

the SA maps have been expressed in different formats for increased applicability and interest purposes.

6.2 ATMOSPHERIC CORROSION MAPS FOR THE GREATER JOHANNESBURG METROPOLITAN AREA (GJMA)

6.2.1 GJMA - Industrial Corrosion Index (ICI) Map

The ICI Map for the GJMA is established on the corrosivity indices derived via the *aluminium wire-on-copper* bolt (CLIMAT) units, manufactured as per ASTM G116:2004 procedures (Section 3.2.4) and exposed at 22 sites in the GJMA, during August to September 2014 (**Figure 5.22 & Appendix G – Table G.1**). According to the resultant IDW interpolated map (**Figure 6.1**), refer also to Section 3.5, the ICI corrosivity rating for the region is mostly NEGLIGIBLE (**Table 2.1**) (Carter 1982), with the Chloorkop (Modderfontein) area, located north-east of the CoJ, exhibiting a MODERATE (in the 1.1 to 2 range) ICI rating. This is likely due to the emissions of chlorine, caustic soda and chloralkali derivative plants in the Chloorkop area (NCP Chlorchem 2011-2017), causing Cl^- to be deposited on surfaces (**Figure 4.54**), encouraging corrosion. Overall, however, the average ICI for the GJMA measured 0.3 ± 0.2, 95% CI [0.2, 0.4], over the 12-month exposure period.

The ICI results (**Figures 4.11 - 4.12**, as well as **Appendix G – Table G.1**) indicated that the impact of industrial pollution on the GJMA atmosphere is significantly more during spring and summer than in autumn and winter. The GJMA also exhibits an increase in the general corrosivity of the atmosphere, towards the eastern side, partly attributed to the dispersion of pollutants from Chloorkop (**Figures 5.16 & 5.17**), and the Kelvin A & B Power Station areas, as well as the presence of a large airport, OR Tambo International, in the region. Other 'land-use' areas, where elevated micro corrosive atmospheres may be anticipated, are shown by a brownish-orange coloured legend.

The estimated level of uncertainty of the map is about 30%, due to the introduction of systematic errors of measurement during the chemical cleaning and weighing procedures utilised during the corrosion monitoring process, including that the map is based on a one-year corrosion monitoring period only and that readings were taken at merely 22 sites. Also, no duplicate measurements were taken per 90-day exposure period.

MAP NOT PUBLICLY AVAILABLE

Figure 6.1 IDW interpolated atmospheric corrosion map of the Greater Johannesburg Metropolitan Area – based on yearly average Industrial Corrosion Indices (ICI), as measured during August 2013 to September 2014. (Base map – ArcGIS).

6.2.2 GJMA – 12-Month Mild Steel Corrosion Map

Figure 6.2 is based on the 12-month corrosion rate of low-carbon steel (**Appendix C – Table C.1**), exposed per ISO 9223 and ISO 9226 procedures (Section 3.2.2.1), at more than 50 sites in the GJMA, during August 2013 to September 2014 (**Table 4.1 & Figure 5.39**). As shown via the derived IDW interpolated map (**Figure 6.2**), the average 12-month corrosion rate of mild steel in the GJMA measures about 20 ± 4 μm/a, 95% CI [18 μm/a, 22 μm/a], yielding an overall C2 (*low*) corrosivity rating (**Table 2.2**), although to the upper end of this category (**Table 5.7**). However, the corrosivity of the GJMA rises to a C3 (*moderate*) category on the eastern and south-eastern sides of the region, due to pollution emanating from the Brakpan and Dunnottar, and likely Secunda and Emalahleni (Witbank) areas (**Figures 5.4 & 5.5**).

Two outlier sites have been excluded from this map, Kagiso-Randfontein and Palmridge (refer to Section 5.2.6), to prevent skewing of the results. Counter to the ICI map (**Figure 6.1**), several sites on the eastern side of the map display higher corrosion rates of mild steel than measured at the Chloorkop (Modderfontein) area. This is possible since the flat mild steel panels have been positioned at an angle of 45° with the horizontal, allowing only the partial collection of pollutants. However, concerning the (ICI) wire-on-bolt and open wire helix (WH) units (**Figures 6.4 - 6.5**), the vertical positioning of the units allowed the collection of pollutants from all directions (Leitch 2006; Knotkova et al. 2010), giving increased values for other industrial and mining zones.

Ignoring the outlier sites, the 12-month corrosion rate of mild steel in the GJMA varies from about 14-27 μm/a, with a possibility for higher rates near mines, coal-fired power stations and other air-polluting areas, indicated by a brownish-orange 'land-use' legend. The estimated level of uncertainty of the map is about 15%, due to the experimental uncertainties of measurement introduced during the chemical cleaning and weighing procedures, and that the map is based on a one-year corrosion monitoring period only. The increased accuracy may be qualified by the fact that the measurements were taken at more than 50 sites in the GJMA and that duplicate specimens were exposed per exposure period, as well as that the 12-month results correlated strongly, 0.99 ($P \leq 0.01$) and 1 ($P \leq 0.01$), with the 18 and 24-month data, respectively.

MAP NOT PUBLICLY AVAILABLE

Figure 6.2 IDW interpolated atmospheric corrosion map of the Greater Johannesburg Metropolitan Area – based on the 12-month corrosion rate of mild steel, as measured during August 2013 to September 2014. (Base map – ArcGIS).

6.2.3 GJMA – 12-Month Hot-dip Galvanised Mild Steel Corrosion Map

Figure 6.3 is based on the 12-month corrosion rate of hot-dip galvanised mild steel (**Appendix C – Table C.2**), exposed, as per slightly modified ISO 9226 procedures, at 21 sites in the GJMA, during August 2013 to September 2014 (**Appendix J – Table J.1**). The derived IDW interpolated map (**Figure 6.3**) shows that the average 12-month corrosion rate of hot-dip galvanised mild steel in the GJMA is about 0.7 ± 0.3 μm/a, 95% CI [0.6 μm/a, 0.8 μm/a], varying between 0.4 μm/a (on the West Rand at Kya Sand) and 1.4 μm/a (at the Chloorkop-Modderfontein area).

Like the ICI and 12-month mild steel corrosion maps for the GJMA (**Figures 6.1 - 6.2**), the higher corrosivity of the East Rand is distinguishable. Also, of note is that the hot-dip galvanised map (**Figure 6.3**) compares statistically more meaningfully (**Appendix K – Table K.1**) with the ICI map (**Figure 6.1)** than with the mild steel chart (**Figure 6.3**). The difference is attributed to the likelihood that the ICI-couple is a better indicator of the expected corrosion rate of hot-dip galvanising than mild steel. In terms of the revised ISO 9223:2012 rating scheme for zinc (**Table 5.7**), the expected corrosivity for the region is primarily Upper-C2 (**Appendix C – Table C.2**) *low-moderately* corrosive (**Table 5.7**), with a possibility for a higher corrosivity (C3) rating near mines, power stations and other potential industrial areas, indicated by a brownish-orange 'land-use' legend.

Based on the experimental uncertainties of measurement introduced during the chemical cleaning and weighing procedures, utilised during the corrosion monitoring process, including that the map is derived from a 12-month corrosion monitoring period only and that the corrosion rates were determined at merely 21 sites, the estimated level of uncertainty of the map is about 20%. The higher degree of certainty of the map, compared to the ICI chart, is due to the increased surface area of measurement (flat panel versus wire specimens) and the duplicate measurements per exposure period, including that the 12-month corrosion rates of hot-dip galvanising steel correlated significantly with the 18- and 24-month corrosion rates, 0.88 ($P \leq 0.01$) and 0.92 ($P \leq 0.01$), respectively.

MAP NOT PUBLICLY AVAILABLE

Figure 6.3 IDW interpolated atmospheric corrosion map of the Greater Johannesburg Metropolitan Area – based on the 12-month corrosion rate of hot-dip galvanised mild steel, as measured during August 2013 to September 2014. (Base map – ArcGIS).

6.2.4 GJMA – 12-Month Aluminium Wire Helix Corrosion Map

As per ISO 9226:1992 procedures (Section 3.2.5), **Figure 6.4** is founded on the 12-month corrosion rate measurement of coiled, thermal spraying (>99% pure) aluminium wire (**Appendix C – Table C.3**), exposed at 22 sites in the GJMA, during August 2013 to September 2014 (**Figure 5.26 & Appendix H – Table H.1**). **Figure 6.4** presents the derived IDW interpolated map, revealing that the average 12-month corrosion rate of pure aluminium is about 0.2 ± 0.1 μm/a, 95% CI [0.1 μm/a, 0.2 μm/a], varying from close to zero on the western to north-western side of the GJMA, to near 0.4 μm/a on the East Rand, at the Chloorkop-Modderfontein area. However, shifting towards to Eastern Highveld region, the possibility of higher readings cannot be excluded due to the significant air-pollution effects originating from the Secunda and Emalahleni (Witbank) areas (**Figures 5.4 & 5.5**).

The aluminium map (**Figure 6.4**) compares statistically meaningfully (**Appendix K – Table K.1**) with the hot-dip galvanised map (**Figure 6.3**), and only slightly lesser with the mild steel corrosion map (**Figure 6.2**). The correlation between the ICI map (**Figure 6.1**) and aluminium chart (**Figure 6.4**) is also statistically significant within a 95% CL.

The estimated level of uncertainty of the map is about 25%, based on the experimental uncertainties of measurement introduced during the chemical cleaning and weighing procedures, including that the map is based on a 12-month corrosion monitoring period only and corrosion rates were recorded at merely 22 sites. Also, no duplicate measurements were done. The slightly higher degree of certainty of the map, compared to the ICI chart, may be attributed to the increased statistical significance of the correlation between the hot-dip galvanising and aluminium charts ($P \leq 0.05$) (**Appendix K – Table K.1**).

MAP NOT PUBLICLY AVAILABLE

Figure 6.4 IDW interpolated atmospheric corrosion map of the Greater Johannesburg Metropolitan Area – based on the 12-month corrosion rate of aluminium, as measured during August 2013 to September 2014. (Base map – ArcGIS).

6.2.5 GJMA – 12-Month Zinc Wire Helix Corrosion Map

Figure 6.5 is based on the 12-month corrosion rate of > 99% pure zinc (**Appendix C – Table C.4**), prepared and exposed per ISO 9226:1992 procedures (Section 3.2.5), at 22 sites in the GJMA, during August 2013 to September 2014 (**Figure 5.27 & Appendix H – Table H.1**). **Figure 6.5** shows that the average 12-month corrosion rate of pure zinc in the GJMA is about 0.8 ± 0.3 μm/a, 95% CI [0.6 μm/a, 0.9 μm/a], yielding an overall C3 (*moderate*) corrosivity rating (**Table 2.2**) (International Organization for Standardization 2012a), however, to the lower end of this category (**Table 5.7**).

Like the maps mentioned above**,** the zinc corrosion chart of the GJMA indicates an increase in the corrosivity of the region towards the north-eastern to eastern sides, particularly near the Chloorkop (Modderfontein) area. However, the impact of the Kagiso-Randfontein (West Rand) and Brakpan (East Rand) mining areas on the corrosivity of the region is also of note, including of the Braamfontein locale due to its elevation (**Appendix B – Table B.1**). The increased corrosivity of the Buccleuch (Sandton) highway interchange is also notable.

As may be expected, the correlation between the pure zinc (**Figure 6.5**) and the hot-dip galvanised (**Figure 6.3**) maps is of statistical most importance (**Appendix K – Table K.1**), although it is still high in the case of the mild steel corrosion chart (**Figure 6.2**). Conversely, the correlation between the ICI (**Figure 6.1**) and zinc (**Figure 6.5**) charts is statistically insignificant within a 95% CL (**Appendix K – Table K.1**).

The estimated level of uncertainty of the map is about 25%, based on the experimental uncertainties of measurement introduced during the chemical cleaning and weighing procedures, including that the map is based on a 12-month corrosion monitoring period only and corrosion rates were taken at merely 22 sites. Also, no duplicate measurements were done. However, the slightly higher degree of certainty of the map, compared to the aluminium (**Figure 6.4**) chart, may be attributed to the very high correlation between the hot-dip galvanising and zinc charts ($P \leq 0.05$) (**Appendix K – Table K.1**).

MAP NOT PUBLICLY AVAILABLE

Figure 6.5 IDW interpolated atmospheric corrosion map of the Greater Johannesburg Metropolitan Area – based on the 12-month corrosion rate of zinc, as measured during August 2013 to September 2014. (Base map – ArcGIS).

6.2.6 GJMA – 12-Month Copper Wire Helix Corrosion Map

Figure 6.6 is based on the 12-month corrosion rate measurement of coiled, thermal spraying (>99% pure) copper wire (**Appendix C – Table C.5**), as per ISO 9226:1992 procedures (Section 3.2.5), exposed at 22 sites in the GJMA, during August 2013 to September 2014 (**Figure 5.28 & Appendix H – Table H.1**). The derived IDW interpolated map, **Figure 6.6**, shows that the average 12-month corrosion rate of pure copper is about 0.6 ± 0.2 μm/a, 95% CI [0.5 μm/a, 0.6μm/a], bordering on the C2-C3 corrosivity range (**Tables 2.2 & 5.7**) (International Organization for Standardization 2012a). Like the maps mentioned above, the increased corrosivity of the Chloorkop-Modderfontein, Brakpan and Kagiso-Randfontein areas, due to mining and industrial activity, are of note. Conversely, however, regarding the copper map, the southern parts of the GJMA also tend to stand out from a corrosivity point of view, particularly near Alrode's refining industry, manufacturing and engineering zone, situated near the Katlehong, Tokoza and Vosloorus 'township' areas. This zone is seen as an SO_2 'hotspot' regarding the "*Highveld priority area air quality management plan*" (DEA 2011).

The copper map (**Figure 6.6**) compares statistically best (**Appendix K – Table K.1**) with the zinc (**Figure 6.4**) and hot-dip galvanised steel (**Figure 6.3**) maps. Notwithstanding, its correlations with the aluminium (**Figure 6.5**) and mild steel (**Figure 6.2**) charts are also of statistical importance. Conversely, the relationship between the copper (**Figure 6.6**) and ICI (**Figure 6.1**) maps, is insignificant within a 95% CL.

The estimated level of uncertainty of the map is about 25%, based on the experimental uncertainties of measurement introduced during the chemical cleaning and weighing procedures, as well as that the map is based on a 12-month corrosion monitoring period and corrosion rates were taken at 22 sites only. Also, no duplicate measurements were done. The slightly higher degree of certainty of the map, compared to the ICI chart, may be attributed to the increased statistical meaningful correlations with the zinc, hot-dip galvanised steel, aluminium and mild steel charts ($P \leq 0.05$) (**Appendix K – Table K.1**).

MAP NOT PUBLICLY AVAILABLE

Figure 6.6 IDW interpolated atmospheric corrosion map of the Greater Johannesburg Metropolitan Area – based on the 12-month corrosion rate of copper, as measured during August 2013 to September 2014. (Base map – ArcGIS).

6.3 ATMOSPHERIC CORROSION MAPS FOR SOUTH AFRICA

Figures 6.7 - 6.12 present atmospheric corrosion maps for South Africa, including in some instances, for Lesotho and Swaziland. These maps have been derived from the data presented in **Figures 4.1 - 4.7**, **5.5**, **5.8 - 5.9**, **5.15**, **5.26 - 5.28 & 5.39**, **Tables 4.1**, **5.1 & 5.2**, as well as **Appendices J & H (Tables J.1 & H.1)**. The data include 12-month corrosion rates of mild steel, hot-dip galvanised steel, aluminium, zinc and copper, measured over many years, by various researchers (CSIR 1975; Callaghan 1991; Nixon 1991,1993; Gross & Nixon 1993; Janse van Rensburg 1994, 2010, 2015; Gnoinski & Ramothlola 1994; Leitch 1999, 2003, 2006; Eskom, 2010-2016), as well as during the latest corrosion study.

The corrosion monitoring procedures used were similar to those described in the ISO 9226 (1992 and 2012) standards (International Organization for Standardization 1992c, 2012d). However, as mentioned in Section 3.1, the level of uncertainty of the old data is high, likely 30% or more, due to the estimation of the locations of some of the sites and that measurements were done over many years, possibly slightly changing from one year to the next. Other issues that could influence the level of accuracy are: variable starting times, different climatic and pollution conditions on a year-to-year basis, dissimilar sample exposure angles, different grades of low-carbon steel, hot-dip galvanised steel, aluminium, zinc and copper materials used, varying descaling and chemical cleaning procedures utilised, as well as different weighing accuracies employed.

6.3.1 South Africa – 12-Month Mild Steel Corrosion Map

Figures 6.7 & 6.8 reveal that the highest atmospheric corrosivity is typically encountered along South Africa's coastline, particularly nearest to the sea (< 150 m), in the *extreme* - 200 to 700 µm (CX) range (**Table 2.2**). Refer also to **Tables 2.2 & 5.7**. This is due to the surf action and white-caps in the ocean (Callaghan 1992; Cole et al. 2003; Janse van Rensburg 2019; Alcántara et al. 2017), whereby chlorides are whipped-up by the wind and transported inland (**Figure 2.6**) (Maskew Miller Longman (Pty) Ltd 2013). However, in calmer seawater areas, e.g. harbours, protective bays, lagoons or more landscaped terrains, as well as elevated places, the atmosphere within 150 m from the ocean is likely to be near the C5-M (*very high*) corrosive category

(Section 5.1.1 & **Figure 6.8**). It may also change due to topographical (**Figure 2.8** (Maskew Miller Longman (Pty) Ltd 2013) and **Figures 4.1, 5.3 & 5.7 - 5.8**), biome (**Figure 2.9**) (OpenStax CNX 2017) and infrastructure shielding effects (Cole et al. 2003; Janse van Rensburg 2010). Consequently, a high degree of uncertainty, 35-40%, exists regarding the corrosivity ratings within the first 30 km from the ocean.

Moving inland, the corrosivity of South Africa macro atmosphere decreases rapidly, about 80% (Section 5.1.1), within 150-1000 m from the ocean (**Figure 5.5**), where a *high to very high* (Upper-C4 to Mid-C5) (**Table 5.7 & Figure 6.8**) corrosivity, as per ISO 9223:2012, likely applies. This decrease may be ascribed to the settling of chloride-rich aerosols via gravitational pull, turbulence diffusion and momentum-dominated impact (Cottis et al. 2010). However, salinity in the atmosphere still tends to affect the corrosion rate of mild steel up to 30 km from the ocean. Thereafter, **Figure 5.13**, the 12-month corrosion rate of mild steel is less than 40 µm/a, representing an ISO 9223:2012 corrosivity range of C3 (*moderate*) and *lower* (C1-C2), with slight increases expected in the Central Highveld, Vaal Triangle, Eastern Highveld and Mpumalanga areas (**Figures 6.7 and 6.8**). The lowest atmospheric corrosivity is predicted for South Africa' desert, and semi-arid plateau (**Figure 5.2**), with reduced values, also indicated for the North West and Limpopo Provinces. The reduced change for the zone between the KwaZulu-Natal, Mpumalanga and Gauteng Provinces, may be ascribed to the sub-tropical nature of the area (Winter et al. 2013; Maskew Miller Longman (Pty) Ltd 2016), observed in **Figure 2.6** (Maskew Miller Longman (Pty) Ltd) 2013), **Figure 2.7** (Evwind 2017), **Figure 2.9** (OpenStax CNX 2017), and **Figure 5.2**. (Archive.cnx.org 2017).

MAP NOT PUBLICLY AVAILABLE

Figure 6.7 Atmospheric corrosion map of South Africa – based on the 12-month corrosion rate of mild steel. (Base map – ArcGIS).

MAP NOT PUBLICLY AVAILABLE

Figure 6.8 Atmospheric corrosion map of South Africa – based on ISO 9223:2012 corrosivity rating scheme. (Base map – ArcGIS).

6.3.2 South Africa – 12-Month Hot-dip Galvanised Steel and Pure Zinc Corrosion Maps

Figures 6.9 & 6.10 show similar trends than observed for the mild steel corrosion maps, with the highest predicted corrosivity ratings given for South Africa's coastline, i.e. within the first 1000 m. The corrosivity rating decreases to the *moderate* (C3) category, within 1-3 km from the ocean, with an expected corrosion rate of hot-dip galvanising and zinc of about 1.2 ± 0.4 µm/a, 95% CI [0.3 µm/a, 2.1 µm/a] and 3.7 (1.5) µm/a, 95% CI [2.4 µm/a, 4.9 µm/a], respectively. The reduced corrosion rate of hot-dip galvanising compared to pure zinc may be attributed to the presence of Zn-Fe alloy layers in the case of hot-dip galvanised coating (McEwan 2004), providing better corrosion protection, than zinc's natural protective oxide layer.

Similar to the observations for the mild steel corrosion maps, reduced corrosion rates for hot-dip galvanised steel and pure zinc may also be expected for South Africa's desert and semi-arid regions, in the C1 to Low-C2 (**Tables 2.2 & 5.7**) (International Organization for Standardization 2012a) range, increasing towards the Free State, North West, Gauteng and Limpopo Provinces, mainly in the C2 - ISO 9223:2012 category. However, **Figure 6.11** shows that the corrosion rate of pure zinc is lightly enhanced in the Mpumalanga region, due to the elevated air-pollution levels in the Sasol Secunda, Emalahleni (Witbank) and Middelburg areas (**Figure 5.4**). Conversely, these variations are not reflected in the hot-dip galvanised steel chart (**Figure 6.9**).

The impact of the sub-tropical zone (Winter et al. 2013; Maskew Miller Longman (Pty) Ltd 2016), between the KwaZulu-Natal, Mpumalanga and Gauteng Provinces, is also reflected in the maps. On an average basis, for all sites located more than 30 km away from the ocean, the estimated corrosion rates of hot-dip galvanised steel and zinc are about 0.8 ± 0.4 µm/a, 95% CI [0.6 µm/a, 0.9 µm/a] and 1.0 ± 0.6 µm/a, 95% CI [0.8 µm/a, 1.2µm/a], respectively.



Figure 6.9 Atmospheric corrosion map of South Africa – based on the 12-month corrosion rate of hot-dip galvanised mild steel.

(Base map – ArcGIS).

MAP NOT PUBLICLY AVAILABLE

Figure 6.10 Atmospheric corrosion profiling of South Africa – based on the 12-month corrosion rate of pure zinc. (Base map – ArcGIS).

6.3.3 South Africa – 12-Month Aluminium Corrosion Map

Similar to the mild steel, hot-dip galvanised mild steel and pure zinc corrosion maps, **Figure 6.11** reveals the highest predicted corrosion rate of aluminium along South Africa's coastline, about 2.2 ± 1.1, 95% CI [1.2 µm/a, 3.2 µm/a] on average (within the first 150 m), decreasing to approximately 1.0 ± 0.5 µm/a, 95% CI [0.7 µm/a, 1.3 µm/a] in the 150-1000 m zone. In contrast to the above-mentioned maps, these rates are per **Table 5.7** (adapted from International Organization for Standardization 2012a) equivalent to Lower-C4 to Mid-C3 corrosive environments, clearly indicating that aluminium is less sensitive with respect to the corrosivity of atmospheric environments and that the map potentially reflects an even higher level of uncertainty than the mild steel, hot-dip galvanised steel and pure zinc corrosion charts. The general slow corrosion rate of aluminium under South Africa's coastal conditions may be explained by the formation of protective oxide layers (Graedel 1989; Lobnig et al. 1996; Leygraf et al. 2016), which tend to corrode by way of pitting, rather than general corrosion mode (Leygraf et al. 2016).

Moving 30 km inland, the corrosivity decreases to about 0.3 ± 0.4, 95% CI [0.2 µm/a, 0.4 µm/a], falling in the C1 to Upper-C2 range (**Table 5.7**), which tends to correspond better with the ISO 9223 ratings for the mild steel, hot-dip galvanising and pure zinc corrosion charts. Moreover, the impact of South Africa's inland industrial, mining and power generating locations in the Vaal Triangle, Secunda, Emalahleni (Witbank), Middelburg and Lephalale areas are reflected in the aluminium map.

MAP NOT PUBLICLY AVAILABLE

Figure 6.11 Atmospheric corrosion map of South Africa – based on the 12-month corrosion rate of pure aluminium. (Base map – ArcGIS).

6.3.4 South Africa – 12-Month Copper Corrosion Map

The 12-month copper corrosion map for South Africa is given in **Figure 6.12**, revealing that the highest corrosion rate of copper is typically expected to be along South Africa's coastline, in the *extreme* (CX) corrosive range (**Tables 2.2 & 5.7**) (International Organization for Standardization 2012a). However, like the mild steel, hot-dip galvanised mild steel, zinc and aluminium charts, the expected corrosion rate of copper decreases significantly, > 50%, within the first 1000 m from the ocean, and a further 20% within 3-30 km from the sea.

According to the map, the desert and semi-desert areas of South Africa rate C1 to Lower-C2 corrosive, while at central industrial, mining and power generating locations, increased corrosion rates of copper are reflected, attaining an Upper-C4 (*high*) (**Table 5.7**) rating in the Sasolburg and Mpumalanga areas.

Noteworthy is that this map has also been used to develop a bronze map for South Africa, as discussed in **Appendix T**.

6.3.5 South Africa – Corrosion Map Correlations

The different South African maps vary slightly regarding their classifications of the atmospheric corrosivity of the countrywide environments. The strengths and weaknesses of the associations of these different maps are presented in **Table 6.1**. As shown, the zinc and hot-dip galvanised charts present the highest statistical relationship, followed by the aluminium vs mild steel, and aluminium vs hot-dip galvanising maps.

Table 6.1 Significant (95%) rank correlations between the different corrosion maps for South Africa.

Metal type	Mild steel	HD galv.	Zinc	Aluminium	Copper
Mild steel	1.00	0.66	0.79	0.78	0.69
HD galv.		1.00	0.79	0.78	0.66
Zinc			1.00	0.54	0.59
Aluminium				1.00	0.74
Copper					1.00

Note: – HD denotes hot-dip galvanising.



Figure 6.12 Atmospheric corrosion profiling of South Africa – based on the 12-month corrosion rate of pure copper. (Base map – ArcGIS).

6.3.6 Comparison of GJMA and SA Maps with those Produced for other Countries

Due to regional, topographical, meteorological, pollution and corrosion monitoring variations, comparisons of the GJMA and SA maps with those produced by other international researchers are difficult. However, as discussed in Section 2.1.9, Methodology A, as per Li et al.'s (2013) classification, was mainly followed regarding the latest atmospheric corrosion study, i.e. direct measurements of the corrosion rates of metals in areas of interest. Similar procedures were used by Callaghan (199), King et al. (1982), Martin & King (1981) and Natesan et al. (2015), i.e. contour-based mapping based on site-specific measurements. However, pertaining to the Natesan et al. (2015) and latest corrosion studies, mapping was also done using geoprocessing software.

While the present trend is to combine corrosion rate measurements, with climatological variables and deposition rates of atmospheric contaminants, this strategy could not be wholly followed during the latest study, mainly due to cost constraints. However, as stated by Tullmin & Roberge (2000), a grid pattern of sites can provide detailed corrosion mapping of regions, which can be valuable for planning, plant design and maintenance of infrastructure points of view.

In contrast to the classification of environments using climatological results and the deposition rates of atmospheric pollutants only, e.g. ISO 9223 and 9225, (International Organization of Standardization 2012a, 2012c), the latest study also enabled examination of the morphology and chemical composition of the corrosion product of the mild steel exposed at the different GJMA sites, including the effects of the GJMA's atmosphere on the degradation of organic materials.

CHAPTER 7

CONCLUSIONS

The variations in the atmospheric corrosivity of the Greater Johannesburg Metropolitan Area (GJMA), as well as the rest of South Africa (SA), were investigated. Measurements of the atmospheric corrosion of mild steel, hot-dip galvanised steel, aluminium, zinc and copper were similarly carried out. Furthermore, seasonal fluctuations about the Industrial (ICI), Marine (MCI) and Atmospheric (ACI) Corrosion Indices were examined. The photochemical ageing effects of polymeric materials due to exposure to the GJMA atmosphere were likewise studied.

7.1 ATMOSPHERIC CORROSIVITY OF SOUTH AFRICA (SA)

7.1.1 Analysis and mapping of existing (published and unpublished) corrosion data about SA's macro atmosphere revealed that the air within the first 150 m from the coast, representing approximately 0.03% of the country's surface area, may potentially be classified as Upper-C5-M (*very high*) to CX (*extreme*) marine corrosive in terms of mild steel, hot-dip galvanising, zinc and copper, based on the ISO 9223 rating system. However, the unpredictability of the corrosivity of the atmosphere along the coastline is substantial (likely more than 35%), depending, amongst others, on the surf action and white-caps in the ocean, including altitude, topography, temperature and onshore wind flow.

7.1.2 Between 150 m to 1000 m from the sea, the environment is potentially rated Mid-C4 (*high*) to Mid-C5 (*very high*) marine corrosive, about 0.2% of SA's total land surface area of approximately 1.2 million km^2. From 1-3 km from the coast, the atmosphere is likely classified as *moderate* (C3) to *high* (C4) corrosive (about 0.5% of the surface area), between 10 km and 30 km inland, *moderate* (C3) marine corrosive, near 5% of SA's surface area, and for the approximate 93% remaining inland locations, *very low* (C1) to potentially *high* (C4) corrosive, e.g. at high-polluting industrial installations.

Furthermore, the results showed that in the desert and semi-arid (non-industrial) areas, the corrosivity of the environment is better classified C1 (*very low*) to Low-C2 (*low*) corrosive, whereas in urban industrial places, the atmosphere is preferably ranked *low* (C2) to *moderate* (C3) corrosive, with a potential for *high* (C4) corrosive 'hotspots', in heavy industrial locations.

7.1.3 Concerning the mild steel corrosion rates, the study showed that the corrosivity of SA's coastal environments decreases rapidly, about 80%, within 150-1000 m from the ocean, which primarily can be attributed to the settling, diffusion and impact of airborne salts originating from the sea. Shielding effects caused by vegetation, infrastructure and landscape formations also play essential roles. The results furthermore revealed that the changes in the corrosion rates of the hot-dip galvanised steel, zinc, aluminium and copper, within the first 150 m from the coast, measured around 22% (for copper), 55% for aluminium, and approximately 63-65% for pure zinc and hot-dip galvanised steel.

However, all five metal types covered in the study exhibited 86% and above decrease in corrosion rates from 30 km or more from the coast. Relationships between the reductions in the various corrosion rates with increasing altitude were also derived, revealing strong statistically meaningful ($P \leq 0.05$) correlations.

7.1.4 In the central inland areas, the corrosivity of the atmosphere reduced above the Great South African Escarpment. This change was less noticeable in the sub-tropical regions stretching between KwaZulu-Natal and the Mpumalanga Provinces. In the North West, Limpopo and Gauteng Provinces, the corrosivity of the environment decreased notably. However, the effects of industrial activity on the corrosivity of the inland atmosphere were found in the Vaal Triangle, GJMA, Secunda, Emalahleni (Witbank), Middelburg and Lephalale areas, which were mainly attributed to the presence of large open-cast mines, steel-processing plants, petrochemical and power generating facilities, as well as general industrial pollution.

7.2 ATMOSPHERIC CORROSIVITY OF THE GREATER JOHANNESBURG METROPOLITAN AREA (GJMA)

7.2.1 Industrial, Marine and Atmospheric Corrosion Indices

7.2.1.1 Based on the Industrial Corrosion Indices (ICI), derived via the exposure of *aluminium-on-copper bolt* (CLIMAT) devises to the GJMA's atmosphere, it was found (within a 95% CL) that the region is most corrosive during spring and summer (particularly during spring). This is owing to the average increases in precipitation and %RH in the atmosphere (TOW), at the start of the rainy season, combined with ambient and substrate temperature rises, as well as changing wind patterns. Also, during the daytime, especially during summer, convection potentially forces pollutants to ground level, via so-called looping. Moreover, moisture likely becomes trapped in crevices and therefore, accelerate localised corrosion. The latter phenomenon particularly applies to wire-on-bolt units, which are potentially more prone to the retention of moisture.

7.2.1.2 Only one site rated MODERATELY corrosive regarding the CLIMAT ICI classification scheme, i.e. Chloorkop, during autumn. The rest of the 22 main GJMA sites all ranked NEGLIGIBLE, owing to their respectively reduced ICI, MCI and ACI values, for all four seasons, which were generally applicable to rural and suburban areas, with a MODERATE ICI implying a typical urban environment. The results also showed the that CLIMAT procedure, as per ASTM G116 standard, was less than ideal for comparing the corrosivities of inland urban atmospheres. However, it adequately reflected the seasonal variations of the corrosivity of the GJMA and showed that the East Rand locales, demonstrated the highest ICI and MCI.

7.2.1.3 Correspondences of the average MCI vs ACI, and ICI vs ACI data were determined as statistically inconsequential ($P > 0.05$), with both the ICI and MCI devices reacting more with corrodents in the atmosphere than the ACI units. Contrarywise, the difference in the average ACI values for the rainy versus the non-rainy seasons was found to be exceptionally statistically meaningful. Similarly, the difference between the mean ACI values for spring and summer was established of very high statistical importance, demonstrating that the ACI unit is a useful tool for measuring the changing moisture levels in the atmosphere, specifically from one season to the next.

Regarding the ACI, the highest overall measurements were recorded for the Kagiso-Randfontein site, likely due to the presence of dust and amorphous carbon, found to be present in the corrosion product, potentially promoting TOW and exhibiting reduced pH. At Delta Park, the opposite was proven to be the case.

7.2.2 Aluminium, Zinc, and Copper Wire Helix (WH) Corrosion Rates

7.2.2.1 The mean 12-month corrosion rates of aluminium, zinc and copper wire helices (Al-WH, Zn-WH & Cu-WH), exposed in the GJMA as per the dated ISO 9226:1992 procedure, demonstrated typical to lower measurements than reported for other urban and industrial areas, in other countries, i.e.:

- Al-WH : 0.2 ± 0.1 μm/a, 95% CI [0.1 μm/a, 0.2 μm/a];
- Zn-WH : 0.8 ± 0.3 μm/a, 95% CI [0.6 μm/a, 0.9 μm/a]; and
- Cu-WH : 0.6 ± 0.2 μm/a, 95% CI [0.5 μm/a, 0.6μm/a].

7.2.2.2 Regarding the Al-WH results, based on the former ISO 9223:1992 corrosivity rating scheme, six of the GJMA sites (27%) coincided with the *moderate* (C3) corrosivity category, while the remaining 16 locales (73%), rated *low* (C2) corrosive. Concerning the Zn-WH data, twelve sites (54%) rated *moderately* (C3) corrosive, while the remaining ten locales (46%), rated *low* (C2) corrosive. Conversely, about the Cu-WH-unit results, 36% (eight) fell in the *moderate* (C3) corrosive category, while the remaining 14 locales (64%), rated *low* (C2) corrosive (also as per ISO 9226:1992). The results revealed that the corrosivity ratings for the GJMA per metal type were different and overstated in the old SA corrosion maps.

On the other hand, since ISO open wire helix devices tend to give higher corrosion rate measurements than flat metal panels, the latest GJMA corrosivity ratings were still slightly overestimated. Similar observations have been made in other international corrosion studies.

7.2.2.3 Statistically meaningful relationships, within a 95% CL, were established for the yearly mean ICI and MCI data, versus the Al-WH 12-month corrosion rates. However, about the 12-month Zn-WH corrosion rates, the ICI and MCI relationships were only significant within a 90% CL, while the Cu-WH results, indicated a positive correlation merely with the MCI data, also within a 90% CL. Accordingly, the results showed that the 12- month

corrosion rates of the Al-WH devices correlated better with the CLIMAT results, compared to the Zn-WH or Cu-WH units, likely because the Al-WH and wire-on-bolt devices were manufactured from pure aluminium wire. Aluminium is also affected by Cl^- and sulphur dioxide (SO_2) in the atmosphere.

7.2.2.4 Like the CLIMAT devices, the ISO open wire helix units demonstrated sensitivity concerning Cl^-, SO_2, and TOW. Conversely, however, the highest corrosion rates were recorded at the Kagiso-Randfontein locale, regarding the ISO devices, followed by the Chloorkop site - the latter site demonstrating the highest ICI, MCI and ICI. This variation between the CLIMAT and ISO open wire helix results was attributed to the presence of mine dust on the metal surfaces at the Kagiso-Randfontein locale, increasing TOW, and reducing the pH of the corrosion product. (The latter site is next to a gold mine tailing dump and brick manufacturing facility.) However, at Chloorkop, Cl^- was identified as the key corrosive species involved in the atmospheric corrosion process.

7.2.2.5 From a regional perspective, like the CLIMAT data, the Al-WH, Zn-WH and Cu-WH 12- month corrosion rates showed that the East Rand demonstrated the highest corrosivity, e.g. at Chloorkop and Brakpan. Also, it was found that Kagiso-Randfontein, Chloorkop, Brakpan, Aeroport, Alrode, Braamfontein, Buccleuch, Chamdor and Rosherville were potentially more corrosive, since all these locales are linked to increased industrial, mining and vehicle-related activity in the GJMA.

7.2.2.6 Very high statistically meaningful correlations (within a 99% CL) were also derived for the Al-WH, Zn-WH and Cu-WH results. However, it was shown that the corrosivity rankings per site, based on the 12-month corrosion rates of the open wire helix devices, did not always coincide. Furthermore, while the open wire helix procedure has been withdrawn from the current ISO 9226:2012 standard, the latest GJMA study showed that these units are highly effectual at accumulating gaseous and particulate pollutants from the atmosphere, inexpensive to make, effortless to place at a site, and relatively easy to camouflage or hide from theft.

7.2.3 Mild Steel Corrosion Rates

7.2.3.1 Exposures of flat low-carbon steel coupons to the GJMA atmosphere demonstrated an average 6-month corrosion rate (determined during Spring 2013 and Summer 2013-2014) of 31 ± 7 μm/a, 95% CI [28 μm/a, 35 μm/a], which decreased by about 36% to

20 ± 4 μm/a, 95% CI [18 μm/a, 22 μm/a] after 12 months of exposure. These measurements were made at the 21 main corrosion monitoring sites in the GJMA. However, once the data of the more than 30 mini sites were included in the calculations, the average 12-month corrosion rate of mild steel in the GJMA changed to 20 ± 4 μm/a, 95% CI [19 μm/a, 21 μm/a], indicating a slightly higher confidence regarding the mean value.

After 18 months, the average corrosion rate of the mild steel decreased to about 17 ± 4 μm/a, 95% CI [15 μm/a, 18 μm/a], and after 24 months, to 14 ± 3 μm/a, 95% CI [12 μm/a, 15 μm/a]. By applying these results, long-term projections of the corrosivity of the GJMA could be made, although, based on four exposure periods, 6-, 12-, 18- and 24-months, only. Even so, the results agreed with the average 10-year and steady-state corrosion rates that are given in the ISO 9224:2012 standard for mild steel exposed to *moderate* (C3) corrosive environments, and lower than given in Callaghan's map for the urban (inland) environments.

Regarding the 12-month corrosion rates of mild steel, used for the corrosivity classification of the environments based on ISO 9226:2012, only Brakpan and Dunnottar rated *medium* (C3) corrosive - both situated near old gold mine tailing dumps. Conversely, all the other GJMA sites rated *low* (C2) corrosive, though, to the upper end of this category. Nonetheless, due to the slight uncertainty of measurement of the mild steel corrosion rates, determined as less than 5% per duplicate measurements, the C3 ranking of the Chloorkop, Bonaero Park and Aeroport sites, all located on the East Rand, was warranted. Conversely, Kagiso-Randfontein was identified as a West Rand 'hotspot', while the Newtown site demonstrated the shielding effects that buildings may have on the corrosivity of an environment, and the Palmridge locale, the impact of elevation.

Elevation also apparently influenced the corrosion rates of mild steel at the Braamfontein, Florida Hills, Durban Deep, Krugersdorp, Princess, and Kliprivierberg sites, measuring approximately 18 μm/a at ~1.9 km altitude, and near 16 μm/a at ~1.4 km elevation, e.g. at Dainfern Ridge, Diepsloot, Kya Sand and Lanseria. Furthermore, local weather data supported this finding, showing that the highest rainfall in the GJMA often corresponds with the rocky ridge that runs east-west across the area.

Although, the impact of business and industrial activities in these areas, could not be excluded.

7.2.3.2 The mild steel corrosion results confirmed with more certainty the measured corrosivity of the GJMA, compared to the CLIMAT and ISO-WH unit data, due to the taking of duplicate measurements per exposure period, the application of multiple cycles of exposures, over more extended periods, as well as an increase in the number of sites involved, i.e. more than 50 locations. Consequently, based on a revised ISO 9223:2012 classification scheme, the corrosivities of the different regions of the GJMA were rated as:

- Upper-C2 (*low-moderate*) corrosive in the East Rand, Southern Suburbs and Central JHB Suburbs; and
- Mid-C2 (*low*) corrosive in the Northern Suburbs and West Rand.

The results furthermore showed that concerning the inland Highveld area, the old Callaghan map was based on local pockets of industrial corrosion, while Leitch's (2006) chart, rated the area as *medium* (C3) and *high* (C4) corrosive, which was also excessive.

7.2.3.3 OR Tambo International Airport was found to potentially influence the corrosivity of the GJMA atmosphere, e.g. at the Aeroport and Bonearo Park sites, attributed to emissions from the aircraft jet engines. The presence of oil-like stains on the mild steel panels exposed at two of the sites near the airport also supported this finding, although further work needs to be done in this regard.

7.2.3.4 The 6-, 12-, 18- and 24-month corrosion rates of mild steel (MSP) showed only weak correlations with the CLIMAT results. However, much stronger, statistically significant relationships (within a 95% CL) were found in relation with the ISO open wire helix data, affirmative that the WH results compared better with the MSP corrosion data. Also, the 6-, 12-, 18- and 24-month corrosion rates of mild steel demonstrated very high correlations with each other, found to be statistically meaningful within a 95% CL.

7.2.3.5 Furthermore, the mild steel results showed that the seasonal and yearly variations in the corrosion rates between the different locations stabilised significantly with time and

that Cu-WH devices were seemingly more precise in determining the corrosivity of urban/industrial areas than aluminium or zinc wire coils.

7.2.3.6 The influence of heavy traffic routes on the local corrosivity of the GJMA, by way of soot, NO_x and CO emissions, was established as low, confirming similar findings made by other scholars that traffic pollution does not seem to influence the corrosivity of regions significantly.

7.2.4 Hot-dip Galvanised Mild Steel (GSP) Corrosion Rates

7.2.4.1 Concerning hot-dip galvanised steel, the average 12-month corrosion rate in the GJMA measured 0.7 ± 0.3 μm/a, 95% CI [0.6 μm/a, 0.8 μm/a], decreasing by about 14% to 0.6 ± 0.2 μm/a, 95% CI [0.5 μm/a, 0.7 μm/a], after 18 months of exposure. However, after 24 months, the average corrosion rate of hot-dip galvanised steel demonstrated only minor additional stabilisation, 0.6 ± 0.2 μm/a, 95% CI [0.5 μm/a, 0.6 μm/a], attributed to the likely formation of zinc carbonate protective films on the metal surfaces.

7.2.4.2 In contrast with the mild steel, high correlations were established between the 12-month hot-dip galvanised steel corrosion rates and the CLIMAT ICI and MCI data, suggesting that the CLIMAT devices were better indicators of the impact of atmospheric pollutants on the 12-month corrosion rate of hot-dip galvanised steel, rather than of uncoated carbon steel. Also, the relationships between the 12-month corrosion rates of aluminium, zinc and copper wire, including the hot-dip galvanised rates, were statistically solid, while it was somewhat weaker regarding the mild steel data, although still meaningful within a 95% CL.

High correlations also existed between the 12-, 18 and 24-months corrosion rates of the hot-dip galvanised mild steel specimens. As a result, long-term projections concerning the corrosion rate of hot-dip galvanising were made possible, falling into the average 10-year and steady-state ranges given in ISO 9224:2012 for zinc exposed to *low* (C2) corrosive environments. However, the long-term projection was derived from only three exposure periods, likely affecting the accuracy thereof.

7.2.4.3 Additionally, the hot-dip galvanised results indicated that the corrosion rate of hot-dip galvanised sheeting in the Highveld area was overstated in Callaghan's map. The

regional hot-dip galvanised results furthermore agreed with the other metal types, namely that the GJMA exhibits higher corrosivity in the East Rand, followed by the Southern Suburbs, with Kagiso-Randfontein being a local 'hotspot' on the West Rand.

7.2.5 Optical Surface Characterisation, Morphology and Chemical Analysis of the Mild Steel Corrosion Products Formed at the Main and Mini Sites in the GJMA

7.2.5.1 Agreeing with other corrosion studies, optical surface characterisation of the corrosion products of the mild steel exposed at the main and mini sites in the GJMA revealed that the corrosion products formed were different, and depended on the area, time and conditions of exposure. For example, at Kagiso-Randfontein, the yellowish colour of the corrosion product was attributable, using scanning electron microscopy-energy dispersive X-ray (SEM-EDS) analysis, to the deposition of fine tailing from a nearby gold mine dump.

7.2.5.2 Attenuated total reflectance (ATR) - Fourier transform infrared (FTIR) and Raman spectroscopy analyses also showed that the formation of rust on carbon steel is complex and varied with different exposure conditions. Nonetheless, considering the 12- month mild steel corrosion products formed at the sites in the GJMA, the main crystalline structure identified was lepidocrocite (γ-FeOOH), stated as typical for rust layers of only a few years old in rural and urban environments.

The yellow coloured areas within the rust layers, while less prevalent than the reddish (γ-FeOOH) areas, was found to be due to a mixture of γ-FeOOH and α-FeOOH (goethite), the latter said to often coincide with the former iron oxide and more prevalent in SO_2 polluted areas. Occasional black oxides or particles were also found to correspond to either amorphous carbon or magnetite (Fe_3O_4), e.g. at Chloorkop, Aeroport, Alexandra, Lenasia and Nasrec. At the Chloorkop site, β-FeOOH (akageneite) and $Fe(OH_3)$ (ferric hydroxide) were detected in the rust products, the former iron oxide known to develop in polluted chloride environments. The EDS results furthermore reinforced this finding.

Conversely, at the Kagiso-Randfontein locale, the main constituents of the mild steel corrosion product were established as γ-FeOOH, α-FeOOH, quartz and amorphous carbon - the quartz likely originating from a nearby gold mine tailing dump and the

amorphous carbon, due to the incomplete combustion of coal, stemming from a nearby brick manufacturing facility and 'township' area. The presence of carbon in the Kagiso-Randfontein mild steel corrosion product, thought to be sticky and acidic, likely assisted in the reduction of the pH value of the corrosion product – subsequently, confirmed by way of pH measurements.

7.2.5.3 Apart from oxygen (O) and carbon (C), SEM-EDS analyses of the corrosion products revealed the presence of aluminium (Al), silicon (Si), phosphorus (P), sulphur (S), chlorine (Cl), potassium (K), calcium (Ca) and iron (Fe). The C and P were linked to bird droppings on the corroded surfaces, while the Al and Si were associated with the occurrence of dust, ash and other particulate matter, e.g. PM_{10}, on the metal surfaces, known to be hygroscopic, thus promoting TOW.

Sulphur-bearing corrodents, e.g. at Springs, Dalpark and Aeroport, including particulate matter were considered the primary pollution drivers of the atmospheric corrosion processes of mild steel in the GJMA, consistent with most urban and industrial environments. However, around Dalpark and Aeroport, the corrosion processes were possibly also encouraged by air pollution affected by aviation fuel combustion, emanating from the nearby airports. Furthermore, Chloorkop exhibited detectable levels of chlorine in the corrosion product of the mild steel panels, due to the presence of a closely situated chloralkali mining and industrial industry. Moreover, the Durban Deep and Kagiso-Randfontein results indicated the presence of sand and ash, explaining the yellowish-white spots observed on the corroded metal surfaces.

7.2.5.4 One of the most important findings of the current study is that the average 12-month corrosion rates of mild steel at the different GJMA sites corresponded linearly (r = 0.92) with every 20 mg/m^2 rise in the concentration of water-soluble salts in the corrosion product, determined by way of the Bresle procedure, and statistically meaningful within a 99% CL. The link was associated with the hygroscopic nature of salts, likely causing wetting of the steel surfaces below the CRH. A substantial escalation in the water-soluble salt levels on the metal surfaces, with an increase in exposure time, was also found.

The high correlation between the water-soluble salts levels of the rusted surfaces and their measured 12-month corrosion rates suggested that potentially a new procedure

can be developed for the rapid classification of corrosive environments. Alternatively, it may be used as an indicator of the corrosivity of environments, in combination with existing atmospheric corrosion models, e.g. ISO 9223:2012 and ISO 9226:2012. However, further work is required in this regard.

7.2.5.5 The average pH of the mild steel corrosion products of the main and mini sites averaged at pH4.9 ± 0.3, 95% CI [pH4.8, pH4.9], with the Kagiso-Randfontein locale exhibiting the lowest value, pH4.3. The relationship, slightly negative, between the pH data versus the 12-month corrosion rates of the mild steel panels, of the various locations, was established as statistically meaningful within a 90% CL.

7.2.6 Effects of the GJMA's Atmosphere on Organic Coatings

7.2.6.1 The impact of the corrosiveness of the GJMA's atmosphere on organic coatings indicated measurable changes regarding their average dry film thicknesses (DFTs), gloss levels, colours, chemical structures, as well as the extent of chalking and dirt retention. Nonetheless, the differences in the average DFTs of the coatings, following 24 months of exposure in the GJMA, were primarily ascribed to shrinkage of the coatings, with possible further volatilisation of the organic components, due to ultraviolet (UV) light exposure, rather than because of atmospheric pollution.

7.2.6.2 The highest chalking and gloss loss rates were determined for a typical alkyd high-gloss enamel coating, while an exterior-quality acrylic emulsion paint, at Aeroport, Braamfontein and Chloorkop, demonstrated maximum levels of dust and soot retention.

Furthermore, modest ($r > 5$) to high ($r > 7$) linear correlations, within a 95% CL, were found between the 12-month corrosion rates of mild steel, galvanised steel, aluminium, zinc and copper, and the changes in gloss levels of polysiloxane and water-based acrylic coatings, indicating that the changes were associated with the corrosive conditions of the atmosphere, rather than by UV light radiation.

7.2.6.4 Moreover, concerning the corrosiveness of the GJMA environment, medium to strong linear correlations, within a 95% CL, were found between the total colour differences (ΔE) of the coated samples exposed at the sites and the associated 12-month corrosion rates of mild steel, galvanised steel, aluminium, zinc and copper. This was valid for the polysiloxane, water-based acrylic and alkyd high-gloss enamel coatings, alluding to the

likelihood that the varying corrosiveness of the environment strongly influenced the slight colour changes.

7.2.6.5 The changes in the chemical structures of the upper facing surfaces of two water-based acrylic coatings, assessed via FTIR analysis, displayed medium to strong negative correlations ($P \leq 0.05$) with their respective chalking, loss of gloss, and colour variation data. The chemical structural changes were also found to be significantly ($P \leq 0.01$) influenced by the varying corrosive levels of the atmosphere.

Moreover, the coating systems exposed at the Kagiso-Randfontein and Aeroport sites appeared most affected by UV light radiation and pollution in the atmosphere - the degradation of the organic coatings at the Aeroport locale, likely being influenced by the Kelvin A and B Power Stations and the nearby OR Tambo International Airport, highlighted in air quality reports as problem areas.

7.2.7 Physical, Meteorological and Pollution Effects on the Corrosivity of the GJMA

7.2.7.1 The corrosivity of the GJMA was found to be associated with altitude (at sites situated along the high ridge between Mogale City and Edenvale), elevation above ground level (Braamfontein and Palmridge), shielding/shading effects (Delta Park and Jabavu-Soweto) and the presence of large water bodies (Bonaero Park), including changing meteorological and air pollution effects.

7.2.7.2 The impacts of the climatic factors on the corrosivity of the GJMA were diverse, involving ambient temperature (maximum and minimum), relative humidity, wind, rainfall and pollution, particularly SO_2, NO_2 and PM_{10} particulate matter.

7.2.7.3 Regarding temperature, the results hinted to the possibility that while daily and seasonal temperature fluctuations may influence atmospheric corrosion in the GJMA, mainly when elevated, the associations were linked primarily with the rainy seasons of the year, spring and summer. The association between temperature and increased RH in the atmosphere during the rainy seasons was also evident.

Nonetheless, the average diurnal fluctuation in the GJMA during the study period was more than 10°C, likely promoting the condensation of moisture on metal surfaces, particularly during winter, due to the dry, cold and windless conditions.

7.2.7.4 The results indicated that %RH is not the sole driving force behind the atmospheric corrosion processes in the GJMA, likely because for most of the year, as well within 24- hour cycles, the %RH of the GJMA is below the average CRH for nearly all clean metal surfaces, given as 66%. Moreover, it is likely that the 2011 to mid-2015 El Niño event, resulting in one of South Africa's worst drought periods, might have affected the corrosivity measurements for the GJMA. However, also realised is that the effects of the drought on the interior regions of the GJMA during 2014-2015 would have been reduced.

Comparisons of the seasonal rainfall data versus the average cyclic changes in the ICI, MCI and ACI values for the Central and East Rand areas, revealed high correlations, although statistically insignificant ($P > 0.10$), due to the limited period of measurement. Nonetheless, these findings proposed that the average rainfall per area play a vital role in the corrosivity of the GJMA, in comparison with the average RH values, concurring with other scholars' results. However, the correlation for RH vs the corrosion data is uncertain, due to the limited duration of the study, warranting further investigation.

7.2.7.5 Cyclic wind trends for at least two of the GJMA regions corresponded strongly ($P \leq 0.05$) with the seasonal ICI values, namely, higher wind speeds during spring and summer, followed by a reduction during autumn and then an escalation during winter. Moreover, the correlation between the seasonal changes in the wind speed versus the average cyclic ACI values for the East Rand was statistically meaningful within a 99% CL. These findings strongly supported the understanding that the wind patterns significantly influence atmospheric corrosion in the GJMA, particularly concerning their impact on the industrial (ICI) and general atmospheric (ACI) conditions.

7.2.7.6 Apart from a seasonal impact of sunlight on the corrosivity of the GJMA, the results of the different organic coatings exposed to the Highveld atmosphere indicated several other factors that also play a role regarding the solar degradation of organic materials, e.g. shielding/shading effects, colours and compositions of the exposed materials. In this regard, Kagiso-Randfontein (West Rand), Aeroport (East Rand) and Chloorkop (East Rand) exhibited a higher photochemical breakdown of the organic coatings than the average GJMA site.

7.2.7.7 Historical pollution data for eight of the 22 main GJMA test locales, coinciding with air quality monitoring stations of the City of Johannesburg Metropolitan Municipality, suggested that the galvanic wire-on-bolt-couples (CLIMAT units) were, at least partially, affected by the PM_{10} particulate matter in the atmosphere. This was because particulate matter likely becomes trapped in the crevices between the wire and bolt surfaces, promoting wetting, increased TOW and corrosion. Conversely, concerning the ISO open wire helix surfaces, without crevices, the results proposed that the wind likely causes drying of the surfaces, while in the case of the flat mild steel panels, the 45° angle of the surfaces probably allows for the partial collection of the particulate matter, causing increased wetting and corrosion of the surfaces.

7.2.7.8 A strong correlation (statistically significant within a 95% CL) was found between the 12-month zinc corrosion data of six of the GJMA sites and their respective SO_2 results, indicating that this pollutant is a major player regarding the corrosion of zinc in the GJMA, as well as for that matter, of hot-dip galvanised steel.

Conversely, the associations between the SO_2 levels and the 12-month corrosion rates of aluminium and copper were less meaningful, although hinting to a likelihood that the copper wire helices were best suited for the detection of SO_2 pollution than aluminium and mild steel devices, also about the ICI and MCI results.

7.2.7.9 Historical NO_2 and NO concentrations for four and three of the GJMA sites, sustained that the eastern to north-eastern regions are influenced most by pollution and corrosivity. Also, the data proposed that motor vehicle emissions might have an impact on the corrosion processes at Buccleuch, situated in the middle of the intersection at the 'Buccleuch' interchange between the N1 and N3 highways. This finding was also maintained by dated $PM_{2.5}$ particulate (dust) matter and CO levels for the Buccleuch interchange area, which showed that during spring and summer, maximum $PM_{2.5}$ and CO concentrations of 100 µg/m^3 and 7 ppm, respectively, were possible.

7.2.7.10 Ozone (O_3) concentrations for five of the air quality/corrosion monitoring sites in the GJMA showed that tropospheric O_3 is of concern when it comes to the long-term durability of organic materials. Also, during the daytime, the levels of O_3 at Delta Park were found to surpass those of the other locales, most likely due to the oxygen-rich environment created by the trees. The latter phenomenon is providing clarification

regarding the high 12-month corrosion rate of mild steel at Delta Park, compared with the other seven air quality/corrosion monitoring locales.

7.2.7.11 Conflicting with the Department of Environmental Affairs' statement that "*acid rain over South Africa is not as serious an issue as previously thought*", the latest GJMA study showed that the atmospheric corrosion results related strongly to an interpolated map of the total (dry plus wet) acid deposition rates in meq/m^2 per year for Gauteng and other regions of South Africa. In this regard, the eastern parts of Gauteng (including the GJMA), exhibit increased signs of acid deposition, especially moving towards the Eastern Highveld, due to the presence of ten coal-fired power stations, several smelters, open-cast coal mines, including a sizeable synthetic fuel production plant.

7.3 ATMOSPHERIC CORROSION MAPS FOR SOUTH AFRICA AND THE GJMA

Medium-scale vector-based atmospheric corrosion maps for the GJMA were developed. These maps were subsequently merged with small-scale national corrosion maps for South Africa (SA), derived using the latest and historical (published and unpublished) corrosion monitoring results. The SA maps were expressed in different formats for increased applicability and interest purposes.

7.3.1 Atmospheric Corrosion Maps for the GJMA

7.3.1.1 Inverse Distance Weighted (IDW) interpolated corrosion maps for the GJMA were established on the corrosivity ICI results, derived using the *aluminium wire-on-copper* bolt (CLIMAT) units (manufactured as per ASTM G116:2004), as well as the 12-month corrosion rates of mild steel and hot-dip galvanised steel, as per ISO 9226:2012, and the 12-month corrosion rates of aluminium, zinc and copper, as per ISO 9226:1992 procedures.

7.3.1.2 The estimated accuracies of these maps vary between 15% and 35%, determined by the systematic errors of measurement introduced during the chemical cleaning and weighing procedures, utilised during the different monitoring processes, the periods of atmospheric exposure (Autumn 2013 to Winter 2014), the number of sites involved, as well as whether duplicate measurements were made per exposure period.

7.3.1.3 The 12-month mild steel corrosion map is considered the most accurate regarding the varying corrosivity of the GJMA, estimated at 15%, since the measurements were taken

at more than 50 sites, duplicate specimens were employed per exposure period, as well as the 12-month mild steel results correlated strongly, 0.99 ($P \leq 0.01$) and 1 ($P \leq 0.01$), with the 18 and 24-month corrosion data, respectively.

7.3.1.4 However, the aluminium map, derived using the 12-month corrosion rates of aluminium, as per the ISO 9226:1992 open wire helix procedure, compares statistically meaningfully with the hot-dip galvanised map, and only slightly less with the mild steel corrosion map. The correlation between the ICI map and aluminium chart is also statistically significant within a 95% CL. Of most importance is the correlation between the pure zinc and the hot-dip galvanised maps, while the relationships between the ICI and zinc maps are statistically insignificant within a 95% CL.

7.3.1.5 In contrast to the mild steel, hot-dip galvanised mild steel, aluminium and zinc maps, the copper chart tends to stand out from a corrosivity point of view concerning the southern parts of the GJMA, particularly near Alrode's refining, manufacturing and engineering industrial zone, situated near the Katlehong, Tokoza and Vosloorus 'township' areas. This agrees with view of the Department of Environmental Affairs, which regards this area as an SO_2 'hotspot' concerning their "*Highveld priority area air quality management plan*".

7.3.1.6 Moreover, the copper map compares statistically best with the zinc and hot-dip galvanised steel maps. Notwithstanding, the correlations with the aluminium and mild steel charts are also of statistical importance. Conversely, the relationship between the copper and ICI maps is insignificant within a 95% CL.

7.3.2 Atmospheric Corrosion Maps for South Africa

7.3.2.1 The atmospheric corrosion maps for South Africa, including in some instances, for Lesotho and Swaziland, have been derived from the results of the current corrosion study, including the 12-month corrosion rates of mild steel, hot-dip galvanised steel, aluminium, zinc and copper, measured over many years, by various scholars, per similar procedures described in the ISO 9226 (1992 and 2012) standards.

7.3.2.2 Due to the estimation of the locations of some of the old sites and that the measurements were done over many years, the level of uncertainty of these SA maps is relatively high, likely 35% to 40%, particularly concerning the first 30 km from the

ocean. Other issues that influence the level of uncertainty are variable starting times, different climatic and pollution conditions on a year-to-year basis, dissimilar sample exposure angles, different grades of low-carbon steel, hot-dip galvanised steel, aluminium, zinc and copper materials used, varying descaling and chemical cleaning procedures utilised, as well as different weighing accuracies achieved.

7.3.2.3 Generally, the maps show a rapid decrease in the corrosivity of the country's atmosphere within a short distance span from the ocean, ascribed to the settling of chloride-rich aerosols via gravitational pull, turbulence diffusion and momentum-dominated impact. The lowest atmospheric corrosivity is predicted for South Africa's desert, and semi-arid plateau, with reduced values, also indicated for the North West and Limpopo Provinces, although not to the same extreme.

However, regarding the zinc corrosion map, the corrosivity of the atmosphere is slightly enhanced in the Mpumalanga region due to the high levels of air pollution in the Sasol Secunda, Emalahleni (Witbank) and Middelburg areas. Conversely, these variations are not reflected in the hot-dip galvanised steel chart, considered to be due to the higher resistance of the zinc-iron alloys layers to atmospheric corrosion. Moreover, the impact of the sub-tropical zone, between the KwaZulu Natal, Mpumalanga and Gauteng Provinces, is reflected in the maps.

7.3.2.4 Concerning the aluminium map, contrary to the other charts, the 150-1000 m zone from the coast was found to be equivalent to Lower-C4 to Mid-C3 corrosive environments. This proposed that aluminium is not only less sensitive concerning the measurement of the corrosivity of atmospheric environments, but the map likely reflects a higher level of uncertainty compared to the mild steel, hot-dip galvanised steel and pure zinc corrosion charts. The general slow corrosion rate of aluminium under South Africa's coastal conditions may be explained by the formation of protective oxide films that tend to corrode by way of pitting, rather than general corrosion.

7.3.2.5 Finally, due to regional, topographical, meteorological, pollution and corrosion monitoring variations, comparisons of the GJMA and SA maps with those produced by other international scholars have proven difficult. However, of note is that while the latest GJMA and SA maps are based on the direct measurements of the corrosion rates of metals in different areas, followed by mapping using geoprocessing software, the

current international trend is to combine corrosion rate measurements, with climatological variables and deposition rates of atmospheric contaminants. Regrettably, this strategy could not be followed during this study, mainly due to cost constraints. Notwithstanding, a grid pattern or contour-based corrosion mapping of sites is useful when it comes to the forecasting of potential corrosion problems, from research, design, construction, maintenance, operations and public perspectives.

Also, in contrast to other international maps derived by way of climatological results and the deposition rates of atmospheric pollutants, this study enabled the examination of the morphology and chemical composition of the corrosion product of the mild steel exposed at the different GJMA sites, including the effects of the GJMA's atmosphere on the degradation of organic materials.

CHAPTER 8

RECOMMENDATIONS AND FUTURE PERSPECTIVE

More and more people are migrating to large metropolitan areas. This trend is recognised globally and is expected to continue in the future, leading to increased deterioration of urban environments. While historically it was believed that human activity resulted in only localised or regional environmental changes, scholars now recognise that the impact of humanity is also causing global effects (Botkin & Keller 2010).

From a South African perspective, the development of more comprehensive corrosion maps of SA's atmosphere needs to be done, particularly pertaining to the corrosion profiling of the country's large metropolitan areas. The impact of global warming and climate change on the environment also requires proper investigation. This can only be achieved if more scholars, including academic, state and public institutions, invest in the atmospheric corrosion field. A continuous study of South Africa's atmosphere (macro, meso and micro environments) therefore, is encouraged, with emphasis that needs to be placed on the following cities: Cape Town, Durban, Port Elizabeth, East-London, Bloemfontein, Sasolburg, Secunda, Mpumalanga, Rustenburg and Phalaborwa.

Additionally, it is recommended that the influence of airports on the corrosivity of the environment be thoroughly investigated, particularly relating to their impact on organic materials. Moreover, the relationship between the average corrosion rate of mild steel with every 20 mg/m^2 rise in the concentration of water-soluble salts in the corrosion product warrants further investigation.

Finally, it needs to be said that atmospheric corrosion is a natural phenomenon that affects all economies. Global cooperation to combat this problem is therefore important to ensure the sustainability and protection of all human heritage and built environments.

REFERENCES

2OceansVibe News, 2013. *Johannesburg is the 7th most polluted city in the world.* [Online]
Available at: http://www.2oceansvibe.com/2013/01/17/johannesburg-is-the-7th-most-polluted-city-in-the-world/comment-page-1/
[Accessed 11 April 2016].

About.com - Part of the New York Times Company, 2012. *London Metal Exchange (LME) Prices.* [Online]
Available at: http://metals.about.com/cs/utilities/l/blprices.htm
[Accessed 1 July 2012].

Adams, M., 2014. *Irrefutable proof we are all being sprayed with poison: 571 tons of toxic lead 'chemtrailed' into America's skies every year.* [Online]
Available at: http://www.naturalnews.com/045563_aviation_fuel_toxic_lead_heavy_metals_pollution.html
[Accessed 1 April 2017].

Adikari, A., De S. Munasinghe, R. & Jayatileke, S., 2014. Prediction of atmospheric corrosion - A review. *Engineer*, XLVII(01), pp. 75-83.

AECI Paints, n.d. *Corrosion map of Southern Africa.* Johannesburg: AECI Paints.

AFSA, 2011. *Corrosion resistance of aluminium and protective measures where appropriate.* 1st Edn. Bedfordview: Aluminium Federation of South Africa.

Airliners.net, 2004. *Fuel dumping over homes?.* [Online]
Available at: http://www.airliners.net/forum/viewtopic.php?t=275153
[Accessed 1 April 2017].

Airshed, 2008. Air quality impact assessment for the proposed new remote apron stands at OR Tambo International Airport (Johannesburg), Report. No.: APP/08/ACSA_JHB-01 Rev 0, June 2008. Midrand: Airshed Planning Professionals (Pty) Ltd.

Airports Company South Africa, n.d. *OR Thambo International Airport.* [Online]
Available at: http://www.airports.co.za/airports/or-tambo-international/the-airport/about-or-tambo
[Accessed 10 April 2016].

AkzoNobel, 2015. *Dulux Steel Primer - Technical data sheet.* [Online]
Available at: s://7009b4c5dfb144578bce-95944689bbf5cfecfed588c2a67511bf.ssl.cf3.rackcdn.com/tds/3dulux22prepsteelprimer-2015-approved.pdf
[Accessed 13 August 2017].

AkzoNobel, 2016. *Dulux Gloss Enamel - Technical data sheet.* [Online]
Available at: /7009b4c5dfb144578bce-95944689bbf5cfecfed588c2a67511bf.ssl.cf3.rackcdn.com/tds/3dulux51trimsglossenamel-2016-approved.pdf
[Accessed 13 August 2017].

Alcántara, J., Chico, B., Diaz, I., De la Fuente, D., Morcillo, M., 2015. Airborne chloride deposits and its effects on marine atmospheric corrosion of mild steel. *Corrosion Science,* Volume 97, pp. 74-88.

Alcántara, J., de la Fuente, D., Chico, B., Simancas, J., Díaz, I. & Morcillo, M., 2017. Marine atmospheric corrosion of carbon steel: A review. *Materials*, 10(4), doi:10.3390/ma10040406.

Allam, I.M., Arlow. J.S. & Saricimen, H., 1991. Initial stages of atmospheric corrosion of steel in the Arabian Gulf. *Corrosion Science,* 32 (4), pp. 417-432.

American Society for Testing and Materials, 2000. *Marine corrosion in tropical environments.* West Conshohocken: ASTM International.

Annegarn, H., Storms, H., van Grieken, R. & Booth-Jones, B., 1987. Composition and size of individual particles from a gold mine atmosphere. *Mining Science and Technology*, 5(2), pp. 111-119.

Annegarn, H., 2007. *Air quality management and climate change: A call for local action.* [Online]
Available at: http://www.joburg-

archive.co.za/2007/pdfs/air_quality/annegarnaqm_presentation.pdf
[Accessed 11 April 2016].

Anthanassiadis, Y., 1969. *United States Environmental Protection Agency - Air pollution aspects of phosphorus and its compound.* [Online]
Available at:
https://nepis.epa.gov/Exe/ZyNET.exe/91008110.TXT?ZyActionD=ZyDocument&Client=EPA&Index=Prior+to+1976&Docs=&Query=&Time=&EndTime=&SearchMethod=1&TocRestrict=n&Toc=&TocEntry=&QField=&QFieldYear=&QFieldMonth=&QFieldDay=&IntQFieldOp=0&ExtQFieldOp=0&XmlQuery=&
[Accessed 2012 February 2017].

Antunesa, R., Costa, I. & Araújo de Faria, D., 2003. Characterization of corrosion products formed on steels in the first months of atmospheric exposure. *Materials Research*, 6(3), pp. 403-408.

ArcelorMittal South Africa, 2017. *Datasheet: C 1.1- Availability, properties and tolerances - Galvanised material - Hot-dip galvanised cold rolled and hot rolled steel substrate.* [Online]
Available at:
https://flatsteel.arcelormittalsa.com/fspcatalogue/DataSheets/Coated/Web_datasheet_c1.1.pdf
[Accessed 21 May 2017].

Archive.cnx.org, 2017. *Geography.* [Online]
Available at: http://archive.cnx.org/contents/d5717376-e429-4585-a1ee-98767a736cfd@1/climate-regions
[Accessed 9 April 2017].

Arrive Alive, 2017. *Minibus taxis and road safety.* [Online]
Available at: https://www.arrivealive.co.za/Minibus-Taxis-and-Road-Safety
[Accessed 19 August 2017].

Arroyave, C., Echeverria, F., Herrera, F., Delgado, J. & Aragon, D., 2002. NO_2 measurements in atmospheric corrosion studies. In: H. Townsend (Ed.). *Outdoor Atmospheric Corrosion.* West Conshohocken: ASTM International, pp. 88-102.

ASM International, 2006. Corrosion: environments and industries. In: D. Cramer & S. Covino (Eds.). *ASM Handbook.* Ohio, United States: ASM International.

ASTM International, 1986. *ASTM G92-86 - Standard practice for the preparation, cleaning and evaluation of corrosion test specimens.* West Conshohocken: ASTM International.

ASTM International, 1990. *ASTM G15-90 - Standard terminology relating to corrosion and corrosion testing.* West Conshohocken: ASTM International.

ASTM International, 2003a. *ASTM G1 - Standard practice for preparing, cleaning and evaluating corrosion test specimens.* West Conshohocken: ASTM International.

ASTM International, 2003b. *ASTM B826 - Standard test method for monitoring atmospheric corrosion by electrical resistance probes.* West Conshohocken: ASTM International.

ASTM International, 2004. *ASTM G116-99 - Standard practice for conducting wire-on-bolt test for atmospheric galvanic corrosion.* West Conshohocken: ASTM International.

ASTM International, 2009. *ASTM D1014: Standard practice for conducting exterior exposure tests of paints and coatings on metal substrates.* West Conshohocken: ASTM International.

ASTM International, 2013. *ASTM E284: Standard terminology of appearance.* West Conshohocken: ASTM International.

ASTM International, 2014. *ASTM G4-1: Standard guide for conducting corrosion tests in field applications.* West Conshohocken: ASTM International.

Aviation Environment Federation (UK), 2000-2018. What are the airport's impacts? [Online]
Available at: https://www.aef.org.uk/uploads/PlanningGuide2.pdf
[Accessed 29 July 2018].

Azue, J. (Ed.), 1999. *Environmental Impacts of Mining Activities*. 1st Edn. Berlin: Springer-Verslag.

Baboian, R., 2000. *Corrosion-doctors.org - Glossary - Airport corrosion.* [Online] Available at: http://corrosion-doctors.org/AtmCorros/ncn-environment.htm [Accessed 21 May 2017].

Badea, G., Cret, P., Lolea, M. & Setel, A., 2011. Studies of carbon steel corrosion in atmospheric conditions. *Acta Technica Corviniensis - Bulletin of Engineering*, Tome IV, pp. 25-18.

Balasubramaniam, R. & Ramesh Kumar, A.V., 2000. Characterization of Delhi iron pillar rust by X-ray diffraction, Fourier transform infrared spectroscopy and Mossbauer spectroscopy. *Corrosion Science,* Volume 42, pp. 2085-2101.

Ballance, J. & Duncan, J., 1985. Wind-borne transport and deposition of sea-salt in New Zealand. *New Zealand Journal of Technology*, Volume 1, pp. 239-244.

Barnett, W., 2006. Walter's corner - The atmospheric corrosion rate is not always what it seems to be!. *Hot Dip Galvanizing Today,* 3(1), pp. 36-37.

Barrett, J. & Malati, M., 1998. *Fundamentals of inorganic chemistry: An introductory text for degree studies.* West Sussex: Horwood Publishing Limited.

Barton, K., 1976. *Protection Against Atmospheric Corrosion*. London: John Wiley & Sons.

Beirle, S., Platt, U., Wenig, M. & Wagner, T., 2003. Weekly cycle of NO_2 by GOME measurements: a signature of anthropogenic sources. *Atmospheric Chemistry and Physics,* Volume 3, pp. 2225-2232.

Bell, A., 1982. A corrosion map of Melbourne. *ECOS Magazine,* Issue 33, pp. 10-12.

Bennett, D., 2017. *Sciencing - How do temperature inversions influence air pollution?.* [Online]
Available at: http://sciencing.com/temperature-inversions-influence-air-pollution-10038430.html
[Accessed 19 August 2017].

Binggelli, C. (Ed.), 2012. *Interior Graphics Standards.* 2nd Edn. New Jersey: John-Wiley & Sons, Inc.

Biodiversity and Conservation Biology Department, 2012. *VWC Environ Facts - Global warming.* [Online]
Available at: http://www.bcb.uwc.ac.za/encfacts/facts/gwarming.htm
[Accessed 29 July 2012].

Bitcon, J., 2014. *Atmospheric corrosivity at Australian and overseas airbases and airports*, Victoria: Commonwealth of Australia.

Bohlweki Environmental (Pty) Ltd, 2002. *Environmental impact assessment for the proposed Gautrain rapid rail link between Johannesburg, Pretoria and Johannesburg International Airport.* Midrand, Bohlweki Environmental (Pty) Ltd, 2002.

Bokobza, L., Bruneel, J. & Couzi, M., 2013. Raman spectroscopic investigation of carbon-based materials and their composites. Comparison between carbon nanotubes and carbon black. *Chemical Physics Letters*, Volume 590, pp. 153-159.

Botkin, D. & Keller, E., 2010. *Environmental Science.* 7th Edn. Asia: John Wiley & Sons, Inc.

Brand South Africa, 2017. *South Africa's population.* [Online]
Available at: https://www.brandsouthafrica.com/people-culture/people/south-africas-population
[Accessed 19 August 2017].

British Standards Institution, 2000. *BS EN 12500:2000 - Protection of metallic materials against corrosion. Corrosion likelihood in atmospheric environment. Classification, determination and estimation of corrosivity of atmospheric environments*. London, British Standards Institution.

British Standards Institution, 2018. BSI.Shop. [Online]
Available at:
https://shop.bsigroup.com/ProductDetail/?pid=000000000030020548
[Accessed 27 June 2018].

Brown, P. & Masters, L., 1982. Factors affecting the corrosion of metals in the atmosphere. In: W. Ailor (Ed.), *Atmospheric Corrosion.* New York: John Wiley & Sons, pp. 31-50.

Brunt, D., 1952. *Physical and Dynamical Meteorology.* 2nd Edn. Cambridge: Cambridge University Press.

BusinessTech, 2016a. *Rand vs the dollar: 1978 – 2016*.
[Online]
Available at: https://businesstech.co.za/news/finance/116372/rand-vs-the-dollar-1978-2016/
[Accessed 9 April 2017].

BusinessTech, 2016b. *The most polluted city in South Africa is not where you expect.*
[Online]
Available at: https://businesstech.co.za/news/lifestyle/123495/the-most-polluted-city-in-south-africa-is-not-where-you-expect/
[Accessed 1 May 2017].

California Environmental Protection Agency, 2015. *Facts about ozone and health.*
[Online]
Available at: http://www.arb.ca.gov/research/aaqs/caaqs/ozone/ozone-fs.pdf
[Accessed 18 June 2016].

Calitz, J. & Potgieter, J., 2005. Corrosion of overhead power transmission conductors in marine environments. *Transactions of the South African Institute of Electrical Engineers*, 96(4), pp. 306-311.

Callaghan, B., 1991. *Atmospheric Corrosion Testing in Southern Africa - Results of a Twenty-year National Programme.* Pretoria: Scientia Publishers.

Callaghan, B., 2012. *An informal discussion related to the development of his corrosion map of Southern Africa* [Interview] (30 July 2012).

Carter, V.E. (Ed.), 1982. *Corrosion Testing for Metal Finishing: Institute of Metal Finishing.* London: Butterworth Scientific (in association with the Institute of Metal Finishing).

Castaneda, A., Corvo, F., Howland, J. & Marrero, R., 2018. Penetration of marine aerosol in a tropical coastal city: Havana. *Atmósfera* 31(1), pp. 87-104.

Castillo, R.F. (Ed.), 2011. *Relative Humidity: Sensors, Management and Environmental Effects (Environmental Science, Engineering and Technology)*. London, Nova Science Pub. Inc.

Chempedia.info, 2015. *Big Chemical Encyclopedia - Aluminium alloys atmospheric corrosion.* [Online]
Available at: http://chempedia.info/info/156854/
[Accessed 7 September 2018].

Chico, B., de la Fuente, D., Díaz, I., Simancas, J. & Morcillo, M., 2017. Annual atmospheric corrosion of carbon steel worldwide. An integration of ISOCORRAG, ICP/UNECE and MICAT databases. *Materials*, 10(601), pp. 1-26.

City Lodge Blog, 2012. *Ten things you didn't know about Johannesburg.* [Online]
Available at: http://clhg.com/blog/2012/09/ten-things-you-didnt-know-about-johannesburg/
[Accessed 10 April 2016].

City of Johannesburg, n.d. *Roads.* [Online]
Available at:
http://joburg.org.za/index.php?option=com_content&task=view&id=58&Itemid=71
[Accessed 10 April 2016].

City of Johannesburg, 2003. *State of the Environment Report 2003.* [Online]
Available at: http://www.joburg-archive.co.za/2003/budget/idp/annex3.pdf
[Accessed 10 April 2016].

City of Johannesburg, 2006. *Telecommunications.* [Online]
Available at:
http://www.joburg.org.za/index.php?option=com_content&task=view&id=95&Itemid=9
[Accessed 10 April 2016].

City of Johannesburg, 2007a. *City plans makeover for Ellis Park Precinct.* [Online]
Available at:

http://www.joburg.org.za/index.php?option=com_content&task=view&id=441&Itemid=168
[Accessed 10 April 2016].

City of Johannesburg, 2007b. *Interpreting the figures.* [Online]
Available at:
http://joburg.org.za/index.php?option=com_content&task=view&id=404&Itemid=52
[Accessed 10 April 2016].

City of Johannesburg, 2007c. *Summary of COJ air quality monitoring results - July to September 2006.* [Online]
Available at: http://www.joburg-archive.co.za/2007/pdfs/summary_report2006.pdf
[Accessed 11 April 2016].

City of Johannesburg, 2008. *Why the gold came to the reef.* [Online]
Available at:
http://joburg.org.za/index.php?option=com_content&task=view&id=274&Itemid=51
[Accessed 10 April 1996].

City of Johannesburg, 2009. *State of the environment report 2008.* [Online]
Available at: http://www.joburg-archive.co.za/2009/pdfs/report_evironment/enviro_land.pdf
[Accessed 10 April 2016].

City of Johannesburg, 2010. *Trains.* [Online]
Available at:
http://joburg.org.za/index.php?option=com_content&task=view&id=64&Itemid=71
[Accessed 11 April 2016].

City of Johannesburg, 2012. *Climate change affects health.* [Online]
Available at:
http://www.joburg.org.za/index.php?option=com_content&view=article&id=7972:climate-change-affects-health&catid=121:health&Itemid=202#ixzz46joQXNBb
[Accessed 24 April 20-16].

City of Johannesburg, 2013. *Water, water... everywhere.* [Online]
Available at:
http://www.joburg.org.za/index.php?option=com_content&id=1104&Itemid=168%20J
[Accessed 10 April 2016].

Clean Planet Solutions, 2015. *Clean Planet Solution - Air pollution.* [Online]
Available at: http://cleanplanetsolution.com/?page_id=2591
[Accessed 1 May 2017].

ClimaTemps.com, 2017a. *ClimaTemps.com - Relative Humidity in Johannesburg, South Africa.* [Online]
Available at: http://www.johannesburg.climatemps.com/humidity.php
[Accessed 1 May 2017].

ClimaTemps.com, 2017b. *Johannesburg Climate & Temperature.* [Online]
Available at: http://www.johannesburg.climatemps.com/
[Accessed 1 May 2017].

Cole, I., Ganther, W. & Norberg, P., 1999. *A new approach to predicting wetness on a metal surface and its complication to atmospheric corrosion - Paper 394*. 14th International Corrosion Congress, 27 September to 1 October 1999,Cape Town, International Corrosion Congress & Corrosion Institute of Southern Africa.

Cole, I., Paterson, D. & Ganther, W., 2003a. Holistic model for atmospheric corrosion Part 1 - Theoretical framework for production, transportation and deposition of marine salts. *Corrosion Engineering, Science and Technology*, 38(2), pp. 129-134.

Cole, I. S., Ganther, W.D., Paterson, D.A., King, G.A., Furman, S.A. & Lau, D., 2003b. Holistic model for atmospheric corrosion: Part 2 - Experimental measurement of deposition of marine salts in a number of long range studies. *Corrosion Engineering, Science and Technology*, 38(4), pp. 259-266.

Cole, I. S., Paterson, D.A., Ganther, W.D., Neufeld, A., Hinton, B., McAdam, G., McGeachie, M., Jeffery, L., Chotimongkol, L., Bhamornsut, C., Hue, N.V. & Purwadaria, S., 2003c. Holistic model for atmospheric corrosion - Part 3 - Effect

of natural and man made landforms on deposition of marine salts in Australia and SouthEast Asia. *Corrosion Engineering Science and Technology*, 38(4), pp. 267-274.

Cole, I., Chan, W., Trinidad, G. & Paterson, D., 2004a. Holistic model for atmospheric corrosion Part 4 – Geographic information system for predicting airborne salinity. *Corrosion Engineering, Science and Technology*, 39(1), pp. 89-96.

Cole, I. & Paterson, D., 2004b. Holistic model for atmospheric corrosion Part 5 – Factors controlling deposition of salt aerosol on candles, plates and buildings. *Corrosion Engineering, Science and Technology*, 39(2), pp. 125-130.

Cole, I., Lau, D. & Paterson, D., 2004c. Holistic model for atmospheric corrosion - Part 6 - from wet aerosol to salt deposit. *Corrosion Engineering Science and Technology*, 39(3), pp. 209- 218.

Cole, I. & Paterson, D., 2006. Mathematical models of dependence of surface temperatures of exposed metal plates on environmental parameters. *Corrosion Engineering, Science and Technology,* 41(1), pp. 67-76.

Cole, I., Paterson, D. & Lau, D., 2007. Holistic modelling of gas and aerosol deposition and the degradation of cultural objects. In: D. Creagh & D. Bradley (Eds.). *Physical Techniques in the Study of Art, Archaeology And Cultural Heritage*. Amsterdam: Elsevier, pp. 1871-1731.

Cole, I., Azmat, N., Kanta, A. & Venkatraman, M., 2009. What really controls the atmospheric corrosion of zinc? Effect of marine aerosols on atmospheric corrosion of zinc. *International Materials Review*, 54(3), pp. 117-133.

Cole I.S. & Paterson D.A., 2010. Possible effects of climate change on atmospheric corrosion in Australia. *Corrosion Engineering, Science and Technology*, 45:19–26.

Cole, I., Muster, T., Paterson, D. & Furman, S., 2011. Multi-scale modelling of the corrosion of metals under atmospheric corrosion. *Electrochemica Acta*, 56(4).

Cole, I. & Paterson, D., 2013. Holistic model for atmospheric corrosion Part 7 – Cleaning of salt from metal surfaces. *Corrosion Engineering, Science and Technology*, 42(2), pp. 106-111.

Cole, I., 2017. Recent progress and required developments in atmospheric corrosion of galvanised steel and zinc. *Materials*, 10(11), p. 1288.

Colloby, D., 1995. *Environmental contributions to atmospheric corrosion - Eskom Report TRR/S95/205,* Johannesburg: Eskom Holdings SOC Limited.

Compton, K. & Mendizza, A., 1955a. Galvanic couple corrosion studies by means of the threaded bolt and wire test. *Symposium, STP 175 (ASTM)*, pp. 116-125.

Compton, K., Mendizza, A. & Bradley, W., 1955b. Atmospheric galvanic couple corrosion. *Corrosion*, Volume 11, p. 383.

Consumer Protection Act No. 68 (2008).

Cook, D. C., Van Orden, A.C., Reyes, J., Oh, S.J., Balasubramanian, R., Carpio.J.J; Townsend, H.E., 2000. *Atmospheric corrosion in marine environments along the Gulf of Mexico*. In: S. Dean, G. Delgadillo & J. Bushman (Eds.). Marine Corrosion in Tropical Environments. West Conshohocken: ASTM International, pp. 75-97.

Cook, A., Padovanib, C. & Davenport, A., 2017. Effect of nitrate and sulfate on atmospheric corrosion of 304L and 316L stainless steels. *Journal of The Electrochemical Society*, 164(4), pp. C148-C163.

Cooper, M., n.d. *City of Johannesburg.* [Online]
Available at: http://www.johannesburg.info/johannesburg-statistics/
[Accessed 10 April 2016].

Corrosion Source, 2018. Corrosion of steel alloys in CO_2 environments. [Online].
Available at:
https://www.corrosionsource.com/FreeContent/1/Corrosion+of+Steel+Alloys+in+CO2+Environments
[Accessed 24 August 2018].

Corvo, F., Perez, T., Dzibb, L.R., Martin, Y., Castañeda, A., Gonzalez, E. & Perez, J., 2008. Outdoor-indoor corrosion of metals in tropical coastal atmospheres. *Corrosion Science*, 50(1), pp. 220-230.

Costa, J., 1987. *Corrosion mapping for Catalonia, Spain*. Madras, India, 10th International Congress on Metallic Corrosion. Vol 1: Sessions 1-4.

Cottis, R.A., Graham, M.J., Lindsay, R., Lyon, S.B., Richardson, J.A., Scantlebury, J.D. & Stott, F.H., 2010. *Shreir's Corrosion - Volume 2.* 4th Edn. Amsterdam, Elsevier Publications.

CSIR, 1975. *Results of the four-year atmospheric exposure programme (Report C.CHEM 330),* Pretoria: Council for Scientific and Industrial Research.

Cui, F., Presuel-Moreno, F. & Kelly, R., 2005. Computational modelling of cathodic limitations on localized corrosion of wetted SS 316L at room temperature. *Corrosion Science*, Volume 47, pp. 2987-3005.

Cui, Z. Y., Li, X.G., Xiao, K., Dong, C.F., Liu, Z.Y. & Wang, L.W., 2017. Study on corrosion behavious of zinc exposed in coastal-industrial atmospheric environments. *Materials Chemistry and Physics*, Volume 198, pp. 243-249.

Davenport, A.J., Guo, L., Mi, N., Mohammed-Ali, H., Ghahari, M., Street, S.R., Laycock, N.J., Rayment, T., Reinhard, C., Padovani, C. & Krouse, D, 2014. Mechanistic studies of atmospheric pitting corrosion of stainless steel for ILW containers. C*orrosion Engineering, Science and Technology*, 49(6), pp. 514-520.

De Wet, T., Patel, L., Korth, M. & Forrester, C., 2008. *Johannesburg poverty and livelihood study,* Johannesburg: Centre for Social Development in Africa - University of Johannesburg.

Dean, S.W., Delgadillo, G.H. & Bushman, J.B. (Eds.), 2000. *Marine Corrosion in Tropical Environments.* West Conshohocken: American Society for Testing of Materials (ASTM International).

Dean, S., Bushman, J. & Choker, V., 2005. Chapter 65: Highways, tunnels and bridges. In: R. Baboian, (Ed.). *Corrosion Tests and Standards: Application and Interpretation.* 2nd Edn. West Conshohocken: ASTM International, pp. 706-716.

Dean, S.W. & Reiser, D.B., 2002. Analysis of long-term atmospheric corrosion rates from ISOCORRAG program. In: H. Townsend, (Ed.). *Outdoor Atmospheric Corrosion, ASTM STP 1421.* West Conshohocken: ASTM International, pp. 3-18.

de Faria, D., Venancio Silva, A. & de Oliveira, M., 1997. Raman microspectroscopy of some iron oxides and oxyhydroxides. *Journal of Raman Spectroscopy*, Volume 28, pp. 873-878.

de la Fuente, D., Diaz, I., Simancas, C. B. & Morcillo, M., 2011. Long-term atmospheric corrosion of mild steel. *Corrosion Science*, Volume 53, pp. 604-617.

Del Angel, E., Vera, R. & Corvo, F., 2015. Atmospheric corrosion of galvanised steel in different environments in Chile and Mexico. *International Journal of Electrochemical Science,* Volume 10, pp. 7985-8004.

Delgado, D. & Vera, R., 2013. Evaluation of the atmospheric corrosion indices at different sites in Chile using (CLIMAT) wire-on-bolt test. *International Journal of Electrochemical Science,* Volume 8, pp. 7687-7701.

DEA (Department of Environmental Affairs), 2011. *Highveld priority area air quality management plan*. [Online]
Available at:
http://www.saaqis.org.za/documents/HIGHVELD%20PRIORITY%20AREA%20AQMP.pdf
[Accessed 2 September 2018].

DEA (Department of Environmental Affairs), 2013. *Department of Environmental Affairs conclude Air Quality Governance Lekgotla.* [Online]
Available at:
https://www.environment.gov.za/mediarelease/airquality_governance_lekgotla
[Accessed 28 May 2017].

DEA (Department of Environmental Affairs), 2017a. *SAAQIS - South African Air Quality Information System.* [Online]
Available at: http://www.saaqis.org.za/AQLineGraph.aspx
[Accessed 20 May 2017].

DEA (Department of Environmental Affairs), 2017b. *Chapter 10 - Air quality.* [Online]
Available at:
https://www.environment.gov.za/sites/default/files/reports/environmentoutlook_chapter10.pdf
[Accessed 20 May 2017].

Dictionary.Com, 2016. *www.dictionay.com.* [Online]
Available at: http://www.dictionary.com/browse/electrolyte
[Accessed 2016 June 2016].

Doyle, D. & Goddard, H., 1966. *Rapid determination of corrosivity of an atmosphere to aluminium.* Proceedings of the 3rd International Congress of Metallic Corrosion, Moscow, Volume 1.

Doyle, D.P & Godard, H., 1969. *Rapid determination of corrosivity of an atmosphere to aluminium*. Proceedings of the 3rd International Congress on Metallic Corrosion, Moscow, Volume 4, pp. 429-437.

Doyle, D. & Wright, T., 1971. *A rapid method for predicting adequate service lives for overhead conductors in marine atmospheres - Paper 71, CP 172-PWR*. The Institute of Electrical and Electronic Engineers (IEEE), Winter Power Meeting, New York: IEEE.

Doyle, D. & Wright, T., 1982. Rapid methods for determining atmospheric corrosivity and corrosion resistance. In: W. Ailor, (Ed.). *Atmospheric Corrosion*. New York: J. Wiley and Sons, Inc., pp. 227-243.

Druzik, J., 1985. Ozone: The Intractable Problem. *Waac: Newsletter,* September, 7(3), pp. 3-9.

Dulux Protective Coatings, 2012. *Dulux Protective Coatings technical information and advice - Duramax GPE ZP (3.10.2).* [Online]
Available at:
http://www.duluxprotectivecoatings.com.au/technotespdf/3.10.2%0Duremax%20GPE%20ZP.pdf
[Accessed 26 July 2012].

Duram, 2012. *Duram Smart Paint - NS4 Anti-rust coating - Data sheet.* [Online] Available at: http://www.jotun.com/Datasheets/Download?url=%2FTDS%2FTDS__515__Jotamastic+87__Euk__GB.pdf [Accessed 2017 August 2017].

Du Toit, J., 2001. *Provincial Characteristics of South Africa.* Rivonia, South Africa: The SA Financial Sector Forum.

Du Toit, A., 1926. Physical geography for South African schools. Cambridge: Cambridge University Press.

Efunda, 2016. *Atlas Copco.* [Online] Available at: http://www.efunda.com/materials/corrosion/corrosion_basics.cfm [Accessed 18 June 2016].

Egoli Gas, n.d. *Egoli Gas - About Us.* [Online] Available at: http://egsite.co.za/about-us.html [Accessed 11 April 2016].

Elcometer Limited, 2014. *Elcometer - Inspection Equipment.* Manchester: Elcometer Limited.

Encyclopaedia Britannica, 2008a. *"Electrolyte" - Encyclopaedia Britannica 2008 Ultimate Reference Suite,* Chicago: Encyclopaedia Britannica.

Encyclopaedia Britannica, 2008b. *"Verkhoyansk" - Encyclopaedia Britannica 2008 Ultimate Reference Suite,* Chicago: Encyclopaedia Britannica.

Encyclopaedia Britannica, 2008c. *"Panama City" - Encyclopaedia Britannica 2008 Ultimate Reference Suite.,* Chicago: Encyclopaedia Britannica.

Encyclopaedia Britannica, 2008d. *"Aluminium" - Encyclopaedia Britannica 2008 Ultimate Reference Suite,* Chicago: Encyclopaedia Britannica.

Encyclopaedia Britannica, 2008e. *"Copper" - Encyclopaedia Britannica 2008 Ultimate Reference Suite,* Chicago: Encyclopaedia Britannica.

Encyclopaedia Britannica, 2016. *"Alkyd resin - Chemical compound".* [Online]
Available at: https://www.britannica.com/science/alkyd-resin
[Accessed 21 March 2017].

Encyclopaedia Brittanica, 2018a. *"Atmosphere"*. [Online]
Available at: https://www.britannica.com/science/atmosphere
[Accessed 6 October 2018].

Encyclopaedia Brittanica, 2018b. "*Carbon dioxide*". [Online]
Available at: https://www.britannica.com/science/carbon-dioxide
[Accessed 6 October 2018].

Encyclopaedia Brittanica, 2018c. "*Electrochemical reaction*". [Online]
Available at: https://www.britannica.com/science/electrochemical-reaction
[Accessed 15 June 2018].

Encyclopaedia Brittanica, 2018d. "*Deliquescence*". [Online]
Available at: https://www.britannica.com/science/deliquescence
[Accessed 15 June 2018].

Encyclopaedia Brittanica, 2018d. "*Nitrate*". [Online]
Available at: https://www.britannica.com/science/nitrate
[Accessed 6 October 2018].

Encyclopedia.Com, 2008. *What is acid rain?.* [Online]
Available at: http://www.encyclopedia.com/topic/acid_rain.aspx
[Accessed 18 June 2016].

Engineering News, 2008. *Busiest freeways in southern hemisphere.* [Online]
Available at: http://www.engineeringnews.co.za/article/busiest-freeways-in-southern-hemisphere-2008-09-26.
[Accessed 10 April 2016].

England, W., Bennette, M., Greenhalgh, D. J. S. & Knights, C., 1986. The characterization by Raman spectroscopy of oxide scales formed on a 20Cr・25Ni・Nb stabilized stainless steel. *Corrosion Science*, 26(7), pp. 537-545.

EPA News, 2014. *New global corrosion cost study discussed at August meeting in Malaysia.* [Online]
Available at:
https://www.nace.org/uploadedFiles/Publications/Newsletters/EAPA_News_Fall_14_PROOF.pdf
[Accessed 9 April 2017].

Eskom, 1988. *"Lethabo – phoenix of the nineties",* Johannesburg: The Communication Department. Johannesburg: Eskom Holdings SOC Limited.

Eskom, 2010-2016. *Unpublished data.* Johannesburg: Eskom Holdings SOC Limited.

Eskom, 2017. *Kusile power station project.* [Online]
Available at:
http://www.eskom.co.za/Whatweredoing/NewBuild/Pages/Kusile_Power_Station.aspx
[Accessed 1 December 2017].

Evitts, R., 1997. *Modelling of crevice corrosion*, Ottawa: Department of Chemical Engineering. Ph.D Thesis, University of Saskatchewan, Saskatoon, Saskatchewan, Canada.

Evans, U.R., 1926. The fundamental principals of corrosion. *Journal of the Society of Chemical Industry*, 45(30), pp. 504-516.

Evwind, 2017. *Enel brings two new South African PV plants.* [Online]
Available at: https://www.evwind.es/2017/02/06/enel-brings-two-new-south-african-pv-plants/58722
[Accessed 16 August 2017].

Federer, C., 1971. *Effects of trees in modifying urban microclimate*. In: Trees and Forests in an Urbanizing Environment. Massachusetts : University of Massachusetts , pp. 23-28.

Feliu, S., Morcillo, M. & Feliu, S. (Jr), 1993. The prediction of atmospheric corrosion from meteorological and pollution parameters - II. Long-term factors. *Corrosion Science*, 34(3), pp. 415-422.

FitzGerald, K., Nairn, J., Skennerton, G. & Atrens, A., 2006. Atmospheric corrosion of copper and the colour, structure and composition of natural patinas on copper. *Corrosion Science*, 48(9), pp. 2480-2509.

Foax, L.J., Tidblad, J., Kucera, V., Hicks, K., Kuylenstierna, J., Dawei, Z., Kai Wing, N.G; Saha, D., Das, S., Zandi, M., Galang, R., Ramiz, A.M., Pradhan, B.B., Arachchi, W.R., Chantra, W., Hong Lien, L.T., Dombo, G., Chissico, M.L., Lungu, C. & Mmari, A.G., 2009. *Atmospheric corrosion effects of air pollution on materials and cultural property in Asia and Africa - Paper 2682*. NACE International.

Fontana, M., 1987. *Corrosion Engineering.* 3rd Edn. New York: McGraw-Hill International Editions.

Francis, R., 1987. *The morphology of corrosion products on steel*. 10th International Congress on Metallic Corrosion. Madris, India, Oxford and IBH Publishing Co., pp. 121-130.

Frankel, G., 1998. Pitting corrosion of metals - A review of the critical factors. *Journal of the Electrochemical Society*, 145, p. 2186.

Frankel, G. & Sridharb, N., 2008. Understanding localized corrosion. *Materials Today*, 11(10), pp. 38-44.

Freudenberger, J., Gollner, J., Hellmaier, M., Mook, G., Saage, H., Srivastava, V. & Wendt, U., 2009. Material Science and Engineering. In: K. Grote & E. Antonsson, (Eds.). *Springer Handbook of Mechanical Engineering, Volume 10.* New York: Springer Science & Business Media, pp. 75-218.

Friel, J. & Nungesser, E., 2012. Acrylic polymers and coating binders. In: J. Koleske, (Ed.). *Paint and Coating Testing Manual – 15th edition of the Gardner - Sward Handbook.* West Conshohocken: ASTM International, pp. 49-64.

Frith, A., n.d. *Census 2011.* [Online]
Available at: http://census2011.adrianfrith.com/
[Accessed 9 April 2016].

Fyfe, D., 1994. *Corrosion*. Oxford: Butterworth Heinemann,.

Galvanizers Association of Australia, 2011. *Coating thickness and factors influencing thickness.* [Online]
Available at: https://www.gaa.com.au/index.php?page=coating-thickness-and-factors-influencing-thickness
[Accessed 16 August 2017].

Gauteng Conference Centre, 2016. *Johannesburg.* [Online]
Available at: http://www.gautengcc.co.za/johannesburg.htm
[Accessed 10 April 2016].

Gauteng Department of Agriculture and Rural Development, 2011. *Gauteng - State of the Environment Report - 2011.* [Online]
Available at:
www.royalhaskoningdhv.com/~/media/.../files/global/.../soe_gauteng.pdf
[Accessed 11 April 2016].

Gauteng Provincial Government, 2017. *The Gauteng pollution buffer zone guidelines - March 2017.* [Online]
Available at:
www.gdard.gpg.gov.za/Gauteng%Provincial%20EMF/Approved%20Gauteng%20Pollution%20Buffer%20Zone%Guideline%202017.pdf
[Accessed 28 May 2017].

Gautrain, n.d. *The Gautrain.* [Online]
Available at: http://www.gautrain.co.za/about/about-gautrain/gautrain/
[Accessed 10 April 2016].

Geoview.info, 2017. *Verkykkop.* [Online]
Available at: http://za.geoview.info/verkykkop,944247
[Accessed 14 April 2017].

Gnoinski, J. & Ramothlola, J., 1994. *Progress Report No. 3 - Monitoring of atmospheric corrosion in the Eastern Transvaal Highveld (Report No. 940062),* Division of Materials Science and Technology. Johannesburg: Council for Scientific Industrial Research.

Google Inc., 2016a. *Johannesburg - Google Maps.* [Online]
Available at: https://www.google.co.za/maps/@-26.1737569,28.2310493,85326m/data=!3m1!1e3
[Accessed 9 April 2016].

Google Inc., 2016b. *City+parks+areas+in+johannesburg/@-26.1849555,27.9607188,11z - Google Maps.* [Online]
Available at: https://www.google.co.za/maps/search/city+parks+areas+in+johannesburg/@-26.1849555,27.9607188,11z
[Accessed 11 April 2016].

Google Inc., 2017a. *Greater Johannesburg Metropolitan Area.* [Online]
Available at: https://www.google.co.za/maps/place/Greater+Johannesburg+Metropolitan+Area/@-26.2142883,27.6841737,10z/data=!3m1!4b1!4m5!3m4!1s0x1e950966aff4e0fb:0x2dc747f800e591b0!8m2!3d-26.1704415!4d27.9717606
[Accessed 20 April 2017].

Google Inc., 2017b. *Fort Sherman.* [Online]
Available at: https://www.google.co.za/maps/search/fort+sherman/@11.6156889,-91.8001334,6337232m/data=!3m1!1e3
[Accessed 29 November 2017].

Google, 2018. *Richards Bay*. [Online]
Available at: https://www.google.co.za/maps/place/Richards+Bay/@-28.7672282,31.9876048,20514m/data=!3m1!1e3!4m5!3m4!1s0x1efa1877da2312b7:0x9fcd92a09e577160!8m2!3d-28.7807276!4d32.0382856
[Accessed 18 July 2018].

Graedel, T., Franey, J. & Kammlott, G., 1984. Ozone- and photon-enhanced atmospheric sulfidation of copper. *Science,* Volume 224, p. 599.

Graedel, T., 1989. Corrosion mechanisms for aluminum exposed to the atmosphere. *Journal of the Electrochemical Society*, 134(4), pp. 204C-212C.

Graedel, T., 1996. Gildes model studies of aqueous chemistry. I. Formulation and potential applications of the multi-regime model. *Corrosion Science*, 38(12), p. 2153–2180.

Graedel, T. & Leygraf, C., 2001. Scenarios for atmospheric corrosion in the 21st centuary. *The Electrochemical Society Interface*, Winter, pp. 24-30.

Greenpeace Afrique, 2014. *Pour la fin du Charbon*. [Online]
Available at: http://www.greenpeace.org/africa/fr/notre-action/changement-climatique/Pour-la-fin-du-charbon-en-Afrique-du-Sud/
[Accessed 15 July 2018].

Gregory, S. & Smith, K., 1967. Local temperature and humidity contrasts around small lakes and reservoirs. *RMets - Weather*, 22(12), pp. 497-505.

Gross, C. & Nixon, M., 1993. *Review of corrosion data for the proposed nuclear sites of the Eastern, Southern and Western Coasts - Eskom Report TRR/S93/091,* Johannesburg: Eskom Holdings SOC Limited.

Grøntoft, T., 2011. Climate change impact on building surfaces and facades. *International Journal of Climate Change Strategies and Management*, 3(4), pp. 374-385.

Guttman, H., 1982. Atmospheric and weather factors in corrosion testing. In: W. Ailor, (Ed.). *Atmospheric Corrosion.* New York: J. Wiley and Sons, Inc., pp. 51-84.

Hardy, C. & Nel, A., 2015. *Data and techniques for studying the urban heat island effect in Johannesburg.* 36th International Symposium on Remote Sensing of Environment, 11-15 May 2015, Berlin, Germany.

Hare, C., 1992. *The degradation of coatings by ultraviolet light and electromagnetic radiation.* [Online]
Available at: https://www.q-lab.com/documents/public/70ccb209-bf41-4da0-bb80-964d597fc728.pdf
[Accessed 1 April 2017].

Haynie, F., 1988. The degradation of metals in the atmosphere. In: S. Dean & T. Lee (Eds.). *ASTM STP 965. Philadephia: American Society for Testing and Materials*, pp. 282-289.

HDGASA, 2005. Corrosion resistance of hot dip galvanized coatings. *Hot Dip Galvanizing Today,* 2(2), pp. 39-45.

Held, G., Snyman, G. & Scheifinger, H., 1993. Seasonal variation and trends of particulates of the Southern Africa Highveld: 1982 - 1990. *The Clean Air Journal,* 8(8), pp. 4-11.

Hernandez, F.J., Santana, J.J., Souta, S., Gonzales, S. & Morales, J., 2011. Characterization of the atmospheric corrosion of aluminium in Archipelagic subtropical environments. *Int. J. Electrochem. Sci.,* Volume 6, pp. 6567-6580.

Heusler, K.E. & Cartledge, G.H., 1961. The influence of iodide ions and carbon monoxide on the anodic dissolution of active iron. *Journal of the Electrochemical Society*, 108(8), pp. 732-740.

Hiller, J., 1966. Phasenumwandlungen im rost werkst. *Werkstoffe und Korrosion. - Materials and Corrosion*, 17(11), pp. 943-951.

Holewinski, D. & Zeigler, A., 1979. *Guidelines for removing hazardous trees from highway rights-of-way*. Michigan: Asplundh Environmental Services: Michigan Department of Transportation.

Huang, C. & Lavenburg, G., 2011. *Impacts of bird droppings and deicing salts on highway structures: monitoring, diagnosis and prevention.* Delaware: Delaware Center for Transportation.

International Organization for Standardization, 1984. *ISO 7224-3: Paints and varnishes - Colorimetry - Part 3: Calculation of colour differences.* Geneva: International Organization for Standardization (ISO).

International Organization for Standardization, 1992a. *ISO 9223: Corrosion of metals and alloys - Corrosivity of atmospheres - Classification.* Geneva: International Organization for Standardization (ISO).

International Organization for Standardization, 1992b. *ISO 9224: Corrosion of metals and alloys - Corrosivity of atmospheres - Guiding values for the corrosivity categories.* Geneva: International Organization for Standardization (ISO).

International Organization for Standardization, 1992c. *ISO 9226: Corrosion of metals and alloys - Corrosivity of atmospheres - Determination of corrosion rate of standard specimens for the evaluation of corrosivity.* Geneva: International Organization for Standardization (ISO).

International Organization for Standardization, 1998a. *ISO 12944-2: Paints and varnishes - Corrosion protection of steel structures by protective paint systems - Part 2: Classification of environments.* Geneva: International Organization for Standardization (ISO).

International Organization for Standardization, 1998b. *ISO 12944-5: Paints and varnishes – Corrosion protection of steel structures by protective systems. Part 5: Protective paint systems.* Geneva: International Organization for Standardization (ISO).

International Organization for Standardization, 1998c. *ISO 12944-6: Paints and varnishes – Corrosion protection of steel structures by protective systems. Part 6: Laboratory performance test methods.* Geneva: International Organization for Standardization (ISO).

International Organization for Standardization, 1998d. *ISO 8502-9: Preparation of steel substrates before application of paints and related products - Tests for the assessment of surface cleanliness - Part 9: Field method for the conductometric determination of water-soluble salts.* Geneva: International Organization for Standardization (ISO).

International Organization for Standardization, 1999. *ISO 1461: Hot dip galvanized coatings on fabricated iron and steel articles — Specifications and test methods*. Geneva: International Organization for Standardization (ISO).

International Organization for Standardization, 2003a. *ISO 4628-2: Paints and varnishes - Evaluation of degradation of coatings - Designation of quantity and size of defects, and of intensity of uniform changes in appearance Part 2:*

Assessment of degree of blistering. Geneva: International Organization for Standardization (ISO).

International Organization for Standardization, 2003b. *ISO 4628-3: Paints and varnishes - Evaluation of degradation of paint coatings - Designation of intensity, quantity and size of common types of defect Part 3: Designation of degree of rusting.* Geneva: International Organization for Standardization (ISO).

International Organization for Standardization, 2003c. *ISO 4628-5: Paints and varnishes - Evaluation of degradation of coatings - Designation of quantity and size of defects, and of intensity of uniform changes in appearance Part 5: Assessment of degree of flaking.* Geneva: International Organization for Standardization (ISO).

International Organization for Standardization, 2004a. *ISO 1514: Paints and varnishes - Standard panels for testing.* Geneva: International Organization for Standardization (ISO).

International Organization for Standardization, 2004b. *ISO 2810: Paints and varnishes - Natural weathering of coatings - Exposure and assessment.* Geneva: International Organization for Standardization (ISO).

International Organization for Standardization, 2006. *ISO 8502-6: Preparation of steel substrates before application of paints and related products - Tests for the assessment of surface cleanliness - Part 6: Extraction of soluble contaminants for analysis - The Bresle method.* Geneva: International Organization for Standardization (ISO).

International Organization for Standardization, 2007b. *ISO 2808: Paints and varnishes - Determination of film thickness.* Geneva: International Organization for Standardization (ISO).

International Organization for Standardization, 2010. *ISO 1513: Paints and varnishes - Examination and preparation of samples for testing.* Geneva: International Organization for Standardization (ISO).

International Organization for Standardization, 2011. *ISO 4628-6: Paints and varnishes - Evaluation of degradation of coatings - Designation of quantity and*

size of defects, and of intensity of uniform changes in appearance - Part 6: Assessment of degree of chalking by tape method. Geneva: International Organization for Standardization (ISO).

International Organization for Standardization, 2012a. *ISO 9223 - International Standard - Corrosion of metals and alloys - Corrosivity of atmospheres - Classification, determination and estimation.* Geneva: International Organization for Standardization (ISO).

International Organization for Standardization, 2012b. *ISO 9224: International Standard - Corrosion of metals and alloys - Corrosivity of atmospheres - Guiding values for the corrosivity categories.* Geneva: International Organization for Standardization (ISO).

International Organization for Standardization, 2012c. *ISO 9225 - Corrosion of metals and alloys - Corrosivity of atmospheres - Measurement of pollution.* Geneva: International Organization for Standardization (ISO).

International Organization for Standardization, 2012d. *ISO 9226 : Corrosion of metals and alloys - Corrosivity of atmospheres - Determination of corrosion rate of standard specimens for the evaluation of corrosivity.* Geneva: International Organization for Standardization (ISO).

International Organization for Standardization, 2014. *ISO 2813: Paints and varnishes - Determination of specular gloss of non-metallic paint films at 20°, 60° and 85°.* Geneva: International Organization for Standardization (ISO).

International Organization for Standardization, 2018a. *ISO 12944-5: Paints and varnishes – Corrosion protection of steel structures by protective systems. Part 5: Protective paint systems.* Geneva: International Organization for Standardization (ISO).

International Organization for Standardization, 2018b. *ISO 12944-6: Paints and varnishes – Corrosion protection of steel structures by protective systems. Part 6: Laboratory performance test methods.* Geneva: International Organization for Standardization (ISO).

Janse van Rensburg, D., 1994. *Environmental contributions to atmospheric corrosion, Research Report TRR/S94/194/djvr,* Johannesburg: Eskom Holdings SOC Limited.

Janse van Rensburg, D., 2000. Acceptable protective coatings - An historical overview (1991 - 2000) and future direction, Research Report RES/RE00/11072, Johannesburg: Eskom Holdings SOC Limited.

Janse van Rensburg, D., 2005. *Corrosion index map - Scan Report No. RES/SC/05/26612,* Johannesburg: Eskom Holdings SOC Limited.

Janse van Rensburg, D., 2010. *TX and DX corrosion index map 2009/2010, Research Report No RES/RR/09/31095,* Johannesburg: Eskom Holdings SOC Limited.

Janse van Rensburg, D., 2011. *Accelerated versus natural (real-life) exposure testing of corrosion protection systems.* Johannesburg, IIR Corrosion Control Conference.

Janse van Rensburg, D., 2015. *Unpublished Orytech corrosion monitoring results, dating between 2010 to 2015.* Johannesburg: Orytech (Pty) Ltd.

Janse van Rensburg, D. & Calitz, J., 2004. Corrosion and corrosion protection. In: *The Fundamentals and Practice of Overhead Line Maintenance*. Johannesburg: Crown Publications cc., pp. 109-137.

Jeon, E.C., Son, H.K. & Sa, J.H., 2009. Emission characteristics and factors of selected odorous compounds at a wastewater treatment plant. *Sensors,* 9(1), pp. 311-326.

Johannesburg City Parks and Zoo, 2016. *Welcome to Joburg Zoo.* [Online] Available at: http://www.jhbcityparks.com/index.php/zoo [Accessed 11 April 2016].

Jonathan Ball Publishers, 2014. *Op Pad in Suid-Afrika - Verken Suid-Afrika Streek vir Streek.* 3rd Edn. Cape Town: Jonathan Ball Publishers (Pty) Ltd.

Jonckie, 2011. *Traffic survey reveals alarming facts about congested traffic in Johannesburg.* [Online] Available at: http://roadsafety.co.za/2011-07/traffic-survey-reveals-alarming-

facts-about-congested-traffic-in-jhb/
[Accessed 10 April 2016].

Josipovic, M., Annegarn, H.J., Kneen, M.A., Pienaar, J.J. & Piketh, S.J., 2011. Atmospheric dry and wet deposition of sulphur and nitrogen species and assessment of critical loads of acidic deposition exceedance in South Africa. *South African Journal of Science*, 107 (3/4)(Art. #478), p.10.

Jotun, 2014. *Waterfine Topcoat - Technical data sheet.* [Online]
Available at: http://www.nor-maali.fi/files/7814/2563/2274/WaterFine_Topcoat.TDS.eng.pdf
[Accessed 13 August 2017].

Jotun, 2016. *Hardtop AS - Technical data sheet.* [Online]
Available at: http://www.nor-maali.fi/files/9514/9259/0756/Hardtop_AS.TDS.eng.pdf
[Accessed 13 August 2017].

Jotun, 2017a. *Jotamastic 87 - Technical data sheet.* [Online]
Available at: http://www.jotun.com/Datasheets/Download?url=%2FTDS%2FTDS__515__Jotamastic+87__Euk__GB.pdf
[Accessed 13 August 2017].

Jotun, 2017b. *Hardtop Optima - Technical data sheet.* [Online]
Available at: http://www.jotun.com/Datasheets/Download?url=%2FAG%2FAG__9600__Hardtop+Optima__Euk__GB.pdf
[Accessed 13 August 2017].

Junior Worldmark Encyclopedia of World Cities, n.d. *Johannesburg.* [Online]
Available at: http://www.encyclopedia.com/topic/Johannesburg.aspx
[Accessed 11 April 2016].

Kamimura, T., Nau, S., Tazaki, T., Kuzushita, K. & Morimoto, S., 2002. Mossbauer spectroscopic study of rust formed on a weathering steel and a mild steel

exposed for a long term in an industrial environment. *Materials Transactiions.* 43, pp. 694-703.

Kansai Plascon, 2013. *Plascon Multi-surface Primer - Technical data sheet.* [Online] Available at: http://www.plascon.co.za/Datasheets/TDS%20-%20WUP%201%20Multi-surface%20Primer.pdf [Accessed 13 August 2017].

Kansai Plascon, 2017. *Wall & All - Technical data sheet.* [Online] Available at: http://www.plascon.co.za/Datasheets/WAA%20(A)%20Wall+All%20+TWA%20Tintbases%20-%20TDS2017Feb.pdf [Accessed 13 August 2017].

Keene, L., Halada, G., Clayton, C. & McKnight, S., 2004. *Degradation mechanisms of military coating systems*. [Online] Available at: http://www.dtic.mil/dtic/tr/fulltext/u2/a433190.pdf [Accessed 2018 August 9].

Keiser, J. & Brown, C. H. R., 1982. Use of Raman spectroscopy in iron corrosion studies. *American Laboratory*, 14(4), pp. 17-124.

Kelly, R., Keene, W. & Fuentes, J., 2007. *Atmospheric corrosion driven by naturally generated reactive halogens*. Charlottesville: University of Virginia.

Kelvin Power, n.d. *Kelvin information summary.* [Online] Available at: http://www.kelvinsale.com/pdf/Kelvin-Information-Summary.pdf [Accessed 10 April 2016].

Kerrod, R., 1983. *Purnell's Concise Dictionary of Science.* Bristol: Purnell Publishers Limited.

King, G., Martin, K. & Moresby, J., 1982. *A detailed corrosivity survey of Melbourne,* Highett, Australia: CSIRO - Division of Building Research.

Klassen, R. & Roberge, P., 2000. *Modeling the effects of local topography on atmospheric corrosivity - Paper No. 272*. Proceedings of NACE 2000 Conference, Orlando, Florida, March 26-31, NACE International.

Knotkova, D., 2005. 2005 F.N Speller Award Lecture: Atmospheric corrosion - Research, testing and standardization. *Corrosion,* 61(8), pp. 723-738.

Knotkova, D. & Kreislova, K., 2007. Atmospheric corrosion and conservation of copper and bronze. *WIT Transactions on State-of-the-art in Science and Engineering*, Volume 28, pp. 107-142.

Knotkova, D., Kreislova, K. & Dean, S.W. (Jr.) (Eds.), 2010. *ISOCORRAG - International Atmospheric Corrosion Programme - Summary of Results.* West Conshohocken: ASTM International.

Kramer, P.J. & Kozlowski, T.T., 1960. *Physiology of trees*. New Yolk, McGraw-Hill Co.

Kreislova, K., 2015. Prediction of long-term corrosion rates of copper alloys objects. *Materials and Corrosion*, July, pp. 1-11.

Krouse, D., Laycock, N. & Padovani, C., 2014. Modelling pitting corrosion of stainless steel in atmospheric exposures to chloride containing environments. *Callaghan Innovation Research Papers*, 49(6), pp. 521-528.

Kruger, A., Retief, J. & Goliger, A., 2013. Strong winds in South Africa: Part 2 Mapping of updated statistics. *Journal of the South Africa Institution of Civil Engineering*, 55(2), pp. ISSN 2309-8775.

Kucera, V. & Mattsson, E., 1987. Atmospheric corrosion. In: F. Mansfeld (Ed.). *Corrosion Mechanisms*. New York: Dekker, pp. 211-284.

Kusmierek, E. & Chrzescijanska, E., 2015. Atmospheric corrosion of metals in industrial city environment. *Data Brief*, Jun (3), pp. 149-154.

Larroumet, D., Greenfield, D., Akid, R. & Yarwood, J., 2007. Raman spectroscopic studies of the corrosion of model iron electrodes in sodium chloride solution. *Journal of Raman Spectroscopy*, Volume 38, pp. 1577-1585.

Laudone, G., Matthews, G. & Gane, P., 2003. Coating shrinkage during evaporation: observation, measurement and modelling within a network structure. [Online] Available at: https://www.omya.com/Documents/Publications/25%20Coating%20Shrinkage%20During%20Evaporation.pdf

[Accessed 17 October 2018].

Learner, T., 2017. *Modern Paints.* [Online]
Available at: https://www.nap.edu/read/11413/chapter/11
[Accessed 2 April 2017].

Leitch, J., 1994. *Interpretation of CLIMAT results* [Interview] 1994.

Leitch, J., 1999. *A corrosivity profile of Southern Africa using ISO 9223 methodology.* 14th International Corrosion Congress, Cape Town, South Africa, September 27 to October 1, International Corrosion Council and Corrosion Institute of Southern Africa, pp. 1-10.

Leitch, J., 2000. *Corrosion-doctors.org - Glossary - Airport corrosion.* [Online]
Available at: http://corrosion-doctors.org/AtmCorros/ncn-environment.htm
[Accessed 21 May 2017].

Leitch, J., 2003. *The atmospheric corrosivity profile of Southern Africa - An Update.* 7th International Corrosion Conference, Gauteng, South Africa, Corrosion Institute of Southern Africa.

Leitch, J., 2006. *The corrosivity regions of Southern Africa - Long term trends and implications of material selection.* 8th International Corrosion Conference, Johannesburg, South Africa, 14-15 November, Corrosion Institute of Southern Africa and South Africa Institute of Mining and Metallurgy, pp. 1-10.

Leonard, T., 2015. *Historical Dictionary of Panama.* Lanham (Maryland): Rowman & Littlefield.

Lewis, P., 2012. Inorganic colored pigments. In: J. Koleske, (Ed.). *Paint and Coating Testing Manual – 15th Edition of the Gardner - Sward Handbook.* West Conshohocken: ASTM International, pp. 234-238.

Leygraf, C., Odnevall Wallinder, I., Tidblad, J. & Graedel, T., 2016. *Atmospheric corrosion.* 2nd Edn. Hoboken: John Wiley & Sons, Inc.

Linarca, E. & Geert, B., 2002. *Climates & Weather Explained.* London: Routledge.

Lindstrom, R., Maurice, V. K. L. & Marcus, P., 2007. *The use of electrochemical scanning tunnelling microscopy (EC-STM) in corrosion analysis.* Cambridge: Woodhead Publishing Limited.

Li, J., Maier, B. & Frankel, G., 2011. Corrosion of an Al-Mg-Si alloy under $MgCl_2$ solution droplets. *Corrosion Science*, 53, p. 10.

Li, Z., Marston, N. & Jones, M., 2013. *Update of New Zealand's atmospheric corrosivity map - Study report SR 288,* New Zealand: BRANZ (ISSN: 1179-6197).

Li, S. & Hihara, L., 2015. A micro-Raman spectroscopic study of marine atmospheric corrosion of carbon steel: The effect of akaganeite. *Electrochemical Society*, 162(9), pp. C495-502.

Lloyd, G., n.d. *Atmospheric corrosion*. [Online]
Available at: http://www.npl.co.uk/upload/pdf/atmospheric_corrosion.pdf
[Accessed 12 June 2018].

Llewellyn, D. & Hudd, R., 1998. *Steels - Metallurgy and Applications*. 3rd Edn. Oxford: Butterworth-Heinemann.

Lobo, H. & Bonilla, J. (Eds.), 2003. *Handbook of Plastics Analysis.* New York: Marcel Decker Inc.

Lobnig, R.E., Siconolfi, D.J., Psoto-Kelty, L., Grundmeier, G., Frankenthal, R.P., Stratmann, M. & Sinclair, J.D., 1996a. Atmospheric corrosion of zinc in the presence of ammonium sulfate particles. *Journal of the Electrochemical Society*, 143(5).

Lobnig, R.E., Siconolfi, R.D., Maisano, J., Grundmeier, O., Sfreckel, H., Frankenthal, R.P. & Stratmann, M., 1996b. Atmospheric corrosion of aluminum in the presence of ammonium sulfate particles. *Journal of the Electrochemical Society*, 143(4), pp. 1175-1182.

Local Government, 2016. *The local government handbook - A complete guide to the municipalities of South Africa - City of Johannesburg Metropolitan Municipality (JHB).* [Online]

Available at: http://www.localgovernment.co.za/metropolitans/view/2/City-of-Johannesburg-Metropolitan-Municipality
[Accessed 10 April 2016].

London Metal Exchange, 2012. *London Metal Exchange, "Price graphs – LME Zinc price graph (between 2001 and 2012).* [Online]
Available at: http://www.lme.com/zinc_graphs.asp.
[Accessed 1 July 2012].

Lourens, A. S., Beukes, J.O., van Zyl, P.G., Fourie, G.D., Burger, J.W., Pienaar, J.J., Read, C.E. & Jordaan, J.H., 2011. Spatial and temporal assessment of gaseous pollutants in the Highveld of South Africa. *South African Journal of Science*, 107(1-2), pp. 1-8.

Lourens, A., 2012. *Air quality in the Johannesburg-Pretoria megacity, its regional influence and identification of parameters that could mitigate pollution*. M.Sc Thesis, Potchefstroom: North-west University.

Lu, G. & Wong, D. W., 2008. An adaptive inverse-distance weighting spatial interpolation technique. *Computer and Geosciences*, 34(9), pp. 1044-1055.

Maier, B. & Frankel, G., 2011. Pitting corrosion of bare stainless steel 304 under chloride solution droplets. *Journal of the Electrochemical Society*, Volume 157, pp. C301-C312.

Manana, M., 2011. *The impact of the Gautrain service disruptions due to cable theft on the viability of modernised public transport and commuter confidence (subject for discussion).* [Online]
Available at: http://www.pa.org.za/hansard/2011/august/31/proceedings-of-the-national-assembly-wednesday-31-/the-impact-of-the-gautrain-service-disruptions-due
[Accessed 10 April 2016].

Mansfield, F., 1979. Atmospheric corrosion rates. *Corrosion*, 30(1), pp. 38-42.

Maps-streetview.com, 2017. *Grabouw maps - road map, satellite view and street view.* [Online]

Available at: https://www.maps-streetview.com/South-Africa/Grabouw/ [Accessed 9 April 2017].

Malatse, M. & Ndlovu, S., 2015. The viability of using the Witwatersrand gold mine tailings for brickmaking. J*ournal of the Southern African Institute of Mining and Metallurgy*, 115(4), pp. ISSN 2411-9717.

Mark, H., 2007. *Encyclopedia of Polymer Science and Technology.* 3rd Edn. New Jersey: John Wiley and Sons Inc.

Martin, K. & King, G., 1981. Corrosion around Australia. *Corrosion Australasia*, Volume 6, pp. 10-15.

Maskew Miller Longman (Pty) Ltd, 2013. *Pearson - Platinum High School Atlas.* Cape Town: HarperCollins Publishers (Pty) Ltd.

Maskew Miller Longman (Pty) Ltd, 2016. *Pearson - Platinum High School Atlas.* 6th Edn. Cape Town: Maskew Miller Longman (Pty) Ltd.

Mathee, A. & von Schirnding, Y., 2003. Air quality and health in the Greater Johannesburg. In: G. McGranahan & F. Murray, (Eds.). *Air Pollution & Health in Rapidly Developing Countries.* Stockholm: Earthscan Publications Ltd, pp. 206-218.

Mayuchi, L., 2008. *City of Johannesburg State of Energy Report 2008.* [Online] Available at: http://www.cityenergy.org.za/uploads/resource_48.pdf [Accessed 11 April 2016].

McEwan, J. (Ed.), 2004. *Corrosion Control in Southern Africa.* Johannesburg: Corrosion Institute of Southern Africa.

Meira, G.R., Andrade, C., Padaratz, I.J., Alonso, C. & Borba, C. (Jr), 2007. Chloride penetration into concrete structures in the marine atmosphere zone – Relationship between deposition of chlorides on the wet candle and chlorides accumulated into concrete. *Cement and Concrete Composites*, 29(9), pp. 667-676.

Meira, G.R., Andrade, C., Alonso, C., Padaratz, I.J. & Borba, C. (Jr), 2008. Modelling sea-salt transport and deposition in marine atmosphere zone – A tool for corrosion studies. *Corrosion Science*, 50(9), pp. 2724-2731.

Melchers, R., 2015. Time dependent development of aluminium pitting corrosion. *Advances in Materials Science and Engineering*, Article ID 215712, pp. 1-10.

Merchak, P., 2012. Colored organic pigments. In: J. Koleske, (Ed.). *Paint and Coating Testing Manual – 15th Edition of the Gardner - Sward Handbook.* West Conshohocken: ASTM International, pp. 215-233.

Mi, N., 2013. Synchrotron X-ray studies of atmospheric pitting corrosion of stainless steel. Ph.D Thesis, Birmingham: University of Birmingham,

Microsoft, 2017. *Microsoft Excel - Pearson function.* [Online]
Available at: https://support.office.com/en-us/article/PEARSON-function-0c3e30fc-e5af-49c4-808a-3ef66e034c18?NS=EXCEL&Version=16&SysLcid=1033&UiLcid=1033&AppVer=ZXL160&HelpId=xlmain11.chm60360&ui=en-US&rs=en-US&ad=US
[Accessed 15 April 2017].

Mikhailov, A., Tidblad, J. & Kucera, V., 2004. The classification system of ISO 9223 standard and the dose–response functions assessing the corrosivity of outdoor atmospheres. *Protection of Metals*, 40(6), pp. 541-550.

Mikhailovsky, Y., 1982. Theoretical and engineering principals of atmospheric corrosion of metal. In: W. Ailor, (Ed.). *Atmospheric Corrosion.* New York: John Wiley & Sons, pp. 85-106.

Miller, M., Brook, P. & Eyers, C., 2010. *Research Project EASA.2008/C11 - Reduction of sulphur limits in aviation.* [Online]
Available at: https://www.easa.europa.eu/system/files/dfu/2009-SULPHUR-Reduction%20of%20sulphur%20limits%20in%20aviation%20fuel%20standards-Final%20Report.pdf
[Accessed 2 February 2017].

Misawa, T., Asami, K., Hashimoto, K. & Shimodaira, S., 1974. The mechanism of atmospheric rusting and the protective amorphous rust on low alloy steel. *Corrosion Science*, 14(4), pp. 279-289.

Mohammed Ali, H., *2016. Atmospheric pitting corrosion of stainless steel, Birmingham*: Ph.D Thesis, Birmingham: University of Birmingham.

Mokgatlhe, B. & Janse van Rensburg, D., 2012. *Corrosion monitoring at Lephalale, Kendal and Elandsfontein (2009 - 2012) - Report RES/RR/11/33538,* Johannesburg: Eskom Holdings SOC Limited.

Montgomery, E., Curren, J., Calle, L. & Kolody, M., 2011. *Timescale correlation between marine atmospheric exposure and accelerated testing.* [Online] Available at: http://www.nace.org/cstm/Store/Product.aspx?id=77abd502-5cd0-e111-a853-0050569a007b [Accessed 18 June 2016].

Moolman, S., 2012. *Zincor closure bodes well for zinc industry's future.* [Online] Available at: http://www.miningweekly.com/article/zincor-closure-bodes-well-for-zinc-indystrys-future-s012-04-20 [Accessed 26 July 2012].

Morcillo, M., Otero, E., Chico, B. & de la Fuente, D., 2010. Atmospheric corrosion studies in a decommissioned nuclear power plant. [Online] Available at: http://digital.csic.es/bitstream/10261/84757/1/Libro_nuclear_power_plant.pdf [Accessed 29 July 2018].

Morcillo, M., De la Fuente, D. & Cano, I., 2011. Atmospheric corrosion of mild steel. *Revista De Metalurgia,* 47(5), pp. 426-444.

Morcillo, M., Chico, B., de la Fuente, D. & Simancas, J., 2012. Review Article - Looking back on contributions in the field of atmospheric corrosion offered by the MICAT Ibero-American Testing Network. *International Journal of Corrosion,* 2012 (ID 8244365), p. 24.

Morcillo, M., Alcantara, J., Diaz, I., Chico, B., Simancas, J. & De la Fuente, D., 2015. Marine atmospheric corrosion of carbon steel. *Revista de Metalurgia,* 51(2), pp. 1-18.

Morcillo, M., Wolthuis, R., Alcántara, J. Chico, B., Díaz, I. & de la Fuente, D., 2016. Scanning electron microscopy/Micro-Raman: A very useful technique for characterizing the morphologies of rust phases formed on carbon steel in atmospheric exposures. *Corrosion*, 72(8), pp. 1044-1054.

Morton, S., 2013. *Atmospheric pitting corrosion of AA7075-T6 under evaporating droplets*. Thesis, Ohio: Ohio State University.

Morton, S. & Frankel, G., 2013. Atmospheric pitting corrosion of AA7075-T6 under evaporating droplets with and without inhibitors. *Materials and Corrosion*, 65(4), pp. 351-361.

Mowrer, N., 2003. *Polysiloxanes.* [Online]
Available at:
http://extra.ivf.se/kemi/common/downloads/Kunskapsarkiv/Polysiloxaner/presentation_polysiloxanes.pdf
[Accessed 28 March 2017].

Mustafe, A., 2005. *FTIR studies on 2K polyurethane paint*. M.Sc Thesis, Singapore: Department of Physics, University of Singapore.

My Cyberwall, 2017. *Weather, climate, and vegetation of South Africa - Rainfall.* [Online]
Available at: https://www.mycyberwall.co.za/get-smart/geography/grade-5/rainfall
[Accessed 18 August 2017].

NACE International, 2002. *NACE International 2002 glossary of corrosion-related terms*. [Online]
Available at:
https://www.nace.org/uploadedFiles/Corrosion_Central/Corrosion_101/GlossaryOfTerms.pdf
[Accessed 23 June 2018].

Natesan, M., Venkatachari, G. & Palaniswamy, N., 2015. *Corrosivity and durability maps of India.* [Online]
Available at: http://krc.cecri.res.in/ro_2005/013-2005.pdf
[Accessed 24 July 2015].

Nauer, G., Strecha, P., Brinda-Konopik, N. & Liptay, G., 1985. Spectroscopic and thermoanalytical characterization of standard substances for the identification of reaction products on iron electrodes. *Journal of Thermal Analysis,* 30(4), pp. 813-830.

NCP Chlorchem, 2011-2017. *NCP Chlorchem - Home.* [Online]
Available at: http://www.ncp.co.za/
[Accessed 1 May 2017].

Nelson, D., 2012. Alkyds and polyesters. In: J. Koleske, (Ed.). *Paint and Coating Testing Manual – 15th Edition of the Gardner - Sward Handbook.* West Conshohocken: ASTM International, pp. 65-71.

News24, 2014. *News24 Breaking News.First - WHO: Johannesburg's air is deadly.* [Online]
Available at: http://www.News24.com/Green/News/WHO-Jozis-air-is-deadly-20140516
[Accessed 1 May 2017].

News24, 2015. *News24 Breaking News First - Drought grips South Africa.* [Online]
Available at: http://www.News24.com/SouthAfrica/News/drought-grips-south-africa-20151115
[Accessed 1 May 2017].

Nixon, M., 1991. *Environmental contributions to atmospheric corrosion - Interim report on continuous monitoring – Research Report TRR/S91/143,* Johannesburg: Eskom Holdings SOC Ltd.

Nixon, M., 1993. *Environmental contributions to atmospheric corrosion.* 10th European Corrosion Congress, Barcelona, Spain, 5 to 8 July 1993, International Corrosion Council (ICC).

Nixon, M. & Janse van Rensburg, D., 1992. *Environmental contributions to atmospheric corrosion - Progress Report - Research Report TRR/S92/168,* Johannesburg: Eskom Holdings SOC Limited.

Northcott, K., 1999. *Environmental contributions to atmospheric corrosion - Paper No. 364.* 4th International Corrosion Congress, Cape Town, South Africa, September 27 to October 1, 1999, International Corrosion Council and Corrosion Institute of Southern Africa.

Nowak, D., 2002. *The effects of urban trees on air quality.* [Online] Available at: http://www.nrs.fs.fed.us/units/urban/local-resources/downloads/Tree_Air_Qual.pdf [Accessed 24 April 2016].

Nuttall, S. & Mbembe, A., 2007. Afropolis: From Johannesburg. *PMLA,* 122(1), pp. 281-288.

O'Donnell, A., White, R., Bronkhorst, R. & le R. Fourie, F., n.d. *The results of an atmospheric exposure programme on agricultural wire in South Africa.* [Online] Available at: http://www.izasa.org/Documents/Technical/Exposure%20Progamme%20on%20Agricultural%20Wire%20in%20SA%20-%20paper%20046.pdf [Accessed 2 January 2016].

OpenStax CNX, 2017. *Natural Science - Ecosystems and the environmental balance.* [Online] Available at: http://archive.cnx.org/contents/669116d7-d148-4af9-905d-4dcdf17cde56@1#graphics1.png [Accessed 17 August 2017].

Osborne, D., 1989. Corrosion in potable water systems: The Johannesburg experience. *Water SA,* 15(4), pp. 201-206.

Oxford University Press Southern Africa (Pty) Ltd, 2006. *Oxford Secondary Atlas for South Africa.* Cape Town: Oxford University Press Southern Africa (Pty) Ltd.

Oxford University Press, 2004. *Oxford Junior Atlas vir Suid-Africa.* Cape Town, South Africa: ABC Press.

Oxford University Press, 2016. *Oxford South African Thematic Atlas.* Cape Town: Oxford University Press.

Parekh, S., Pandya, A. & Kadiya, H., 2012. Progressive atmospheric corrosion study of metals like mild steel, zinc and aluminium in Urban Station of Ahmedabad District. *International Journal of ChemTech Research*, 4(4), pp. 1770-1774.

Payne, H.F., 1961. *Organic Coating Technology - Volume 2 : Pigments and Pigmented Coatings*. New York, John Wiley & Sons, Inc..

Petzer, G. & Kornelius, G., 2007. *Umfolozi-Empangeni transmission line and substation atmospheric corrosion study.* Midrand: Airshed Planning Professionals (Pty) Ltd (on behalf of BKS (Pty) Ltd).

Pietersen, D., Holtzhausen, J. & Vosloo, W., 2004. *An investigation into the methodology to develop an insulator pollution severity application map for South Africa.* AFRICON, Cape Town, pp. 1-7.

Piketh, S., Mabusela, X. & Slabbert, G., 2007. *Air quality management - Climate change: A call to local action.* [Online]
Available at: http://www.joburg-archive.co.za/2007/pdfs/air_quality/changeworkshop_presentation.pdf
[Accessed 11 April 2016].

Powder-lak, 2013. *Powder-lak (Pty) Ltd Series 1000 Premium paints - technical information.* [Online]
Available at: http://www.powderlak.co.za/wp-content/uploads/Series-10004.pdf
[Accessed 13 August 2017].

Pourbaix, M., 1982. The linear bilogarithmic law for atmospheric corrosion. In: W. Ailor (Ed.). *Atmospheric Corrosion*. New York: J. Wiley & Sons, p. 107.

Pretorius, I., Piketh, S., Burger, R. & Neomagus, H., 2015. A perspective on South African coal fired power station emissions. *Journal of Energy in South Afrrica,* 26(3), pp. 27-40.

Q-Lab Corporation, 2015. *Q-Panel - Steel panels (Specification Bulletin LP-0862-A).* [Online]

Available at: https://www.q-lab.com/documents/public/53630802-cc1d-47d8-a9c4-f59006bc2990.pdf
[Accessed 19 May 2017].

Raman, A., Kuban, B. & Razvan, A., 1991. The application of infrared spectroscopy to the study of atmospheric rust systems - I. Standard spectra and illustrative applications to identify rust phases in natural atmospheric corrosion products. *Corrosion Science,* 32(12), pp. 1295-1306.

Raunio, M., 2015. *Basic approaches and goals for crevice corrosion modelling - Report VTT-R-02078-15.* Finland: VTT Technical Resource Centre of Finland.

Readers' Digest, 1978. *Reader's Digest Library of Modern Knowledge.* 1st Edn. London: The Readers' Digest Association Limited.

Rice, D.W., Peterson, P., Rigby, E.B., Phipps, P.B.P., Cappell, R.J. & Tremoureux, R., 1981. Atmospheric corrosion of copper and silver. *Journal of the Electrochemical Society*, 128(2), pp. 275-284.

Rincon, A., De Rincon, A.F.M. & Loaiza, E., 2000. Measurement of pollution atmospheres in a tropical region and its atmospheric corrosion map. *Corrosion Reviews,* 18(6), pp. 473-487.

Ríos-Rojas, J., Escobar-Ocampo, D., Hernández-García, E. & Arroyave, C., 2015. Atmospheric corrosivity in Bogota as a very high-altitude metropolis questions international standards. *DYNA*, 82(190), pp. 128-137.

Rivera, N., Kaur, N., Hesterberg, D., Ward, C., Austin, R. & Duckworth, O., 2015. Chemical composition, speciation, and elemental associations in coal fly ash samples related to the Kingston ash spill. *Energy Fuels,* 29(2), p. 954–967.

Roberge, P., 2011. Atmospheric corrosion. In: R. Revie, (Ed.). *Uhlig's Corrosion Handbook.* 3rd Edn. Hoboken, New Jersey: A. John Wiley & Sons, Inc., pp. 299-326.

Roberge, P.R., 2012. *Handbook of Corrosion Engineering.* 2nd Edn. New York: The McGraw-Hill Companies, Inc.

Rohli, R., 2017. *Just the Fact 101 - Textbook Key facts - Climatology.* 3rd Edn. Texas: Cram 101.

Rozenfeld, I., 1972. *Atmospheric Corrosion of Metals*. Houston: NACE International.

Salas, B.V., Wiener, M.S., Badilla, G.L., Beltran, M.C., Zlatev, R., Stoycheya, M., Diaz, J.O., Osuna, L.V. & Gaynor, J.T., 2012. *H_2S pollution and its effect on corrosion of electronic components*. [Online]
Available at:
https://www.researchgate.net/publication/300386396_H2S_Pollution_and_Its_Effect_on_Corrosion_of_Electronic_Components
[accessed 21 October 2018].

Sandenberg, R., 2016. *Kenote 1*. AfriCORR'16, Midrand, July 25-29. Corrosion Institute of Southern Africa.

Santana, J.J., Santana, J., Gonzalez, J.E., De La Fuente, D., Chico, B. & Morcillo, M., 2001. Atmospheric corrosivity map for steel in Canary Isles. *British Corrosion Journal,* 36(4), pp. 266-271.

Schinderholtz, E. & Kelly, R., 2012. Wetting phenomena and time of wetness in atmospheric corrosion: *A review. De Gruyter*, pp. 1-36.

Schindelholz, E., Tsui, L. & Kelly, R., 2014. Hygroscopic particle behavior studied by interdigitated array microelectrode impedance sensors. *The Journal of Physical Chemistry*, 118(1), pp. 167-177.

Schultz, W. & Thiele, M., 2012. *General Hot-dip Galvanizing - Materials, Technologies, Layer Formation, Properties and Defects.* Germany: Eugen G. Leuze Verslag KG, D-88348 Bad Saulgrau.

Schwarz, M., 1965. Untersuchungen über dir wirkung des eisen (II)-sulfates beim atmosphärischen rosten una beim unterrosten von anstrichen. *Werkstoffe und Korrosion*, 16(1), pp. 93-103.

Seinfeld, J. & Pandis, S., 1997. *Atmospheric chemistry and physics; from air pollution to climate change.* New York: Wiley Interscience.

Shuters-Macmillan, 1996. *Shuters-Macmillan - Nuwe Sekondere Skoolatlas vir Suid Afrika.* Pietermaritzburg: Macmillan Education Ltd.

Sica, Y., Kenny, E., Portella, K. & Campos Filho, D., 2007. Atmospheric corrosion performance of carbon steel, galvanized steel, aluminum and copper in the North Brazilian Coast. *Sociedade Brasileira de Química* , 18(1), pp. 153-166.

Simillion, H., Dolgikh, O., Terryn, H. & Deconinck, J., 2014. Atmospheric corrosion modeling. *Corrosion Reviews*, 32, pp. 73-100.

SGS, 2012. *Ambient air quality monitoring report*. Prepared for the Richards Bay Clean Air Association, Durban: SGS.

Skerry, B., Johnson, J. & Wood, G., 1988. Corrosion in smoke, hydrocarbon and SO_2 polluted atmospheres - III. The general behaviour of zinc. *Corrosion Science*, 28(7), pp. 721-727.

Slabbert, M., 1986. *Cost implications of metallic corrosion for the South African economy in the sectors of mining, power generation, shipping, and transportation - Report No. M251,* Randburg: Mintek.

Slamova, K., Glaser, R., Schill, C., Wiesmeier, S. & Köhl, M., 2012. Mapping atmospheric corrosion in coastal regions: Methods and results. *Journal of Photonics for Energy,* 2(1), pp. 022003-1-022003-11.

Smith, B., 1999. *Infrared Spectral Interpretation - A Systematic Approach.* Boca Raton: CRC Press.

Snow Report, 1853 - 2016. *History of snow in South Africa: 1853 – 2016.* [Online] Available at: http://snowreport.co.za/history-of-snow-in-south-africa-1853-2014/ [Accessed 19 August 2017].

South Africa.info, 2015. *Geography and climate - Gauteng Province, South Africa.* [Online]
Available at:
http://www.southafrica.info/about/geography/gauteng.htm#.VwurY_l95D8
[Accessed 11 April 2016].

South African Bureau of Standards, 1998a. *SANS ISO 12944-1: Paints and varnishes — Corrosion protection of steel structures by protective systems - Part 1: General introduction.* Pretoria: South African Bureau of Standards.

South African Bureau of Standards, 1998b. *SANS ISO 12944-2: Paints and varnishes – Corrosion protection of steel structures by protective systems.* Pretoria: South African Bureau of Standards.

South African Bureau of Standards, 1998c. *SANS ISO 12944-6: Paints and varnishes – Corrosion protection of steel structures by protective systems. Part 6: Laboratory performance test methods.* Pretoria: South African Bureau of Standards.

South African Bureau of Standards, 2013. *SANS 1796: South African National Standard - Application of durable organic powder coatings for architectural aluminium.* Pretoria: SABS Standards Division.

South African History Online, 2011. *Discovery of the gold in 1884.* [Online]
Available at: http://www.sahistory.org.za/discovery-gold-1884
[Accessed 10 April 1996].

South African Iron and Steel Institute, 2012. *Members – ArcelorMittal South Africa Limited.* [Online]
Available at: http://www/saisi.co.za
[Accessed 26 July 2012].

South African Tours and Travel.com, 2016. *Enjoy South Africa 's climate, delightfully mild and pleasant all year round.* [Online]
Available at: http://www.south-africa-tours-and-travel.com/south-africa-climate.html
[Accessed 18 August 2017].

SAWS (South African Weather Services), 2014. *Temperature and rain data for Johannesburg.* Pretoria: SA Weather Services.

SAWS (South African Weather Services), 2017. *Weather data for South Africa and the GJMA (2007 to 2016).* Pretoria: SA Weather Services.

Spasojević, P.M., Panić, V.V., Džunuzović, J.V., Marinković, A.D., Woortman, A.J.J., Loos, K. & Popović, I.G., 2015. *High performance alkyd resins synthesized from postconsumer PET bottles.* [Online]
Available at: http://pubs.rsc.org/-/content/articlehtml/2015/ra/c5ra11777a
[Accessed 4 April 2017].

Spence, J.W., Haynie, F.H., Lipfert, F.W., Cramer, S.D. & Donald, L.G., 1992. *Corrosion*, 48(12), pp. 1009-1019.

Stassen, W., 2015. *Gauteng's mine dumps brimming with radioactive uranium.* [Online]
Available at: http://www.health-e.org.za/2015/10/15/gautengs-mine-dumps-brimming-with-radioactive-uranium/
[Accessed 10 April 2016].

Statistics South Africa, 2004. *South African statistics 2003.* [Online]
Available at:
https://www.statssa.gov.za/publications/SAStatistics/SAStatistics2003.pdf
[Accessed 11 April 2016].

Statistics South Africa, 2017a. *Stats SA - City of Johannesburg.* [Online]
Available at: http://www.statssa.gov.za/?page_id=993&id=city-of-johannesburg-municipality
[Accessed 1 December 2017].

Statistics South Africa, 2017b. *Mid-year population estimates.* [Online]
Available at: http://www.statssa.gov.za/publications/PO3022017
[Accessed 26 December 2017].

Sterling, T., 2004. *Transpiration – Water Movement through Plants*. [Online]
Available at:
https://www.sciencemag.org/site/feature/misc/webfeat/vis2005/show/transpiration.pdf
[Accessed 11 August 2018].

Still, A., Gertzen, D. & Ricketson, C., 2004. *Improved service delivery through a performance based management contract.* Proceedings of the 2004 Water

Institute of Southern Africa (WISA) Biennial Conference, Cape Town, South Africa.

Stoye, D. & Freitag, W. (Eds)., 2008. *Paints, Coatings and Solvents.* 2nd Edn. New York: Wiley - VCH.

Stratmann, M., Bohnenkamp, K. & Ramchandran, T., 1987. The influence of copper upon the atmospheric corrosion of iron. *Corrosion Science*, 27(9), p. 905–926.

Stratmann, M., 1990. The atmospheric corrosion of iron — A discussion of the physico-chemical fundamentals of this omnipresent corrosion process - invited review. *Berichte der Bunsengesellschaft - Physical Chemistry Chemical Physics*, 94, pp. 626-639.

Street, S.R., Mi, N., Cook A.J., Mohammed-Ali, H.B., Guo, L., Rayment, T. & Davenport, A.J., 2015. Atmospheric pitting corrosion of 304L stainless steel: the role of highly concentrated chloride solutions. *Faraday Discussions*, 180, pp. 251-265.

Syed, S., 2006. Atmopsheric corrosion of materials. *Emirates Journal for Engineering Research,* 11(1), pp. 1-24.

Schweitzer, P., 1999. *Atmospheric Degradation and Corrosion Control*. New York: Marcel Dekker Inc.

Summitt, R. & Fink, F., 1980. *PACER LIME: An Environmental corrosion severity classification system*. Michigan: Michigan State University.

Sun, S., Zheng, Q., Wen, J. & Li, D., 2009. Atmospheric corrosion of aluminium in the northern Taklamakan Desert environment. *Materials and Corrosion*, 61(10), pp. 852-859.

Tahir, H. & Yousif, T., 2013. Modeling the effect of urban trees on relative humidity in Khartoum State. *Journal of Forest Products and Industries*, 2(5), pp. 20-24.

Tator, K., 2015. Coating deterioration. In: K. Tator, (Ed.). *ASM Handbook*, *Volume 5B, Protective Organic Coatings*. Materials Park (OH): ASM International, pp. 462-473.

Tétreault, J., Cano, E., van Bommel, M., Scott, D., Dennis, M., Barthés-Labrousse, M., Minel, L. & Robbiola, L., 2013. Corrosion of copper and lead by formaldehyde, formic and acetic acid vapours. *Studies in Conservation,* 48(4), pp. 237-250.

Tengs, T., 2016. How accurate are longitude and latitude in Google Maps?. [Online] Available at: http://buyingandsellingland.com/how-accurate-are-longitude-and-latitude-in-google-maps/ [Accessed 9 July 2018].

The Economist, 2013. *Choked.* [Online] Available at: http://www.economist.com/blogs/graphicdetail/2013/01/daily-chart-11?fsrc=rss [Accessed 11 April 2016].

The Gale Encyclopedia of Science, 2008. *Atmosphere, composition and structure.* [Online] Available at: http://www.encyclopedia.com/article-1G2-2830100209/atmosphere-composition-and-structure.html [Accessed 1 May 2016].

The World Bank, 2017. *South Africa.* [Online] Available at: http://www.worldbank.org/en/country/southafrica [Accessed 9 April 2017].

Thibeau, R. & Heidersbach, R., 1978. Applied spectra of possible corrosion products of iron. *Applied Spectroscopy*, 32(6), pp. 532-535.

Thornton, J.A., Kercher, J.P., Riedel, T.P., Wagner, N.L., Cozic, J., Holloway, J.S., Dubé, W.P., Wolfe, G.M., Quinn, P.K., Middlebrook, A.M., Alexander, B. & Brown, S.S., 2010. A large atomic chlorine source inferred from mid-continental reactive nitrogen chemistry. *Nature*, 464(7286): 271-4.

Tidblad, J., Mikhailov, A. & Kucera, V., 1999. *Model for calculation of time of wetness using relative humidity and temperature data*. Paper 337.2 Sep 26 - Oct 1, Cape Town, International Corrosion Congress.

Tidblad, J., Kucera, V., Samie, F., Das, S.N., Bhamornsut, C., Chow Peng, L., Lung So, K., Dawei, Z., Thi Hong Lien, L., Schollenberger, H., Lungu, C.V. & Simbi,

D., 2007. Exposure programme on atmospheric corrosion effects of acidifying pollutants in tropical and subtropical climates. *Water Air Soil Pollution: Focus (2007) 7,* pp. 241-247.

Torres-Mendoza, V., Rodrigues-Gomez, F. Garcia-Ochoa, E. & Genesca, F., 2006. The assessment of natural atmosphere corrosivity by the use of electrochemical noise analysis. *Anti-Corrosion Methods and Materials*, 53(6), pp. 348-356.

Tsutsumi, Y., Nishikata, A. & Tsuru, T., 2007. Pitting corrosion mechanism of Type 304 stainless steel under a droplet of chloride solutions. *Corrosion Science*, 49(3), pp. 1394-1407.

Tullmin, M. & Roberge, 2000. Atmospheric corrosion. In: R. W. Revie, (Ed.). *Uhlig's Corrosion Handbook,* 2nd Edn. New York: John Wiley & Sons, Inc. pp1.

Uhlig, H., 1963. *Corrosion and Corrosion Control.* 1st Edn. Unites States of America: John Wiley & Sons, Inc.

United Nations Human Settlements Programme (UN-Habitat), 2014. *The state of African cities 2014 - Re-imagaing sustainable urban transitions.* [Online]
Available at: https://unhabitat.org/books/state-of-african-cities-2014-re-imagining-sustainable-urban-transitions
[Accessed 18 June 2016].

University of Wisconsin, 2018. *Atlas of the biosphere - Annual total precipitation*. [Online]
Available at: https://nelson.wisc.edu/sage/data-and-models/atlas/maps/anntotprecip/atl_anntotprecip.jpg
[Accessed 25 July 2018].

US Environmental Protection Agency, 2016. *What is acid rain?.* [Online]
Available at: https://www.epa.gov/acidrain/what-acid-rain
[Accessed 18 June 2016].

Van Tienhoven, A., 1999. *Status of air pollution in South Africa.* [Online]
Available at: http://www.sei.se/rapidc/pdfs/Airpoll.Africa.pdf
[Accessed 19 July 2012].

Vargel, C., 2004. *Corrosion of Aluminium*. Amsterdam: Elsevier.

Vera, R., Rosales, B. & Tapia, C., 2003. Effect of the exposure angle in the corrosion rate of plain carbon steel in a marine atmosphere. *Corrosion Science*, 45(2), pp. 321-337.

Vera, R. & Ossandon, S., 2014. On the prediction of atmospheric corrosion of metals and alloys in Chile using artificial neural networks. *International Journal of Electrochemical Science,* Volume 9, pp. 7131-7151.

Vernon, W., 1931. A laboratory study of the atmospheric corrosion of metals. Part I. *Transactions of the Faraday Society*, 27, p. 265.

Vernon, W., 1934. Basic copper carbonate and patina. *Journal of the Chemical Society,* Volume 1934, pp. 1853-1859.

Vidal, J., 2011. *South Africa - where climate change may trigger a toxic timebomb.* [Online]
Available at: http://www.theguardian.com/environment/blog/2011/nov/26/south-africa-mining-indutrsy-johannesburg-pollution
[Accessed 11 12 2012].

Virtual Chembook, 2003. *Acid rain effects on buildings.* [Online]
Available at: http://chemistry.elmhurst.edu/vchembook/196buildings.html
[Accessed 18 June 2016].

Vosloo, W., 2002. *A comparison of the performance of high-voltage insulator materials in a severely polluted coastal environment*. Ph.D Thesis, Stellenbosch: University of Stellenbosch.

Wallinder, I., Korpinen, T. & Sundberg, R., 2002. Atmospheric corrosion of naturally and pre-patinated copper roofs in Singapore and Stockholm - Runoff rates and corrosion product formation. In: H. Townsend, (Ed.). *Outdoor Atmospheric Corrosion.* Phila: ASTM International, pp. 230-244.

Wallinder, I., Wallinder, O. & Leygraf, C., 2003. Influence of surface treatment of 304L stainless steel on atmospheric corrosion resistance in an urban and a marine environment. *Corrosion*, 59(3), pp. 220-227.

Weldon, D., 2012. Infrared spectroscopy. In: J. Koleske, (Ed.). *Paint and Coating Testing Manual – 15th Edition of the Gardner-Sward Handbook.* West Conshohocken: ASTM International, pp. 895-907.

Wexler, A., Haynes, W. & Lide, D.R., 2011. *CRC Handbook of Chemistry and Physics: A Ready-Reference Book of Chemical and Physical Data*. Boca Raton: CRC Press.

Whitmore, P., Cass, G. & Druzik, J., 1987. The ozone fading of traditional natural organic colourants on paper. *Journal of the American Institute for Conservation,* 26(1), pp. 45-58.

Why Joburg.com, 2016. *The history of Johannesburg.* [Online]
Available at: http://www.whyjoburg.com/history.html
[Accessed 10 April 2016].

Wiegand, P. (Ed.), 2007. *Oxford Secondary Atlas for South Africa.* Cape Town: Oxford University Press.

Wikipedia.com, 2017a. *Greater Johannesburg.* [Online]
Available at: https://en.wikipedia.org/wiki/Greater_Johannesburg
[Accessed 5 March 2017].

Wikipedia.com, 2017b. *Great Escarpment, Southern Africa.* [Online]
Available at: https://en.wikipedia.org/wiki/Great_Escarpment,_Southern_Africa
[Accessed 18 August 2017].

Williams, K., Smith, B. & Hayward, I., 1995. New horizons in Raman microscopy and raman imgaging. *International Labmate*, 20(3).

Winter, K., Oelofse, C. & Bottaro, J., 2013. *Oxford Senior Atlas vir Suider-Afrika.* 13th Edn. Cape Town: Oxford University Press Southern Africa (Pty) Ltd.

World Weather Online, 2017. *Johannesburg, Gauteng monthly climate average, South Africa.* [Online]
Available at: https://www.worldweatheronline.com/johannesburg-weather-averages/gauteng/za.aspx
[Accessed 20 May 2017].

Yale Data Driven, 2016. *Visual and digital media - Interactive air pollution map: Fine particulates and nitrogen dioxide.* [Online]
Available at: http://visuals.datadriven.yale.edu/airmap_2016/
[Accessed 11 June 2017].

Yibas, B., van Tonder, D., Netili, F., Rust, U., Wade, P. & Maree, J., 2010. *Mine water management in the Witwatersrand gold field with special emphasis on acid mine drainage - Report to the Inter-ministerial Committee on Acid Mine Drainage*. Pretoria: Department of Mineral Resources.

Yocom, J., 2012. The deterioration of materials in polluted atmospheres. *Journal of the Air Pollution Control Association*, 8(3), pp. 203-208.

Yousif, A. & Haddad, R., 2013. Photodegradation and photostabilization of polymers, especially polystyrene: review. *Springerplus,* 2(398).

Zunckel, M., John, J., Taviv, R. & Naidoo, M., 2005. *Technical compilation to inform the State of Air Report 2005.* Pretoria: CSIR-Natural Resources and the Environment.

APPENDICES

APPENDIX A

Table A.1 The different zones and populations of the CoJ Metropolitan Municipality's section of the GJMA – Source: Frith (2016).

Name	Population	Area (km²)
Alexandra	179 624	6.91
Chartwell	1 728	9.07
City of Johannesburg NU	9 933	289.84
Dainfern	6 601	4.08
Diepsloot	138 329	12.00
Drie Ziek	35 622	7.53
Ebony Park	22 309	1.63
Ennerdale	71 815	21.33
Farmall	1 051	5.01
Itsoseng	5 243	0.58
Ivory Park	184 383	9.21
Johannesburg	957 441	334.81
Kaalfontein	46 147	4.96
Kagiso	5 182	0.57
Kanana Park	21 005	6.82
Lakeside	23 503	3.78
Lanseria	4 788	1.83
Lawley	33 136	6.09
Lehae	13 380	3.50
Lenasia	89 714	20.28
Lenasia South	37 110	13.98
Lucky 7	0	0.11
Malatjie	2 321	0.18
Mayibuye	22 178	1.16
Midrand	87387	152.87
Millgate Farm	172	0.88
Orange Farm	76 767	12.16
Poortjie	11 153	2.43
Rabie Ridge	4 1204	3.33
Randburg	337 053	167.98
Randfontein Estate Gold Mine	0	9.19
Rietfontein	196	2.17
Roodepoort	326 416	161.50
Sandton	222 415	143.54
Soweto	1 271 628	200.03
Stretford	61 141	7.38
Tshepisong	53 260	6.56
Vlakfontein	27 291	4.63
Zakariyya Park	6 200	1.96
Zevenfontein	0	3.10

In addition to the above 4.4 million people, the following populated areas (**Tables A.2-A.4**) were included in the study area, as part of the Greater Johannesburg metropolis.

Table A.2 Sections of the Ekurhuleni Metropolitan Municipality forming part of the GJMA – Source: Frith (2016).

Name	Population	Area (km²)
Alberton	121 536	77.16
Benoni	158 777	175.55
Boksburg	260 321	162.35
Brakpan	73 080	182.81
Edenvale	49 292	20.03
Geluksdal	14 489	3.16
Germiston	255 863	143.27
Katlehong	407 294	55.36
Kempton Park	171 575	149.05
Kwa-Thema	103 727	14.70
Nigel	38 318	139.07
Springs	121 610	183.50
Tembisa	463 109	42.80

Table A.3 Sections of the Mogale Local Municipality included in the GJMA study – Source: Frith (2016).

Name	Population	Area (km²)
Kagiso	115 802	14.17
Krugersdorp	140 643	247.22
Mogale City NU	19 757	981.54

Table A.4 Sections of the Randfontein Local Municipality included in the GJMA study – Source: Frith (2016).

Name	Population	Area (km²)
Randfontein Estate Gold Mine	654	24.39
Green Hills	9 135	4.81
Green Hills Ext 3	1 037	0.25

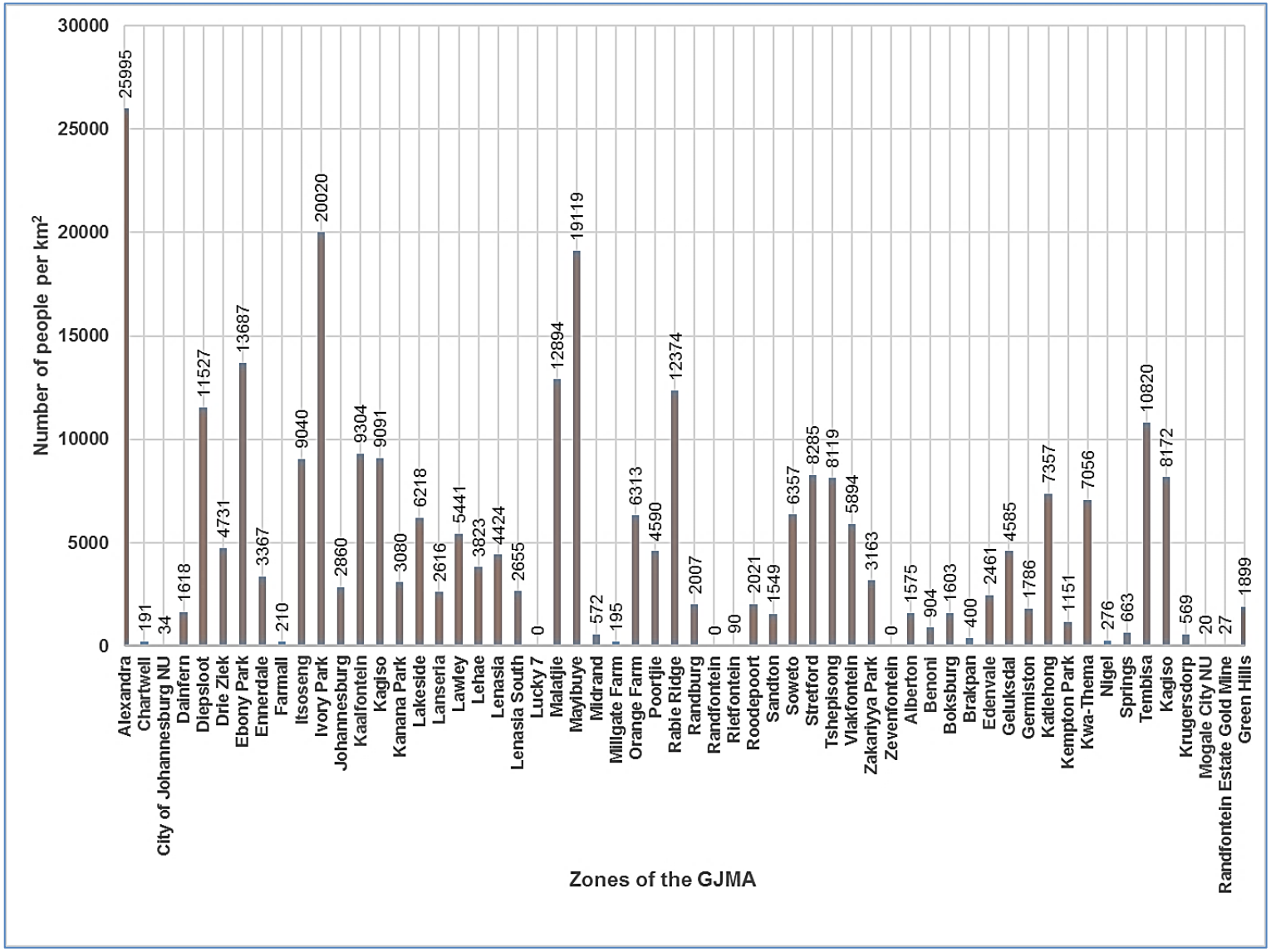


Figure A.1 Population densities of the different towns and suburbs of the GJMA study area - Based on Frith's (2016) adaptations of South African Statistic's 2011 Census data.

APPENDIX B

Table B.1 Geographical information and general descriptions of the main atmospheric corrosion monitoring locations in the GJMA.

Main site no.	Site name	Date installed	GPS coordinates		General environment	Estimated height above ground level (m)	Surrounding terrain	Altitude (km)
S1	**Florida Hills**	20 August 2013	S26°09'59.0"	E27°55'27.1"	Residential	3.0	Flat	1.8
S2	**Alexandra**	21 August 2013	S26°06'24.9"	E28°06'39.1"	Township	3.0	Flat to hilly	1.5
S3	**Ivory Park**	21 August 2013	S25°59'34.0"	E28°12'14.3"	Township	2.0	Flat	1.6
S4	**Diepsloot**	21 August 2013	S25°55'19.0"	E28°01'07.8"	Township	2.0	Flat to hilly	1.4
S5	**Buccleuch**	21 August 2013	S26°02'42.8"	E28°05'56.8"	Traffic/business	3.5	Flat to hilly	1.5
S6	**Newtown**	21 August 2013	S26°12'18.5"	E28°01'55.5"	Traffic/business	3.5	Flat & built-up	1.7
S7	**Delta Park**	21 August 2013	S26°07'29.7"	E28°00'31.4"	Recreational park	2.0	Flat to hilly	1.6
S8	**Chamdor**	22 August 2013	S26°09'33.8"	E27°47'59.4"	Industrial	4.0	Flat & built-up	1.7
S9	**Orange Farm**	23 August 2013	S26°28'45.7"	E27°52'00.6"	Township	3.5	Flat	1.6
S10	**Jabavu (Soweto)**	23 August 2013	S26°15'09.3"	E27°52'19.7"	Township	2.0	Flat	1.6
S11	**Brakpan**	28 August 2013	S26°13'16.4"	E28°21'30.2"	Mining/park	3.0	Flat	1.6
S12	**Alrode**	29 August 2013	S26°18'30.3"	E28°07'05.5"	Industrial	1.5	Flat	1.6
S13	**Kagiso-Randfontein**	30 August 2013	S26°07'47.5"	E27°46'18.3"	Mining/industrial	3.0	Flat to hilly	1.7
S14	**Ruimsig**	03 September 2013	S26°04'04.6"	E27°51'00.4"	Residential	3.0	Flat to hilly	1.5
S15	**Kya Sand**	03 September 2013	S26°00'53.0"	E27°57'08.2"	Business/industrial	2.0	Flat to hilly	1.4
S16	**Midrand**	03 September 2013	S25°58'24.4"	E28°07'58.7"	Business/industrial	2.5	Flat to hilly	1.6
S17	**Aeroport**	04 September 2013	S26°07'09.1"	E28°12'28.3"	Industrial	5.0	Flat & built-up	1.7
S18	**Nasrec**	05 September 2013	S26°14'04.0"	E27°59'06.3"	Business/mining	2.0	Flat	1.7
S19	**Rosherville**	05 September 2013	S26°13'43.9"	E28°06'54.1"	Industrial	1.5	Flat to hilly	1.7
S20	**Chloorkop**	05 September 2013	S26°04'24.9"	E28°11'19.4"	Business/industrial	2.5	Flat to hilly	1.7
S21	**Bonaero Park**	08 September 2013	S26°7'11"	E28°15'58.0"	Residential	1.5	Flat	1.7
S22	**Braamfontein**	09 September 2013	S26°11'35.3"	E28°01'47.6"	Business	30	Flat & built-up	1.8

Table B.2 Geographical information and general descriptions of the mini atmospheric corrosion monitoring locations in the GJMA.

Mini site no.	Site name	Date installed	GPS coordinates		General environment	Estimated height above ground level (m)	Surrounding terrain	Altitude (km)
M1	**Princess**	22 August 2013	S26°08'07.1"	E27°51'17.0"	Business/township	4.0	Flat to hilly	1.8
M2	**Nigel**	28 August 2013	S26°26'10.4"	E28°29'23.8"	Residential	2.0	Flat	1.6
M3	**Geluksdal**	28 August 2013	S26°19'49.6"	E28°21'41.5"	Business/industrial	2.0	Flat	1.6
M4	**Dunnottar**	28 August 2013	S26°19'12.5"	E28°27'28.8"	Rural	2.0	Flat to hilly	1.6
M5	**Springs**	28 August 2013	S26°15'53.9"	E28°26'32.3"	Residential	2.0	Flat/open country	1.6
M6	**Dalpark**	28 August 2013	S26°14'33.3"	E28°18'02.1"	Field/business	2.0	Flat/open country	1.6
M7	**Elspark**	28 August 2013	S26°15'46.0"	E28°13'59.2"	Residential/business	2.5	Flat & built-up	1.6
M8	**Wadeville**	28 August 2013	S26°16'00.4"	E28°10'19.0"	Industrial/business	2.0	Flat & built-up	1.6
M9	**Durban Deep**	29 August 2013	S26°10'26.2"	E28°52'00.9"	Industrial/mining	2.5	Flat to hilly	1.8
M10	**Doornkop**	29 August 2013	S26°12'49.8"	E28°48'02.3"	Industrial/mining	3.0	Flat to hilly	1.7
M11	**Lenasia**	29 August 2013	S26°18'48.7"	E27°51'03.4"	Residential/business	3.0	Flat & built-up	1.6
M12	**Ennerdale**	29 August 2013	S26°24'35.4"	E27°51'13.7"	Residential/business	2.0	Flat & built-up	1.6
M13	**Eikenhof**	29 August 2013	S26°19'43.6"	E27°57'56.2"	Field/farming	2.0	Flat to hilly	1.5
M14	**Kliprivierberg**	29 August 2013	S26°18'12.1"	E28°00'41.5"	Residential/field	2.0	Hilly/open country	2
M15	**Kliprivier**	29 August 2013	S26°25'37.8"	E28°05'06.5"	Industrial	2.5	Flat & built-up	2.5
M16	**Palmridge**	29 August 2013	S26°23'12.0"	E28°08'37.1"	Residential/industrial	30.0-40.0	Flat & built-up	1.6
M17	**Walkerville**	29 August 2013	S26°24'13.6"	E27°57'49.3"	Field/farming	3.0	Flat to hilly/open country	1.7
M18	**Randfontein**	30 August 2013	S26°09'36.3"	E27°41'35.0"	Residential/business	3.0	Flat & built-up	1.7
M19	**Krugersdorp**	03 September 2013	S26°06'24.7"	E27°48'04.0"	Residential/business	2.5	Flat & built-up	1.8
M20	**Honeydew**	03 September 2013	S26°04'17.0"	E27°55'22.6"	Residential/industrial/business/traffic	3.0	Hilly & built-up	1.6
M21	**Lanseria**	03 September 2013	S26°56'03.8"	E27°55'23.2"	Industrial/business/traffic	3.0	Hilly/open-country	1.4
M22	**Bryanston**	03 September 2013	S26°03'45.8"	E28°00'39.0"	Residential/field	3.0	Flat/open-country	1.5

Table B.2 *continued*.

Mini site no.	Site name	Date installed	GPS coordinates		General environment	Estimated height above ground level (m)	Surrounding terrain	Altitude (km)
M23	Dainfern Ridge	03 September 2013	S25°59'23.5"	E28°00'21.2"	Residential	3.0	Flat to hilly/built-up	1.4
M24	Kyalami	03 September 2013	S25°58'41.9"	E28°03'29.9"	Residential/field	3.0	Flat open-country	1.5
M25	Newclare	04 September 2013	S26°11'23.2"	E27°58'08.0"	Residential/industrial/business /traffic	3.0	Flat to hilly/built-up	1.7
M26	Gillooy's	04 September 2013	S26°10'16.7"	E28°07'42.2"	Residential/business/traffic	3.0	Flat to hilly/open country	1.6
M27	Eastleigh	04 September 2013	S26°07'41.0"	E28°09'11.9"	Residential/industrial/business /traffic	3.0	Flat to hilly/built-up	1.6
M28	Esselen Park	04 September 2013	S26°02'04.0"	E28°14'50.3"	Residential/industrial/field	3.0	Flat	1.6
M29	Kempton Park	04 September 2013	S26°05'56.0"	E28°14'00.7"	Residential/business/traffic	3.0	Flat/built-up	1.7
M30	Northmead/Benoni	04 September 2013	S26°10'37.3"	E28°19'08.9"	Residential/industrial/business /traffic	2.5	Flat to hilly/built-up	1.6
M31	Eastrand Mall	04 September 2013	S26°10'33.8"	E28°14'38.3"	Residential/business/traffic	3.0	Flat	1.7
M32	Rosettenville/Southhills	05 September 2013	S26°15'18.6"	E28°03'20.7"	Residential/business/traffic	3.0	Hilly/built-up	1.8
M33	Houghton	05 September 2013	S26°08'51.6"	E28°03'45.2"	Residential/business/traffic	3.0	Flat to hilly/wooded/built-up	1.7
M34	Morningside	05 September 2013	S26°04'14.9"	E28°03'49.8"	Residential/business/traffic	3.0	Flat to hilly/wooded/built-up	1.5
M35	Balmoral	12 September 2013	S26°11'49.0"	E28°11'50.8"	Residential/business	2.0	Flat/built-up	1.7

APPENDIX C

Table C.1 Typical physical and chemical properties of the low-carbon (mild) steel flat metal panels used for corrosion monitoring, and preparation of the hot-dip galvanised and coated mild steel specimens.

Parameter	Description/result
General	Cold-rolled, low-carbon steel
Thickness	0.8 mm
Finish	Dull matte
Roughness	25-65 (micro-inches)
ASTM specification	A1008 / 1010
Fe. steel specification	QQ-S-698
Temper	¼ hard
Hardness (Rockwell)	B50-B65
Tensile (psi)	54 000
Manganese	0.25-0.60% maximum
Carbon	0.13% maximum
Phosphorous	0.04% maximum
Sulphur	0.05% maximum

Table C.2 Typical physical and chemical properties of the hot-dip galvanised coating.

Parameter	Description/result
General	Substrate - cold-rolled, low-carbon steel as per **Table A.2**
Thickness	0.8 mm – mild steel substrate Zinc coating ~ 50 µm
Finish	Shiny, with spangled effect

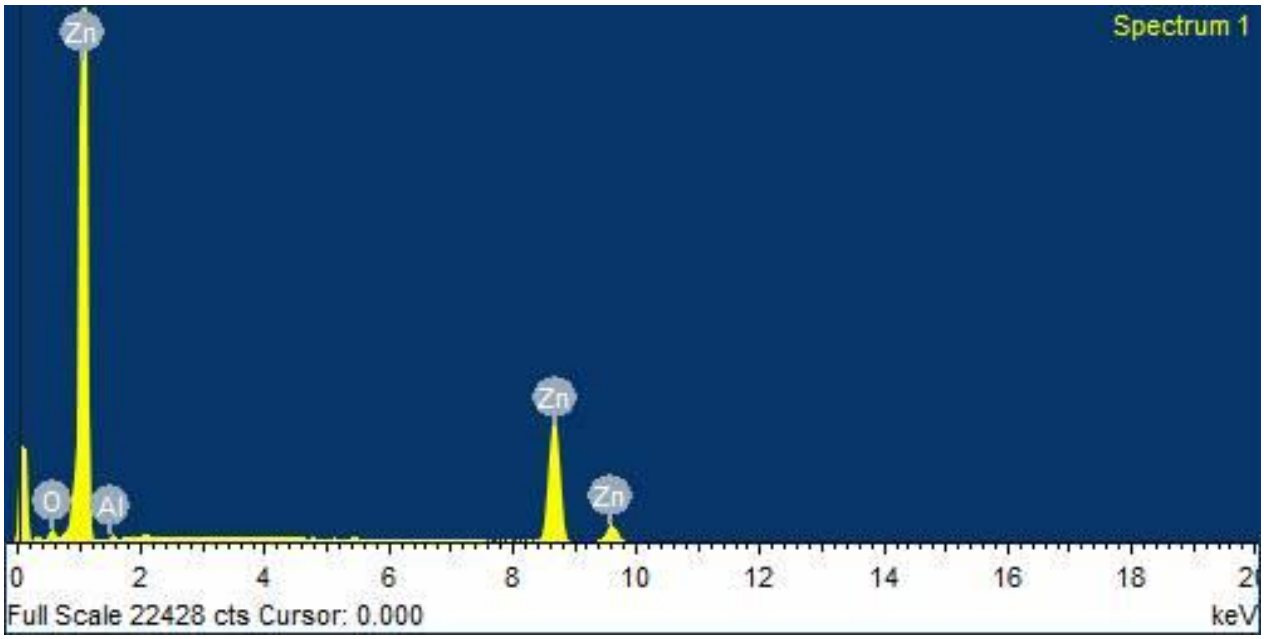


Figure C.1 EDS spectrograph of the elemental composition of surface for the hot-dip galvanised coating.

Table C.3 Typical physical and chemical properties of the aluminium wire used for manufacturing of the ISO WH-Al units.

Parameter	Description/result
General	Thermal spraying wire
Thickness	2.0 mm
Specifications	Grade 1100, BS EN 573-3. EN AW-1100 99.0%, ISO 209:2007, AWS C2.25/C2.25M:2012
Composition	
Element	**% Weight**
Al Min	99.0
Si + Fe Max	0.95
Cu Min-Max	0.05-0.20
Mn Max	0.05
Zn Max	0.10
Others Each	0.05

Table C.4 Typical physical and chemical properties of the zinc wire used for manufacturing of the ISO WH-Zn units.

Parameter	Description/result
General	Thermal spraying wire
Thickness	2.0 mm
Specifications	BS EN 1179 base material Z1: 2003 & ISO 752:2004 EN ISO 14919:2015 AWS C2. 25/C2M:2012
Composition	
Element	**% Weight**
Zn Min	99.990
Al Max	0.001
Cu Max	0.001
Pb Max	0.003
Cd Max	0.003
Fe Max	0.002
Sn Max	0.001

Table C.5 Typical physical and chemical properties of the copper wire used for manufacturing of the ISO WH-Cu units.

Parameter	Description/result
General	Thermal spraying wire
Thickness	2.0 mm
Specifications	DIN EN 10204-3.1
Composition	
Element	**% Weight or ppm**
Cu Min	99.9%
Ag Max	10 ppm
Al Max	1 ppm
As Max	1 ppm
Bi Max	0.4 ppm
Fe Max	2 ppm
O Max	257 ppm
Pb Max	1 ppm
S Max	4 ppm
Sb Max	1 ppm
Se Max	0.9 ppm
Te Max	1.0 ppm
Zn Max	1 ppm

APPENDIX D

Elcometer 135A & 135B Bresle Patches

The Elcometer 135A Bresle Sampler is a self-adhesive rubber film patch with a sealed compartment for sampling of soluble impurities from steel surfaces with a suitable solvent.

The Elcometer 135A Bresle Samplers are also part of the Elcometer 138/2 Surface Contamination Kit.



Elcometer 135A

Elcometer 135B Bresle Patches are used to determine surface chloride contamination and are self-adhesive rubber film patches with a sealed compartment for sampling soluble impurities from steel surfaces with a suitable solvent.

Elcometer Bresle Patches are also available as part of the Elcometer 138 Bresle Salt Kit.



Elcometer 135B

STANDARDS:
ISO 8502-6

Technical Specification

Part Number	Description	Tests per kit
E135----A25	Elcometer 135 Bresle Sampler	25
E135----A	Elcometer 135 Bresle Sampler	50
E135----B	Elcometer 135B Bresle Sampler	25
Test Area	1250mm², 12.5cm² (1.93sq inches)	
Sample Volume	2.6ml ± 0.6ml	
Dimensions	52 x 52mm (2.0 x 2.0")	

APPENDIX E

Infrared control spectra of the different coatings.

System A - Water-based acrylic coating

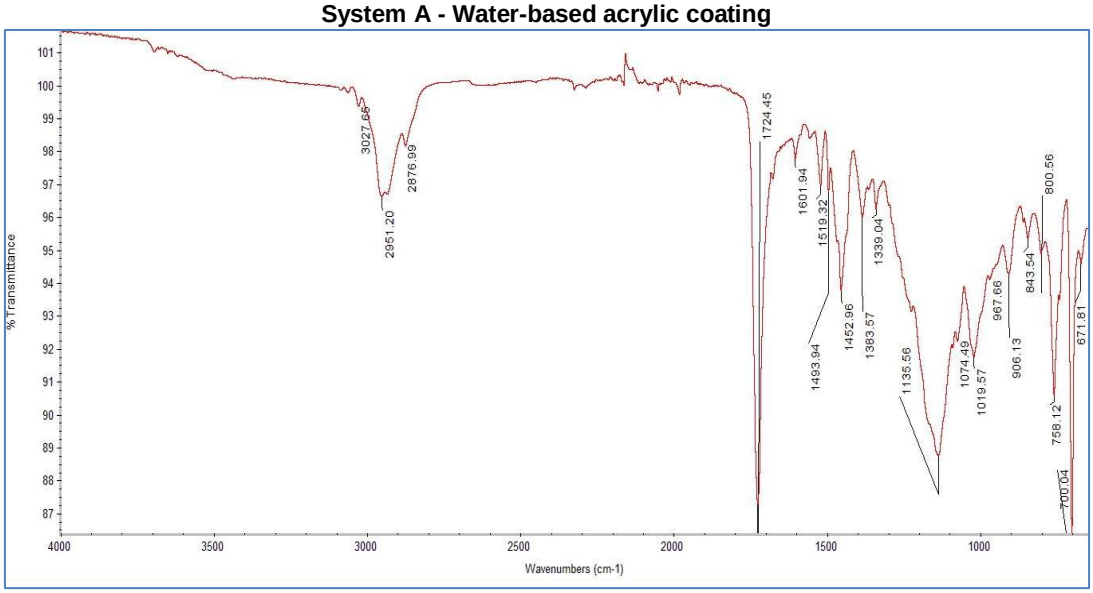


Figure E.1 Typical peaks associated with the acrylic binder are the frequencies of the single C-H stretching bands at 2951 cm^{-1} and 2876 cm^{-1}, the overall profile of the C-H stretching region, strong C=O stretching at 1724 cm^{-1}, and skeletal vibrations at 1195 cm^{-1} (Learner 2017).

System B - Polysiloxane coating

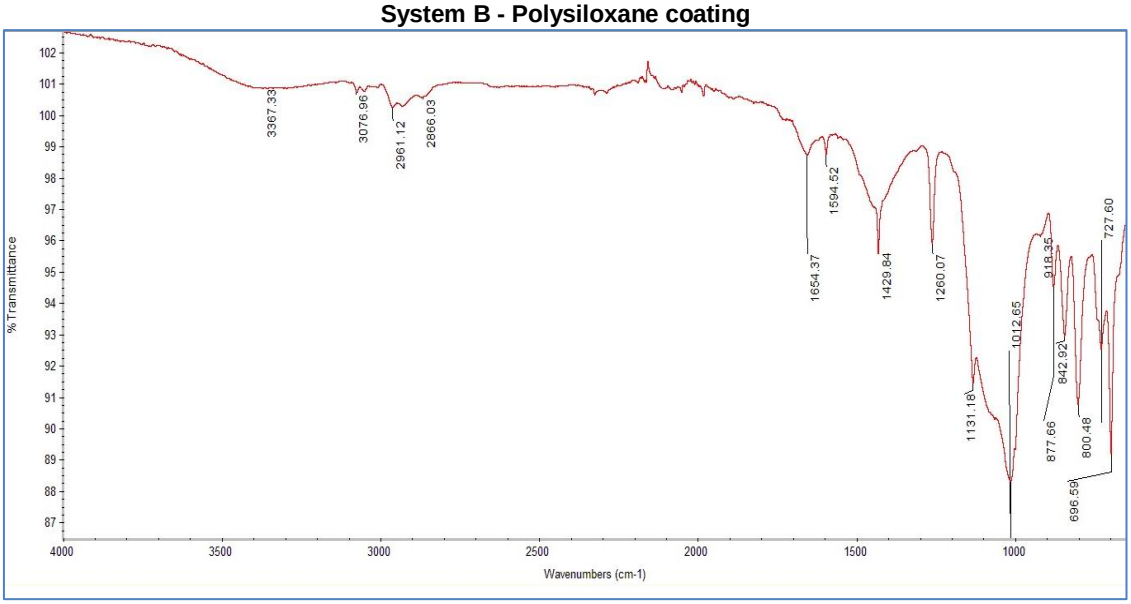


Figure E.2 Typical peaks associated with the polysiloxane binder are the Si-O-Si peaks between 1012 cm^{-1} and 1131cm^{-1} and the very intense Si-CH_3 peak at 1260 ± 5 cm^{-1} and $Si(CH_3)_2$ peak at 800 ± 10 cm^{-1} (Smith 1999; Lobo & Bonilla 2003).

System C - Polyurethane coating

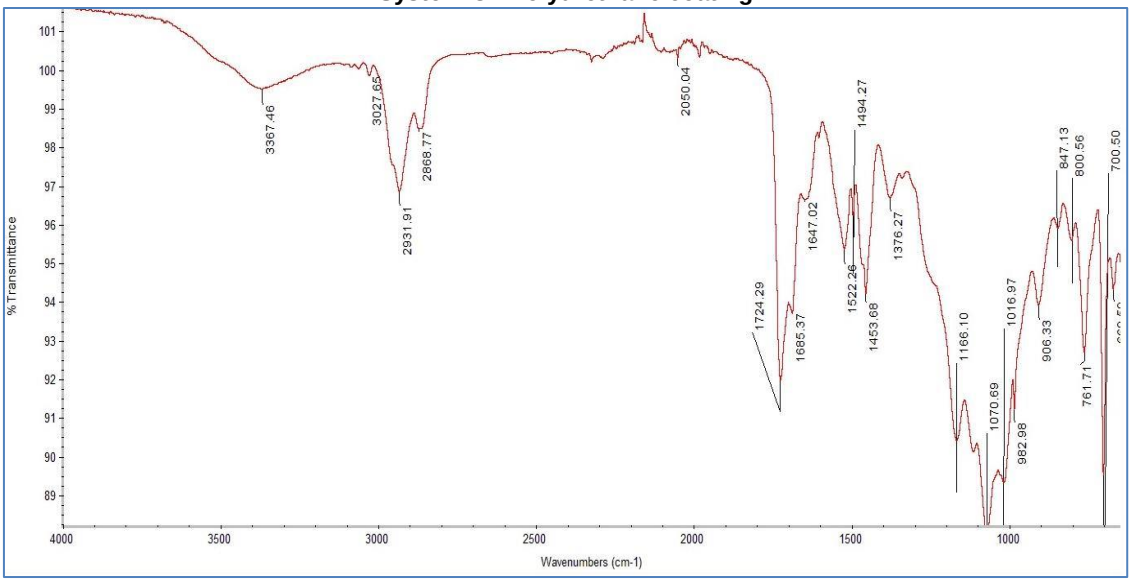


Figure E.3 Peaks associated with the acrylic polyurethane binder are the single -NH (amine) stretch vibration at 3367 cm^{-1}, -C=O (carbonyl) urethane vibration at 1724 cm^{-1} and -C=O urea peak at 1685 cm^{-1} (Mustafe 2005)**.**

System D - Water-based acrylic (anti-corrosion) coating

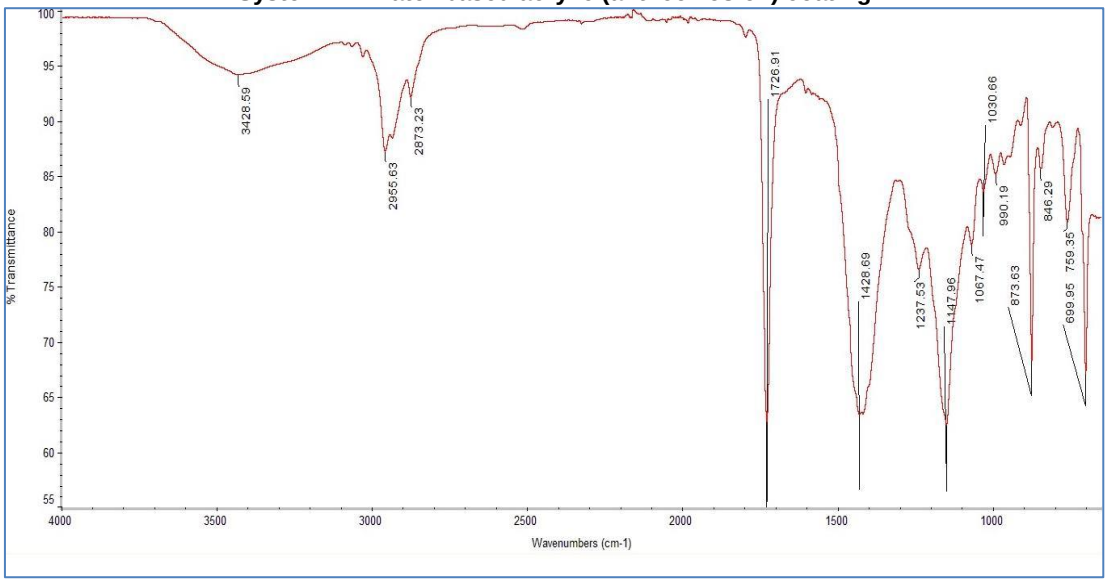


Figure E.4 Typical peaks associated with the acrylic binder are the frequencies of the -OH peak at 3428 cm^{-1} - indicative of water (Lobo & Bonilla 2003), C-H stretching bands at 2955 cm^{-1} and 2873 cm^{-1}, the overall profile of the C-H stretching region, C=O stretching at 1726 cm^{-1}, and skeletal vibrations at 1147 cm^{-1} - all indicative of an acrylic emulsion (Learner 2017).

System E - Water-based acrylic coating

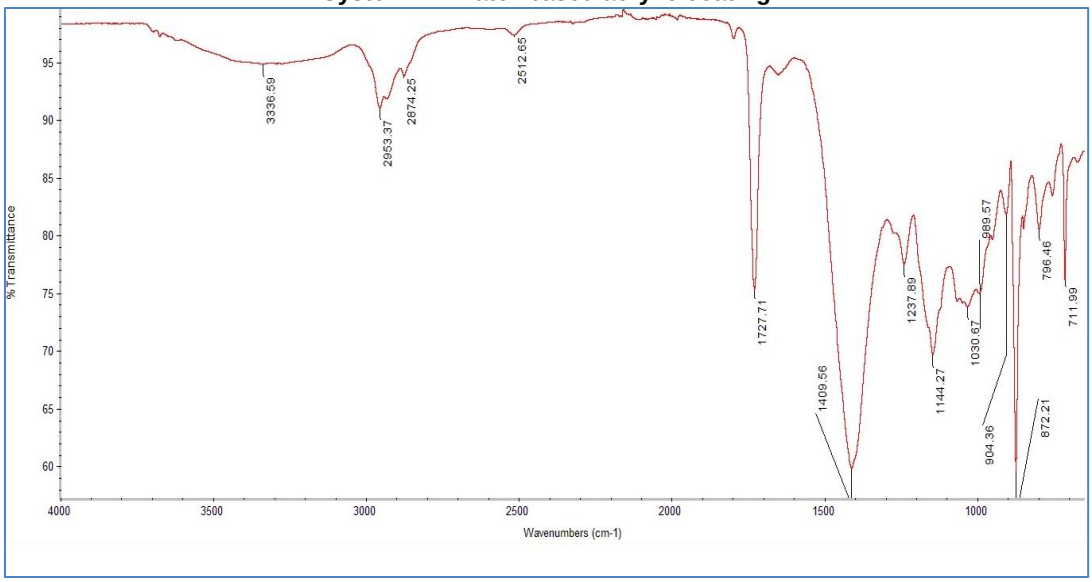


Figure E.5 Typical peaks associated with the acrylic binder are the frequencies of the -OH peak at 3428 cm^{-1} - indicative of water (Lobo & Bonilla 2003), C-H stretching bands at 2955 cm^{-1} and 2873 cm^{-1}, the overall profile of the C-H stretching region, C=O stretching at 1726 cm^{-1}, and skeletal vibrations at 1147 cm^{-1} - all indicative of an acrylic emulsion (Learner 2017).

System F - Polyester powder coating

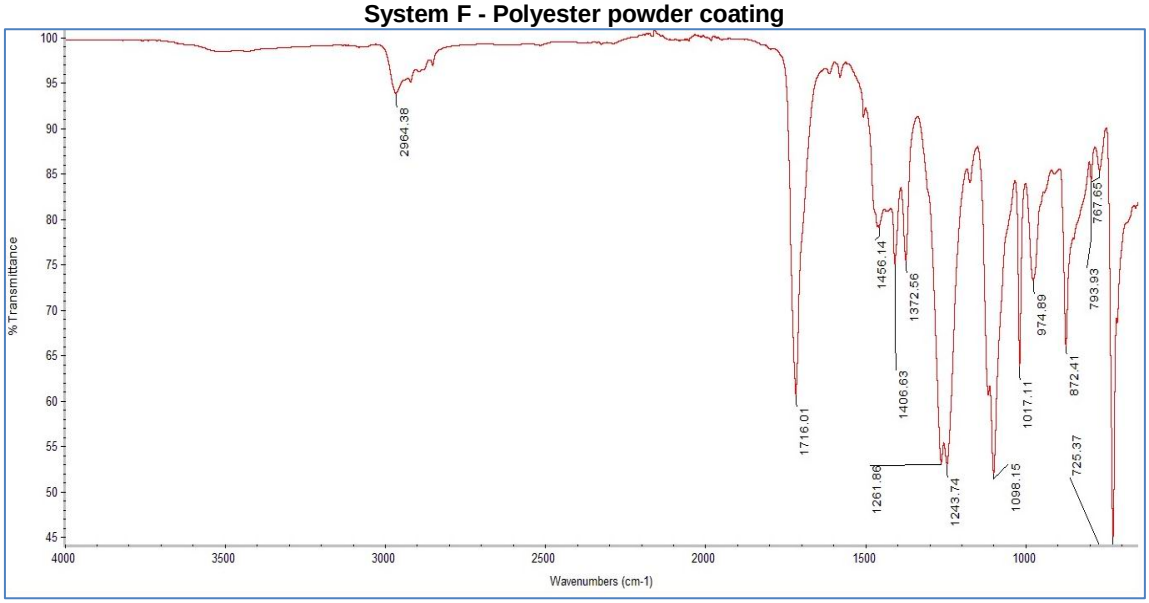


Figure E.6 Typical peaks associated with the polyester binder are the functional groups of an ester (C=O) at 1716 cm^{-1}, and skeletal vibrations of the C-O group at 1098 cm^{-1} (Spasojević et al. 2015).

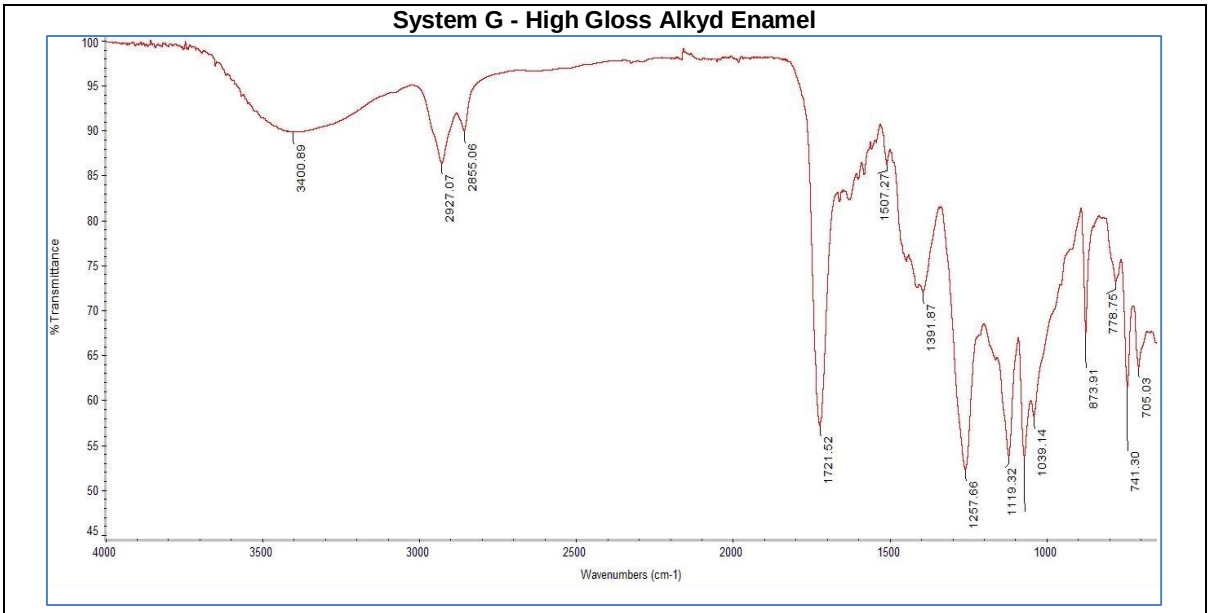


Figure E.7 Typical peaks associated with the alkyd binder are the frequencies of the C-H stretching bands at 2927 cm^{-1} and 2855 cm^{-1}, C=O stretching at 1721 cm^{-1}, and skeletal C-O vibrations between 1257 cm^{-1} and 1039 cm^{-1} (Spasojević et al. 2015).

APPENDIX F

FIGURES B.1 – B228 Photographs of the GJMA exposure sites.

Site: Florida Hills			
Surrounding Shelter and Environment			
 **North**	 **East**	 **South**	 **West**
Site: Alexandra			
Surrounding Shelter and Environment			
 **North**	 **East**	 **South**	 **West**
Site: Ivory Park			
Surrounding Shelter and Environment			
 **North**	 **East**	 **South**	 **West**

Site: Diepsloot

Surrounding Shelter and Environment

North	East	South	West
			

Site: Buccleuch

Surrounding Shelter and Environment

North	East	South	West
			

Site: Newtown

Surrounding Shelter and Environment

North	East	South	West
			

Site: Delta Park

Surrounding Shelter and Environment

North	East	South	West
			

Site: Chamdor

Surrounding Shelter and Environment

North	East	South	West
			

Site: Orange Farm

Surrounding Shelter and Environment

North	East	South	West
			

Site: Jabavu (Soweto)

Surrounding Shelter and Environment



North



East



South



West

Site: Brakpan

Surrounding Shelter and Environment



North



East



South



West

Site: Alrode

Surrounding Shelter and Environment



North



East



South



West

Site: Kagiso-Randfontein

Surrounding Shelter and Environment



North



East



South



West

Site: Ruimsig

Surrounding Shelter and Environment



North



East



South



West

Site: Kya Sand

Surrounding Shelter and Environment



North



East



South



West

Site: Midrand

Surrounding Shelter and Environment

North	East	South	West
			

Site: Aeroport

Surrounding Shelter and Environment

North	East	South	West
			

Site: Nasrec

Surrounding Shelter and Environment

North	East	South	West
			

Site: Rosherville

Surrounding Shelter and Environment



North



East



South



West

Site: Chloorkop

Surrounding Shelter and Environment



North



East



South



West

Site: Bonaero Park

Surrounding Shelter and Environment



North



East



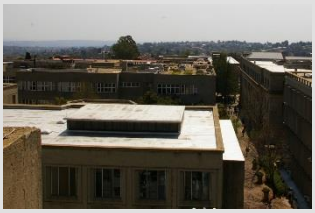
South



West

Site: Braamfontein

Surrounding Shelter and Environment



North



East



South



West

Site: Princess

Surrounding Shelter and Environment



North



East



South



West

Site: Nigel

Surrounding Shelter and Environment



North



East



South



West

Site: Geluksdal

Surrounding Shelter and Environment



North



East



South



West

Site: Dunnottar

Surrounding Shelter and Environment



North



East



South



West

Site: Springs

Surrounding Shelter and Environment



North



East



South



West

Site: Dalpark

Surrounding Shelter and Environment



North



East



South



West

Site: Elspark

Surrounding Shelter and Environment



North



East



South



West

Site: Wadeville

Surrounding Shelter and Environment



North



East



South



West

Site: Durban Deep

Surrounding Shelter and Environment



North



East



South



West

Site: Doornkop

Surrounding Shelter and Environment



North



East



South



West

Site: Lenasia

Surrounding Shelter and Environment



North



East



South



West

Site: Ennerdale

Surrounding Shelter and Environment

North	East	South	West
			

Site: Eikenhof

Surrounding Shelter and Environment

North	East	South	West
			

Site: Kliprivierberg

Surrounding Shelter and Environment

North	East	South	West
			

Site: Kliprivier

Surrounding Shelter and Environment

North	East	South	West
			

Site: Palmridge

Surrounding Shelter and Environment

North	East	South	West
			

Site: Walkerville

Surrounding Shelter and Environment

North	East	South	West
			

Site: Randfontein

Surrounding Shelter and Environment

North	East	South	West
			

Site: Krugersdorp

Surrounding Shelter and Environment

North	East	South	West
			

Site: Honeydew

Surrounding Shelter and Environment

North	East	South	West
			

Site: Lanseria

Surrounding Shelter and Environment

North	East	South	West
			

Site: Bryanston

Surrounding Shelter and Environment

North	East	South	West
			

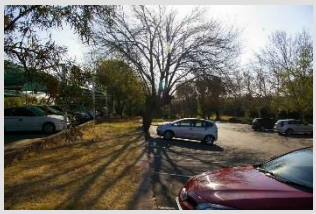
Site: Dainfern Ridge

Surrounding Shelter and Environment

North	East	South	West
			

Site: Kyalami

Surrounding Shelter and Environment

North	East	South	West
			

Site: Newclare

Surrounding Shelter and Environment

North	East	South	West
			

Site: Gillooy's

Surrounding Shelter and Environment

North	East	South	West
			

Site: Eastleigh

Surrounding Shelter and Environment



North



East



South



West

Site: Esselen Park

Surrounding Shelter and Environment



North



East



South



West

Site: Kempton Park

Surrounding Shelter and Environment



North



East



South



West

Site: Northmead

Surrounding Shelter and Environment

North	East	South	West
			

Site: Eastrand Mall

Surrounding Shelter and Environment

North	East	South	West
			

Site: Rosettenville

Surrounding Shelter and Environment

North	East	South	West
			

Site: Houghton

Surrounding Shelter and Environment



North



East



South



West

Site: Morningside

Surrounding Shelter and Environment



North



East



South



West

Site: Balmoral

Surrounding Shelter and Environment



North



East



South



West

APPENDIX G

Table G.1 ICI, MCI and ACI (CLIMAT) results (as percentage weight loss) for the periods Spring 2013 to Winter 2014 for the different main GJMA sites, with an uncertainty of measurement of about 5%.

Exposure Site	Spring 2013			Summer 2014			Autumn 2014			Winter 2014			12-month averages		
	ICI	MCI	ACI	ICI	MCI	ACI	ICI	MCI	ACI	ICI	MCI	ACI	ICI	MCI	ACI
Aeroport	0.54	0.11	0.11	0.16	0.09	0.08	0.04	0.00	0.02	0.11	0.00	0.06	0.21	0.05	0.07
Alexandra	0.58	0.09	0.12	0.70	0.14	0.06	0.13	0.03	0.03	0.09	0.08	0.04	0.37	0.34	0.06
Alrode	0.34	0.02	0.06	0.08	0.29	0.09	0.02	0.04	0.02	0.14	0.03	0.01	0.14	0.38	0.04
Bonaero Park	0.18	0.14	0.13	0.24	0.15	0.03	0.02	0.03	0.04	0.31	0.07	0.01	0.19	0.39	0.05
Braamfontein	0.28	0.00	0.13	0.15	0.18	0.03	0.00	0.00	0.03	0.14	0.10	0.01	0.14	0.28	0.05
Brakpan	0.70	0.25	0.12	1.26	0.28	0.05	0.63	0.44	0.07	0.22	0.12	0.01	0.70	1.09	0.06
Buccleuch	0.32	0.03	0.06	0.27	0.04	0.07	0.04	0.03	0.03	0.02	0.00	0.05	0.16	0.10	0.05
Chamdor	0.40	0.01	0.10	0.29	0.15	0.04	0.19	0.10	0.01	0.34	0.20	0.01	0.30	0.45	0.04
Chloorkop	1.44	1.03	0.09	1.43	0.44	0.05	0.81	0.73	0.01	0.82	0.81	0.02	1.12	3.01	0.04
Delta Park	0.48	0.06	0.05	0.74	0.16	0.03	0.04	0.14	0.01	0.22	0.08	0.00	0.37	0.43	0.02
Diepsloot	0.22	0.00	0.11	0.37	0.11	0.04	0.04	0.08	0.01	0.10	0.02	0.05	0.18	0.20	0.05
Florida Hills	0.45	0.04	0.12	0.21	0.26	0.03	0.07	0.07	0.01	0.00	0.00	0.05	0.18	0.37	0.05
Ivory Park	0.92	0.12	0.10	0.51	0.26	0.03	0.08	0.14	0.05	0.15	0.00	0.05	0.42	0.53	0.06
Jabavu (Soweto)	0.46	0.00	0.20	0.38	0.05	0.03	0.10	0.01	0.01	0.48	0.07	0.00	0.36	0.13	0.06
Kagiso-Randfontein	0.35	0.06	0.15	0.36	0.18	0.07	0.19	0.01	0.08	0.28	0.24	0.03	0.30	0.49	0.08
Kya Sand	0.34	0.07	0.06	0.34	0.07	0.06	0.20	0.15	0.06	0.13	0.00	0.01	0.25	0.28	0.05
Midrand	0.12	0.00	0.14	0.84	0.18	0.07	0.13	0.08	0.01	0.17	0.67	0.09	0.31	0.93	0.08
Nasrec	0.44	0.00	0.13	0.15	0.15	0.06	0.03	0.00	0.06	0.27	0.02	0.04	0.22	0.16	0.07
Newtown	0.19	0.00	0.10	0.12	0.08	0.03	0.00	0.00	0.02	0.08	0.00	0.05	0.10	0.08	0.05
Orange Farm	0.44	0.37	0.13	0.23	0.03	0.03	0.00	0.00	0.02	0.13	0.14	0.01	0.20	0.54	0.05
Rosherville	0.49	0.00	0.11	0.85	0.33	0.03	0.17	0.06	0.01	0.11	0.01	0.07	0.40	0.40	0.05
Ruimsig	0.53	0.05	0.07	0.42	0.12	0.03	0.17	0.03	0.07	0.22	0.00	0.07	0.34	0.21	0.06
Average	**0.46**	**0.11**	**0.11**	**0.46**	**0.17**	**0.05**	**0.14**	**0.10**	**0.03**	**0.20**	**0.12**	**0.03**	**0.32**	**0.49**	**0.05**

APPENDIX H

Table H.1 12-month helix wire corrosion rates (in µm/a) for the GJMA, measured during August-September 2013 to August-September 2014, with an uncertainty of measurement of about 5%.

Exposure Site	ISO-WH		
	Al	Zn	Cu
Aeroport	0.23	0.95	0.60
Alexandra	0.03	0.58	0.41
Alrode	0.20	0.65	0.71
Bonaero Park	0.17	0.64	0.45
Braamfontein	0.19	0.95	0.60
Brakpan	0.21	0.97	0.73
Buccleuch	0.19	1.02	0.57
Chamdor	0.14	0.94	0.62
Chloorkop	0.41	1.33	0.78
Delta Park	0.04	0.53	0.49
Diepsloot	0.07	0.46	0.37
Florida Hills	0.07	0.62	0.45
Ivory Park	0.24	0.68	0.45
Jabavu (Soweto)	0.11	0.74	0.44
Kagiso-Randfontein	0.42	1.74	1.02
Kya Sand	0.09	0.50	0.41
Midrand	0.16	0.64	0.56
Nasrec	0.15	0.76	0.57
Newtown	0.12	0.71	0.47
Orange Farm	0.20	0.80	0.57
Rosherville	0.17	0.79	0.62
Ruimsig	0.01	0.59	0.50

APPENDIX I

Table I.1 Measured 6-, 12-, 18- and 24-month corrosion rates of mild steel at 21 of the main GJMA sites, during August 2013 to September 2015 (with an uncertainty of measurement of about 5%).

Main exposure site	MSP Corrosion Rates (µm/a)				ISO 9223 rating
	6 Months	12 Months	18 Months	24 Months	
Aeroport	39	24	20	15	C2
Alexandra	25	17	15	12	C2
Alrode	31	21	18	15	C2
Bonaero Park	38	24	21	17	C2
Braamfontein	29	20	14	12	C2
Brakpan	46	26	23	17	C3
Chamdor	32	18	13	10	C2
Chloorkop	38	24	20	17	C2
Delta Park	30	20	18	15	C2
Diepsloot	22	14	13	10	C2
Florida Hills	29	19	17	13	C2
Ivory Park	29	19	15	12	C2
Jabavu (Soweto)	24	14	13	11	C2
Kagiso-Randfontein	49	33	27	21	C3
Kya Sand	26	18	15	12	C2
Midrand	31	20	17	13	C2
Nasrec	32	21	17	14	C2
Newtown	22	14	11	9	C2
Orange Farm	28	18	15	12	C2
Rosherville	34	21	16	14	C2
Ruimsig	26	16	13	11	C2
Average	**31**	**20**	**17**	**13**	**C2**

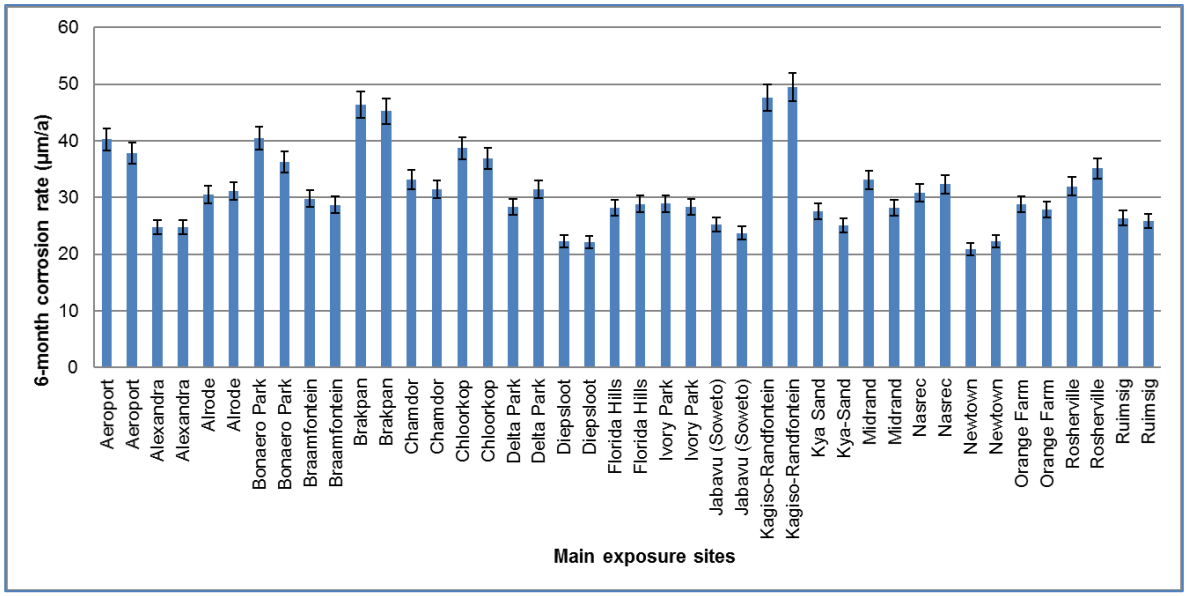


Figure I.1 Measured 6-month corrosion rates of duplicate sets of mild steel panels (MSP) at 21 of the main exposure sites.

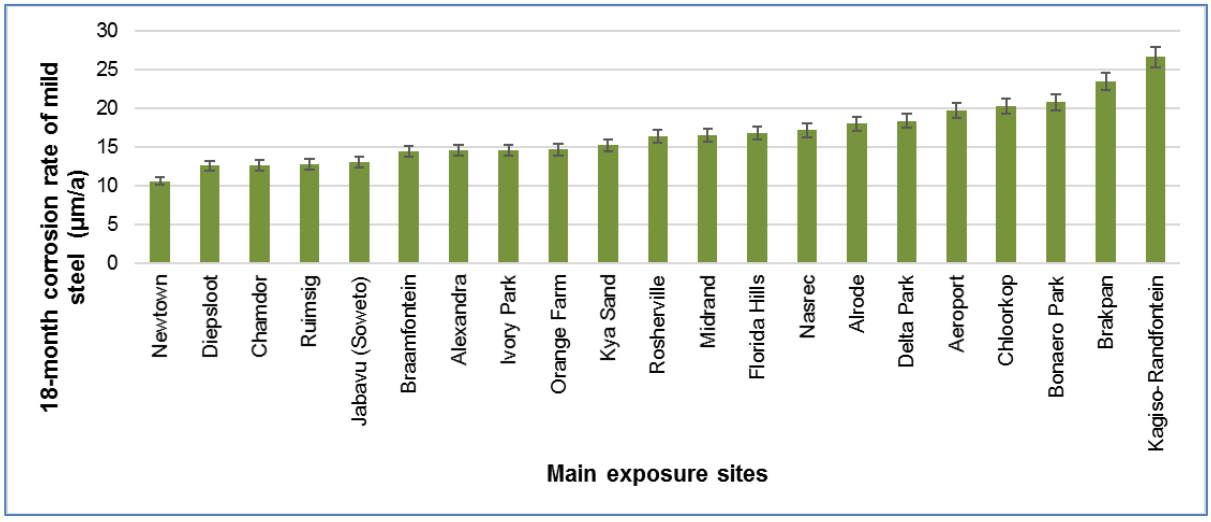


Figure I.2 Measured corrosion rates of mild steel after 18 months of exposure at the main sites in the GJMA.

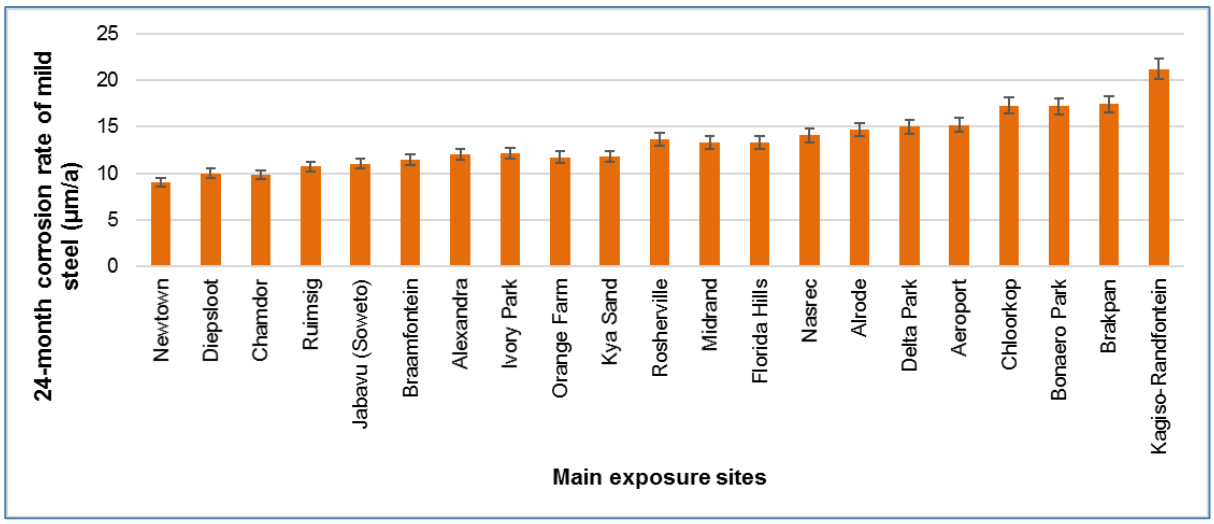


Figure I.3 Measured 24-month corrosion rates of mild steel at the main GJMA sites.

APPENDIX J

Table J.1 12-, 18- and 24-month corrosion rates of hot-dip galvanised steel specimens exposed at 21 of the main GJMA sites, with an uncertainty of measurement of about 5%.

Main exposure site	GSP corrosion rates (μm/a)			ISO 9223 rating
	12 Months	18 Months	24 Months	
Aeroport	0.8	0.7	0.8	C3
Alexandra	0.6	0.5	0.4	C2
Alrode	0.7	0.5	0.5	C2
Bonaero Park	0.8	0.6	0.5	C2
Braamfontein	0.7	0.6	0.5	C2
Brakpan	0.8	0.7	0.7	C3
Chamdor	0.8	0.7	0.7	C2
Chloorkop	1.4	0.8	0.9	C3
Delta Park	0.5	0.5	0.5	C2
Diepsloot	0.4	0.4	0.4	C2
Florida Hills	0.6	0.5	0.5	C2
Ivory Park	0.7	0.8	0.6	C2
Jabavu (Soweto)	0.7	0.5	0.5	C2
Kagiso-Randfontein	1.5	1.3	1.2	C3
Kya Sand	0.4	0.4	0.4	C2
Midrand	0.6	0.5	0.5	C2
Nasrec	0.6	0.6	0.5	C2
Newtown	0.5	0.4	0.4	C2
Orange Farm	0.8	0.5	0.5	C2
Rosherville	0.7	0.5	0.6	C2
Ruimsig	0.4	0.4	0.4	C2
Average	**0.7**	**0.6**	**0.6**	**C2**

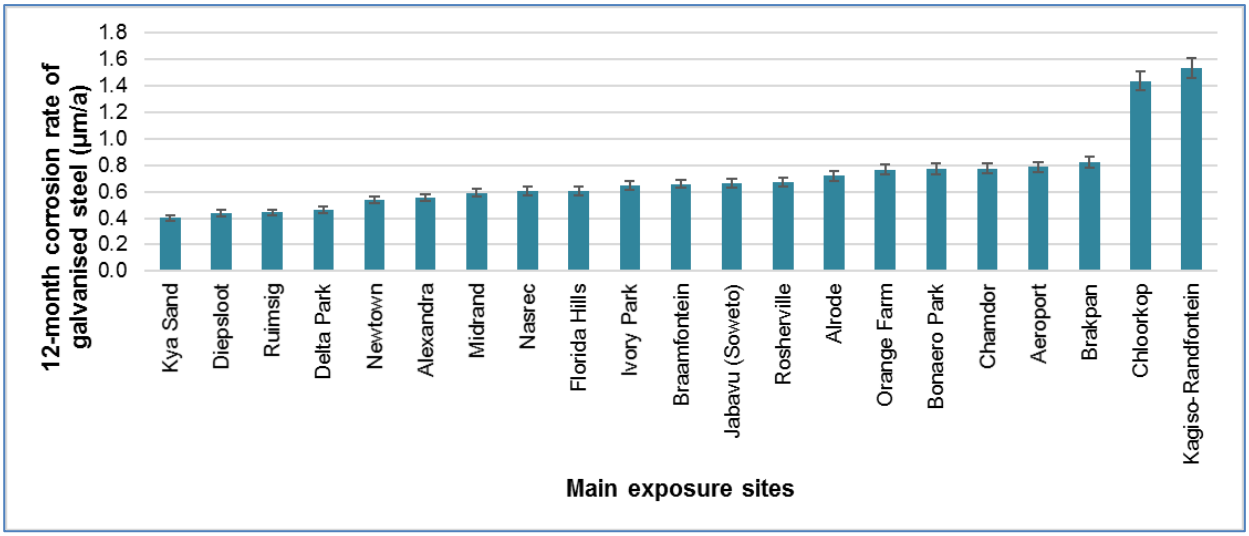


Figure J.1 Average 12-month corrosion rates of duplicate sets of hot-dip galvanised steel panels (GSP) at 21 of the main exposure sites.

APPENDIX K

Table K.1 Pearson's product-moment correlation coefficients between the different corrosion monitoring results measured for the main GJMA sites.

Corrosion data	Avg. ICI	Avg. MCI	Avg. ACI	12-month Al-WH	12-month Zn-WH	12-month Cu-WH	6-month MSP	12-month MSP	18-month MSP	24-month MSP	12-month GSP-	18-month GSP	24-month GSP
	r-value	*r*-value	*r*-value	*r*-value	*r*-value	*r*-value	*r*-value	*r*-value	*r*-value	*r*-value	*r*-value	*r*-value	*r*-value
Avg. ICI	1	0.89	-0.08	0.44	0.37	0.36	0.39	0.31	0.36	0.40	0.52	0.33	0.48
Avg. MCI		1	-0.13	0.58	0.41	0.43	0.38	0.35	0.37	0.42	0.62	0.35	0.48
Avg. ACI			1	0.26	0.32	0.28	0.31	0.33	0.28	0.26	0.24	0.38	0.34
12-month-Al-WH				1	0.87	0.81	0.72	0.76	0.65	0.68	0.91	0.85	0.87
12-month-Zn-WH					1	0.88	0.75	0.75	0.63	0.64	0.94	0.91	0.94
12-month-Cu-WH						1	0.80	0.82	0.72	0.72	0.85	0.81	0.86
6-month - MSP							1	0.96	0.93	0.90	0.75	0.80	0.84
12-month - MSP								1	0.99	0.95	0.78	0.82	0.82
18-month - MSP									1	1	0.70	0.71	0.74
24-month - MSP										1	0.73	0.71	0.74
12-month - GSP											1	0.88	0.92
18-month - GSP												1	0.92
24-month - GSP													1

Note: Values ≥ 0.41 indicate statistical importance within a 95% CL

Appendix L

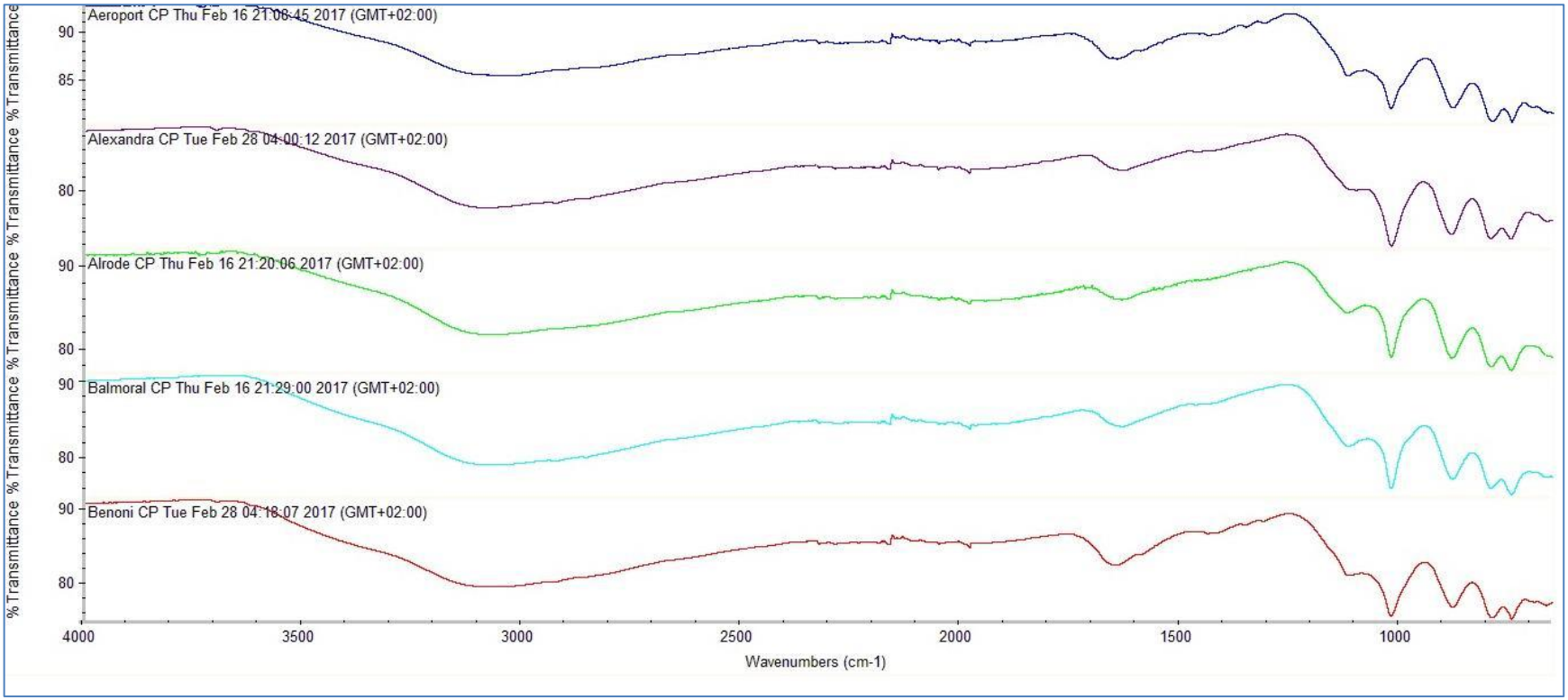


Figure L.1 Typical FTIR spectra of the rust layers of the mild steel samples exposed at different sites – Note the similarity of the spectra.

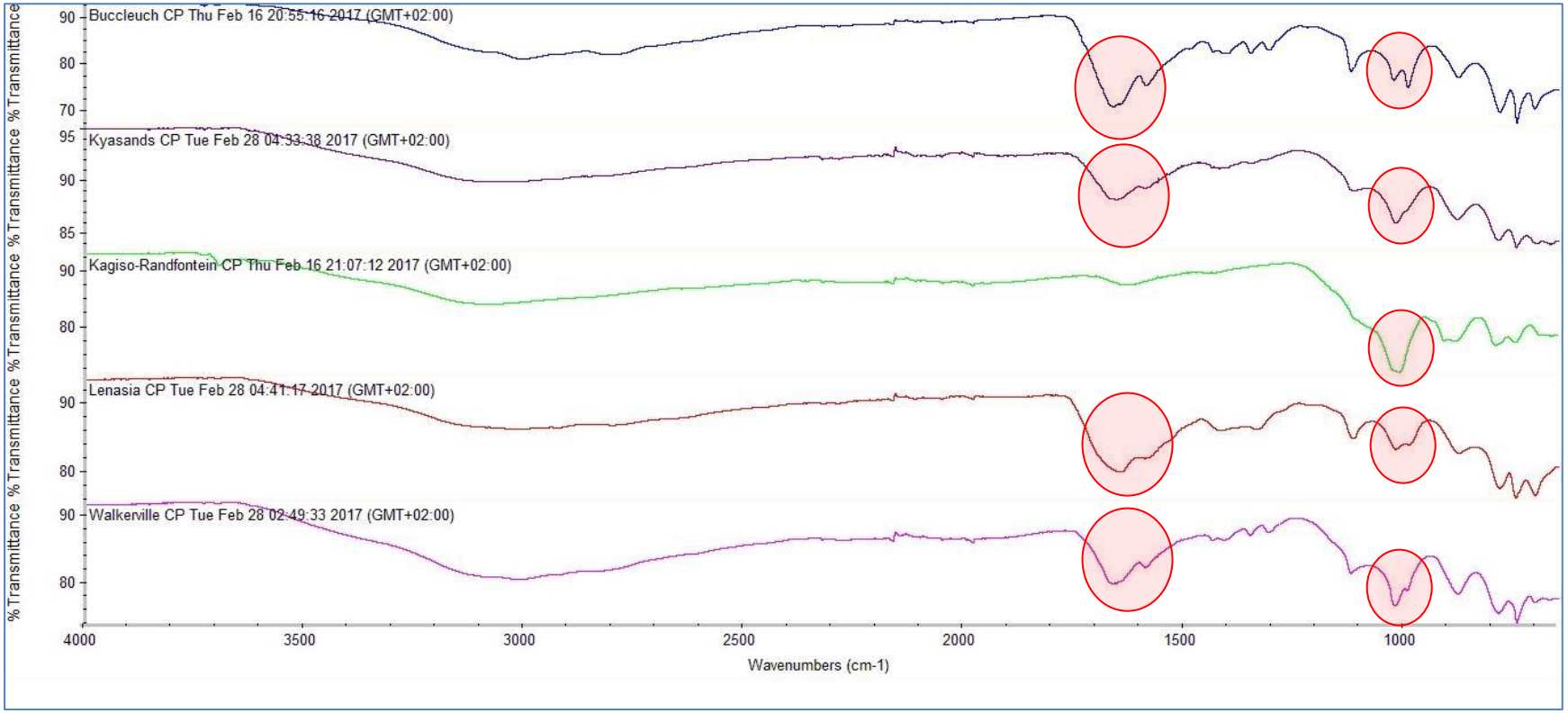


Figure L.2 Outlier spectra regarding the typical FTIR spectrum of the corrosion product of mild steel in the GJMA area.

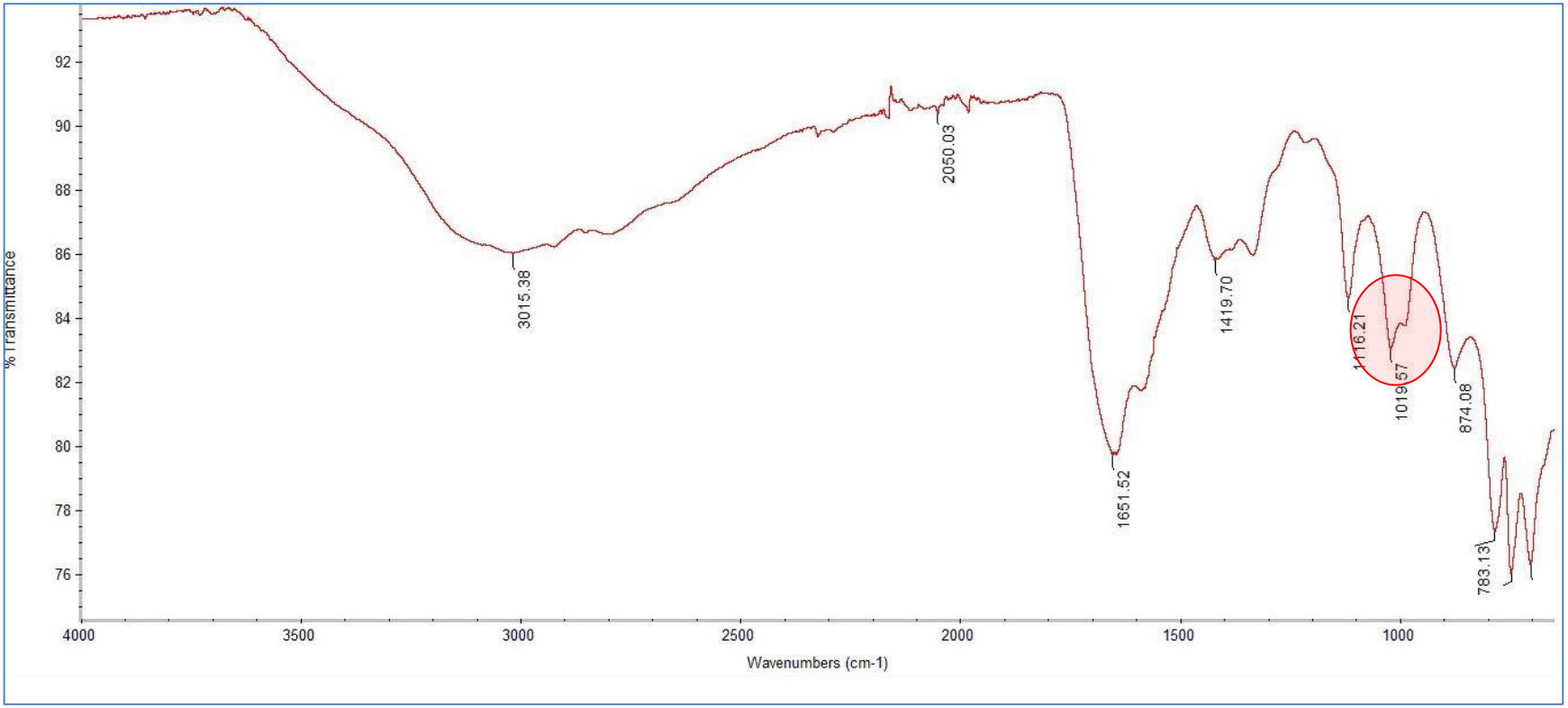


Figure L.3 FTIR spectrum of the corrosion product of mild steel exposed at the Lenasia site for 12 months.

APPENDIX M

Table M.1 Raman spectral bands of the mild steel corrosion products formed at selected sites in the GJMA.

Exposure Site	Position	Wavenumbers ($\tilde{\nu}$)								
		cm^{-1}	cm^{-1}	cm^{-1}	cm^{-1}	cm^{-1}	cm^{-1}	cm^{-1}	cm^{-1}	cm^{-1}
Aeroport	A	634								
	B	250	300	388	485	558	690	996	1116	1309
	C	250	300	388	479	556	683	989	1294	
	D	143	252	298	386	530	684	1311		
	E	250	304	384	534	610	686	1306		
	F	108	627	1000	1041	1233	1292	1422	1501	1646
	G	248	396	703	1354	1603				
Alexandra										
	A	127	201	248	462					
	B	131	248	373	539	653	1302			
	C	250	302	394	554	690	1314			
	D	248	379	655	1306					
	E	246	298	386	483	532	668	1297		
Chloorkop										
	A	217	283	394	723	1395				
	B	250	304	386	528	714	1299			
	C	250	314	405	532	716	1337			
	D	250	306	392	719	1330				
	E	317	400	536	719	1356				
	F	141	248	304	390	504, 545	723	991	1357	
	G	248	386	1120						
	H	248	308	379	537	655	1301			
	I	248	315, 350, 379		528	658	989	1306		
Kagiso-Randfontein										
	A	315	466	1393		1611				
	B	215, 248	300	384	536	662, 681	1311		1605	
	C	252	390	695	993	1347		1611		
	D	1376		1606						
	E	250	302	386						
Lenasia										
	A	250	381	534	651	1313			1616	
	B	252	300	388	692	1299	1659			
	C	248	382	536	653	1309				
	D	250	300	390	530	653	1308			
	E	248	308	384	528	662	1302			
	F	252	308	394	688					
Nasrec										
	A	135	248	302	384	539	686	989	1316	
	B	159	246	302, 340	384	692	1005	1294		
	C	250	306, 350	381	536	651	1062	1295		
	D	396	1352	1600						
	E	1062	1129	1294	1414	1441				

Appendix N

Table N.1 SEM-EDS results of the mild steel corrosion products from the GJMA sites.

Site name	Aluminium as % oxide	Phosphor as % oxide	Silicon as % oxide	Sulphur as % oxide	Chlorine as % oxide	Potassium as % oxide	Calcium as % oxide	Iron as % oxide
Aeroport	2.56		3.31	2.91				91.21
Alexandra	3.99		4.01	1.65				90.34
Alrode	2.01		3.55	1.74				92.7
Balmoral			1.38	2.53				96.09
Bonaero Park	1.71		4.03	2.59				93.38
Braamfontein	0.74		3.54	2.51				93.93
Brakpan	3.08		3.82	2.04				90.16
Bryanston	1.02		0.71	0.96				97.3
Buccleuch	3.44		2.89	1.48				92.19
Chamdor	1.42		6.23	2.17				91.6
Chloorkop	1.9		1.55	2.16	0.75			93.64
Dainfern Ridge			2.19	1.61				96.21
Dalpark		4.09	6.54	3.11		2.42		83.85
Delta Park	1.29		0.89	1.12				96.7
Diepsloot	1.59		1.81	1.01				95.59
Dunnottar	1.75		2.3	2.22				93.72
Durban Deep	3.14		8.64	0.8				87.42
Eastleigh	1.19		1.26	1.48				96.07
Eastrand Mall			2.27	2.33				95.4
Eikenhof	1.67		1.94	1.51				94.88
Elspark			4.92	2.58				92.5
Ennerdale	2.13		2.83	1.73				93.31
Esselenpark	1.30		1.24	1.58				95.89
Florida Hills	1.24		2.01	1.76				96.23
Geluksdal	2.40		3.44	1.87				92.29
Gillooy's	1.66		1.86	1.83				94.66
Houghton	0.83		1.05	1.27				
Ivory Park	1.99		5.85	1.45				92.7
Jabavu (Soweto)	1.29		1.37	1.38				95.95
Kagiso-Randfontein	11.06		17.2	2.51				69.22
Kempton Park	1.66		1.22	1.58				95.54
Kliprivier	3.91		6.55	1.69			0.42	87.44
Kliprivierberg	1.99		2.11	1.72				94.19
Krugersdorp	1.33		2.03	1.72				94.92

Table N.1 *Continued*.

Site name	Aluminium as % oxide	Phosphor as % oxide	Silicon as % oxide	Sulphur as % oxide	Chlorine as % oxide	Potassium as % oxide	Calcium as % oxide	Iron as % oxide
Kyalami	1.58		0.65	1.31				96.46
Kya Sand	1.02		0.74	1.18				97.06
Lanseria			3.38	1.61				95.01
Lenasia	2.98		3.73	1.7				91.58
Midrand	2.12		2	1.62				96.38
Morningside	0.92		0.58	1.37				97.12
Nasrec			2.96	2.38				94.65
Newclare	0.93		0.86	1.53				96.69
Newtown	1.66		2.78	1.3			0.28	93.98
Nigel			5.97	2.23				91.8
Orange farm	1.97		3.46	1.83				94.71
Palmridge			4.6	1.52				93.87
Princess	2.37		2.83	1.52				93.28
Randfontein	1.08		1.52	1.35				96.05
Rosherville	1.37		1.92	2.01				96.07
Ruimsig	1.13		0.03	1.2				96.64
Springs			5.53	3.43				90.94
Wadeville	3.46		5.49	2.76				88.29
Walkerville	3.55		5.28	2.08				89.08

APPENDIX O

Table O.1 Dry film thicknesses (DFTs) of the coated samples before (BE) and after (AE) exposure at the main GJMA sites, with an uncertainty of measurement of about 2.5 µm.

Exposure site	System A		System B		System C		System D		System E		System F		System G	
	DFT (µm)		DFT (µm)		DFT (µm)		DFT (µm)		DFT (µm)		DFT (µm)		DFT (µm)	
	BE	AE	BE	AE	BE	AE	BE	AE	BE	AE	BE	AE	BE	AE
Aeroport	189	177	138	136	176	207	74	61	108	70	69	64	131	114
Alexandra	185	196	186	197	160	120	74	58	128	66	76	73	139	125
Alrode	110	102	196	182	113	115	67	64	144	64	76	68	109	88
Bonaero Park	154	143	182	185	213	210	72	53	91	67	51	46	128	125
Braamfontein	100	90	205	212	135	225	62	44	148	87	49	39	126	103
Brakpan	114	122	195	210	120	185	54	45	112	80	71	58	118	104
Chamdor	159	158	180	203	110	105	70	52	173	94	69	66	117	120
Chloorkop	177	170	181	195	200	226	72	57	145	60	63	57	107	98
Delta Park	176	166	177	170	111	86	74	69	119	64	57	49	131	113
Diepsloot	108	102	218	218	190	189	74	51	115	72	62	52	131	111
Florida Hills	101	91	181	197	135	100	79	62	105	65	65	56	114	104
Ivory Park	102	92	181	158	190	153	70	57	88	57	50	41	146	131
Jabavu (Soweto)	140	127	152	143	176	108	68	53	159	94	63	57	124	108
Kagiso-Randfontein	100	96	141	141	148	96	68	47	138	55	54	46	116	105
Kya Sand	134	128	155	146	194	93	66	63	120	71	66	60	115	94
Midrand	155	153	257	266	198	185	75	63	112	80	62	56	117	105
Nasrec	156	137	257	301	170	184	76	63	151	47	44	37	137	113
Newtown	166	147	180	176	95	148	71	58	242	95	55	49	144	119
Orange Farm	87	75	205	209	106	110	82	70	155	89	68	58	117	97
Rosherville	169	169	186	184	234	171	84	65	98	59	64	57	137	127
Ruimsig	107	97	258	309	94	130	79	69	146	59	66	59	133	123
Average	**138**	**130**	**191**	**197**	**156**	**150**	**72**	**58**	**133**	**71**	**62**	**55**	**126**	**111**
% Variation	**24**	**27**	**18**	**24**	**27**	**32**	**9**	**13**	**26**	**20**	**14**	**17**	**9**	**11**
Note: DFT denotes dry film thickness, BE – before exposure and AE – after exposure.														

Table O.2 Percentage change in the average dry film thicknesses (DFTs) of the different coated samples after 24 months of exposure at the main GJMA sites, with an accuracy of measurement of about 2.5 µm, with an uncertainty of measurement of about 1%.

System	System A	System B	System C	System D	System E	System F	System G
Generic description	**2 x ST epoxy + 1 x WBA topcoat**	**2 x ST epoxy + 1 x PS topcoat**	**2 x ST epoxy + 1 x PU topcoat**	**1 x WBA Primer + 2 x WBA topcoat**	**1 x WBA Primer + 2 x WBA topcoat**	**Polyester Powder Coating**	**1 x Alkyd Primer + 2 x Alkyd topcoat**
Exposure Site	**%**	**%**	**%**	**%**	**%**	**%**	**%**
Aeroport	6	1	-18	17	35	8	13
Alexandra	-6	-6	25	21	49	3	10
Alrode	7	7	-1	4	55	11	19
Bonaero Park	7	-2	1	26	26	10	2
Braamfontein	10	-3	-67	29	42	19	18
Brakpan	-7	-8	-55	17	29	18	12
Chamdor	0	-13	5	26	46	4	-3
Chloorkop	4	-8	-13	21	58	9	9
Delta Park	6	4	23	7	46	13	14
Diepsloot	5	0	0	31	38	15	15
Florida Hills	10	-9	26	21	39	13	9
Ivory Park	10	13	19	18	35	18	10
Jabavu (Soweto)	9	6	39	22	41	10	13
Kagiso-Randfontein	3	0	35	32	60	15	9
Kayasands	4	6	52	4	41	9	19
Midrand	1	-4	6	15	29	9	10
Nasrec	12	-17	-8	17	69	16	17
Newtown	11	2	-55	18	61	11	18
Orange Farm	13	-2	-4	15	43	14	17
Rosherville	0	1	27	23	40	11	7
Ruimsig	10	-20	-38	12	60	11	7
Average	**6**	**-2**	**0**	**19**	**45**	**12**	**12**

NOTES
ST – surface tolerant
WBA – water-based acrylic
PU - polyurethane
PS – poly-siloxane

APPENDIX P

Table P.1 Degree of chalking and dirt retention results, with a level of uncertainty of about 20%.

Site	System A	System B	System C	System D	System E	System F	System G	SUM
Aeroport	1	1	2	1	2	2	3	12
Alexandra	1	1	1	1	1	1	2	8
Alrode	1	1	1	1	2	2	2	9
Bonaero Park	1	1	2	1	2	2	3	11
Braamfontein	1	1	2	1	2	2	3	12
Brakpan	1	1	1	1	2	2	2	10
Chamdor	1	1	1	1	2	2	3	10
Chloorkop	1	1	2	1	2	2	3	12
Delta Park	1	1	1	1	1	2	3	10
Diepsloot	1	1	1	1	1	2	2	9
Florida Hills	1	1	1	1	1	1	2	8
Ivory Park	1	1	1	1	1	2	3	10
Jabavu (Soweto)	1	1	1	1	2	2	3	10
Kagiso-Randfontein	1	1	1	1	2	2	3	11
Kya Sand	1	1	1	1	2	2	2	9
Midrand	1	1	2	1	2	2	3	11
Nasrec	1	1	2	1	2	2	3	11
Newtown	2	1	1	1	2	2	3	11
Orange Farm	1	1	2	1	2	2	3	11
Rosherville	1	1	1	1	2	2	3	10
Ruimsig	1	1	1	1	1	1	3	9
SUM	**22**	**21**	**27**	**21**	**31**	**33**	**57**	**210**
Average	**1**	**1**	**1**	**1**	**1**	**2**	**3**	**10**

Rating – 1 – Slight, 2 – Moderate, 3 – Severe.

APPENDIX Q

Table Q.1 Average 60° specular gloss levels (in GU) of the coated samples before exposure at the different GJMA sites, with an uncertainty of measurement of about 2.5%.

Coating system	System A	System B	System C	System D	System E	System F	System G
	2 x ST epoxy + 1 x WBA topcoat	2 x ST epoxy + 1 x PS topcoat	2 x ST epoxy + 1 x PU topcoat	1 x WBA Primer + 2 x WBA topcoat	1 x WBA Primer + 2 x WBA topcoat	Polyester Powder Coating	1 x Alkyd Primer + 2 x Alkyd topcoat
Florida Hills	40.3	70.8	74.9	26.7	4.7	65.9	80.4
Alexandra	46.8	57.9	69.1	24.7	4.9	66.9	81.4
Ivory Park	39.4	61.2	71.0	27.4	4.7	67.2	82.1
Diepsloot	39.7	54.7	70.6	24.0	5.0	68.8	81.7
Newtown	50.0	57.6	63.5	24.7	5.1	67.9	81.4
Delta Park	41.7	66.8	60.1	24.1	5.0	67.9	80.6
Chamdor	42.8	59.5	72.7	26.3	5.2	67.9	81.1
Orange Farm	37.6	67.0	66.7	27.2	5.0	67.8	80.0
Jabavu (Soweto)	48.6	72.2	65.1	27.0	5.2	67.0	80.5
Brakpan	52.6	68.2	65.1	23.9	5.1	66.9	80.0
Alrode	45.1	53.3	62.0	26.5	5.0	68.3	78.7
Kagiso-Randfontein	40.2	73.0	58.0	22.0	5.2	66.5	82.1
Ruimsig	37.0	63.3	73.4	25.3	5.2	69.0	80.8
Kya Sand	48.3	65.5	60.6	27.8	5.0	65.5	80.1
Midrand	40.3	68.8	49.2	25.3	5.0	68.0	78.5
Aeroport	45.0	66.3	54.5	25.0	5.0	68.0	81.1
Nasrec	34.2	84.2	64.5	22.1	5.1	67.5	77.7
Rosherville	35.9	75.0	64.7	25.6	4.9	67.1	77.5
Chloorkop	34.0	69.2	59.5	25.5	5.2	69.2	79.5
Bonaero Park	45.2	67.1	48.2	24.0	4.8	67.1	80.7
Braamfontein	37.6	74.1	62.5	23.6	4.9	67.6	79.1
Average	42.0	66.5	63.6	25.2	5.0	67.5	80.2
SD	5.3	7.5	7.3	1.6	0.1	0.9	1.3
% Variation	12.6	11.2	11.4	6.5	3.0	1.4	1.7
NOTE: ST denotes surface tolerant, WBA – water-based acrylic, PU – polyurethane, PS – polysiloxane and GU – gloss units.							

Table Q.2 Average 60° specular gloss levels of the coated samples after 24 months of exposure at the different GJMA sites (before cleaning), with an uncertainty of measurement of about 2.5%.

Coating system	System A	System B	System C	System D	System E	System F	System G
	2 x ST epoxy + 1 x WBA topcoat	2 x ST epoxy + 1 x PS topcoat	2 x ST epoxy + 1 x PU topcoat	1 x WBA Primer + 2 x WBA topcoat	1 x WBA Primer + 2 x WBA topcoat	Polyester Powder Coating	1 x Alkyd Primer + 2 x Alkyd topcoat
Florida Hills	17.8	32.4	26.6	9.8	5.6	22.0	2.8
Alexandra	15.3	24.1	15.1	7.5	6.2	8.5	1.1
Ivory Park	16.5	31.5	18.7	8.0	6.2	11.5	1.3
Diepsloot	16.0	25.9	11.3	6.9	6.8	13.5	1.2
Newtown	16.2	28.0	12.8	8.9	6.9	11.7	1.4
Delta Park	16.6	31.6	20.7	6.2	7.1	17.6	2.5
Chamdor	18.1	23.4	19.1	5.0	5.1	21.2	1.8
Orange Farm	17.0	27.2	26.0	8.8	5.7	18.6	1.4
Jabavu (Soweto)	21.1	33.7	13.3	9.9	5.9	54.4	1.6
Brakpan	20.6	26.2	13.3	8.2	5.8	16.7	1.6
Alrode	19.8	18.9	16.3	9.3	5.5	21.4	1.5
Kagiso-Randfontein	16.6	32.3	19.1	6.8	4.8	23.3	1.3
Ruimsig	18.0	32.6	17.8	11.1	8.5	24.9	2.0
Kayasands	18.9	32.2	20.7	8.4	5.7	21.7	1.4
Midrand	18.1	32.2	7.5	8.6	6.4	28.9	1.6
Aeroport	15.9	24.6	4.8	7.8	5.0	9.6	1.5
Nasrec	19.3	32.1	8.6	7.8	6.2	16.7	1.8
Rosherville	21.6	32.2	14.6	8.5	6.1	17.9	1.7
Chloorkop	13.5	27.7	2.9	7.0	5.0	20.4	1.5
Bonaero Park	15.9	33.0	10.3	7.5	5.8	16.1	1.6
Braamfontein	18.4	34.8	3.8	8.2	5.5	9.3	2.0
Average	**17.7**	**29.4**	**14.4**	**8.1**	**6.0**	**19.3**	**1.7**
SD	11.7	14.4	46.2	16.7	14.2	50.3	24.9
% Variation	17.8	32.4	26.6	9.8	5.6	22.0	2.8

NOTE: ST denotes surface tolerant, WBA – water-based acrylic, PU – polyurethane, PS – polysiloxane and GU – gloss units.

Table Q.3 Changes in the average 60° specular gloss levels (in GU) of the different coated samples after 24 months of exposure at the GJMA sites (after cleaning), with an uncertainty of measurement of about 2.5%.

Coating system	System A	System B	System C	System D	System E	System F	System G
	2 x ST epoxy + 1 x WBA topcoat	2 x ST epoxy + 1 x PS topcoat	2 x ST epoxy + 1 x PU topcoat	1 x WBA Primer + 2 x WBA topcoat	1 x WBA Primer + 2 x WBA topcoat	Polyester Powder Coating	1 x Alkyd Primer + 2 x Alkyd topcoat
	GU	**GU**	**GU**	**GU**	**GU**	**GU**	**GU**
Florida Hills	17.8	32.4	26.6	9.8	5.6	22.0	2.8
Alexandra	15.3	24.1	15.1	7.5	6.2	8.5	1.1
Ivory Park	16.5	31.5	18.7	8.0	6.2	11.5	1.3
Diepsloot	16.0	25.9	11.3	6.9	6.8	13.5	1.2
Newtown	16.2	28.0	12.8	8.9	6.9	11.7	1.4
Delta Park	16.6	31.6	20.7	6.2	7.1	17.6	2.5
Chamdor	18.1	23.4	19.1	5.0	5.1	21.2	1.8
Orange Farm	17.0	27.2	26.0	8.8	5.7	18.6	1.4
Jabavu (Soweto)	21.1	33.7	13.3	9.9	5.9	54.4	1.6
Brakpan	20.6	26.2	13.3	8.2	5.8	16.7	1.6
Alrode	19.8	18.9	16.3	9.3	5.5	21.4	1.5
Kagiso-Randfontein	16.6	32.3	19.1	6.8	4.8	23.3	1.3
Ruimsig	18.0	32.6	17.8	11.1	8.5	24.9	2.0
Kayasands	18.9	32.2	20.7	8.4	5.7	21.7	1.4
Midrand	18.1	32.2	7.5	8.6	6.4	28.9	1.6
Aeroport	15.9	24.6	4.8	7.8	5.0	9.6	1.5
Nasrec	19.3	32.1	8.6	7.8	6.2	16.7	1.8
Rosherville	21.6	32.2	14.6	8.5	6.1	17.9	1.7
Chloorkop	13.5	27.7	2.9	7.0	5.0	20.4	1.5
Bonaero Park	15.9	33.0	10.3	7.5	5.8	16.1	1.6
Braamfontein	18.4	34.8	3.8	8.2	5.5	9.3	2.0
Average	**17.7**	**29.4**	**14.4**	**8.1**	**6.0**	**19.3**	**1.7**
%Variation	11.7	14.4	46.2	16.7	14.2	50.3	24.9

NOTE: ST denotes surface tolerant, WBA – water-based acrylic, PU – polyurethane, PS – polysiloxane and GU – gloss units.

APPENDIX R

Table R.1 Measured colour coordinates of Coating System A before exposure, with an uncertainty of measurement of about 1%.

Colour Co-ordinates of Standard Reference Sample (White)

	*L**	*a**	*b**	*C**	*h**
Standard (White)	100	0.0	0.0	0.0	0.0

		Sample Colour Co-ordinates				
Site	**Sample No**	***L****	***a****	***b****	***C****	***h****
Florida Hills	**A1**	31.3	-24.5	23.0	33.6	136.8
Alexandra	**A2**	31.2	-24.7	23.2	33.9	136.8
Ivory Park	**A3**	31.2	-24.8	23.3	34.0	136.8
Diepsloot	**A4**	31.1	-24.7	23.3	34.0	136.7
Newtown	**A6**	31.2	-24.8	23.5	34.2	136.6
Delta Park	**A7**	31.2	-24.8	23.3	34.0	136.7
Chamdor	**A8**	31.3	-24.7	23.3	34.0	136.7
Orange Farm	**A9**	31.4	-24.9	23.6	34.6	136.6
Jabavu (Soweto)	**A10**	31.4	-24.8	23.3	34.0	136.7
Brakpan	**A11**	31.6	-24.9	23.6	34.3	136.5
Alrode	**A12**	31.3	-24.8	23.3	34.0	136.7
Kagiso-Randfontein	**A13**	31.5	-24.6	23.4	34.0	136.4
Ruimsig	**A14**	31.2	-24.8	23.5	34.2	136.6
Kya Sand	**A15**	31.3	-24.7	23.3	31.0	136.7
Midrand	**A16**	31.3	-24.7	23.3	33.9	136.6
Aeroport	**A17**	31.3	-24.7	23.4	34.1	136.5
Nasrec	**A18**	31.0	-24.8	23.4	34.1	136.7
Rosherville	**A19**	31.2	-24.8	23.3	34.0	136.8
Chloorkop	**A20**	31.7	-24.8	24.3	34.8	135.5
Bonaero Park	**A21**	31.8	-25.1	23.8	34.6	136.4
Braamfontein	**A22**	31.5	-24.5	23.6	34.0	136.1
	Average	31.3	-24.8	23.4	34.0	136.6
	SD	0.2	0.1	0.3	0.7	0.3
	% Variation	0.6	-0.5	1.1	2.2	0.2

Table R.2 Measured colour coordinates of Coating System B before exposure, with an uncertainty of measurement of about 1%.

Colour Co-ordinates of Standard Reference Sample (White)

	*L**	*a**	*b**	*C**	*h**
Standard (White)	100	0.0	0.0	0.0	0.0

		Sample Colour Co-ordinates				
Site	**Sample No**	***L****	***a****	***b****	***C****	***h****
Florida Hills	**B1**	30.0	-17.1	22.3	28.1	127.5
Alexandra	**B2**	29.7	-17.2	22.6	28.4	127.3
Ivory Park	**B3**	29.9	-17.5	23.6	29.4	126.5
Diepsloot	**B4**	30.0	-17.3	23.5	29.2	126.4
Newtown	**B6**	29.9	-17.6	23.7	29.5	126.5
Delta Park	**B7**	29.8	-17.3	23.1	28.9	126.8
Chamdor	**B8**	29.6	-17.3	22.9	28.7	127.1
Orange Farm	**B9**	29.4	-17.4	23.4	29.1	126.6
Jabavu (Soweto)	**B10**	29.2	-17.4	23.2	29.0	126.9
Brakpan	**B11**	29.3	-17.4	23.2	28.9	126.8
Alrode	**B12**	29.9	-17.6	23.8	29.6	126.4
Kagiso-Randfontein	**B13**	29.2	-17.3	23.1	28.9	126.9
Ruimsig	**B14**	29.4	-17.4	23.6	29.3	126.4
Kya Sand	**B15**	29.7	-17.2	23.6	29.2	126.0
Midrand	**B16**	30.1	-17.7	24.4	30.1	126.1
Aeroport	**B17**	30.1	-17.5	24.1	29.8	126.0
Nasrec	**B18**	30.1	-17.7	24.2	30.0	126.2
Rosherville	**B19**	29.6	-17.4	23.0	28.8	127.1
Chloorkop	**B20**	29.5	-17.4	23.1	28.9	127.0
Bonaero Park	**B21**	29.7	-17.4	22.7	28.6	127.5
Braamfontein	**B22**	29.4	-17.3	22.9	28.7	127.1
	Average	29.7	-17.4	23.3	29.1	126.7
	SD	0.3	0.2	0.5	0.5	0.5
	% Variation	1.0	-0.9	2.3	1.7	0.4

Table R.3 Measured colour coordinates of Coating System C before exposure, with an uncertainty of measurement of about 1%.

Colour Co-ordinates of Standard Reference Sample (White)

	*L**	*a**	*b**	*C**	*h**
Standard (White)	100	0.0	0.0	0.0	0.0

		Sample Colour Co-ordinates				
Site	**Sample No**	***L****	***a****	***b****	***C****	***h****
Florida Hills	**C1**	30.0	-20.5	24.5	31.9	130.0
Alexandra	**C2**	30.1	-20.5	24.4	31.9	130.0
Ivory Park	**C3**	30.0	-20.5	24.5	32.0	130.0
Diepsloot	**C4**	30.1	-20.5	24.4	31.9	130.1
Newtown	**C6**	30.4	-20.5	24.6	32.0	129.9
Delta Park	**C7**	30.7	-20.7	24.8	32.3	129.8
Chamdor	**C8**	30.4	-20.4	24.4	31.8	130.0
Orange Farm	**C9**	30.0	-20.5	24.4	31.9	130.0
Jabavu (Soweto)	**C10**	30.0	-20.5	24.4	31.9	130.0
Brakpan	**C11**	30.1	-20.6	24.5	32.0	130.0
Alrode	**C12**	30.1	-20.5	24.6	32.0	129.9
Kagiso-Randfontein	**C13**	30.1	-20.4	24.2	31.7	130.2
Ruimsig	**C14**	29.9	-20.5	24.4	31.9	130.0
Kya Sand	**C15**	30.1	-20.4	24.3	31.7	129.9
Midrand	**C16**	30.2	-20.2	24.2	31.6	129.8
Aeroport	**C17**	30.2	-20.5	24.4	31.9	129.9
Nasrec	**C18**	30.1	-20.5	24.6	32.0	129.8
Rosherville	**C19**	30.2	-20.4	24.5	31.9	129.8
Chloorkop	**C20**	30.1	-20.5	24.5	32.0	129.9
Bonaero Park	**C21**	30.1	-20.4	24.4	31.8	129.9
Braamfontein	**C22**	29.9	-20.4	24.5	31.9	129.8
	Average	30.1	-20.5	24.5	31.9	129.9
	SD	0.2	0.1	0.1	0.1	0.1
	% Variation	0.6	-0.5	0.6	0.4	0.1

Table R.4 Measured colour coordinates of Coating System D before exposure, with an uncertainty of measurement of about 1%.

Colour Co-ordinates of Standard Reference Sample (White)

	*L**	*a**	*b**	*C**	*h**
Standard (White)	100	0.0	0.0	0.0	0.0

		Sample Colour Co-ordinates				
Site	**Sample No**	***L****	***a****	***b****	***C****	***h****
Florida Hills	**D1**	27.4	-11.8	5.0	12.8	157.0
Alexandra	**D2**	27.3	-11.9	4.9	12.9	157.4
Ivory Park	**D3**	27.1	-12.0	5.0	13.0	157.5
Diepsloot	**D4**	27.5	-11.7	4.8	12.6	157.8
Newtown	**D6**	27.3	-11.7	4.9	12.7	157.2
Delta Park	**D7**	27.5	-11.8	4.9	12.7	157.6
Chamdor	**D8**	27.2	-11.9	5.1	12.9	156.9
Orange Farm	**D9**	27.1	-11.9	4.8	12.9	157.9
Jabavu (Soweto)	**D10**	27.2	-12.1	5.1	13.1	157.1
Brakpan	**D11**	27.0	-11.3	4.8	12.2	157.1
Alrode	**D12**	27.3	-12.0	4.8	13.0	158.2
Kagiso-Randfontein	**D13**	27.3	-11.2	4.6	12.1	157.4
Ruimsig	**D14**	27.2	-11.8	4.7	12.7	158.2
Kya Sand	**D15**	27.1	-12.1	5.1	13.1	157.2
Midrand	**D16**	27.3	-12.0	4.9	12.9	157.9
Aeroport	**D17**	27.3	-11.9	4.8	12.8	158.0
Nasrec	**D18**	27.5	-11.5	4.7	12.6	158.4
Rosherville	**D19**	27.3	-12.0	5.0	13.0	157.4
Chloorkop	**D20**	27.3	-11.9	5.0	12.9	157.3
Bonaero Park	**D21**	27.5	-11.7	4.7	12.6	158.0
Braamfontein	**D22**	27.2	-11.6	4.8	12.6	157.5
	Average	27.3	-11.8	4.9	12.8	157.6
	SD	0.1	0.2	0.1	0.3	0.4
	% Variation	0.5	-2.0	3.0	2.0	0.3

Table R.5 Measured colour coordinates of Coating System E before exposure, with an uncertainty of measurement of about 1%.

Colour Co-ordinates of Standard Reference Sample (White)

	*L**	*a**	*b**	*C**	*h**
Standard (White)	100	0.0	0.0	0.0	0.0

		Sample Colour Co-ordinates				
Site	**Sample No**	***L****	***a****	***b****	***C****	***h****
Florida Hills	**E1**	39.4	-16.1	9.7	18.8	148.9
Alexandra	**E2**	39.5	-15.9	9.9	18.8	148.3
Ivory Park	**E3**	39.5	-16.2	10.0	19.0	148.4
Diepsloot	**E4**	39.4	-16.2	9.8	18.9	148.9
Newtown	**E6**	39.3	-16.2	9.6	18.8	149.5
Delta Park	**E7**	39.3	-16.1	9.8	18.9	148.7
Chamdor	**E8**	39.4	-16.2	9.9	19.0	148.5
Orange Farm	**E9**	39.2	-16.1	9.7	18.8	148.8
Jabavu (Soweto)	**E10**	39.3	-16.2	10.0	19.1	148.2
Brakpan	**E11**	39.2	-16.1	9.9	18.9	148.4
Alrode	**E12**	39.4	-16.2	10.2	19.1	147.8
Kagiso-Randfontein	**E13**	39.1	-16.0	9.7	18.7	148.9
Ruimsig	**E14**	39.2	-16.2	9.9	19.0	148.5
Kya Sand	**E15**	39.2	-16.1	9.8	18.8	148.7
Midrand	**E16**	39.4	-16.1	10.0	19.0	148.2
Aeroport	**E17**	39.5	-16.0	10.0	18.9	147.9
Nasrec	**E18**	39.5	-16.1	9.9	18.9	148.4
Rosherville	**E19**	39.4	-16.0	9.9	18.8	148.3
Chloorkop	**E20**	39.3	-16.1	9.8	18.9	148.8
Bonaero Park	**E21**	39.3	-15.6	10.0	18.6	147.5
Braamfontein	**E22**	39.7	-15.9	9.8	18.7	148.3
	Average	39.4	-16.1	9.9	18.9	148.5
	SD	0.1	0.1	0.1	0.1	0.4
	% Variation	0.4	-0.9	1.4	0.7	0.3

Table R.6 Measured colour coordinates of Coating System F before exposure, with an uncertainty of measurement of about 1%.

Colour Co-ordinates of Standard Reference Sample (White)

	*L**	*a**	*b**	*C**	*h**
Standard (White)	100	0.0	0.0	0.0	0.0

		Sample Colour Co-ordinates				
Site	**Sample No**	***L****	***a****	***b****	***C****	***h****
Florida Hills	**F1**	38.8	-25.6	31.6	40.7	129.0
Alexandra	**F2**	38.8	-25.6	31.7	40.7	128.9
Ivory Park	**F3**	38.9	-25.7	31.9	40.9	128.9
Diepsloot	**F4**	38.9	-25.6	31.6	40.7	129.0
Newtown	**F6**	38.8	-25.7	31.8	40.9	128.9
Delta Park	**F7**	38.8	-25.6	31.7	40.8	128.9
Chamdor	**F8**	38.7	-25.6	31.7	40.8	129.0
Orange Farm	**F9**	38.9	-25.4	31.1	40.1	129.3
Jabavu (Soweto)	**F10**	39.0	-25.5	31.4	40.4	129.1
Brakpan	**F11**	38.8	-25.6	31.8	40.8	128.9
Alrode	**F12**	38.8	-25.6	31.9	40.9	128.8
Kagiso-Randfontein	**F13**	39.0	-25.3	31.2	40.1	129.0
Ruimsig	**F14**	38.9	-25.6	31.7	40.7	128.9
Kya Sand	**F15**	38.8	-25.6	31.6	40.7	128.9
Midrand	**F16**	38.8	-25.6	31.7	40.8	128.9
Aeroport	**F17**	38.8	-25.5	31.5	40.5	129.0
Nasrec	**F18**	39.1	-25.5	31.2	40.3	129.2
Rosherville	**F19**	39.0	-25.5	31.3	40.3	129.1
Chloorkop	**F20**	38.9	-25.6	31.6	40.6	129.0
Bonaero Park	**F21**	38.8	-25.6	31.8	40.8	128.9
Braamfontein	**F22**	38.9	-25.5	31.5	40.5	129.1
	Average	38.9	-25.6	31.6	40.6	129.0
	SD	0.1	0.1	0.2	0.3	0.1
	% Variation	0.2	-0.4	0.7	0.6	0.1

Table R.7 Measured colour coordinates of Coating System G before exposure, with an uncertainty of measurement of about 1%.

Colour Co-ordinates of Standard Reference Sample (White)

	*L**	*a**	*b**	*C**	*h**
Standard (White)	100	0.0	0.0	0.0	0.0

		Sample Colour Co-ordinates				
Site	**Sample No**	***L****	***a****	***b****	***C****	***h****
Florida Hills	**G1**	29.5	-19.9	18.6	27.3	136.9
Alexandra	**G2**	29.4	-20.0	18.9	27.5	136.5
Ivory Park	**G3**	29.3	-19.4	18.4	26.7	136.5
Diepsloot	**G4**	29.4	-20.0	18.9	27.5	136.7
Newtown	**G6**	29.4	-20.0	18.8	27.4	136.8
Delta Park	**G7**	29.4	-19.9	18.8	27.4	136.6
Chamdor	**G8**	29.5	-19.9	18.8	27.4	136.7
Orange Farm	**G9**	29.5	-19.8	18.8	27.3	136.5
Jabavu (Soweto)	**G10**	29.4	-20.0	18.9	27.5	136.7
Brakpan	**G11**	29.3	-19.9	18.9	27.4	136.5
Alrode	**G12**	29.3	-20.4	20.3	28.8	135.2
Kagiso-Randfontein	**G13**	29.5	-19.9	19.2	27.7	136.0
Ruimsig	**G14**	29.3	-19.8	18.7	27.2	136.6
Kya Sand	**G15**	29.4	-19.7	18.8	27.2	136.3
Midrand	**G16**	29.4	-19.7	18.8	27.2	136.4
Aeroport	**G17**	29.4	-19.9	18.8	27.4	136.7
Nasrec	**G18**	29.4	-19.7	19.1	27.5	136.0
Rosherville	**G19**	29.4	-19.8	19.0	27.5	136.1
Chloorkop	**G20**	29.5	-20.0	18.9	27.6	136.6
Bonaero Park	**G21**	29.4	-20.0	18.8	27.4	136.8
Braamfontein	**G22**	29.5	-19.8	18.8	27.3	136.4
	Average	29.4	-19.9	18.9	27.4	136.5
	SD	0.1	0.2	0.4	0.4	0.4
	% Variation	0.2	-0.9	1.9	1.4	0.3

Table R.8 Colour changes (ΔE) per sample after exposure at the GJMA, with an uncertainty of measurement of about 1%.

	Coating system							
Exposure site	**System A**	**System B**	**System C**	**System D**	**System E**	**System F**	**System G**	**System H**
Florida Hills	3	2	7	5	1	10	12	40
Alexandra	9	4	9	7	5	10	14	58
Ivory Park	4	3	9	7	5	10	13	51
Diepsloot	4	3	9	7	5	10	13	50
Newtown	6	5	10	6	5	10	12	54
Delta Park	5	3	7	7	6	10	13	50
Chamdor	6	6	9	8	6	9	13	56
Orange Farm	4	6	9	7	6	9	13	54
Jabavu (Soweto)	3	3	6	5	5	5	13	40
Brakpan	4	7	8	7	5	9	13	52
Alrode	4	4	9	6	5	9	15	51
Kagiso-Randfontein	5	8	9	7	7	8	16	60
Ruimsig	3	5	8	7	2	9	14	47
Kya Sand	3	5	7	6	5	9	13	48
Midrand	4	3	12	6	5	9	13	52
Aeroport	5	4	12	6	6	10	13	57
Nasrec	4	5	11	5	6	9	14	55
Rosherville	3	6	11	7	6	9	13	54
Chloorkop	6	7	13	7	7	8	13	61
Bonaero Park	4	6	10	7	6	10	13	57
Braamfontein	4	5	13	6	6	10	13	56
Average	**4**	**5**	**9**	**6**	**5**	**9**	**13**	**53**
SD	**1**	**2**	**2**	**1**	**1**	**1**	**1**	**6**
% V	**32**	**33**	**22**	**11**	**27**	**12**	**7**	**11**

APPENDIX S

Table S.1 QCheck™ correlations (matches) before cleaning between the FTIR 'fingerprints' of the different coated specimens after exposure at the main GJMA sites and their respective control spectra.

Main exposure sites	System A	System B	System C	System D	System E	System F	System G	Average
	Correlations with control spectra							
Diepsloot	0.91	0.98	0.73	0.84	0.65	0.83	0.39	0.76
Kagiso-Randfontein	0.91	0.94	0.87	0.75	0.42	0.92	0.55	0.77
Ivory Park	0.91	0.97	0.89	0.86	0.60	0.89	0.46	0.80
Alexandra	0.90	0.96	0.88	0.82	0.72	0.90	0.47	0.81
Aeroport	0.89	0.94	0.75	0.88	0.61	0.93	0.70	0.81
Midrand	0.92	0.96	0.81	0.87	0.67	0.93	0.56	0.82
Chloorkop	0.91	0.96	0.76	0.87	0.59	0.92	0.72	0.82
Orange Farm	0.90	0.97	0.85	0.87	0.68	0.93	0.57	0.82
Bonaero Park	0.93	0.95	0.88	0.85	0.62	0.96	0.63	0.83
Newtown	0.86	0.97	0.84	0.87	0.63	0.95	0.71	0.83
Delta Park	0.93	0.97	0.92	0.83	0.66	0.90	0.64	0.84
Braamfontein	0.91	0.98	0.86	0.87	0.61	0.95	0.71	0.84
Rosherville	0.94	0.97	0.81	0.88	0.62	0.95	0.73	0.84
Nasrec	0.94	0.97	0.86	0.87	0.65	0.96	0.79	0.86
Kya Sand	0.94	0.96	0.90	0.89	0.77	0.89	0.69	0.87
Ruimsig	0.94	0.97	0.90	0.90	0.64	0.95	0.80	0.87
Alrode	0.95	0.97	0.92	0.90	0.61	0.96	0.81	0.87
Chamdor	0.95	0.90	0.90	0.90	0.70	0.94	0.82	0.87
Brakpan	0.95	0.98	0.91	0.91	0.71	0.95	0.74	0.88
Florida Hills	0.94	0.98	0.88	0.91	0.74	0.97	0.74	0.88
Jabavu (Soweto)	0.96	0.98	0.94	0.93	0.79	0.97	0.89	0.92
Average	**0.92**	**0.96**	**0.86**	**0.87**	**0.65**	**0.93**	**0.67**	**0.84**
SD	**0.02**	**0.02**	**0.06**	**0.04**	**0.08**	**0.03**	**0.13**	**0.04**
% Var	**2.7**	**2.0**	**6.8**	**4.5**	**11.9**	**3.7**	**19.6**	**4.6**

Table S.2 QCheck™ correlations (matches) after cleaning between the FTIR 'fingerprints' of the different coated specimens after exposure at the main GJMA sites and their respective control spectra.

Main exposure sites	System A	System B	System C	System D	System E	System F	System G	Average
	Correlations with control spectra							
Kagiso-Randfontein	0.96	0.95	0.93	0.51	0.55	0.96	0.68	0.79
Aeroport	0.91	0.96	0.83	0.61	0.63	0.95	0.71	0.80
Midrand	0.91	0.97	0.88	0.66	0.66	0.95	0.59	0.80
Delta Park	0.92	0.95	0.94	0.62	0.66	0.95	0.57	0.80
Braamfontein	0.94	0.97	0.86	0.65	0.65	0.96	0.62	0.81
Diepsloot	0.92	0.96	0.90	0.69	0.71	0.95	0.56	0.81
Ivory Park	0.94	0.97	0.92	0.66	0.67	0.96	0.59	0.82
Alexandra	0.91	0.98	0.93	0.66	0.70	0.92	0.63	0.82
Orange Farm	0.95	0.96	0.93	0.66	0.68	0.95	0.65	0.82
Bonaero Park	0.94	0.98	0.92	0.64	0.66	0.96	0.67	0.82
Chloorkop	0.95	0.97	0.92	0.63	0.65	0.97	0.70	0.83
Nasrec	0.96	0.97	0.91	0.67	0.67	0.96	0.66	0.83
Chamdor	0.97	0.97	0.90	0.61	0.66	0.96	0.75	0.83
Kya Sand	0.94	0.98	0.91	0.72	0.72	0.96	0.62	0.84
Rosherville	0.96	0.98	0.94	0.65	0.68	0.97	0.67	0.84
Newtown	0.93	0.98	0.92	0.69	0.71	0.95	0.67	0.84
Brakpan	0.97	0.98	0.94	0.68	0.72	0.97	0.64	0.84
Alrode	0.97	0.97	0.94	0.64	0.70	0.96	0.71	0.84
Ruimsig	0.96	0.96	0.93	0.69	0.69	0.95	0.73	0.84
Florida Hills	0.95	0.98	0.94	0.69	0.74	0.96	0.64	0.84
Jabavu (Soweto)	0.98	0.98	0.97	0.68	0.75	0.98	0.91	0.89
Average	**0.94**	**0.97**	**0.92**	**0.65**	**0.68**	**0.96**	**0.67**	**0.83**
SD	**0.02**	**0.01**	**0.03**	**0.04**	**0.04**	**0.01**	**0.08**	**0.02**
% Var	**2.3**	**1.0**	**3.4**	**6.7**	**6.4**	**1.2**	**11.4**	**2.6**

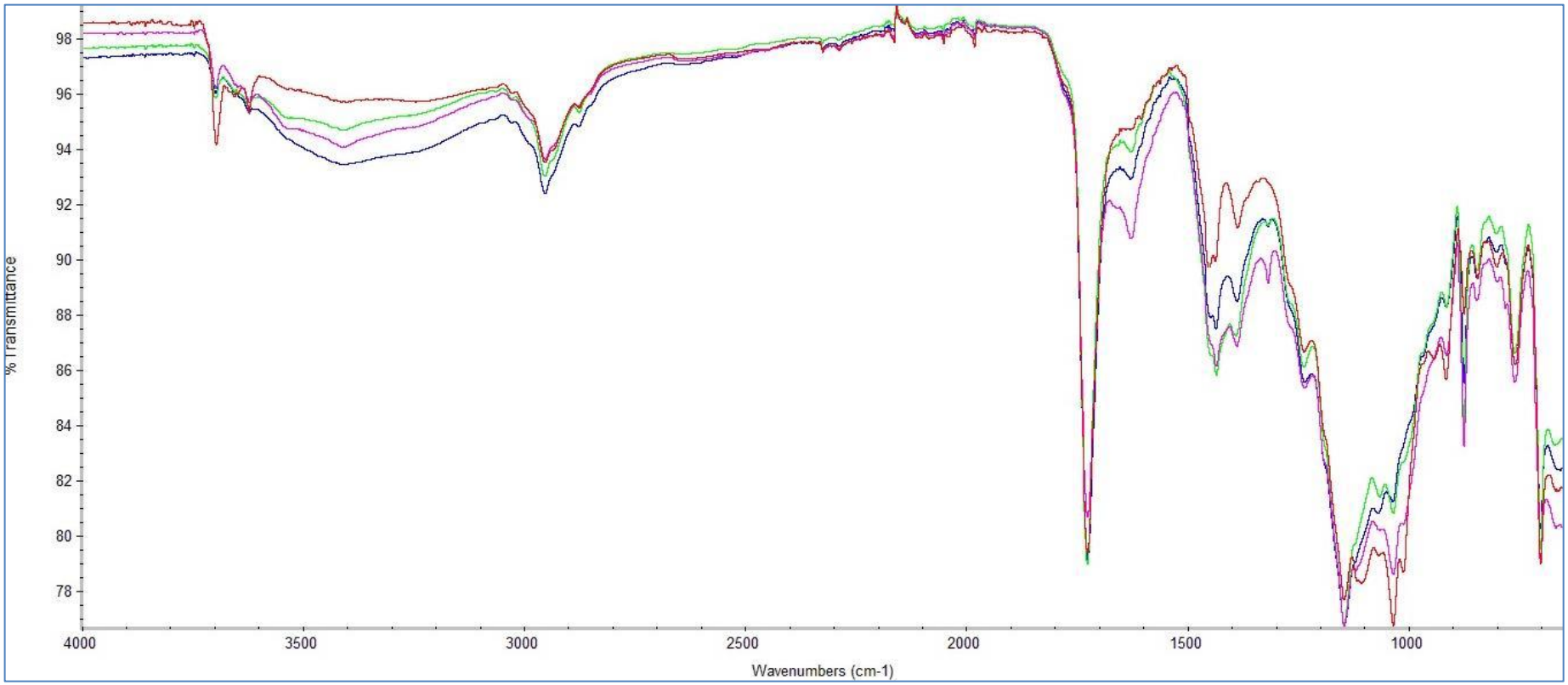


Figure S.1 Changes in the amplitudes/intensities of the peaks of the functional groups of **System D**, i.e. the water-based acrylic coating, at Aeroport (dark blue), Jabavu (Soweto) (purple), Kagiso-Randfontein (green) and Newtown (red), after 24 months of exposure at the main sites in the GJMA.

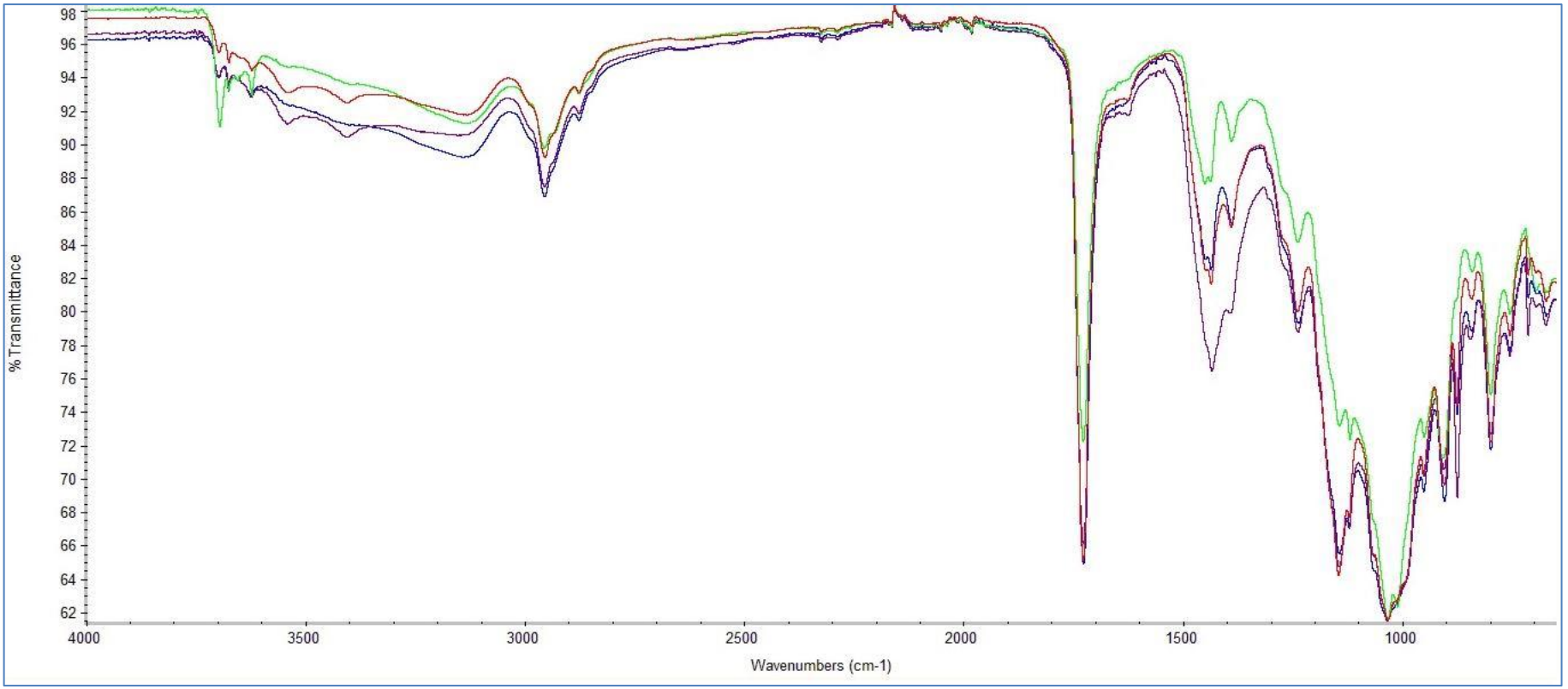


Figure S.2 Changes in the amplitudes/intensities of the peaks of the functional groups of **System E** (water-based acrylic coating) at Aeroport (dark blue), Jabavu (Soweto) (purple), Kagiso-Randfontein (green) and Newtown (red), after 24 months of exposure at the main sites in the GJMA.

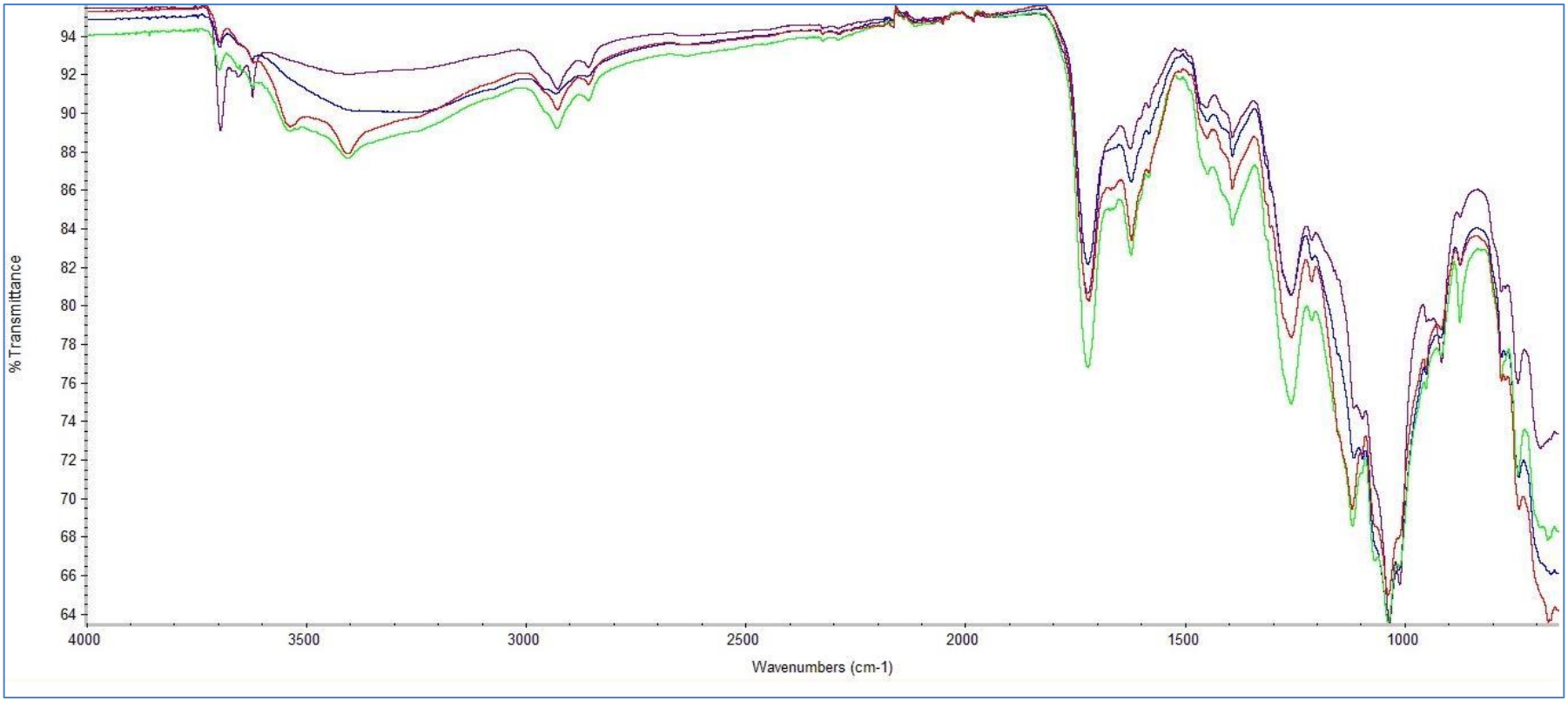


Figure S.3 Changes in the amplitudes/intensities of the peaks of the functional groups of **System G** (alkyd high gloss enamel coating) at Aeroport (dark blue), Jabavu (Soweto) (purple), Kagiso-Randfontein (green) and Newtown (red), after 24 months of exposure at the main sites in the GJMA.

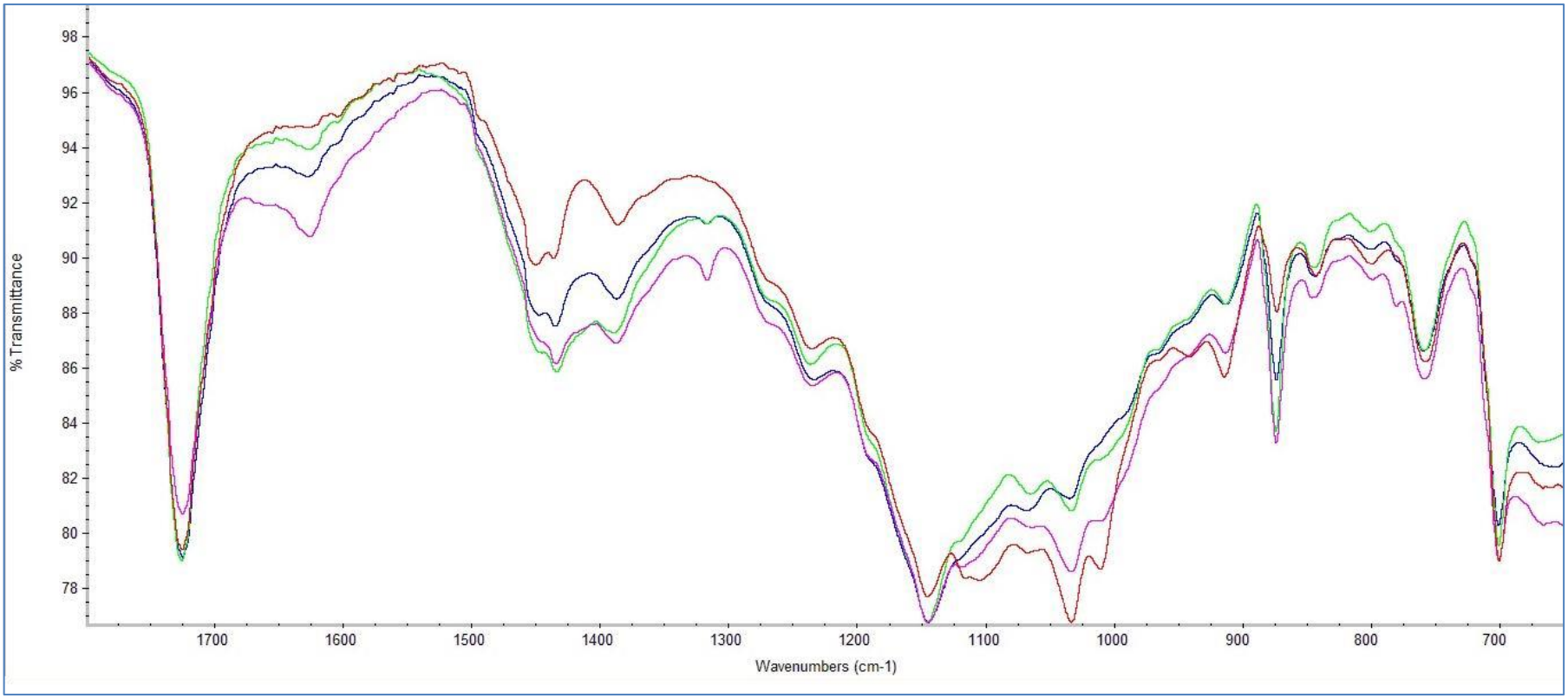


Figure S.4 Reduced intensities of the FTIR peaks of **System D** (water-based acrylic coating) at Aeroport (dark blue), Jabavu (Soweto) (purple), Kagiso-Randfontein (green) and Newtown (red), after 24 months of exposure at the main sites in the GJMA.

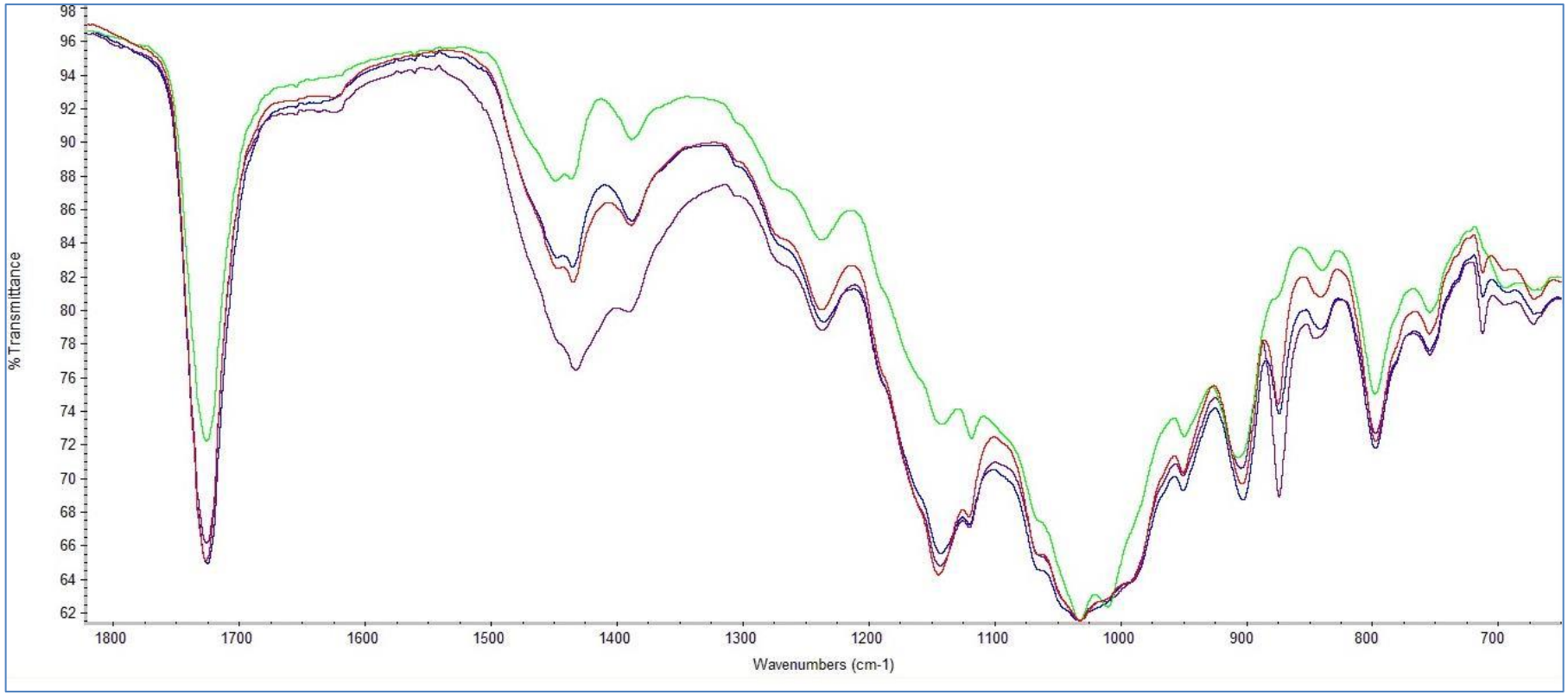


Figure S.5 Reduced intensities of the FTIR peaks of **System E** (water-based acrylic coating) at Aeroport (dark blue), Jabavu (Soweto) (purple), Kagiso-Randfontein (green) and Newtown (red), after 24 months of exposure at the main sites in the GJMA.

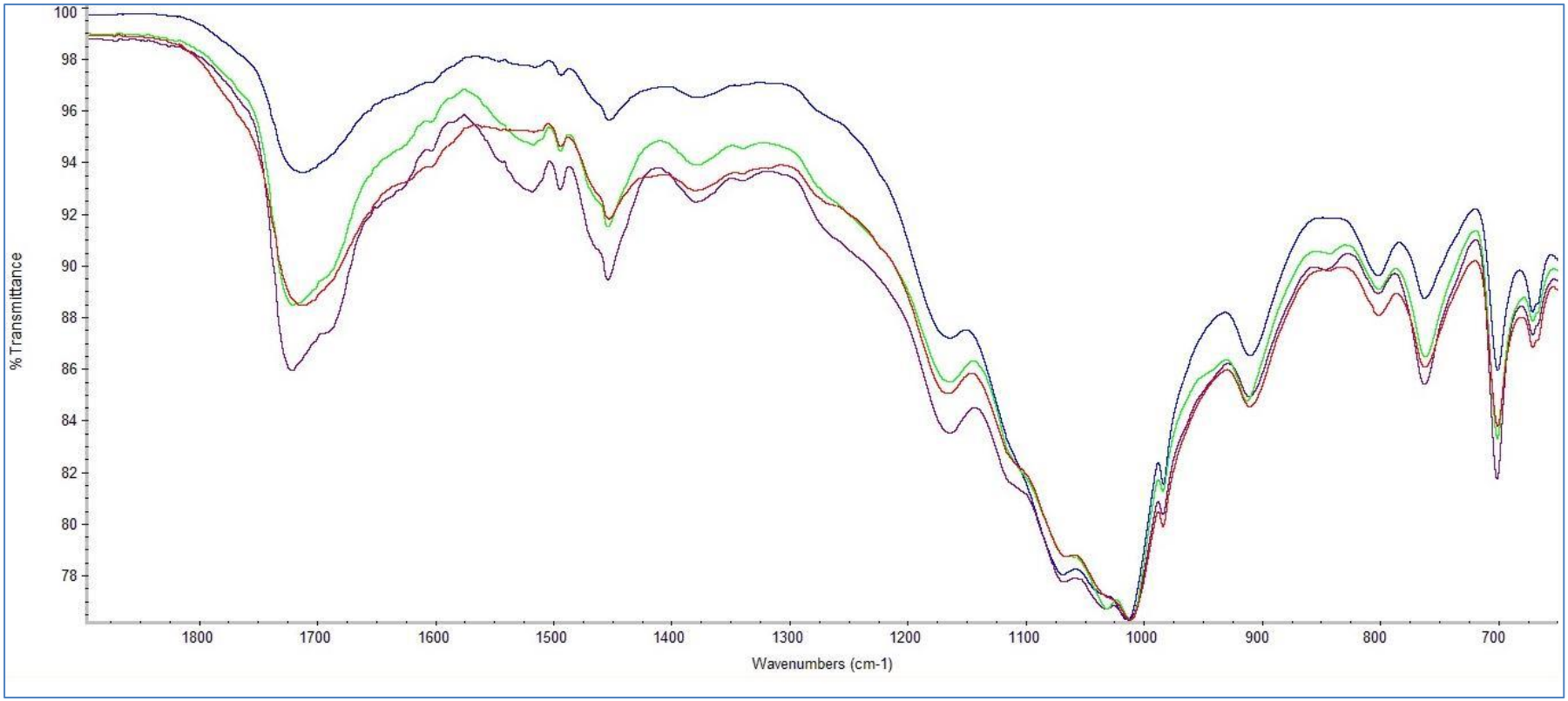


Figure S.6 Reduced changes of the FTIR peaks of **System C** (aliphatic acrylic polyurethane coating) at Aeroport (dark blue), Jabavu (Soweto) (purple), Kagiso-Randfontein (green) and Newtown (red), after 24 months of exposure at the main sites in the GJMA.

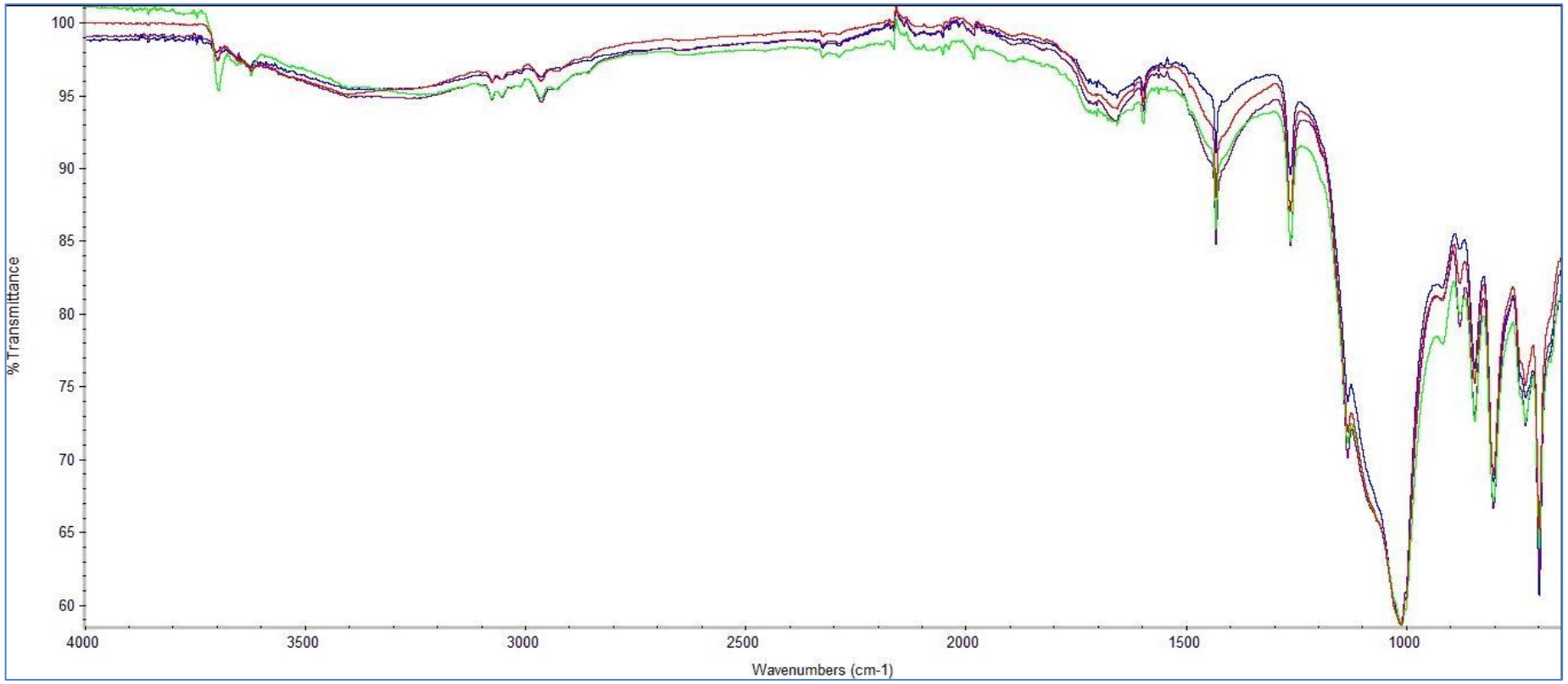


Figure S.7 Reduced changes in the intensities of the FTIR peaks of **System B** (polysiloxane coating) at Aeroport (dark blue), Jabavu (Soweto) (purple), Kagiso-Randfontein (green) and Newtown (red), after 24 months of exposure at the main sites in the GJMA.

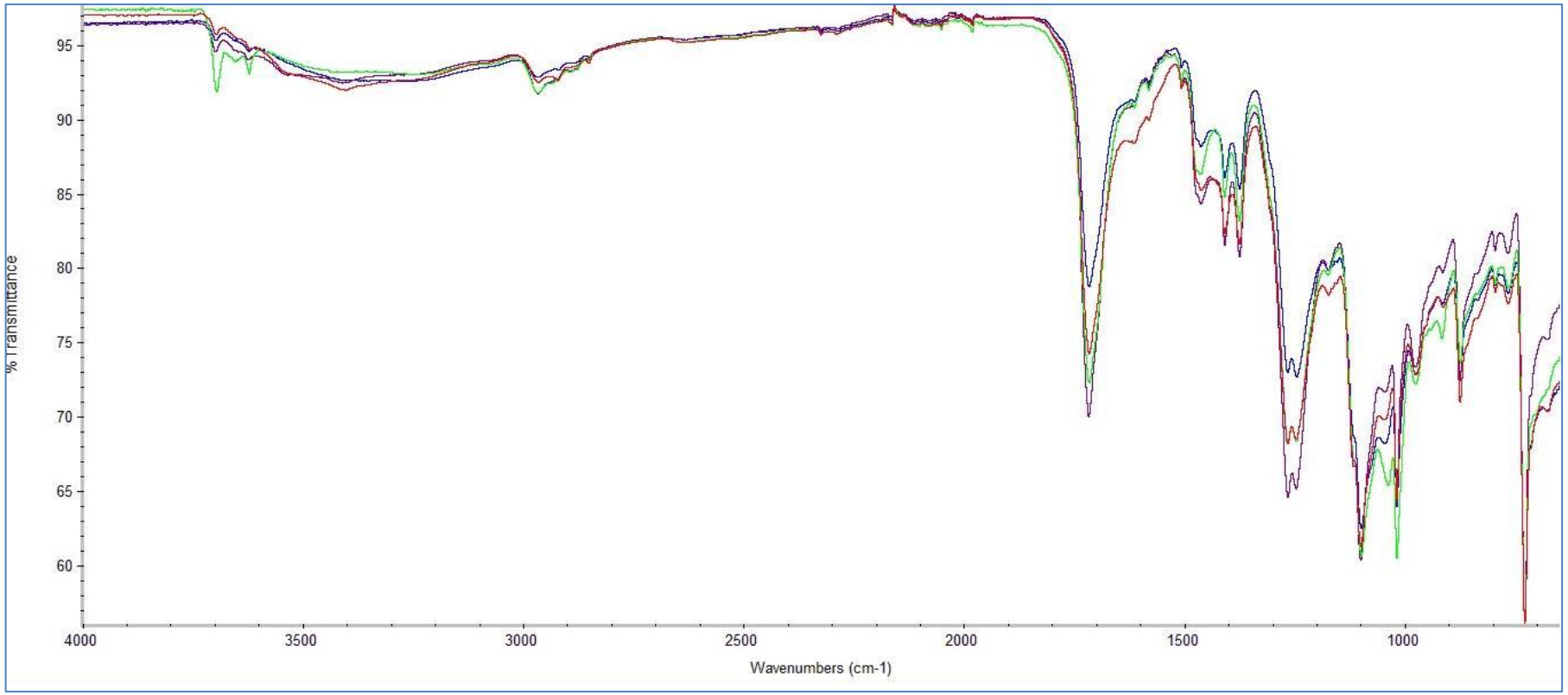


Figure S.8 Reduced changes in the intensities of the FTIR peaks of **System F** (polyester powder coating) at Aeroport (dark blue), Jabavu (Soweto) (purple), Kagiso-Randfontein (green) and Newtown (red), after 24 months of exposure at the main sites in the GJMA.

APPENDIX T

Table T.1 List of papers prepared for publishing.

No.	Title of paper	Journal
1	Corrosion map of South Africa' s macro atmosphere	South African Journal of Science
2	Atmospheric corrosion profiling of the Greater Johannesburg Metropolitan Area (GJMA)	Journal of Environmental Management
3	Residual life expectancies of select bronze statues in South Africa	South African Journal of Science
4	Photochemical degradation of organic materials in the Greater Johannesburg Metropolitan Area (GJMA)	South African Journal of Science

Table T.2 List of presentations given at conferences and seminars

No.	Title of presentation	Conference
1	Atmospheric corrosion profiling of the Greater Johannesburg Metropolitan Area – The start of a new corrosion map	AfriCORR – 2014 Conference in Pretoria (28 to 30 July 2014)
2	A preliminary updated atmospheric corrosivity map of South Africa - based on historical published and unpublished data	AfriCORR – 2016 Conference in Midrand (25 to 29 July 2016)
3	Atmospheric corrosion of zinc and hot-dip galvanising in South Africa (8 June 2017);	Corrosion Institute of Southern Africa – Gauteng branch
4	Atmospheric corrosion of zinc and hot-dip galvanising in South Africa (22 June 2017)	Corrosion Institute of Southern Africa - Western Cape branch
5	Atmospheric corrosion maps of South Africa and the Greater Johannesburg Metropolitan Area (GJMA).	AfriCORR – 2018 Conference in Johannesburg (28 t0 30 July 2018)